

**EXPERIMENTAL AND THEORETICAL VIBRATIONAL
SPECTROSCOPIC STUDIES OF
DIKETOPIPERAZINES**

BY

AHSAN ALI KHAN

[B.Pharm., MSc]

A thesis submitted in partial fulfilment of the requirements of the
University of Greenwich for the Degree of Doctor of Philosophy

January, 2017

Department of Pharmaceutical, Chemical & Environmental Sciences
Faculty of Engineering & Science
University of Greenwich
Central Avenue
Chatham Maritime
Kent ME4 4TB, UK



UNIVERSITY
of
GREENWICH

DECLARATION

“I certify that the work contained in this thesis, or any part of it, has not been accepted in substance for any previous degree awarded to me, and is not concurrently being submitted for any degree other than that of Doctor of Philosophy being studied at the University of Greenwich. I also declare that this work is the result of my own investigations, except where otherwise identified by references and that the contents are not the outcome of any form of research misconduct.”

_____ (Ahsan Ali Khan) (Candidate)



PhD Supervisors

_____ (Dr Andrew Mendham)

_____ (Prof. B.Z. Chowdhry)

Date: 27/01/2017

ACKNOWLEDGEMENTS

I am grateful to THE ALMIGHTY ALLAH (swt) for giving me the strength to complete my doctoral dissertation.

I am thankful to Dr Andrew P. Mendham and Prof. Babur Z. Chowdhry for the invaluable guidance, support and encouragement they have given to me as my doctoral thesis supervisors.

My sincere thanks to Dr Trevor J. Dines (University of Dundee) for helping and supplying me with the necessary computer programs and data for normal coordinate analysis of spectroscopic (FTIR/Raman) data. I also appreciate Dr Bruce D. Alexander's help for his assistance and support for the teaching and training I have received in computational chemistry.

I am very thankful to my parents, friends and relatives for their support, motivation and encouragement throughout my PhD studies at Greenwich University and boosting my moral in completing the work undertaken to date.

Thanks to all the technical staff members particularly Mark Allen, Devyani Amin, Dr Cris Laphorn, Dr Iain Goodall and Dr Ian Slipper of the University of Greenwich for their time to guide and assist me in my research.

The research reported in this doctoral thesis was made possible by a University of Greenwich "V.C., PhD Scholarship" awarded to Dr A. P. Mendham; I am grateful to the University of Greenwich and Dr Mendham for the aforementioned studentship.

Ahsan Ali Khan

ABSTRACT

Experimental and theoretical vibrational spectroscopic studies of diketopiperazines

The diketopiperazine (DKP) cyclo(L-homoCySH-L-homoCySH) (C-CySH) has been synthesised by a method reported in the literature. DFT calculations of molecular structures and their associated vibrational modes were conducted at the B3LYP/aug-cc-pVTZ level. The two calculated minimum energy structures of C-CySH display boat conformations, with C_1 and C_2 symmetry. The solid state Raman and IR spectra for C-CySH and its deuterated isotopomer are reported. The strong band at 1662 cm^{-1} observed in IR and at 1663 cm^{-1} in the Raman spectrum is assigned to the C=O stretching mode (*cis* amide I mode). On deuteration the *cis* amide I band shows a downward shift of around 54 cm^{-1} in the Raman spectrum; this can be attributed to stronger coupling and high N-H character compared with other DKPs. The *cis* amide II mode is found at 1506 cm^{-1} (Raman). This band is found at a significantly higher wavenumber than that of other DKPs where the ring, essentially, adopts a boat conformation.

The degradation of D-cycloserine was examined by $^1\text{H-NMR}$ spectroscopy. The resulting degradation products, 3,6-bis(aminoxymethyl)-piperazine-2,5-dione (AMDKP) and 3,6-dimethylene-piperazine-2,5-dione (DMDKP), were synthesised and their Raman and IR spectra obtained in both the solid and aqueous solution state (AMDKP) and in the solid state only (DMDKP). DFT calculations of molecular structures and their associated vibrational modes were conducted at the B3LYP/aug-cc-pVTZ level. The calculated minimum energy structures of AMDKP (C_2) and DMDKP (C_{2h}) have boat and planar conformations, respectively. Due to intermolecular hydrogen bonding with neighbouring molecules it is suggested that in AMDKP, the N-H bonds of the DKP appear at lower wavenumbers (between 3165 cm^{-1} and 3182 cm^{-1}) compared with the aminoxymethyl side-chain NH_2 vibrations (between $\sim 3204\text{ cm}^{-1}$ and 3342 cm^{-1}) in both solid state IR and Raman spectra. The strong bands located at 1659 cm^{-1} and 1655 cm^{-1} in the IR and Raman spectra are assigned to the C=O stretching mode (*cis* amide I mode) in AMDKP. The *cis* amide II vibration is detected at 1502 cm^{-1} in AMDKP. In DMDKP, the *cis* amide II mode is located at 1499 cm^{-1} and shifts to lower wavenumbers on *N*-deuteration (by $\sim 50\text{ cm}^{-1}$). It is hypothesised that due to the resonance effect associated with the dimethylene side-chain in DMDKP, the *cis* amide II mode may have a dramatic effect on its location compared to planar or near-planar DKPs.

Investigations of the Raman and IR spectra, of the DKPs N,N'-diacetyl-cyclo(Gly-Gly) (DAGG) and N,N'-dimethyl-cyclo(Gly-Gly) (DMGG) are reported and compared/contrasted with the parent DKP cyclo(Gly-Gly) in both the solid (powdered) and aqueous states. DFT calculations of the

structures of the isolated molecules, in the gas phase, and their associated vibrational modes were conducted using the hybrid SCF-DFT B3LYP method in conjunction with the aug-cc-pVTZ basis set. The calculated minimum energy structures of DAGG and DMGG both display boat conformations with C_2 symmetry. The Raman and IR spectra for DAGG show a significant decrease in wavenumber of the ring amide C-N stretching vibration compared to the parent DKP, resulting from a shortening of the ring C=O and lengthening of the C-N bonds. Unlike DAGG, there is no significant difference in C-N bond lengths for DMGG.

IR and Raman spectra of histidine containing DKPs, cyclo(L-His-L-Pro) (CHP), cyclo(D-His-L-Pro) (CDHP) and cyclo(L-Ala-L-His) (CAH), are reported in both the solid and solution state. Conformational analyses were carried out for the two tautomers of each molecule. DFT calculations of molecular structures and their associated vibrational modes were conducted at the B3LYP/aug-cc-pVTZ level. The experimental vibrational spectroscopic results are discussed together with the calculated data obtained for the lowest energy conformers of the two tautomers. The strong bands at 1645 and 1648 cm^{-1} (infra-red) and at 1649 and 1650 cm^{-1} in the Raman spectra of CHP and CDHP are assigned to the (C=O) stretch mode (*cis* amide I mode). In the case of CAH, this mode appears at 1671 cm^{-1} in the IR spectrum and at 1662 cm^{-1} in the Raman spectrum. The *cis* amide II mode is found at 1495, 1498 and 1496 cm^{-1} in the solid-state Raman spectra of CHP, CDHP and CAH, respectively. In the solution state this band is found at 1518, 1512 and 1523 cm^{-1} in the Raman spectra of CHP, CDHP and CAH, respectively. This mode shows a downward shift of $\sim 10\text{-}20 \text{ cm}^{-1}$ in the Raman spectra of CHP, CDHP and CAH in D_2O .

Investigations of the IR and Raman spectra of 2,3-DKP, 2,6-DKP and hexahydropyrimidine-4,5-dione (4,5-HHP) are reported and compared/contrasted with the 2,5-DKP regioisomer in both the solid (powdered) and aqueous states. DFT calculations at the B3LYP/aug-cc-pVTZ level, were employed in order to obtain the minimum energy structures of the three compounds. Due to intermolecular hydrogen bonding with neighbouring molecules it is suggested that in the case of 2,6-DKP, two N-H stretching bands are observed at different wavenumbers owing to the presence of N-H groups in different locations. Compared to the amide I mode of 2,5-DKP (located at $\sim 1655 \text{ cm}^{-1}$) in the solid state Raman spectrum, it is apparent that the vibrational bands for the ring C=O stretch of 2,3-DKP and 2,6-DKP appear at a significantly higher wavenumber ($\sim 40\text{-}50 \text{ cm}^{-1}$). The decrease in wavenumbers (cm^{-1}) of the C-N stretching vibrations (*cis* amide II) in 2,3-DKP, 2,6-DKP and 4,5-HHP can be attributed to the strong coupling of C-N vibrations with N-H in-plane-bending and CH_2 bending vibrations.

Ahsan Ali Khan [B.Pharm., MSc]

OVERVIEW OF THESIS

Chapter one provides a brief background and introduction to the subject area of the research reported in this report; namely diketopiperazines (DKPs).

Chapter two is divided into two parts. The first part focusses on an introduction to the theoretical aspects of the techniques used to obtain the vibrational spectra of the DKPs investigated; the second part describes different computational methods (DFT calculations and normal coordinate analysis) used to obtain the optimized molecular geometry, minimized energy and assign the vibrational bands in the spectra of DKPs.

Chapter three provides a list of the chemical reagents used in the research reported herein, together with the instrumentation used for FT-IR and Raman analysis. In addition computational methods used (DFT calculations) for structural determination, together with band assignments are discussed.

Chapter four reports on the theoretical and experimental vibrational spectroscopic studies of a sulphur containing DKP, cyclo(L-homoCySH-L-homoCySH); (C-CySH) is a cyclic di-amino acid peptide containing a DKP ring with two-homocysteinyl side-chains attached on either side of the ring. DKPs containing sulphur groups have been recognised for their diverse biological activities and pharmacological applications, thus making cyclo(L-homoCySH-L-homoCySH) an excellent research target for theoretical, experimental vibrational spectroscopic studies (solid state) and for investigating the conformation of the DKP ring in the gas phase.

Chapter five reports on the experimental vibrational and theoretical spectroscopic studies of the degradation products of D-cycloserine (3,6-bis(aminoxymethyl)-2,5-piperazinedione, AMDKP and 3,6-dimethylene-2,5-piperazinedione, DMDKP). Potentially, D-cycloserine is recognised for its broad spectrum therapeutic bioactivity against a wide variety of bacteria. This has led us to investigate the physico-chemical properties of its degradation products experimentally using FT-IR and Raman spectroscopy in the solid state and theoretically using DFT methods in the gas phase in order to compare and contrast the conformation of the DKP rings.

Chapter 6 reports on the IR and Raman studies of N,N'-diacetyl-cyclo(Gly-Gly) (DAGG) and N,N'-dimethyl-cyclo(Gly-Gly) (DMGG). These are the derivatives of the 2,5-DKP with N,N'-diacetyl or N,N'-dimethyl substitutions on either side of the DKP ring, with decreased effect of intermolecular hydrogen bonding seen in the parent DKP. This study determined the effect of

hydrogen bonding on the vibrational spectra of the DAGG and DMGG in solid and solution states using DFT methods in the gas phase in comparison to the parent DKP.

Chapter 7 reports the vibrational spectroscopic studies of the histidine-containing DKPs, cyclo(L-His-L-Pro) (CHP), cyclo(D-His-L-Pro) (CDHP) and cyclo(Ala-His) (CAH) together with conformational analyses of the two tautomeric forms of each compound. CHP has been recognised for its potent therapeutic activity, and this has led us to investigate the physico-chemical properties of CHP together with other DKPs (CDHP and CAH) experimentally using IR and Raman spectroscopy in the solid and solution state and theoretically using DFT methods in the gas phase to compare and contrast the conformation of the DKP rings.

Chapter 8 reports on the experimental and vibrational spectroscopic studies on the regioisomers of DKPs (2,3-DKP, 2,6-DKP and 4,5-HHP). This study have been carried out in order to compare and contrast the vibrational spectra of the regioisomers with 2,5-DKP in both solid and solution states and using DFT calculations in the gas phase.

Chapter 9 provides a summary of the work presented in the thesis and a brief discussion of possible future research prospects related to DKPs.

Chapter 10 provides appendices of the work not included in the main body of the thesis, namely the analytical data for the characterization of the DKPs examined.

CONTENTS

DECLARATION.....	II
ACKNOWLEDGMENTS.....	III
ABSTRACT.....	IV
OVERVIEW OF THESIS.....	VI
CONTENTS.....	VIII
FIGURES.....	XIV
TABLES.....	XXI
ABBREVIATIONS.....	XXIV
PUBLICATIONS AND CONFERENCE PRESENTATIONS.....	XXVI
Chapter 1: Introduction.....	1
1.1 Introduction to diketopiperazines.....	1
1.2 Physico-chemical properties of DKPs.....	2
1.2.1 Solubility of DKPs.....	2
1.2.2 Stability of DKPs.....	2
1.2.3 Absorption and transportation of DKPs.....	2
1.3 Biological properties of diketopiperazines.....	3
1.4 Sulphur containing diketopiperazine.....	3
1.5 Synthesis of diketopiperazines.....	4
1.6 Structure and conformation of diketopiperazines.....	9
1.7 References.....	13
Chapter 2: Theoretical Aspects of Instrumental Techniques and Computational Methods.....	17
2.1 Theoretical aspects of instrumental techniques.....	17
2.1.1 Introduction to spectroscopy.....	17
2.1.2 Vibrational spectroscopy.....	17
2.2 Molecular vibrations.....	18
2.2.1 Vibrational modes.....	21
2.2.2 Classification of fundamental vibrations.....	21
2.2.3 Non-fundamental vibrations.....	22
2.2.3.1 Overtones.....	23
2.2.3.2 Combination and difference bands.....	23
2.2.3.3 Fermi resonance.....	23

2.2.4	Intensities of vibrational bands.....	24
2.2.5	Theory of infra-red absorption.....	25
2.2.6	Raman scattering.....	27
2.2.7	Selection rules.....	30
2.2.8	Selection rules for infra-red absorption and Raman scattering.....	30
2.2.9	Infra-red versus Raman spectroscopy.....	31
2.2.10	Introduction to molecular symmetry.....	32
2.2.11	Group theory.....	33
2.2.12	Symmetry operations and symmetry elements.....	33
2.2.13	Point groups.....	34
2.2.14	Character Tables.....	35
2.3	Computational chemistry.....	37
2.3.1	Molecular mechanics.....	38
2.3.2	Electronic structure methods.....	38
2.3.3	<i>Ab-initio</i> methods.....	39
2.3.4	Semi-empirical methods.....	40
2.3.5	Electron correlation methods.....	40
2.3.6	Møller-Plesset perturbation theory.....	40
2.3.7	Density functional theory.....	42
2.3.7.1	DFT methods.....	43
2.3.8	Basis sets.....	43
2.3.9	Geometry optimization.....	44
2.3.10	Frequency calculations.....	45
2.3.11	Normal coordinate analysis (NCA).....	46
2.4	Nuclear Magnetic Resonance.....	46
2.4.1	Principles of NMR.....	46
2.4.2	Chemical shift.....	47
2.5	Mass spectrometry.....	49
2.6	References.....	50
Chapter 3:	Experimental	54
3.1	Chemical reagents.....	54
3.1.1	Synthesis.....	54
3.1.2	Deuteration.....	55
3.2	Vibrational spectroscopy.....	55

3.2.1	Raman spectroscopy.....	55
3.2.2	Solid and solution state Raman spectra.....	56
3.2.3	Attenuated total reflectance (ATR).....	56
3.2.4	Solid and solution state IR spectra.....	57
3.3	DFT calculations.....	57
3.4	Molecular orbital analysis.....	59
3.5	Molecular electrostatic potential.....	59
3.6	Hirshfeld surface analysis.....	60
3.7	References.....	60
Chapter 4: Theoretical and Experimental Vibrational Spectroscopic Studies of a Sulphur containing Diketopiperazine.....		62
4.1	Introduction.....	62
4.2	Experimental.....	62
4.2.1	Materials.....	63
4.2.2	Synthesis.....	63
4.2.3	Vibrational spectroscopy and instrumental details.....	64
4.2.4	DFT calculations.....	64
4.3	Results and discussion.....	64
4.3.1	Geometry optimization.....	64
4.3.2	Vibrational assignments.....	71
4.3.3	Spectral region >2000 cm ⁻¹	71
4.3.4	Spectral region 1250-1700 cm ⁻¹	71
4.3.5	Spectral region 850-1350 cm ⁻¹	73
4.3.6	Spectral region 500-850 cm ⁻¹	73
4.3.7	Spectral region < 500 cm ⁻¹	74
4.4	Molecular orbital analysis.....	82
4.5	Hirshfeld surface analysis.....	84
4.6	Conclusions.....	87
4.7	References.....	96
Chapter 5: Theoretical and Experimental Vibrational Spectroscopic Studies of the Degradation Products of D-Cycloserine.....		97
5.1	Introduction.....	97
5.2	Experimental.....	98
5.2.1	Materials.....	98

5.2.2	Synthesis.....	98
5.2.3	Vibrational spectroscopy and instrumental details.....	99
5.2.4	DFT calculations.....	99
5.3	NMR spectroscopy of the degradation of CS	99
5.4	Results and discussion.....	100
5.4.1	NMR spectroscopy.....	100
5.4.2	Geometry optimization.....	100
5.4.3	Vibrational assignments.....	108
5.4.4	Spectral region $>2000\text{ cm}^{-1}$	108
5.4.5	Spectral region $1250\text{-}1700\text{ cm}^{-1}$	109
5.4.6	Spectral region $850\text{-}1350\text{ cm}^{-1}$	112
5.4.7	Spectral region $500\text{-}850\text{ cm}^{-1}$	112
5.4.8	Spectral region $< 500\text{ cm}^{-1}$	113
5.5	Molecular orbital analysis.....	126
5.6	Molecular electrostatic potential.....	128
5.7	Hirshfeld surface analysis.....	129
5.8	Conclusions.....	132
5.9	References.....	140
Chapter 6: Vibrational Spectroscopic Studies of the Cyclic Di-Amino Acid Peptides <i>N, N'</i>-Diacetyl-cyclo(Gly-Gly) and <i>N, N'</i>-Dimethyl-cyclo(Gly-Gly).....		
6.1	Introduction.....	142
6.2	Experimental.....	143
6.2.1	Materials.....	143
6.2.2	Synthesis.....	143
6.2.3	Vibrational spectroscopy and instrumental details.....	143
6.2.4	DFT calculations.....	143
6.3	Results and discussion.....	143
6.3.1	Geometry optimization.....	144
6.3.2	Vibrational assignments.....	151
6.3.3	Wavenumber region $>2000\text{ cm}^{-1}$	151
6.3.4	Wavenumber region $1200\text{-}1700\text{ cm}^{-1}$	153
6.3.5	Wavenumber region $900\text{-}1200\text{ cm}^{-1}$	155
6.3.6	Wavenumber region $500\text{-}900\text{ cm}^{-1}$	156
6.3.7	Wavenumber region $< 500\text{ cm}^{-1}$	157

6.4	Molecular orbital analysis.....	164
6.5	Molecular electrostatic potential.....	166
6.6	Hirshfeld surface analysis.....	167
6.7	Conclusions.....	171
6.8	References.....	179
Chapter 7:	Vibrational Spectroscopic Studies of Histidine Containing Cyclic Dipeptides in the Solid State and in Aqueous Solution: Conformational Analysis and DFT Calculations.....	180
7.1	Introduction.....	180
7.2	Experimental.....	182
7.2.1	Materials.....	182
7.2.2	Vibrational spectroscopy and Instrumental details.....	183
7.2.3	DFT calculations.....	183
7.3	Results and discussion.....	183
7.3.1	Geometry optimization.....	183
7.3.2	Conformational analysis.....	184
7.3.3	Vibrational assignments.....	201
7.3.4	Spectral region $>2000\text{ cm}^{-1}$	201
7.3.5	Spectral region $1250\text{-}1700\text{ cm}^{-1}$	202
7.3.6	Spectral region $850\text{-}1350\text{ cm}^{-1}$	204
7.3.7	Spectral region $500\text{-}850\text{ cm}^{-1}$	205
7.3.8	Spectral region $< 500\text{ cm}^{-1}$	205
7.4	Molecular orbital analysis.....	238
7.5	Conclusions.....	241
7.6	References.....	242
Chapter 8:	IR and Raman Spectroscopic Studies of the Regioisomers of Diketopiperazine: Solid State and Aqueous Solution, DFT Calculations, HOMO-LUMO and Hirshfeld Surface Analysis	245
8.1	Introduction.....	245
8.2	Experimental.....	246
8.2.1	Materials.....	246
8.2.2	Synthesis.....	246
8.2.3	Vibrational spectroscopy and instrumental details.....	247
8.2.4	DFT calculations.....	247
8.3	Results and discussion.....	247

8.3.1	Geometry optimization.....	247
8.3.2	Vibrational assignments.....	255
8.3.3	Wavenumber region above 2000 cm ⁻¹	256
8.3.4	Wavenumber region 1200-1700 cm ⁻¹	257
8.3.5	Wavenumber region 900-1200 cm ⁻¹	260
8.3.6	Wavenumber region 500-900 cm ⁻¹	260
8.3.7	Wavenumber region < 500 cm ⁻¹	261
8.4	Molecular orbital analysis.....	282
8.5	Molecular electrostatic potential.....	285
8.6	Hirshfeld surface analysis.....	285
8.7	Conclusions.....	297
8.8	References.....	298
9.0	Overall Conclusions and Future Work.....	300
9.1	Overall conclusions.....	300
9.1.1	DFT calculations.....	300
9.1.2	N-H stretching vibrations.....	301
9.1.3	<i>Cis</i> amide I vibrations.....	302
9.1.4	<i>Cis</i> amide II vibrations.....	303
9.2	Future work.....	304
9.3	References.....	305
10.0	APPENDIX.....	307

FIGURES

Figure 1.1.	Structure of DKP.....	1
Figure 1.2.	Dipeptide ester cyclization reaction.....	5
Figure 1.3.	Amino acid condensation.....	6
Figure 1.4.	<i>Cis</i> and <i>trans</i> isomers in peptides.....	9
Figure 1.5.	Schematic representation of different conformation in DKPs.....	11
Figure 2.1.	An illustration of vibrational excitation in IR (top) and Raman (bottom) spectroscopy.....	18
Figure 2.2.	Potential energy plot for a harmonic oscillator.....	19
Figure 2.3.	Morse potential curve for an anharmonic oscillator.....	20
Figure 2.4.	Types of vibrations in a diatomic molecule.....	22
Figure 2.5.	Example of intensity and frequency shifts due to Fermi resonance.....	24
Figure 2.6.	Energy level diagram for vibrational transitions.....	25
Figure 2.7.	Schematic representation of energy transitions.....	27
Figure 2.8.	Flow chart for determining point groups.....	35
Figure 2.9.	Character table for C _{2v} point group.....	36
Figure 2.10.	Flow chart for quantum mechanical calculations of molecular structure.....	46
Figure 2.11.	Nuclear spin of nucleus.....	47
Figure 2.12.	Influence of a magnetic field on nuclei of atoms.....	47
Figure 2.13.	The quantum energy levels in NMR.....	48
Figure 2.14.	¹ H-NMR chemical shifts.....	48
Figure 2.15.	Typical example of ionisation of a molecule followed by fragmentation.....	49
Figure 2.16.	Schematic diagram of a mass analyser.....	50
Figure 3.1.	LabRam Raman spectrometer.....	55
Figure 3.2.	Perkin Elmer Spectrum Two UATR FTIR spectrometer.....	56
Figure 3.3.	A multiple reflection ATR system.....	57
Figure 4.1.	Structure of C-CySH.....	63
Figure 4.2.	Atom numbering scheme for C-CySH.....	65
Figure 4.3.	Potential energy plot for C-CySH.....	65
Figure 4.4.	The three asymmetric structures of C-CySH in a crystallographic unit cell.....	66

Figure 4.5.	Calculated structures of C-CySH.....	66
Figure 4.6.	Calculated (A=C ₁ symmetry, B= C ₂ symmetry molecules) and experimental (C) IR spectra for C-CySH.....	80
Figure 4.7.	Calculated (A=C ₁ symmetry, B= C ₂ symmetry molecules) and experimental (C) Raman spectra for C-CySH.....	81
Figure 4.8.	Calculated (A=C ₁ symmetry, B= C ₂ symmetry molecules) and experimental (C) Raman spectra for C-CySH.....	81
Figure 4.9.	Calculated (A=C ₁ symmetry, B= C ₂ symmetry molecules) and experimental (C) Raman spectra for <i>N,S</i> -deuterated C-CySH.....	82
Figure 4.10.	HOMO-LUMO plots with orbital composition of the C ₁ molecule of C-CySH.....	83
Figure 4.11.	HOMO-LUMO plots with orbital composition of the C ₂ molecule of C-CySH.....	83
Figure 4.12.	Hirshfeld surface mapped with d_{norm} as transparent to visualize the orientation of the three asymmetric molecules of C-CySH.....	85
Figure 4.13.	Hirshfeld surfaces for the three molecules (A, B and C) of C-CySH mapped with (a) shape index (b) curvedness.....	85
Figure 4.14.	2D Fingerprint plots for the intermolecular contacts in molecules A, B and C of C-CySH.....	86
Figure 5.1.	Structures of (a) AMDKP and (b) DMDKP.....	98
Figure 5.2.	Reaction scheme for the synthesis of D-cycloserine derivatives.....	99
Figure 5.3.	¹ H-NMR spectra (part) highlighting the degradation of CS in the presence of 120 μL of glacial acetic acid.....	100
Figure 5.4.	Atom numbering scheme for (a) AMDKP and (b) DMDKP.....	101
Figure 5.5.	Calculated structures of (a) AMDKP, (b) DMDKP and (c) X-ray structure of DMDKP.....	101
Figure 5.6.	Potential energy plot for AMDKP.....	102
Figure 5.7.	Calculated (top) and experimental (bottom) solid state IR spectra for AMDKP.....	121
Figure 5.8.	Calculated (top) and experimental (bottom) solid state Raman spectra for AMDKP.....	122
Figure 5.9.	Calculated (top) and experimental (bottom) solid state IR spectra for <i>N</i> -deuterated AMDKP.....	122

Figure 5.10.	The calculated (top) and experimental (bottom) solid state Raman spectra for <i>N</i> -deuterated AMDKP.....	123
Figure 5.11.	Calculated (top) and experimental (bottom) solid state IR spectra for DMDKP.....	123
Figure 5.12.	Calculated (top) and experimental (bottom) solid state IR spectra for <i>N</i> - deuterated DMDKP.....	124
Figure 5.13.	Calculated (top) and experimental (bottom) solid state Raman spectra for DMDKP.....	124
Figure 5.14.	Calculated (top) and experimental (bottom) solid state Raman spectra for <i>N</i> -deuterated DMDKP.....	125
Figure 5.15.	Experimental non-deuterated (top) and <i>N</i> -deuterated (bottom) solution state Raman spectra of AMDKP.....	125
Figure 5.16.	Experimental non-deuterated (top) and <i>N</i> -deuterated (bottom) solution state IR spectra of AMDKP.....	126
Figure 5.17.	HOMO-LUMO plots with orbital compositions of AMDKP.....	127
Figure 5.18.	HOMO-LUMO plots with orbital compositions of DMDKP.....	127
Figure 5.19.	(a) MEP energy surface and (b) contour map (MEP) for AMDKP.....	128
Figure 5.20.	(a) MEP energy surface and (b) contour map (MEP) for DMDKP.....	129
Figure 5.21.	Hirshfeld surface mapped with d_{norm} showing all close contacts in DMDKP.....	130
Figure 5.22.	Hirshfeld surfaces of DMDKP mapped with (a) shape index (b) curvedness (c) stacking interactions in DMDKP.....	130
Figure 5.23.	2D Fingerprint plots for the intermolecular contacts in DMDKP.....	131
Figure 6.1.	Atom numbering scheme for (A) DAGG and (B) DMGG.....	143
Figure 6.2.	Experimental (a), calculated (planar) (b) and boat (c)) structure of DMGG.....	144
Figure 6.3.	Experimental (A and B) and calculated (C) structure of DAGG.....	144
Figure 6.4.	Calculated (top) and experimental (bottom) solid state Raman spectra for DAGG.....	161
Figure 6.5.	Calculated (top) and experimental (bottom) solid state IR spectra for DAGG.....	162
Figure 6.6.	Calculated (A) planar (B) boat conformers and (C) experimental solid state Raman spectra of DMGG.....	162

Figure 6.7.	Calculated (A) planar (B) boat conformers and (C) experimental solid state IR spectra of DMGG.....	163
Figure 6.8.	Solution state Raman spectra of (top) DMGG and (bottom) DAGG.....	163
Figure 6.9.	Solution state IR spectra of (top) DMGG and (bottom) DAGG.....	164
Figure 6.10.	HOMO-LUMO plots with orbital compositions of DAGG.....	165
Figure 6.11.	HOMO-LUMO plots with orbital compositions of DMGG.....	165
Figure 6.12.	(a) Molecular electrostatic potential energy surface and (b) contour map (MEP) of DAGG.....	166
Figure 6.13.	(a) Molecular electrostatic potential energy surface and (b) contour map (MEP) of DMGG.....	167
Figure 6.14.	Hirshfeld surface mapped with d_{norm} showing all close contacts in (A1, B1) front view and (A2, B2) back view of molecule A and B of DAGG respectively.....	168
Figure 6.15.	Hirshfeld surface mapped with d_{norm} showing all close contacts in DMGG.....	169
Figure 6.16.	Hirshfeld surfaces mapped with shape index (left) and curvedness (right) for molecules A and B of DAGG.....	169
Figure 6.17.	Hirshfeld surfaces of DMGG mapped with (a) shape index (b) curvedness.....	169
Figure 6.18.	2D Fingerprint plots for all the intermolecular contacts in molecules A and DAGG.....	170
Figure 6.19.	2D Fingerprint plots for all the intermolecular contacts in DMGG.....	171
Figure 7.1.	Structures of (A) CHP (B) CDHP and (C) CAH with their tautomeric forms.....	182
Figure 7.2.	Atom numbering scheme of (A) N^{ϵ} -protonated (B) N^{δ} -protonated tautomers of CHP and CDHP and (C) N^{ϵ} -protonated (D) N^{δ} -protonated tautomers of CAH.....	184
Figure 7.3.	Potential energy scan of CHP.....	186
Figure 7.4.	Potential energy scan of (A) N^{ϵ} (B) N^{δ} -tautomeric forms of CHP.....	187
Figure 7.5.	Potential energy scan of CDHP.....	189
Figure 7.6.	Potential energy scan of (A) N^{ϵ} (B) N^{δ} -tautomeric forms of CDHP.....	189
Figure 7.7.	Potential energy scan of CAH.....	191
Figure 7.8.	Potential energy scan of (A) N^{ϵ} (B) N^{δ} -tautomeric forms of CAH.....	191

Figure 7.9.	Calculated (A) N ^ε -protonated (B) N ^δ -protonated tautomers and (C) experimental solid state Raman spectra of CHP.....	206
Figure 7.10.	Calculated (A) N ^ε -protonated (B) N ^δ -protonated tautomers and (C) experimental solid state IR spectra of CHP.....	207
Figure 7.11.	Calculated (A) N ^ε -protonated (B) N ^δ -protonated tautomers and (C) experimental solid state Raman spectra of CDHP.....	207
Figure 7.12.	Calculated (A) N ^ε -protonated (B) N ^δ -protonated tautomers and (C) experimental solid state IR spectra of CDHP.....	208
Figure 7.13.	Solution state Raman spectra of (A) CAH (B) CHP and (C) CDHP in H ₂ O.....	208
Figure 7.14.	Solution state Raman spectra of (A) CAH (B) CHP and (C) CDHP in D ₂ O.....	209
Figure 7.15.	Solution state IR spectra of (A) CAH (B) CHP and (C) CDHP in H ₂ O...	209
Figure 7.16.	Solution state IR spectra of (A) CAH (B) CHP and (C) CDHP in D ₂ O...	210
Figure 7.17.	Calculated (A) N ^ε -protonated (B) N ^δ -protonated tautomers and (C) experimental solid state Raman spectra of CAH.....	210
Figure 7.18.	Calculated (A) N ^ε -protonated (B) N ^δ -protonated tautomers and (C) experimental Solid state IR spectra of CAH.....	211
Figure 7.19.	Calculated (A) N ^ε -deuterated (B) N ^δ -deuterated tautomers of CHP and (C) experimental solid state Raman spectra of <i>N</i> -deuterated CAH.....	211
Figure 7.20.	Calculated (A) N ^ε -deuterated (B) N ^δ -deuterated tautomers and (C) experimental solid state IR spectra of <i>N</i> -deuterated CAH.....	212
Figure 7.21.	HOMO-LUMO plots of lowest energy conformer of (A) N ^ε and (B) N ^δ -tautomeric forms of CHP.....	238
Figure 7.22.	HOMO-LUMO plots of the lowest energy conformer of (A) N ^ε and (B) N ^δ -tautomeric forms of CDHP.....	239
Figure 7.23.	HOMO-LUMO plots of the lowest energy conformer of (A) N ^ε and (B) N ^δ -tautomeric forms of CAH.....	239
Figure 8.1.	Atom numbering scheme of (a) 2,3-DKP (b) 2,6-DKP and (c) 4,5-HHP.	247
Figure 8.2.	Calculated structures of 2,3-DKP (a) skew-boat (d) planar, 2,6-DKP (b) half-chair (e) planar, 4,5-HHP (c) half-chair (f) planar and 2,5-DKP (g) boat together with X-ray structures of (h) 2,3-DKP and (i) 2,5-DKP.....	248
Figure 8.3.	Solid state IR spectra of (A) 2,5-DKP (B) 2,6-DKP (C) 4,5-HHP and (D) 2,3-DKP.....	276

Figure 8.4.	Solid state Raman spectra of (A) 2,5-DKP (B) 2,6-DKP (C) 4,5-HHP and (D) 2,3-DKP.....	276
Figure 8.5.	Solid state IR spectra of <i>N</i> -deuterated (A) 2,5-DKP (B) 2,6-DKP (C) 4,5-HHP and (D) 2,3-DKP.....	277
Figure 8.6.	Solid state Raman spectra of <i>N</i> -deuterated (A) 2,5-DKP (B) 2,6-DKP (C) 4,5-HHP and (D) 2,3-DKP.....	277
Figure 8.7.	Solution state IR spectra of (A) 2,5-DKP (B) 2,6-DKP (C) 4,5-HHP and (D) 2,3-DKP.....	278
Figure 8.8.	Solution state Raman spectra of (A) 2,5-DKP (B) 2,6-DKP (C) 4,5-HHP and (D) 2,3-DKP.....	278
Figure 8.9.	Solution state IR spectra of <i>N</i> -deuterated (A) 2,5-DKP (B) 2,6-DKP (C) 4,5-HHP and (D) 2,3-DKP.....	279
Figure 8.10.	Solution state Raman spectra of <i>N</i> -deuterated (A) 2,5-DKP (B) 2,6-DKP (C) 4,5-HHP and (D) 2,3-DKP.....	279
Figure 8.11.	Calculated IR spectra of (A) half-chair (B) planar (2,6-DKP) (C) Half-chair (D) planar (4,5-HHP) and (E) skew-boat (F) planar (2,3-DKP).....	280
Figure 8.12.	Calculated Raman spectra of (A) half-chair (B) planar (2,6-DKP) (C) Half-chair (D) planar (4,5-HHP) and (E) skew-boat (F) planar (2,3-DKP).....	280
Figure 8.13.	Calculated IR spectra of <i>N</i> -deuterated (A) half-chair (B) planar (2,6-DKP) (C) half-chair (D) planar (4,5-HHP) and (E) skew-boat (F) planar (2,3-DKP).....	281
Figure 8.14.	Calculated Raman spectra of <i>N</i> -deuterated (A) half-chair (B) planar (2,6-DKP) (C) half-chair (D) planar (4,5-HHP) and (E) skew-boat (F) planar (2,3-DKP).....	281
Figure 8.15.	HOMO-LUMO plots of (A) 2,3-DKP (B) 2,6-DKP (C) 4,5-HHP and (D) 2,5-DKP and their molecular electrostatic potential energy surface (MEP) are shown in a,b,c and d, respectively.....	283
Figure 8.16.	Hirshfeld surfaces of (A) 2,3-DKP (B) 2,5-DKP mapped with (a,d) d_{norm} showing all close contacts (b,e) shape index (c,f) curvedness.....	286
Figure 8.17.	2D Fingerprint plots for all the intermolecular contacts in (A) 2,3-DKP and (B) 2,5-DKP.....	287
Figure 10.1.	^1H -NMR spectrum of C-CySH.....	308
Figure 10.2.	^{13}C -NMR spectrum of C-CySH.....	309

Figure 10.3.	^1H -NMR spectrum of AMDKP.....	309
Figure 10.4.	^{13}C -NMR spectrum of AMDKP.....	310
Figure 10.5.	^1H -NMR spectrum of DMDKP.....	311
Figure 10.6.	^{13}C -NMR spectrum of DMDKP.....	311
Figure 10.7.	^1H -NMR spectrum of DAGG.....	312
Figure 10.8.	^{13}C -NMR spectrum of DAGG.....	312
Figure 10.9.	^1H -NMR spectrum of DMGG.....	313
Figure 10.10.	^{13}C -NMR spectrum of DMGG.....	314
Figure 10.11.	^1H -NMR spectrum of 2,3-DKP.....	314
Figure 10.12.	^{13}C -NMR spectrum of 2,3-DKP.....	315
Figure 10.13.	DEPT-135 spectrum of 2,3-DKP.....	315
Figure 10.14.	^1H -NMR spectrum of 2,6-DKP.....	316
Figure 10.15.	^{13}C -NMR spectrum of 2,6-DKP.....	316
Figure 10.16.	HMBC spectrum of 2,6-DKP.....	317
Figure 10.17.	^1H -NMR spectrum of 4,5-HHP.....	317
Figure 10.18.	^{13}C -NMR spectrum of 4,5-HHP.....	318
Figure 10.19.	HMBC spectrum of 4,5-HHP.....	318
Figure 10.20.	The mass spectrum (ES-) of C-CySH.....	319
Figure 10.21.	MS ES+ spectrum of AMDKP.....	320
Figure 10.22.	MS ES- spectrum of AMDKP.....	320
Figure 10.23.	MS ES+ spectrum of DMDKP.....	320
Figure 10.24.	MS ES- spectrum of DMDKP.....	321
Figure 10.25.	MS ES- spectrum of DAGG.....	321
Figure 10.26.	MS ES+ spectrum of DMGG.....	321
Figure 10.27.	The chromatogram and mass spectrum of 2,3-DKP.....	322
Figure 10.28.	The chromatogram and mass spectrum of 2,6-DKP.....	323
Figure 10.29.	The chromatogram and mass spectrum of 4,5-HHP.....	324

TABLES

Table 1.1.	Different methods for the synthesis of DKPs.....	6
Table 1.2.	List of different DKP structures/ ring conformations.....	12
Table 2.1.	List of point groups with description and examples.....	34
Table 2.2.	Mulliken symbols/description.....	37
Table 3.1.	List of chemical reagents.....	54
Table 4.1.	Calculated bond lengths (Å), bond angles and dihedral angles (°) for C-CySH in comparison with the X-ray structure.....	67
Table 4.2.	Calculated DKP ring torsional angles and degree of folding (°) of the calculated structure in comparison with the X-ray structure.....	70
Table 4.3.	Experimental and calculated (scaled) vibrational band wavenumbers (cm ⁻¹) for non-deuterated <i>N,S</i> -C-CySH.....	74
Table 4.4.	Experimental and calculated (scaled) vibrational band wavenumbers (cm ⁻¹) for <i>N,S</i> -deuterated C-CySH.....	77
Table 4.5.	Definitions of symmetry-adapted internal coordinates for C-CySH.....	88
Table 5.1.	Calculated bond lengths (Å), bond angles and dihedral angles (°) for DMDKP in comparison with the X-ray structure.....	102
Table 5.2.	Calculated bond lengths (Å), bond angles and dihedral angles (°) for AMDKP.....	104
Table 5.3.	Experimental and calculated vibrational band wavenumbers (cm ⁻¹) for non-deuterated AMDKP.....	113
Table 5.4.	Experimental and calculated vibrational band wavenumbers (cm ⁻¹) for <i>N</i> -deuterated AMDKP.....	116
Table 5.5.	Experimental and calculated vibrational band wavenumbers (cm ⁻¹) for non-deuterated DMDKP.....	118
Table 5.6.	Experimental and calculated vibrational band wavenumbers (cm ⁻¹) for <i>N</i> -deuterated DMDKP.....	119
Table 5.7.	Definitions of symmetry-adapted internal coordinates for AMDKP and DMDKP.....	134
Table 6.1.	Comparison of calculated bond lengths for DAGG with the X-ray geometry.....	145
Table 6.2.	Comparison of calculated bond lengths for DMGG with the X-ray geometry.....	148

Table 6.3.	Comparison of calculated bond lengths for DAGG with the X-ray geometry bond lengths for cyclo(Gly-Gly).....	152
Table 6.4.	Comparison of calculated bond lengths for DMGG with the X-ray geometry bond lengths for cyclo(Gly-Gly).....	152
Table 6.5.	Experimental and calculated wavenumber assignments (in cm^{-1}) for DAGG vibrational bands.....	157
Table 6.6.	Experimental and calculated wavenumber assignments (in cm^{-1}) for DMGG vibrational bands.....	159
Table 6.7.	Definitions of symmetry-adapted internal coordinates for DAGG and DMGG.....	173
Table 7.1.	Structures and conformational energies of CHP.....	185
Table 7.2.	Structures and conformational energies of CDHP.....	188
Table 7.3.	Structures and conformational energies of CAH.....	190
Table 7.4.	Comparison of the DKP ring geometries of the lowest energy conformers of the calculated structures with other DKPs.....	192
Table 7.5.	The calculated bond lengths, bond angles and dihedral angles of the lowest energy conformer of N^{ϵ} and N^{δ} - tautomeric forms of CHP and CDHP.....	193
Table 7.6.	The calculated bond lengths, bond angles and dihedral angles of the lowest energy conformer of the N^{ϵ} and N^{δ} - tautomeric forms of CAH.....	197
Table 7.7.	Experimental and calculated vibrational band wavenumbers (cm^{-1}) for CHP.....	213
Table 7.8.	Experimental and calculated vibrational band wavenumbers (cm^{-1}) for CDHP.....	217
Table 7.9.	Experimental and calculated vibrational band wavenumbers (cm^{-1}) for non-deuterated CAH.....	223
Table 7.10.	Experimental and calculated vibrational band wavenumbers (cm^{-1}) for <i>N</i> -deuterated CAH.....	227
Table 7.11.	Definitions of symmetry-adapted internal coordinates for CHP, CDHP and CAH.....	231
Table 7.12.	HOMO-LUMO composition of the lowest energy conformer of N^{ϵ} and N^{δ} - tautomeric forms of CHP and CDHP.....	240
Table 7.13.	HOMO-LUMO composition of the lowest energy conformer of N^{ϵ} and N^{δ} - tautomeric forms of CAH.....	241

Table 8.1.	Calculated bond lengths (Å), bond angles and dihedral angles (°) for 2,3-DKP.....	249
Table 8.2.	Calculated bond lengths (Å), bond angles and dihedral angles (°) for 2,6-DKP.....	250
Table 8.3.	Calculated bond lengths (Å), bond angles and dihedral angles (°) for 4,5-HHP.....	252
Table 8.4.	Calculated energy values, conformation and vibrational modes for non-constrained and constrained molecules of 2,3-DKP, 2,6-DKP and 4,5-HHP..	255
Table 8.5.	Comparison of calculated bond lengths for 2,3-DKP, 2,6-DKP and 4,5-HHP with the X-ray geometry bond lengths for 2,5-DKP.....	255
Table 8.6.	Experimental and calculated vibrational band wavenumbers (cm ⁻¹) for non-deuterated 2,3-DKP.....	262
Table 8.7.	Experimental and calculated vibrational band wavenumbers (cm ⁻¹) for <i>N</i> -deuterated 2,3-DKP.....	264
Table 8.8.	Experimental and calculated vibrational band wavenumbers (cm ⁻¹) for non-deuterated 2,6-DKP.....	266
Table 8.9.	Experimental and calculated vibrational band wavenumbers (cm ⁻¹) for <i>N</i> -deuterated 2,6-DKP.....	268
Table 8.10.	Experimental and calculated vibrational band wavenumbers (cm ⁻¹) for non-deuterated 4,5-HHP.....	271
Table 8.11.	Experimental and calculated vibrational band wavenumbers (cm ⁻¹) for <i>N</i> -deuterated 4,5-HHP.....	273
Table 8.12.	HOMO-LUMO composition of the lowest energy conformers of 2,3-DKP, 2,6-DKP, 4,5-HHP and 2,5-DKP.....	284
Table 8.13.	Definitions of symmetry-adapted internal coordinates for 2,6-DKP.....	288
Table 8.14.	Definitions of symmetry-adapted internal coordinates for 2,3-DKP.....	291
Table 8.15.	Definitions of symmetry-adapted internal coordinates for 4,5-HHP.....	295
Table 10.1.	¹ H- and ¹³ C-NMR shifts for C-CySH.....	308
Table 10.2.	¹ H- and ¹³ C-NMR shifts for AMDKP.....	310
Table 10.3.	¹ H- and ¹³ C-NMR shifts for DMDKP.....	310
Table 10.4.	¹ H- and ¹³ C-NMR shifts for DAGG.....	313
Table 10.5.	¹ H- and ¹³ C-NMR shifts for DMGG.....	313

ABBREVIATIONS

Symbol	Description
ATR	-Attenuated total reflectance
aug	-Augmented (diffuse) functions
B3LYP	-Becke, 3-parameter, Lee-Yang-Parr
cc-pVTZ	-correlation-consistent polarised valence triple-zeta basis sets
cm	-centimetre
DFT	-Density functional theory
DKP	-Diketopiperazine
ΔE	-change in energy
$^{\circ}\text{C}$	-degrees Celsius
β	-degree of folding
μ	-dipole moment
ρ	-depolarization ratio
E	-electromagnetic radiation
Eq	-equation
$h\nu_0$	-energy of incident photon
$h\nu_R$	-energy of scattered photon
$h_R(\nu_0 - \nu_1)$	-emitted photon with less energy
$h_R(\nu_0 + \nu_1)$	-emitted photon with higher energy
FT	-Fourier transform
ν	-frequency
g/mm	-grooves per millimetre
He-Ne	-helium/neon
\hat{H}	-Hamiltonian operator
I	-intensity
I_0	-intensity of incident light
I_R	-intensity of Raman scattering
IR	-infra-red
K	-Kelvin
mg	-milligram

ml	-millilitre
mm	-millimetre
M_r	-molecular weight
mW	-milliwatt
γ	-magnetogyric ratio
MS	-mass spectroscopy
α	-molecular polarizability
β_0	-magnetic field
NMR	-nuclear magnetic resonance
q	-nuclear displacement
Q_k	-normal coordinate
σ	-shielding constant
P_{nm}	-transition polarizability
SCF	-self consistent field
λ	-wavelength
$\tilde{\nu}$	-wavenumber

Abbreviations for vibrational modes

ν = stretch, δ = deformation, τ = twist, ρ = rocking, ω = wagging, s = symmetric,
as = asymmetric, ip = in-plane, op = out-of-plane

PUBLICATIONS AND CONFERENCE PRESENTATIONS

Publications in preparation

Ahsan A. Khan, Trevor J. Dines, Babur Z. Chowdhry, Andrew P. Mendham, Experimental and Theoretical Vibrational Spectroscopic Studies of a Sulphur containing Diketopiperazine (To be submitted 2017) (*J. Raman. Spectrosc.*)

Ahsan A. Khan, Trevor J. Dines, Babur Z. Chowdhry, Andrew P. Mendham, Experimental and Theoretical Vibrational Spectroscopic Studies of the Degradation Products of D-Cycloserine (To be submitted 2017) (*Phys. Chem. Chem. Phys.*)

Ahsan A. Khan, Trevor J. Dines, Babur Z. Chowdhry, Andrew P. Mendham, Spectroscopic Studies of the Cyclic Di-Amino Acid Peptides, *N, N'*- Diacetyl- Cyclo(Gly-Gly) and *N, N'*-Dimethyl- Cyclo(Gly-Gly) (To be submitted 2017) (*J. Raman. Spectrosc.*)

Ahsan A. Khan, Trevor J. Dines, Babur Z. Chowdhry, Andrew P. Mendham, Vibrational Spectroscopic Studies of Histidine Containing Cyclic Dipeptides in the Solid State and in Aqueous Solution: Conformational Analysis and DFT Calculations (To be submitted 2017) (*J. Chem. Phys.*)

Ahsan A. Khan, Trevor J. Dines, Babur Z. Chowdhry, Andrew P. Mendham, IR and Raman Spectroscopic Studies of the Regioisomers of Diketopiperazine: Solid and Aqueous States and DFT Calculations (To be submitted 2017) (*Phys. Chem. Chem. Phys.*)

Ahsan A. Khan, Trevor J. Dines, Babur Z. Chowdhry, Andrew P. Mendham, Theoretical and Experimental Vibrational Spectroscopic Studies of *Cis* and *Trans* Amides in Cyclic Diamides: DFT Calculations, HOMO-LUMO and Hirshfeld Surface Analysis (To be submitted 2017) (*Chem. Eur. J.*)

Ahsan A. Khan, Trevor J. Dines, Babur Z. Chowdhry, Andrew P. Mendham, Experimental and Theoretical Vibrational Spectra of Proline-Containing Cyclic Dipeptides: Conformational Analysis, DFT Calculations and Hirshfeld Surface Analysis (To be submitted 2017) (*J. Chem. Phys.*)

Conference poster presentations

Ahsan Ali Khan, Andrew Paul Mendham, Babur Zahurridin Chowdhry, Trevor John Dines; Abstract MoP-P-IC: Vibrational spectroscopic studies of *cis* and *trans* cyclic diamides. XXV International Conference on Raman Spectroscopy, (ICORS 2016), Fortaleza, Brazil (14-19 August 2016).

Ahsan Ali Khan, Babur Zahurridin Chowdhry, Andrew Paul Mendham, Trevor John Dines, Perry Devo; Abstract P-004 -Theoretical and Experimental Vibrational Spectroscopic Studies of Sulphur Containing Diketopiperazines-pp.,66-67. II International Turkish Congress on Molecular Spectroscopy, (TURCMOS 2015), Antalya, Turkey (13-18 September, 2015).

Chapter 1: Introduction

1.1. Introduction to diketopiperazines

2, 5-Diketopiperazines (DKPs; Fig 1.1) are the “simplest” cyclic di-amino acid peptides obtained by the condensation of two α -amino acids. For example, cyclo(Gly-Gly) was first synthesized by Curtius and Goebel¹ in 1888 and was also the first compound containing a peptide bond to be studied by X-ray crystallography in 1938.² Moreover, DKPs are often produced as degradation products of polypeptides, especially in processed foods and beverages.³ DKPs occur in abundance in natural products, and this skeletal subunit is often found in a variety of compounds in diverse organisms, including bacteria and fungi, either alone or embedded in more complex structures. They are recognised for their ability to bind to a wide range of cellular receptors, and they also possess several characteristic features that make them a valuable framework as privileged scaffolds for the design of drug libraries and, hence, in drug discovery. DKPs are small molecular weight molecules, incorporating heterocyclic rings in which the stereochemistry can be controlled at up to four positions and functional group diversity can be introduced in up to six positions. They act as molecular scaffolds in drug discovery because of their stability against proteolysis. The rigid back-bone helps to mimic a preferential peptide conformation without the unwanted physical and metabolic properties of proteins. Most DKPs are chirally enriched molecules and easily synthesized using robust chemistry making them attractive for combinatorial drug discovery.⁴

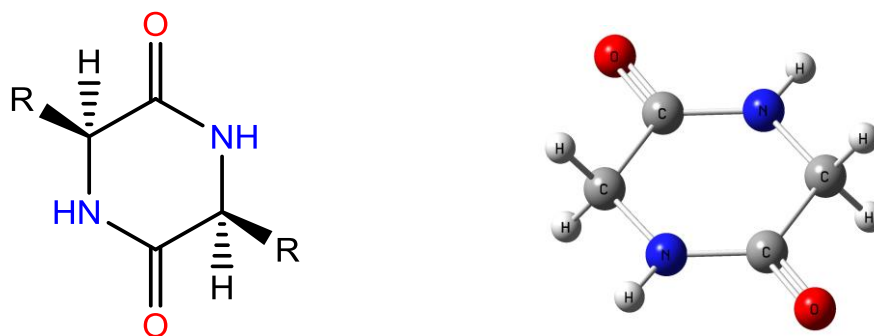


Figure 1.1. Structure of DKP (R=H).

The biogenesis and physicochemical properties of DKPs have been previously studied and piperazines are well known for their important biological properties.⁵ DKPs are considered to be very useful because of their various biological properties and constitute an effective source of novel, biologically active products. The chemical, biological and pharmacological properties of the regioisomers of DKP have been previously studied.⁶ Although most DKPs are isolated from

natural sources, there are methods available for their synthesis based mainly on the reactions of linear di-amino acid peptides in solution or via solid-phase synthesis.^{7, 8}

1.2. Physico-chemical properties of DKPs

1.2.1. Solubility of DKPs

DKPs are neutral and do not exist as zwitterions. DKPs have the capability of forming hydrogen bonds with certain solvents via the two *cis*-amide groups in the DKP ring. In contrast, they may give rise to hydrophobic interactions; the extent of which is determined by the R1 and R2 substituents. The solubility of the non-ionic DKPs is still less than those with short alkyl groups.⁹

1.2.2. Stability of DKPs

There is a paucity of data relating to the stability of DKPs. However, a recent study on the kinetics of DKP formation involving the intramolecular aminolysis of Phe-Pro-*p*-nitroaniline (Phe-Pro-*p*NA) to cyclo(Phe-Pro) (Phe-Pro-DKP) in solution was studied as a function of pH, temperature and buffer concentration. In the pH range studied, Phe-Pro-DKP was the only product generated upon degradation of Phe-Pro-*p*NA. From this study it was found that Phe-Pro-DKP was stable between pH values 3 and 8, while at low pH (<3) and high pH (>8) it undergoes hydrolysis to the linear dipeptide, Phe-Pro-OH.¹⁰

In an another study, the stability of cyclo(Gly-Gly), cyclo(Gly-Trp) and cyclo(Trp-Trp), was examined at various temperatures and pH values; it was found that the naturally occurring *cis*-fused DKP were relatively stable compared to their *trans*-fused counterparts, but also displayed pH sensitive instability below pH 3 and greater than pH 9.¹¹ These findings showed that within a reasonable pH range, pharmaceutical formulations consisting of a DKP and a drug would yield relatively stable products provided no significant drug-excipient interactions occurred.

1.2.3. Absorption and transportation of DKPs

Once ingested, peptides must be transported to the systemic circulation without being metabolized in order to exert their pharmacological effects, but the overall absorption of linear peptides is poor due to metabolic degradation by peptidases. Peptides and other peptidomimetics are transported across the cell membrane by peptide transporters (PET1 and PET2). Both transporters are driven electrochemically, via a gradient of protons across the intestinal or renal brush border membrane,

in the lumen-to-cytoplasm direction.¹² Mizuma *et. al.*,¹³ also reported the uptake of DKPs via the PET1 peptide transporters. They noted that the cellular uptake of the DKPs was pH dependent, and that it was inhibited by the addition of PET1 substrates which indicates PET1-mediated transport of the DPKs.

1.3. Biological properties of DKPs

DKPs display interesting chemical properties such as proteolytic resistance, conformational rigidity; accepting and donating functional groups that favour hydrogen bonding and interaction with biological targets.⁴ However, these compounds show common properties, easily obtained by conservative synthetic procedures, which favour structural uniformity as a function of substitution of side-chains and functional groups. Such attributes are helpful in the DKPs acquiring favourable pharmacokinetic and pharmacodynamic properties, which promotes their development as pharmacological agents.¹⁴ DKPs exhibit promising antimicrobial (antibacterial, antifungal, antiviral), and antitumor biological activities.¹⁵ Cyclo(L-Leu-L-Pro), also known as Gancidin W, has been identified as a potent inhibitor of twelve vancomycin-resistant enterococci (VRE) strains, including *Enterococcus faecalis* and *E. faecium* species.¹⁶ DKPs have also been established as decomposition products of certain drugs; for example, the aminopenicillin antibiotic, amoxicillin upon degradation converts-via cyclization-to its more stable six-membered ring product, amoxicillin-2,5-diketopiperazine. The chemically stable form of this compound has been detected in waste water samples.¹⁷

The DKP-motif is considered a novel brain shuttle for the delivery of drugs which have limited ability to cross the blood-brain barrier,¹⁸ and has been proposed as an ideal candidate for the rational development of new neurotherapeutic agents. DKP derivatives have shown remarkable neuroprotective and nootropic activity. Two major classes of DKPs, the “thyrotropin-releasing hormone (TRH)-related” and the unsaturated derivatives have already been used to demonstrate significant protection against neurotoxicity in different in-vitro environments suggesting they may have a future for in-vivo therapy of neuronal degeneration via several different mechanisms of action.¹⁸

1.4. Sulphur containing DKPs

DKPs containing sulphur groups have also been used, mainly in medicine and biosynthesis, as they are renowned for their diverse biological activities.¹⁹ Many sulphur containing DKP derivatives, including gliotoxins and epidithiodiketopiperazines, have demonstrated anti-cancer

activities increasing their use in many different medicines and antibiotics.¹⁹ Cyclo(Met-Pro) has been identified in beef. Sensory evaluations indicate that although not strong, cyclo(Met-Pro) possess different taste effects at different concentrations.²⁰

In recent years, homocysteine, in particular, has achieved the status of an important amino acid in many fundamental biological and medicinal processes.²¹ Homocysteine is also an important intermediate for in vivo methionine metabolism. The biological significance of homocysteine and its DKP grew extensively in 1962 when it was confirmed that children with mental retardation, accelerated growth and propensity to thrombosis of arteries and veins excreted homocysteine in their urine.²¹ The epipolythiodioxopiperazines (ETPs) constitute one group of fungal toxins, which has been established as a fungal metabolite possessing antiviral, antibacterial and cytostatic properties.²²

In the case of cyclo-L-cystine and its metabolites, 3,6-epi(dithio- and tetrathio-)2,5-piperazinedione, X-ray studies and quantum chemical calculations have confirmed the helicity of the di- and tetra-sulphide bonds in the DKP ring. Each sulphur atom is closer to the adjacent carbon atom rather than the adjacent nitrogen atom in epi-dithio-DKP and the inner sulphur atoms closer to the adjacent nitrogen and the outer sulphur atoms closer to the adjacent carbons in epi-tetrathio-DKP, triggering biological activity.¹⁹ Another study identified the DKP cyclo(L-Pro-L-Tyr), found in cell free *Pseudomonas aeruginosa* culture supernatants, that was shown to activate the *N*-acylhomoserine lactone (AHL) biosensor.²³ It has also been confirmed that DKPs containing the amino acid proline possess specialised characteristics allowing them to mimic specific domains such as β -turns and loop motifs which play an important role in protein folding.²⁴

1.5. Synthesis of diketopiperazines

DKPs are generally obtained by the condensation of two amino acids or by the degradation of polypeptides. Recent scientific studies have outlined key advances in the synthesis of DKPs employing many different methods that have been frequently used for their synthesis.⁴

Dipeptide ester cyclization

This is a common method of synthesis and involves linear di-amino acid peptides being substituted with an amide group at one terminal and an ester at the other terminal in order to achieve spontaneous cyclization. Careful selection of reaction conditions is required to limit racemisation; the reaction can occur at several pH values but all other conditions must be controlled appropriately.⁴ The typically employed route utilizes a nitrogen-protected α -amino acid

(Fig. 1.2(a)) and an α -amino acid ester (Fig. 1.2(b)). On deprotection, the dipeptide coupled product (Fig. 1.2(c)) gives the amino dipeptide ester (Fig. 1.2(d)), which can then cyclize *in situ* to form the desired molecule (Fig. 1.2(e)). To achieve this, the amide bond must assume the *cis*-orientation. If this is prevented, electronically or sterically, the rate of cyclization can be poor. Under these circumstances, heating in an acidic or basic medium is often used to enhance the formation of the ring (Table 1.1).

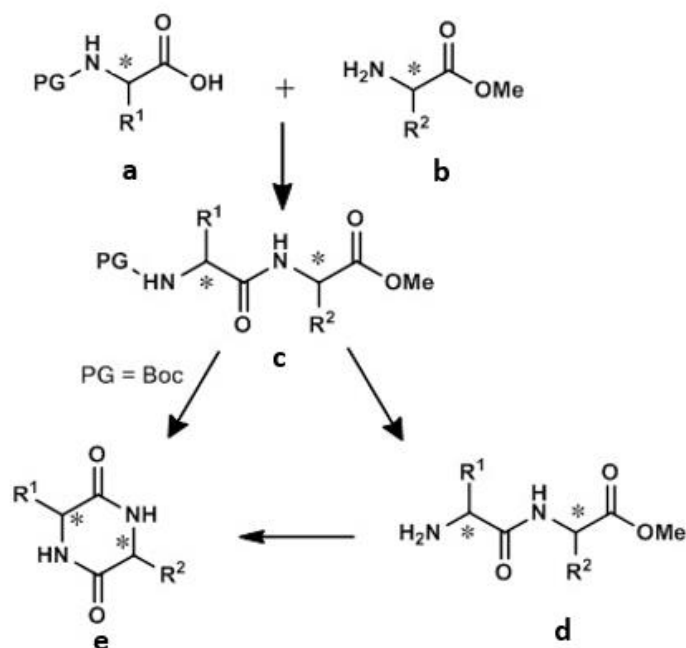


Figure 1.2. Dipeptide ester cyclization reaction (PG = protecting group).⁴

Amino acid condensation

This method involves the direct condensation of two amino acids to form the DKP ring (Fig. 1.3). This method of synthesis suffers from a poor yield of product²⁵ and one of the amino acids is often needed to react with “phosgene” before reacting with the other amino acid.²⁶ Another approach has been to use “gas-solid phase” conditions, whereby gaseous amino acids are condensed on to a silica surface. Studies have been undertaken to develop this approach and although it has promise, this method is prone to produce racemates and specialised reaction conditions are also required.^{27a} The use of peptide coupling reagents has been reported to facilitate 2,5-DKP formation (e.g., glycine polypeptide dimerization). A recent improvement in this chemistry was improved by using amide bond-coupling reagents (HBTU/DMAP) with 400 W irradiation in DMF to produce yields of 85-95% in short reaction times (5 min) without epimerization.^{27b}

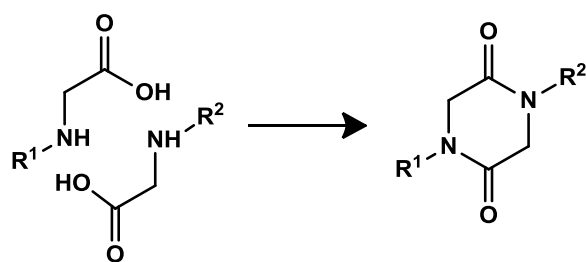
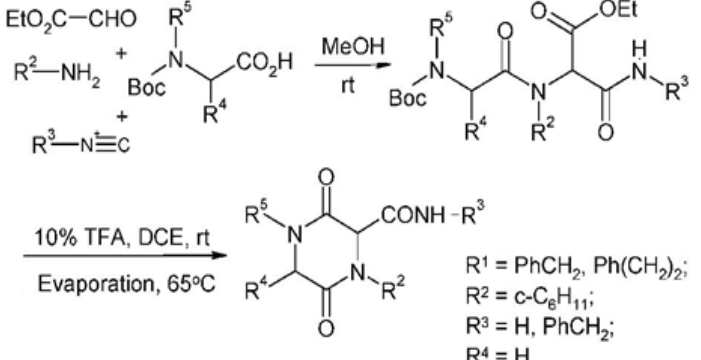
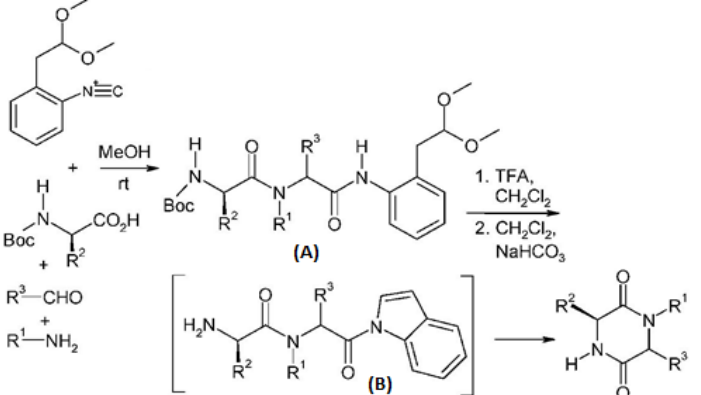
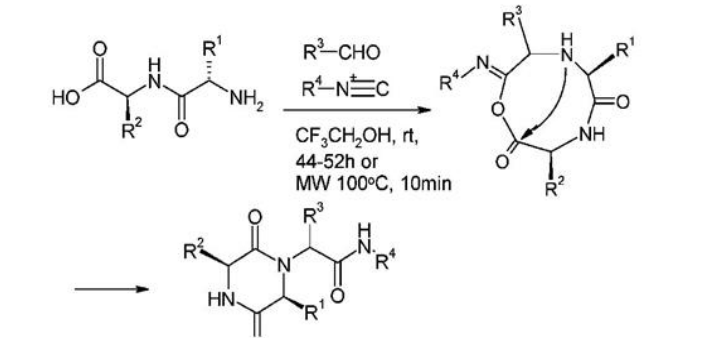
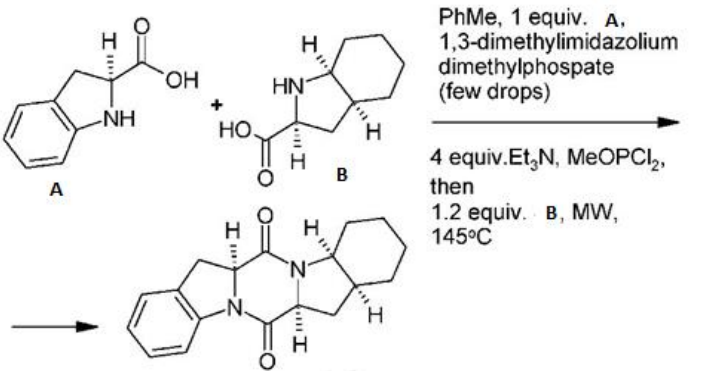


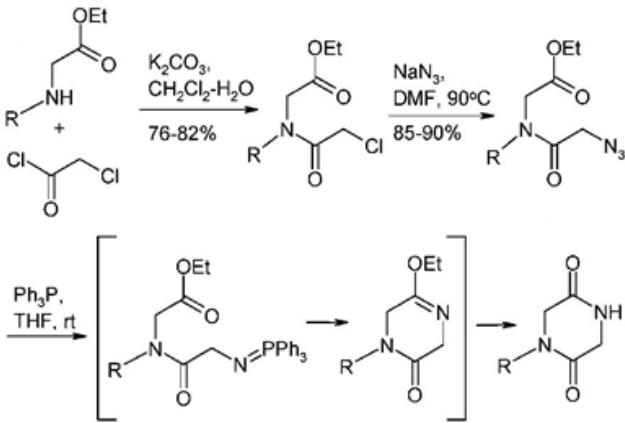
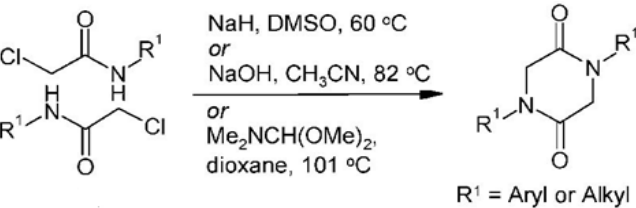
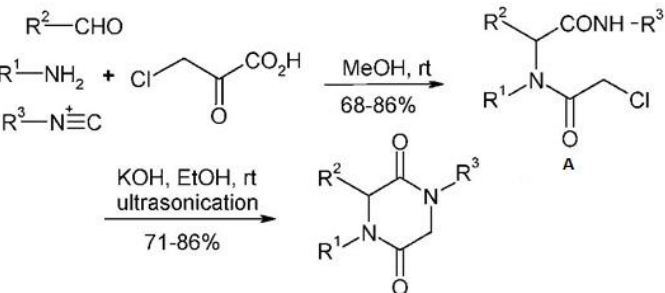
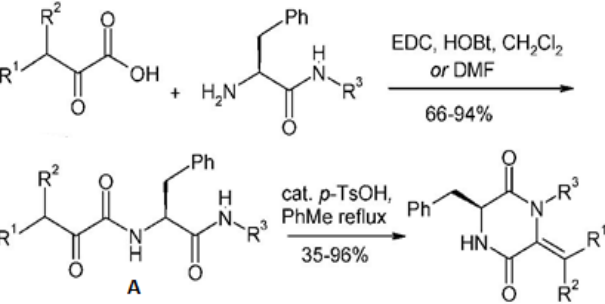
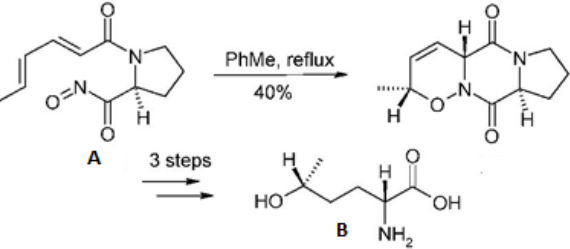
Figure 1.3. Amino acid condensation.

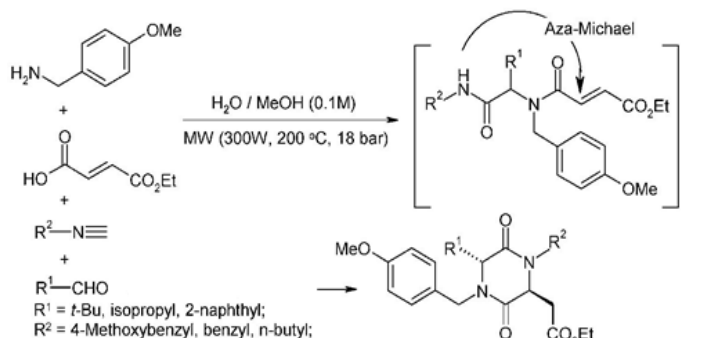
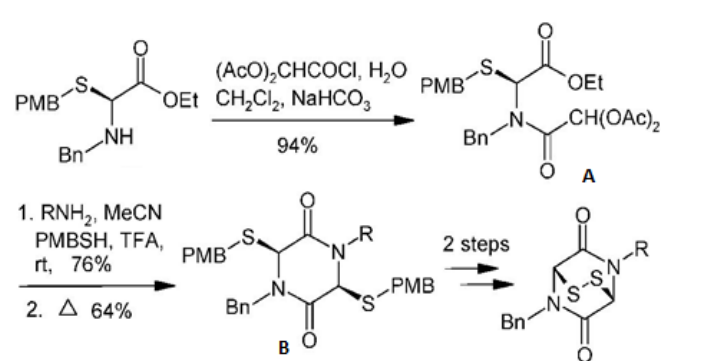
Other methods used in the synthesis of DKPs are listed in Table 1.1

Table 1.1. Different methods used for the synthesis of DKPs.

Name	Schematic representation of the synthetic procedure	Description
Base-catalysed dipeptide ester cyclization ²⁸		Yield 95%
Acid-catalysed dipeptide ester cyclization ²⁹		Yield 28%
Cleavage induced cyclization (solid phase synthesis) ³⁰		Intramolecular aminolysis of resin bound dipeptide (yield: 83%).
Cyclization via intermediate <i>N</i> -acyliminium ion ³¹	<p>R¹ = alkyl, aryl; R² = H, alkyl, aryl; R³ = H, Me, PhCH₂</p>	Excellent yield with expulsion of a cyclohexyliminium cation.

<p><i>N</i>-4 Carboxamide template³² (cyclization)</p>	 <p> $\text{EtO}_2\text{C}-\text{CHO} + \text{R}^2-\text{NH}_2 + \text{Boc}-\text{N}(\text{R}^5)-\text{CH}(\text{R}^4)-\text{CO}_2\text{H} + \text{R}^3-\text{N}\equiv\text{C} \xrightarrow[\text{rt}]{\text{MeOH}}$ </p> <p> $\xrightarrow[\text{Evaporation, } 65^\circ\text{C}]{10\% \text{ TFA, DCE, rt}}$ </p> <p> $\text{R}^1 = \text{PhCH}_2, \text{Ph}(\text{CH}_2)_2;$ $\text{R}^2 = \text{c-C}_6\text{H}_{11};$ $\text{R}^3 = \text{H}, \text{PhCH}_2;$ $\text{R}^4 = \text{H},$ </p>	<p>Deprotection and cyclization of tripeptide moiety furnishing excellent yield of DKP-carboxamide template.</p>
<p>Cyclization <i>via</i> indolamide intermediate³³</p>	 <p> $\xrightarrow[\text{rt}]{\text{MeOH}}$ (A) </p> <p> 1. TFA, CH_2Cl_2 2. CH_2Cl_2, NaHCO_3 </p> <p>(B)</p>	<p>Mild acidic post-Ugi activation of (A) involving simultaneous Boc removal and indolamide formation (B) followed by cyclization to give the <i>N</i>-substituted DKP.</p>
<p><i>N</i>-4 Glycinamide template <i>via</i> dipeptide³⁴</p>	 <p> $\xrightarrow[\text{MW } 100^\circ\text{C, 10min}]{\text{R}^3-\text{CHO}, \text{R}^4-\text{N}\equiv\text{C}, \text{CF}_3\text{CH}_2\text{OH, rt, 44-52h}}$ </p>	<p>Microwave-assisted Ugi reaction involving dipeptide, aldehydes and isocyanides. This reaction forms a nine-membered intermediate which on ring contraction gives the DKP.</p>
<p>Non-symmetrical 2,5-DKPs <i>via</i> amino acid condensation³⁵</p>	 <p> $\xrightarrow[\text{then } 1.2 \text{ equiv. B, MW, } 145^\circ\text{C}]{\text{PhMe, 1 equiv. A, 1,3-dimethylimidazolium dimethylphosphate (few drops), 4 equiv. Et}_3\text{N, MeOPCl}_2}$ </p>	<p>Microwave-assisted stereoselective preparation of unsymmetrical DKPs from unprotected amino acids (yield: 81%).</p>

<p>Aza-Wittig cyclization³⁶</p>		<p>Formation of DKP by intramolecular aza-Wittig reaction followed by hydrolysis of the resulting imino ether.</p>
<p>Cyclization via chloro acetamides³⁷</p>	 <p>R¹ = Aryl or Alkyl</p>	<p>The ring closure of α-haloacetamides in the presence of a base gives 1,4-disubstituted-DKPs.</p>
<p>Synthesis via Ugi-4CR/ intramolecular <i>N</i>-alkylation³⁸</p>	 <p>R¹ = 4-ClC₆H₄CH₂; PhCH₂; c-C₆H₁₁; R² = 4-ClC₆H₄, 4-MeO₆H₄, 2-naphthyl, 4-BrC₆H₄, CH₃; R³ = c-C₆H₁₁, PhCH₂;</p>	<p>Treatment of α-haloacetamide adducts with ethanolic KOH using ultrasonication results in the formation of DKPs.</p>
<p>Cyclization via <i>N</i>-α-Ketoacylamino acid amides³⁹</p>		<p><i>N</i>-α-Ketoacylamino acid amides (A) undergoes acid-catalysed cyclization to give excellent yield and enantiomeric excess (EE) DKPs.</p>
<p>Cyclization via Diels-Alder reaction⁴⁰</p>		<p>Stereospecific intramolecular Diels-Alder reaction of <i>N</i>-sorbyl-L-Pro (A) gives DKP in the synthesis of B.</p>

<p>Cyclization via Michael Addition⁴¹</p>	 <p> $\text{H}_2\text{N}-\text{C}_6\text{H}_4-\text{OMe}$ $\text{HO}-\text{C}(\text{O})-\text{CH}=\text{CH}-\text{CO}_2\text{Et}$ $\text{R}^2-\text{N}\equiv$ R^1-CHO $\text{R}^1 = t\text{-Bu, isopropyl, 2-naphthyl};$ $\text{R}^2 = 4\text{-Methoxybenzyl, benzyl, n-butyl};$ </p>	<p>Ugi/intramolecular <i>aza</i>-Michael reaction of four components under the influence of protic solvents, bifunctional substrates and microwaves gives excellent yield of DKPs.</p>
<p>Epithio-DKPs via tandem cyclization⁴²</p>	 <p> $(\text{AcO})_2\text{CHCOCl, H}_2\text{O}$ $\text{CH}_2\text{Cl}_2, \text{NaHCO}_3$ 94% A 1. $\text{RNH}_2, \text{MeCN}$ $\text{PMBSH, TFA, rt, 76\%}$ B 2. Δ 64% 2 steps </p>	<p>A is a diastereomeric mixture formed by three-component ring closure, on heating gives the thermodynamically stable <i>cis</i>-isomer (B) which forms epithio-DKPs.</p>

1.6. Structure and conformation of diketopiperazines

Cis and *trans* refer to geometric isomers; *cis* refers to an isomer where both hydrogen and oxygen atoms of the amide groups are on the same side (in the case of DKPs). *Trans* refers to an isomer where the functional groups are on opposite sides.⁴³ Fig. 1.4 shows the difference between *cis* and *trans* amides in a peptide.

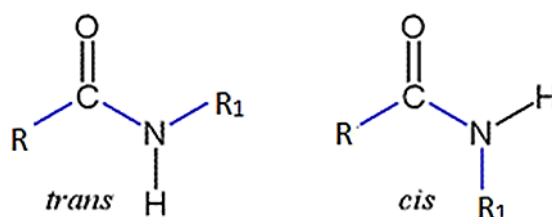


Figure 1.4. *Cis* and *trans* amide isomers in peptides.

The vast majority of linear peptides possess amide bonds in the *trans* configuration, whereas in DKPs the amide groups adopt a *cis* conformation.⁴⁴

The molecular and X-ray structures of DKPs (piperazine-2, 5-diones) have been studied as these molecules are the simplest class of cyclic dipeptides containing two *cis*-amide groups and have

two hydrogen bond acceptors and two hydrogen bond donor sites which are essential for binding to cellular receptors and enzymes. 2, 5-DKPs can be described as diverse compounds in terms of structural conformation due, as stated previously, to the six positions in which substituents can be added and up to four positions in which their stereochemistry can be controlled. Although they are semi-rigid and conformationally constrained heterocycles, they are deemed to possess molecular flexibility because the six membered ring can exist in a flat, planar conformation or a slightly puckered boat conformation with only a few kJ mol^{-1} difference in energy between the planar and boat forms.⁴⁴

The conformation of unsubstituted DKPs e.g., cyclo(Gly-Gly) has been the subject of considerable studies in recent times. Recent vibrational spectral analysis has confirmed that cyclo(Gly-Gly) (Fig. 1.5(a)) adopts a planar *cis* conformation in the solid state.⁴⁴ A study of cyclo(Gly-Gly) by microwave spectroscopy in the gas phase suggests that the compound, in isolation, does not adopt a planar structure but displays a boat conformation with C_2 symmetry.⁴⁵ The vibrational spectra and *ab initio* calculations of cyclo(Gly-Gly) in the gas phase also favours the boat conformation as the minimum energy conformer over the planar structure, which is found to be a transition state in the gas phase. The difference in the energy between planar and boat conformers was found to be 1.3-1.7 kJ mol^{-1} , which suggests that crystal lattice forces and hydrogen bonding may force the molecule into a planar structure in the solid state.⁴⁶ Several other studies have shown that *cis* di-substituted and tri-substituted DKP compounds in the solid state usually adopt twist-boat or flattened boat conformations, particularly when the substituents are aryl-methyl groups.⁴⁷ X-ray crystallographic studies of symmetrically substituted DKPs such as cyclo(L-Asp-L-Asp)⁴⁸, cyclo(L-Ala-L-Ala)⁴⁹, cyclo(L-Met-L-Met)⁵⁰ and cyclo(L-Glu-L-Glu)⁵¹ have confirmed that the boat conformation is favoured in the solid state (Fig. 1.5 (a)). Exceptions include cyclo(L-homoCySH-L-homoCySH)⁵² and cyclo(L-Ser-L-Ser)⁵³ where the DKP ring is near-planar with two substituted alkyl side-chains on the C_α atoms being folded above the ring. However, DFT calculations and vibrational spectroscopy studies of cyclo(L-Ser-L-Ser) suggest that the boat conformation is preferred in aqueous solution and the gas phase.⁵⁴ Previous vibrational spectroscopic studies and DFT calculations of unsymmetrical substituted DKPs, such as cyclo(Gly-Val),⁵⁵ cyclo(His-Phe),⁵⁶ and cyclo(Leu-Gly)⁵⁷ have also highlighted the *cis* amide characteristics of these molecules and the boat conformer is preferred as the minimum energy conformer in the gas phase. The substituents present in the DKP can induce dramatic effects on the conformation of the ring, due to the avoidance of steric interactions between the two substituted side-chains on the C_α atoms. From previous vibrational spectroscopic studies on DKPs it has been

suggested that the wavenumber location of the amide II mode plays a crucial role in determining which conformer the DKP ring adopts in the solid state.^{44,54}

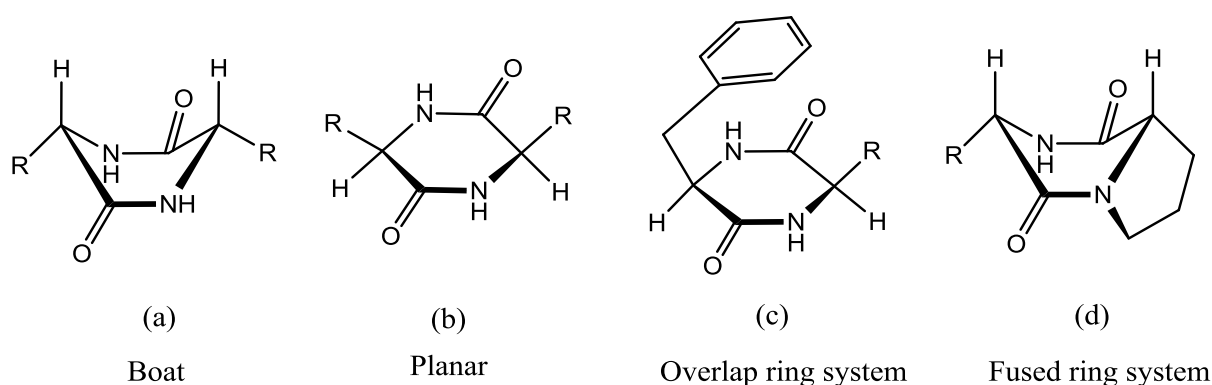


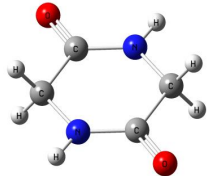
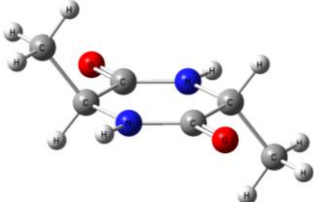
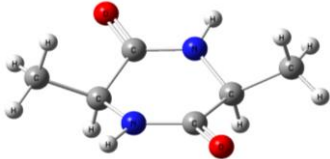
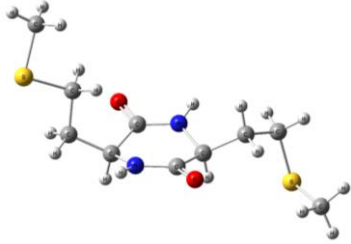
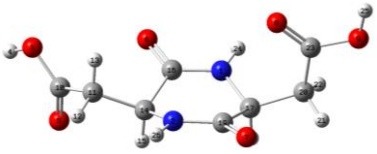
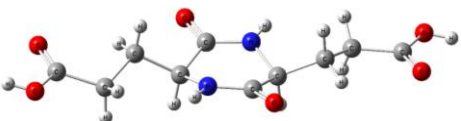
Figure 1.5. Schematic representation of different conformations in DKPs.¹

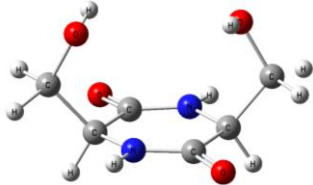
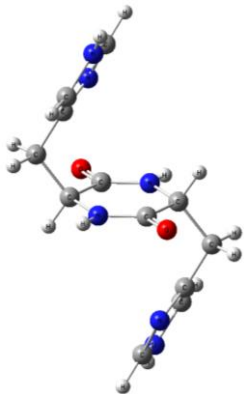
The conformation of the DKP ring varies depending on the number and molecular nature of substituents on the ring. Symmetric substituted DKP rings e.g., cyclo(Gly-Gly) and α -dimethyl-cyclo(Gly-Gly) usually adopt a planar conformation in the solid and solution state (Fig. 1.5 (b)), whereas the symmetric *trans*-di-substituted DKPs, e.g., cyclo(D-*t*BuGly-L-*t*BuGly) and cyclo(D-Ala-L-Ala) vary from planar to flattened-chair conformation.⁴⁷ Aromatic substituted side-chains on DKP have a tendency to overlap with the DKP ring (Fig. 1.5(c)); a phenomenon suggested by ¹H-NMR studies in the solution state.⁵⁸ In proline containing cyclic dipeptides, the DKP ring is fused with the five-membered proline ring which imposes rigidity and constrains the structure to a stable boat conformation^{59,60} (Fig. 1.5(d)). The *cis*-amide in the DKP ring forms hydrogen bonds between adjacent molecules. This enables the DKPs to exist as well-organized structures that are important in e.g., crystal engineering^{61,62} and as liquid gelators.^{63,64}

The formation of intermolecular hydrogen bonds (N-H...O) between adjacent DKP molecules allows the development of molecular assemblies which can be studied using NMR and X-ray crystallographic techniques.⁶⁵ X-ray crystallographic studies of the unsubstituted DKP cyclo(Gly-Gly) show that the ring is planar and forms linear “tape structures” in which the adjacent molecules are connected by two hydrogen bonds.⁶⁶ The majority of substituted DKPs adopt the linear tape alignment in the solid state.⁴⁴ However, cyclo(D-Ala-L-Ala)⁶⁷ and cyclo(L-His-D-His)⁶⁸ forms layer-type structures. Studies of cyclo(Glu-Glu) suggests that the crystalline molecule exists in two different polymorphic forms⁵¹; the hydrogen bonding in form 1 is described as layers and as a chain in form 2. A previously reported crystal structure of DKPs suggests that the choice of substitution can have a significant impact on the preferred packing arrangement.⁵² The substitution

of carboxylic acid groups at the 3rd and 6th position of the DKP ring resulted in “layered structures”,⁶⁹ whereas the substitution by bulky spirocyclic groups favoured the tape orientation.⁷⁰ The conformation and X-ray structures of selected, substituted DKPs are shown in Table 1.1.

Table 1.1. List of different DKP structures/ring conformations.

Name	Conformation	X-ray structure
Cyclo(Gly-Gly) ⁷¹	Essentially planar (deviation ~1°)	
Cyclo(D-Ala-L-Ala) ⁶⁷	Nearly planar (deviation ~2.5°)	
Cyclo(L-Ala-L-Ala) ⁴⁹	Puckered twist boat	
Cyclo(L-Met-L-Met) ⁵⁰	Boat	
Cyclo(L-Asp-Asp) ⁴⁸	Boat	
Cyclo(Glu-Glu) ⁵¹	Boat	

Cyclo(L-Ser-L-Ser) ⁵³	Nearly planar (deviation ~4°)	
Cyclo(L-His-D-His) ⁶⁸	Planar	

1.7. References

1. T. Curtius, F. Goebel, *J. Prakt. Chem.*, 1888, 37, 150.
2. R. B. Corey, *J. Am. Chem. Soc.*, 1938, 60, 1598.
3. A. D. Borthwick, N. C. Da Costa, *Crit. Rev. Food Sci. Nutr.*, 2017, 57, 718.
4. A. D. Borthwick, *Chem. Rev.*, 2012, 112, 3641.
5. W. Herz, H. Grisebach, G. W. Kirby, “*Fortschritte der Chemie Organischer Naturstoffe/ Progress in the Chemistry of Organic Natural Products*”, Springer-Verlag (Vienna), 1975, 51.
6. D. T Witiak, Y. Wei, *Prog. Drug. Res.*, 1990, 35, 249.
7. M. B. Martins, I. Carvalho, *Tetrahedron*. 2007, 63, 9923.
8. W. R. Li, J. H Yang, *J. Comb. Chem.*, 2002, 4, 106.
9. V. Crescenzi, A. Cesaro, E. Russo, *Int. J. Pept. Protein. Res.*, 1973, 5, 427.
10. C. Goolcharran R. T. Borchardt, *J. Pharm. Sci.*, 1998, 87, 283.
11. G. D. Grant, “*The Medicinal Chemistry of Cyclo(Trp-Trp), Cyclo(Gly-Trp) and Cyclo(Gly-Gly)*” PhD thesis, University of Port Elizabeth, 2002.
12. S. Nussberger, M. Hediger, *Exp. Nephrol.*, 1995, 3, 211.
13. T. Mizuma, T. Narasaka, S. Awazu, *Biol. Pharm. Bull.*, 2003, 26, 1625.
14. D. X. Wang, M. T. Liang, G. J. Tian, H. Lin, H. Q. Liu, *J. Comb. Chem.*, 2002, 5, 109.
15. M. P. de Carvalho, W. R. Abraham, *Curr. Med. Chem.*, 2012, 19, 3564.

16. K. H. Rhee, *J. Gen. Appl. Microbiol.*, 2002, 48, 321.
17. A. Lamm, I. Gozlan, A. Rotstein, D. Avisar, *J. Environ. Sci. Health. Part A.*, 2009, 44, 1512.
18. C. Cornacchia, I. Cacciatore, L. Baldassarre, A. Mollica, F. Feliciani, F. Pinnen, *Mini. Rev. Med. Chem.*, 2012, 12, 2.
19. A. Gregory, M. Przybylska, *J. Am. Chem. Soc.*, 1978, 100, 943.
20. M. Chen, M. Dewis, K. Kraut, D. Merritt, L. Reiber, L. Trinnaman, N. Da Costa. *J. Food Sci.*, 2009, 74, C100.
21. K. S. McCully, *J. Sci. Exp.*, 2001, 15, 5.
22. A. Taylor, *Microb. Toxins*, 1971, 7, 337.
23. M. T. G. Holden et al, *Mol. Microbiol.*, 1999, 33, 1254.
24. J. C. Monbaliu, F. K. Hansen, L. K. Beagle, M. J. Panzner, P. J. Steel, E. Todadze, C. V. Stevens, A. R. Katritzky, *Chem. Eur. J.*, 2012, 18, 2632.
25. M. Falorni, G. Giacomelli, A. Porcheddu, M. Taddei, *Eur. J. Org. Chem.*, 2000, 8, 1669.
26. A. Gonzalez, S. L Vorobeva, A. Linares, *Tetrahedron*, 1995, 6, 1357.
27. (a) V. A. Basiuk, T. Y. Gromovoy, A. A. Chuiko, V. A. Soloshonok, V. P. Kukhar, *Synthesis*, 1992, 5, 449. (b) V. Santagada, F. Fiorino, E. Perissutti, B. Severino, S. Terracciano, G. Cirino, G. Caliendo, *Tetrahedron Lett*, 2003, 44, 1145.
28. P. S. Baran, C. A. Guerrero, E. J. Corey, *J. Am. Chem. Soc.*, 2003, 125, 5628.
29. A. C. Durow, G. C. Long, S. J. O'Connell, C. L. Willis, *Org. Lett.*, 2006, 8, 5401.
30. A. L. Kennedy, A. M. Fryer, J. A. Josey, *Org. Lett.*, 2002, 4, 1167.
31. C. Hulme, M. M. Morrissette, F. A. Volz, C. J. Burns, *Tetrahedron Lett.*, 1998, 39, 1113.
32. C. Hulme, M. P. Cherrier, *Tetrahedron Lett.*, 1999, 40, 5295.
33. C. R. Rhoden, D. G. Rivera, O. Kreye, A. K. Bauer, B. Westermann, L. A. Wessjohann, *J. Comb. Chem.*, 2009, 11, 1078.
34. S. Cho, G. Keum, S. B. Kang, S. Y. Han, Y. Kim, *Mol. Diversity*, 2003, 6, 283.
35. M. Jainta, M. Nieger, S. Bräse, *Eur. J. Org. Chem.*, 2008, 32, 5418.
36. K. C. Majumdar, K. Ray, S. Ganai, *Synlett.*, 2010, 14, 2122.
37. A. Hazra, P. Paira, P. Palit, S. Banerjee, N. B. Mondal, N. P. Sahu, *J. Chem. Res.*, 2007, 7, 381.
38. S. Marcaccini, R. Pepino, M. C. Pozo, *Tetrahedron Lett.*, 2001, 42, 2727.
39. Y. Yamazaki, Y. Mori, A. Oda, Y. Okuno, Y. Kiso, Y. Hayashi, *Tetrahedron*, 2009, 65, 3688.
40. T. Sheradsky, E. R. Silcoff, *Molecules*, 1998, 3, 80.
41. S. Santra, P. R. Andreana, *Org. Lett.*, 2007, 9, 5035.

42. A. E. Aliev, S. T. Hilton, W. B. Motherwell, D. L. Selwood, *Tetrahedron Lett.*, 2006, 47, 2387.
43. G. Patrick, *Organic Chemistry*, Bios Scientific, London, 2004.
44. A. P. Mendham, T. J. Dines, M. J. Snowden, B. Z. Chowdhry, R. Withnall. *J. Raman Spectrosc.*, 2009, 40, 1478.
45. F. L. Bettens, R. P. A. Bettens, R. D. Brown, P. D. Godfrey. *J. Am. Chem. Soc.*, 2000, 122, 5856.
46. J. D. Hirst, B. J. Persson, *J. Phys. Chem. A.*, 1998, 102, 7519.
47. J. C. MacDonald, G. M. Whitesides, *Chem. Rev.*, 1994, 94, 2383.
48. A. P. Mendham, R. A. Palmer, B. S. Potter, T. J. Dines, B. Z. Chowdhry, *J. Chem. Crystallogr.*, 2010, 40, 1074.
49. E. J. Sletten, *J. Am. Chem. Soc.*, 1970, 92, 172.
50. A. P. Mendham, B. S. Potter, R. A. Palmer, T. J. Dines, J. C. Mitchell, R. Withnall, B. Z. Chowdhry, *J. Raman Spectrosc.*, 2010, 41, 148.
51. A. P. Mendham, R. A. Palmer, B. S. Potter, T. J. Dines, M. J. Snowden, R. Withnall, B. Z. Chowdhry, *J. Raman Spectrosc.*, 2010, 41, 288.
52. A. P. Mendham, J. Spencer, B. Z. Chowdhry, T. J. Dines, M. Mujahid, R. A. Palmer, G. Tizzard, S. Coles, *J. Chem. Crystallogr.*, 2011, 41, 1328.
53. G. G. Fava, M. F. Belicchi, *Acta Crystallogr., Sect. B.* 1981, 37, 625.
54. A. P. Mendham, T. J. Dines, M. J. Snowden, R. Withnall, B. Z. Chowdhry, *J. Raman Spectrosc.*, 2009, 40, 1508.
55. S. Celik, A. E. Ozel, S. Akyuz, G. Agaeva, *J. Mol. Struct.*, 2011, 993, 341.
56. S. Celik, A. E. Ozel, S. Akyuz, S. Kecel, *Vib. Spectrosc.*, 2012, 61, 54.
57. S. Celik, A. E. Ozel, S. Akyuz, *Vib. Spectrosc.*, 2016, 83, 57.
58. K. D. Kopple, M. Ohnishi, *J. Am. Chem. Soc.*, 1969, 91, 962.
59. V. Madison, P. E. Young, E. R. Blout, *J. Am. Chem. Soc.*, 1976, 98, 5358.
60. Z. Li, S. Mukamel, *J. Phys. Chem. Part A.*, 2007, 111, 11579.
61. G. T. R. Palmore, M. T. McBride, *J. Chem. Soc., Chem. Commun.*, 1998, 1, 145.
62. S. Palacin, D. N. Chin, E. E. Simanek, J. C. MacDonald, G. M. Whitesides, M. T. McBride, G. T. R. Palmore, *J. Am. Chem. Soc.*, 1997, 119, 11807.
63. Z. Xie, A. Zhang, L. Ye, Z. Feng, *Soft Matter*. 2009, 5, 1474.
64. (a) Y. Yang, M. Suzuki, M. Kimura, H. Shirai, K. Hanabusa, *Chem. Commun.*, 2004, 11, 1332. (b) K. Hanabusa, H. Fukui, M. Suzuki, H. Shirai, *Langmuir*, 2005, 21, 10383.
65. G. T. R. Palmore, J. C. MacDonald, "The Amide Linkage: Selected Structural Aspects"; In

- Chemistry, Biochemistry, and Material Science; A. Greenberg, C. M. Breneman, J. F. Liebman, Eds.; John Wiley & Sons, Inc., New York, 2000, 291.
66. R. B. Corey, *J. Am. Chem. Soc.*, 1938, 60, 1598.
67. E. Benedetti, P. Corradini, C. Pedone, *J. Phys. Chem.*, 1969, 73, 2891.
68. E. Benedetti, A. Bavoso, B. Di Blasio, V. Pavone, C. Pedone, L. Paolillo, M. D'Alagni, *Int. J. Pept. Protein Res.*, 1988, 31, 220.
69. K. A. Lyssenko, D. A. Lenev, R. G. Kostyanovsky, *Tetrahedron*, 2002, 58, 8525.
70. S. Palacin, D. N. Chin, E. E. Simanek, J. C. MacDonald, G. M. Whitesides, M. T. McBride, G. T. R. Palmore. *J. Am. Chem. Soc.*, 1997, 119, 11807.
71. R. Degeilh, R. E. Marsh, *Acta Crystallogr.*, 1959, 12, 1007.

Chapter 2: Theoretical Aspects of Instrumental Techniques and Computational Methods

2.1. Theoretical aspects of instrumental techniques

2.1.1. Introduction to spectroscopy

Electromagnetic radiation is a form of energy that may behave either as a particle or as a wave. The word photon is used as a term to define a particle representing a quantum of light or other electromagnetic radiation. The terms wavelength (λ) and frequency (ν) are used to describe the wave nature of energy. Spectroscopy is the study interaction of matter with electromagnetic radiation. It involves the absorption, emission or scattering of electromagnetic radiation by atoms or molecules followed by interpretation of spectral parameters in order to extract structural and other physico-chemical information pertaining to the system under investigation. The frequency (ν) and wavelength (λ) of the radiation are inversely related by the equation,

$$\nu = c / \lambda \quad (2.1)$$

When a molecule interacts with an electromagnetic radiation, a transfer of energy from photons to molecules may occur such that:

$$\Delta E = h\nu = hc/\lambda = hc\tilde{\nu} \quad (2.2)$$

Here, ΔE is the difference in energy between two quantized states, h is Planck's constant (6.626×10^{-34} Joule/sec), c is the velocity of light and $\tilde{\nu}$ is the wavenumber (which is the number of waves per unit length). Since, the wavenumber is directly proportional to the energy and frequency, it is inversely proportional to the wavelength which makes it more suitable to use.

2.1.2. Vibrational spectroscopy

The vibrational spectroscopic profile of a molecule is, with certain exceptions, considered to be unique. Vibrational frequencies can be determined by using two fundamental techniques.

- 1 Infra-red (IR) spectroscopy was introduced by Coblenz² in 1905. The vibration in the molecule is based on the direct absorption of photons from electromagnetic radiation (Fig. 2.1).
- 2 Raman spectroscopy was first predicted theoretically by Smekal³ in 1923 and later observed by the Indian scientist Sir C.V. Raman⁴ in 1928 and thus denoted the Raman effect. Compared to IR spectroscopy, Raman involves the inelastic scattering (ν_R) of the monochromatic

radiation (ν_0) used for exciting molecules. Whereas the elastic scattering (ν_0) is represented by a thicker arrow (Fig. 2.1).

In many cases IR and Raman spectroscopy provide complementary information for the molecules with the same or different vibrational transitions. Hence, IR and Raman spectra are plotted in a corresponding way to allow comparison. The ordinate axis refers to the extent of absorbed light (IR) and relative intensities (Raman) plotted against the wavenumber (cm^{-1}). The principle information obtained from vibrational spectroscopy are the energies of vibrational transitions and the strength of their interaction with IR or ultraviolet/visible radiation i.e. the vibrational band intensities.

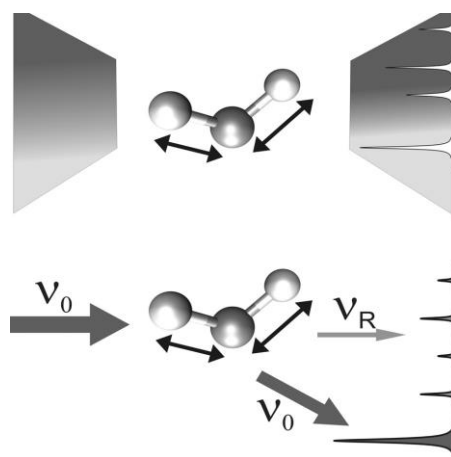


Figure 2.1. An illustration of vibrational excitation in IR (top) and Raman (bottom) spectroscopy.^{5a}

2.2. Molecular vibrations

The relationship between molecular structure and vibrational frequencies can be described by classical mechanics. In order to understand the concept of molecular vibrations in a molecule, it is important to consider the atoms in a molecule as a group of point masses that are connected together *via* intramolecular interactions resembling mass-less springs.⁵ If we denote m_a and m_b as the masses of the atoms in a diatomic molecule, A and B, upon displacement by Δx a restoring force F_x acts on the molecules A and B, which according to Hooke's law is given as:

$$F_x = -k\Delta x \quad (2.3)$$

Here k is the force constant, which is the measure of the strength of the bond or the rigidity of the spring via which atoms are connected in a molecule.

Hooke's law states that the vibrational frequency in the molecule increases with the increase in strength of the bond or rigidity of the spring and decreases with increase in the masses of diatomic molecules⁶:

$$\tilde{\nu} = \frac{1}{2\pi c} \sqrt{\frac{k}{\mu}} \quad (2.4)$$

where, the reduced masses is given by,

$$\mu = \frac{m_a m_b}{m_a + m_b} \quad (2.5)$$

The potential energy can be defined as the energy possessed by a body by virtue of its position in a system; for a diatomic molecule the potential energy (V) is given as,

$$V = \frac{1}{2} kx^2 \quad (2.6)$$

The kinetic energy (T) can be defined as the energy possessed by a body by virtue of its motion; it is given as:

$$T = \frac{1}{2} m_a \left(\frac{dx_a}{dt} \right)^2 + \frac{1}{2} m_b \left(\frac{dx_b}{dt} \right)^2 \quad (2.7)$$

The total energy (E) is, therefore,

$$E = V + T \quad (2.8)$$

If potential energy is plotted as a function of position (x), the resulting parabolic potential (Fig. 2.2), is termed a harmonic oscillator.

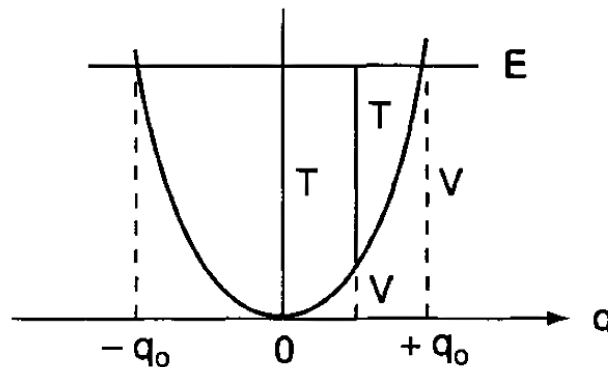


Figure 2.2. Potential energy plot for a harmonic oscillator.⁷

The quantum mechanical approach^{8,9} for determining the vibrations in a diatomic molecule is to treat the vibrations as the motion of a single particle with mass μ whose potential energy is expressed by equation 2.6. The Schrödinger wave equation for such a system is given as:

$$\frac{d^2\psi}{dx^2} + \frac{8\pi^2\mu}{\hbar^2} \left(E - \frac{1}{2} kx^2 \right) \psi = 0 \quad (2.9)$$

where \hbar is the reduced Planck constant.

The (energy) eigen values can be obtained from the above equation as:

$$E_n = \left(n + \frac{1}{2} \right) \hbar\omega \quad (2.10)$$

Here, ω is the frequency of oscillation where, n is the vibrational quantum number with values of 0, 1, 2, 3....

The vibrational frequency in both classical and quantum mechanics is the same. However, in classical mechanics E is 0 when x is zero. Whereas, in quantum mechanics the lower energy state ($n=0$) has an energy of $\frac{1}{2} \hbar\omega$, as shown in Fig. 2.2. The energy changes only in units of $\hbar\omega$. The energy change is continuous in classical mechanics. The energy difference between the two successive vibrational levels in a harmonic oscillator is always the same ($\hbar\omega$). In reality, the system behaves as an anharmonic oscillator corresponding to an asymmetric energy difference and the potential energy is approximated by the Morse potential function¹⁰ (Fig. 2.3).

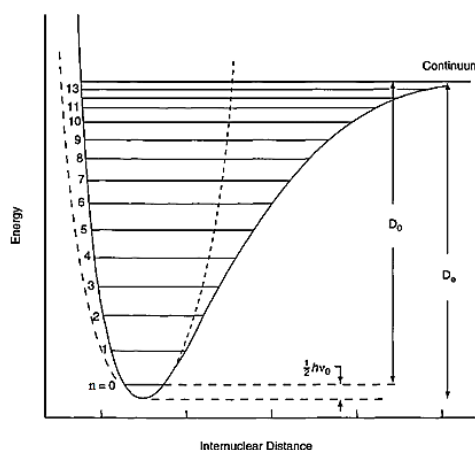


Figure 2.3. Morse potential curve for an anharmonic oscillator.⁷

The potential energy of an anharmonic oscillator is given as,

$$V = D_e (1 - e^{-\beta r})^2 \quad (2.11)$$

Where, β is the measure of the depth of the curvature in a potential well and D_e is the dissociation energy. After solving the Schrödinger equation for the anharmonic oscillator the eigen values are given as,

$$E_n = \hbar\omega_e \left(n + \frac{1}{2}\right) - h\chi_e\omega_e \left(n + \frac{1}{2}\right)^2 + \dots, \quad (2.12)$$

where ω_e is the frequency of oscillation, and $\chi_e\omega_e$ indicates the extent of anharmonicity. From Fig. 2.3, the energy difference in the vibrational levels decreases with increase in n and the energy levels in an anharmonic oscillator are no longer equidistant. The transitions involving $\Delta n = \pm 1$ are allowed for an harmonic vibration. However, the transitions involving $\Delta n = \pm 1, \pm 2, \pm 3$ are allowed for an anharmonic vibration, i.e., overtones (see section 2.2.3.1). Maxwell-Boltzmann law,¹¹ the magnitude of vibrational energy is such that the $n = 0$ level is *significantly* populated at room temperature. Hence, the $\Delta n = \pm 1$ harmonic transitions, $n = 0 \leftrightarrow 1$ appear strongly in both IR and Raman spectra. However, some weak overtones from anharmonic transitions also appear in IR and Raman spectra.

2.2.1 Vibrational modes

A normal mode is defined as an independent, synchronous motion of atoms, or group of atoms. Normal modes are used to describe different vibrational motions in a molecule. Each mode can be characterised by its symmetry and the type of motion associated with it. The degree of freedom is the number of variables required to describe the motion in a molecule. For N atoms in a molecule in 3-D space, three coordinates (x, y, z) are sufficient to describe its $3N$ degrees of freedom. Since, the atoms are bonded together; the motions are not purely translational. The rotational motions can be described in terms of the x, y, z axes; of the six motions three constitute translational motions and the remaining three constitute the rotational motions. Hence, for a non-linear molecule, $3N-6$ degrees of freedom constitutes the vibrational motion. For a linear molecule, there will be two rotational motions around its axis resulting in $3N-5$ degrees of freedom for vibration.¹²

2.2.2. Classification of fundamental vibrations

Vibrations in diatomic and triatomic molecules are defined by stretching and bending modes. For larger molecular weight molecules, there will be several vibrations due to the interaction of different atoms in the system. The vibrations can be classified based on the change in the bond lengths, bond angles and torsional angles as follows.

1 Stretching (ν): this vibration is characterised by a change in the bond length.

- 2 Bending (δ): this vibration is characterised by a change in the angle between two bonds.
- 3 Scissoring (ρ): a change in bond angle, when the two atoms move towards and away from each other.
- 4 Rocking (γ): where one or more bond angle changes between the groups of atoms during the vibration.
- 5 Wagging (ω): a change in bond angle of two atoms such that, two atoms move to one side of the plane. They move up and down the plane.
- 6 Twisting (τ): during the course of vibration, one atom moves above the plane and other moves below the plane.
- 7 Torsion modes: a change in torsional angle (the angle between two planes) i.e. the rotation of alkyl (methyl) group.

Out of four bending vibrations, scissoring and rocking vibrations correspond to in-plane deformation; wagging and twisting modes corresponds to out-of-plane deformation. According to molecular symmetry rules, the normal modes of vibration can be symmetric, if the atoms in a bond move in the same phase, and asymmetric if the atoms moves in the opposite direction. (Fig. 2.4)

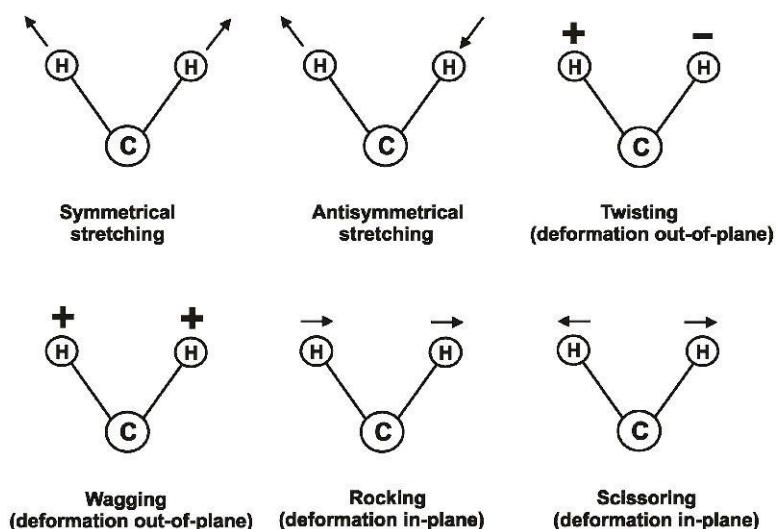


Figure 2.4. Types of vibrations in a diatomic molecule.¹³

2.2.3. Non-fundamental vibrations

The excitation from the ground state (ν_0) to the vibrational state ν_1 results in fundamental vibrations. However, some low intensity bands are also detected which usually arise from

non-fundamental vibrations such as overtones, combination and difference bands¹⁴ or Fermi resonance.¹⁵

2.2.3.1. Overtones

Overtone arise due to excitation from the ground state to higher energy state, which resembles the integral multiples of fundamental frequencies in the spectra. The energy required for an overtone to occur is twice the fundamental transition; $\nu = \pm 1$ are the most commonly occurring, and the probability of overtones rapidly decreases as $\nu = \pm n$ increases (assuming the energy level spacing of a harmonic oscillator). However, overtone frequencies are not exact integral multiples because of anharmonicity with non-uniform energy levels and are usually less than a multiple of the fundamental frequency, given in equation 2.12. The wavenumber, $\tilde{\nu}_n$, of each overtone is given by the expression:

$$\tilde{\nu}_n = n \tilde{\nu}_f - (n + n^2) \tilde{\nu}_f \chi_e \quad (2.13)$$

2.2.3.2. Combination and difference bands

A combination band arises when two or more fundamental vibrations are excited simultaneously. The transition occurs from the ground state to a new combinational energy level (which is not involved in fundamental transitions). The combinational level contains two different normal modes with n quantum numbers and involves the excitation of one photon into two different vibrations by increasing two vibrational quantum numbers, by one each. The energy of such a photon corresponds to a frequency almost equal to the sum of frequencies of two photons required to excite the two vibrations separately. These transitions are allowed in an anharmonic oscillator.

Difference bands appear due to the transition from a lower excited energy level (usually of low frequency) of one vibration to the higher excited level (high frequency) of another vibration. The transition, in this case, uses the existing energy levels; the population of the lower excited level will be higher compared to the higher excited state and thus the intensity will be low for higher frequencies provided the transitions are anharmonic. The frequency of a difference band is exactly equal to the frequency difference of two different fundamental bands.¹⁴

2.2.3.3. Fermi resonance

Fermi resonance is the splitting of two vibrational bands, usually a fundamental vibration and either a combination band or an overtone. The wave function for these two vibrations blend

according to the harmonic approximation, and the result is a change in intensity and a shift in wavenumber in the spectra. As a result, two strong bands appear, instead of a strong and a weak band in the spectra.¹⁵

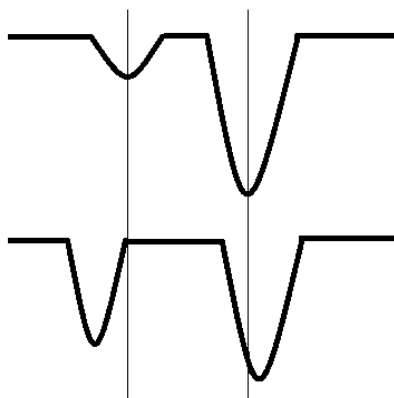


Figure 2.5. Example of intensity and frequency shifts due to Fermi resonance.

If the energies of two states are similar and symmetry requirements are satisfied, mixing occurs, and the resulting vibration can be described as a linear combination of two interacting bands. Fig. 2.5 shows the intensity and wavenumber shifts due to Fermi resonance. The top band represents the non-interacting fundamental vibrations, and the bottom bands show the change in bands as a result of Fermi resonance. They move away from each other, as the two energy levels are split such that one band increases and other band decreases in energy. Such bands are known as “Fermi doublets.”¹⁶

2.2.4. Intensities of vibrational bands

The intensity of a vibrational band is the second important parameter, besides the frequencies of normal mode in the vibrational spectra. The intensity (IR) is proportional to the transition from a vibrational energy state n to another vibrational energy state, m ; typically (but not necessarily) corresponding to the vibrational ground and excited states, respectively. However, quantum mechanical treatments are required to understand the probability of transitions, induced by the interaction of molecules with electromagnetic radiation. Generally, the transition probability, P_{nm} , is given by,

$$P_{nm} = \langle \psi_m^* | \hat{\Omega} | \psi_n \rangle \quad (2.14)$$

Where, ψ_m and ψ_n are the wave functions for the vibrational states and $\hat{\Omega}$ is the operator that describes the perturbation of the molecule with the electromagnetic radiation.⁵

2.2.5. Theory of infra-red absorption

Infrared (IR) spectroscopy is an important analytical techniques, mainly used in the structure elucidation/identification of organic compounds. The technique is based on the absorption of radiation by a chemical substance in the infrared region. IR spectroscopy is based on the principle that when a compound is exposed to IR radiations, the atoms selectively absorb radiation of specific wavelength resulting in vibrations in the molecule. The multitude of vibrations occurring simultaneously produces a complex absorption spectrum that is characteristic of the functional groups that constitute the molecule and also its overall molecular configuration.⁵

The vibrations in a molecule occur due to the vibrational transitions from the ground state to an excited vibrational state (Fig. 2.6, infrared absorption). The difference in energy between the two vibrational states is related to the frequency of the incident radiation (equation 2.15).¹⁷ The intensity of transmitted radiation is measured at each frequency. The infra-red region can be divided into three spectral regions; near infra-red (13,000-4000 cm^{-1}), mid infra-red (4000-450 cm^{-1}) and far infra-red (450-10 cm^{-1}).

$$\Delta E = E_2 - E_1 = h\nu \quad (2.15)$$

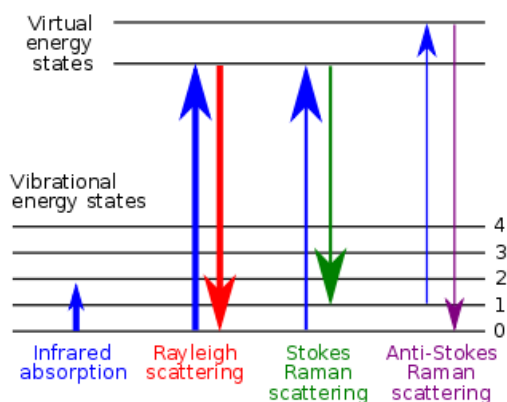


Figure 2.6. Energy level diagram for vibrational transitions.¹⁷

The transitions from the ground state to higher vibrational states results from the absorption of a photon from the IR radiation; this process is controlled by the electrical dipole moment operator $\hat{\mu}_q$, given as,

$$\hat{\mu}_q = \sum_{\alpha} e_{\alpha} q_{\alpha} \quad (2.16)$$

Where, e_α is the effective charge of the atom α and q_α is the distance to the centre of gravity of the molecule in Cartesian coordinates ($q = x, y, z$). The IR intensity for the vibrational transition $n \rightarrow m$ associated with non-zero dipole moment $[\mu_q]_{nm}$, is expressed as the scalar product of the vector of $\hat{\mu}_q$ and the electric field:

$$I_{nm,IR} \propto ([\mu_x]_{nm}^2 + [\mu_y]_{nm}^2 + [\mu_z]_{nm}^2) \quad (2.17)$$

Where $[\mu_q]_{nm}$ is the integral:

$$[\mu_q]_{nm} = \langle \psi_m^* | \hat{\mu}_q | \psi_n \rangle \quad (2.18)$$

One can easily see that a vibrational transition $n \rightarrow m$ in the IR spectrum only occurs if it is associated with a non-zero transition dipole moment. To determine whether a mode is IR active within the harmonic approximation, $\hat{\mu}_q$ is expanded in a Taylor series with respect to the normal mode, Q_k ; the series is restricted to linear terms and given as,

$$\hat{\mu}_q = \mu_q^0 + \sum_{k=1}^{3N-6} \hat{\mu}_q^k Q_k \quad (2.19)$$

$$\text{Where, } \hat{\mu}_q^k = \left(\frac{\partial \mu_q}{\partial Q_k} \right)_0 \quad (2.20)$$

Using equation 2.14, the transition probability is given by:

$$[\hat{\mu}_q] = \langle \psi_m^* | \hat{\mu}_q | \psi_n \rangle = \mu_q^0 \langle \psi_m^* | \psi_n \rangle + \sum_{k=1}^{3N-6} \hat{\mu}_q^k \langle \psi_m^* | Q_k | \psi_n \rangle \quad (2.21)$$

The first term in equation 2.21 is equal to zero since the vibrational wave functions ψ_m and ψ_n are orthogonal. Thus, a non-zero transition probability is achieved if two conditions are satisfied. Firstly, in equation 2.21, the dipole moment with respect to the normal mode, Q_k , must not be equal to zero, which explains/shows that the vibrational mode is related to the change in the dipole moment. Secondly, the term $\langle \psi_m^* | Q_k | \psi_n \rangle \neq 0$ must be non-zero, which is the situation when the vibrational quantum numbers m and n differ by one. This suggests that, within harmonic approximations the fundamental vibrational modes are IR active.⁵ Equation 2.21 holds for all three Cartesian coordinates ($q = x, y, z$), such that only one non-zero electric dipole moment is sufficient to allow IR activity with respect to Q_k (equation 2.17).

2.2.6. Raman scattering

Raman spectroscopy is based on inelastic scattering of photons by irradiating the molecules with monochromatic radiation. Typically, laser beams in the UV, visible or near infra-red regions are used to irradiate samples.^{5,18} A portion of photons from the incident laser are scattered inelastically such that the energy of the incident photons ($h\nu_0$) differs from the scattered photon ($h\nu_{vib}$) (Fig. 2.7) as,

$$\Delta E = h\nu_0 \pm h\nu_{vib} \quad (2.22)$$

According to the law of conservation of energy, the energy difference in the molecule corresponds to the energy difference due to the transitions between two vibrational states. Thus, the above equation can be written as,

$$\Delta E = E_2 - E_1 = h\nu_0 - h\nu_{vib} \quad (2.23)$$

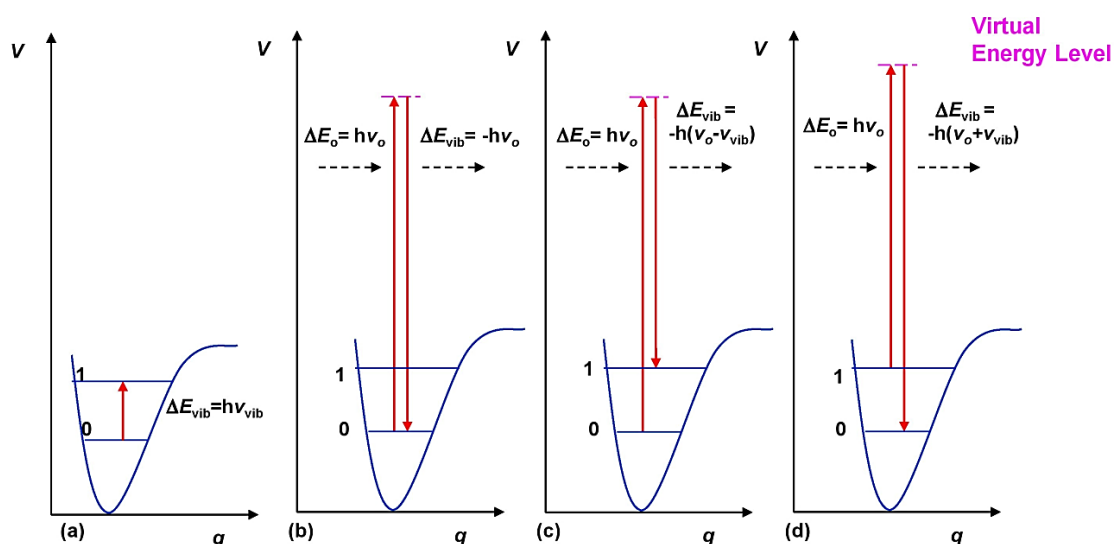


Figure 2.7. Schematic representation of energy transitions in: (a) IR, (b) Rayleigh scattering, (c) Stokes Raman scattering, and (d) anti-Stokes Raman scattering.²¹

The vibrations in a molecule appear between ($4000-10\text{ cm}^{-1}$) in Raman spectra including the far infra-red region ($450-10\text{ cm}^{-1}$). A Raman spectrum is a plot of the intensity of the shifted scattered light versus frequency (cm^{-1}), which is unique to each sample based on its molecular structure. Raman scattering provides information about molecular vibrations, which can be useful in identification and quantification of compounds. The technique relates to infra-red spectroscopy as the spectra from both techniques describes the vibrational transitions in a molecule. Raman scattering occurs due to the change in polarizability of a molecule. Polarizability (α) is a measure

of the distortion of the electron cloud in a molecule to produce an electric dipole moment (μ) under the influence of an electric field (E) of a light wave.¹⁹ This relationship can be defined as:

$$\mu = \alpha E \quad (2.24)$$

However, the above relation does not hold in actual molecules since both polarizability and electric field are vectors consisting of three components in Cartesian coordinates (x, y, z). Thus, equation 2.24 must be written as,

$$\begin{aligned} \mu_x &= \alpha_{xx}E_x + \alpha_{xy}E_y + \alpha_{xz}E_z \\ \mu_y &= \alpha_{yx}E_x + \alpha_{yy}E_y + \alpha_{yz}E_z \\ \mu_z &= \alpha_{zx}E_x + \alpha_{zy}E_y + \alpha_{zz}E_z \end{aligned} \quad (2.25)$$

Equation 2.25 can be further simplified as:

$$\begin{bmatrix} \mu_x \\ \mu_y \\ \mu_z \end{bmatrix} = \begin{bmatrix} \alpha_{xx} & \alpha_{xy} & \alpha_{xz} \\ \alpha_{yx} & \alpha_{yy} & \alpha_{yz} \\ \alpha_{zx} & \alpha_{zy} & \alpha_{zz} \end{bmatrix} \begin{bmatrix} E_x \\ E_y \\ E_z \end{bmatrix} \quad (2.26)$$

The above matrix is termed a polarizability tensor. According to quantum mechanics, the vibrational mode is Raman active if one of these components in equation 2.26 changes during the vibration.⁷

The scattering process can be explained on the basis of classical theory. When a molecule interacts with an electromagnetic wave of frequency ν_0 , the oscillating electric field (E) can be given as,

$$E = E_0 \cos(2\pi\nu_0 t) \quad (2.27)$$

E_0 is the vibrational amplitude and ν_0 is the frequency of the laser. If a diatomic molecule is irradiated by this light, an electric dipole moment μ_{ind} is induced:

$$\mu_{ind} = \alpha E = \alpha E_0 \cos(2\pi\nu_0 t) \quad (2.28)$$

where α is the polarizability. This quantity, which is actually a tensor, varies with time as it describes the response of the electron distribution to the movements of the nuclei that oscillate with the normal mode frequency ν_k , with change in time (t) can be expressed as,

$$\alpha = \alpha_0(\nu_0) + \left(\frac{\partial \alpha}{\partial Q_k} \right)_0 (2\pi\nu_k t) \quad (2.29)$$

where, $\left(\frac{\partial\alpha}{\partial Q_k}\right)$ is the rate of change of α with respect to the change in Q_k ; on combining equations 2.28 and 2.29, we obtain:

$$\mu_{ind} = E_0 \left[\alpha_0 \cos(2\pi\nu_0 t) + \left(\frac{\partial\alpha}{\partial Q_k}\right)_0 Q_k \cos[2\pi(\nu_0 + \nu_k)t] + \left(\frac{\partial\alpha}{\partial Q_k}\right)_0 Q_k \cos[2\pi(\nu_0 - \nu_k)t] \right] \quad (2.30)$$

The sum of the three terms in equation 2.30 corresponds to polarizabilities that depend on different frequencies. The first term is the frequency of the incident radiation, ν_0 , the second and third term gives frequencies for Stokes ($\nu_0 - \nu_k$) and anti-Stokes ($\nu_0 + \nu_k$) that differ from ν_0 by the frequency of the normal mode. The frequency of radiation that remains unchanged after scattering is referred as elastic scattering or Rayleigh scattering whereas the inelastic (frequency-shifted) scattering is referred as Raman scattering (Figs. 2.6 and 2.7); when the frequency of scattered radiation is lower than ν_0 , the molecule remains in a higher excited vibrational state. This process is known as Stokes scattering. If the molecule loses energy (by starting from a higher vibrational excited state), the process is denoted as anti-Stokes scattering.²⁰

At ambient temperature, the energies of most of the normal modes are higher than the thermal energy, such that the molecules predominantly exist in the vibrational ground state. The band intensities of Stokes and anti-Stokes scattering is mainly dependent on the population of molecules in the ground state and excited vibrational levels. Stokes scattering occurs when the molecule is essentially in the vibrational ground state, while for anti-Stokes scattering the molecule, which is in the excited vibrational state, relaxes back to ground state. Therefore, Stokes lines are much more intense than anti-Stokes lines, as governed by the Boltzmann distribution of the vibrational state population.¹¹

The intensity of Raman scattering^{20, 21} is given by,

$$I_R = Kl \left(\frac{\partial\alpha}{\partial Q_k}\right)^2 \omega^4 \quad (2.31)$$

where, K is a constant which includes the speed of light, l is the power of incident radiation, ω is the frequency of incident light, α is the molecular polarizability and Q_k is the normal mode (vibrational coordinate). The intensity of Raman scattering is proportional to the incident laser power and the fourth power of the frequency of the incident radiation. Experimentally, the intensity of Stokes scattering can be expressed as:

$$I = KCI_0(\nu_i)^4 \quad (2.32)$$

where, K is a constant, C is the concentration of the sample responsible for the scattering, I_0 is the intensity of the incident laser beam and ν_i is the frequency of the incident radiation. Classical theory correctly predicts that Raman scattering should be weaker than Rayleigh scattering and the Raman scattering is dependent on the intensity of incident laser and on sample concentration. Using classical theory, the ratio of Stokes intensity to anti-Stokes can be stated as:

$$[(\nu_0 - \nu_k) / (\nu_0 + \nu_k)]^4 \quad (2.33)$$

2.2.7. Selection rules

Both infrared and Raman spectroscopies provide a unique spectral fingerprint of a material. The vibrational bands in the spectra are caused due to molecular or lattice vibrations. Although the spectral features of infra-red and Raman spectra can be interpreted in a similar way, the spectra appear slightly different depending upon the nature of the vibrations. The vibrations of a molecule (symmetric and antisymmetric vibrations of normal modes) are given by the corresponding information from infra-red and Raman spectra.

Using vibrational selection rules, it is possible to predict whether a molecular vibration is infra-red or Raman active or both. During the interaction between photons and molecules, the total angular momentum in the electronic ground state has to be conserved. As a consequence of this requirement only specific vibrational transitions are possible.

Rule of mutual exclusion

If a molecule has a centre of symmetry, then no vibrations can be both infra-red and Raman active, and vice versa.⁶ In the absence of a molecule with a centre of symmetry, some vibrations (but not necessarily all) may be both infra-red and Raman active.

2.2.8. Selection rules for infra-red absorption and Raman scattering

A vibration is infra-red active, if the dipole moment μ , in a molecule changes during the vibration. The intensity of an infra-red absorption band, I_{IR} , is dependent on the change in dipole moment μ :

$$I_{IR} \propto \left(\frac{\partial \mu_q}{\partial Q_k} \right)^2 \quad (2.34)$$

where Q_k is the normal coordinate.

A vibration is Raman active, if the polarizability in a molecule changes during the vibration. The intensity of a Raman active band (I_{Raman}) is dependent on the change in the polarizability α :

$$I_{Raman} \propto \left(\frac{\partial \alpha}{\partial Q_k}\right)^2 \quad (2.35)$$

As a consequence of the selection rules, both infra-red and Raman spectroscopy provide detailed information about the functional groups present in a molecule. Raman spectroscopy especially contributes to the characterisation of the carbon backbone of organic molecules or polymers.

2.2.9. Infra-red versus Raman spectroscopy

Although infra-red and Raman spectroscopies provide similar information pertaining to vibrational frequencies in a molecule, there are many advantages and disadvantages unique to each technique.

Advantages (of Raman spectroscopy)

1. As mentioned earlier (section 2.2.8), the selection rules are significantly different between infra-red and Raman spectroscopies. Thus, some vibrations are only Raman-active while others are only infra-red active. The mutual exclusion rule holds for molecules possessing a centre of symmetry. However, in molecules with high symmetry point groups only totally symmetric vibrations are Raman-active.
2. Some vibrations are inherently weak in infra-red and strong in Raman spectra. Examples includes stretching vibrations of C=C, C≡C, S—S, C—S and P=S bonds. Generally, non-polar (covalent) bonds are stronger in Raman and polar bonds (ionic) are stronger in infra-red. Stretching vibrations are stronger than bending modes in both IR and Raman, because stretching frequencies are of higher energy resulting in larger dipole moments and polarizabilities.
3. In Raman spectroscopy, only a small amount of sample is needed to obtain Raman spectra. However, care is still needed to avoid thermal degradation of the sample due to the intense laser light. Nevertheless, this is an advantage compared to infra-red spectroscopy when only small quantities of samples are available.
4. Raman spectra of aqueous sample solutions can be obtained without major interference from water since water is a weak Raman scatterer. Therefore, Raman spectroscopy is ideal for studying biological compounds in aqueous solution. In contrast, infra-red spectroscopy suffers from the strong absorption of water.

5. Raman spectra of air-sensitive and/or hygroscopic materials can be obtained by placing the compounds in sealed glass tubing. This is not possible in infra-red spectroscopy since glass tubing absorbs infra-red radiation.^{17,20,21}
6. The vibrations in the region from (4000-50 cm^{-1}), which includes the far infra-red region, (450-50 cm^{-1}) can be recorded using Raman spectroscopy. Mostly, lattice mode vibrations and ring breathing vibrations are detected in this region. In contrast, beam splitters, gratings, filters and detectors must be changed to cover the far infra-red region.
7. In Raman spectra, the measurement of depolarization ratios may provide reliable information regarding the symmetry of a normal vibration in solution (discussed in following section). However, such information cannot be obtained from infra-red spectra.

Disadvantages (of Raman spectroscopy)

1. A laser source is necessary to detect weak Raman scattering. If the excitation intensity of the laser is too high, it may thermally decompose the sample.²³
2. For samples with substantial fluorescence background, it may be difficult to differentiate the Raman signal from the background unless an excitation source of higher wavelength (in near-IR region) is used.
3. Raman scattering is not very sensitive for analysing samples in the solution state (high concentrations of samples are usually required for analysis), unless, techniques such as SERS or SERRS are used.
4. It is more difficult to obtain rotation-vibration and rotational spectra with high resolution in Raman compared to IR spectroscopy. This is because Raman spectra are, usually, obtained in the visible region where high resolving power is difficult to obtain.
5. A Raman spectrometer is much more expensive compared to a conventional FT-IR spectrophotometer, although less expensive models are available which are portable, smaller and suitable for some forms of data processing.^{18,21, 22}

2.2.11. Introduction to molecular symmetry

Symmetry is a powerful mathematical tool and an important aspect of chemistry. An understanding of symmetry is important in e.g. crystallography, spectroscopy, and solving quantum mechanical calculations. The symmetry properties of molecules allow us to predict e.g., optical activity, vibrational spectra and hybridization. To comprehend the concept of symmetry it is essential to understand the following.

2.2.12. Group theory

Group theory provides a systematic treatment of symmetry in chemical systems within a mathematical framework. Once the symmetry of a molecule is established, group theory provides a valuable set of tools to gain insight into the physical and chemical properties of a system.¹⁸ Some applications of group theory include:

1. predicting whether a given molecule will be polar or chiral.
2. inspecting chemical bonding and visualizing molecular orbitals.
3. investigating vibrational motions in a molecule.

2.2.13. Symmetry operations and symmetry elements

A symmetry operation is a well-defined transformation of a molecule that produces a new orientation that is indistinguishable from the original. Typical symmetry operations include rotations, reflections, and centre of inversions. Each symmetry operation has a symmetry element which is the plane, axis, point or line corresponding to the symmetry operation being carried out. The symmetry element consists of all the points that stay in the same place when the symmetry operation is performed. For example, a reflection is carried out in a plane; a rotation is carried out around an axis, while an inversion is carried out at a point. The symmetry elements and related operations^{5,7} that a molecule may possess are as follows.

- 1 The identity (E) operation represents a rotation of 360° and leaves the entire molecule unchanged, causing no change in the molecule. Every molecule possesses this symmetry.
- 2 An n -fold axis of symmetry, C_n is a rotation through the angle $360^\circ/n$, which leaves the molecule unchanged. Some molecules have more than one C_n axis; the one with greatest value of n is termed the principal axis. All linear molecules including diatomic molecules have C_∞ axis because rotation at any angle leaves the molecule in the same orientation.
- 3 A plane of symmetry (σ) is a reflection operation with respect to a mirror plane. They are divided into three types: a vertical mirror plane (σ_v), containing a principal rotation axis; a horizontal mirror plane (σ_h), perpendicular to a principal axis of rotation and a dihedral mirror plane (σ_d) which bisects the dihedral angle made by the principal axis of rotation and two adjacent C_2 axes perpendicular to the principal axis of rotation.
- 4 A centre of symmetry (i) is an inversion operation carried out through the centre of symmetry. Inversion consists of passing each point through the centre of inversion and out to the same distance on the other side of the molecule.

5 An improper rotation-reflection axis (S_n) operation consists of rotation through an angle $360^\circ/n$ about the axis, followed by a reflection operation in a plane perpendicular to the axis. The identity and C_n rotations are the only two operations that may actually be carried out on a molecule. Hence, they are referred as *proper symmetry operations*. Reflection (σ), improper rotation-reflection and centre of inversion operations can only be imagined, as it is not possible to invert or turn a molecule into its mirror image without affecting the arrangement of chemical bonds. Hence, these operations are termed *improper symmetry operations*.

2.2.14. Point groups

The overall symmetry of a molecule is described by a set of symmetry operations; this set of operations is defined as the *point group* of the molecule. This is due to the fact that there is at least one point in space that remains unchanged regardless of which symmetry operation is applied. For labelling point groups, the two systems of notation called the *Schoenflies* and *Hermann-Mauguin* systems are used. Of the two systems, the *Hermann-Mauguin* (international) system is preferred in crystallography, because they can easily be used to include the translational symmetry elements, which specify the directions of the symmetry axes.²⁴ The molecular point groups, with examples, are listed in Table 2.1.

Table 2.1. List of point groups with descriptions and examples.

Point group	Description	Example
C_1	Contains only an identity operation (E) as the C_1 rotation is a rotation by 360°	Bromochlorofluoromethane (C_1)
C_i	Contains the identity (E) and a centre of inversion (i).	1,2-Dichloro-1,2-dibromoethane (C_i)
C_s	Contains the identity (E) and plane of reflection (σ).	Hypochlorous acid, thionyl chloride (C_s)
C_n	Contains the identity (E) and an n -fold axis of rotation.	Hydrogen peroxide (C_2)
C_{nv}	Contains the identity (E), an n -fold axis of rotation, and n vertical mirror planes (σ_v).	Water (C_{2v}), ammonia (C_{3v})
C_{nh}	Have the identity (E), an n -fold axis of rotation, and a horizontal mirror plane (σ_h).	Boric acid (C_{3h}), planar diketopiperazine (C_{2h})
D_n	Have the identity (E), an n -fold axis of rotation with C_2 rotation axis, perpendicular to the principal axis.	Cyclohexane twist form (D_2)
D_{nh}	Contains the same symmetry elements as D_n , but with the addition of a horizontal mirror plane (σ_h).	Ethene (D_{2h}), boron trifluoride (D_{3h}), xenon tetrafluoride (D_{4h}).
D_{nd}	Contains the same symmetry elements as D_n with the addition of n dihedral mirror planes.	Ethane (D_{3d}), allene (D_{2d})
S_n	Contains the identity and one S_n axis.	1,2-Dibromo-1,2-dichloroethylene (S_2)

T_d	Contains all the symmetry elements of a regular tetrahedron, including the identity, three- C_2 axes, four C_3 axes, three S_4 axes and six dihedral mirror planes.	Methane (T_d)
T T_h	Same as T_d but no planes of reflection. Same as for T but contains a centre of inversion.	$C_{60}Br_{24}$ (T_h)
O_h O	The group of the regular octahedron. Same as O_h but with no planes of reflection.	Sulphur hexafluoride (O_h)

It is thus quite straightforward to classify a molecule in terms of its point group. However, certain rules still need to be followed as suggested by Zeldin²⁵ and outlined in Fig. 2.8.

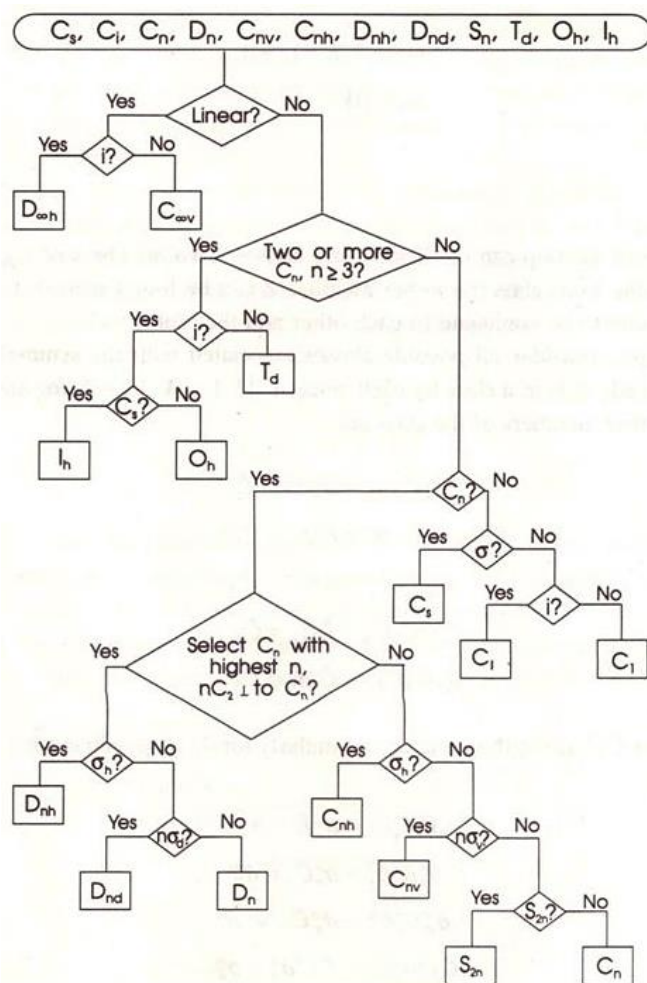


Figure 2.8. Flow chart for determining point groups.²⁶

2.2.15. Character tables

Each point group has a complete set of possible symmetry operations that can be listed conveniently in a matrix transformation known as a character table. The systematic analysis of the symmetry properties of molecules is carried out using character tables. Prior to interpreting the

character table, it is necessary to understand the terms *irreducible* and *reducible representations*. A reducible representation is the transformation of similar matrices into the same block form (matrices of the same dimension in the same positions). A representation is said to be *irreducible*, when a matrix cannot be reduced further. The number of reducible representations of symmetry operations is infinite but there is a small finite number of irreducible representations. The reducible representations can be reduced to a linear combination of irreducible representations using the formula^{5,18}:

$$n_{\Gamma} = \frac{1}{h} \sum_x n_x \chi_R \chi_{ir} \quad (2.37)$$

Where, n_{Γ} is the total number of appearances for irreducible representation, h is the order of the group, n_x is the number of operations in the symmetry class, χ_{ir} are the characters from irreducible representation for a particular class and χ_R are the characters from reducible representation for a particular class. The number of irreducible representations is always equal to the number of classes of the symmetry point group.

Name of the point group (Schoenflies symbol)	Symmetry Operations arranged by class				Order of the group (sum of the coefficients of each class)
C_{2v}	E	C_2	$\sigma_v(xz)$	$\sigma_v(yz)$	$h = 4$
Symmetry Species, Γ (Irred. Rep)	A_1	1	1	1	z, x^2, y^2, z^2
	A_2	1	1	-1	R_z, xy
	B_1	1	-1	1	x, R_y, xz
	B_2	1	-1	-1	y, R_x, yz
Characters 1 = symmetric -1 = antisymmetric					
functions					

Figure 2.9. Character table for the C_{2v} point group.

Fig. 2.9 shows the character table for the point group C_{2v} . The short hand notation system that describes the symmetry of an irreducible representation are known as Mulliken symbols (Table 2.2).²⁷ The functions in the last column of the character table provide information about infra-red, Raman and activities of normal vibrational modes.¹⁸ The x, y, z coordinates relate to translational motion and infra-red activity. R_x, R_y, R_z are the rotational motions about the respective axis. The quadratic functions $xy, yx, zy, x^2, y^2, z^2$ relate to Raman activity.

Table 2.2. Mulliken symbols/descriptions.

Mulliken symbols	Description
A	Symmetric with respect to the principle axis of rotation.
B	Antisymmetric with respect to the principle axis of rotation
E	Doubly degenerate (E=2)
T	Triply degenerate (E=3)
g	Symmetric to centre of inversion
u	Antisymmetric to centre of inversion
Subscript 1	Symmetric to C ₂ rotation perpendicular to principle axis
Subscript 2	Antisymmetric to C ₂ rotation perpendicular to principle axis
Superscript '	Symmetric with respect to a horizontal plane of symmetry (σ_h)
Superscript ''	Antisymmetric with respect to a horizontal plane of symmetry (σ_h)

2.3. Computational chemistry

Computational chemistry is a branch of chemistry concerned with determining theoretical properties of molecules. A computational chemistry approach allows scientists to simulate chemical structures and reactions, based on the fundamental laws of physics and chemistry.²⁸ It uses mathematical approximations and computer programs (rather than or in conjunction with experimental studies) to predict the structure, reactivity, kinetics and other properties of molecules. Ideally, some methods can be used to model unstable intermediates, molecules in the transition state and their reactions which is impossible to obtain by experimental observations. Therefore, the calculations can be used to predict and interpret experimental results. Quantum chemical calculations are the basis for computational chemistry, performed on a wide range of molecules by means of suitable computer programs.^{28, 29}

There are two broad areas in computational chemistry dedicated to the structure and reactivity of molecules: molecular mechanics and electronic structure methods. Both perform the same basic type of calculations (except computation of vibrational frequencies, which can only be performed using electronic structure methods).

- Computing the energy of a specific molecular structure (atoms or nuclei and electrons arranged in 3D space).

- Geometry optimization; a procedure that attempts to elucidate the minimum energy structure of the molecule, which often approximates the specified starting structure.
- Computing the vibrational frequencies resulting from interatomic motions within a molecule.

2.3.1. Molecular mechanics

Molecular mechanics (MM) is a computational method that uses a wide amount of experimentally derived parameters (structural characteristics) to predict the chemical properties of molecules. MM simulation is based on the classical laws of physics and neglects the explicit treatment of electrons in molecular systems. Instead, the calculations are based on the interactions amongst the nuclei. Therefore, molecular mechanics calculations cannot be used to study the molecular properties which depend on electronic details. MM models are used to predict the energy of a molecule as a function of its conformation. This allows the prediction of relative energies between different conformers as well as transition states and equilibrium geometries, which correspond to local minima of the potential energy surface. Applications includes analysis of reaction mechanisms by predicting the most possible pathway for the reaction and alternatively, by analysing steric factors to predict the stereo-specificity and kinetics of a reaction,³⁰ and studies of crystal properties (*e.g.* packing, density).^{31, 32}

2.3.2. Electronic structure methods

Electronic structure methods are based on the laws of quantum mechanics^{33, 34} rather than classical physics for their computations. According to quantum mechanics the energy and other related properties of a molecule can be obtained by solving the Schrodinger equation²⁸:

$$\hat{H}\Psi = E\Psi \quad (2.38)$$

The solution of the above equation provides wave functions, Ψ , which describes the probability of finding the electrons within molecules, \hat{H} is the Hamiltonian operator which characterises the total energy of any given wave function, as well as the eigenvalues E . In order to calculate eigenvalues, the Hamiltonian operator can be split into different energies given as:

$$H = T_e(r) + T_n(R) + V_{n-e} + V_e(r) + V_n(R) \quad (2.39)$$

where, e and n refer to electrons and nuclei, respectively, V is the potential energy, V_{n-e} is the potential energy due to attraction, T is the kinetic energy and r and R refer to the position of electrons and nuclei, respectively. However, the exact solution to the Schrodinger equation is not

computationally practical. Electronic structure methods are characterised by their various mathematical approximations to its solution which include the following.

- 1 The Born-Oppenheimer (BO) approximation, which states that because the mass of electrons is much less than that of nuclei, electrons move much more rapidly compared to the motion of the nucleus. Hence, the nuclear motion can be considered to be fixed. Thus the electronic part can be reduced assuming the electrons are in the ground state. By solving the time-independent Schrodinger equation, the electronic Hamiltonian, \hat{H}_e , can be obtained.
- 2 The Linear Combination of Atomic Orbitals (LCAO) approximation relates to the wave function ψ , which is assumed to be the total wave function, that can be expressed as the sum of smaller functions called basis functions, ϕ :

$$\psi = \sum_i c_i \phi_i \quad (2.40)$$

Where, ϕ_i are the atomic orbitals and c_i is a weighting factor in relation to the overall contribution to the molecular orbitals. There are two major classes of electronic structure methods.

2.3.3. *Ab Initio* methods

Ab initio methods are based on laws of quantum mechanics; *ab initio* means “from first principles”. This implies that no (or few) assumptions are made, and that the method is ‘pure’ from a theoretical standpoint. *Ab initio* methods use a series of rigorous mathematical expressions to obtain approximate solutions to the Schrödinger equation. They are not limited to any specific class of system and provide highly quantitative predictions for a broad range of systems. The simplest *ab initio* method originally developed by Hartree and Fock (HF) ³⁵ uses the variational principle (which states that the calculated energy will be higher than the exact solution) to obtain the constants, c_i , which enables the Roothaan-Hall matrix equation to be solved ³⁶:

$$FC = SC_\epsilon \quad (2.41)$$

$$\text{Det}|F - \epsilon_a S| = 0 \quad (2.42)$$

Where, F is the Fock matrix, C is the matrix of constants c_i , S is the orbital overlap matrix, ϵ is the diagonal matrix of orbital energies and ϵ_a the energy level matrix of the system. HF method utilizes a self-consistent field (SCF) procedure to solve the variational principle equations. The SCF process uses an iterative methodology of finding the optimum wave function and is time consuming and computationally very complicated. The major drawback of the HF-SCF method is that it does not account for electron correlation.

2.3.4. Semi-empirical methods

Semi-Empirical (SE) methods use parameters derived from experimental data to solve the calculations used for geometry optimization/energy minimization. SE methods start with the general form of *ab initio* HF calculations, but make numerous approximations for the various integrals³⁷; these integrals are approximated by functions with empirical parameters which are adjusted to improve the agreement with experimental data.³² As a result, SE methods are very fast, applicable to relatively larger weight molecules, and may give accurate results when applied to molecules that are similar to the molecules used for parameterization. In contrast to *ab initio* methods, SE calculations are comparatively less computationally demanding and provide accurate quantitative predictions of structure and energies of molecules and fairly reasonable qualitative descriptions of molecular systems. Semi-empirical methods have been designed for biological and typical organic systems and tend to be inaccurate for problems involving the prediction of activation barriers, chemical transitions and hydrogen-bonding which generally lack parameterization.

2.3.5. Electron correlation methods

When using HF approximations, interactions between electrons are treated as the average density of all other electrons. The probability of finding any one electron at a particular position is independent of the positions of the other electrons in space.³⁸ Since two electrons cannot be in the same position at the same time, the electrons must move to avoid each other, *i.e.* their motion must be correlated. However, the HF-SCF method fails to account for electron correlation (the energy contribution arising from electrons interacting with one another). For systems where such properties are important, HF results may not be satisfactory. For this reason various methods have been developed which account for electron correlation. Such methods are referred as *post* HF-SCF methods because they add correlation corrections to the HF model.

2.3.6. Møller-Plesset perturbation theory

Perturbation theory is a well-established qualitative approach to electron correlation. Perturbation theory is based upon dividing the Hamiltonian into two parts:

$$\hat{H} = \hat{H}_0 + \lambda V \quad (2.43)$$

Where λ is an arbitrary real parameter and V is a *perturbation correction* applied to the unperturbed Hamiltonian, \hat{H}_0 , which is assumed to be small in comparison to it. The solution is expressed as a Taylor series in λ , the perturbation strength, as:

$$E = E^{(0)} + \lambda E^{(1)} + \lambda^2 E^{(2)} + \dots \quad (2.44)$$

$$\Psi = \Psi^{(0)} + \lambda \Psi^{(1)} + \lambda^2 \Psi^{(2)} + \dots \quad (2.45)$$

The expressions obtained by perturbation theory are not exact. However, accurate results can be obtained as long as the Taylor expansion parameter, λ , is very small. The energy and perturbed wave function are expanded and the Schrodinger equation becomes:

$$\hat{H}\Psi = E\Psi$$

$$(\hat{H}_0 + \lambda V) (\Psi^{(0)} + \lambda \Psi^{(1)} + \lambda^2 \Psi^{(2)} + \dots) = (E^{(0)} + \lambda E^{(1)} + \lambda^2 E^{(2)} + \dots) (\Psi = \Psi^{(0)} + \lambda \Psi^{(1)} + \lambda^2 \Psi^{(2)} + \dots) \quad (2.46)$$

In the above equation, \hat{H}_0 is defined as the sum of one-electron Fock operators:

$$\hat{H}_0 = \sum_i F^i \quad (2.47)$$

F^i is the Fock operator acting on the i^{th} electron. The zeroth-order equation is solely the Schrödinger equation for the unperturbed system:

$$\hat{H}_0 \Psi^{(0)} = E^{(0)} \Psi^{(0)} \quad (2.48)$$

Equation 2.48 is then expressed in powers of λ to obtain energy corrections:

$$\begin{aligned} E^{(0)} &= \langle \Psi^{(0)} | \hat{H}_0 | \Psi^{(0)} \rangle \\ E^{(1)} &= \langle \Psi^{(0)} | V | \Psi^{(0)} \rangle \\ E^{(2)} &= \langle \Psi^{(0)} | V | \Psi^{(1)} \rangle \end{aligned} \quad (2.49)$$

such that the first energy correction is larger than second and so forth.

Moller-Plesset (MP) perturbation theory³⁹ adds non-iterative correlation corrections to Hartree-Fock theory. It considers the unperturbed Hamiltonian \hat{H}_0 as the sum of one-electron Fock operators, and treats electron correlation as the perturbation to the zeroth-order Hamiltonian. By using zeroth and first order, an expression for the energy equivalent to the Hartree-Fock energy can be obtained. Improvements in HF-SCF can be achieved by including second and higher order terms. MP methods encounter size extensivity issues by scaling the predicted energy for each order of perturbation with the number of non-interacting particles in infinite systems with different

numbers of electrons, such as crystal lattices. The commonly used perturbation methods can be truncated at second order (MP2), third order (MP3) and higher orders (MP4 and MP5). Qualitatively, MP2 accounts for 80-90% of the correlation energy and describes the correlation between pairs of electrons. MP3 accounts for 90-95% of the correlation energy and also describes the interaction between electron pairs. MP methods of any higher degree are generally not used because they are computationally demanding and require considerable processing time. However, they can be used for very simple systems when precise calculations are necessary.^{40,41}

2.3.7. Density functional theory

Density functional theory (DFT) is a quantum mechanical method used to investigate the electronic structure of many body systems, especially in condensed matter physics and computational chemistry. Like Hartree-Fock other traditional electronic structure methods are based on the complicated many-body electronic wave function. DFT does not depend on electronic wave functions but, instead, it uses electronic density as the fundamental parameter. The electron density is a function of three variables and is very simple to deal with both theoretically and practically compared to the many-body wave function which is dependent on three spatial variables, $3N$ variables for each of the N -electrons.

DFT was put into a firm theoretical footing by Hohenberg-Kohn theorems.⁴² The first Hohenberg-Kohn theorem states that the density is a physical entity and governs all ground state properties of the system; i.e., $E = E[\rho]$, where ρ is the density in the ground state of the system. The second theorem states that a variational principle guides the aforementioned energy density functional $E[\rho]$. If ρ' is not the ground state density of the above system, then:

$$E[\rho'] > E[\rho] \quad (2.50)$$

In 1965, the above theorems were practically enunciated by Kohn and Sham as DFT.⁴³ The Kohn-Sham theory is shown in its simplest form (equation 2.51), which is described as the mathematical expression of electron densities and their subsequent correlation to molecular energies,

$$E_{DFT}[\rho] = T[\rho] + E_{ne}[\rho] + J[\rho] + E_{xc}[\rho] \quad (2.51)$$

Where, E is the energy, T is the kinetic energy of the electrons, E_{ne} is the energy from electron-nuclear attraction, J is the energy from electron-electron repulsion, and E_{xc} is the electron-electron exchange-correlation energy. The foregoing terms are the functions of a function, the electron density ρ , which itself is a function of the three (x , y , and z) positional coordinates. As such, the

individual terms T , J , E_{xc} and E_{ne} are termed functionals. The task then is to determine the values of each of these four functionals. There are a great number of approximations that attempt to calculate the electron exchange-correlation energy. The electron correlation feature addresses how an electron interacts, or “sees” another electron in an atom or molecule. The electron exchange describes a quantum mechanical property of electrons that is related to their exchange between a fermion and a boson (a *fermionic* or *bosonic* electron); a consequence of Pauli’s exclusion principle, which states that no two fermions (half-integer spin particles) have the same quantum state.

2.3.7.1. DFT methods

DFT methods are complex and different, but can be divided into the following three classes.

- 1 *Local density approximation (LDA)*. The LDA is determined based on the properties of electron density. The critical assumption of this approximation is that, for a molecule with numerous electrons in the gas phase, the density is uniform throughout the molecule. This is not the case for molecules, where the electron density is distinctly non-uniform. This approximation does, however, work well with electronic band structures of solids, which describes the range of energies in which electrons are permitted or not permitted (forbidden). Outside of this application, however, local density approximations are not very satisfactory.
- 2 Methods that combine the *gradient correction factor* with the electron density calculations. Mathematically, a gradient is a function that measures the rate of change in any property. In this case, the gradient is used to account for the non-homogeneity of the electron density, and hence is known as the *gradient-corrected method* (also known as a *non-local method*).
- 3 Methods that are a combination of an exchange energy to the Hartree-Fock approximation and a DFT approximation to the exchange energy, all combined with a functional that incorporates electron correlation. These methods are known as *hybrid* methods and are, at present, the most popular and, in practice, widely used DFT methods.
- 4 Dispersion methods (DFT-D) are recent developments in DFT in order to accurately model the physical and chemical interaction that occurs in molecules due to dispersion forces (van der Waals forces).

2.3.8. Basis sets

Modern quantum chemical calculations are usually performed via a predetermined set of basis functions. *Ab initio* electronic structure programs such as Gaussian 09 use Gaussian type atomic

functions as basis functions. A basis set is the mathematical expression formed by the linear combination of atomic orbitals (LCAO) within a system (to approximate the total electronic wave functions) used to perform quantum mechanical calculations. The wave functions are represented as vectors, which correspond to the components of the coefficients as a linear combination of the basis functions in the basis set used. The operators are then represented as matrices. When quantum mechanical calculations are performed, it is common to use basis sets comprising of a finite number of atomic orbitals, centred at each atomic nucleus within the molecule. Primarily, atomic orbitals were classical Slater orbitals, resembling a set of functions, which decompose exponentially as the distance from the nuclei increases. These Slater-type orbitals⁴⁴ could be approximated as linear combinations of Gaussian orbitals. It is easier to calculate and overlap other integrals with Gaussian basis functions and this results in low computation cost of several basis sets comprised of Gaussian-type orbitals (GTOs); the smallest number of basis functions, required to represent all the electrons on each atom are called minimal basis sets. The most common additions to minimal basis sets are polarisation functions, denoted by an asterisk*. Polarization functions can also be added to lighter atoms such as hydrogen and helium, indicated by two asterisks**. When polarisation is added to this basis set, a p-function is added to the basis set. This adds some additional needed flexibility within the basis set, effectively allowing molecular orbitals involving the hydrogen atoms to be more asymmetric about the hydrogen nucleus. Similarly, d-type functions can be added to a basis set with valence p-orbitals, and f-functions to a basis set with d-orbitals and so on. The particular notation indicates exactly which and how many functions are added to the basis set, such as (d, p). Other common functions added to basis sets are diffuse functions, denoted by a plus sign, +. Two plus signs (++) indicates that diffuse functions are also added to lighter atoms such as hydrogen and helium. These additional basis functions may be important when considering anions, atoms with lone-pair electrons and larger molecular weight systems.

2.3.9. Geometry optimization

Optimization of the geometry of any molecule is the first step in a quantum mechanical calculation. This is usually performed on non-interacting isolated molecules, assumed to be in the gas phase. Geometry optimization is a procedure that attempts to ascertain the lowest energy/minimum energy of a molecule in close proximity to the specified starting structure. The atomic positions in the molecule are adjusted during the computation until the minimum energy is reached. Whenever possible, the experimentally obtained geometry (e.g., from X-ray crystallographic data) can be used as a starting point for geometry optimization. The geometry of the molecule can be generated

using molecular editing and visualizing programs such as ChemDraw, MolDraw,⁴⁵ with reasonable values of bond lengths, bond angles and dihedral angles. The initial molecular structure can also be built using computer software such as Gaussian 09 and its graphical user interface, called GaussView.⁴⁶

2.3.10. Frequency calculations

Vibrational spectra of molecules in their ground and excited states can be computed by using the Gaussian 09 program. Frequency calculation are effective only at stationary points (local minima) on the potential energy surface; for this reason it is essential to obtain geometry optimization of the molecule being investigated prior to undertaking frequency calculations. The output of the program predicts the frequencies and intensities of vibrational bands. Besides this, the calculations also provide data which describe the displacements of the molecule as it undergoes normal modes of vibrations. Molecular frequencies depend on the second derivative of energy with respect to the nuclear position. Analytically, second derivatives are provided by DFT (B3LYP), Hartree-Fock and Moller-Plesset perturbation theory (MP2). An optimized geometry is used as the input for the frequency calculation. The frequency calculations should be performed using the same level of theory and basis set as the one that was used to obtain the optimized geometry of the molecule.^{29,47,48} Harmonic force fields obtained from quantum mechanical calculations are widely used for the calculation of vibrational frequencies and the normal modes of vibrations.^{49,50} This opened the way to calculate the frequencies and intensities of spectral bands with a minimum degree of uncertainty and finding the rational explanation for a number of physical and chemical properties of substances.

However, in several modern quantum mechanical calculations of vibrational spectra performed at various levels of approximation, the calculated frequencies are higher in comparison to their experimental counterparts. This is a consequence of the more or less systematic overestimation of the force constants in the Hartree-Fock method.⁵¹ This overestimation of the force constants depends on the basis set employed and to the not-so regular discrepancies in applications of the Moller-Plesset perturbation theory.³⁹ Such calculations require empirical corrections. To improve the agreement between calculated and experimental vibrational frequencies, quantum-mechanical force fields are corrected in one way or another; e.g., by using scaling factors which are the empirical corrections estimated from the experimental vibrational spectra of small molecules with reliable frequency assignments. Fig. 2.10 shows a typical flow chart explaining the quantum mechanical calculations for a molecule.

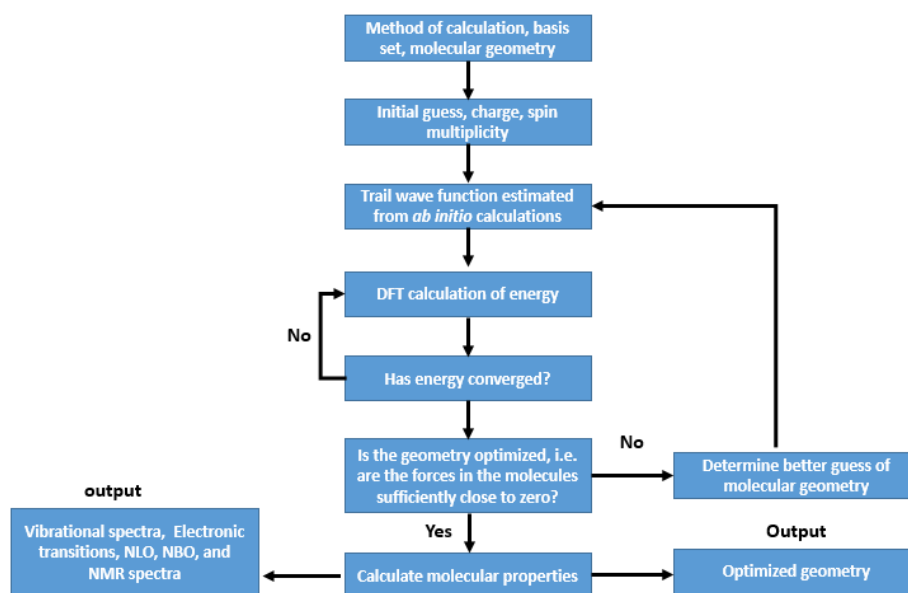


Figure 2.10. Flow chart for quantum mechanical calculations of molecular structure.

2.3.11. Normal co-ordinate analysis (NCA)

Detailed description of vibrational modes can be studied by means of normal coordinate analysis. Normal coordinate analysis is a procedure for calculating the vibrational frequencies which relates the observed frequencies of preferably the harmonic infrared and Raman frequencies to the force constants, equilibrium geometry and the atomic masses of the oscillating system. NCA has proven to be a useful tool in assigning vibrational bands but its predictive ability depends on reliable intramolecular force constants.

2.4. Nuclear magnetic resonance

Nuclear magnetic resonance spectroscopy uses radio-frequency (RF) waves to induce transitions between different nuclear energy states in a magnetic field. Generally, the energy involved in the radio-frequencies used is very small for an atom or a molecule to vibrate, rotate or cause excitation, but sufficient to change the direction of nuclear spin of an atom in a molecule (Fig 2.11). To carry out the absorption of radiation by the nuclei, an external magnetic field of several Tesla (τ) must be applied that results in the development of selected energy states leading to absorption.

2.4.1. Principles of NMR

A nucleus with an odd mass number (A) or an odd atomic number (Z) possesses a nuclear spin. The spinning of charged species generates a magnetic field.

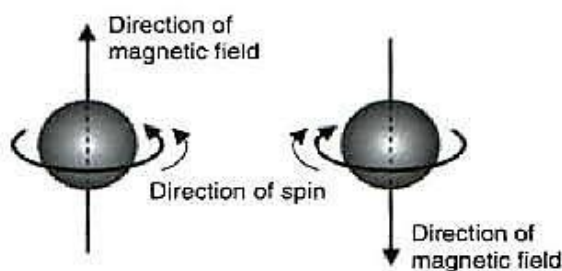


Figure 2.11. Nuclear spin of charged nucleus.⁵²

In the absence of a magnetic field the nuclei are arranged randomly. In the presence of a magnetic field some of the nuclei align themselves parallel to the applied magnetic field and some anti-parallel (Fig 2.12).

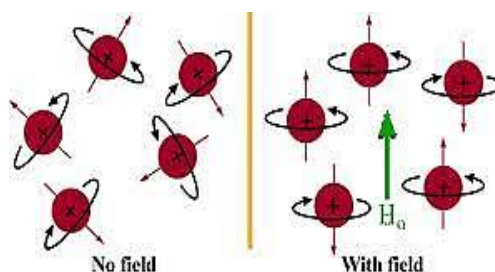


Figure 2.12. Influence of a magnetic field on nuclei of atoms.⁵²

2.4.2. Chemical shift

The electrons revolving around the nucleus in an atom or a molecule shields the nucleus from the externally applied magnetic field. These electrons generate a small magnetic field, known as the secondary magnetic field or induced magnetic field, which can act against or in favour of the applied magnetic field. For the most useful nuclei which are usually referred to “spin $\frac{1}{2}$ ” nuclei, there are two quantum states (higher state and lower state) that have the same energy in the absence of an external magnetic field. At thermal equilibrium, exactly one half of the amount of nuclei will be in the higher state and the other half will be in the lower state. For nuclei to emit an NMR signal, its proton(s) need to be elevated from a lower energy level to a higher energy level. If the small induced magnetic field favours the applied magnetic field, then only a small externally applied field will be required for a proton to change its spin. In this case a proton is considered to be deshielded, while the absorption of radiation is referred to as downfield. Therefore, a stronger applied magnetic field is required for a shielded proton to resonate and give an accurate NMR signal and vice versa, (Fig. 2.13).^{52, 54}

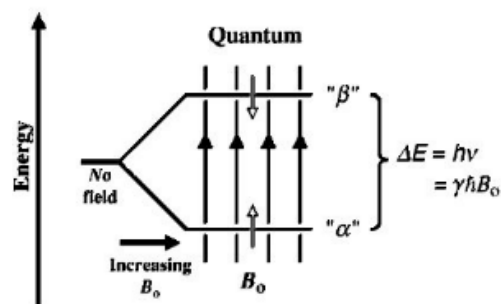


Figure 2.13. The quantum energy levels in NMR.⁵²

$$\nu = \frac{\gamma \beta_0}{2\pi} \quad (2.52)$$

ν is the resonance frequency of a nuclei, γ represents the magnetogyric ratio and β_0 is the magnetic field.¹⁸

In NMR not all protons resonate at the same frequency, variability can depend on a number of factors mainly due to the fact that protons in a molecule are surrounded by electrons (electronic shielding) and exist in different chemical environments to each other resulting in different resonance frequencies.¹⁸ The equation determining the relationship between shielding and resonance frequency of a nuclei is:

$$\nu = \frac{\gamma \beta_0 (1 - \sigma)}{2\pi} \quad (2.53)$$

Where σ represents the shielding constant.⁵³

Electron withdrawing groups such as halogens contribute to the de-shielding effect. While electron donating groups such as alkyl groups contribute to the shielding effect. Chemical shift refers to the difference in shifts in the NMR signal when compared to a reference compound (internal standard) due to shielding and de-shielding effects by the electrons. The proton, ^1H , chemical shifts are shown in Fig. 2.14.

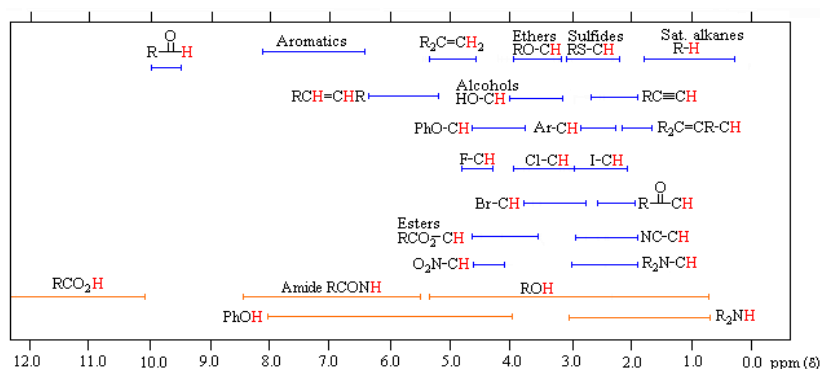


Figure 2.14. ^1H proton chemical shifts.

A reference substance is added, to the solution or to another tube which is placed in the sample holder help determine the frequencies of every proton in the sample as they are measured relative to the resonance frequencies of the protons in the reference in solution.

Therefore, the chemical shifts which are measured with reference to an internal standard (such as tetramethyl silane, TMS) helps to determine the electronic environment of the proton which in turn influences the region where the proton would absorb in the NMR spectrum.⁵⁴

2.5. Mass spectrometry

Mass spectrometry is a powerful analytical technique that deals with the determination of the elemental composition of a sample upon converting it to rapidly moving charged particles. The principle behind this technique is that when the sample is exposed to a high voltage electric current, it loses electrons and is converted to positively charged ions. The magnetic or electric field acting on these moving charged ions (positive ions), deflects them along a circular path on a radius that is a function of their mass (m) to charge (z) ratio. i.e, m/z.

The sample is loaded into mass spectrometer and is vaporized. The vaporized sample components are then passed into an ion source where they are exposed to a beam of electrons. These electrons initially convert the sample molecules into molecular ions (a molecule whose one electron is lost) and then to smaller ions (cations which are the decomposition products of molecular ions). This is then allowed to undergo fragmentation which gives a radical and an ion with an even number of electrons or a molecule and a new radical cation (Fig. 2.15). The molecular ions can be separated in the mass spectrometer according to their m/z ratio (z = charge number) and are detected in terms of abundance.⁵⁵

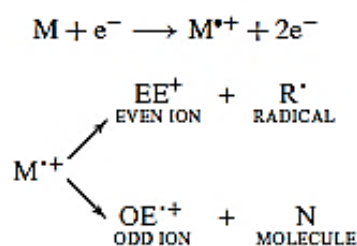


Figure 2.15. Typical example of ionisation of a molecule followed by fragmentation.⁵⁵

The fragments are pushed from the ionisations source into the magnetic sector where a magnetic field deflects the moving ions around the curved path shown in the diagram below. Separation of ions occurs via a magnetic field and the results are determined by the m/z ratio, with fragments of lower mass deflecting more than heavier fragment ions. The resolution is dependent on the ions

moving through the magnet sector with the same momentum and is altered continuously to achieve the maximum number of responses from each molecular fragment present. This means that the ions reach the detector where the m/z is determined according to their momentum which is a product of velocity and mass. The amount of energy required to accelerate the fragments and allow it to reach the detector is specific to any one fragment and such equipment is known for being very sensitive.⁵⁶

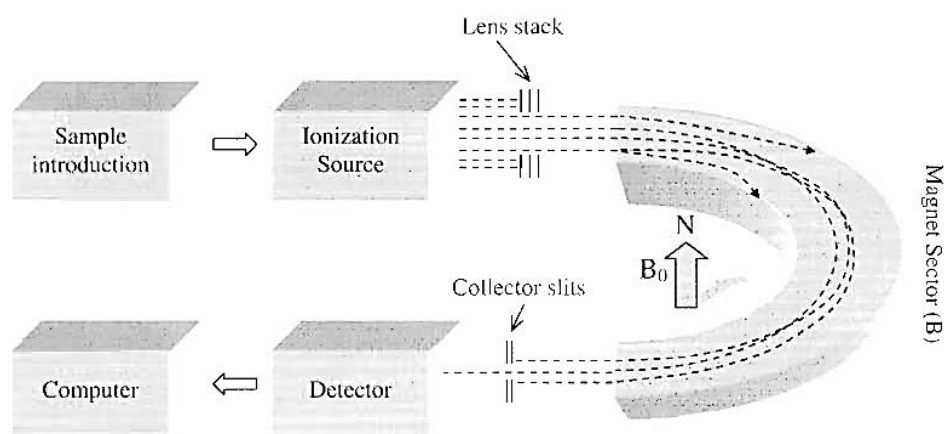


Figure 2.16. Schematic diagram of a mass analyzer.⁵⁶

In mass spectrometry there are multiple ions sources available the oldest, simplest and most talked about is electron ionization or electron impact (EI). This ionization technique works well with organic compounds and works in gas phase inducing various fragments from a molecule. This ionisation technique involves bombarding the sample in the gas phase with electrons, the accelerated electrons collide a number of interactions can occur. The interactions possible are the loss of an electron, electron capture and simple excitation of a molecule. The loss of an electron being the most likely to occur, these positive ions can then fragment providing segments of the molecule so analysis can commence.¹⁸ Mass spectrometry is a useful analytical technique because it can provide the molecular mass of the compound present and ultimately map the structure. This technique is very sensitive and thus will detect samples with very low concentrations down to parts per trillion; also it can be used to measure the molecular weight of large biological molecules with masses of $> 100,000$ Daltons.¹⁸

2.6. References

1. R. A. Serway, J. W. Jewett, "*Physics for scientists and engineers*", 6th ed, Thomson Brooks Cole, 2004.
2. W. W. Coblenz, "*Investigations of Infra-red Spectra*", Carnegie institution of Washington,

- 1905.
3. A. Smekal, *Naturwissenschaften*, 1923, 11, 873.
 4. C. V. Raman, *Ind. J. Phys.*, 1928, 2, 387.
 5. (a) F. Siebert, P. Hildebrandt “*Vibrational Spectroscopy in Life Science*”, Verlag GmbH & Co. KGaA, Weinheim, 2008. (b) E. B. Wilson, J. C. Decius, P.C. Cross, “*Molecular Vibrations: The Theory of Infrared and Raman Vibrational Spectra*”, McGraw Hill, New York, 1995.
 6. C. N. Banwell, E. M. McCash, “*Fundamentals of Molecular Spectroscopy*”, 4th ed, McGraw Hill, 2008.
 7. J. R. Ferraro, K. Nakamoto, C. W. Brown, “*Introductory Raman Spectroscopy*”, 2nd ed, Academic Press, San Diego, 2003.
 8. G. W. King, “*Spectroscopy and Molecular Structure*”, Holt, Rinehart and Winston, New York, 1964.
 9. H. Eyring, J. Walter, G. E. Kimball, “*Quantum Chemistry*.” John Wiley, 1944.
 10. P. M. Morse, *Phys. Rev.*, 1928, 34, 57.
 11. J. A. Bittencourt, “*Fundamentals of Plasma Physics*”, 3rd ed, Springer New York, 2013.
 12. L. D. Landau, Lifschitz, “*E. M. Mechanics*”, 3rd ed, Oxford, England, 1976.
 13. A. Nawrocka, J. Lamorska, “*Determination of Food Quality by Using Spectroscopic Methods*”, Prof. Stanisław Grundas (Ed.), InTech, 2013.
 14. N. B. Colthup, L. H. Daly, S. E. Wiberley. “*Introduction to Infrared and Raman Spectroscopy*”, 3rd Ed, Academic Press, New York-London, 1965.
 15. J. B. Lambert, H. F. Shurvell, D. A. Lightner, R. G. Cooks, “*Organic Structural Spectroscopy*”, Prentice Hall, 1998.
 16. P. Kondratyuk, *Spectrochim. Acta Mol. Biomol. Spectrosc.*, 2005, 61, 589.
 17. L. M. Harwood, T. D. W. Claridge, “*Introduction to Organic Spectroscopy*”, Oxford University Press, 1997.
 18. A. Vogel, J. Mendham, “*Vogel's textbook of quantitative chemical analysis*”, 6th ed, Harlow: Prentice Hall. 1999.
 19. B. Schrader, D. S. Moore, *Pure & Appl. Chem.*, 1997, 69, 1451.
 20. C. Y. Huang, G. Balakrishnan, T. G. Spiro, *J. Raman Spectr.*, 2006, 37, 277.
 21. E. Smith, G. Dent, “*Modern Raman Spectroscopy*”, John Wiley & Sons, Chichester, 2005.
 22. A. Fadini, F. M. Schnepel, “*Vibrational spectroscopy Methods and Applications*”, Ellis Horwood Ltd. John Wiley & Sons, New York, 1989.

23. T. Vankeirsbilck, A. Vercauteren, W. Baeyens, G. Van der Weken, F. Verpoort, G. Vergote, J. P. Remon, *Trends Analyt. Chem.*, 2002, 21, 869.
24. D. E. Sands, "*Crystal Systems and Geometry. Introduction to Crystallography*", Mineola, New York: Dover Publications, 1993.
25. M. Zeldin, *J. Chem. Educ.*, 1966, 43, 17.
26. P. F. Bernath, "*Spectra of Atoms and Molecules*", Oxford University Press, 2015.
27. F. A. Cotton, "*Chemical Applications of Group Theory*", 3rd ed. New York, Wiley, 1990.
28. J. B. Foresman, Æ. Frisch, "*Exploring chemistry with electronic structure methods*", 2nd ed, Gaussian Inc, Pittsburgh, PA, 1996.
29. J. B. Foresman "*Ab Initio Techniques in Chemistry: Interpretation and Visualization*", ACS Books, Washington, D.C, 1997.
30. M. B. Hursthouse, G. P. Moss, K. D. Sales, *Annu. Rep. Prog. Chem. Sect. B: Org. Chem.*, 1978, 75, 23.
31. K. Y. Ohno, K. Ueda, A. Imamura, *J. Phys. Chem.*, 1996, 100, 4701.
32. D. C. Sorescu, B. M. Rice, D. L. Thompson, *J. Phys. Chem. A.*, 1998, 102, 8386.
33. A. Szabo, N. Ostlund, "*Modern Quantum Chemistry: Introduction to Advanced Electronic Structure Theory*", 2nd ed, Dover Publications, 1996.
34. P. Atkins, R. Friedman, "*Molecular Quantum Mechanics*", 4th ed, Dover Publications, 1996.
35. D. R. Hartree, "*The Calculation of Atomic Structures*", New York, Wiley, 1957; V. Fock, *Z. Phys.*, 1930, 62, 795.
36. (a) C. C. J. Roothaan, *Revs. Mod. Phys.*, 1951, 23, 69. (b) G. G. Hall, *Proc. R. Soc. A.*, 1951, 205, 541.
37. (a) J. Sadley, "*Semi-Empirical Methods of Quantum Chemistry*", Wiley, 1985. (b) M. C. Zerner, *Rev. Comp. Chem.*, 1991, 2, 313. (c) T. Bredow, K. Jug, *Theor. Chem. Acc.*, 2005, 1, 113.
38. S. Bell, T. J. Dines, B. Z. Chowdhry, R. Withnall, *J. Chem. Ed.*, 2007, 84, 1364.
39. C. Møller, M. S. Plesset, *Phys. Rev.*, 1934, 46, 618.
40. F. Jensen, "*Introduction to Computational Chemistry*", John Wiley & Sons, Chichester, 1999.
41. I. N. Levine, "*Quantum Chemistry*", 5th Ed. Prentice Hall, Upper Saddle River, NJ, 2002.
42. P. Hohenburg, W. Kohn, *Phys. Rev.*, 1964, 136, B864.
43. W. Kohn, L. J. Sham, *Phys. Rev.*, 1965, 140, A1133.
44. J. C. Slater, *Phys. Rev.*, 1930, 36, 57.
45. P. Ugliengo, D. Viterbo, G. Chiari, *Z Kristallogr.*, 1993, 207, 9.
46. R. Dennington, T. Keith, J. Millam, *Semichem Inc.*, Shawnee Mission, KS, 2009.

47. C. C. Chambers, D. L. Thomson, *J. Phys. Chem.*, 1995, 99, 15881.
48. D. B. Cook, "*Handbook of Computational Quantum Chemistry*", Oxford University Press, Oxford, UK, 1997.
49. E. B. Brame, I. G. Grasselli, "*Infrared and Raman Spectroscopy*", Marcel Dekker Inc, New York, 1976.
50. S. J. Cyvin, "*Molecular Vibrations and Mean Square Amplitudes*", Elsevier, Amsterdam, 1968.
51. W. J. Hehre, L. Radom, P. V. R. Schleyer, J. A. Pople, "*Ab initio Molecular Orbital Theory*", Wiley, New York, 1986.
52. N. Jacobsen, "*NMR spectroscopy explained*", Hoboken, Wiley, 2007.
53. J. Schraml, J. M. Bellama, "*Two dimensional NMR spectroscopy*", Wiley, 1976.
54. R. Shankar, "*Textbook for pharmaceutical analysis*", 2005.
55. E. Hoffmann, V. Stroobant, "*Mass spectrometry*", 3rd Ed. Chichester, West Sussex, England: J. Wiley, 2007.
56. R. Silverstein, F. Webster, D. Kiemle, "*Spectrometric identification of organic compounds*", 7th ed. Hoboken, N. J. Wiley, 2005.

Chapter 3: Experimental

3.1. Chemical reagents

The chemical reagents used in the experimental studies are listed in Table 3.1.

Table 3.1. List of chemical reagents.

Chemical name	Chemical formula	Mol. Wt (g/mol)	Supplier	Purity
DL-Homocysteine thiolactone hydrochloride	C ₄ H ₇ NOS · HCl	153.63	Sigma Aldrich	99%
Sodium bicarbonate	NaHCO ₃	84.00	Fisher Scientific	99%
D-Cycloserine	C ₃ H ₆ N ₂ O ₂	102.02	Alfa Aesar	99%
Glacial acetic acid	CH ₃ CO ₂ H	60.05	Fisher Scientific	99%
Cyclo(Gly-Gly)	C ₄ H ₆ N ₂ O ₂	114.10	Sigma Aldrich	99%
Acetic anhydride	C ₄ H ₆ O ₃	102.09	Fisher scientific	99%
Sarcosine anhydride	C ₆ H ₁₀ N ₂ O ₂	142.16	Alfa Aesar	99%
Cyclo(His-Pro)	C ₁₁ H ₁₄ N ₄ O ₂	234.25	Bachem	99%
Cyclo(His-D-Pro)	C ₁₁ H ₁₄ N ₄ O ₂	234.25	Bachem	99%
Cyclo(Ala-His)	C ₉ H ₁₂ N ₄ O ₂	208.22	Bachem	99%
2,6-DKP	C ₄ H ₆ N ₂ O ₂	114.10	Fluorochem	>95%
Ethylenediamine	C ₂ H ₈ N ₂	60.10	Alfa Aesar	99%
Diethyl oxalate	C ₄ H ₆ O ₄	146.14	Alfa Aesar	99%
Methanol	CH ₃ OH	32.04	Fisher Scientific	99%
Absolute Ethanol	CH ₃ CH ₂ OH	46.06	Fisher Scientific	99%
Deionised water	H ₂ O	18.02	Milli-Q-system	99%
Deuterium oxide	D ₂ O	20.03	Sigma-Aldrich	99.98 (Atom %)
Deuterated methanol	MeOD	33.05	Sigma-Aldrich	99.9 (Atom %)

3.1.1. Synthesis

The synthesis of the compounds C-CySH, AMDKP, DMDKP, DAGG and 2,3-DKP, were carried out by the methods reported in the literature (see sections 4.2.2, 5.2.2, 6.2.2 and 8.2.2) using the chemical reagents listed in Table 3.1. The purity of the synthesised compounds was checked using ¹H and ¹³C-NMR spectroscopy, mass spectrometry and CHN analysis and found to be > 98% (see Appendix).

3.1.2. Deuteration

Deuteration was undertaken by dissolving ~5 mg of each compound in 5 ml D₂O and the powdered *N*-deuteriated isotopomers were recovered after evaporation of the solvent followed by drying using a hot air oven (60 °C). Additionally, deuterated methanol was used for deuterating samples of AMDKP. The deuteration process was repeated at least an additional two-three times, in order to improve the percentage yield of the deuteration product.

3.2. Vibrational spectroscopy

3.2.1. Raman spectroscopy

The Raman spectra of the samples and their *N*-deuterated derivatives was acquired using a LabRam Raman spectrometer (Horiba Jobin Yvon).¹ The Labram is an integrated Raman system equipped with 1800 lines/mm grating, edge filter and high sensitivity Peltier-cooled CCD detector. Each sample was excited using a He-Ne 8 mW laser at a wavelength of 632.8 nm with the laser mounted on the back of the instrument. The Raman spectra were collected on a microscope slide at room temperature using an Olympus BX40 microscope, with an objective of x100 magnification coupled confocally to a 300 mm focal length spectrograph to focus and collect the scattering on the samples.² The Raman instrument was calibrated using the ν_1 line of silicon at 520.7 cm⁻¹. Centring of the silicon line was checked by using the frequencies of the principal lines of a neon lamp.

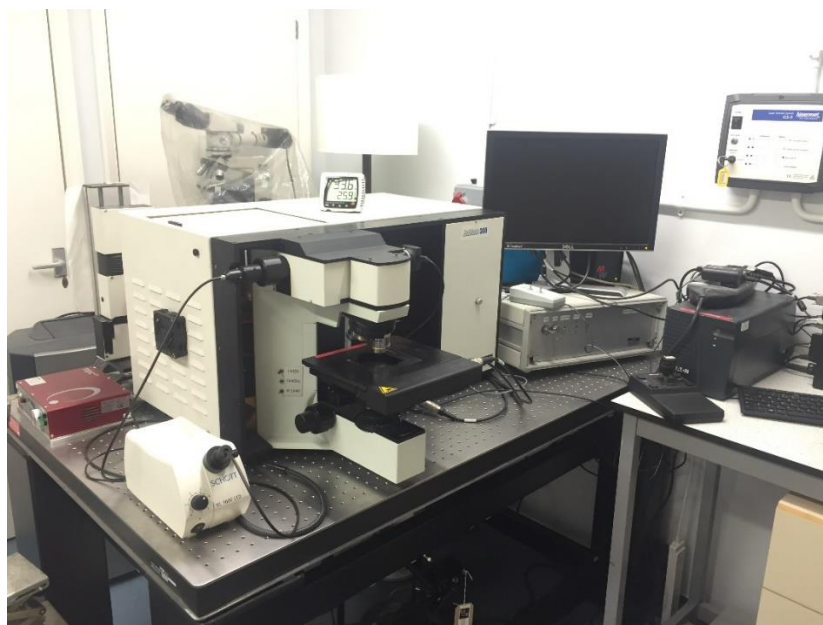


Figure 3.1. LabRam Raman spectrometer.

3.2.2. Solid and solution state Raman spectra

The solid state Raman spectra of non-deuterated and *N*-deuterated samples were collected on a microscope slide using a microscope objective of x100 magnification to focus the helium-neon laser beam. If there appeared to be a problem from polarisation effects, the spectra were re-collected using x10 microscope objective to focus the laser beam. Solution phase (H₂O/D₂O) spectra (20 scans, scan time 30 s each) were acquired using a 1 cm path length quartz cuvette. The concentration of the samples used was ~70 mg/mL. A 40 mm focal length macro lens was used to focus the laser beam, and collect the back scattered light in these experiments. A back scattering geometry was used in all experiments.

3.2.3. Attenuated total reflectance (ATR)

The Perkin Elmer Spectrum Two UATR FT-IR spectrometer (Fig. 3.2) is a versatile ATR accessory ideal for the analysis of solids, liquids, pastes and gels.³ The UATR employs a diamond ZnSe crystal, which is composed of a diamond ATR with a zinc selenide focusing element which is in direct contact with the diamond. The focusing element provides interfacing optics for the IR radiation into the diamond crystal. Both components of the Diamond ZnSe ATR work over the spectral range of interest for the majority of applications and have similar refractive indices.



Figure 3.2. Perkin Elmer Spectrum Two UATR FT-IR spectrometer.³

The radiation enters the focusing element through the flat surface typically about 5 cm by 1 cm. The number of reflections at each surface of the crystal is usually between five and ten, depending on the length and thickness of the crystal and the angle of incidence.³ To allow reflection within the diamond, the focusing crystal has a small cavity at the centre of its surface (Fig. 3.3). The

radiation undergoes internal reflection in the diamond which is in contact with the sample and then exits the crystal at a point which is diametrically opposite to the point of entry. The shorter optical path within the ATR reduces the loss of energy through the crystal caused by internal reflections. The Diamond ZnSe crystal has the benefits of diamond (hardness and chemical resistance) and the cost effectiveness of zinc selenide. For obtaining the best spectrum two things should be taken into consideration, the sample must be in direct contact with the ATR crystal, because the evanescent wave or bubble only extends beyond the crystal $0.5\ \mu\text{m} - 5\ \mu\text{m}$. And the refractive index of the crystal must be significantly greater than that of the sample or else internal reflectance will not occur; the light will be transmitted rather than internally reflected in the crystal.³ Typically, ATR crystals have refractive index values between 2.38 and 4.01 at $2000\ \text{cm}^{-1}$.

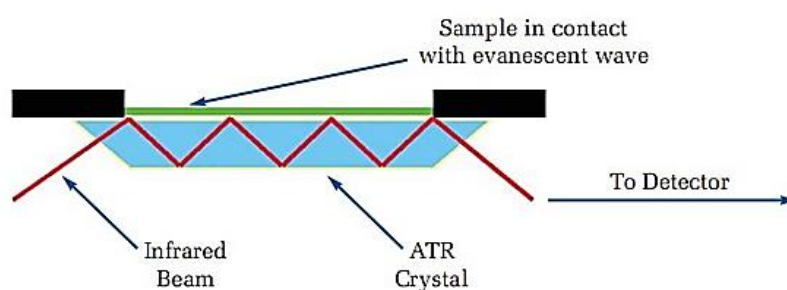


Figure 3.3. A multiple reflection ATR system.³

3.2.4. Solid and solution state IR spectra

IR spectra (32 scans) were recorded on Perkin Elmer Spectrum Two UATR FTIR spectrometer operating at a resolution of $4\ \text{cm}^{-1}$, data interval of $2\ \text{cm}^{-1}$ and a scan speed of $0.2\ \text{cm/s}$ in the $450\text{-}4000\ \text{cm}^{-1}$ range. The ATR sample base plate was equipped with a diamond ZnSe crystal. As with all FTIR measurements, an infrared background is collected, in this case, from the clean ATR crystal. The solid state IR spectra of samples were collected by placing 2-5 mg of the sample on the ATR crystal and pressure was applied with the aid of a pressure arm in order to obtain the spectra; likewise solution spectra (32 scans) were obtained using sample concentrations of $\sim 70\ \text{mg/mL}$.

3.5. DFT calculations

DFT calculations for the DKPs were performed using the *Gaussian 09* program.⁴ The geometry obtained was generated from *Gaussian* (GUI) software GaussView. Geometry optimisation and calculations of vibrational spectra were performed using the hybrid SCF-DFT method B3LYP,

incorporating Becke's exchange-energy functional⁵ and Lee-Yang-Parr correlation-energy functional⁶ together with the aug-cc-pVTZ basis set.⁷ Geometry optimisation was conducted assuming the molecules to have C₂ symmetry and vibrational spectra were calculated at the optimised geometry, for each molecule. For computation of the potential energy distributions (PEDs) associated with the vibrational modes, the Cartesian force constants obtained from the *Gaussian 09* output were converted to force constants expressed in terms of internal coordinates. Scaling factors were applied to the force constants before input to a normal coordinate analysis program derived from those of Schachtsneider.⁸ A full set of internal coordinates, including all bond angles and torsional angles, was reduced to a set of 3*N*-6 symmetry-adapted internal coordinates, by construction of local symmetry coordinates where appropriate, e.g. for methylene groups as well as for the in-plane and out-of-plane deformations of the six-membered DKP ring. Scaling is necessary to match the calculated harmonic vibrations with the observed vibrations, which are anharmonic. Previously reported DFT calculations on DKPs employed a large number of scale factors to give the best fit to the experimental spectra.⁹

For N-H and C=O stretches, in particular, low scaling factors were necessary because of intermolecular hydrogen-bonding in the solid and solution state. However, this method is not entirely satisfactory and the better approach would be to calculate the anharmonic fundamentals to compare with experimental data. Due to the absence of hydrogen bonding in DAGG and DMGG this approach is preferred over the Pulay SQM-FF method.¹⁰ Anharmonic corrections at the B3LYP/aug-cc-pVTZ level can be computationally demanding and time consuming. However, the combination of anharmonic corrections computed at low level with the harmonic frequencies computed at high level of theory can be an effective method for large molecular weight molecules.¹¹ In our calculations firstly we have optimised the structure followed by anharmonic calculations using the B3LYP/cc-pVDZ level of theory. The anharmonic corrected fundamentals were thus obtained using the harmonic fundamentals obtained at the B3LYP/aug-cc-pVTZ level in combination with the B3LYP/cc-pVDZ anharmonicity constants.

Due to the hydrogen bonding effects the above method could not be used for other compounds. Furthermore, the PEDs from anharmonic fundamentals indicates that there is a difference of 150-200 cm⁻¹ for the N-H and ~100 cm⁻¹ for C=O stretching vibrations compared to the experimental data. The differences between calculated and experimental vibrational wavenumbers are attributed to incomplete inclusion of electronic correlation effects and the neglect of anharmonicity. In order to account for the deviation of the calculated and the observed frequencies scaling factors were

used. Pulay *et al.*¹⁰ introduced a formula for the scaling of force constants, f_{ij} , expressed in terms of internal coordinates i and j :

$$f_{ij}' = \sqrt{S_i S_j} f_{ij}$$

where S_i and S_j are the scale factors associated with internal coordinates i and j . In these calculations the scale factors were as follows: NH stretch 0.80; CH stretch 0.91; NH & CH deformation 0.92; C=O stretch 0.86 (except for 2,3-DKP and 2,6-DKP, 0.88 was used); others: 0.98. These scale factors are identical to those used for other cyclic dipeptides.⁹

IR and Raman intensities were computed from the dipole and polarizability derivatives of the *Gaussian 09* output obtained within the harmonic approximation of B3LYP/aug-cc-pVTZ calculations. Thus the band wavenumbers were corrected for anharmonicity, but not the IR and Raman intensities in DAGG, DMGG. Simulated IR and Raman spectra, calculated by convolution with a Lorentzian line shape (full width at half-maximum = 10 cm⁻¹).

3.6. Molecular orbital analysis

The highest occupied molecular orbital (HOMO) and lowest unoccupied molecular orbital (LUMO) energies of the compounds were calculated at their optimised geometries. HOMO is an electron donor that donates an electron. Whereas, LUMO acts an electron acceptor that contain vacant places to accept electrons. The energy gap between HOMO and LUMO is very useful in determining the way the molecule interacts with other species and hence, regarded as the Frontier molecular orbitals (FMO's) in quantum chemistry. A molecule with small HOMO-LUMO energy gap is more polarizable and is generally associated with low thermodynamic stability and high chemical reactivity.¹² A smaller energy gap increases the ease of excitation from HOMO to LUMO. It is easy for LUMO to accept electrons when the energy of LUMO is low and similarly for HOMO to donate electrons when the energy of HOMO is high. Furthermore, the energy gap between HOMO and LUMO is a critical parameter in determining molecular electrical conveyance properties.^{13,14} The composition of HOMO and LUMO were calculated using the Becke method utilising *Multwfn 3.3.9* program.¹⁵

3.7. Molecular electrostatic potential

Molecular electrostatic potential (MEP) mapped surface illustrates the charge distributions of molecules and can be useful in investigating the correlation between molecular structures with its

physiochemical properties, including drugs and biomolecules.¹⁶ The total electron density mapped with molecular electrostatic potential (MEP) surface have been plotted for the optimised geometries. The importance of MEP lies in the fact that it consecutively displays molecular shape, size, as well as negative, positive and neutral electrostatic potential regions in terms of colour grading. The electrostatic potential values of the surface are represented by different colours with an increasing order (red < orange < yellow < green < blue). The red area indicates the strongest electrostatic repulsion and blue coloured area indicates the strongest attraction. The increase in negative potential is shown from yellow to red colour, with the maximum negative potential in red colour (preferred site for electrophilic attack), green represent the zero potentials and the maximum positive region, (preferred site for nucleophilic attack) is represented in deep blue colour.

3.8. Hirshfeld surface analysis

Molecular Hirshfeld surfaces and 2D fingerprint plots for the compounds were generated using *Crystal Explorer 3.1*¹⁷ based on the results obtained from single X-ray diffraction studies. In the absence of X-ray data, the Hirshfeld surfaces for AMDKP, CHP, CAH, CDHP, 2,6-DKP and 4,5-HHP could not be obtained. The normalized contact (d_{norm}) is the ratio incorporating the distances of any surface point to the closest exterior (d_e) and interior (d_i) atom and the van der Waals (vdW) radii of the atom.¹⁸⁻²⁰ The negative value of d_{norm} indicates that the sum of the relevant vdW radii is larger than the sum of d_i and d_e values, which is visualised as red colour and considered as the closest contact on Hirshfeld surface. The contacts with positive d_{norm} values are longer than the sum of vdW radii, and are coloured with blue whereas the d_{norm} values equal to zero with the intermolecular distances close to vdW radii are visualized as white colour. All these regions are of particular interest and enable the identification of the important intermolecular interactions.²⁰ The 2D fingerprint plot of d_e and d_i displays the existence of different types of intermolecular interactions in the crystal.²¹

3.9. References

1. LabRam user manual, ISA, Dilor, Jobin Yvon, France, 1998.
2. CCD Detection User Manual, Spectrum One, 1996.
3. Text: courtesy of Perkin-Elmer, UK.
4. M. J. Frisch, G. W. Trucks, H. B. Schlegel, G. E. Scuseria, M. A. Robb, J. R. Cheeseman, G. Scalmani, V. Barone, B. Mennucci, G. A. Petersson, H. Nakatsuji, M. Caricato, X. Li, H. P. Hratchian, A. F. Izmaylov, J. Bloino, G. Zheng, J. L. Sonnenberg, M. Hada, M. Ehara, K. Toyota, R. Fukuda, J. Hasegawa, M. Ishida, T. Nakajima, Y. Honda, O. Kitao, H. Nakai, T.

- Vreven, J. A. Montgomery, Jr., J. E. Peralta, F. Ogliaro, M. Bearpark, J. J. Heyd, E. Brothers, K. N. Kudin, V. N. Staroverov, R. Kobayashi, J. Normand, K. Raghavachari, A. Rendell, J. C. Burant, S. S. Iyengar, J. Tomasi, M. Cossi, N. Rega, J. M. Millam, M. Klene, J. E. Knox, J. B. Cross, V. Bakken, C. Adamo, J. Jaramillo, R. Gomperts, R. E. Stratmann, O. Yazyev, A. J. Austin, R. Cammi, C. Pomelli, J. W. Ochterski, R. L. Martin, K. Morokuma, V. G. Zakrzewski, G. A. Voth, P. Salvador, J. J. Dannenberg, S. Dapprich, A. D. Daniels, O. Farkas, J. B. Foresman, J. V. Ortiz, J. Cioslowski, D. J. Fox, Gaussian, Inc., Wallingford CT, 2009.
5. A. D. Becke, *J. Chem. Phys.*, 1993, 98, 5648.
 6. C. Lee, W. Yang, R. G. Parr, *Phys. Rev. B.*, 1988, 37, 785.
 7. T. H. Dunning Jr, *J. Chem. Phys.*, 1989, 90, 1007.
 8. J. A. Schachtschneider, “*Vibrational analysis of polyatomic molecules, parts V and VI*”, Technical Report Nos. 231 and 57, Shell Development Co.: Houston, 1964–1965.
 9. A. P. Mendham, R. A. Palmer, B. S. Potter, T. J. Dines, M. J. Snowden, R. Withnall, B. Z. Chowdhry, *J. Raman Spectrosc.*, 2009, 40, 1478.
 10. P. Pulay, G. Fogarasi, F. Pang, J. E. Boggs, A. Vargha, *J. Am. Chem. Soc.*, 1983, 105, 7037.
 11. V. Barone, *Chem. Phys. Lett.*, 2004, 383, 528.
 12. D. F. V. Lewis, C. Loannides, D. V. Parke, *Xenobiotica*, 1994, 24, 401.
 13. K. Fukui, *Science*, 1982, 218, 747.
 14. P. Udhayakala, T. V. Rajendiran, S. Seshadri, S. Gunasekaran, *J. Chem. Pharm. Res.*, 2011, 3, 610.
 15. T. Lu, F. Chen, *J. Comput. Chem.*, 2012, 33, 580.
 16. E. Scrocco, J. Tomasi, *Curr. Chem.*, 1973, 42, 95.
 17. S. K. Wolff, D. J. Grimwood, J. J. McKinnon, D. Jayatilaka, M. A. Spackman, Crystal Explorer 3.1, University of Western Australia, Perth, Australia, 2007.
 18. F. L. Hirshfeld, *Theor. Chim. Acta*, 1977, 44, 129.
 19. M. A. Spackman, D. Jayatilaka, *Cryst. Eng. Comm.*, 2009, 11, 19.
 20. M. A. Spackman, J. J. McKinnon, *Cryst. Eng. Comm.*, 2002, 4, 378.
 21. J. Bernstein, R. E. Davis, L. Shimoni, N. L. Chang, *Angew. Chem. Int. Ed. Eng.*, 1995, 34, 1555.

Chapter 4: Theoretical and Experimental Vibrational Spectroscopic Studies of a Sulphur containing Diketopiperazine

4.1. Introduction

Research relating to synthetic and naturally occurring DKP derivatives is an area of significant scientific interest due, in part, to their potential pharmacological applications. DKPs containing sulphur groups have been recognised for their diverse biological activities and their potential uses in clinical medicine. For example, a range of epidithiodiketopiperazines have been investigated for both antimicrobial and anticancer activities.¹ In recent years homocysteine, in particular, has achieved the status of an important amino acid in many fundamental medicinal and biological processes. Homocysteine and its derivatives have also been used in the treatment of diseases caused by ageing and various vascular diseases. In addition, the thiol-containing DKPs have been identified as potent inhibitors of matrix metalloproteinases.² Moreover, the ring bridging in DKP by a disulphide group at the 3,6 positions has been established as a potent metabolite possessing antibacterial, antiviral and cytostatic properties.³ Another study identified the sulphur containing DKP cyclo(L-Met-L-Pro) in beef; sensory evaluations indicate that although not strong, it possess different taste effects at different concentrations.⁴ Studies of proline-containing DKPs have revealed specialised characteristics of the molecules which allows them to mimic specific domains such as β -turns and loop motifs, playing an important role in the protein field.⁵ Cyclo-L-cystine is considered an important model for the theoretical understanding of the optical properties and chirality of disulphides.⁶ X-ray studies of the bridged disulphide cyclo-L-cystine show that the DKP ring exists in a twisted boat form with the C-S-S-C bridge across the C_α atoms.⁷ The cyclic disulphide L-cysteinyl-L-cysteine molecule crystallises in the orthorhombic crystal system, containing a *cis*-peptide unit and a right-handed disulphide bridge with a dihedral angle of 94° around the -S-S- bond.⁸

In the bridged DKP ring of 3,6-epidithio-2,5 piperazinedione the disulphide linkage occurs at the 3,6 position.^{9,10} This is mainly due to steric hindrance caused by the intramolecular electrostatic attraction between the positive carbon atoms of the amide and the lone-pair of electrons on the sulphur atoms as well as the repulsion between the lone-pairs on the nitrogen and sulphur atoms.^{9,10} Taylor *et.al* first isolated 3,6-epitetrathio- N^1, N^4 -dimethyl-2,5-piperazinedione.¹¹ The tetrasulphide bridge in the molecule is twisted, such that the outer sulphur atoms are closer to the carbons of the carbonyl group and the inner sulphur atoms are closer to the amide nitrogen atoms.

The conformational preferences of the bridged DKP ring were investigated by extended Hückel method and *ab initio* and the geometries of the compounds have been reported.¹² Cyclo-L-cystine and 3,6-epi(dithio and tetrathio) DKPs display C₂ symmetry, with a twofold axis passing through the centre of the disulphide bridge.

The X-ray structure of cyclo(L-homoCySH-L-homoCySH) (C-CySH) has been reported.¹³ The crystals are orthorhombic, consisting of three asymmetric molecules A, B and C per unit cell. In all three molecules, the DKP ring appears to be essentially planar and the carbonyl (C=O) oxygen atoms are co-planar in individual cases. There have been no previous reports of vibrational spectroscopic studies on C-CySH. Hence, the IR and Raman spectroscopic studies of C-CySH and its *N,S*-deuterated isotopomer in the solid (powdered) state are reported herein. In addition, the previously reported X-ray structure and the vibrational frequencies of the molecule are compared with the results acquired from B3LYP/aug-cc-pVTZ calculations.

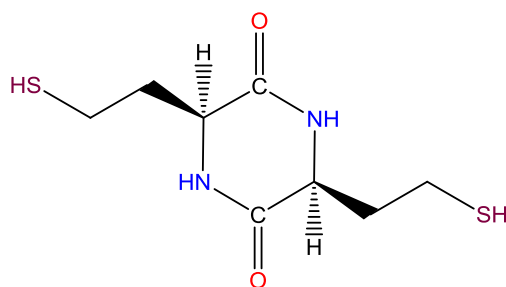


Figure 4.1. Structure of C-CySH.

4.2. Experimental

4.2.1. Materials

See sections 3.1 to 3.1.2 in Chapter 3.

4.2.2. Synthesis

The synthesis of C-CySH was carried out by the method reported by DuVigneaud *et al.* (see Appendix).¹⁴ The purity of the compound was checked using ¹H-NMR, ¹³C-NMR spectroscopy and CHN analysis and found to be > 98% (see Appendix). Spectroscopic grade deuterium oxide (99.98 %) were obtained from Sigma-Aldrich Ltd (Poole, Dorset, UK). Deuteration was carried out by dissolving 5 mg C-CySH in 5 ml D₂O and the powdered *N,S*-deuterated isotopomer was recovered after evaporation of D₂O followed by drying using a hot air oven at 60 °C.

4.2.3. Vibrational spectroscopy and instrumental details

See sections 3.2, 3.2.1, 3.2.3, 3.2.3 and 3.2.4 in Chapter 3.

4.2.4. DFT calculations

See section 3.5 in Chapter 3

4.3. Results and discussion

4.3.1. Geometry optimization

C-CySH ($C_8H_{14}N_2O_2S_2$) consists of 28 atoms and has 78 normal vibrational modes. The atom numbering scheme is shown in Fig. 4.2. The calculated bond angles, bond lengths and torsional angles are compared with the X-ray structure in Table 4.1. In order to verify the minimum energy conformations of the L-homoCySH side-chains of C-CySH we carried out an energy profile calculation at the HF/3-21G level using the Spartan'14 program,¹⁵ by rotating the exocyclic (CC) and (CS) bonds ($\tau(1) = \tau(H24-C12-C13-C14)$ and $\tau(H19-C8-C9-C10)$, $\tau(2) = \tau(C12-C13-C14-S2)$ and $\tau(C8-C9-C10-S1)$, $\tau(3) = \tau(C13-C14-S2-H16)$ and $\tau(C9-C10-S1-H15) = \pm 180^\circ$) on either side of the DKP ring (Fig. 4.3). In these calculations an idealised C_2 symmetry was assumed. Geometry optimisation was carried at higher level (B3LYP /aug-cc-pVTZ) using the initial geometry from the Spartan'14 output, leading to a minimum energy optimised structure whose energy (-1369.93615495 a.u.) is 2.172 kJ mol⁻¹ lower than that of the asymmetric structure (C_1 symmetry) favoured in the solid state (-1369.93532731 a.u.). However, in both cases the molecule deviates slightly from planarity towards a boat conformation with the two L-homoCySH side-chains folded above the ring. The previously reported X-ray crystallographic structure of C-CySH suggests that the DKP rings in A, B and C are essentially planar with the two side-chains on the same side of the DKP ring (Fig. 4.4) and, therefore, maintain a pseudo C_2 symmetry with respect to other features of the molecule.¹³ However, there are significant differences in the orientations of the side chains (Table 1) which shows that all three molecules have C_1 symmetry. Hence, the calculated gas phase structures with C_1 and C_2 symmetry are taken into account as shown in Fig. 4.5. In comparison with cyclo(L-Met-L-Met), single X-ray crystal studies¹⁶ suggest that in the solid state the molecule adopts a slightly distorted boat conformation. It is important to note that the calculated gas phase structure is based on a single isolated molecule, and does not account for intermolecular interactions such as hydrogen bonding and/or crystal packing forces. Due to

approximate C_2 symmetry in the DKP ring, it is assumed that the DKP ring vibrations may be treated using local C_2 symmetry.

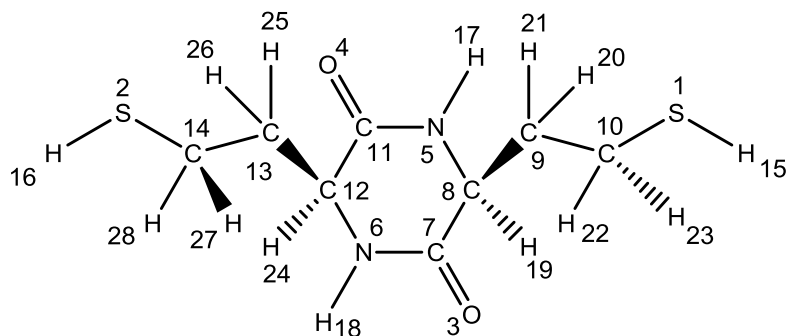


Figure 4.2. Atom numbering scheme for C-CySH.

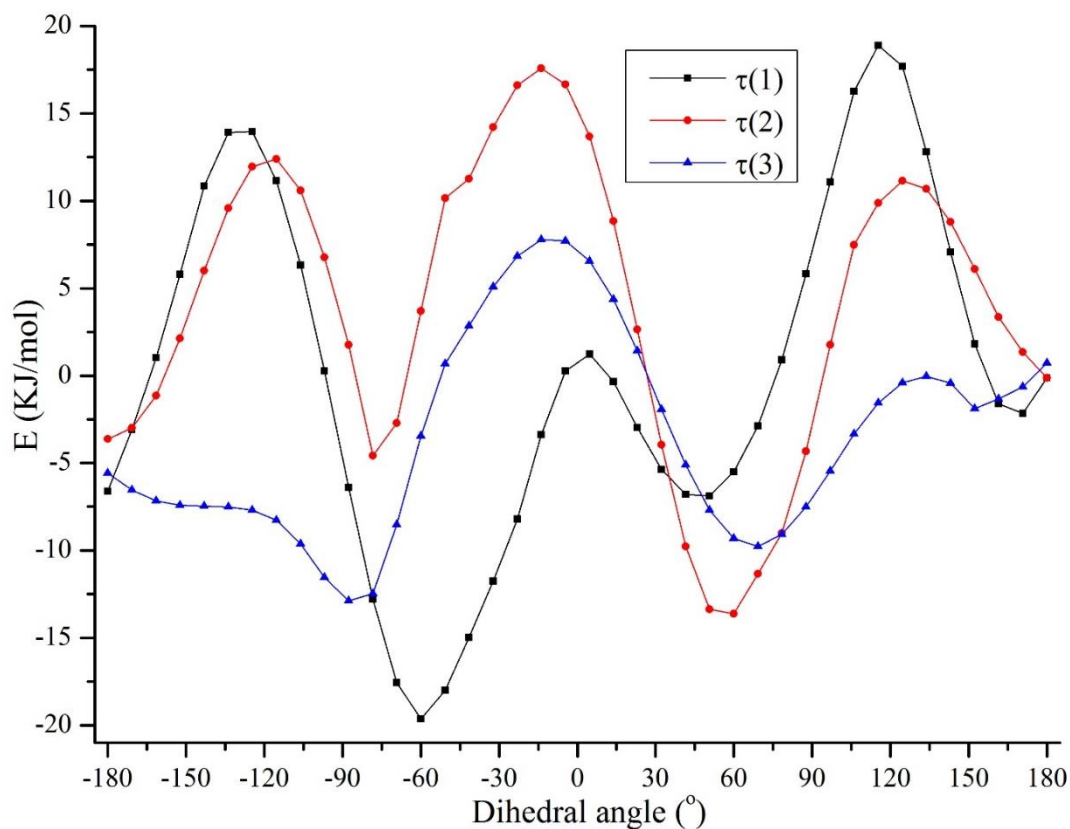


Figure 4.3. Potential energy plot for C-CySH.

Where, $\tau(1) = \tau(\text{H24-C12-C13-C14})$ and $\tau(\text{H19-C8-C9-C10})$

$\tau(2) = \tau(\text{C12-C13-C14-S2})$ and $\tau(\text{C8-C9-C10-S1})$

$\tau(3) = \tau(\text{C13-C14-S2-H16})$ and $\tau(\text{C9-C10-S1-H15})$

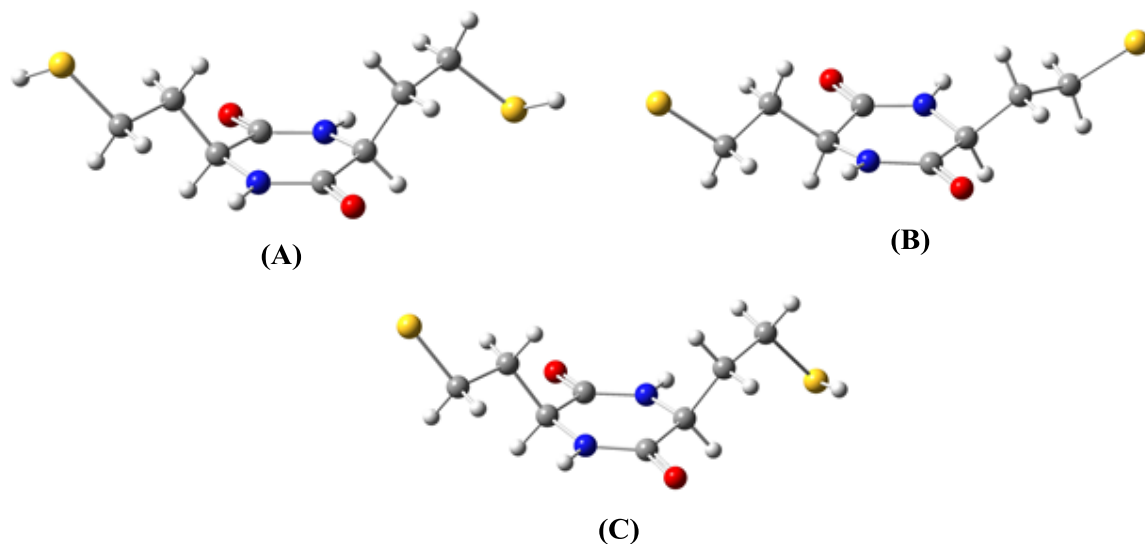


Figure 4.4. The three asymmetric structures of C-CySH in a crystallographic unit cell.

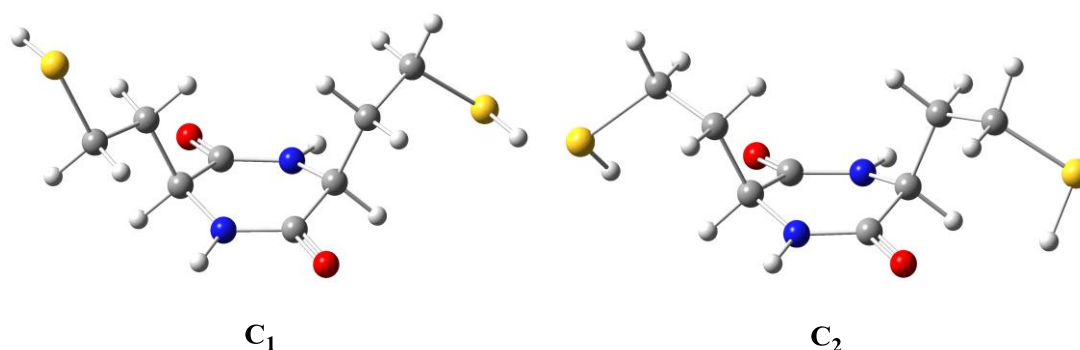


Figure 4.5. Calculated structures of C-CySH.

The calculated bond lengths for C-CySH are generally in good correlation with the X-ray data, apart from the N-C, N-H and C=O bonds. The calculated N-C, N-H and C=O bond lengths are 1.35, 1.00, 1.22 Å, respectively. The X-ray data shows that the N-C, N-H and C=O bond lengths are 1.312-1.340, ~0.88, ~1.240 Å, respectively. The calculated bond angles are very similar to those obtained from the X-ray data, although there is a difference of ~0.5-2° between the two sets of data. This is mainly due to the effect of intermolecular forces such as hydrogen bonding. The three dihedral angles ω , ψ , ϕ are mainly responsible for determining the geometry of the peptide units in the ring. Davies and Khaled first reported the degree of folding (β) for the simplest cyclic dipeptide cyclo(Gly-Gly).¹⁷ By examining $C_\alpha-N-C'-C_\alpha$, $N-C'-C_\alpha-N$ and $C'-N-C_\alpha-C'$ dihedral angles the geometry of the ring can be determined. A good measure of folding of the DKP ring can be established by taking the average of $N-C_\alpha-C_\alpha-N$ (β_1) and $C_\alpha-C'-C'-C_\alpha$ (β_2).

Table 4.1. Calculated bond lengths (Å), bond angles and dihedral angles (°) for C-CySH in comparison with the X-ray structure.¹³

Bond lengths (Å)	X-ray structure ¹³			Calculated (B3LYP/aug-cc-pVTZ)	
	Molecule A	Molecule B	Molecule C	C ₂ symmetry	C ₁ symmetry
H(28)-C(14)	0.9897	0.9904	0.9904	1.0856	1.0899
H(27)-C(14)	0.9903	0.9902	0.9897	1.0889	1.0902
H(26)-C(13)	0.9905	0.9897	0.9905	1.0944	1.0903
H(25)-C(13)	0.9903	0.9892	0.9893	1.0923	1.0916
H(24)-C(12)	1.0011	0.9991	0.9992	1.0899	1.0914
H(23)-C(10)	0.9896	0.9908	0.9897	1.0889	1.0900
H(22)-C(10)	0.9895	0.9895	0.9893	1.0856	1.0879
H(21)-C(9)	0.9892	0.9905	0.9891	1.0944	1.0905
H(20)-C(9)	0.9895	0.9898	0.9887	1.0923	1.0943
H(19)-C(8)	0.9996	1.0005	0.9995	1.0899	1.0897
H(18)-N(6)	0.8800	0.8803	0.8805	1.0097	1.0088
H(17)-N(5)	0.8798	0.8807	0.8800	1.0097	1.0092
H(16)-S(2)	1.1627	-	-	1.3455	1.3459
H(15)-S(1)	1.0478	-	1.0323	1.3455	1.3462
C(14)-C(13)	1.5159	1.5110	1.5124	1.5277	1.5244
C(14)-S(2)	1.8011	1.8095	1.8016	1.8388	1.8349
C(13)-C(12)	1.5317	1.5324	1.5213	1.5441	1.5438
C(12)-C(11)	1.5077	1.5132	1.5083	1.5222	1.5259
C(12)-N(6)	1.4744	1.4566	1.4500	1.4588	1.4579
C(11)-N(5)	1.3176	1.3393	1.3384	1.3526	1.3538
C(11)-O(4)	1.2441	1.2422	1.2366	1.2222	1.2190
C(10)-S(1)	1.8048	1.8187	1.8118	1.8388	1.8388
C(10)-C(9)	1.5159	1.5461	1.5242	1.5277	1.5265
C(9)-C(8)	1.5192	1.5478	1.5202	1.5441	1.5410
C(8)-N(5)	1.4671	1.4607	1.4520	1.4588	1.4573
C(8)-C(7)	1.5246	1.5104	1.5296	1.5222	1.5231
C(7)-N(6)	1.3123	1.3133	1.3256	1.3526	1.3565
C(7)-O(3)	1.2413	1.2499	1.2358	1.2222	1.2188
Bond angles (°)					
S(2)-C(14)-C(13)	115.6354	110.6093	113.6241	115.1025	113.8386
S(2)-C(14)-H(27)	108.4030	109.4890	108.8265	105.0123	103.5928
S(2)-C(14)-H(28)	108.3558	109.4079	108.7698	107.7038	108.8756
C(13)-C(14)-H(27)	108.4099	109.5212	108.8616	108.9612	111.3747
C(13)-C(14)-H(28)	108.3603	109.6080	108.8769	111.7130	111.1397
H(27)-C(14)-H(28)	107.3893	108.1642	107.7212	107.9343	107.5954
C(12)-C(13)-C(14)	114.2196	111.8470	112.6923	116.0240	113.0550
C(12)-C(13)-H(25)	108.7011	109.2964	109.1183	106.8915	109.5837
C(12)-C(13)-H(26)	108.7229	109.1806	109.0937	108.9657	107.2499

C(14)-C(13)-H(25)	108.6922	109.2260	109.0235	109.1627	109.5975
C(14)-C(13)-H(26)	108.6852	109.2593	109.0542	108.6915	109.7795
H(25)-C(13)-H(26)	107.6256	107.9495	107.7370	106.7174	107.3989
C(13)-C(12)-H(24)	107.2488	107.9757	106.9046	107.7981	108.3425
C(13)-C(12)-C(11)	109.9662	109.3285	109.9488	111.2992	109.3591
C(13)-C(12)-N(6)	112.1963	111.4922	112.7102	112.0808	113.6020
H(24)-C(12)-C(11)	107.3159	107.8782	106.8760	107.8540	104.8190
H(24)-C(12)-N(6)	107.2409	107.8529	106.8111	105.3325	107.8700
C(11)-C(12)-N(6)	112.5721	112.1502	113.1722	112.1128	112.3875
O(4)-C(11)-C(12)	117.8550	119.0969	118.3527	120.3249	120.2207
O(4)-C(11)-N(5)	122.5757	121.2110	122.5287	122.7751	123.0985
C(12)-C(11)-N(5)	119.5644	119.6502	119.1183	116.8998	116.6784
C(9)-C(10)-S(1)	114.5900	112.3969	115.1739	115.1025	115.7782
C(9)-C(10)-H(22)	108.5913	109.1713	108.4128	111.7130	109.7130
C(9)-C(10)-H(23)	108.6433	109.0665	108.4687	108.9612	111.2043
S(1)-C(10)-H(22)	108.6067	109.0904	108.5457	107.7038	108.7342
S(1)-C(10)-H(23)	108.6037	109.1532	108.5414	105.0123	104.0671
H(22)-C(10)-H(23)	107.5913	107.8580	107.4413	107.9343	106.8750
C(8)-C(9)-C(10)	111.2868	110.6974	114.8158	116.0240	115.2308
C(8)-C(9)-H(20)	109.2719	109.5370	108.5796	106.8915	109.2568
C(8)-C(9)-H(21)	109.4085	109.4544	108.5480	108.9657	107.2036
C(10)-C(9)-H(20)	109.3952	109.5166	108.5946	109.1627	107.7345
C(10)-C(9)-H(21)	109.4468	109.4823	108.5632	108.6915	110.1258
H(20)-C(9)-H(21)	107.9672	108.1085	107.5070	106.7174	106.9996
C(9)-C(8)-H(19)	106.9672	107.4595	107.8518	107.7981	107.9113
C(9)-C(8)-N(5)	112.1663	111.1374	111.6466	112.0808	113.4334
C(9)-C(8)-C(7)	111.7426	110.4907	108.3703	111.2992	109.1864
H(19)-C(8)-N(5)	106.9521	107.3355	107.8227	105.3325	107.6320
H(19)-C(8)-C(7)	106.9564	107.3509	107.8670	107.8540	105.5069
N(5)-C(8)-C(7)	111.6789	112.7980	113.0896	112.1128	112.7427
O(3)-C(7)-C(8)	117.3981	118.1688	118.0609	120.3249	120.4282
O(3)-C(7)-N(6)	122.4885	122.5318	123.5804	122.7751	122.7685
C(8)-C(7)-N(6)	120.0795	119.1150	118.3585	116.8998	116.8029
H(18)-N(6)-C(12)	116.4591	116.1547	115.8334	117.8235	118.3776
H(18)-N(6)-C(7)	116.5837	116.1336	115.9820	114.7004	114.2269
C(12)-N(6)-C(7)	126.9571	127.7117	128.1845	127.2822	127.1651
H(17)-N(5)-C(11)	116.0198	117.2676	116.3734	114.7004	114.7011
H(17)-N(5)-C(8)	116.0948	117.1732	116.3631	117.8235	117.8100
C(11)-N(5)-C(8)	127.8854	125.5591	127.2635	127.2822	127.4868
C(14)-S(2)-H(16)	106.2166	-	-	96.3517	96.9776
C(10)-S(1)-H(15)	95.7969	-	84.9258	96.3517	97.1959
Dihedral angles (°)					
H(28)-C(14)-C(13)-H(26)	-62.6968	49.8178	63.8592	60.0393	62.0609
H(28)-C(14)-C(13)-H(25)	54.1666	-68.5608	-178.7529	176.0824	179.7935

H(28)-C(14)-C(13)-C(12)	175.7235	170.6561	-57.4420	-63.1216	-57.6447
H(27)-C(14)-C(13)-H(26)	-178.9504	68.6098	-178.9630	-59.1221	-177.9802
H(27)-C(14)-C(13)-H(25)	-62.0870	-173.5128	-61.5751	56.9210	-60.2477
H(27)-C(14)-C(13)-C(12)	59.4699	-52.3900	59.7358	177.7170	62.3142
S(2)-C(14)-C(13)-H(26)	59.1264	-172.8736	-57.5212	-176.7297	-61.3100
S(2)-C(14)-C(13)-H(25)	175.9898	-54.9961	59.8667	-60.6866	56.4226
S(2)-C(14)-C(13)-C(12)	-62.4533	66.1267	-178.8224	60.1094	178.9844
H(28)-C(14)-S(2)-H(16)	27.1801	-	-	40.4514	-60.8808
H(27)-C(14)-S(2)-H(16)	143.4276	-	-	155.3025	-175.1703
C(13)-C(14)-S(2)-H(16)	-94.6456	-	-	-84.8868	63.7133
H(26)-C(13)-C(12)-N(6)	-177.5741	165.4628	171.5907	64.2667	175.5884
H(26)-C(13)-C(12)-C(11)	56.3177	40.8849	44.3114	-62.1864	49.1426
H(26)-C(13)-C(12)-H(24)	-60.0663	-76.2333	-71.3522	-177.6491	-64.5665
H(25)-C(13)-C(12)-N(6)	65.5370	47.5902	54.1265	-50.7089	59.3060
H(25)-C(13)-C(12)-C(11)	-60.5713	-76.9877	-73.1529	-177.1620	-67.1399
H(25)-C(13)-C(12)-H(24)	-176.9553	165.8940	171.1835	67.3753	179.1511
C(14)-C(13)-C(12)-N(6)	-56.0151	-73.4918	-67.1305	-172.7159	-63.2635
C(14)-C(13)-C(12)-C(11)	177.8767	161.9303	165.5901	60.8310	170.2906
C(14)-C(13)-C(12)-H(24)	61.4927	44.8120	49.9265	-54.6316	56.5816
N(6)-C(12)-C(11)-N(5)	-8.5812	8.1248	-7.1414	-18.7036	-18.9344
N(6)-C(12)-C(11)-O(4)	172.2021	-174.2004	172.6881	161.4168	161.6128
H(24)-C(12)-C(11)-N(5)	-126.3441	-110.5025	-124.4386	-135.7396	-135.8237
H(24)-C(12)-C(11)-O(4)	54.4392	67.1723	55.3910	44.3807	44.7235
C(13)-C(12)-C(11)-N(5)	117.3140	132.3177	119.8798	107.3076	108.2007
C(13)-C(12)-C(11)-O(4)	-61.9027	-50.0075	-60.2907	-72.5721	-71.2521
C(11)-C(12)-N(6)-C(7)	10.0805	-13.0770	5.8192	23.7365	24.3720
C(11)-C(12)-N(6)-H(18)	-170.0347	166.8647	-174.3092	-161.6203	-161.4881
H(24)-C(12)-N(6)-C(7)	127.8877	105.5652	123.1544	139.2505	139.4242
H(24)-C(12)-N(6)-H(18)	-52.2275	-74.4931	-56.9740	-46.1064	-46.4360
C(13)-C(12)-N(6)-C(7)	-114.5999	-136.0574	-119.7332	-102.6990	-100.4629
C(13)-C(12)-N(6)-H(18)	65.2850	43.8843	60.1384	71.9442	73.6769
C(12)-C(11)-N(5)-C(8)	-0.7501	7.2915	0.8927	-4.3194	-2.9715
C(12)-C(11)-N(5)-H(17)	179.2715	-172.5729	-179.0615	-179.1051	177.5558
O(4)-C(11)-N(5)-C(8)	178.4280	-170.3328	-178.9294	175.5570	176.4640
O(4)-C(11)-N(5)-H(17)	-1.5504	9.8027	1.1165	0.7713	-3.0086
H(23)-C(10)-S(1)-H(15)	-140.6802	-	168.7951	155.3025	179.4664
H(22)-C(10)-S(1)-H(15)	-23.9494	-	52.3094	40.4514	65.8268
C(9)-C(10)-S(1)-H(15)	97.6528	-	-69.4130	-84.8868	-58.1830
H(23)-C(10)-C(9)-H(21)	-177.1919	176.9430	-170.0628	-59.1221	-175.8876
H(23)-C(10)-C(9)-H(20)	-59.0848	-64.6857	-53.4607	56.9210	-59.5213
H(23)-C(10)-C(9)-C(8)	61.7591	56.1913	68.2705	177.7170	62.7192
H(22)-C(10)-C(9)-H(21)	66.0641	59.3186	-53.6881	60.0393	-57.8689
H(22)-C(10)-C(9)-H(20)	-175.8288	177.6899	62.9140	176.0824	58.4974
H(22)-C(10)-C(9)-C(8)	-54.9850	-61.4332	-175.3548	-63.1216	-179.2621

S(1)-C(10)-C(9)-H(21)	-55.5465	-61.8657	68.1061	-176.7297	65.6301
S(1)-C(10)-C(9)-H(20)	62.5606	56.5056	-175.2918	-60.6866	-178.0035
S(1)-C(10)-C(9)-C(8)	-176.5956	177.3825	-53.5606	60.1094	-55.7630
H(21)-C(9)-C(8)-C(7)	46.0723	44.9668	57.2695	-62.1864	54.5822
H(21)-C(9)-C(8)-N(5)	172.3652	170.9802	-177.5345	64.2667	-178.7663
H(21)-C(9)-C(8)-H(19)	-70.6681	-71.8590	-59.2554	-177.6491	-59.6204
H(20)-C(9)-C(8)-C(7)	-71.9400	-73.4001	-59.3162	-177.1620	-61.0354
H(20)-C(9)-C(8)-N(5)	54.3529	52.6134	65.8798	-50.7089	65.6161
H(20)-C(9)-C(8)-H(19)	171.3196	169.7741	-175.8411	67.3753	-175.2380
C(10)-C(9)-C(8)-C(7)	167.1438	165.7351	178.9445	60.8310	177.5444
C(10)-C(9)-C(8)-N(5)	-66.5633	-68.2515	-55.8596	-172.7159	-55.8041
C(10)-C(9)-C(8)-H(19)	50.4034	48.9093	62.4196	-54.6316	63.3418
C(7)-C(8)-N(5)-C(11)	9.0046	-17.9674	6.8026	23.7365	21.2523
C(7)-C(8)-N(5)-H(17)	-171.0170	161.8972	-173.2432	-161.6203	-159.2893
H(19)-C(8)-N(5)-C(11)	125.7016	100.0728	125.9727	139.2505	137.1914
H(19)-C(8)-N(5)-H(17)	-54.3201	-80.0626	-54.0732	-46.1064	-43.3502
C(9)-C(8)-N(5)-C(11)	-117.3228	-142.6908	-115.7308	-102.6990	-103.5027
C(9)-C(8)-N(5)-H(17)	62.6556	37.1738	64.2234	71.9442	75.9557
N(5)-C(8)-C(7)-N(6)	-7.5340	12.9408	-8.0171	-18.7036	-16.1426
N(5)-C(8)-C(7)-O(3)	170.4011	-171.8670	171.8667	161.4168	164.1035
H(19)-C(8)-C(7)-N(6)	-124.2283	-105.0903	-127.1616	-135.7396	-133.3460
H(19)-C(8)-C(7)-O(3)	53.7068	70.1019	52.7222	44.3807	46.9001
C(9)-C(8)-C(7)-N(6)	119.0247	138.0166	116.3233	107.3076	110.9018
C(9)-C(8)-C(7)-O(3)	-63.0402	-46.7911	-63.7929	-72.5721	-68.8521
C(8)-C(7)-N(6)-C(12)	-1.8096	2.1658	1.9264	-4.3194	-6.2225
C(8)-C(7)-N(6)-H(18)	178.3057	-177.7758	-177.9450	-179.1051	179.4307
O(3)-C(7)-N(6)-C(12)	-179.6361	-172.8065	-177.9505	175.5570	173.5251
O(3)-C(7)-N(6)-H(18)	0.4792	7.2518	2.1781	0.7713	-0.8217

Table 4.2. Calculated DKP ring torsional angles and degree of folding ($^{\circ}$) of the calculated structure in comparison with the X-ray structure.¹³

Torsional angles ($^{\circ}$)	Calc. structure		X-ray ¹³	X-ray ¹³	X-ray ¹³
	C ₁	C ₂	(A)	(B)	(C)
C _{α} -C'-N-C _{α} (ω)	-6.22, -2.97	-4.31	-1.8, -0.7	2.2, 7.4	2.1, 1.0
C'-N-C _{α} -C' (ϕ)	21.25, 23.27	23.73	10.0, 9.1	-13.1, -18.0	5.7, 6.8
N-C'-C _{α} -N (ψ)	-18.93, -16.14	-18.7	-8.6, -7.5	8.1, 13.0	-7.2, -8.1
Degree of folding (β)	-21.82	-23.05	-9.6	14.0	-7.6

The X-ray crystal structure of C-CySH indicates that the DKP ring in all three molecules is nearly planar, the peptide torsional angles ω , ϕ , and ψ along with (the pseudo torsional angle) β in comparison to the calculated structure are given in Table 2. The DKP ring in the three asymmetric

molecules display a small deviation from C_2 symmetry (planarity) as the pairs of peptide dihedral angles, from either side of the ring, are almost equivalent.¹³ The ring torsional angles of the calculated minimum energy structure of C-CySH with C_1 and C_2 symmetry are slightly different compared to those obtained from the X-ray structure. By contrast the DFT calculations, based upon the assumption of an isolated molecule, predict significant deviation from planarity ($\beta=21.8^\circ$ (C_1) and 23° (C_2)) towards a boat conformation.

4.3.2. Vibrational assignments

The experimental and calculated IR and Raman spectra of C-CySH in the solid state are shown in Figs. 4.6 and 4.7, and those for the *N,S*-deuterated isotopomer are shown in Figs. 4.8 and 4.9. Experimental and calculated band wavenumbers (cm^{-1}) and assignments in terms of potential energy distribution (PEDs) of C-CySH and its *N,S*-deuterated isotopomer are given in Tables 4.3 and 4.4, respectively.

4.3.3. Spectral region $>2000 \text{ cm}^{-1}$

The bands found in this region are mainly due to C-H, N-H, N-D, S-H and S-D stretching modes. The vibrational wavenumbers for N-H stretching band for C-CySH can be easily located due to their large downward shift on *N*-deuteration. The N-H stretch is found at 3162 cm^{-1} in the Raman spectrum, shifting to 2301 cm^{-1} upon deuteration. In the IR spectrum $\nu(\text{NH})$ appears as an intense band at 3184 cm^{-1} , shifting to 2324 cm^{-1} upon deuteration. However, the IR spectrum shows clearly that 100% deuteration had not occurred despite repeating the process three times. The group of bands in the $2970\text{-}2850 \text{ cm}^{-1}$ region are attributed to C-H stretching modes, as evidence by the lack of shift on deuteration. These bands are less intense in the IR than in the Raman spectra. S-H stretching gives rise to a band at 2560 cm^{-1} in the Raman spectrum and one at 2553 cm^{-1} in the IR. These bands shift considerably on deuteration, appearing at 1865 cm^{-1} in the Raman spectrum and a very weak band at 1840 cm^{-1} in the IR spectrum. However, the Raman spectrum shows that 100% deuteration has not occurred.

4.3.4. Spectral region $1250\text{-}1700 \text{ cm}^{-1}$

The bands found in this region are attributed to amide group vibrations (combinations of C=O stretch, C-N stretch and N-H in-plane bending) and modes involving C-H bending, $C_\alpha\text{-H}$ bending, CH_2 scissoring, twisting and wagging. The strong band at 1662 cm^{-1} in the IR and at 1663 cm^{-1} in the Raman spectrum is assigned to the *cis* amide 1 mode, involving principally C=O stretching.

On deuteration this band shifts to lower wavenumber appearing at 1651 cm^{-1} in the IR and at 1609 cm^{-1} in the Raman spectrum. From previous studies of DKPs^{18, 19} it is suggested that the C=O stretch contribution, with respect to N-H in plane bending, is larger in compounds with *cis* amide groups compared with those possessing *trans* amide groups. As a consequence deuteration causes a greater shift to lower wavenumber for the *cis* amide I band. It is noteworthy that *cis* amide I shows downward shift of around 54 cm^{-1} in Raman spectrum, this can be attributed to the larger contribution from N-H in-plane bending in the *cis* amide I mode, with respect to the amide I mode of a *trans* amide. For example, it is observed in linear L-Met-L-Met that the *trans* amide I mode shows a downward shift of only 6 cm^{-1} upon *N*-deuteration.¹⁶

The *cis* amide II mode is found at 1506 cm^{-1} in the Raman spectrum of C-CySH. This mode is mainly due to C-N stretching, with a decreased contribution from N-H in plane bending compared with that of a *trans* amide. This band is found at a significantly higher wavenumber than that of other DKPs where the ring essentially adopts a boat conformation, cyclo-L-Met-L-Met ($\sim 1493\text{ cm}^{-1}$).¹⁶ In other cyclic di-amino acid peptides where the DKP ring is planar or near planar,¹⁹ such as cyclo(Gly-Gly), cyclo(D-Ala-L-Ala) and cyclo(L-Ala-Gly) the *cis* amide II was found at $\sim 1520\text{ cm}^{-1}$. For cyclo(L-Ala-L-Ala), where the *cis* amide II was found at $\sim 1508\text{ cm}^{-1}$, the DKP ring exists in a twist-boat conformation.¹⁹ However, the increase in the strain on the DKP ring due the attachment of bulky substituents on the C_{α} atoms may also influence the location of the *cis* amide II mode.¹⁶ The calculated band position for the *cis* amide II vibration is located at $\sim 1471\text{ cm}^{-1}$, significantly lower than the observed position (1506 cm^{-1}). On deuteration the *cis* amide II band shifts to 1489 cm^{-1} , revealing a shoulder at 1510 cm^{-1} . This shift is in good agreement with both the calculated spectrum and *cis* amide II deuterium shifts observed in other DKPs.^{18, 19, 20} The weak band at 1510 cm^{-1} in the Raman spectrum of *N,S*-deuterated C-CySH could be the result of anharmonic vibrations. By contrast, the amide II mode has significantly high N-H in-plane bending character for *trans* amides and it is observed in linear L-Met-L-Met that the *trans* amide II mode shows a downward shift of 66 cm^{-1} upon *N*-deuteration.^{16, 18}

IR and Raman bands in the $1410\text{-}1480\text{ cm}^{-1}$ region can be ascribed to CH_2 , CH symmetric and asymmetric bending modes of C-CySH. Specific bands have been assigned by reference to the computed spectra. From previous observations in DKPs, vibrations involving N-H in-plane bending are expected in this region, but no large shifts are observed in IR and Raman spectra. However, small shifts are observed in the region ($\sim 1350\text{ cm}^{-1}$ to 1420 cm^{-1}) of the C-H bending modes on deuteration, which is indicative of little N-H character. The band located at 1342 cm^{-1} in the Raman spectrum has been assigned to the N-H in-plane bending vibration. It was not

possible to locate the asymmetric N-H in-plane bending vibrational band in the IR and Raman spectra but it is likely that such a band is hidden beneath the broad bands assigned to C-H bending vibrations.

IR and Raman bands located between 1220 and 1335 cm^{-1} are assigned to vibrations of mixed character. The DFT calculations indicate that these bands are mainly due to modes involving C_α -H bending, C_α -H wagging, C_α -H twisting, CH_2 wagging and CH_2 twisting motions. On deuteration the broad Raman band at 1342 cm^{-1} vanishes and sharp bands, which are assigned to N-D bending vibrations, appear at 1227 cm^{-1} . This observation fits well with the previously reported N-H in-plane bend shift in DKPs on *N*-deuteration.¹⁹ Generally most of the bands due to C-H bending vibrations show little shift on deuteration, but some are shifted by 5-10 cm^{-1} .

4.3.5. Spectral region 850-1350 cm^{-1}

The vibrations observed in this region are due to N- C_α and C-C stretching as well as CH_2 rocking and C-S bending vibrations. The bands located at 1030 cm^{-1} and 1180 cm^{-1} in both the IR and Raman spectra of C-CySH are assigned to mixed C-C, N- C_α stretching vibrations which also involve CH_2 rocking and C-S bending motion. Additionally the bands at 966 cm^{-1} in IR (968 cm^{-1} in the Raman spectrum) have been assigned to C-C stretching with little contribution from C-S bending vibration. The assignments of other IR and Raman bands in the 900–1100 cm^{-1} region were less straightforward but are facilitated by comparison with the DFT calculated spectra, which show that these vibrations involve combinations of N- C_α , C-C stretching as well as CH_2 rocking and C-S bending.

4.3.6. Spectral region 500-850 cm^{-1}

In this region, there are two peptide group vibrations: C=O bending, N-H out-of-plane bending, as well as C-S stretching modes and in-plane DKP ring stretching/deformation. Bands due to N-H out-of-plane bending modes have been assigned by comparison with the IR and Raman spectra of deuterated C-CySH and also from the previous IR and Raman data relating to other DKPs. The broad band found at 835 cm^{-1} in the IR spectrum (819 cm^{-1} in Raman) can be assigned to N-H out-of-plane bending as these bands are shifted upon deuteration to 577 cm^{-1} (IR) and 511 cm^{-1} (Raman). Previous work on other CDAPs has shown that the specific NH out-of-plane bending band is quite difficult to find and has as a wide-ranging feature centred $\sim 820 \text{ cm}^{-1}$ in the IR spectrum.^{18,19,20} These band positions are not in good agreement with the DFT calculations, which do not account for hydrogen bonding effects. Bands due to C-S stretching can be easily located at

649 and 626 cm^{-1} in the Raman spectrum (678 and 647 cm^{-1} in IR), which display very small shifts on deuteration. By comparison, C-S stretching in cyclo(L-Met-L-Met) gives rise to strong Raman bands at 721 and 636 cm^{-1} .¹⁶ The medium intensity Raman bands located from 620 to 760 cm^{-1} can be assigned to vibrations that are principally C=O out-of-plane bending, although there are also contributions from C-S stretching and bending motions.

4.3.7. Spectral region < 500 cm^{-1}

There are some weak bands observed in the Raman spectrum below 500 cm^{-1} , which are due to vibrations from C=O, C-N, C-S, C-C bending motions and C-S torsional vibrations together with vibrations involving DKP ring stretching and bending. A medium intensity band centred at 469 cm^{-1} in the IR spectrum (appearing as a weak band in the Raman spectrum) is tentatively assigned to a C=O out-of-plane bend; on deuteration, it increases in intensity and shifts down in wavenumber by 6 cm^{-1} indicative of a small contribution from N-H out-of-plane bending. The bands in the 200-400 cm^{-1} region of the Raman spectrum are predominantly due to C-C, C=O, C-C-S bending motion and C-S torsional vibrations. The attachment of the side chain on the C_α atom also gives rise to C-C-C bending vibrations in this region as well as the bending modes of the DKP ring. The bands located between 50 and 200 cm^{-1} are mainly due to torsional vibrations of the aliphatic side chain attached to the C_α atom, ring torsional vibrations and lattice vibrations. These bands show no significant shift on N-deuteration, indicative of very little N-H contributions to these modes.

Table 4.3. Experimental and calculated (scaled) vibrational band wavenumbers (cm^{-1}) for non-deuterated *N,S*-C-CySH (solid phase).

IR	Raman	Calc. C ₁	%PEDs	Calc. C ₂	%PEDs
3320					
	3162	3207 A	99 $\nu_s(\text{N6H18})$	3198 A	100 $\nu_s(\text{NH})$
3184		3202 A	99 $\nu_s(\text{N5H17})$	3196 B	100 $\nu_{as}(\text{NH})$
3090	3112				
3045	3046				
2961		2962 A	89 $\nu_{as}(\text{CH}_2^\wedge)$	2990 B	11 $\nu_s(\text{CH}_2')$, 88 $\nu_{as}(\text{CH}_2)$
	2981	2959 A	49 $\nu_{as}(\text{CH}_2')$, 48 $\nu_{as}(\text{CH}_2'')$	2990 A	11 $\nu_s(\text{CH}_2')$, 88 $\nu_{as}(\text{CH}_2)$
	2957	2941 A	24 $\nu_s(\text{C8H19})$, 56 $\nu_{as}(\text{CH}_2^*)$	2932 A	11 $\nu_{as}(\text{CH}_2')$, 74 $\nu_s(\text{CH}_2)$, 10 $\nu_s(\text{CH})$
	2942	2937 A	51 $\nu_{as}(\text{CH}_2'')$, 44 $\nu_{as}(\text{CH}_2')$	2932 B	11 $\nu_{as}(\text{CH}_2')$, 79 $\nu_s(\text{CH}_2')$
		2931 A	74 $\nu_s(\text{C8H19})$, 13 $\nu_{as}(\text{CH}_2^*)$	2930 A	80 $\nu_s(\text{CH})$, 13 $\nu_s(\text{CH}_2)$
2933		2919 A	86 $\nu_s(\text{CH}_2^\wedge)$	2930 B	86 $\nu_s(\text{CH})$
	2919	2914 A	60 $\nu_s(\text{C12H24})$, 25 $\nu_s(\text{CH}_2')$, 15 $\nu_s(\text{CH}_2'')$	2913 A	81 $\nu_{as}(\text{CH}_2)$

		2906 A	27 $\nu_s(\text{C12H24})$, 68 $\nu_s(\text{CH}_2'')$	2912 B	10 $\nu_s(\text{CH}_2)$, 81 $\nu_{as}(\text{CH}_2)$
	2895	2898 A	10 $\nu_s(\text{C12H24})$, 68 $\nu_s(\text{CH}_2')$, 17 $\nu_s(\text{CH}_2')$	2875 A	92 $\nu_s(\text{CH}_2)$
2890		2879 A	79 $\nu_s(\text{CH}_2^*)$, 19 $\nu_{as}(\text{CH}_2^*)$	2873 B	90 $\nu_s(\text{CH}_2)$
	2575				
2553	2560	2543 A	99 $\nu_s(\text{S2H16})$	2551 A	100 $\nu_s(\text{SH})$
2542		2543 A	99 $\nu_s(\text{S1H15})$	2551 B	100 $\nu_{as}(\text{SH})$
1662	1663	1644 A	65 $\nu_s(\text{C11=O4})$, 10 $\nu_{as}(\text{NC})$	1639 B	62 $\nu_s(\text{C=O})$, 12 $\nu_s(\text{NC})$, 11 $\delta_{ip}(\text{NH})$
		1643 A	66 $\nu_s(\text{C7=O3})$, 10 $\delta_{ip,s}(\text{NH})$	1634 A	66 $\nu_s(\text{C=O})$, 10 $\nu_s(\text{NC})$, 12 $\delta_{ip}(\text{NH})$
	1506	1460 A	23 $\nu_s(\text{NC})$, 17 $\delta_{ip,s}(\text{NH})$	1474 A	23 $\nu_s(\text{NC})$, 15 $\delta_{ip,s}(\text{NH})$, 11 $\nu_s(\text{CC}\alpha)$, 14 $\omega(\text{CCH})$
1481					
1457		1456 A	80 $\delta(\text{CH}_2')$, 13 $\delta(\text{CH}_2'')$	1450 B	91 $\delta(\text{CH}_2)$
		1449 A	91 $\delta(\text{CH}_2^*)$	1444 A	91 $\delta(\text{CH}_2)$
		1442 A	91 $\delta(\text{CH}_2^\wedge)$	1431 B	10 $\nu_s(\text{C=O})$, 12 $\nu_s(\text{NC})$, 10 $\delta_{ip}(\text{NH})$, 43 $\delta(\text{CH}_2')$, 10 $\omega(\text{CCH})$
	1430	1438 A	13 $\delta(\text{CH}_2')$, 85 $\delta(\text{CH}_2'')$	1426 A	98 $\delta(\text{CH}_2')$
		1427 A	17 $\nu_s(\text{C11=O4})$, 28 $\nu_{as}(\text{NC})$, 14 $\delta_{ip,as}(\text{NH})$	1423 B	11 $\nu_s(\text{C=O})$, 13 $\nu_s(\text{NC})$, 54 $\delta(\text{CH}_2')$
		1388 A	16 $\nu_{as}(\text{NC})$, 14 $\nu_{as}(\text{C}\alpha\text{C})$, 52 $\delta_{ip,as}(\text{NH})$, 13 $\delta_{ip}(\text{C11=O4})$	1393 B	17 $\nu_s(\text{NC})$, 15 $\nu_s(\text{CC}\alpha)$, 41 $\delta_{ip}(\text{NH})$, 10 $\delta_{ip}(\text{C=O})$
	1342	1356 A	10 $\nu_s(\text{NC}\alpha)$, 35 $\delta_{ip,s}(\text{NH})$	1352 A	12 $\nu_s(\text{C=O})$, 35 $\delta_{ip}(\text{NH})$, 22 $\omega(\text{CH}_2)$
1336		1342 A	12 $\delta(\text{C9C8H19})$, 66 $\omega(\text{CH}_2^*)$	1342 B	56 $\omega(\text{CH}_2)$
		1332 A	66 $\omega(\text{CH}_2')$, 12 $\omega(\text{CH}_2'')$	1320 A	10 $\delta_{ip}(\text{NH})$, 50 $\omega(\text{CH}_2)$, 12 $\tau(\text{CH}_2')$
	1319	1323 A	10 $\tau(\text{CH}_2^*)$, 12 $\delta(\text{C13C12H24})$, 11 $\nu_{as}(\text{NC}\alpha)$, 12 $\tau(\text{CH}_2')$	1311 A	33 $\delta(\text{CCH})$, 40 $\tau(\text{CH}_2)$, 13 $\omega(\text{CH}_2')$
1291		1290 A	16 $\nu_s(\text{NC})$, 12 $\delta_{ip,s}(\text{NH})$, 10 $\tau(\text{CH}_2')$	1305 B	25 $\delta(\text{CCH})$, 38 $\tau(\text{CH}_2)$, 21 $\omega(\text{CH}_2')$
	1288	1282 A	11 $\tau(\text{CH}_2^*)$, 55 $\omega(\text{CH}_2^\wedge)$	1293 A	21 $\nu_s(\text{NC})$, 33 $\omega(\text{CCH})$, 20 $\tau(\text{CCH})$
		1271 A	24 $\delta(\text{C13C12H24})$, 35 $\omega(\text{CH}_2'')$	1291 B	12 $\nu_s(\text{NC}\alpha)$, 25 $\omega(\text{CCH})$, 13 $\tau(\text{CCH})$, 13 $\omega(\text{CH}_2)$, 11 $\tau(\text{CH}_2')$
	1268	1268 A	11 $\omega(\text{C13C12H24})$, 30 $\tau(\text{CH}_2'')$, 28 $\tau(\text{CH}_2')$	1276 A	20 $\delta(\text{CCH})$, 64 $\omega(\text{CH}_2')$
		1256 A	15 $\omega(\text{C9C8H19})$, 10 $\omega(\text{CH}_2^\wedge)$, 25 $\delta(\text{C9C8H19})$	1273 B	27 $\delta(\text{CCH})$, 57 $\omega(\text{CH}_2')$
1233	1233	1219 A	11 $\delta(\text{C13C12H24})$, 20 $\omega(\text{CH}_2')$, 34 $\omega(\text{CH}_2'')$	1207 A	12 $\omega(\text{CH}_2)$, 48 $\tau(\text{CH}_2')$
1187	1193	1185 A	14 $\rho(\text{C9C8H19})$, 13 $\delta(\text{C9C8H19})$, 36 $\tau(\text{CH}_2^*)$, 17 $\omega(\text{CH}_2^\wedge)$	1204 B	14 $\omega(\text{CH}_2)$, 48 $\tau(\text{CH}_2')$
		1171 A	11 $\tau(\text{C9C8H19})$, 53 $\tau(\text{CH}_2^\wedge)$	1154 A	10 $\nu_s(\text{NC}\alpha)$, 10 $\delta(\text{CCH})$, 30 $\tau(\text{CH}_2)$, 11 $\tau(\text{CH}_2')$
1144	1144	1153 A	11 $\rho(\text{C13C12H24})$, 34 $\tau(\text{CH}_2'')$, 22 $\tau(\text{CH}_2')$	1147 B	11 $\rho(\text{CCH})$, 40 $\tau(\text{CH}_2)$, 18 $\tau(\text{CH}_2')$
1102	1101	1122 A	31 $\nu_s(\text{NC}\alpha)$, 11 $\delta_{ip,s}(\text{NH})$	1117 A	30 $\nu_s(\text{NC}\alpha)$, 11 $\delta_{ip}(\text{NH})$, 10 $\tau(\text{CH}_2)$, 13 $\tau(\text{CH}_2')$

	1080	1082 A	10 $\nu_s(\text{C}^*\text{C}^\wedge)$, 10 $\delta(\text{C}^\wedge\text{S1H15})$, 16 $\rho(\text{CH}_2^*)$	1079 B	27 $\nu_s(\text{NC}_\alpha)$, 14 $\nu_s(\text{C}_\alpha\text{C}')$, 12 $\nu_s(\text{C}'\text{C}^*)$
	1061	1081 A	27 $\nu_s(\text{C}_\alpha\text{C}^*)$, 16 $\nu_s(\text{C}^*\text{C}^\wedge)$, 16 $\nu_{\text{as}}(\text{NC}_\alpha)$	1061 A	40 $\nu_s(\text{C}_\alpha\text{C}')$, 25 $\nu_s(\text{C}'\text{C}^*)$, 14 $\rho(\text{CH}_2)$
		1062 A	25 $\nu_s(\text{C}_\alpha\text{C}')$, 13 $\nu_s(\text{C}'\text{C}''')$, 11 $\rho(\text{CH}_2')$, 10 $\rho(\text{CH}_2'')$	1053 B	35 $\nu_s(\text{C}_\alpha\text{C}')$, 14 $\delta(\text{CSH})$, 15 $\rho(\text{CH}_2)$
1038	1040	1029 A	57 $\nu_s(\text{C}'\text{C}''')$, 10 $\rho(\text{C13C12H24})$	1032 B	25 $\nu_s(\text{NC}_\alpha)$, 27 $\nu_s(\text{C}'\text{C}^*)$, 12 $\rho(\text{CH}_2)$
1004		989 A	14 $\nu_s(\text{C}_\alpha\text{C}^*)$, 15 $\rho(\text{CH}_2^\wedge)$, 12 $\delta(\text{C}^\wedge\text{S1H15})$	1021 A	26 $\rho(\text{CH}_2')$, 26 $\delta(\text{CSH})$
966		972 A	51 $\nu_s(\text{C}_\alpha\text{C}')$, 17 $\delta_{\text{ip}}(\text{Ring-3})$	969 B	15 $\nu_s(\text{C}'\text{C}^*)$, 11 $\rho(\text{CCH})$, 21 $\rho(\text{CH}_2)$, 12 $\delta_{\text{ip}}(\text{Ring-3})$
	968	952 A	11 $\nu_s(\text{C}_\alpha\text{C}^*)$, 24 $\nu_s(\text{C}^*\text{C}^\wedge)$, 10 $\delta_{\text{ip}}(\text{Ring-3})$	955 A	28 $\nu_s(\text{C}_\alpha\text{C}')$, 12 $\rho(\text{CCH})$, 30 $\rho(\text{CH}_2)$
		941 A	14 $\nu_{\text{as}}(\text{C}_\alpha\text{C})$, 11 $\delta_{\text{ip}}(\text{Ring-3})$	931B	19 $\nu_s(\text{C}_\alpha\text{C}')$, 30 $\rho(\text{CH}_2')$, 20 $\delta(\text{CSH})$, 13 $\delta_{\text{ip}}(\text{Ring-3})$
	889	867 A	22 $\delta(\text{C}''\text{S2H16})$	904 A	18 $\nu_s(\text{C}_\alpha\text{C}')$, 10 $\rho(\text{CH}_2)$, 29 $\delta(\text{CSH})$
		849 A	19 $\delta(\text{C}^\wedge\text{S1H15})$, 14 $\delta(\text{C}''\text{S2H16})$, 11 $\nu_{\text{as}}(\text{C}_\alpha\text{C})$	837 B	24 $\delta(\text{CSH})$, 38 $\delta_{\text{ip}}(\text{Ring-3})$
		801 A	12 $\rho(\text{CH}_2^\wedge)$, 21 $\delta(\text{C}^\wedge\text{S1H15})$	801 B	30 $\nu_s(\text{C}_\alpha\text{C})$, 13 $\nu_s(\text{NC})$
791		773 A	10 $\rho(\text{CH}_2'')$, 21 $\delta_{\text{ip}}(\text{Ring-3})$	785 A	14 $\nu_s(\text{NC})$, 15 $\rho(\text{CH}_2')$, 24 $\delta(\text{CSH})$
753	759	754 A	17 $\rho(\text{CH}_2^\wedge)$, 14 $\nu_s(\text{C}''\text{S2})$, 15 $\delta_{\text{op}}(\text{C7=O3})$, 11 $\rho(\text{CH}_2'')$	746 A	68 $\delta_{\text{op}}(\text{C=O})$
725	728	737 A	15 $\nu_s(\text{C}''\text{S2})$, 15 $\delta_{\text{op}}(\text{C7=O3})$, 14 $\rho(\text{CH}_2'')$	719 B	56 $\delta_{\text{op}}(\text{C=O})$
	698 690	711 A	65 $\delta_{\text{op}}(\text{C11=O4})$	704 B	15 $\nu_s(\text{C}_\alpha\text{C}')$, 38 $\rho(\text{CH}_2')$, 11 $\delta(\text{CSH})$, 11 $\delta_{\text{op}}(\text{C=O})$
678	672	697 A	21 $\nu_s(\text{C}''\text{S2})$, 11 $\delta_{\text{op}}(\text{C7=O3})$, 23 $\rho(\text{CH}_2'')$, 10 $\delta(\text{C}''\text{S2H16})$	690 A	13 $\delta_{\text{ip}}(\text{C=O})$, 11 $\rho(\text{CH}_2)$, 40 $\rho(\text{CH}_2')$
	662	668 A	12 $\nu_s(\text{C}_\alpha\text{C})$, 10 $\nu_s(\text{C}_\alpha\text{C}^*)$, 17 $\delta_{\text{op}}(\text{C7=O3})$, 10 $\nu_s(\text{C}''\text{S2})$	651 A	80 $\nu_s(\text{CS})$
647	649	638 A	55 $\nu_s(\text{C}'\text{S1})$	648 B	78 $\nu_s(\text{CS})$
622	626	615 A	55 $\nu_s(\text{C}'\text{S1})$, 37 $\delta_{\text{ip}}(\text{C7=O3})$	612 A	35 $\nu_s(\text{C}_\alpha\text{C})$, 17 $\delta_{\text{ip}}(\text{C=O})$, 11 $\delta_{\text{ip}}(\text{Ring-2})$, 14 $\delta_{\text{op}}(\text{NH})$
835		580 A	54 $\delta_{\text{op}}(\text{N5H17})$, 29 $\delta_{\text{op}}(\text{N6H18})$	564 A	73 $\delta_{\text{op}}(\text{NH})$
	819 506	557 A	20 $\delta_{\text{op}}(\text{N5H17})$, 60 $\delta_{\text{op}}(\text{N6H18})$	559 B	87 $\delta_{\text{op}}(\text{NH})$
	493 469	496 A	12 $\nu_s(\text{C}_\alpha\text{C})$, 10 $\delta(\text{C8C}^\wedge\text{C}^*)$, 36 $\delta_{\text{ip}}(\text{Ring-1})$	474 A	28 $\delta_{\text{ip}}(\text{C=O})$, 44 $\delta_{\text{ip}}(\text{Ring-1})$
469		465 A	11 $\delta(\text{C8C}^\wedge\text{C}^*)$, 51 $\delta_{\text{ip}}(\text{C11=O4})$	450 B	23 $\delta(\text{C}_\alpha\text{C}^*)$, 21 $\delta(\text{C}'\text{C}^*\text{S})$
	462	446 A	16 $\nu_s(\text{NC}_\alpha)$, 62 $\delta_{\text{ip}}(\text{Ring-2})$	446 A	15 $\nu_s(\text{NC}_\alpha)$, 67 $\delta_{\text{ip}}(\text{Ring-2})$
	425	416 A	15 $\delta_{\text{ip}}(\text{C7=O3})$, 16 $\rho(\text{C13C12H24})$	416 A	17 $\delta(\text{C}_\alpha\text{C}^*)$, 34 $\delta(\text{C}'\text{C}^*\text{S})$, 12 $\delta_{\text{ip}}(\text{Ring-1})$
	386	403 A	12 $\rho(\text{C9C8H19})$, 35 $\delta_{\text{ip}}(\text{C11=O4})$	399 B	16 $\nu_s(\text{NC}_\alpha)$, 11 $\nu_s(\text{C}_\alpha\text{C})$, 57 $\delta_{\text{ip}}(\text{C=O})$
		370 A	14 $\rho(\text{C9C8H19})$, 26 $\delta(\text{C}^*\text{C}^\wedge\text{S1})$, 10 $\delta_{\text{ip}}(\text{Ring-1})$	340B	28 $\tau(\text{CCH})$, 14 $\delta(\text{C}_\alpha\text{C}^*)$

	325	292 A	12 ω (C13C12H24), 19 τ (C13C12H24), 4 δ (C'C''S2)	324 A	28 τ (CCH), 12 δ (C α C'C*), 19 τ (CS), 13 δ_{op} (Ring-2)
	312	243 A	25 δ (C12C'C''), 10 τ (C''S2)	319 A	84 τ (CS)
		237 A	69 τ (C^AS1)	315 B	94 τ (CS)
	255	217 A	12 δ (C*C^AS1), 39 τ (C''S2)	286 B	14 τ (CCH), 32 δ (C'C*S), 12 τ (C'C*)
	237	213 A	46 τ (C''S2)	268 A	19 τ (CCH), 27 δ (C'C*S), 14 τ (C'C*)
	215	177 A	17 ω (C9C8H19), 13 τ (C^AS1), 21 τ (C9C8H19), 17 δ (C8C^C*),	193 B	19 τ (CCH), 26 ω (CCH), 26 δ (C α C'C*), 10 δ_{op} (C=O)
	140	125 A	10 δ (C12C'C''), 10 δ (C'C''S2), 27 δ_{op} (Ring-1), 19 τ (C'C'')	190 A	16 τ (CCH), 18 ω (CCH), 13 δ (C α C'C*),
	121	111 A	12 δ_{op} (Ring-2), 12 τ (C*C^A), 11 δ (C12C'C''), 14 δ_{op} (Ring-1)	127 B	13 δ (C'C*S), 28 δ_{op} (Ring-1), 38 τ (C'C*)
	90	105 A	15 τ (C*C^A), 10 τ (C12C'), 11 τ (C'C'')	102 A	18 δ (C α C'C*), 18 δ (C'C*S), 13 τ (C α C'), 27 τ (C'C*)
	79	83 A	17 δ_{op} (Ring-2), 49 τ (C12C'), 25 τ (C'C'')	76 A	99 δ_{op} (Ring-2)
		70 A	51 δ_{op} (Ring-2), 20 δ_{op} (Ring-1), 13 τ (C12C')	67 B	75 δ_{op} (Ring-1), 21 τ (C'C*)
		51 A	15 δ_{op} (Ring-2), 12 τ (C*C^A), 32 δ_{op} (Ring-1), 19 τ (C'C'')	50 A	49 τ (C α C'), 40 τ (C'C*)
		28 A	64 τ (C8C*), 22 τ (C*C^A)	34 B	77 τ (C α C'), 18 τ (C'C*)
		20 A	81 δ_{op} (Ring-3)	27 A	84 δ_{op} (Ring-3), 17 τ (C α C')

Table 4.4. Experimental and calculated (scaled) vibrational band wavenumbers (cm⁻¹) for *N,S*-deuterated C-CySH (solid phase).

IR	Raman	Calc. (C ₁)	%PEDs	Calc. (C ₂)	%PEDs
		2962 A	89 ν_{as} (CH ₂ [^])	2990 B	11 ν_s (CH ₂ [']), 88 ν_{as} (CH ₂ ['])
	2955	2959 A	49 ν_{as} (CH ₂ [']), 48 ν_{as} (CH ₂ ^{''})	2989 A	11 ν_s (CH ₂ [']), 88 ν_{as} (CH ₂ ['])
		2941 A	24 ν_s (C8H19), 56 ν_{as} (CH ₂ [*])	2932 A	11 ν_{as} (CH ₂ [']), 74 ν_s (CH ₂ [']), 10 ν_s (CH)
2928		2937 A	51 ν_{as} (CH ₂ ^{''}), 44 ν_{as} (CH ₂ ['])	2932 B	11 ν_{as} (CH ₂ [']), 79 ν_s (CH ₂ ['])
	2925	2931 A	74 ν_s (C8H19), 13 ν_{as} (CH ₂ [*])	2930 A	80 ν_s (CH), 13 ν_s (CH ₂ ['])
		2918 A	86 ν_s (CH ₂ [^])	2930 B	86 ν_s (CH)
		2914 A	60 ν_s (C12H24), 25 ν_s (CH ₂ [']), 15 ν_s (CH ₂ ^{''})	2913 A	81 ν_{as} (CH ₂)
		2906 A	27 ν_s (C12H24), 68 ν_s (CH ₂ ^{''})	2912 B	10 ν_s (CH ₂), 81 ν_{as} (CH ₂)
2855	2855	2898 A	10 ν_s (C12H24), 68 ν_s (CH ₂ [']), 17 ν_s (CH ₂ ^{''})	2875 A	92 ν_s (CH ₂)
		2879 A	79 ν_s (CH ₂ [*]), 19 ν_{as} (CH ₂ [*])	2873 B	90 ν_s (CH ₂)
		2351 A	99 ν_s (N6D18)	2344 A	99 ν_s (ND ₂)
2324	2301 2137	2347 A	99 ν_s (N5D17)	2343 B	99 ν_s (ND ₂)
1840		1826 A	100 ν_s (S2D16)	1832 B	100 ν_s (SD)
	1865 1678	1826 A	100 ν_s (S1D15)	1832 A	100 ν_{as} (SD)

1651		1632 A	72 $\nu_s(\text{C11}=\text{O4}), 11 \nu_{as}(\text{NC})$	1625 B	70 $\nu_s(\text{C}=\text{O}), 12 \nu_s(\text{NC})$
	1609	1628 A	75 $\nu_s(\text{C7}=\text{O3})$	1618 A	75 $\nu_s(\text{C}=\text{O})$
	1510	1456 A	85 $\delta(\text{CH}_2')$, 14 $\delta(\text{CH}_2'')$	1456 A	22 $\nu_s(\text{NC}), 11 \omega(\text{CCH}), 35 \delta(\text{CH}_2)$
1448		1450A	94 $\delta(\text{CH}_2^*)$	1449 B	92 $\delta(\text{CH}_2)$
	1489	1443 A	91 $\delta(\text{CH}_2^\wedge)$	1440 A	12 $\nu_s(\text{NC}), 63 \delta(\text{CH}_2)$
		1438 A	14 $\delta(\text{CH}_2')$, 81 $\delta(\text{CH}_2'')$	1427 B	89 $\delta(\text{CH}_2')$
	1427	1435 A	31 $\nu_s(\text{NC}), 11 \nu_{as}(\text{C}_\alpha\text{C}), 10 \omega(\text{C9C8H19})$	1425 A	95 $\delta(\text{CH}_2')$
		1417 A	10 $\nu_s(\text{C11}=\text{O4}), 39 \nu_{as}(\text{NC}), 11 \omega(\text{C13C12H24})$	1418 B	12 $\nu_s(\text{C}=\text{O}), 33 \nu_s(\text{NC}), 14 \omega(\text{CCH})$
1354	1349	1343 A	10 $\delta(\text{C9C8H19}), 69 \omega(\text{CH}_2^*)$	1353 B	13 $\omega(\text{CCH}), 52 \omega(\text{CH}_2)$
1335	1331	1333 A	66 $\omega(\text{CH}_2')$, 11 $\omega(\text{CH}_2'')$	1330 A	65 $\omega(\text{CH}_2)$
		1326 A	15 $\omega(\text{C9C8H19}), 16 \tau(\text{CH}_2^*), 13 \delta(\text{C9C8H19})$	1312 B	29 $\delta(\text{CCH}), 31 \tau(\text{CH}_2), 12 \omega(\text{CH}_2')$
		1314 A	15 $\delta(\text{C13C12H24}), 12 \nu_s(\text{NC}_\alpha), 13 \omega(\text{C13C12H24}), 20 \tau(\text{CH}_2')$	1311 A	33 $\delta(\text{CCH}), 39 \tau(\text{CH}_2), 13 \omega(\text{CH}_2')$
	1283	1281 A	18 $\tau(\text{CH}_2^*), 52 \omega(\text{CH}_2^\wedge)$	1302 A	11 $\nu_s(\text{NC}_\alpha), 37 \omega(\text{CCH}), 20 \tau(\text{CCH})$
1298		1273 A	20 $\delta(\text{C13C12H24}), 35 \omega(\text{CH}_2''), 13 \omega(\text{C13C12H24})$	1293 B	19 $\omega(\text{CCH}), 11 \tau(\text{CCH}), 13 \omega(\text{CH}_2), 12 \tau(\text{CH}_2')$
	1262	1269 A	28 $\tau(\text{CH}_2''), 28 \tau(\text{CH}_2')$	1275 A	20 $\delta(\text{CCH}), 64 \omega(\text{CH}_2')$
1279		1262 A	10 $\omega(\text{C9C8H19}), 15 \omega(\text{CH}_2^\wedge), 24 \delta(\text{C9C8H19})$	1273 B	23 $\delta(\text{CCH}), 60 \omega(\text{CH}_2')$
1234		1223 A	11 $\tau(\text{C13C12H24}), 10 \omega(\text{CH}_2')$, 25 $\omega(\text{CH}_2'')$	1219 A	19 $\nu_s(\text{NC}_\alpha), 11 \nu_s(\text{C}_\alpha\text{C}), 13 \tau(\text{CCH}), 18 \tau(\text{CH}_2')$
	1228	1214 A	13 $\nu_s(\text{NC}_\alpha), 10 \nu_{as}(\text{NC}_\alpha), 10 \delta_{ip,as}(\text{ND})$	1209 B	31 $\nu_s(\text{NC}_\alpha), 28 \delta_{ip}(\text{ND}), 20 \delta_{ip}(\text{CO})$
1197	1197	1202 A	17 $\nu_{as}(\text{NC}_\alpha), 13 \delta_{ip,as}(\text{ND}), 13 \omega(\text{CH}_2'')$	1199 B	13 $\omega(\text{CH}_2), 44 \tau(\text{CH}_2')$
		1182 A	12 $\rho(\text{C9C8H19}), 23 \tau(\text{CH}_2^*), 13 \delta(\text{C9C8H19}), 16 \omega(\text{CH}_2^\wedge), 11 \tau(\text{CH}_2^\wedge)$	1194 A	12 $\omega(\text{CH}_2), 11 \tau(\text{CH}_2), 24 \tau(\text{CH}_2')$
1177		1148 A	19 $\tau(\text{CH}_2^*), 46 \tau(\text{CH}_2^\wedge)$	1143 B	39 $\tau(\text{CH}_2), 22 \tau(\text{CH}_2')$
	1163	1141 A	10 $\rho(\text{C13C12H24}), 33 \tau(\text{CH}_2''), 24 \tau(\text{CH}_2')$	1138 A	37 $\tau(\text{CH}_2), 31 \tau(\text{CH}_2')$
1086					
	1066	1069 A	14 $\nu_s(\text{C}_\alpha\text{C}^*), 32 \nu_s(\text{C}^*\text{C}^\wedge), 17 \rho(\text{CH}_2^*), 10 \nu_s(\text{C}_\alpha\text{C}')$	1061 A	38 $\nu_s(\text{C}_\alpha\text{C}'), 34 \nu_s(\text{C}'\text{C}^*), 11 \rho(\text{CH}_2)$
1049	1041	1053 A	39 $\nu_s(\text{C}'\text{C}''), 11 \rho(\text{CH}_2')$	1057 B	29 $\nu_s(\text{C}_\alpha\text{C}'), 36 \nu_s(\text{C}'\text{C}^*), 13 \rho(\text{CH}_2)$
		1025 A	11 $\nu_s(\text{C}_\alpha\text{C}'), 18 \nu_s(\text{C}'\text{C}''), 13 \rho(\text{CH}_2'), 11 \rho(\text{CH}_2''), 11 \rho(\text{C13C12H24})$	1031 B	17 $\nu_s(\text{C}_\alpha\text{C}'), 13 \rho(\text{CCH}), 16 \rho(\text{CH}_2), 10 \tau(\text{CH}_2')$
		1015 A	16 $\nu_s(\text{C}_\alpha\text{C}'), 11 \rho(\text{CH}_2^\wedge), 14 \nu_s(\text{C}'\text{C}''), \delta_{ip,s}(\text{ND})$	1007 A	14 $\nu_s(\text{C}_\alpha\text{C}'), 12 \delta_{ip}(\text{ND}), 24 \rho(\text{CH}_2')$
984		990 A	25 $\nu_s(\text{C}_\alpha\text{C}^*), 19 \delta_{ip,s}(\text{ND})$	961 B	35 $\nu_s(\text{C}'\text{C}^*), 10 \rho(\text{CCH}), 15 \rho(\text{CH}_2)$
	974				
960		965 A	22 $\nu_s(\text{C}^*\text{C}^\wedge), 17 \rho(\text{C9C8H19}), 25 \rho(\text{CH}_2^*)$	960 A	36 $\nu_s(\text{C}_\alpha\text{C}'), 10 \rho(\text{CCH}), 19 \rho(\text{CH}_2)$

		945 A	16 $\nu_s(\text{C}_\alpha\text{C}')$, 15 $\nu_s(\text{C}^*\text{C}^\wedge)$, 26 $\delta_{\text{ip}}(\text{Ring-3})$	935 B	21 $\nu_s(\text{NC}_\alpha)$, 30 $\delta_{\text{ip}}(\text{ND})$, 11 $\rho(\text{CH}_2)$
	921	927 A	10 $\nu_s(\text{N-CO})$, 11 $\nu_s(\text{CC}_\alpha)$, 12 $\nu_s(\text{C}_\alpha\text{C}^*)$, 38 $\delta_{\text{ip},s}(\text{ND})$	920 A	18 $\nu_s(\text{NC}_\alpha)$, 49 $\delta_{\text{ip}}(\text{ND})$, 10 $\rho(\text{CH}_2)$
901	903				
879	881	873 A	27 $\rho(\text{CH}_2^\wedge)$, 10 $\nu_s(\text{NC}_\alpha)$, 14 $\delta_{\text{ip},as}(\text{ND})$, 12 $\delta_{\text{ip}}(\text{Ring-3})$	895 B	29 $\rho(\text{CH}_2')$, 35 $\delta_{\text{ip}}(\text{Ring-3})$
	834				
820		819 A	14 $\rho(\text{CH}_2'')$	857 A	12 $\nu_s(\text{C}_\alpha\text{C}')$, 12 $\nu_s(\text{N-CO})$, 28 $\rho(\text{CH}_2')$, 10 $\delta(\text{CSH})$
789					
	769	764 A	19 $\delta_{\text{ip},as}(\text{ND})$, 11 $\rho(\text{CH}_2')$, 15 $\rho(\text{CH}_2'')$	773 B	13 $\rho(\text{CH}_2)$, 16 $\rho(\text{CH}_2')$, 11 $\delta(\text{CSH})$, 27 $\delta_{\text{ip}}(\text{Ring-3})$
		752 A	30 $\delta_{\text{op}}(\text{C7=O3})$, 11 $\rho(\text{CH}_2^*)$	744 A	13 $\rho(\text{CH}_2)$, 57 $\delta_{\text{op}}(\text{C=O})$
734		734 A	12 $\delta_{\text{op}}(\text{C11=O4})$, 12 $\rho(\text{CH}_2')$, 19 $\delta_{\text{ip}}(\text{Ring-3})$	744 B	12 $\nu_s(\text{C}_\alpha\text{C}')$, 15 $\delta_{\text{ip}}(\text{ND})$, 10 $\rho(\text{CH}_2)$, 37 $\delta_{\text{op}}(\text{C=O})$
	729	724 A	44 $\nu_s(\text{C}''\text{S2})$, 15 $\delta_{\text{op}}(\text{C7=O3})$	711 A	14 $\nu_s(\text{N-CO})$, 12 $\delta_{\text{ip}}(\text{C=O})$, 10 $\delta(\text{CSD})$, 13 $\delta_{\text{op}}(\text{C=O})$
		702 A	10 $\nu_s(\text{C}^\wedge\text{S1})$, 46 $\delta_{\text{op}}(\text{C11=O4})$	697 B	19 $\nu_s(\text{CC}_\alpha)$, 12 $\nu_s(\text{C}_\alpha\text{C}')$, 12 $\delta_{\text{ip}}(\text{ND})$, 36 $\delta_{\text{op}}(\text{C=O})$, 40 $\rho(\text{CH}_2')$
672	675	674 A	16 $\delta(\text{C}^\wedge\text{S1D15})$, 16 $\nu_s(\text{C}^\wedge\text{S1})$, 11 $\delta_{\text{op}}(\text{C7=O3})$	651 A	80 $\nu_s(\text{CS})$
657 639		654 A	21 $\nu_s(\text{C}^\wedge\text{S1})$, 11 $\delta_{\text{op}}(\text{C7=O3})$	648 B	77 $\nu_s(\text{CS})$
		609 A	16 $\rho(\text{CH}_2'')$, 72 $\delta(\text{C}''\text{S2D16})$	605 A	16 $\rho(\text{CH}_2')$, 52 $\delta(\text{CSD})$
609	605	603 A	35 $\nu_s(\text{C}^\wedge\text{S1})$, 41 $\delta(\text{C}^\wedge\text{S1D15})$	600 B	16 $\rho(\text{CH}_2')$, 52 $\delta(\text{CSD})$
		599 A	15 $\nu_s(\text{CC}_\alpha)$, 31 $\delta_{\text{ip}}(\text{C7=O3})$, 11 $\delta(\text{C}^\wedge\text{S1D15})$	588 A	30 $\nu_s(\text{CC}_\alpha)$, 10 $\delta_{\text{ip}}(\text{C=O})$, 18 $\delta(\text{CSD})$
		503 A	12 $\delta_{\text{ip}}(\text{C7=O3})$, 26 $\delta_{\text{ip}}(\text{Ring-1})$, 17 $\delta_{\text{op}}(\text{N5D17})$	487 A	16 $\delta_{\text{ip}}(\text{C=O})$, 15 $\rho(\text{CCH})$, 23 $\delta_{\text{ip}}(\text{Ring-1})$, 23 $\delta_{\text{op}}(\text{ND})$
465		468 A	18 $\delta(\text{C8C}^\wedge\text{C}^*)$, 18 $\delta_{\text{op}}(\text{N5D17})$	461 B	20 $\delta(\text{C}_\alpha\text{C}^*\text{C}^*)$, 15 $\delta(\text{C}^*\text{C}^*\text{S})$, 26 $\delta_{\text{op}}(\text{ND})$
	448	458 A	13 $\delta_{\text{ip}}(\text{Ring-1})$, 14 $\delta_{\text{ip}}(\text{Ring-2})$, 12 $\delta_{\text{op}}(\text{N5D17})$	444 A	19 $\delta_{\text{ip}}(\text{C=O})$, 57 $\delta_{\text{ip}}(\text{Ring-2})$
	511	440 A	11 $\nu_s(\text{NC}_\alpha)$, 53 $\delta_{\text{ip}}(\text{Ring-2})$	424 A	28 $\delta_{\text{ip}}(\text{Ring-1})$, 11 $\delta_{\text{ip}}(\text{Ring-1})$, 55 $\delta_{\text{op}}(\text{ND})$
577		423 A	58 $\delta_{\text{op}}(\text{N6D18})$	417 B	18 $\delta_{\text{ip}}(\text{C=O})$, 49 $\delta_{\text{op}}(\text{ND})$
		399 A	26 $\delta_{\text{ip}}(\text{C11=O4})$, 25 $\delta_{\text{op}}(\text{N6D18})$	411 A	22 $\delta(\text{C}_\alpha\text{C}^*\text{C}^*)$, 33 $\delta(\text{C}^*\text{C}^*\text{S})$, 10 $\delta_{\text{op}}(\text{ND})$
		385 A	20 $\delta(\text{C}^*\text{C}^\wedge\text{S1})$, 22 $\delta_{\text{op}}(\text{N5D17})$, 12 $\delta_{\text{ip}}(\text{C11=O4})$	392 B	14 $\nu_s(\text{NC}_\alpha)$, 43 $\delta_{\text{ip}}(\text{C=O})$, 14 $\delta_{\text{op}}(\text{ND})$
		350 A	12 $\rho(\text{C9C8H19})$, 20 $\delta_{\text{op}}(\text{N5D17})$, $\delta_{\text{op}}(\text{Ring-2})$, 11 $\delta(\text{C}^*\text{C}^\wedge\text{S1})$	338 B	27 $\rho(\text{CCH})$, 16 $\delta(\text{C}_\alpha\text{C}^*\text{C}^*)$
	314	284 A	11 $\omega(\text{C13C12H24})$, 18 $\tau(\text{C13C12H24})$, 42 $\delta(\text{C}^*\text{C}''\text{S2})$	298 A	27 $\rho(\text{CCH})$, 13 $\delta(\text{C}_\alpha\text{C}^*\text{C}^*)$, 29 $\delta_{\text{op}}(\text{Ring-2})$
	245	240 A	11 $\nu_s(\text{C}''\text{S2})$, 26 $\delta(\text{C12C}^*\text{C}''')$	282 B	13 $\tau(\text{CCH})$, 30 $\delta(\text{C}^*\text{C}^*\text{S})$, 10 $\tau(\text{C}^*\text{C}^*)$, 12 $\tau(\text{C}_\alpha\text{C}')$
		217 A	14 $\delta(\text{C8C}^\wedge\text{C}^*)$, 20 $\delta(\text{C8C}^\wedge\text{C}^*)$,	270 A	14 $\tau(\text{CCH})$, 25 $\delta(\text{C}^*\text{C}^*\text{S})$,

			17 $\tau(\text{C}^*\text{C}^\wedge)$		11 $\tau(\text{C}'\text{C}^*)$
	201	196 A	14 $\omega(\text{C9C8H19})$, 26 $\tau(\text{C}^\wedge\text{S1})$, 20 $\tau(\text{C9C8H19})$	229 A	93 $\tau(\text{CS})$
		165 A	87 $\tau(\text{C}''\text{S2})$	227 B	97 $\tau(\text{CS})$
		151 A	18 $\delta(\text{C8C}^\wedge\text{C}^*)$, 55 $\tau(\text{C}^\wedge\text{S1})$	188 B	27 $\tau(\text{CCH})$, 18 $\omega(\text{CCH})$, 26 $\delta(\text{C}_\alpha\text{C}'\text{C}^*)$
		124 A	28 $\delta_{\text{op}}(\text{Ring-1})$, 19 $\tau(\text{C}'\text{C}''')$	186 A	17 $\tau(\text{CCH})$, 14 $\omega(\text{CCH})$, 14 $\delta(\text{C}_\alpha\text{C}'\text{C}^*)$
		109 A	11 $\delta_{\text{op}}(\text{Ring-2})$, 12 $\tau(\text{C}^*\text{C}^\wedge)$, 10 $\delta(\text{C12C}'\text{C}''')$, 16 $\delta_{\text{op}}(\text{Ring-1})$	125 B	13 $\delta(\text{C}'\text{C}^*\text{S})$, 29 $\delta_{\text{op}}(\text{Ring-1})$, 38 $\tau(\text{C}'\text{C}^*)$
	117	101 A	11 $\delta_{\text{op}}(\text{Ring-2})$, 15 $\tau(\text{C}^*\text{C}^\wedge)$, 12 $\tau(\text{C}'\text{C}''')$	101 A	18 $\delta(\text{C}_\alpha\text{C}'\text{C}^*)$, 19 $\delta(\text{C}'\text{C}^*\text{S})$, 14 $\tau(\text{C}_\alpha\text{C}')$, 27 $\tau(\text{C}'\text{C}^*)$
	96	79 A	24 $\delta_{\text{op}}(\text{Ring-2})$, 42 $\tau(\text{C12C}')$, 18 $\tau(\text{C}'\text{C}''')$	76 A	100 $\delta_{\text{op}}(\text{Ring-2})$
		68 A	43 $\delta_{\text{op}}(\text{Ring-2})$, 17 $\delta_{\text{op}}(\text{Ring-1})$, 20 $\tau(\text{C12C}')$, 10 $\tau(\text{C}'\text{C}''')$	66 B	76 $\delta_{\text{op}}(\text{Ring-1})$, 21 $\tau(\text{C}'\text{C}^*)$
		50 A	14 $\delta_{\text{op}}(\text{Ring-2})$, 12 $\tau(\text{C}^*\text{C}^\wedge)$, 33 $\delta_{\text{op}}(\text{Ring-1})$, 20 $\tau(\text{C}'\text{C}''')$	48 A	48 $\tau(\text{C}_\alpha\text{C}')$, 41 $\tau(\text{C}'\text{C}^*)$
		28 A	64 $\tau(\text{C8C}^*)$, 23 $\tau(\text{C}^*\text{C}^\wedge)$	33 B	77 $\tau(\text{C}_\alpha\text{C}')$, 18 $\tau(\text{C}'\text{C}^*)$
		20 A	81 $\delta_{\text{op}}(\text{Ring-3})$	26 A	84 $\delta_{\text{op}}(\text{Ring-3})$, 17 $\tau(\text{C}_\alpha\text{C}')$

NB= C'= 9,13 and C* = 10,14 for C₂ symmetry; C* = C9, C[^] = C10, C' = C13, C'' = C14 for C₁ symmetry (Fig. 4.2).

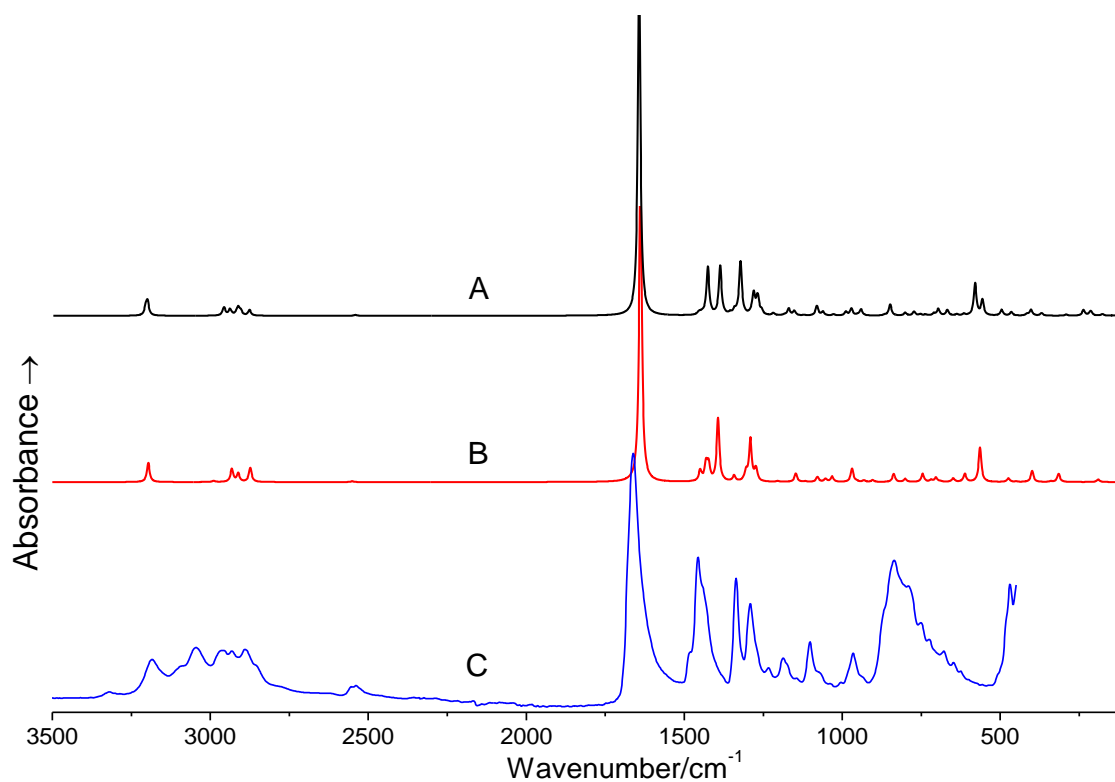


Figure 4.6. Calculated (A=C₁ symmetry, B=C₂ symmetry molecules) and experimental (C) IR spectra for C-CySH.

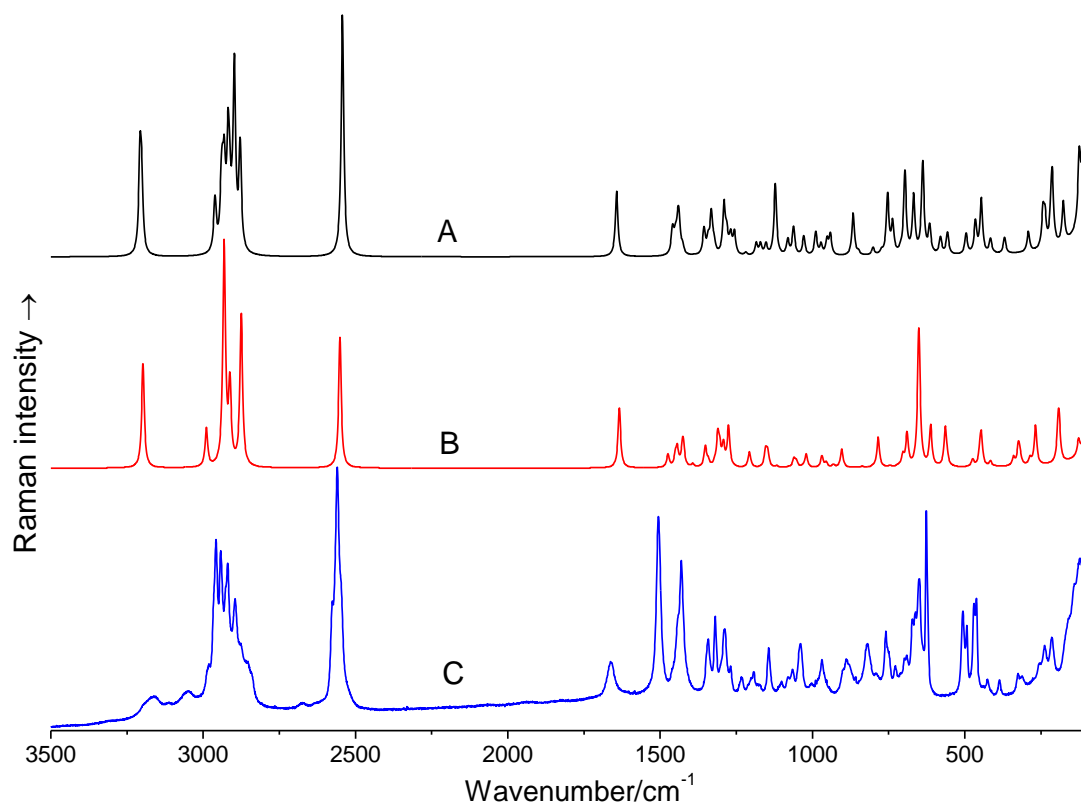


Figure 4.7. Calculated (A= C_1 symmetry, B= C_2 symmetry molecules) and experimental (C) Raman spectra for C-CySH.

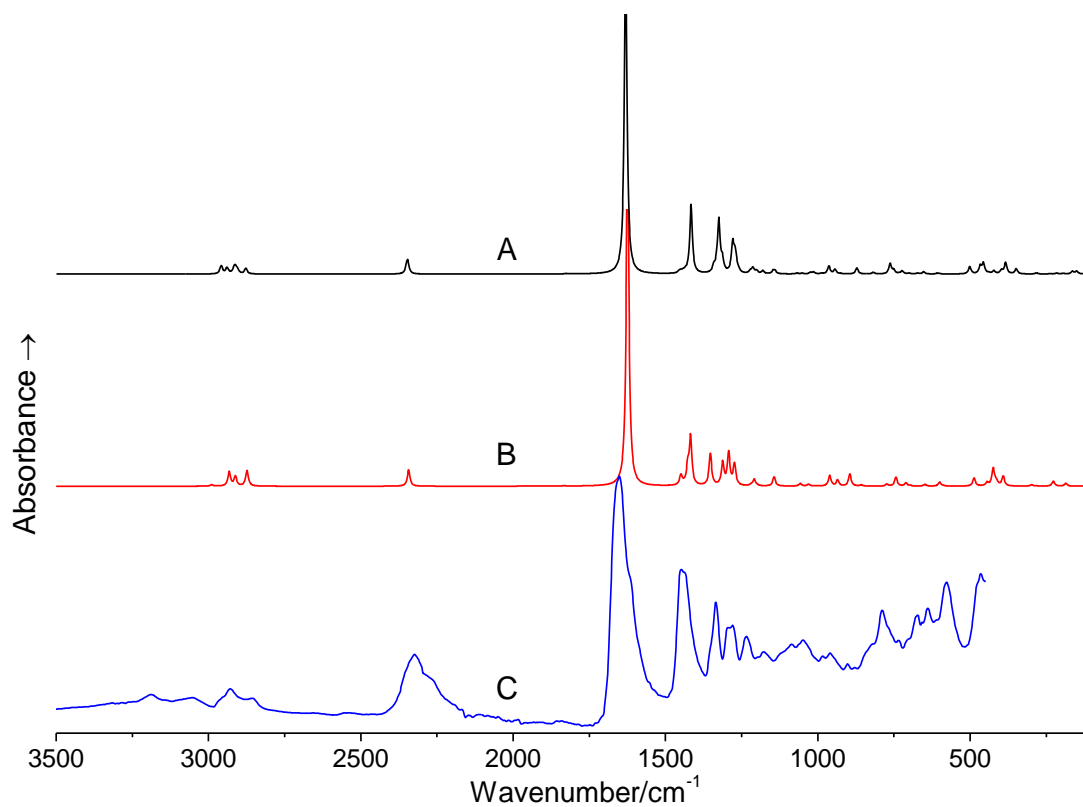


Figure 4.8. Calculated (A= C_1 symmetry, B= C_2 symmetry molecules) and experimental (C) IR spectra for *N,S*-deuterated C-CySH.

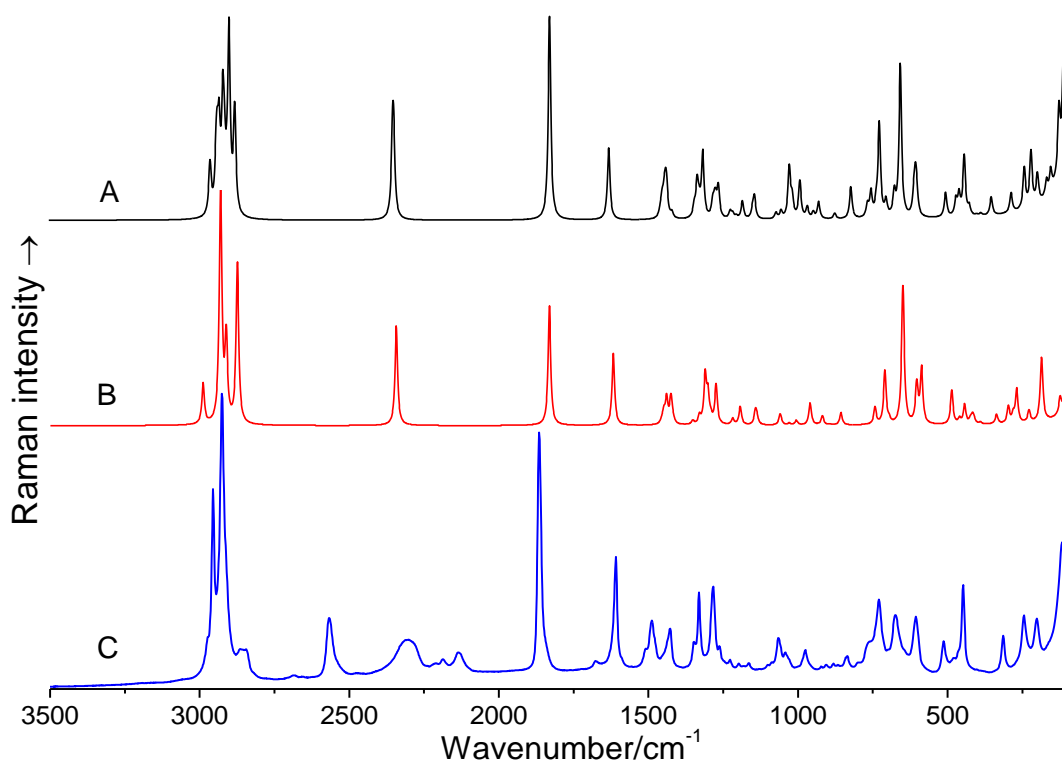


Figure 4.9. Calculated (A= C_1 symmetry, B= C_2 symmetry molecules) and experimental (C) Raman spectra for *N,S*-deuterated C-CySH.

4.4. Molecular orbital analysis

The highest occupied molecular orbital (HOMO) and lowest unoccupied molecular orbital (LUMO) energies of C-CySH (both C_1 and C_2 molecules) were calculated by DFT at the B3LYP/aug-cc-pVTZ level of theory, using Gaussian 09 software. The HOMO energies of C_1 and C_2 are -6.951 eV and -6.763 eV whereas, the LUMO energies are -0.802 eV and -0.711 eV, respectively. The composition of HOMO and LUMO are shown in Figs. 4.10 and 4.11. The analysis of molecular orbitals of C_1 and C_2 show that the HOMO is localized on the sulphur and carbon atoms of the side-chains, partly on the oxygen and nitrogen atoms of the DKP ring whereas the LUMO is localized on the DKP ring and partly on the side-chains. The computed HOMO-LUMO energy gap of C-CySH corresponds to 6.149 eV (C_1) and 6.052 eV (C_2). All the HOMO and LUMO have nodes. The nodes in each HOMO and LUMO are placed symmetrically (in the case of C_2 molecule). The positive phase is red and the negative is green. Since the HOMO-LUMO gap value is relatively large, it is therefore expected that both C_1 and C_2 molecules of C-CySH are less reactive, less polarizable, and chemically relatively stable molecules.

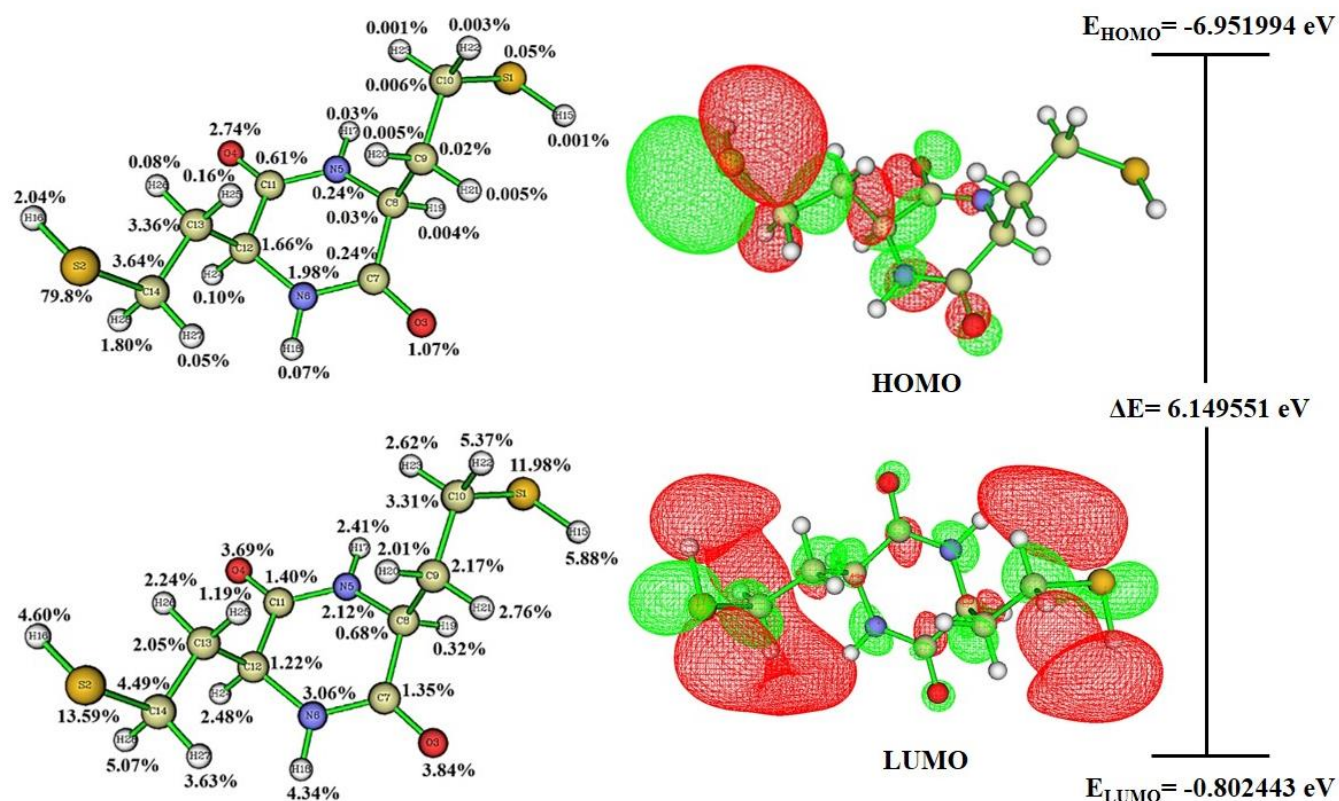


Figure 4.10. HOMO-LUMO plots with orbital composition of the C₁ molecule of C-CySH.

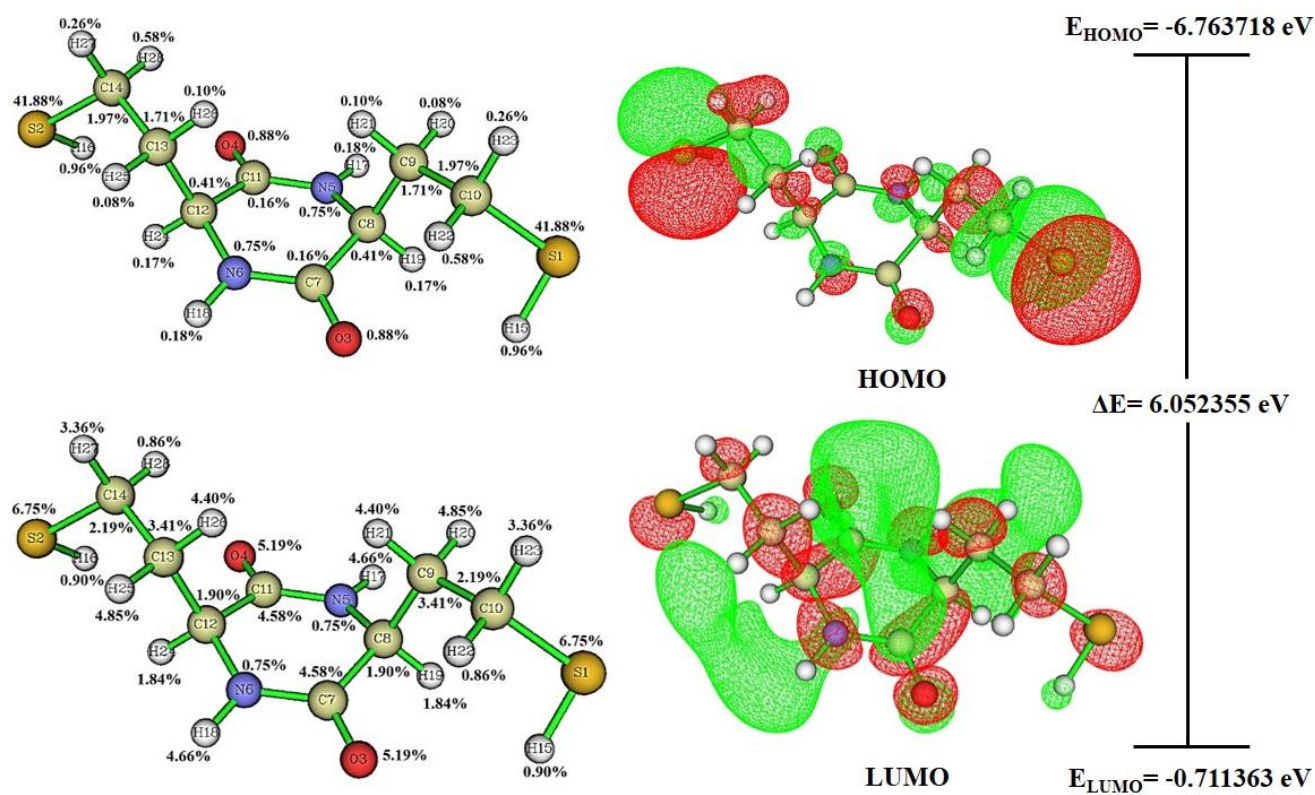


Figure 4.11. HOMO-LUMO plots with orbital compositions of the C₂ molecule for C-CySH.

4.5. Hirshfeld surface analysis

The Hirshfeld surfaces of molecules A, B, and C of C-CySH are illustrated in Fig. 4.12 showing the mapped surface over d_{norm} , curvedness and shape index in Fig. 4.13. The interaction between carboxyl oxygen and amide hydrogen atoms of the DKP ring (C=O--H-N) in all three asymmetric molecules of C-CySH can be seen as the bright red areas on the Hirshfeld surface (Fig. 4.12, labelled as a). The light red spots are due to C-H--O interactions between CH₂ groups on the L-homoCySH side-chains and oxygen atoms of the DKP ring (Fig. 4.12, labelled as b), and other visible red spots on the surface correspond to C_αH--O and S--H/H--S contacts (Fig. 4.12, labelled as c and d). The H--H and O--H intermolecular interactions appear as separate spikes in the 2D fingerprint plot (Fig. 4.13). Corresponding regions are visible in the fingerprint plots where one molecule act as an acceptor ($d_e < d_i$) and other acts as a donor ($d_e > d_i$). The two small broad spikes pointing toward the lower left of the plots are due to H--H hydrogen interactions, encompassing 43% (A), 43.8% (B) and 38.4% (C) of the total Hirshfeld surfaces for each molecule of C-CySH. The $(d_e + d_i)$ for H--H interactions is around 2.3Å. The S--H interactions can be easily located at the around the corners, resembles as “wings” on the 2D fingerprint plot (Fig. 4.14). They comprise about 13.1% (A), 22.2% (B) and 17% (C) of the total Hirshfeld surface with a high $(d_e + d_i)$ value of 2.9Å. The two sharp peaks pointing towards the left corner are due to O--H interactions (~11.8%) in all three molecules. The shortest contact i.e., the minimum $(d_e + d_i)$ value is around 1.8Å shows the importance of these interactions. From the fingerprint plots, the contributions involving different interactions include S--O/S/C atoms, N--H and C--O comprises around 4.5% of the total Hirshfeld surface area for the three asymmetric C-CySH molecules in a unit cell. Curvedness and shape indices can also be used to identify the ways by which neighbouring molecules contact each other and the characteristic packing modes. The shape index of C-CySH shows a red concave region on the surface around the acceptor atom and a blue region around the donor H-atom (Fig. 4.13a). Curvedness is a function of the RMS curvature of the surface and the curvedness maps on the Hirshfeld surface show no flat surface patches which indicates that there is no stacking interaction in the C-CySH molecules (Fig. 4.13b).

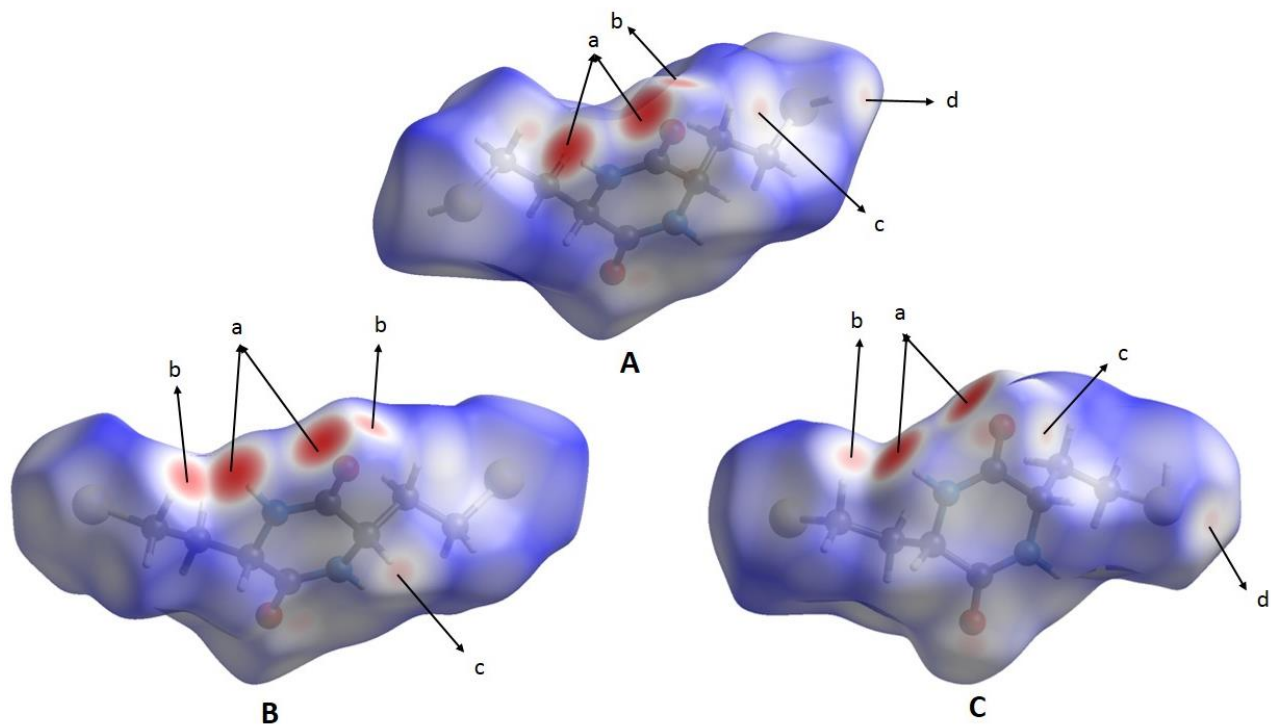


Figure 4.12. Hirshfeld surface mapped with d_{norm} as transparent to visualize the orientation of the three asymmetric molecules of C-CySH.

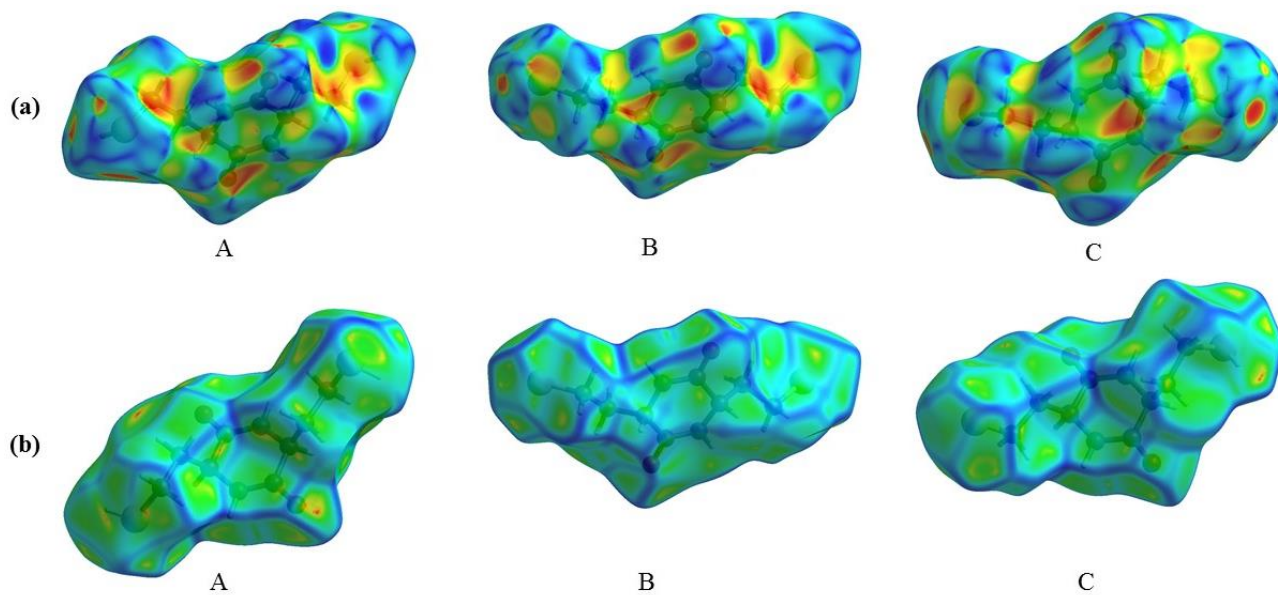


Figure 4.13. Hirshfeld surfaces for the three molecules (A, B and C) of C-CySH mapped with (a) shape index (b) curvedness.

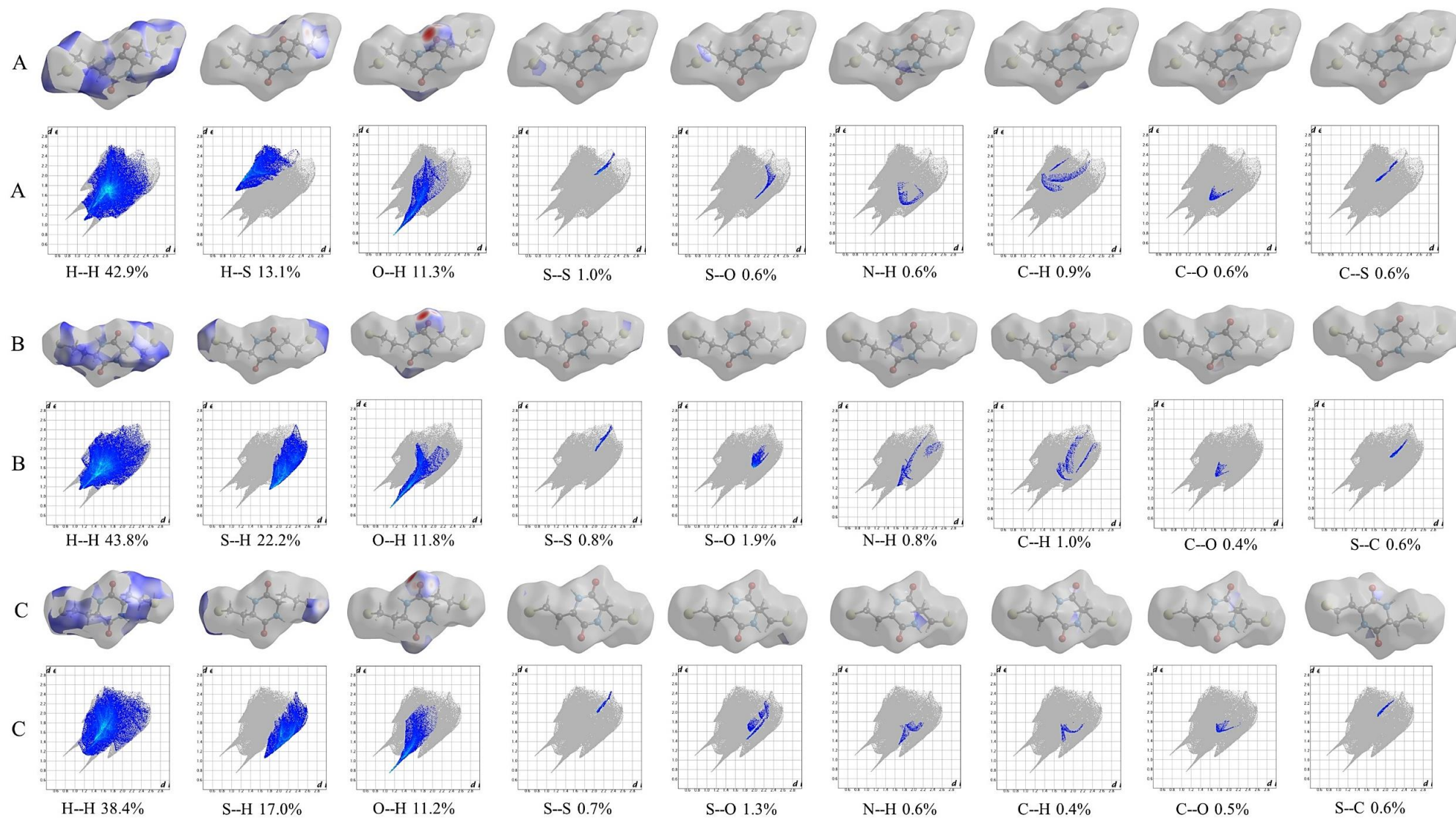


Figure 4.14. 2D Fingerprint plots for the intermolecular contacts in molecules **A**, **B** and **C** of C-CySH.

4.6. Conclusions

Vibrational spectroscopy of cyclo-L-homoCySH (C-CySH), supported by DFT calculations of isolated molecules, has provided an insight into the molecular geometry in the solid state. Energy profile calculations were carried out at the HF/3-21G level for the conformational analysis of the L-homoCySH side-chains on the DKP ring, in the gas phase, assuming an idealised C_2 symmetry. DFT calculations were then carried out at the B3LYP/aug-cc-pVTZ level, using initial geometries from the HF/3-21G calculations, leading to a minimum energy optimised structure of C_2 symmetry whose energy (-1369.93615495 H) is only 2.172 kJ mol⁻¹ lower than that of the asymmetric structure (C_1 symmetry) favoured in the solid state (-1369.93532731 H). However, in both cases (C_1 and C_2 symmetry) the molecule slightly deviates from planarity (degree of folding, $\beta=21.8^\circ$ (C_1) and 23° (C_2)) towards a boat conformer with the two L-homoCySH side chain folded above the ring. The assignments of the amide I and II modes and the nature of the amide vibrations of the *cis* peptide groups in C-CySH have been confirmed by the spectroscopic data and DFT calculations. Differing ring conformations can have a dramatic influence on the location of the *cis* amide II vibration and the signal detected at 1506 cm⁻¹ is similar to the previous observations for cyclo(L-Ala-L-Ala) where the *cis* amide II was found at ~ 1508 cm⁻¹. Hence, it is suggested that the location of the amide II mode plays a crucial role in determining which conformer the DKP ring adopts in the solid state. However, the increase in the strain on the DKP ring due to the attachment of bulky substituents on the C_α atoms may also influence the location of the amide II mode. HOMO and LUMO analysis has been carried out to elucidate the information related to the charge transfer within the molecule. The computed HOMO-LUMO energy gap of C-CySH corresponds to 6.149 eV (C_1) and 6.052 eV (C_2), which implies that both molecules of C-CySH possesses relatively high chemical stability. The Hirshfeld surface analysis and 2D fingerprint plots show the types of intermolecular interactions present in the crystal structure of C-CySH.

Table 4.5. Definitions of symmetry-adapted internal coordinates for C-CySH.

C-CySH- C₂

A symmetry

$$v_s(\text{NH})=1/\sqrt{2}[r(\text{N5H17}) + r(\text{N6H18})]$$

$$v_s(\text{CO})=1/\sqrt{2}[r(\text{C11O4}) + r(\text{C7O3})]$$

$$v_s(\text{NC})=1/\sqrt{2}[r(\text{N5C11}) + r(\text{N6C7})]$$

$$v_s(\text{NC}_\alpha)=1/\sqrt{2}[r(\text{N5C8}) + r(\text{N6C12})]$$

$$v_s(\text{CC}_\alpha)=1/\sqrt{2}[r(\text{C11C12}) + r(\text{C7C8})]$$

$$v_s(\text{C}_\alpha\text{C}')=1/\sqrt{2}[r(\text{C8C9}) + r(\text{C12C13})]$$

$$v_s(\text{C}'\text{C}^*)=1/\sqrt{2}[r(\text{C9C10}) + r(\text{C13C14})]$$

$$v_s(\text{CS})=1/\sqrt{2}[r(\text{C10S1}) + r(\text{C14S2})]$$

$$v_s(\text{SH})=1/\sqrt{2}[r(\text{S1H15}) + r(\text{S2H16})]$$

$$v_s(\text{CH})=1/\sqrt{2}[r(\text{C8H19}) + r(\text{C12H24})]$$

$$v_s(\text{CH}_2)=1/2[r(\text{C9H20}) + r(\text{C9H21})+ r(\text{C13H25}) + r(\text{C13H26})]$$

$$v_{as}(\text{CH}_2)=1/2[r(\text{C9H20}) - r(\text{C9H21})+ r(\text{C13H25}) - r(\text{C13H26})]$$

$$v_s(\text{CH}_2')=1/2[r(\text{C10H22}) + r(\text{C10H22})+ r(\text{C14H27}) + r(\text{C14H28})]$$

$$v_{as}(\text{CH}_2')=1/2[r(\text{C10H22}) - r(\text{C10H22})+ r(\text{C14H27}) - r(\text{C14H28})]$$

$$\delta_{ip}(\text{NH})=1/2[\theta(\text{C8N5H17}) - \theta(\text{C11N5H17}) + \theta(\text{C12N6H18}) - \theta(\text{C7N6H18})]$$

$$\delta_{ip}(\text{CO})=1/2[\theta(\text{N5C11O4}) - \theta(\text{C12C11O4}) + \theta(\text{N6C7O3}) - \theta(\text{C8C7O3})]$$

$$\delta(\text{CH}_2)=1/4\sqrt{3}[(\sqrt{6} + 2)\theta(\text{H20C9H21}) - (\sqrt{6} - 2)\theta(\text{C8C9C10}) - \theta(\text{C8C9H20}) - \theta(\text{C8C9H21}) - \theta(\text{C10C9H20}) - \theta(\text{C10C921})+ (\sqrt{6} + 2)\theta(\text{H25C13H26}) - (\sqrt{6} - 2)\theta(\text{C128C13C14}) - \theta(\text{C12C13H25}) - \theta(\text{C12C13H26}) - \theta(\text{C14C13H25}) - \theta(\text{C14C13H26})]$$

$$\rho(\text{CH}_2)=1/2\sqrt{2}[\theta(\text{C8C9H20}) - \theta(\text{C8C9H21}) + \theta(\text{C10C9H20}) - \theta(\text{C10C921})+ \theta(\text{C12C13H25}) - \theta(\text{C12C13H26}) + \theta(\text{C14C13H25}) - \theta(\text{C14C13H26})]$$

$$\omega(\text{CH}_2)=1/2\sqrt{2}[\theta(\text{C8C9H20}) + \theta(\text{C8C9H21}) - \theta(\text{C10C9H20}) - \theta(\text{C10C921})+ \theta(\text{C12C13H25})+ \theta(\text{C12C13H26}) - \theta(\text{C14C13H25}) - \theta(\text{C14C13H26})]$$

$$\tau(\text{CH}_2)=1/2\sqrt{2}[\theta(\text{C8C9H20}) - \theta(\text{C8C9H21}) - \theta(\text{C10C9H20}) + \theta(\text{C10C921})+ \theta(\text{C12C13H25}) - \theta(\text{C12C13H26}) - \theta(\text{C14C13H25}) + \theta(\text{C14C13H26})]$$

$$\delta(\text{CH}_2')=1/4\sqrt{3}[(\sqrt{6} + 2)\theta(\text{H22C10H23}) - (\sqrt{6} - 2)\theta(\text{C9C10S1}) - \theta(\text{C9C10H22}) - \theta(\text{C9C10H23}) - \theta(\text{S1C10H22}) - \theta(\text{S1C10H23})+ (\sqrt{6} + 2)\theta(\text{H27C14H28})]$$

$$\begin{aligned}
& -(\sqrt{6}-2)\theta(\text{C13C14S2}) - \theta(\text{C13C14H27}) - \theta(\text{C13C14H28}) - \theta(\text{S2C14H27}) - \theta(\text{S2C14H28})] \\
\rho(\text{CH}_2') &= 1/2\sqrt{2}[\theta(\text{C9C10H22}) - \theta(\text{C9C10H23}) + \theta(\text{S1C10H22}) - \theta(\text{S1C10H23}) + \theta(\text{C13C14H27}) - \theta(\text{C13C14H28}) + \theta(\text{S2C14H27}) - \theta(\text{S2C14H28})] \\
\omega(\text{CH}_2') &= 1/2\sqrt{2}[\theta(\text{C9C10H22}) + \theta(\text{C9C10H23}) - \theta(\text{S1C10H22}) - \theta(\text{S1C10H23}) + \theta(\text{C13C14H27}) + \theta(\text{C13C14H28}) - \theta(\text{S2C14H27}) - \theta(\text{S2C14H28})] \\
\tau(\text{CH}_2') &= 1/2\sqrt{2}[\theta(\text{C9C10H22}) - \theta(\text{C9C10H23}) - \theta(\text{S1C10H22}) + \theta(\text{S1C10H23}) + \theta(\text{C13C14H27}) - \theta(\text{C13C14H28}) - \theta(\text{S2C14H27}) + \theta(\text{S2C14H28})] \\
\rho(\text{CCH}) &= 1/2\sqrt{2}[(\theta(\text{N5C8H19}) - \theta(\text{N5C8C9}) + \theta(\text{C7C8H19}) - \theta(\text{C7C8C9}) + (\theta(\text{N6C12H24}) - \theta(\text{N6C12C13}) + \theta(\text{C11C12H24}) - \theta(\text{C11C12C13}))] \\
\omega(\text{CCH}) &= 1/2\sqrt{2}[(\theta(\text{N5C8H19}) + \theta(\text{N5C8C9}) - \theta(\text{C7C8H19}) - \theta(\text{C7C8C9}) + (\theta(\text{N6C12H24}) + \theta(\text{N6C12C13}) - \theta(\text{C11C12H24}) - \theta(\text{C11C12C13}))] \\
\tau(\text{CCH}) &= 1/2\sqrt{2}[(\theta(\text{N5C8H19}) - \theta(\text{N5C8C9}) - \theta(\text{C7C8H19}) + \theta(\text{C7C8C9}) + (\theta(\text{N6C12H24}) - \theta(\text{N6C12C13}) - \theta(\text{C11C12H24}) + \theta(\text{C11C12C13}))] \\
\delta(\text{CCH}) &= 1/\sqrt{2}[\theta(\text{C9C8H19}) + \theta(\text{C13C12H24})] \\
\delta_{\text{op}}(\text{CO}) &= 1/\sqrt{2}[\tau(\text{O4C11N5C12}) + \tau(\text{O3C7N6C8})] \\
\delta_{\text{op}}(\text{NH}) &= 1/\sqrt{2}[\tau(\text{H17N5C11C8}) + \tau(\text{H18N6C7C12})] \\
\delta(\text{C}_\alpha\text{C}'\text{C}^*) &= 1/4\sqrt{3}[(-\sqrt{6}-2)\theta(\text{H20C9H21}) + (\sqrt{6}+2)\theta(\text{C8C9C10}) - \theta(\text{C8C9H20}) - \theta(\text{C8C9H21}) - \theta(\text{C10C9H20}) - \theta(\text{C10C9H21}) - (\sqrt{6}-2)\theta(\text{H25C13H26}) \\
& \quad + (\sqrt{6}+2)\theta(\text{C128C13C14}) - \theta(\text{C12C13H25}) - \theta(\text{C12C13H26}) - \theta(\text{C14C13H25}) - \theta(\text{C14C13H26})] \\
\delta(\text{C}'\text{C}^*\text{S}) &= 1/4\sqrt{3}[(-\sqrt{6}-2)\theta(\text{H22C10H23}) + (\sqrt{6}+2)\theta(\text{C9C10S1}) - \theta(\text{C9C10H22}) - \theta(\text{C9C10H23}) - \theta(\text{S1C10H22}) - \theta(\text{S1C10H23}) - (\sqrt{6}-2)\theta(\text{H27C14H28}) \\
& \quad + (\sqrt{6}+2)\theta(\text{C13C14S2}) - \theta(\text{C13C14H27}) - \theta(\text{C13C14H28}) - \theta(\text{S2C14H27}) - \theta(\text{S2C14H28})] \\
\tau(\text{C}_\alpha\text{C}') &= 1/3\sqrt{2}[\tau(\text{H19C8C9C10}) + \tau(\text{H19C8C9H20}) + \tau(\text{H19C8C9H21}) + \tau(\text{N5C8C9C10}) + \tau(\text{N5C8C9H20}) + \tau(\text{N5C8C9H21}) + \tau(\text{C7C8C9C10}) + \tau(\text{C7C8C9H20}) \\
& \quad + \tau(\text{C7C8C9H21}) + \tau(\text{H24C12C13C14}) + \tau(\text{H24C12C13H25}) + \tau(\text{H24C12C13H26}) + \tau(\text{N6C12C13C14}) + \tau(\text{N6C12C13H25}) + \tau(\text{N6C12C13H26}) \\
& \quad + \tau(\text{C11C12C13C14}) + \tau(\text{C11C12C13H25}) + \tau(\text{C11C12C13H26})] \\
\tau(\text{C}'\text{C}^*) &= 1/3\sqrt{2}[\tau(\text{C8C9C10S1}) + \tau(\text{C8C9C10H22}) + \tau(\text{C8C9C10H23}) + \tau(\text{H20C9C10H22}) + \tau(\text{H20C9C10H23}) + \tau(\text{H20C9C10S1}) + \tau(\text{H21C9C10H22}) \\
& \quad + \tau(\text{H21C9C10H23}) + \tau(\text{H21C9C10S1}) + \tau(\text{C12C13C14S2}) + \tau(\text{C12C13C14H27}) + \tau(\text{C12C13C14H28}) + \tau(\text{H25C13C14H27}) + \tau(\text{H25C13C14H28}) \\
& \quad + \tau(\text{H25C13C14S2}) + \tau(\text{H26C13C14S2}) + \tau(\text{H26C13C14H27}) + \tau(\text{H26C13C14H28})] \\
\tau(\text{C}^*\text{S1}) &= 1/\sqrt{6}[\tau(\text{C9C10S1H15}) + \tau(\text{H22C10S1H15}) + \tau(\text{H23C10S1H15}) + \tau(\text{C13C14S2H16}) + \tau(\text{H27C14S2H16}) + \tau(\text{H28C14S2H16})] \\
\delta(\text{C}^*\text{SH}) &= 1/\sqrt{2}[\theta(\text{C10S1H15}) + \theta(\text{C14S2H16})] \\
\delta_{\text{ip}}(\text{Ring-1}) &= 1/\sqrt{2}[2\theta(\text{C7C8N5}) - \theta(\text{C8N5C11}) - \theta(\text{N5C11C12}) + 2\theta(\text{C11C12N6}) - \theta(\text{C12N6C7}) - \theta(\text{N6C7C8})] \\
\delta_{\text{ip}}(\text{Ring-2}) &= 1/2[\theta(\text{C8N5C11}) - \theta(\text{N5C11C12}) + \theta(\text{C12N6C7}) - \theta(\text{N6C7C8})] \\
\delta_{\text{op}}(\text{Ring-2}) &= 1/\sqrt{2}[2\tau(\text{C12C11N5C8}) - \tau(\text{C11N5C8C7}) - \tau(\text{N5C8C7N6}) + 2\tau(\text{C8C7N6C12}) - \tau(\text{C7N6C12C11}) - \tau(\text{N6C12C11N5})] \\
\delta_{\text{op}}(\text{Ring-3}) &= 1/2[\tau(\text{C11N5C8C7}) - \tau(\text{N5C8C7N6}) + \tau(\text{C7N6C12C11}) - \tau(\text{N6C12C11N5})]
\end{aligned}$$

B symmetry

$$v_{as}(NH)=1/\sqrt{2}[r(N5H17) - r(N6H18)]$$

$$v_{as}(CO)=1/\sqrt{2}[r(C11O4) - r(C7O3)]$$

$$v_{as}(NC)=1/\sqrt{2}[r(N5C11) - r(N6C7)]$$

$$v_{as}(NC_{\alpha})=1/\sqrt{2}[r(N5C8) - r(N6C12)]$$

$$v_{as}(CC_{\alpha})=1/\sqrt{2}[r(C11C12) - r(C7C8)]$$

$$v_{as}(C_{\alpha}C')=1/\sqrt{2}[r(C8C9) - r(C12C13)]$$

$$v_{as}(C'C^*)=1/\sqrt{2}[r(C9C10) - r(C13C14)]$$

$$v_{as}(CS)=1/\sqrt{2}[r(C10S1) - r(C14S2)]$$

$$v_{as}(SH)=1/\sqrt{2}[r(S1H15) - r(S2H16)]$$

$$v_{as}(CH)=1/\sqrt{2}[r(C8H19) - r(C12H24)]$$

$$v_s(CH_2)=1/2[r(C9H20) + r(C9H21) - r(C13H25) - r(C13H26)]$$

$$v_{as}(CH_2)=1/2[r(C9H20) - r(C9H21) - r(C13H25) + r(C13H26)]$$

$$v_s(CH_2')=1/2[r(C10H22) + r(C10H23) - r(C14H27) - r(C14H28)]$$

$$v_{as}(CH_2')=1/2[r(C10H22) - r(C10H23) - r(C14H27) + r(C14H28)]$$

$$\delta_{ip}(NH)=1/2[\theta(C8N5H17) - \theta(C11N5H17) - \theta(C12N6H18) + \theta(C7N6H18)]$$

$$\delta_{ip}(CO)=1/2[\theta(N5C11O4) - \theta(C12C11O4) - \theta(N6C7O3) + \theta(C8C7O3)]$$

$$\delta(CH_2)=1/2\sqrt{3}[(\sqrt{6} + 2)\theta(H20C9H21) - (\sqrt{6} - 2)\theta(C8C9C10) - \theta(C8C9H20) - \theta(C8C9H21) - \theta(C10C9H20) - \theta(C10C921) - (\sqrt{6} + 2)\theta(H25C13H26) + (\sqrt{6} - 2)\theta(C128C13C14) + \theta(C12C13H25) + \theta(C12C13H26) + \theta(C14C13H25) + \theta(C14C13H26)]$$

$$\rho(CH_2)=1/2\sqrt{2}[\theta(C8C9H20) - \theta(C8C9H21) + \theta(C10C9H20) - \theta(C10C921) - \theta(C12C13H25) + \theta(C12C13H26) - \theta(C14C13H25) + \theta(C14C13H26)]$$

$$\omega(CH_2)=1/2\sqrt{2}[\theta(C8C9H20) + \theta(C8C9H21) - \theta(C10C9H20) - \theta(C10C921) - \theta(C12C13H25) - \theta(C12C13H26) + \theta(C14C13H25) + \theta(C14C13H26)]$$

$$\tau(CH_2)=1/2\sqrt{2}[\theta(C8C9H20) - \theta(C8C9H21) - \theta(C10C9H20) + \theta(C10C921) - \theta(C12C13H25) + \theta(C12C13H26) + \theta(C14C13H25) - \theta(C14C13H26)]$$

$$\delta(CH_2')=1/4\sqrt{3}[(\sqrt{6} + 2)\theta(H22C10H23) - (\sqrt{6} - 2)\theta(C9C10S1) - \theta(C9C10H22) - \theta(C9C10H23) - \theta(S1C10H22) - \theta(S1C10H23) - (\sqrt{6} + 2)\theta(H27C14H28) + (\sqrt{6} - 2)\theta(C13C14S2) + \theta(C13C14H27) + \theta(C13C14H28) + \theta(S2C14H27) + \theta(S2C14H28)]$$

$$\rho(CH_2')=1/2\sqrt{2}[\theta(C9C10H22) - \theta(C9C10H23) + \theta(S1C10H22) - \theta(S1C10H23) - \theta(C13C14H27) + \theta(C13C14H28) - \theta(S2C14H27) + \theta(S2C14H28)]$$

$$\omega(CH_2')=1/2\sqrt{2}[\theta(C9C10H22) + \theta(C9C10H23) - \theta(S1C10H22) - \theta(S1C10H23) - \theta(C13C14H27) - \theta(C13C14H28) + \theta(S2C14H27) + \theta(S2C14H28)]$$

$$\begin{aligned}
\tau(\text{CH}_2') &= 1/2\sqrt{2}[\theta(\text{C9C10H22}) - \theta(\text{C9C10H23}) - \theta(\text{S1C10H22}) + \theta(\text{S1C10H23}) - \theta(\text{C13C14H27}) + \theta(\text{C13C14H28}) + \theta(\text{S2C14H27}) - \theta(\text{S2C14H28})] \\
\rho(\text{CCH}) &= 1/2\sqrt{2}[(\theta(\text{N5C8H19}) - \theta(\text{N5C8C9}) + \theta(\text{C7C8H19}) - \theta(\text{C7C8C9}) - (\theta(\text{N6C12H24}) + \theta(\text{N6C12C13}) - \theta(\text{C11C12H24}) + \theta(\text{C11C12C13}))] \\
\omega(\text{CCH}) &= 1/2\sqrt{2}[(\theta(\text{N5C8H19}) + \theta(\text{N5C8C9}) - \theta(\text{C7C8H19}) - \theta(\text{C7C8C9}) - (\theta(\text{N6C12H24}) - \theta(\text{N6C12C13}) + \theta(\text{C11C12H24}) + \theta(\text{C11C12C13}))] \\
\tau(\text{CCH}) &= 1/2\sqrt{2}[(\theta(\text{N5C8H19}) - \theta(\text{N5C8C9}) - \theta(\text{C7C8H19}) + \theta(\text{C7C8C9}) - (\theta(\text{N6C12H24}) + \theta(\text{N6C12C13}) + \theta(\text{C11C12H24}) - \theta(\text{C11C12C13}))] \\
\delta(\text{CCH}) &= 1/\sqrt{2}[\theta(\text{C9C8H19}) - \theta(\text{C13C12H24})] \\
\delta_{\text{op}}(\text{CO}) &= 1/\sqrt{2}[\tau(\text{O4C11N5C12}) - \tau(\text{O3C7N6C8})] \\
\delta_{\text{op}}(\text{NH}) &= 1/\sqrt{2}[\tau(\text{H17N5C11C8}) - \tau(\text{H18N6C7C12})] \\
\delta(\text{C}_\alpha\text{C}'\text{C}^*) &= 1/4\sqrt{3}[(-\sqrt{6} - 2)\theta(\text{H20C9H21}) + (\sqrt{6} + 2)\theta(\text{C8C9C10}) - \theta(\text{C8C9H20}) - \theta(\text{C8C9H21}) - \theta(\text{C10C9H20}) - \theta(\text{C10C9H21}) + (\sqrt{6} - 2)\theta(\text{H25C13H26}) \\
&\quad - (\sqrt{6} + 2)\theta(\text{C128C13C14}) + \theta(\text{C12C13H25}) + \theta(\text{C12C13H26}) + \theta(\text{C14C13H25}) + \theta(\text{C14C13H26})] \\
\delta(\text{C}'\text{C}^*\text{S}) &= 1/4\sqrt{3}[(-\sqrt{6} - 2)\theta(\text{H22C10H23}) + (\sqrt{6} + 2)\theta(\text{C9C10S1}) - \theta(\text{C9C10H22}) - \theta(\text{C9C10H23}) - \theta(\text{S1C10H22}) - \theta(\text{S1C10H23}) + (\sqrt{6} - 2)\theta(\text{H27C14H28}) \\
&\quad - (\sqrt{6} + 2)\theta(\text{C13C14S2}) + \theta(\text{C13C14H27}) + \theta(\text{C13C14H28}) + \theta(\text{S2C14H27}) + \theta(\text{S2C14H28})] \\
\tau(\text{C}_\alpha\text{C}') &= 1/3\sqrt{2}[\tau(\text{H19C8C9C10}) + \tau(\text{H19C8C9H20}) + \tau(\text{H19C8C9H21}) + \tau(\text{N5C8C9C10}) + \tau(\text{N5C8C9H20}) + \tau(\text{N5C8C9H21}) + \tau(\text{C7C8C9C10}) + \tau(\text{C7C8C9H20}) \\
&\quad + \tau(\text{C7C8C9H21}) - \tau(\text{H24C12C13C14}) - \tau(\text{H24C12C13H25}) - \tau(\text{H24C12C13H26}) - \tau(\text{N6C12C13C14}) - \tau(\text{N6C12C13H25}) - \tau(\text{N6C12C13H26}) \\
&\quad - \tau(\text{C11C12C13C14}) - \tau(\text{C11C12C13H25}) - \tau(\text{C11C12C13H26})] \\
\tau(\text{C}'\text{C}^*) &= 1/3\sqrt{2}[\tau(\text{C8C9C10S1}) + \tau(\text{C8C9C10H22}) + \tau(\text{C8C9C10H23}) + \tau(\text{H20C9C10H22}) + \tau(\text{H20C9C10H23}) + \tau(\text{H20C9C10S1}) + \tau(\text{H21C9C10H22}) \\
&\quad + \tau(\text{H21C9C10H23}) + \tau(\text{H21C9C10S1}) - \tau(\text{C12C13C14S2}) - \tau(\text{C12C13C14H27}) - \tau(\text{C12C13C14H28}) - \tau(\text{H25C13C14H27}) - \tau(\text{H25C13C14H28}) \\
&\quad - \tau(\text{H25C13C14S2}) - \tau(\text{H26C13C14S2}) - \tau(\text{H26C13C14H27}) - \tau(\text{H26C13C14H28})] \\
\tau(\text{C}^*\text{S1}) &= 1/\sqrt{6}[\tau(\text{C9C10S1H15}) + \tau(\text{H22C10S1H15}) + \tau(\text{H23C10S1H15}) - \tau(\text{C13C14S2H16}) - \tau(\text{H27C14S2H16}) - \tau(\text{H28C14S2H16})] \\
\delta(\text{C}^*\text{SH}) &= 1/\sqrt{2}[\theta(\text{C10S1H15}) - \theta(\text{C14S2H16})] \\
\delta_{\text{ip}}(\text{Ring-3}) &= 1/\sqrt{6}[\theta(\text{C7C8N5}) - \theta(\text{C8N5C11}) + \theta(\text{N5C11C12}) - \theta(\text{C11C12N6}) + \theta(\text{C12N6C7}) - \theta(\text{N6C7C8})] \\
\delta_{\text{op}}(\text{Ring-1}) &= 1/\sqrt{6}[\tau(\text{C12C11N5C8}) - \tau(\text{C11N5C8C7}) + \tau(\text{N5C8C7N6}) - \tau(\text{C8C7N6C12}) + \tau(\text{C7N6C12C11}) - \tau(\text{N6C12C11N5})]
\end{aligned}$$

N.B. C' = 9 and 13, C* = 10 and 14

C-CySH- C1

$$v_s(\text{N5H17}) = r(\text{N5H17})$$

$$v_s(\text{N6H18}) = r(\text{N6H18})$$

$$v_s(\text{C11=O4}) = r(\text{C11O4})$$

$$v_s(\text{C7=O3}) = r(\text{C7O3})$$

$$v_s(\text{NC}) = 1/\sqrt{2}[r(\text{N5C11}) + r(\text{N6C7})]$$

$$v_{as}(\text{NC}) = 1/\sqrt{2}[r(\text{N5C11}) - r(\text{N6C7})]$$

$$v_s(\text{NC}_\alpha) = 1/\sqrt{2}[r(\text{N5C8}) + r(\text{N6C12})]$$

$$v_{as}(\text{NC}_\alpha) = 1/\sqrt{2}[r(\text{N5C8}) - r(\text{N6C12})]$$

$$v_s(\text{CC}_\alpha) = 1/\sqrt{2}[r(\text{C11C12}) + r(\text{C7C8})]$$

$$v_{as}(\text{CC}_\alpha) = 1/\sqrt{2}[r(\text{C11C12}) - r(\text{C7C8})]$$

$$v_s(\text{C}_\alpha\text{C}') = r(\text{C12C13})$$

$$v_s(\text{C}_\alpha\text{C}^*) = r(\text{C8C9})$$

$$v_s(\text{C}^*\text{C}^\wedge) = r(\text{C9C10})$$

$$v_s(\text{C8H19}) = r(\text{C8H19})$$

$$v_s(\text{C12H24}) = r(\text{C12H24})$$

$$v_s(\text{S1H15}) = r(\text{S1H15})$$

$$v_s(\text{S2H16}) = r(\text{S2H16})$$

$$v_s(\text{C}'\text{C}'') = r(\text{C13C14})$$

$$v_s(\text{C}^\wedge\text{S1}) = r(\text{C10S1})$$

$$v_s(\text{C}^*\text{S2}) = r(\text{C14S2})$$

$$v_s(\text{CH}_2^*) = 1/\sqrt{2}[r(\text{C9H20}) + r(\text{C9H21})]$$

$$v_{as}(\text{CH}_2^*) = 1/\sqrt{2}[r(\text{C9H20}) - r(\text{C9H21})]$$

$$v_s(\text{CH}_2') = 1/\sqrt{2}[r(\text{C13H25}) + r(\text{C13H26})]$$

$$v_{as}(\text{CH}_2') = 1/\sqrt{2}[r(\text{C13H25}) - r(\text{C13H26})]$$

$$v_s(\text{CH}_2^\wedge) = 1/\sqrt{2}[r(\text{C10H22}) + r(\text{C10H22})]$$

$$\begin{aligned}
v_{as}(\text{CH}_2^\wedge) &= 1/\sqrt{2}[r(\text{C10H22}) - r(\text{C10H22})] \\
v_s(\text{CH}_2'') &= 1/\sqrt{2}[r(\text{C14H27}) + r(\text{C14H28})] \\
v_{as}(\text{CH}_2'') &= 1/\sqrt{2}[r(\text{C14H27}) - r(\text{C14H28})] \\
\delta_{ip,s}(\text{NH}) &= 1/2[\theta(\text{C8N5H17}) - \theta(\text{C11N5H17}) + \theta(\text{C12N6H18}) - \theta(\text{C7N6H18})] \\
\delta_{ip,as}(\text{NH}) &= 1/2[\theta(\text{C8N5H17}) - \theta(\text{C11N5H17}) - \theta(\text{C12N6H18}) + \theta(\text{C7N6H18})] \\
\delta_{ip}(\text{C11=O4}) &= 1/\sqrt{2}[\theta(\text{N5C11O4}) - \theta(\text{C12C11O4})] \\
\delta_{ip}(\text{C7=O3}) &= 1/\sqrt{2}[\theta(\text{N6C7O3}) - \theta(\text{C8C7O3})] \\
\delta_{op}(\text{N5H17}) &= \tau(\text{H17N5C11C8}) \\
\delta_{op}(\text{N6H18}) &= \tau(\text{H18N6C7C12}) \\
\delta_{op}(\text{C11=O4}) &= \tau(\text{O4C11N5C12}) \\
\delta_{op}(\text{C7=O3}) &= \tau(\text{O3C7N6C8}) \\
\delta(\text{CH}_2^*) &= 1/2\sqrt{6}[(\sqrt{6} + 2)\theta(\text{H20C9H21}) - (\sqrt{6} - 2)\theta(\text{C8C9C10}) - \theta(\text{C8C9H20}) - \theta(\text{C8C9H21}) - \theta(\text{C10C9H20}) - \theta(\text{C10C921})] \\
\rho(\text{CH}_2^*) &= 1/2[\theta(\text{C8C9H20}) - \theta(\text{C8C9H21}) + \theta(\text{C10C9H20}) - \theta(\text{C10C921})] \\
\omega(\text{CH}_2^*) &= 1/2[\theta(\text{C8C9H20}) + \theta(\text{C8C9H21}) - \theta(\text{C10C9H20}) - \theta(\text{C10C921})] \\
\tau(\text{CH}_2^*) &= 1/2[\theta(\text{C8C9H20}) - \theta(\text{C8C9H21}) - \theta(\text{C10C9H20}) + \theta(\text{C10C921})] \\
\delta(\text{CH}_2') &= 1/2\sqrt{6}[(\sqrt{6} + 2)\theta(\text{H25C13H26}) - (\sqrt{6} - 2)\theta(\text{C12C13C14}) - \theta(\text{C12C13H25}) - \theta(\text{C12C13H26}) - \theta(\text{C14C13H25}) - \theta(\text{C14C13H26})] \\
\rho(\text{CH}_2') &= 1/2[\theta(\text{C12C13H25}) - \theta(\text{C12C13H26}) + \theta(\text{C14C13H25}) - \theta(\text{C14C13H26})] \\
\omega(\text{CH}_2') &= 1/2[\theta(\text{C12C13H25}) + \theta(\text{C12C13H26}) - \theta(\text{C14C13H25}) - \theta(\text{C14C13H26})] \\
\tau(\text{CH}_2') &= 1/2[\theta(\text{C12C13H25}) - \theta(\text{C12C13H26}) - \theta(\text{C14C13H25}) + \theta(\text{C14C13H26})] \\
\delta(\text{CH}_2^\wedge) &= 1/2\sqrt{6}[(\sqrt{6} + 2)\theta(\text{H22C10H23}) - (\sqrt{6} - 2)\theta(\text{C9C10S1}) - \theta(\text{C9C10H22}) - \theta(\text{C9C10H23}) - \theta(\text{S1C10H22}) - \theta(\text{S1C10H23})] \\
\rho(\text{CH}_2^\wedge) &= 1/2[\theta(\text{C9C10H22}) - \theta(\text{C9C10H23}) + \theta(\text{S1C10H22}) - \theta(\text{S1C10H23})] \\
\omega(\text{CH}_2^\wedge) &= 1/2[\theta(\text{C9C10H22}) + \theta(\text{C9C10H23}) - \theta(\text{S1C10H22}) - \theta(\text{S1C10H23})] \\
\tau(\text{CH}_2^\wedge) &= 1/2[\theta(\text{C9C10H22}) - \theta(\text{C9C10H23}) - \theta(\text{S1C10H22}) + \theta(\text{S1C10H23})] \\
\delta(\text{CH}_2'') &= 1/2\sqrt{6}[(\sqrt{6} + 2)\theta(\text{H27C14H28}) - (\sqrt{6} - 2)\theta(\text{C13C14S2}) - \theta(\text{C13C14H27}) - \theta(\text{C13C14H28}) - \theta(\text{S2C14H27}) - \theta(\text{S2C14H28})] \\
\rho(\text{CH}_2'') &= 1/2[\theta(\text{C13C14H27}) - \theta(\text{C13C14H28}) + \theta(\text{S2C14H27}) - \theta(\text{S2C14H28})] \\
\omega(\text{CH}_2'') &= 1/2[\theta(\text{C13C14H27}) + \theta(\text{C13C14H28}) - \theta(\text{S2C14H27}) - \theta(\text{S2C14H28})]
\end{aligned}$$

$$\begin{aligned}
\tau(\text{CH}_2'') &= 1/2[\theta(\text{C13C14H27}) - \theta(\text{C13C14H28}) - \theta(\text{S2C14H27}) + \theta(\text{S2C14H28})] \\
\rho(\text{C9C8H19}) &= 1/2[(\theta(\text{N5C8H19}) - \theta(\text{N5C8C9}) + \theta(\text{C7C8H19}) - \theta(\text{C7C8C9})) \\
\omega(\text{C9C8H19}) &= 1/2[(\theta(\text{N5C8H19}) + \theta(\text{N5C8C9}) - \theta(\text{C7C8H19}) - \theta(\text{C7C8C9}))] \\
\tau(\text{C9C8H19}) &= 1/2[(\theta(\text{N5C8H19}) - \theta(\text{N5C8C9}) - \theta(\text{C7C8H19}) + \theta(\text{C7C8C9}))] \\
\delta(\text{C9C8H19}) &= \theta(\text{C9C8H19}) \\
\rho(\text{C13C12H24}) &= 1/2[\theta(\text{N6C12H24}) - \theta(\text{N6C12C13}) + \theta(\text{C11C12H24}) - \theta(\text{C11C12C13})] \\
\omega(\text{C13C12H24}) &= 1/2[\theta(\text{N6C12H24}) + \theta(\text{N6C12C13}) - \theta(\text{C11C12H24}) - \theta(\text{C11C12C13})] \\
\tau(\text{C13C12H24}) &= 1/2[(\theta(\text{N6C12H24}) - \theta(\text{N6C12C13}) - \theta(\text{C11C12H24}) + \theta(\text{C11C12C13}))] \\
\delta(\text{C13C12H24}) &= \theta(\text{C13C12H24}) \\
\delta(\text{C8C}^*\text{C}^\wedge) &= 1/2\sqrt{6}[-(\sqrt{6} - 2)\theta(\text{H20C9H21}) + (\sqrt{6} + 2)\theta(\text{C8C9C10}) - \theta(\text{C8C9H20}) - \theta(\text{C8C9H21}) - \theta(\text{C10C9H20}) - \theta(\text{C10C921})] \\
\delta(\text{C}^*\text{C}^\wedge\text{S1}) &= 1/2\sqrt{6}[-(\sqrt{6} - 2)\theta(\text{H22C10H23}) + (\sqrt{6} + 2)\theta(\text{C9C10S1}) - \theta(\text{C9C10H22}) - \theta(\text{C9C10H23}) - \theta(\text{S1C10H22}) - \theta(\text{S1C10H23})] \\
\tau(\text{C8C}^*) &= 1/3[\tau(\text{H19C8C9C10}) + \tau(\text{H19C8C9H20}) + \tau(\text{H19C8C9H21}) + \tau(\text{N5C8C9C10}) + \tau(\text{N5C8C9H20}) + \tau(\text{N5C8C9H21}) + \tau(\text{C7C8C9C10}) + \tau(\text{C7C8C9H20}) \\
&\quad + \tau(\text{C7C8C9H21})] \\
\tau(\text{C}^*\text{C}^\wedge) &= 1/3[\tau(\text{C8C9C10S1}) + \tau(\text{C8C9C10H22}) + \tau(\text{C8C9C10H23}) + \tau(\text{H20C9C10H22}) + \tau(\text{H20C9C10H23}) + \tau(\text{H20C9C10S1}) + \tau(\text{H21C9C10H22}) \\
&\quad + \tau(\text{H21C9C10H23}) + \tau(\text{H21C9C10S1})] \\
\tau(\text{C}^\wedge\text{S1}) &= 1/\sqrt{3}[\tau(\text{C9C10S1H15}) + \tau(\text{H22C10S1H15}) + \tau(\text{H23C10S1H15})] \\
\delta(\text{C}^\wedge\text{S1H15}) &= \theta(\text{C10S1H15}) \\
\delta(\text{C12C}'\text{C}'') &= 1/2\sqrt{6}[-(\sqrt{6} - 2)\theta(\text{H25C13H26}) + (\sqrt{6} + 2)\theta(\text{C128C13C14}) - \theta(\text{C12C13H25}) - \theta(\text{C12C13H26}) - \theta(\text{C14C13H25}) - \theta(\text{C14C13H26})] \\
\delta(\text{C}'\text{C}''\text{S2}) &= 1/2\sqrt{6}[-(\sqrt{6} - 2)\theta(\text{H27C14H28}) + (\sqrt{6} + 2)\theta(\text{C13C14S2}) - \theta(\text{C13C14H27}) - \theta(\text{C13C14H28}) - \theta(\text{S2C14H27}) - \theta(\text{S2C14H28})] \\
\tau(\text{C12C}') &= 1/3[\tau(\text{H24C12C13C14}) + \tau(\text{H24C12C13H25}) + \tau(\text{H24C12C13H26}) + \tau(\text{N6C12C13C14}) + \tau(\text{N6C12C13H25}) + \tau(\text{N6C12C13H26}) \\
&\quad + \tau(\text{C11C12C13C14}) + \tau(\text{C11C12C13H25}) + \tau(\text{C11C12C13H26})] \\
\tau(\text{C}'\text{C}'') &= 1/3[\tau(\text{C12C13C14S2}) + \tau(\text{C12C13C14H27}) + \tau(\text{C12C13C14H28}) + \tau(\text{H25C13C14H27}) + \tau(\text{H25C13C14H28}) \\
&\quad + \tau(\text{H25C13C14S2}) + \tau(\text{H26C13C14S2}) + \tau(\text{H26C13C14H27}) + \tau(\text{H26C13C14H28})] \\
\tau(\text{C}''\text{S2}) &= 1/\sqrt{3}[\tau(\text{C13C14S2H16}) + \tau(\text{H27C14S2H16}) + \tau(\text{H28C14S2H16})] \\
\delta(\text{C}''\text{S2H16}) &= \theta(\text{C14S2H16}) \\
\delta_{ip}(\text{Ring-1}) &= 1/\sqrt{12}[2\theta(\text{C7C8N5}) - \theta(\text{C8N5C11}) - \theta(\text{N5C11C12}) + 2\theta(\text{C11C12N6}) - \theta(\text{C12N6C7}) - \theta(\text{N6C7C8})]
\end{aligned}$$

$$\delta_{ip}(\text{Ring-2}) = 1/2[\theta(\text{C8N5C11}) - \theta(\text{N5C11C12}) + \theta(\text{C12N6C7}) - \theta(\text{N6C7C8})]$$

$$\delta_{ip}(\text{Ring-3}) = 1/\sqrt{6}[\theta(\text{C7C8N5}) - \theta(\text{C8N5C11}) + \theta(\text{N5C11C12}) - \theta(\text{C11C12N6}) + \theta(\text{C12N6C7}) - \theta(\text{N6C7C8})]$$

$$\delta_{op}(\text{Ring-1}) = 1/\sqrt{6}[\tau(\text{C12C11N5C8}) - \tau(\text{C11N5C8C7}) + \tau(\text{N5C8C7N6}) - \tau(\text{C8C7N6C12}) + \tau(\text{C7N6C12C11}) - \tau(\text{N6C12C11N5})]$$

$$\delta_{op}(\text{Ring-2}) = 1/\sqrt{12}[2\tau(\text{C12C11N5C8}) - \tau(\text{C11N5C8C7}) - \tau(\text{N5C8C7N6}) + 2\tau(\text{C8C7N6C12}) - \tau(\text{C7N6C12C11}) - \tau(\text{N6C12C11N5})]$$

$$\delta_{op}(\text{Ring-3}) = 1/2[\tau(\text{C11N5C8C7}) - \tau(\text{N5C8C7N6}) + \tau(\text{C7N6C12C11}) - \tau(\text{N6C12C11N5})]$$

N.B- C* = C9, C^ = C10, C' = C13, C'' = C14

4.7. References

1. K. M. Reece, E. D. Richardson, K. M. Cook, T. J. Campbell, S. T. Pisle, A. J. Holly, D. J. Venzon, D. J. Liewehr, C. H. Chau, D. K. Price, W. D Figg, *Mol. Cancer.*, 2014, 13.
2. A. K. Szardenings, V. Antonenko, D. A. Campbell, N. DeFrancisco, S. Ida, L. Shi, N. Sharkov, D. Tien, Y. Wang, M. Navreet., *J. Med. Chem.*, 1999, 42, 1348.
3. A. Taylor, *Microb. Toxin*, 1971, 7, 337.
4. M. T. Holden, S. R. Chhabra, R. de Nys, P. Stead, N. J. Bainton, P. J. Hill, M. Manefield, N. Kumar, M. Labatte, D. England, S. Rice, M. Givskov, G. P. Salmond, G. S. Stewart, B. W. Bycroft, S. Kjelleberg, P. Williams, *Mol. Microbiol.*, 1999, 33, 1254.
5. J. C. M. Monbaliu, F. K. Hansen, L. K. Beagle, M. J. Panzner, P. J. Steel, E. Todadze, C.V. Stevens, A. R. Katritzky, *Chem. Eur. J.*, 2012, 18, 2632.
6. M. Ottnad, P. Hartter, G. Jung, *Hoppe-Seyler's Z. Physiol. Chem.*, 1975, 356, 1011.
7. K. I. Varughese, G. Kartha, *Int. J. Pept. Protein Res.*, 1981, 18, 88.
8. S. Capasso, C. Mattia, L. Mazzarella, R. Puliti, *Acta Crystallogr. Section B.*, 1977, 33, 2080.
9. D. B. Boyd, *J. Am. Chem. Soc.*, 1972, 94, 8799.
10. D. B. Boyd, *J. Phys. Chem.*, 1974, 78, 1554.
11. R. Rahman, S. Safe, A. Taylor, *J. Chem. Soc.*, 1969, 1665.
12. A. R. Gregory, M. Przybylska, *J. Am. Chem. Soc.*, 1978, 100, 943.
13. A. P. Mendham, J. Spencer, M. Mujahid, R. A. Palmer, G. J. Tizzard, T. J. Dines, S. J. Coles, B. Z. Chowdhry, *J. Chem. Crystallogr.*, 2011, 41, 1328.
14. V. du Vigneaud, Wilbur I. Patterson, Madison Hunt, *J. Biol. Chem.*, 1938, 126, 217.
15. Spartan'14 for Windows. Wavefunction, Inc; Irvine, CA, USA: 2013.
16. A. P. Mendham, R. A. Palmer, B. S. Potter, T. J. Dines, J. C. Mitchell, R. Withnall, B. Z. Chowdhry, *J. Raman Spectrosc.*, 2010, 41, 148.
17. D. B. Davies, Md. A. Khaled, *J. Chem. Soc., Perkin Trans.*, 1975, 2, 1238.
18. T. C. Cheam, S. Krimm, *Spectrochim. Acta*, 1984, 40A, 481.
19. A. P. Mendham, T. J. Dines, M. J. Snowden, R. Withnall, B. Z. Chowdhry, *J. Raman Spectrosc.*, 2009, 40, 1478.
20. T. C. Cheam, S. Krimm, *Spectrochim. Acta*, 1988, 44A, 182.

Chapter 5: Experimental and Theoretical Vibrational Spectroscopic Studies of the Degradation products of D-cycloserine

5.1. Introduction

Our interest in the chemistry and biological properties of D-cycloserine (CS) and its derivatives has led us to investigate the physico-chemical properties of the degradation products of CS. CS (D-4-amino-3-isoxazolidone, D-oxamycin and seromycin) is naturally produced by certain strains of *Streptomyces lavendulus*, *Streptomyces garyphalus* and *Streptomyces orchidaceus*.¹ It is well known for its biological activity against a majority of Gram-positive and Gram-negative bacteria and is clinically used as an effective second-line antibiotic against *Mycobacterium tuberculosis* in the treatment of tuberculosis.² In addition, studies have shown that CS is effective in treating cognitive illnesses, such as depression, schizophrenia and Alzheimer's disease.³ From a pharmacological perspective it acts as an antagonist to D-alanine, by inhibiting the enzymes D-alanine racemase and D-alanyl-D-alanine synthetase, thereby blocking the formation of D-alanine which leads to the destruction of the bacterial cell wall.⁴ It also acts as a partial agonist to the glycine recognition site of *N*-methyl-D-aspartate (NMDA) receptors and thus facilitates control of psychiatric disorders.⁵ In bacteria it hinders the formation of cell wall peptidoglycan by blocking the enzyme alanine racemase for the biosynthesis of uridine diphosphate (UDP)-*N*-acetylmuramyl-pentapeptide.⁶ The products formed from CS are also of importance in exhibiting potent biological activities.⁷ The CS dimer has been reported to be at least as effective as CS in inhibiting microbial growth,⁸ and also inhibiting aspartate and other aminotransferases.^{9,10} Under a humid atmosphere CS dimerises to form 3,6-*bis*(aminoxymethyl)-piperazine-2,5-dione.¹¹ (AMDKP, Fig 5.1a).

X-ray crystallographic studies have been used to show that CS monohydrate exists in zwitterionic, ionic CS.H₂O-I and non-ionic CS.H₂O-II forms. The evidence suggests that in both solution and solid states the non-ionic CS.H₂O molecule is responsible for the dimerisation due to nucleophilic attack from the α -amino group of one CS molecule to the carbonyl group of another CS molecule.¹² A kinetic study of the acid-catalysed hydrolysis of AMDKP indicates that the aminoxy groups in the side-chain undergo facile mutarotation in aqueous acid resulting in hydrolytic cleavage of the CS-dimer ring which leads to the formation of a peptide intermediate, β -aminoxy-D-alanyl- β -aminoxy-D-alanine.¹³ However, reaction of the CS-dimer with aqueous base forms 3,6-dimethylene-piperazine-2,5-dione (DMDKP, Fig. 5.1b).

The $^1\text{H-NMR}$, IR and Raman bands of AMDKP in the solid and solution states have been reported.^{11,12,14} CS-monohydrate undergoes dimerization in the presence of water molecules in the solid state.¹² As a function of time, under an applied saturated water vapour pressure, the IR bands at 1580 and 1406 cm^{-1} of CS.H₂O decrease in intensity and new characteristic bands which are identical for the AMDKP appear in a time-span of ~354 hours. In the solution state, CS is converted to the CS-dimer and the equilibrium between CS and the CS-dimer is pH dependent. In 5 % D₂O solution at a pD 6.2, the characteristic band at 1580 cm^{-1} in CS.H₂O-I decreases in intensity and new bands appear at 1650, 1464 and 1342 cm^{-1} as a function of time. These bands coincide with those of the CS-dimer in D₂O solution. This spectral change indicates the conversion of CS to CS-dimer in the solution state.¹¹ The rate of dimerization was enhanced when 50 % methanol was used as a solvent.

No detailed vibrational spectroscopic studies have yet been reported for the degradation products of D-cycloserine. Hence, the IR and Raman spectra of AMDKP (solid state and aqueous solution) and DMDKP (solid state only). Vibrational assignments are supported by DFT calculations of isolated molecules at the B3LYP/aug-cc-pVTZ level.

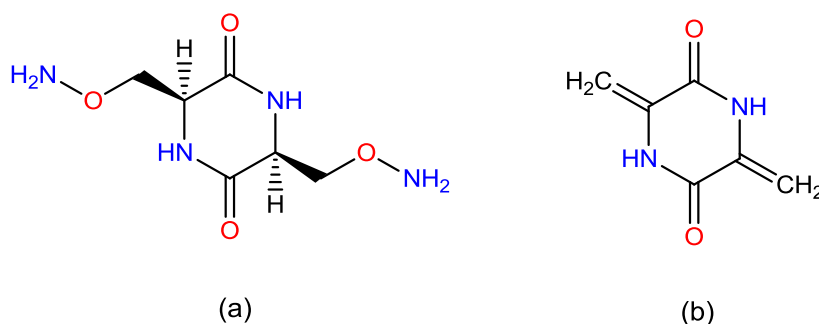


Figure 5.1. Schematic chemical structures of (a) AMDKP and (b) DMDKP.

5.2. Experimental

5.2.1. Materials

See sections 3.1 to 3.1.2 in Chapter 3.

5.2.2. Synthesis

AMDKP and DMDKP were synthesised by methods reported in the literature¹⁴ (see Appendix). The purity of was checked using $^1\text{H-NMR}$, $^{13}\text{C-NMR}$, MS and C, H, N analyses and found to be >98% (see Apeendix). D-cycloserine (99%; Alfa Aesar; Heysham, Lancashire, UK) and glacial

acetic acid (99%) as well as absolute ethanol (99%) were purchased from Fisher Scientific (Loughborough, UK). Spectroscopic grade deuterium oxide (99.98 atom %) and methanol- d_1 (99 atom %) were obtained from Sigma-Aldrich Ltd (Poole, Dorset, UK). Deuteration was carried out by dissolving 5 mg AMDKP in 5 ml methanol-D (MeOD) and 5 mg DMDKP in 5 ml D_2O . The powdered *N*-deuterated isotopomers were recovered after drying (60 °C) using a hot air oven.

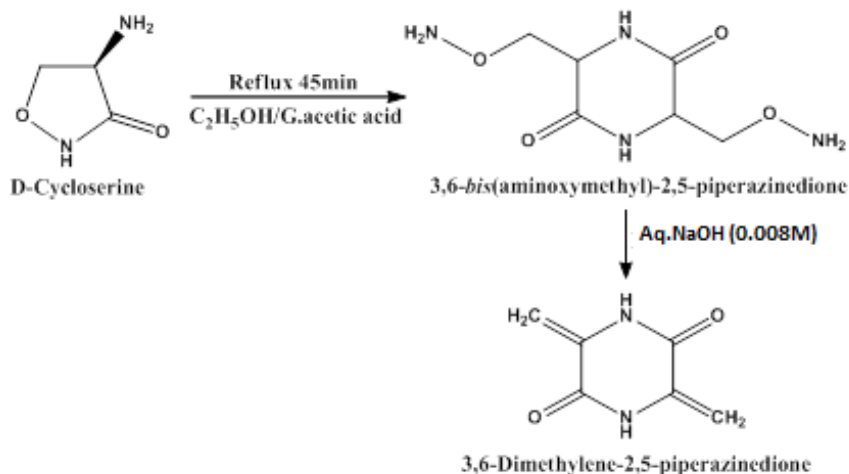


Figure 5.2. Reaction scheme for the synthesis of D-cycloserine derivatives.

5.2.3. Vibrational spectroscopy and Instrumental details

See sections 3.2, 3.2.1, 3.2.2, 3.2.3 and 3.2.4 in Chapter 3.

5.2.4. DFT calculations

See section 3.5 in Chapter 3.

5.3. NMR spectroscopy of the degradation of CS

1H -NMR experiments were used in order to examine the degradation of CS using a JEOL ECP 400 MHz FT NMR spectrometer, incorporating a tuneable H(5) 400 probe. The reaction mixture contained 20 mg CS, 1 ml D_2O and 0.75 ml DMSO- d_6 , and 120 μL of glacial acetic acid placed into a 5 mm NMR borosilicate glass tube and spun at 15 Hz using a single pulse experiment, that had a relaxation delay of 1s, the total number of spectral accumulations were undertaken using 16 scans using a 90° pulse and a width of 10.5 μ seconds. The degradation temperature was maintained at 50° C throughout the acquisition period.

5.4. Results and discussion

5.4.1. NMR spectroscopy

The degradation of D-cycloserine (CS) was characterised by $^1\text{H-NMR}$ spectroscopy whereby the reaction was monitored at different time intervals (Fig. 5.3). The reduction in concentration of CS can be detected by the diminishing signals found within region a. The degradation product 3,6-bis(aminoxymethyl)-2,5-piperazinedione (AMDKP) begins to be produced within 30 min (signals within region b). Finally, after 8 hr, the final degradation product, 3,6-dimethylene-2,5-piperazinedione (DMDKP) (region c) can be detected. It was established that acetic acid catalyses the degradation of CS. Indeed, in the presence of acetic acid degradation of CS occurs within 24 hr.

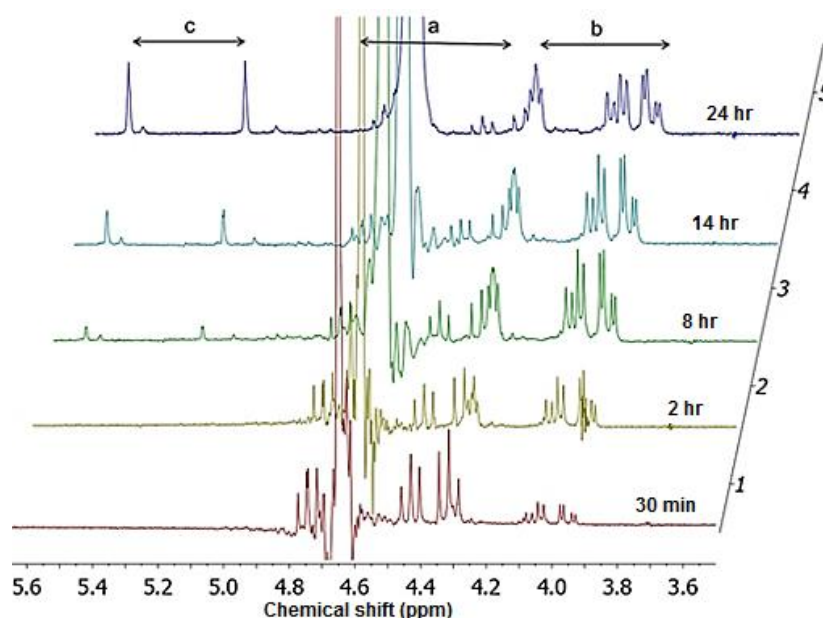


Figure 5.3. $^1\text{H-NMR}$ spectra (part) highlighting the degradation of CS in the presence of 120 μL of glacial acetic acid.

5.4.2. Geometry optimization

The atom numbering scheme and the computed structures for AMDKP and DMDKP together with the X-ray structure of DMDKP are shown in Figs. 5.4 and 5.5. The calculated bond lengths, bond angles, and dihedral angles are compared with the experimental data for DMDKP in Table 5.1. In order to verify the minimum energy conformations of the aminoxymethyl side chains of AMDKP, we carried out an energy profile calculation, assuming an idealised C_2 symmetry, at the HF/3-21G level using the Spartan'14 program,¹⁵ by rotation about the exocyclic (CC) and (CO) bonds ($\tau(1)$

$= \tau(\text{H15-C9-C13-O1})$ and $\tau(\text{H16-C10-C14-O2})$ and $\tau(2) = \tau(\text{C9-C13-O1-N7})$ and $\tau(\text{C10-C14-O2-N8}) = \pm 180^\circ$) on either side of the DKP ring (Fig 5.6). It was found that the $\tau(1)$ have three minimum energy regions ($\sim 70^\circ$ (a), -45° (b) and 160° (c), respectively). The geometry optimisation calculations were carried out at higher level (B3LYP /aug-cc-pVTZ) using the initial geometry from the Spartan'14 output, leading to a minimum energy optimised structure (-755.96777 a.u. (a), -755.96669 a.u. (b) and -755.96083 a.u. (c), respectively). Unfortunately, there is no X-ray data for AMDKP with which to compare these results. It is predicted that the DKP ring in the minimum energy structure (a) of AMDKP adopts a boat conformation with C_2 symmetry in the gas phase. It is important to note that the gas phase calculated structure is based on a single molecule, and does not account for intermolecular interactions such as hydrogen bonding or crystal packing forces in the solid state. From previously reported *ab initio* calculations on a range of DKPs, it is noteworthy that the boat conformation was, consistently, shown to be the most stable conformation in the gas-phase.^{16,17} The X-ray structure and our calculated structure of DMDKP suggests that the DKP ring adopts a planar conformation with C_{2h} symmetry.^{18,19}

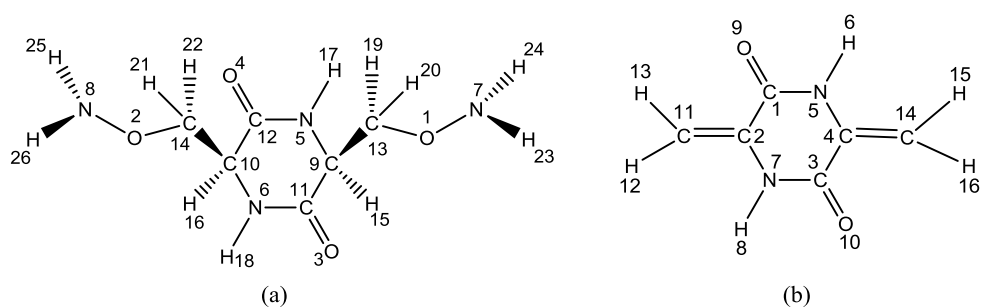


Figure 5.4. Atom numbering scheme for (a) AMDKP and (b) DMDKP.

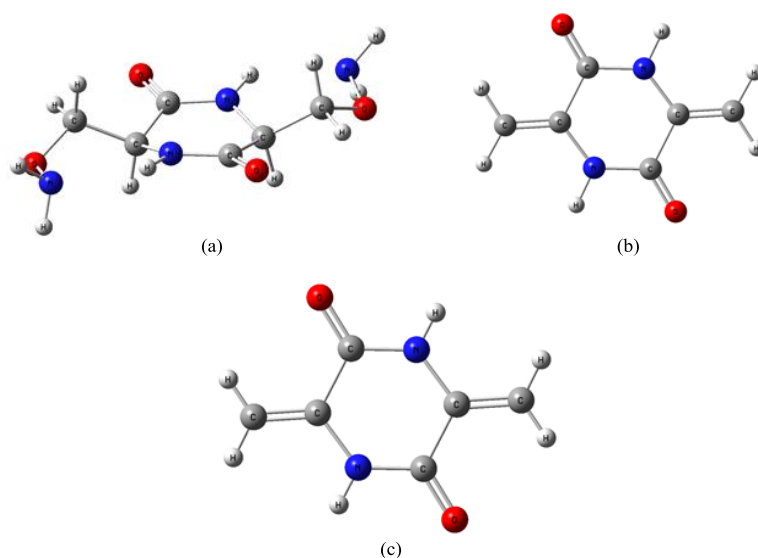


Figure 5.5. Calculated minimum energy structures of (a) AMDKP, (b) DMDKP and (c) X-ray structure of DMDKP.¹⁸

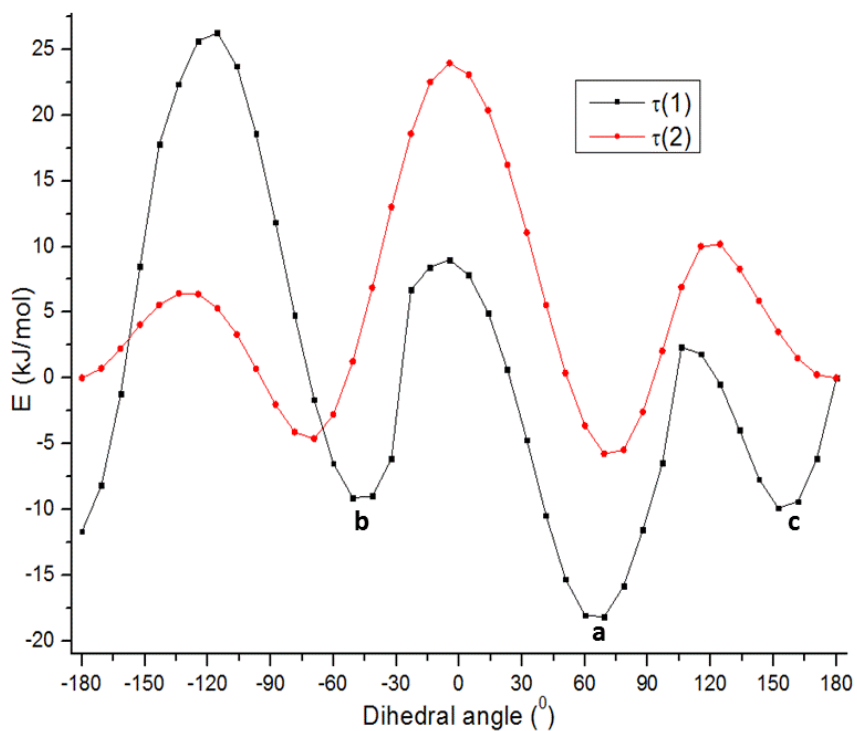


Figure 5.6. Potential energy plot for AMDKP.

Where, $\tau(1) = \tau(\text{H15-C9-C13-O1})$ and $\tau(\text{H16-C10-C14-O2})$

$\tau(2) = \tau(\text{C9-C13-O1-N7})$ and $\tau(\text{C10-C14-O2-N8})$

Table 5.1. Calculated bond lengths (Å), bond angles and dihedral angles (°) for DMDKP in comparison with the X-ray structure.¹⁸

Bond lengths (Å)	Calculated	X-ray ¹⁸
H(16)-C(14)	1.0776	0.9302
H(15)-C(14)	1.0808	0.9300
C(14)-C(4)	1.3334	1.3128
H(13)-C(11)	1.0776	0.9302
H(12)-C(11)	1.0808	0.9300
C(11)-C(2)	1.3334	1.3128
O(10)-C(3)	1.2156	1.2284
O(9)-C(1)	1.2156	1.2284
H(8)-N(7)	1.0100	0.8598
N(7)-C(2)	1.3979	1.3945
N(7)-C(3)	1.3708	1.3368
H(6)-N(5)	1.0100	0.8598
N(5)-C(1)	1.3708	1.3368
N(5)-C(4)	1.3979	1.3945
C(4)-C(3)	1.4961	1.4875

C(2)-C(1)	1.4961	1.4875
Bond angles (°)		
C(4)-C(14)-H(15)	121.9099	119.9928
C(4)-C(14)-H(16)	119.0461	120.0011
H(15)-C(14)-H(16)	119.0441	120.0061
C(2)-C(11)-H(12)	121.9099	119.9928
C(2)-C(11)-H(13)	119.0461	120.0011
H(12)-C(11)-H(13)	119.0441	120.0061
H(8)-N(7)-C(2)	118.1541	116.3559
H(8)-N(7)-C(3)	114.1125	116.2545
C(2)-N(7)-C(3)	127.7334	127.3896
H(6)-N(5)-C(1)	114.1125	116.2545
H(6)-N(5)-C(4)	118.1541	116.3559
C(1)-N(5)-C(4)	127.7334	127.3896
C(14)-C(4)-N(5)	123.1908	122.6544
C(14)-C(4)-C(3)	119.9228	120.8914
N(5)-C(4)-C(3)	116.8864	116.4527
O(10)-C(3)-N(7)	121.5282	122.3826
O(10)-C(3)-C(4)	123.0915	121.4648
N(7)-C(3)-C(4)	115.3802	116.1490
C(11)-C(2)-N(7)	123.1908	122.6544
C(11)-C(2)-C(1)	119.9228	120.8914
N(7)-C(2)-C(1)	116.8864	116.4527
O(9)-C(1)-N(5)	121.5282	122.3826
O(9)-C(1)-C(2)	123.0915	121.4648
N(5)-C(1)-C(2)	115.3802	116.1490
Dihedral angles (°)		
H(16)-C(14)-C(4)-C(3)	0.0000	0.4506
H(16)-C(14)-C(4)-N(5)	180.0000	179.9947
H(15)-C(14)-C(4)-C(3)	180.0000	-179.4689
H(15)-C(14)-C(4)-N(5)	0.0000	0.0752
H(13)-C(11)-C(2)-C(1)	0.0000	-0.4506
H(13)-C(11)-C(2)-N(7)	180.0000	-179.9947
H(12)-C(11)-C(2)-C(1)	180.0000	179.4689
H(12)-C(11)-C(2)-N(7)	0.0000	-0.0752
C(3)-N(7)-C(2)-C(1)	0.0000	1.1191
C(3)-N(7)-C(2)-C(11)	180.0000	-179.3179
H(8)-N(7)-C(2)-C(1)	180.0000	-178.8168
H(8)-N(7)-C(2)-C(11)	0.0000	0.7462
C(2)-N(7)-C(3)-C(4)	0.0000	-1.1161
C(2)-N(7)-C(3)-O(10)	180.0000	178.1956
H(8)-N(7)-C(3)-C(4)	180.0000	178.8198

H(8)-N(7)-C(3)-O(10)	0.0000	-1.8684
C(4)-N(5)-C(1)-C(2)	0.0000	1.1161
C(4)-N(5)-C(1)-O(9)	180.0000	-178.1956
H(6)-N(5)-C(1)-C(2)	180.0000	-178.8198
H(6)-N(5)-C(1)-O(9)	0.0000	1.8684
C(1)-N(5)-C(4)-C(3)	0.0000	-1.1191
C(1)-N(5)-C(4)-C(14)	180.0000	179.3179
H(6)-N(5)-C(4)-C(3)	180.0000	178.8168
H(6)-N(5)-C(4)-C(14)	0.0000	-0.7462
N(5)-C(4)-C(3)-N(7)	0.0000	0.9905
N(5)-C(4)-C(3)-O(10)	180.0000	-178.3281
C(14)-C(4)-C(3)-N(7)	180.0000	-179.4382
C(14)-C(4)-C(3)-O(10)	0.0000	1.2432
N(7)-C(2)-C(1)-N(5)	0.0000	-0.9905
N(7)-C(2)-C(1)-O(9)	180.0000	178.3281
C(11)-C(2)-C(1)-N(5)	180.0000	179.4382
C(11)-C(2)-C(1)-O(9)	0.0000	-1.2432

Table 5.2. Calculated bond lengths (Å), bond angles and dihedral angles (°) for the minimum energy conformer (a) of AMDKP.

Bond lengths (Å)	Calculated
H(26)-N(8)	1.0181
H(25)-N(8)	1.0161
H(24)-N(7)	1.0181
H(23)-N(7)	1.0161
H(22)-C(14)	1.0867
H(21)-C(14)	1.0936
H(20)-C(13)	1.0867
H(19)-C(13)	1.0936
H(18)-N(6)	1.0125
H(17)-N(5)	1.0125
H(16)-C(10)	1.0987
H(15)-C(9)	1.0987
C(14)-C(10)	1.5297
C(14)-O(2)	1.4234
C(13)-O(1)	1.4234
C(13)-C(9)	1.5297
C(12)-O(4)	1.2206
C(12)-N(5)	1.3504
C(12)-C(10)	1.5330
C(11)-C(9)	1.5330
C(11)-N(6)	1.3504

C(11)-O(3)	1.2206
C(10)-N(6)	1.4580
C(9)-N(5)	1.4580
N(8)-O(2)	1.4445
N(7)-O(1)	1.4445
Bond angles (°)	
O(2)-C(14)-C(10)	113.9944
O(2)-C(14)-H(21)	110.4827
O(2)-C(14)-H(22)	104.7832
C(10)-C(14)-H(21)	110.0839
C(10)-C(14)-H(22)	108.2415
H(21)-C(14)-H(22)	109.0094
C(9)-C(13)-O(1)	113.9944
C(9)-C(13)-H(19)	110.0839
C(9)-C(13)-H(20)	108.2415
O(1)-C(13)-H(19)	110.4827
O(1)-C(13)-H(20)	104.7832
H(19)-C(13)-H(20)	109.0094
O(4)-C(12)-N(5)	123.3404
O(4)-C(12)-C(10)	121.4124
N(5)-C(12)-C(10)	115.2448
O(3)-C(11)-C(9)	121.4124
O(3)-C(11)-N(6)	123.3404
C(9)-C(11)-N(6)	115.2448
C(14)-C(10)-H(16)	106.7865
C(14)-C(10)-C(12)	110.2229
C(14)-C(10)-N(6)	111.2270
H(16)-C(10)-C(12)	106.0870
H(16)-C(10)-N(6)	110.4981
C(12)-C(10)-N(6)	111.7778
C(13)-C(9)-H(15)	106.7865
C(13)-C(9)-C(11)	110.2229
C(13)-C(9)-N(5)	111.2270
H(15)-C(9)-C(11)	106.0870
H(15)-C(9)-N(5)	110.4981
C(11)-C(9)-N(5)	111.7778
O(2)-N(8)-H(25)	103.3150
O(2)-N(8)-H(26)	104.6175
H(25)-N(8)-H(26)	105.9820
O(1)-N(7)-H(23)	103.3150
O(1)-N(7)-H(24)	104.6175
H(23)-N(7)-H(24)	105.9820
H(18)-N(6)-C(11)	117.2180
H(18)-N(6)-C(10)	115.6642

C(11)-N(6)-C(10)	126.0670
H(17)-N(5)-C(12)	117.2180
H(17)-N(5)-C(9)	115.6642
C(12)-N(5)-C(9)	126.0670
N(8)-O(2)-C(14)	110.6524
N(7)-O(1)-C(13)	110.6524
Dihedral angles (°)	
H(22)-C(14)-C(10)-N(6)	166.7772
H(22)-C(14)-C(10)-C(12)	42.2188
H(22)-C(14)-C(10)-H(16)	-72.5887
H(21)-C(14)-C(10)-N(6)	47.7208
H(21)-C(14)-C(10)-C(12)	-76.8376
H(21)-C(14)-C(10)-H(16)	168.3549
O(2)-C(14)-C(10)-N(6)	-77.0692
O(2)-C(14)-C(10)-C(12)	158.3724
O(2)-C(14)-C(10)-H(16)	43.5649
H(22)-C(14)-O(2)-N(8)	-171.1540
H(21)-C(14)-O(2)-N(8)	-53.8842
C(10)-C(14)-O(2)-N(8)	70.6928
H(20)-C(13)-O(1)-N(7)	-171.1540
H(19)-C(13)-O(1)-N(7)	-53.8842
C(9)-C(13)-O(1)-N(7)	70.6928
H(20)-C(13)-C(9)-N(5)	166.7772
H(20)-C(13)-C(9)-C(11)	42.2188
H(20)-C(13)-C(9)-H(15)	-72.5887
H(19)-C(13)-C(9)-N(5)	47.7208
H(19)-C(13)-C(9)-C(11)	-76.8376
H(19)-C(13)-C(9)-H(15)	168.3549
O(1)-C(13)-C(9)-N(5)	-77.0692
O(1)-C(13)-C(9)-C(11)	158.3724
O(1)-C(13)-C(9)-H(15)	43.5649
C(10)-C(12)-N(5)-C(9)	8.6993
C(10)-C(12)-N(5)-H(17)	176.4152
O(4)-C(12)-N(5)-C(9)	-170.7400
O(4)-C(12)-N(5)-H(17)	-3.0243
N(5)-C(12)-C(10)-N(6)	23.5617
N(5)-C(12)-C(10)-H(16)	-96.9474
N(5)-C(12)-C(10)-C(14)	147.8031
O(4)-C(12)-C(10)-N(6)	-156.9870
O(4)-C(12)-C(10)-H(16)	82.5039
O(4)-C(12)-C(10)-C(14)	-32.7456
N(6)-C(11)-C(9)-N(5)	23.5617
N(6)-C(11)-C(9)-H(15)	-96.9474
N(6)-C(11)-C(9)-C(13)	147.8031

O(3)-C(11)-C(9)-N(5)	-156.9870
O(3)-C(11)-C(9)-H(15)	82.5039
O(3)-C(11)-C(9)-C(13)	-32.7456
C(9)-C(11)-N(6)-C(10)	8.6993
C(9)-C(11)-N(6)-H(18)	176.4152
O(3)-C(11)-N(6)-C(10)	-170.7400
O(3)-C(11)-N(6)-H(18)	-3.0243
C(12)-C(10)-N(6)-C(11)	-33.3910
C(12)-C(10)-N(6)-H(18)	158.7260
H(16)-C(10)-N(6)-C(11)	84.5086
H(16)-C(10)-N(6)-H(18)	-83.3744
C(14)-C(10)-N(6)-C(11)	-157.068
C(14)-C(10)-N(6)-H(18)	35.0486
C(11)-C(9)-N(5)-C(12)	-33.3910
C(11)-C(9)-N(5)-H(17)	158.7260
H(15)-C(9)-N(5)-C(12)	84.5086
H(15)-C(9)-N(5)-H(17)	-83.3744
C(13)-C(9)-N(5)-C(12)	-157.0680
C(13)-C(9)-N(5)-H(17)	35.0486
H(26)-N(8)-O(2)-C(14)	109.1686
H(25)-N(8)-O(2)-C(14)	-140.0910
H(24)-N(7)-O(1)-C(13)	109.1686
H(23)-N(7)-O(1)-C(13)	-140.0910

The data in Table 5.1 show that there are no significant differences between the X-ray and calculated structures of DMDKP. Indeed, the bond lengths fit quite well with the X-ray crystal data, with the exception of the N–H and C–H bond lengths. For example, the calculated N–H and C–H bond lengths are 1.01 Å and ~1.07 Å, and the experimental bond lengths are ~0.85 Å and 0.93 Å, respectively. These differences can be attributed to the fact that the positions of hydrogen atoms cannot be precisely located by X-ray diffraction techniques. The X-ray structure of DMDKP indicates that the DKP ring in the molecule is planar ($\beta = 0.0^\circ$) and the peptide dihedral angles ω , ϕ , and ψ are -1.11 and 1.11° ; -0.9 and 0.9° ; and -1.1 and 1.11° , respectively. The calculated planar conformation has ring dihedral angles ω , ϕ , ψ and (the pseudo torsional angle) β of 0.0° . There is a good relationship between the dihedral angles of the DKP ring for the X-ray and calculated structures, showing a fairly good fit between the calculated and experimental data. The calculated ring dihedral angles, ω , ϕ , ψ and β (the pseudo torsional angle) for AMDKP are 8.6, -33.3, 23.5 and 30.8° , respectively.

5.4.3. Vibrational assignments

AMDKP ($C_6H_{12}N_4O_4$) consists of 26 atoms and has 72 normal modes, whereas DMDKP ($C_6H_6N_2O_2$) consists of 16 atoms and has 42 normal modes. It is important to note that the mutual exclusion principle holds for the IR and Raman spectra of DMDKP in the solid state, indicating that the molecule has a centre of symmetry. The solid state IR and Raman spectra of non-deuterated and *N*-deuterated AMDKP and DMDKP, together with the calculated IR and Raman spectra are shown in Figs. 5.7-5.14. The solution state IR and Raman spectra of non-deuterated and *N*-deuterated AMDKP are shown in Figs. 5.15 and 5.16. Unfortunately, the aqueous solution state IR and Raman spectra of DMDKP could not be obtained because of its low solubility. The experimental and calculated band wavenumbers (cm^{-1}) and potential energy distribution (PEDs) of vibrational modes of AMDKP and DMDKP and their *N*-deuterated isotopomers are given in Tables 5.3 to 5.6. The assignment of the amide II band for AMDKP is of particular interest. This appears in the Raman spectrum at 1502 cm^{-1} (solid), 1518 cm^{-1} (solution), in agreement with previous observations for cyclo(L-Ala-L-Ala) where the *cis* amide II band was found at ($\sim 1508\text{ cm}^{-1}$) in the solid state.¹⁶

5.4.4. Spectral region $>2000\text{ cm}^{-1}$

The bands found in this region are mainly due to N-H, C-H, N-D stretching modes. The bands located between $\sim 3342\text{ cm}^{-1}$ and 3204 cm^{-1} in both the solid state IR and Raman spectra of AMDKP are assigned to the amine NH_2 stretching vibrations. On *N*-deuteration, these bands shift to lower wavenumber, increase in intensity and becomes complex with the most intense bands appearing at $\sim 2470\text{ cm}^{-1}$ in both the solid state IR and Raman spectra. The amide N-H stretching bands in AMDKP appear at 3182 cm^{-1} and 3047 cm^{-1} in the IR spectrum and at 3165 cm^{-1} and 3049 cm^{-1} in the Raman spectrum in the solid state. On *N*-deuteration, this band shifts down to lower wavenumber and appears as a broad band at 2331 cm^{-1} in the Raman spectrum. In the IR spectrum this band increases in intensity and becomes more complex and shows a large downward shift in wavenumber appearing as three bands, with the most intense band located at 2320 cm^{-1} . It is apparent that the computed N-H and NH_2 vibrations do not match well with the experimental wavenumber locations, because our DFT calculations on isolated molecules do not take account of intermolecular hydrogen bonding. In AMDKP the N-H groups on the DKP ring participate in hydrogen bonding and hence appear at lower wavenumber compared to NH_2 stretching vibrations. The N-H stretching vibrations for DMDKP are observed at 3181 cm^{-1} and a very weak band at 3195 cm^{-1} in the solid state IR and Raman spectra; due to their large downward shift on deuteration

the N-D stretching band for the *N*-deuterated molecule in the Raman spectrum appears as a broad band at 2263 cm⁻¹. In the IR spectra, after *N*-deuteration, multiple bands occur with the most intense band appearing at 2263 cm⁻¹. Two possible explanations underlying the complexity of N-D bands in IR and Raman spectra have been previously suggested, namely anharmonic coupling with low wavenumber modes and Fermi resonance producing several sub-bands.¹⁶

The group of bands in the 2970-2850 cm⁻¹ region are attributed to C-H stretching modes. These bands are less intense in both solid and solution state IR spectra than in the Raman spectra of AMDKP. In DMDKP the alkene (=C-H) stretching bands are located at 3128 and 3032 cm⁻¹ in the Raman spectra. These bands are more complex in the IR spectrum with the most intense band located at 3015 cm⁻¹. Band assignments in this region are facilitated by comparison with the DFT calculations and the lack of shift of C-H modes on *N*-deuteration. The weak band at ~1802 cm⁻¹ in the IR spectra of both non-deuterated and *N*-deuterated DMDKP could be the result of overtones or combination bands.

5.4.5. Spectral region 1250-1700 cm⁻¹

The vibrational bands found in this region are attributed to amide group vibrations (C=O stretch, C-N stretch and N-H in-plane bending), C-H bending, C_α-H bending and CH₂ scissoring, twisting and wagging modes. The strong bands located at 1659 cm⁻¹ and 1655 cm⁻¹ in the IR and Raman spectra of AMDKP in the solid state are assigned to the C=O amide stretch mode (*cis* amide I mode), which is found at 1670 cm⁻¹ in solution. This band appears to have a very weak shoulder at 1636 cm⁻¹ in the solid state Raman spectrum. There is good agreement with the previously reported amide I mode observed at 1664 cm⁻¹ and 1667 cm⁻¹ in the solid and solution state IR spectra of AMDKP.^{11,12} The corresponding Raman band was observed at 1655 cm⁻¹. On *N*-deuteration this band shifts down in wavenumber, and is observed at 1616 cm⁻¹ with a weak shoulder at 1641 cm⁻¹ in the Raman spectrum. In the IR spectrum the amide I mode shifts on *N*-deuteration to 1640 cm⁻¹ and reveals a shoulder, located at 1618 cm⁻¹. From the foregoing observations it is suggested that the coupling of C=O with N-H in-plane bending is higher in compounds with *cis* amide groups compared to *trans* amide groups and, hence, show a larger downward shift on *N*-deuteration.²¹ It is noteworthy that *cis* amide I shows a downward shift of about 39 cm⁻¹ in the Raman spectrum; this can be attributed to stronger coupling and high N-H character in the *cis* amide I mode. However, the downward shift on *N*-deuteration, (~25 cm⁻¹), is indicative of the carbonyl stretch being coupled to N-H in-plane-bending vibrations and is typical of the *cis* amide I conformation.¹⁶

In DMDKP, the bands located in the region 1685 and 1600 cm^{-1} are assigned to vibrations that are quite mixed. The band located at 1681 cm^{-1} in both IR and Raman is assigned to a mixed carbonyl C=O stretching and C=C stretching mode. Interestingly, on *N*-deuteration this mode shifts down in wavenumbers $\sim 4 \text{ cm}^{-1}$ in IR compared to Raman spectra where the downward shift is $\sim 27 \text{ cm}^{-1}$. From our calculated PEDs, the predicted IR active mode (B_u) at 1683 cm^{-1} indicates that there is no N-H character and hence, does not shift to lower wavenumber on *N*-deuteration. Whereas the Raman active mode (A_g) at 1680 cm^{-1} shifts down in wavenumber on *N*-deuteration ($\sim 14 \text{ cm}^{-1}$) and therefore indicates the presence of N-H character (11% N-H in-plane-bend, see Table 3). Hence it is therefore suggested that due to the absence of N-H character, the band observed at 1681 cm^{-1} shows an insignificant shift on *N*-deuteration in the IR spectrum. In the Raman spectrum this mode shows a considerable downward shift and splits into two bands and appears at 1644 and 1625 cm^{-1} respectively. In DMDKP, the corresponding vibrations in both IR and Raman spectra are predominantly due to C=C stretching with a small contribution from C=O stretching and hence, cannot be regarded as a *cis* amide I mode. However, the band located at 1637 cm^{-1} in the IR spectrum shows a downward shift of 30 cm^{-1} and appears at 1607 cm^{-1} and hence indicates the presence of N-H character as suggested from the computed PEDs. This observation does not agree well with the previously reported DKPs where the *cis* amide I is found in between 1690 and 1650 cm^{-1} for the molecules with planar/near planar^{16,23} and boat conformations.^{21, 24, 25} Hence, it can be hypothesised that this is not a typical *cis* amide I mode as observed previously in other DKPs.

The band located at $\sim 1586 \text{ cm}^{-1}$ in both the IR and Raman spectra of AMDKP can be assigned to the NH_2 bending vibration. Previous observations also suggest the location at 1588 and 1596 cm^{-1} in solid and solution state IR spectra and a Raman band at 1594 cm^{-1} in the solid state of AMDKP.^{11,12} The ND_2 bending vibration is clearly located in the IR and Raman spectra as a doublet at 1170 and 1174 cm^{-1} in good agreement with the DFT calculations. The *cis* amide II mode is found at 1502 cm^{-1} in the Raman spectrum of AMDKP. This mode is mainly due to the out of plane $\text{C}_\alpha\text{-C-N}$ stretch, with a small contribution from N-H in-plane bending. This band is found at a significantly higher wavenumber than that of other DKPs where the ring essentially adopts a boat conformation (cyclo(L-Ala-L-Ala)).²¹ In other DKPs, such as cyclo(Gly-Gly), cyclo(D-Ala-L-Ala) and cyclo(L-Ala-Gly) where the DKP ring conformation is planar or near planar, the *cis* amide II band was found at $\sim 1520 \text{ cm}^{-1}$. However, the increase in the strain on the DKP ring-due to the attachment of bulky substituents on the C_α atoms may also influence the location of the amide II mode.²¹ The calculated band position for the amide II vibration is 1454 cm^{-1} which

does not fit well with the experimental result of 1502 cm^{-1} in the solid state. This band appears at 1518 cm^{-1} in solution state Raman spectra. The bands detected in the $1400\text{-}1500\text{ cm}^{-1}$ region are mostly due to C-H bending motions. Upon deuteration the *cis* amide II band in AMDKP shifts to considerably lower wavenumber and appears at 1481 cm^{-1} . This wavenumber shift is in good agreement with both our calculated wavenumbers and other DKPs *cis* amide II shifts after *N*-deuteration.^{16, 20, 22} In contrast, the *trans* amide II mode displays a greater shift on *N*-deuteration e.g. linear L-Met-L-Met shows a downward shift of 66 cm^{-1} .^{20, 21} This can be attributed to a significantly larger N-H in-plane bending contribution in the *trans* amide II mode compared with the *cis* amide II mode.

In DMDKP the *cis* amide II mode is found at 1499 cm^{-1} in the Raman spectra, shifts to 1449 cm^{-1} on *N*-deuteration. It is unusual for a planar DKP molecule to have such a low wavenumber for a *cis* amide II mode with a large shift on *N*-deuteration. The DFT calculations predict a shift of the *cis* amide II mode from 1427 to 1393 cm^{-1} . Hence, it is hypothesised that strong coupling of out-of-phase C_{α} -C-N stretch with a large contribution from N-H in-plane bending, and the resonance effect associated with dimethylene side-chain, the *cis* amide II is at lower wavenumber in DMDKP and exhibits a larger shift on *N*-deuteration, compared with other DKPs. Theoretically from PEDs and experimentally from *N*-deuteration shifts in IR and Raman spectra, it is hypothesised that the assumptions (location in cm^{-1} , coupling and contribution) on *cis* amide I and II modes in DMDKP cannot be made from the experimental data. However, the planar conformation of the DKP ring in DMDKP with C_{2h} symmetry has been confirmed by the rule of mutual exclusion which appears to hold for the IR and Raman spectra of DMDKP in the solid state.

IR and Raman bands in the $1350\text{-}1480\text{ cm}^{-1}$ region can be allocated to CH_2 and CH symmetric and asymmetric bending modes of both AMDKP and DMDKP. Individual bands have been assigned with reference to the calculated PEDs. These vibrations are of significantly mixed character, involving predominantly C-H and CH_2 deformation. From previous observations in DKPs, the N-H bending vibration would be expected in this region but no significant deuterium shifts can be observed in the IR and Raman spectra. However, small shifts are observed for bands in the region $\sim 1375\text{ cm}^{-1}$ to 1260 cm^{-1} on *N*-deuteration, due to the presence of some N-H character, which is confirmed by our calculations. IR and Raman bands located between 1220 and 1346 cm^{-1} are mixed vibrations and this region appears to be quite complex. From the calculated wavenumber locations these bands are attributed to vibrations involving combinations of NH_2 rocking, C_{α} -H bending, C_{α} -H wagging, C_{α} -H twisting, CH_2 wagging and CH_2 twisting motions. However, in

N-deuterated DMDKP a new band appears at 1228 cm⁻¹ in the IR which is absent in the Raman spectrum. The appearance of this band fits well with the previously reported N-H in-plane bend shift in DKPs on *N*-deuteration.¹⁶ From the calculated spectra and from the previous work undertaken on DKPs these assignments have been made possible.^{16,20} Usually, most of these bands are due to C-H bending modes and show little shift on *N*-deuteration, but some bands are shifted by 6-10 cm⁻¹.

5.4.6. Spectral region 850-1350 cm⁻¹

The bands in this region are due to C-O, O-N, N-C_α and C-C stretching as well as CH₂ rocking and NH₂ wagging vibrations. The band located at 1188 cm⁻¹ in both the IR and Raman spectra of AMDKP is assigned to a mixed C-O/O-N stretching vibration together with contributions from NH₂ wagging motion; this band shifts to ~876 cm⁻¹ on *N*-deuteration. The bands at ~1118 cm⁻¹ and ~1074 cm⁻¹ (again in both the IR and Raman spectra) are assigned to N-C_α stretching and C-C stretching vibrations, with contributions from CH₂ rocking motion. Additionally, the band at 828 cm⁻¹ in IR (852 cm⁻¹ in the Raman spectrum) has been assigned to a vibration involving O-N stretching with a small contribution from C-O stretching. The assignment of other IR and Raman bands observed in the 910–1200 cm⁻¹ region is less straightforward because these are attributed to vibrations of mixed character. In DMDKP the band at 1342 cm⁻¹, in IR and in Raman spectra, is assigned to CH₂ bending and NH-in-plane-bending motions with small contribution from C=C stretching vibrations. The band at 1000 cm⁻¹ in IR and at 994 cm⁻¹ in the Raman spectra of DMDKP is assigned to a mode involving N-C_α stretching with a significant contribution from CH₂ rocking motion, and the calculations indicate that the band at 895 cm⁻¹ in the IR spectrum (894 cm⁻¹ in Raman) should be assigned to out-of-plane CH₂ bending.

5.4.7. Spectral region 500-850 cm⁻¹

Various peptide group vibrations are seen in this region, especially C=O and N-H out-of-plane bending modes, and also in-plane DKP ring deformation/stretching modes. The N-H bending modes have been assigned on the basis of *N*-deuteration shift and also from previous IR and Raman data relating to other DKPs. Three bands found in the IR spectrum of AMDKP, at 766, 673 and 649 cm⁻¹, show significant deuteration shifts. These bands are found in the Raman spectrum at 787, 677, 647 cm⁻¹. Previous work on other DKPs has shown that the N-H out-of-plane bending band is quite difficult to find and has an extensive feature centred ~820 cm⁻¹ in the IR spectrum.^{16,20,22} A series of bands around ~850-500 cm⁻¹ in the IR spectrum of DMDKP shift

considerably on *N*-deuteration. Of these bands the one at 844 cm⁻¹ shows a greater shift and appears at 625 cm⁻¹ in the *N*-deuterated IR spectrum. Unfortunately, these bands are not accurately assigned by our DFT calculations (due to hydrogen bonding effects). However, the calculated wavenumbers shows that the vibrations in this region are of mixed character. The N-H out-plane-bending band does not match well with the previous observations in simple DKPs,¹⁶ this might be due the strong hydrogen bonding between the DMDKP molecules in the crystallographic unit lattice. The Raman bands located at 620 and 785 cm⁻¹ are assigned to vibrations that are quite mixed, but contain a significant amount of C=O out-of-plane bending motion both molecules and but also C=CH₂ in- and out-of-plane motion in DMDKP.

5.4.8. Spectral region < 500 cm⁻¹

There are some weak bands observed in the Raman spectrum below 500 cm⁻¹, which are due to vibrations from C=O, O-N, C-O, C-C-O and N-O-C bending motions in AMDKP. The bands in the 200-400 cm⁻¹ region of the Raman spectrum are predominantly due to C-C, C=O, C-C-O bending motions and O-N torsional vibrations, the attachment of the side-chain on the C_α atoms also shows C-C-O and N-O-C bending vibrations in this region as well as the bending modes of the DKP ring. The bands located between 50 and 200 cm⁻¹ are mainly due to torsional vibrations of the aliphatic side-chain attached to the C_α atoms, ring torsional vibrations and lattice vibrations. These bands show no remarkable shift on *N*-deuteration, indicative of very little N-H contributions to these modes. In DMDKP, the vibrational modes below 500 cm⁻¹ are predominantly due to C=O, C-N, C-C, C=CH₂ bending motions and DKP ring bending modes.

Table 5.3. Experimental and calculated vibrational band wavenumbers (cm⁻¹) for non-deuterated AMDKP.

IR (s)	Raman (s)	IR (sol)	Raman (sol)	Calc	%PEDs
	3165			3153 A	100 v _s (NH)
3182				3152 B	100 v _s (NH)
3047	3049				
3340	3342			3145 B	95 v _{as} (NH ₂)
3304	3306			3145 A	95 v _{as} (NH ₂)
	3262			3069 A	95 v _s (NH ₂)
	3244			3069 B	95 v _s (NH ₂)
	2978			2989 A	25 v _s (CH ₂), 75 v _{as} (CH ₂)
2970				2989 B	25 v _s (CH ₂), 75 v _{as} (CH ₂)
2931	2933		2947		

2876				2886 B	74 $\nu_s(\text{CH}_2)$, 25 $\nu_{as}(\text{CH}_2)$
	2873		2890	2886 A	74 $\nu_s(\text{CH}_2)$, 25 $\nu_{as}(\text{CH}_2)$
				2831 B	99 $\nu_s(\text{CH})$
				2829 A	99 $\nu_s(\text{CH})$
	1655 1636		1670	1640 A	67 $\nu_s(\text{C=O})$, 13 $\nu_s(\text{NC})$, 10 $\delta_{ip}(\text{NH})$
1659	1596			1637 B	68 $\nu_s(\text{C=O})$, 13 $\nu_s(\text{NC})$
	1587			1589 A	100 $\delta(\text{NH}_2)$
1586				1588 B	100 $\delta(\text{NH}_2)$
1503	1502		1519	1452 A	10 $\nu_s(\text{C=O})$, 13 $\nu_s(\text{NC})$, 14 $\delta_{ip}(\text{NH})$, 43 $\delta(\text{CH}_2)$
1456	1453	1468	1468	1447 B	97 $\delta(\text{CH}_2)$
	1442			1441 A	10 $\nu_s(\text{NC})$, 10 $\delta_{ip}(\text{NH})$, 56 $\delta(\text{CH}_2)$
				1411 B	13 $\nu_s(\text{C=O})$, 14 $\nu_s(\text{NC})$, 45 $\delta_{ip}(\text{NH})$
1372	1373	1370	1373	1383 B	16 $\nu_s(\text{CC}_\alpha)$, 39 $\nu_s(\text{NC})$, 23 $\delta_{ip}(\text{NH})$, 14 $\delta_{ip}(\text{C=O})$
	1363			1355 A	84 $\omega(\text{CH}_2)$
1364				1350 B	78 $\omega(\text{CH}_2)$
1343	1343	1334		1346 A	34 $\delta_{ip}(\text{NH})$, 14 $\omega(\text{CCH})$
1326	1323 1313		1312	1318 B	11 $\delta(\text{CCH})$, 30 $\omega(\text{CCH})$, 12 $\tau(\text{CCH})$, 24 $\tau(\text{CH}_2)$
				1283 A	10 $\delta_{ip}(\text{NH})$, 22 $\rho(\text{NH}_2)$, 35 $\tau(\text{CH}_2)$
1274				1276 B	54 $\rho(\text{NH}_2)$, 21 $\tau(\text{CH}_2)$
	1262			1273 A	33 $\rho(\text{NH}_2)$, 10 $\delta(\text{CCH})$, 15 $\omega(\text{CCH})$
1255	1254				
				1239 B	24 $\rho(\text{NH}_2)$, 16 $\delta(\text{CCH})$, 14 $\omega(\text{CCH})$, 11 $\tau(\text{CCH})$, 21 $\tau(\text{CH}_2)$
	1237		1234	1237 A	21 $\rho(\text{NH}_2)$, 13 $\delta(\text{CCH})$, 20 $\omega(\text{CCH})$, 14 $\tau(\text{CCH})$, 18 $\tau(\text{CH}_2)$
1228		1225		1227 A	20 $\rho(\text{NH}_2)$, 24 $\delta(\text{CCH})$, 10 $\rho(\text{CCH})$, 18 $\tau(\text{CH}_2)$
				1222 B	18 $\rho(\text{NH}_2)$, 25 $\delta(\text{CCH})$, 11 $\rho(\text{CCH})$, 17 $\tau(\text{CH}_2)$
	1188		1170	1190 A	14 $\nu_s(\text{C-O})$, 11 $\nu_s(\text{O-N})$, 59 $\omega(\text{NH}_2)$
1188				1189 B	13 $\nu_s(\text{C-O})$, 12 $\nu_s(\text{O-N})$, 63 $\omega(\text{NH}_2)$
	1175			1162 A	31 $\nu_s(\text{NC}_\alpha)$, 16 $\tau(\text{CCH})$, 16 $\rho(\text{CH}_2)$
1119	1118	1115		1135 B	37 $\nu_s(\text{NC}_\alpha)$, 16 $\tau(\text{CCH})$, 23 $\rho(\text{CH}_2)$
1072		1054		1085 B	48 $\nu_s(\text{CC})$, 14 $\rho(\text{CH}_2)$
	1074		1082	1060 A	53 $\nu_s(\text{CC})$, 19 $\rho(\text{CH}_2)$
	1011		1025	998 A	58 $\nu_s(\text{C-O})$, 24 $\omega(\text{NH}_2)$
1010		1020		996 B	58 $\nu_s(\text{C-O})$, 23 $\omega(\text{NH}_2)$
978	977			977 A	10 $\nu_s(\text{C}_\alpha\text{C})$, 16 $\nu_s(\text{CC})$, 25 $\rho(\text{CH}_2)$
937	939		943	948 B	37 $\nu_s(\text{NC}_\alpha)$, 25 $\rho(\text{CH}_2)$, 18 $\delta_{ip}(\text{Ring-3})$

				917 B	30 $\nu_s(\text{C}_\alpha\text{C})$, 12 $\delta_{\text{ip}}(\text{Ring-3})$, 16 $\delta_{\text{op}}(\text{C=O})$
	852		876	863 A	77 $\nu_s(\text{O-N})$, 12 $\nu_s(\text{C-O})$
828				862 B	72 $\nu_s(\text{O-N})$, 12 $\nu_s(\text{C-O})$
			855 811	853 A	12 $\nu_s(\text{NC}_\alpha)$, 10 $\delta(\text{CCO})$, 26 $\delta_{\text{op}}(\text{C=O})$
				759 B	11 $\nu_s(\text{CN})$, 20 $\nu_s(\text{C}_\alpha\text{C})$, 14 $\delta_{\text{ip}}(\text{Ring-3})$, 22 $\delta_{\text{op}}(\text{C=O})$
	787		727	719 A	95 $\delta_{\text{op}}(\text{NH})$, 18 $\delta_{\text{op}}(\text{C=O})$
766				709 B	88 $\delta_{\text{op}}(\text{NH})$
673	677		673		
649	647			643 A	25 $\nu_s(\text{C}_\alpha\text{C})$, 10 $\delta_{\text{op}}(\text{NH})$, 30 $\delta_{\text{op}}(\text{C=O})$
				632 B	18 $\nu_s(\text{CC})$, 19 $\delta_{\text{ip}}(\text{Ring-3})$, 29 $\delta_{\text{op}}(\text{C=O})$
			622	604 A	58 $\delta_{\text{ip}}(\text{C=O})$
551	550			537 A	16 $\nu_s(\text{C}_\alpha\text{C})$, 10 $\delta(\text{CCO})$, 16 $\delta_{\text{ip}}(\text{Ring-2})$, 27 $\delta(\text{NOC})$
535	536			519 B	22 $\delta(\text{CCO})$, 19 $\delta_{\text{ip}}(\text{C=O})$, 18 $\delta(\text{NOC})$
478	475		486	477 B	12 $\tau(\text{CCH})$, 11 $\rho(\text{CH}_2)$, 12 $\delta_{\text{ip}}(\text{C=O})$, 35 $\delta(\text{NOC})$
452	453		462	459 A	17 $\nu_s(\text{NC}_\alpha)$, 50 $\delta_{\text{ip}}(\text{Ring-2})$
	419		439	429 A	25 $\delta_{\text{ip}}(\text{Ring-1})$, 20 $\delta(\text{NOC})$
			388	363 A	28 $\rho(\text{CCH})$, 11 $\delta(\text{CCO})$, 24 $\delta(\text{NOC})$
			331	355 B	25 $\rho(\text{CCH})$, 22 $\delta_{\text{ip}}(\text{C=O})$
	296			314 B	11 $\nu_s(\text{C}_\alpha\text{C})$, 43 $\delta(\text{CCO})$, 10 $\delta_{\text{ip}}(\text{C=O})$, 24 $\delta(\text{NOC})$
				277 A	11 $\nu_s(\text{CC})$, 43 $\delta(\text{CCO})$, 23 $\delta_{\text{ip}}(\text{Ring-1})$
	258			249 B	10 $\tau(\text{CCH})$, 68 $\tau(\text{ON})$, 10 $\tau(\text{CC})$
				240 A	12 $\tau(\text{CCH})$, 68 $\tau(\text{ON})$
	204			218 A	10 $\omega(\text{CCH})$, 15 $\tau(\text{CCH})$, 25 $\tau(\text{ON})$, 27 $\tau(\text{C-O})$
				201 B	21 $\tau(\text{ON})$, 43 $\tau(\text{C-O})$
	177		161		
	143		131	143 A	11 $\delta(\text{CCO})$, 41 $\tau(\text{C-O})$, 21 $\tau(\text{CC})$
				121 B	19 $\omega(\text{CCH})$, 23 $\tau(\text{CCH})$, 36 $\tau(\text{C-O})$
			108	107 A	99 $\delta_{\text{op}}(\text{Ring-2})$
	112			105 B	91 $\delta_{\text{op}}(\text{Ring-1})$
	94			73 B	16 $\tau(\text{C-O})$, 72 $\tau(\text{CC})$
				58 A	27 $\tau(\text{C-O})$, 66 $\tau(\text{CC})$
				33 A	94 $\delta_{\text{op}}(\text{Ring-3})$

Table 5.4. Experimental and calculated vibrational band wavenumbers (cm⁻¹) for *N*-deuterated AMDKP.

IR (s)	Raman (s)	IR (sol)	Raman (sol)	Calc.	%PEDs
	2978			2989 A	25 $\nu_s(\text{CH}_2)$, 75 $\nu_{as}(\text{CH}_2)$
2979			2947	2989 B	25 $\nu_s(\text{CH}_2)$, 75 $\nu_{as}(\text{CH}_2)$
2933 2931	2934	2936			
2873			2892	2886 A	74 $\nu_s(\text{CH}_2)$, 25 $\nu_{as}(\text{CH}_2)$
	2871			2866 A	74 $\nu_s(\text{CH}_2)$, 25 $\nu_{as}(\text{CH}_2)$
				2831 B	99 $\nu_s(\text{CH})$
				2829 A	99 $\nu_s(\text{CH})$
2498	2500				
2470	2472			2320 A	98 $\nu_{as}(\text{ND}_2)$
2448	2450			2320 B	98 $\nu_{as}(\text{ND}_2)$
2432 2393 2381	2431 2395 2383				
2342					
	2331			2313 A	99 $\nu_s(\text{ND})$
2320				2313 B	99 $\nu_s(\text{ND})$
2252	2286				
				2217 A	99 $\nu_s(\text{ND}_2)$
				2217 B	99 $\nu_s(\text{ND}_2)$
1640		1650		1628 B	73 $\nu_s(\text{C=O})$, 13 $\nu_s(\text{NC})$
1618	1616		1652	1627 A	75 $\nu_s(\text{C=O})$, 12 $\nu_s(\text{NC})$
1480 1456	1481 1454		1496 1446	1447 A	97 $\delta(\text{CH}_2)$
1456	1442	1458		1446 B	97 $\delta(\text{CH}_2)$
				1418 A	36 $\nu_s(\text{CN})$, 14 $\nu_s(\text{CC}_\alpha)$, 12 $\omega(\text{CCH})$
1366	1374	1373		1391 B	49 $\nu_s(\text{NC})$, 10 $\omega(\text{CH}_2)$
	1350		1372	1355 A	10 $\delta(\text{CCH})$, 82 $\omega(\text{CH}_2)$
1346			1339	1351 B	73 $\omega(\text{CH}_2)$
				1319 B	10 $\delta(\text{CCH})$, 34 $\omega(\text{CCH})$, 14 $\tau(\text{CCH})$, 22 $\tau(\text{CH}_2)$
	1335		1328	1308 A	14 $\nu_s(\text{NC}_\alpha)$, 14 $\delta(\text{CCH})$, 21 $\omega(\text{CCH})$, 20 $\tau(\text{CH}_2)$
1289	1289			1267 B	16 $\delta(\text{CCH})$, 13 $\omega(\text{CCH})$, 10 $\tau(\text{CCH})$, 15 $\tau(\text{CH}_2)$
	1267			1253 A	15 $\omega(\text{CCH})$, 10 $\tau(\text{CCH})$, 58 $\tau(\text{CH}_2)$

1274 1254	1267			1246 B	16 δ (CCH), 21 τ (CH ₂)
				1233 A	44 δ (CCH), 14 ρ (CCH)
1219	1226		1206		
				1196 A	20 ν_s (NC _{α}), 10 ω (CCH), 17 τ (CCH)
				1186 B	20 ν_s (NC _{α}), 23 δ_{ip} (ND), 16 δ (CCH), 23 δ_{ip} (C=O)
1170				1161 B	90 δ (ND ₂)
1146	1174			1160 A	90 δ (ND ₂)
1104	1101	1102		1117 B	10 ν_s (NC _{α}), 16 τ (CCH), 37 ρ (CH ₂)
	1065		1063	1082 A	51 ν_s (C-O), 21 ν_s (O-N), 11 ω (ND ₂)
1061		1059		1080 B	51 ν_s (C-O), 21 ν_s (O-N), 11 ω (ND ₂)
	1052		1035	1074 A	20 ν_s (CC), 10 δ_{ip} (ND), 10 ρ (CCH), 32 ρ (CH ₂)
		1037		1039 B	37 ν_s (CC), 15 δ_{ip} (ND)
1013				1018 A	35 ν_s (CC), 23 δ_{ip} (ND)
	969		981	942 A	22 δ_{ip} (ND), 19 ρ (ND ₂)
965				937 B	45 ρ (ND ₂)
			912	924 A	75 ρ (ND ₂)
924				920 B	50 ρ (ND ₂), 14 ρ (CH ₂), 10 δ_{ip} (Ring-3)
878				873 B	10 ν_s (NC _{α}), 18 δ_{ip} (ND), 34 ω (ND ₂)
	889		892		
	876			871 A	10 ν_s (NC _{α}), 39 ω (ND ₂)
				854 B	63 ν_s (O-N), 21 ν_s (C-O)
	851		859	852 A	65 ν_s (O-N), 16 ν_s (C-O)
833	833			815 B	12 δ_{ip} (ND), 48 ω (ND ₂)
780	783		798	810 A	10 ν_s (NC _{α}), 41 ω (ND ₂), 10 ρ (CH ₂), 10 δ_{op} (C=O)
767				728 B	11 ν_s (CN), 28 ν_s (C _{α} C), 18 δ_{ip} (ND), 14 δ_{ip} (Ring-3), 11 δ_{op} (C=O)
692	699				
	674		677	658 A	21 ν_s (C _{α} C), 11 δ_{op} (ND), 52 δ_{op} (C=O)
666					
642	647			643 B	13 ν_s (CC), 25 δ_{ip} (Ring-3), 43 δ_{op} (C=O)
581	592		596	585 A	50 δ_{ip} (C=O)
539				530 A	17 ν_s (C _{α} C), 19 δ_{ip} (Ring-2), 10 δ (NOC), 31 δ_{op} (ND)
525	527			528 B	11 ν_s (CC), 17 δ_{ip} (C=O), 39 δ_{op} (ND)
				516 A	16 δ (NOC), 56 δ_{op} (ND)
	470			489 B	14 δ (CCO), 52 δ_{op} (ND)
455	454			468 B	12 ρ (CCH), 10 ρ (CH ₂), 10 δ_{ip} (C=O), 32 δ (NOC)
	444		450	457 A	18 ν_s (NC _{α}), 12 δ_{ip} (Ring-1), 46 δ_{ip} (Ring-2)
	407		425	410 A	22 δ_{ip} (Ring-1), 20 δ (NOC), 14 δ_{op} (Ring-2), 11 τ (CC)
			376	353 A	10 δ (CCH), 28 ρ (CCH), 23 δ (NOC)
	339		323	352 B	24 ρ (CCH), 24 δ_{ip} (C=O)

	292			307 B	10 $\nu_s(\text{C}_\alpha\text{C})$, 43 $\delta(\text{CCO})$, 27 $\delta(\text{NOC})$
	249			272 A	29 $\delta(\text{CCO})$, 23 $\delta_{\text{ip}}(\text{Ring-1})$, 11 $\delta(\text{NOC})$
	221			224 A	16 $\omega(\text{CCH})$, 28 $\tau(\text{CCH})$, 15 $\tau(\text{C-O})$
	214			221 B	10 $\omega(\text{CCH})$, 21 $\tau(\text{CCH})$, 22 $\tau(\text{ON})$, 15 $\tau(\text{C-O})$, 15 $\tau(\text{CC})$
	198				
			162	169 A	81 $\tau(\text{ON})$, 14 $\tau(\text{C-O})$
				166 B	59 $\tau(\text{ON})$, 32 $\tau(\text{C-O})$
	143		129	134 A	11 $\delta(\text{CCO})$, 38 $\tau(\text{C-O})$, 23 $\tau(\text{CC})$
	110			113 B	17 $\omega(\text{CCH})$, 21 $\tau(\text{CCH})$, 31 $\tau(\text{C-O})$
			105	106 A	102 $\delta_{\text{op}}(\text{Ring-2})$
				102 B	93 $\delta_{\text{op}}(\text{Ring-1})$
				69 B	17 $\tau(\text{C-O})$, 71 $\tau(\text{CC})$
				55 A	28 $\tau(\text{C-O})$, 62 $\tau(\text{CC})$
				32 A	92 $\delta_{\text{op}}(\text{Ring-3})$

Table 5.5. Experimental and calculated vibrational band wavenumbers (cm^{-1}) for non-deuterated (solid) DMDKP.

IR	Raman	Calculated	%PEDs
	3195	3199 A_g	100 $\nu_s(\text{NH})$
3181		3198 B_u	100 $\nu_s(\text{NH})$
	3128	3116 A_g	96 $\nu_{\text{as}}(\text{CH}_2)$
3042		3116 B_u	96 $\nu_{\text{as}}(\text{CH}_2)$
3015		3019 B_u	95 $\nu_s(\text{CH}_2)$
	3032	3018 A_g	95 $\nu_s(\text{CH}_2)$
2932	2902		
2896			
2831	2832		
1681		1683 B_u	13 $\nu_s(\text{C=O})$, 61 $\nu_s(\text{C=C})$, 11 $\delta_{\text{ip}}(\text{Ring-3})$
	1681	1680 A_g	19 $\nu_s(\text{C=O})$, 43 $\nu_s(\text{C=C})$, 11 $\delta_{\text{ip}}(\text{NH})$, 10 $\delta_{\text{ip}}(\text{Ring-1})$
1637		1640 B_u	58 $\nu_s(\text{C=O})$, 14 $\delta_{\text{ip}}(\text{NH})$
	1600	1629 A_g	58 $\nu_s(\text{C=O})$, 26 $\nu_s(\text{C=C})$
1543			
	1499	1427 A_g	11 $\nu_s(\text{NC})$, 29 $\delta_{\text{ip}}(\text{NH})$, 41 $\delta(\text{CH}_2)$
1470			
	1438		
1414		1415 B_u	10 $\nu_s(\text{C=O})$, 10 $\nu_s(\text{C}_\alpha\text{N})$, 28 $\delta_{\text{ip}}(\text{NH})$, 47 $\delta(\text{CH}_2)$
		1383 A_g	23 $\nu_s(\text{NC}_\alpha)$, 12 $\nu_s(\text{NC})$, 22 $\nu_s(\text{C}_\alpha\text{C})$

1363	1366	1367 B _u	17 $\nu_s(\text{NC}_\alpha)$, 43 $\nu_s(\text{NC})$, 24 $\nu_s(\text{C}_\alpha\text{C})$
1342	1342	1331 B _u	10 $\nu_s(\text{C}=\text{C})$, 39 $\delta_{\text{ip}}(\text{NH})$, 38 $\delta(\text{CH}_2)$
	1303	1328 A _g	14 $\nu_s(\text{C}=\text{C})$, 24 $\delta_{\text{ip}}(\text{NH})$, 50 $\delta(\text{CH}_2)$
1282		1266 B _u	20 $\nu_s(\text{NC}_\alpha)$, 16 $\nu_s(\text{NC})$, 19 $\rho(\text{CH}_2)$, 14 $\delta_{\text{ip}}(\text{C}=\text{O})$, 15 $\delta_{\text{ip}}(\text{C}=\text{CH}_2)$
1193		1239 A _g	21 $\nu_s(\text{NC}_\alpha)$, 36 $\nu_s(\text{NC})$, 26 $\delta_{\text{ip}}(\text{NH})$
	994	974 A _g	12 $\nu_s(\text{NC}_\alpha)$, 67 $\rho(\text{CH}_2)$
1000		970 B _u	23 $\nu_s(\text{NC}_\alpha)$, 39 $\rho(\text{CH}_2)$, 10 $\delta_{\text{ip}}(\text{NH})$, 10 $\delta_{\text{ip}}(\text{C}=\text{O})$
954	909		
	894	896 A _u	95 $\delta_{\text{op}}(\text{CH}_2)$
895		895 B _g	96 $\delta_{\text{op}}(\text{CH}_2)$
		822 B _u	41 $\nu_s(\text{NC}_\alpha)$, 11 $\nu_s(\text{NC})$, 27 $\rho(\text{CH}_2)$
	785	794 B _g	71 $\delta_{\text{op}}(\text{C}=\text{O})$, 12 $\delta_{\text{op}}(\text{C}=\text{CH}_2)$, 17 $\tau(\text{CH}_2)$
		789 A _u	52 $\delta_{\text{op}}(\text{C}=\text{O})$, 37 $\tau(\text{CH}_2)$
757		751 B _u	69 $\delta_{\text{ip}}(\text{Ring-3})$
713		717 A _u	25 $\delta_{\text{op}}(\text{NH})$, 22 $\delta_{\text{op}}(\text{C}=\text{CH}_2)$, 23 $\delta_{\text{op}}(\text{C}=\text{O})$, 49 $\tau(\text{CH}_2)$
		716 B _g	24 $\delta_{\text{op}}(\text{C}=\text{CH}_2)$, 67 $\tau(\text{CH}_2)$
	682	656 A _g	15 $\nu_s(\text{NC}_\alpha)$, 13 $\nu_s(\text{NC})$, 57 $\nu_s(\text{C}_\alpha\text{C})$
844		623 B _g	90 $\delta_{\text{op}}(\text{NH})$, 14 $\tau(\text{CH}_2)$
		612 A _u	90 $\delta_{\text{op}}(\text{NH})$, 12 $\delta_{\text{op}}(\text{Ring-3})$
	620	619 A _g	12 $\rho(\text{CH}_2)$, 60 $\delta_{\text{ip}}(\text{C}=\text{O})$, 16 $\delta_{\text{ip}}(\text{C}=\text{CH}_2)$
517	515	511 A _g	15 $\nu_s(\text{NC}_\alpha)$, 10 $\delta_{\text{ip}}(\text{C}=\text{CH}_2)$, 54 $\delta_{\text{ip}}(\text{Ring-2})$
501			
482	438	435 A _u	31 $\delta_{\text{op}}(\text{C}=\text{O})$, 52 $\delta_{\text{op}}(\text{C}=\text{CH}_2)$
		422 A _g	75 $\delta_{\text{ip}}(\text{Ring-1})$
		406 B _u	14 $\nu_s(\text{NC}_\alpha)$, 14 $\nu_s(\text{C}_\alpha\text{C})$, 64 $\delta_{\text{ip}}(\text{C}=\text{O})$
	390	394 B _g	24 $\delta_{\text{op}}(\text{C}=\text{O})$, 56 $\delta_{\text{op}}(\text{C}=\text{CH}_2)$, 13 $\delta_{\text{op}}(\text{Ring-1})$
	342	328 A _g	22 $\delta_{\text{ip}}(\text{C}=\text{O})$, 55 $\delta_{\text{ip}}(\text{C}=\text{CH}_2)$, 13 $\delta_{\text{ip}}(\text{Ring-2})$
		320 B _u	77 $\delta_{\text{ip}}(\text{C}=\text{CH}_2)$
	189	147 A _u	104 $\delta_{\text{op}}(\text{Ring-3})$
	114	117 B _g	112 $\delta_{\text{op}}(\text{Ring-1})$
		61 B _g	108 $\delta_{\text{op}}(\text{Ring-2})$

Table 5.6. Experimental and calculated vibrational band wavenumbers (cm^{-1}) for *N*-deuterated (solid) DMDKP.

IR	Raman	Calculated	%PEDs
3181			
3126	3129	3116 A _g	96 $\nu_{\text{as}}(\text{CH}_2)$
		3116 B _u	96 $\nu_{\text{as}}(\text{CH}_2)$
3020		3019 B _u	96 $\nu_s(\text{CH}_2)$
	3023	3018 A _g	96 $\nu_s(\text{CH}_2)$

2930			
2900			
2835			
2319	2275		
	2263	2345 A _g	99 v _s (ND)
		2345 B _u	98 v _s (ND)
2263			
2246			
2138			
1677		1683 B _u	15 v _s (C=O), 59 v _s (C=C), 11 δ _{ip} (Ring-3)
	1644	1666 A _g	12 v _s (C=O), 57 v _s (C=C)
	1625	1626 A _g	67 v _s (C=O), 15 v _s (C=C)
1607		1621 B _u	64 v _s (C=O), 13 v _s (C=C)
	1598		
	1449		
1470			
1420	1426	1397 A _g	16 v _s (NC), 63 δ(CH ₂)
1386	1390	1393 B _u	22 v _s (NC _α), 15 v _s (NC), 55 δ(CH ₂)
	1365	1372 A _g	29 v _s (NC _α), 20 v _s (C _α C), 10 ρ(CH ₂)
	1341	1362 B _u	32 v _s (NC), 20 v _s (C _α C), 32 δ(CH ₂)
	1321	1294 A _g	15 v _s (C=C), 14 v _s (NC _α), 35 v _s (NC), 23 δ(CH ₂)
1275		1259 B _u	18 v _s (NC _α), 16 v _s (NC), 24 ρ(CH ₂), 10 δ _{ip} (C=O), 19 δ _{ip} (C=CH ₂)
1228			
1182		1152 B _u	10 v _s (C=C), 12 v _s (C _α C), 39 δ _{ip} (ND), 14 δ _{ip} (C=O)
1118	1126		
1083		1065 A _g	10 δ _{ip} (C=CH ₂), 34 ρ(CH ₂), 35 δ _{ip} (ND), 16 δ _{ip} (C=O)
	950	898 A _g	14 v _s (NC _α), 41 ρ(CH ₂), 42 δ _{ip} (ND)
930		898 B _u	16 v _s (NC _α), 56 ρ(CH ₂), 17 δ _{ip} (ND)
	908	896 A _u	95 δ _{op} (CH ₂)
891	894	895 B _g	96 δ _{op} (CH ₂)
850			
808			
782		791 B _g	72 δ _{op} (C=O), 14 δ _{op} (C=CH ₂), 16 τ(CH ₂)
	786	788 A _u	54 δ _{op} (C=O), 36 τ(CH ₂)
753		750 B _u	11 v _s (C=C), 15 v _s (C _α C), 18 δ _{ip} (ND), 41 δ _{ip} (Ring-3)
		741 B _u	11 v _s (NC), 21 v _s (C _α C), 19 δ _{ip} (ND), 32 δ _{ip} (Ring-3)
721	729	713 B _g	19 δ _{op} (C=CH ₂), 77 τ(CH ₂)
		707 A _u	19 δ _{op} (C=O), 26 δ _{op} (C=CH ₂), 58 τ(CH ₂)
	672	645 A _g	16 v _s (NC _α), 15 v _s (NC), 55 v _s (C _α C)
550	613	594 A _g	56 δ _{ip} (C=O), 14 δ _{ip} (C=CH ₂)
625		515 B _g	79 δ _{op} (ND), 14 δ _{op} (C=O), 32 δ _{op} (C=CH ₂)

501			
	509	506 A _g	14 $\nu_s(\text{NC}_\alpha)$, 11 $\delta_{\text{ip}}(\text{C}=\text{CH}_2)$, 56 $\delta_{\text{ip}}(\text{Ring-2})$
486		484 A _u	49 $\delta_{\text{op}}(\text{ND})$, 15 $\delta_{\text{op}}(\text{C}=\text{O})$, 27 $\delta_{\text{op}}(\text{C}=\text{CH}_2)$
	438	420 A _g	13 $\delta_{\text{ip}}(\text{Ring-1})$
		413 A _u	56 $\delta_{\text{op}}(\text{ND})$, 17 $\delta_{\text{op}}(\text{C}=\text{O})$, 29 $\delta_{\text{op}}(\text{C}=\text{CH}_2)$
	387 366	405 B _u	14 $\nu_s(\text{NC}_\alpha)$, 14 $\nu_s(\text{C}_\alpha\text{C})$, 64 $\delta_{\text{ip}}(\text{C}=\text{O})$
	340	347 B _g	26 $\delta_{\text{op}}(\text{ND})$, 14 $\delta_{\text{op}}(\text{C}=\text{O})$, 34 $\delta_{\text{op}}(\text{C}=\text{CH}_2)$, 20 $\delta_{\text{op}}(\text{Ring-1})$
		327 A _g	21 $\delta_{\text{ip}}(\text{C}=\text{O})$, 55 $\delta_{\text{ip}}(\text{C}=\text{CH}_2)$, 14 $\delta_{\text{ip}}(\text{Ring-2})$
		319 B _u	77 $\delta_{\text{ip}}(\text{C}=\text{CH}_2)$
	184	144 A _u	109 $\delta_{\text{op}}(\text{Ring-3})$
	110 92	116 B _g	117 $\delta_{\text{op}}(\text{Ring-1})$
		61 B _g	109 $\delta_{\text{op}}(\text{Ring-2})$

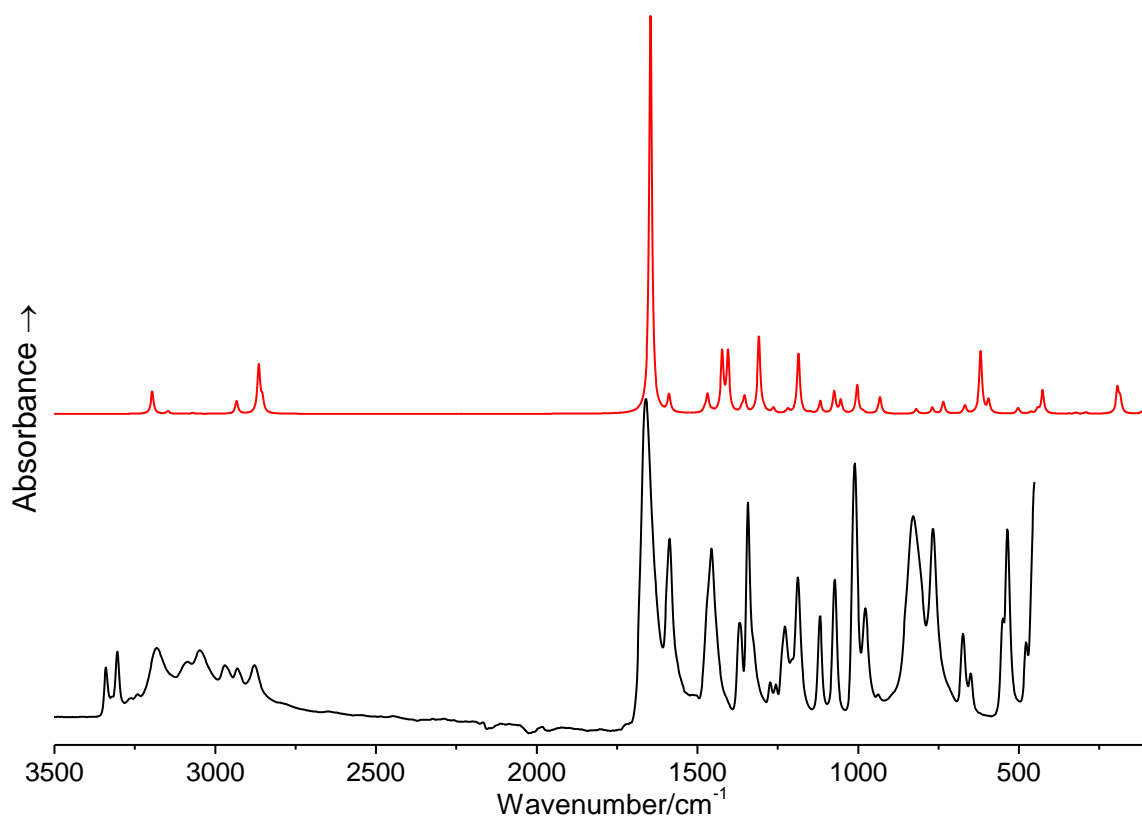


Figure 5.7. Calculated (top) and experimental (bottom) solid state IR spectra for AMDKP.

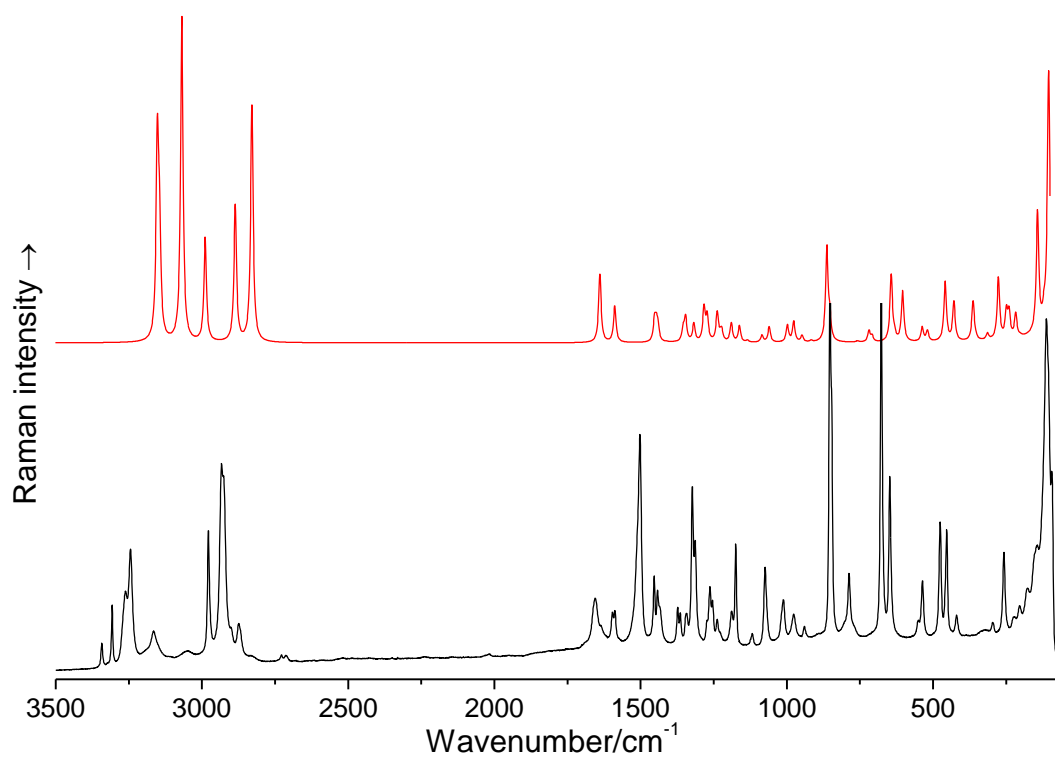


Figure 5.8. Calculated (top) and experimental (bottom) solid state Raman spectra for AMDKP.

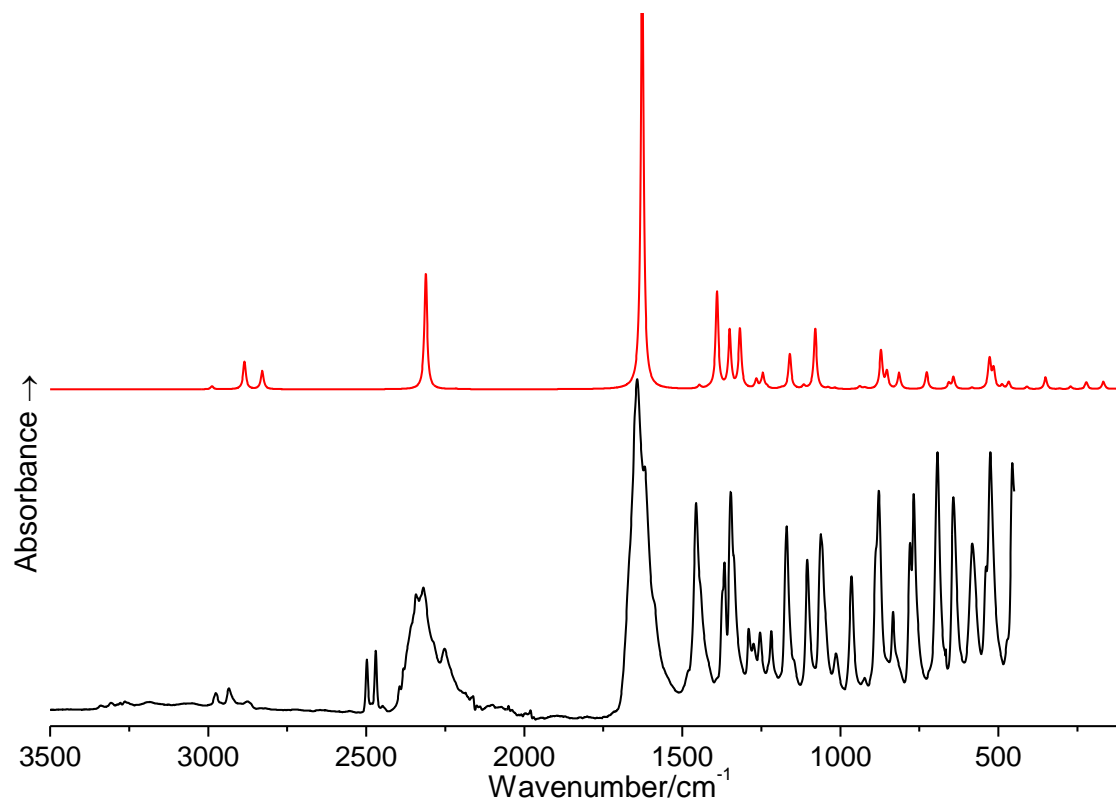


Figure 5.9. Calculated (top) and experimental (bottom) solid state IR spectra for *N*-deuterated AMDKP.

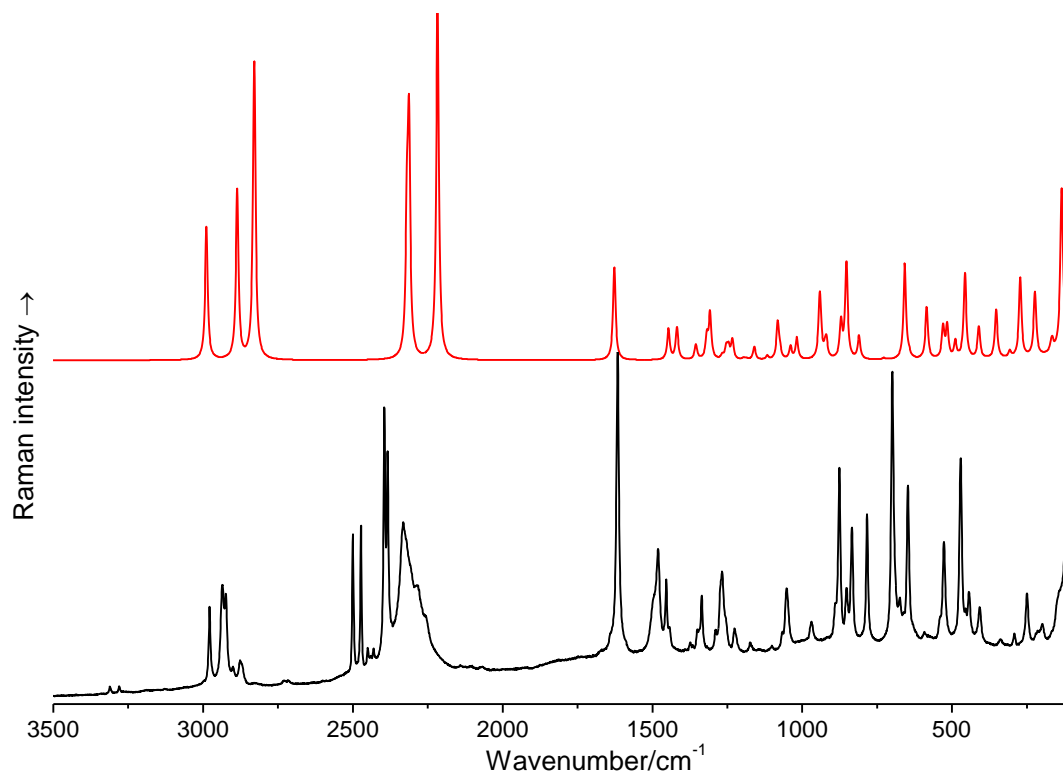


Figure 5.10. Calculated (top) and experimental (bottom) solid state Raman spectra for *N*-deuterated AMDKP.

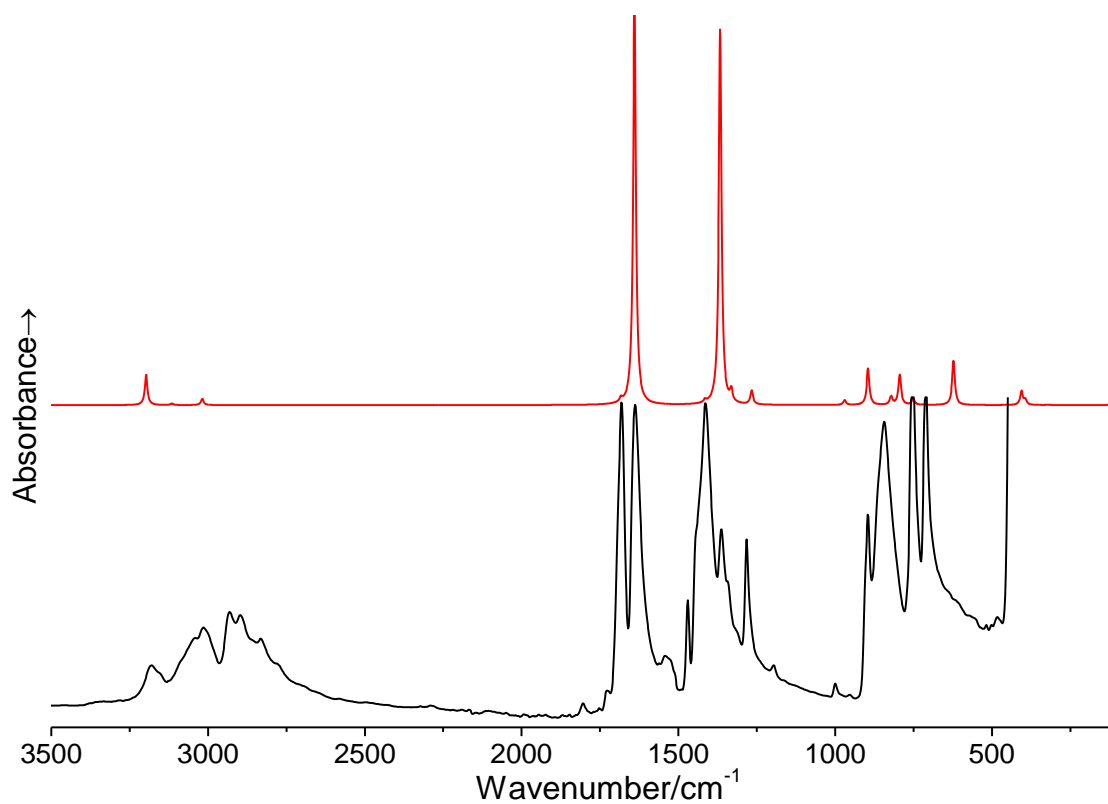


Figure 5.11. Calculated (top) and experimental (bottom) solid state IR spectra for DMDKP.

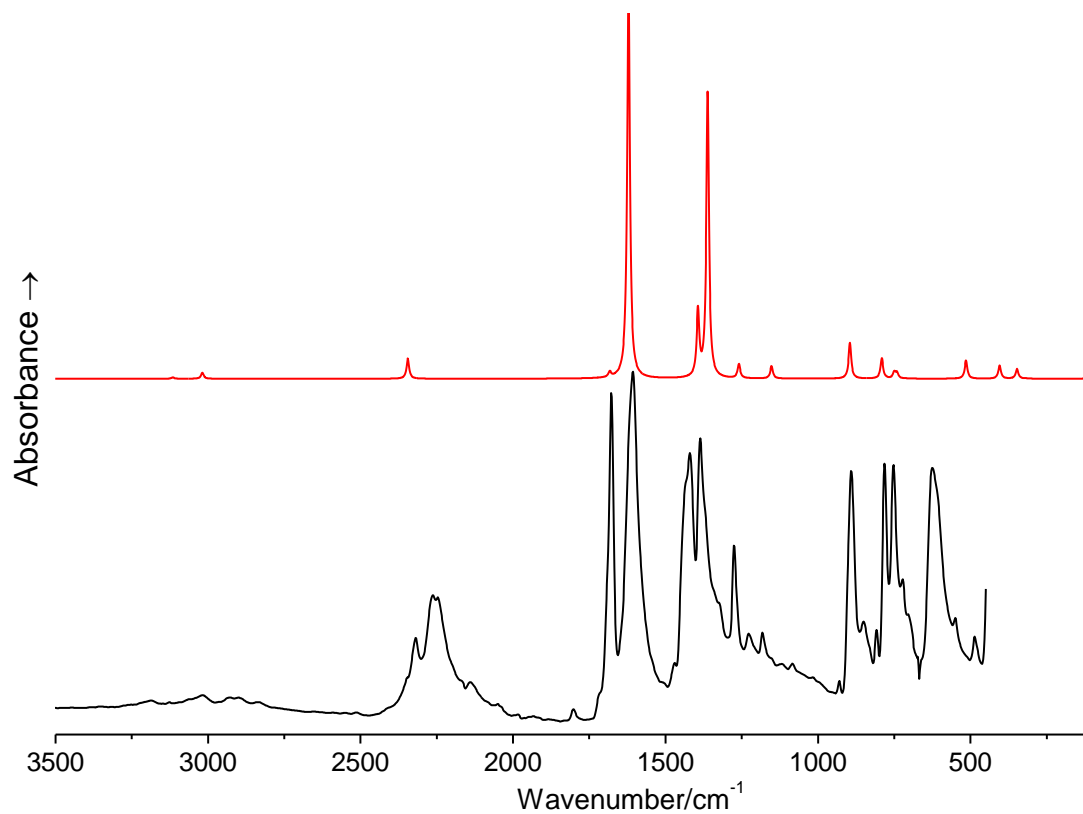


Figure 5.12. Calculated (top) and experimental (bottom) solid state IR spectra for *N*-deuterated DMDKP.

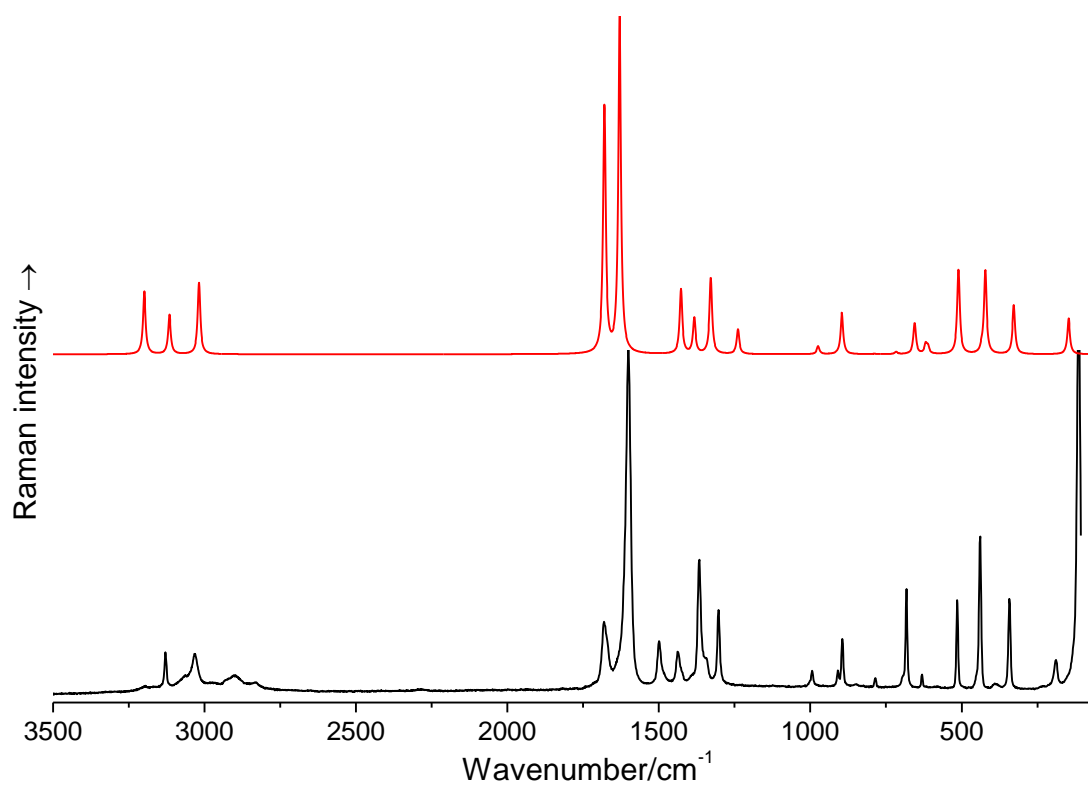


Figure 5.13. Calculated (top) and experimental (bottom) solid state Raman spectra for DMDKP.

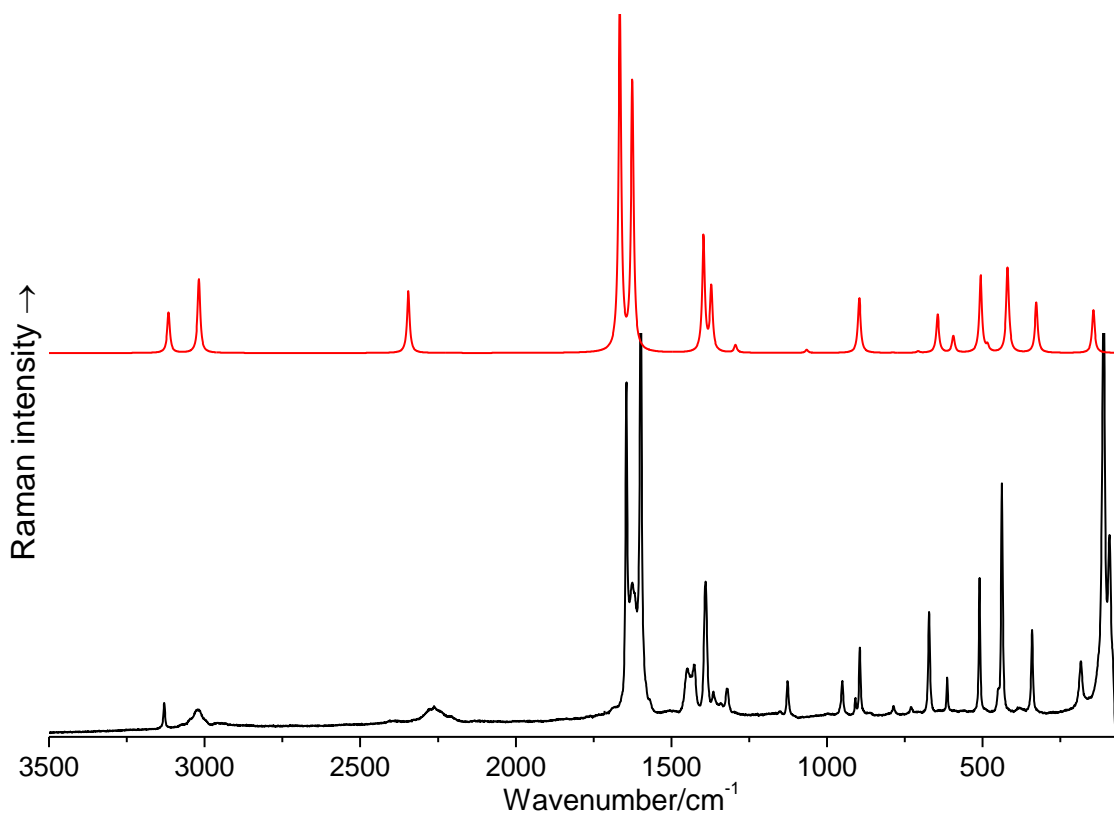


Figure 5.14. Calculated (top) and experimental (bottom) solid state Raman spectra for *N*-deuterated DMDKP.

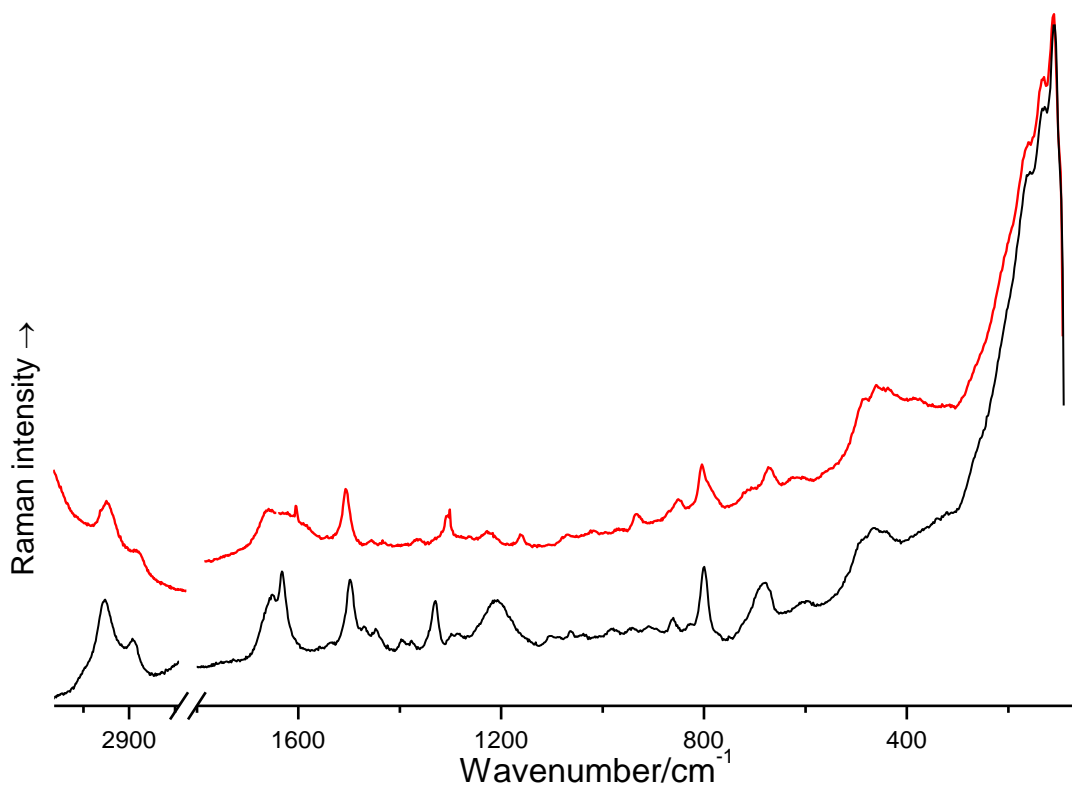


Figure 5.15. Experimental non-deuterated (top) and *N*-deuterated (bottom) solution state Raman spectra of AMDKP.

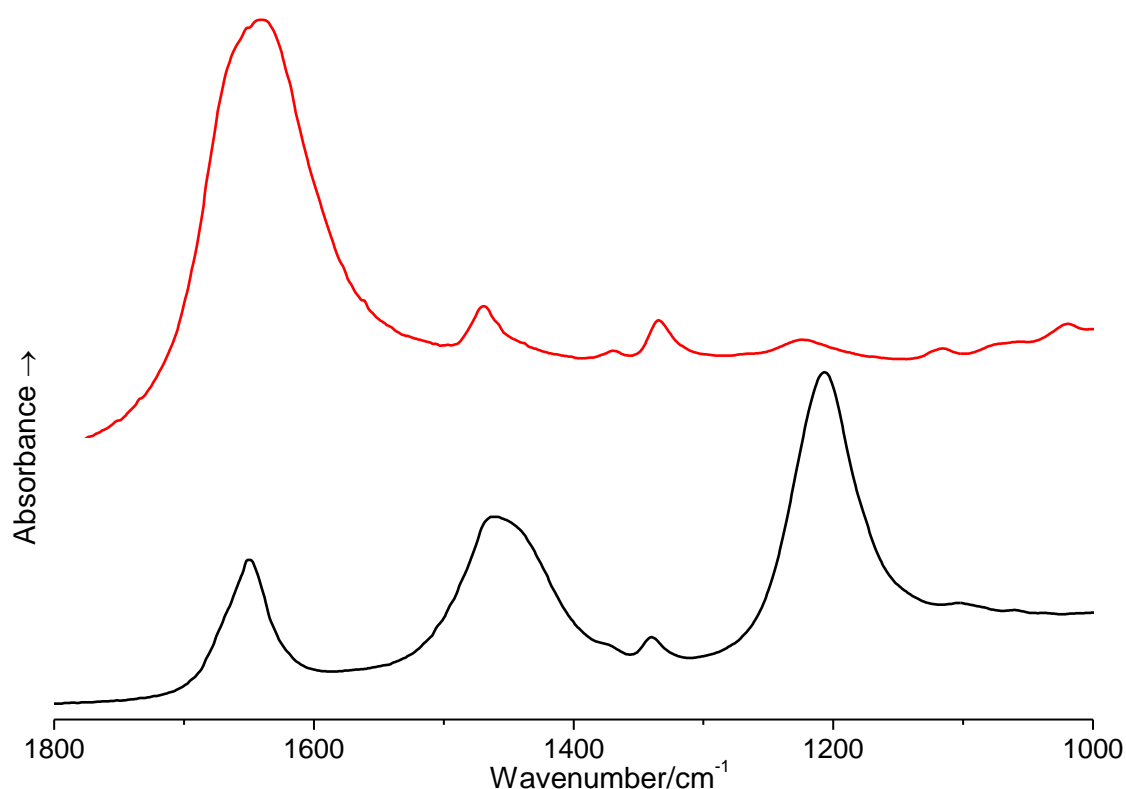


Figure 5.16. Experimental non-deuterated (top) and *N*-deuterated (bottom) solution state IR spectra of AMDKP.

5.5. Molecular orbital analysis

The highest occupied molecular orbital (HOMO) and lowest unoccupied molecular orbital (LUMO) energies of AMDKP and DMDKP were calculated at their optimised geometries. The molecular orbitals (HOMO and LUMO) of AMDKP and DMDKP with their compositions are shown in Figs. 5.17 and 5.18. The HOMO energies of AMDKP and DMDKP are -7.002 eV and -7.034 eV, respectively, whereas, the LUMO energies are -0.620 eV and -2.270 eV. The analyses of molecular orbitals of AMDKP illustrated that the HOMO is localized on the DKP ring whereas the LUMO is localized on the aminoxymethyl side chains and partly on the DKP ring. The computed HOMO-LUMO energy gap of AMDKP is 6.381 eV. In case of DMDKP, the HOMO is localized on nitrogen atoms of DKP ring, double bonds of the 3,6-dimethylene side chains and partly on oxygen atoms of DKP ring, whereas the LUMO is predominantly localized on carbon and oxygen atoms of the DKP ring and CH₂ groups of the 3,6-dimethylene side chains. The computed HOMO-LUMO energy gap for DMDKP is 4.764 eV. Since the HOMO-LUMO gap value is relatively large, it is therefore expected that both AMDKP and DMDKP are not very chemically reactive or polarizable, and are, therefore, relatively stable molecules.

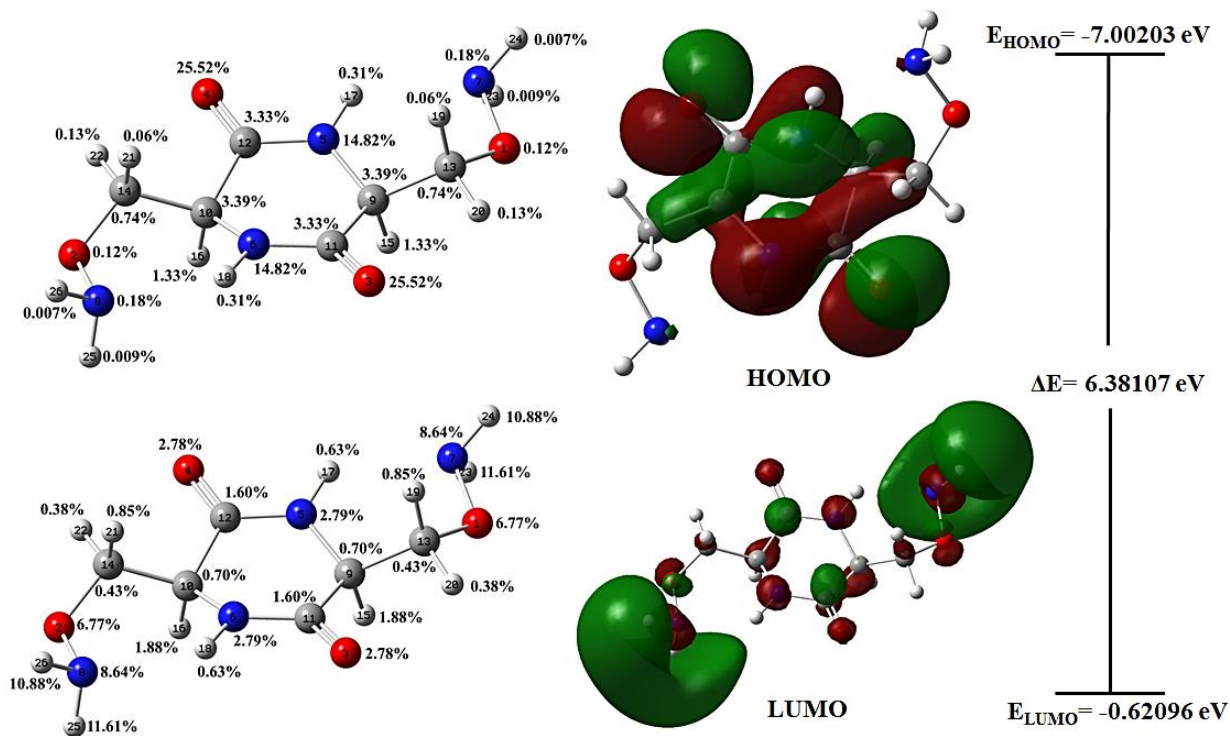


Figure 5.17. HOMO-LUMO plots with orbital compositions of AMDKP.

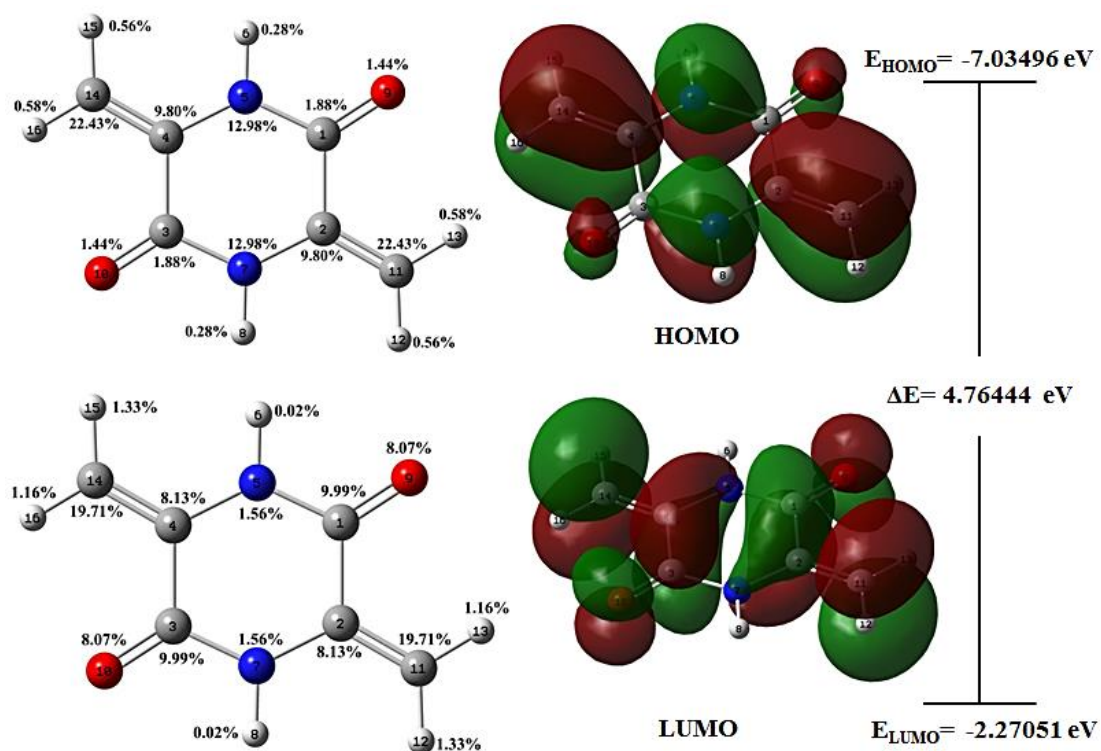


Figure 5.18. HOMO-LUMO plots with orbital compositions of DMDKP.

5.7. Molecular electrostatic potential

The total electron density mapped with molecular electrostatic potential (MEP) surface and the contour map of electrostatic potential (ESP) have been plotted for AMDKP (Fig. 5.19) and DMDKP (Fig. 5.20) molecules at the B3LYP/aug-cc-pVTZ level. The MEP surfaces are in the range between -5.31 (arb. units) (deepest red) and 5.31 (arb. units) (deepest blue) for AMDKP and between -5.74 (arb. units) (deepest red) and 5.74 (arb. units) (deepest blue) for DMDKP. The red area indicates the strongest electrostatic repulsion and blue coloured area indicates the strongest attraction. From the MEP maps of AMDKP (Fig. 5.19a) and DMDKP (Fig. 5.20a), the increase in negative potential is shown from yellow to red colour, with the maximum negative potential in red colour (preferred site for electrophilic attack), green represent the zero potentials and the maximum positive region, (preferred site for nucleophilic attack) is represented in deep blue colour.

The negative potentials are mainly over the electronegative oxygen atoms of the DKP ring, and the oxygen atoms of the aminoxymethyl side-chains (in the case of AMDKP). There is positive potential over the nitrogen and hydrogen atoms of the DKP ring in both AMDKP and DMDKP. This information can be useful in investigating possible sites for intermolecular interactions. The contour map of MEP also clearly indicates the electron rich red lines are around oxygen and nitrogen and electron deficient yellow lines are around hydrogen and carbon atoms in both AMDKP (Fig. 5.19b) and DMDKP (Fig. 5.20b).

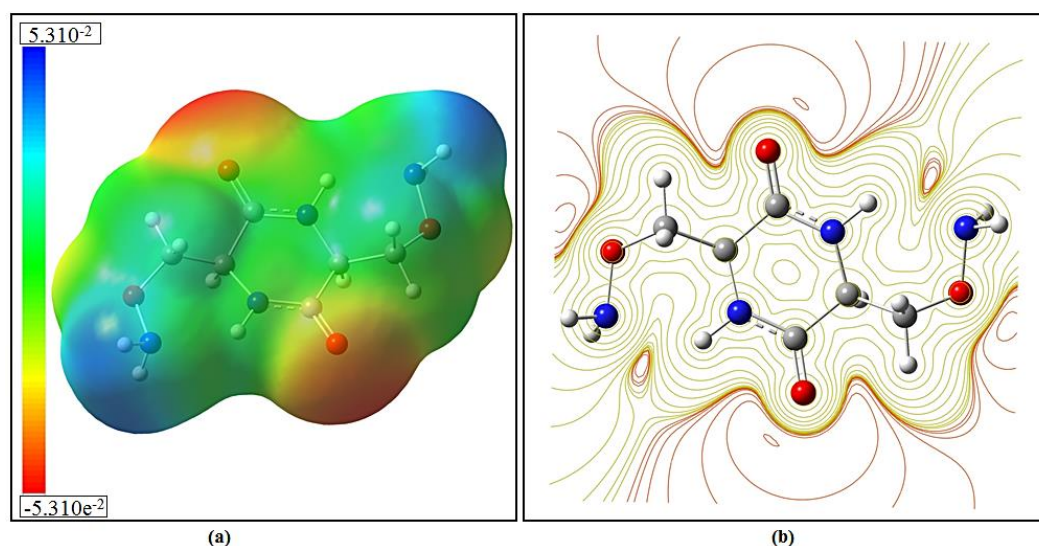


Figure 5.19. (a) MEP energy surface and (b) contour map (MEP) for AMDKP.

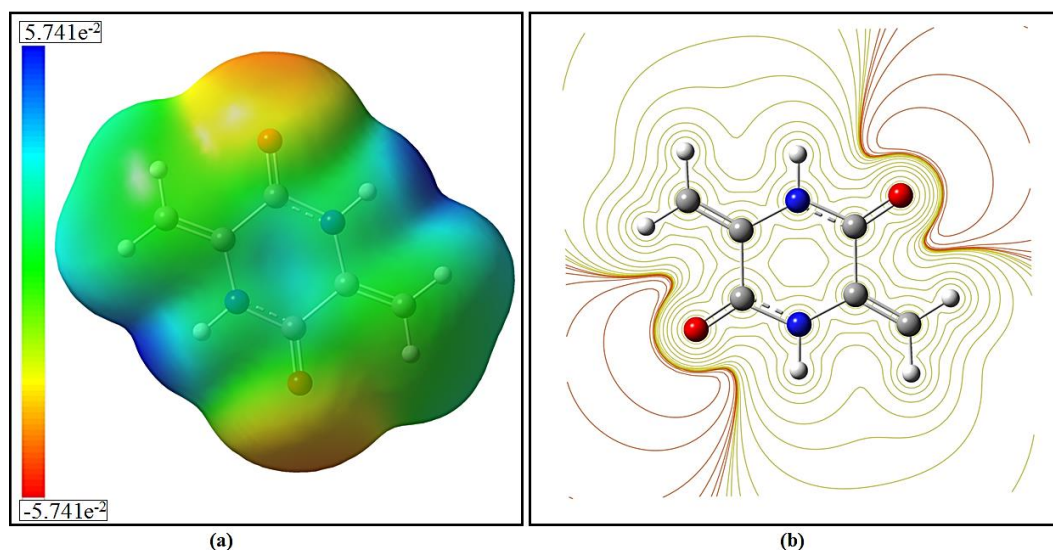


Figure 5.20. (a) MEP energy surface and (b) contour map (MEP) for DMDKP.

5.7. Hirshfeld surface analysis

The Hirshfeld surfaces of DMDKP are illustrated in Fig. 5.21 showing the mapped surface over d_{norm} , curvedness and shape index in Fig. 5.22. The 2D fingerprint plots for all the close contacts in DMDKP are shown in Fig. 5.23. The interactions between the carbonyl oxygen atoms and the hydrogen atoms of the neighbouring molecule O--H (17.6%)/H--O (14.3%) can be seen as the bright red areas on the Hirshfeld surface (Fig. 5.21, labelled as a). The light red spots are due to C--C (2.0%) interactions between the carbonyl atoms of the DKP ring (Fig. 5.21, labelled as b). The H--H and O--H/H--O intermolecular interactions appear as separate spikes in the 2D fingerprint plot (Fig. 5.23). Corresponding regions are visible in the fingerprint plots where one molecule act as an acceptor ($d_e < d_i$) and other acts as a donor ($d_e > d_i$). The small broad region with $(d_e + d_i)$ value around 2.8 Å, pointing toward the lower left of the plots is due to H--H hydrogen interactions, encompassing 32.5 % of the total Hirshfeld surface for DMDKP. The O--H/H--O interactions can be easily located as the sharp spikes on the 2D fingerprint plot (Fig. 5.23). They comprise about 17.6-14.3% of total Hirshfeld surface with a low $(d_e + d_i)$ value of 1.8 Å. The shortest contact i.e., the minimum $(d_e + d_i)$ value is around 1.8 Å shows the importance of O--H interactions on the Hirshfeld surface of DMDKP.

From the fingerprint plots, the contributions involving different interactions includes C--C/H/O, N--O/C/H on the fingerprint plots comprises around C--H (10.9%), C--O/O--C (3-4%), N--H (3.3 %) and N--O (1.7 %) and N--C (0.2%) of the total Hirshfeld surface area for DMDKP (Fig 5.23). Curvedness and shape index can also be used to identify the ways by which the neighbouring molecules contact each another and the characteristic packing modes. The shape index of DMDKP

shows a red concave region on the surface around the acceptor atom and a blue region around the donor H-atom (Fig. 5.22a). Curvedness is a function of the RMS curvature of the surface and the curvedness maps on the Hirshfeld surface shows that the largest flat regions appear near carbonyl carbons of the DKP ring (Fig. 5.22b) and hence, indicates that stacking interaction occur between the molecules of DMDKP (Fig. 5.22c). The type and nature of the interaction of DMDKP molecule is more easily understood using Hirshfeld surface analysis, the results showcase the power of the analysis in mapping out the interactions.

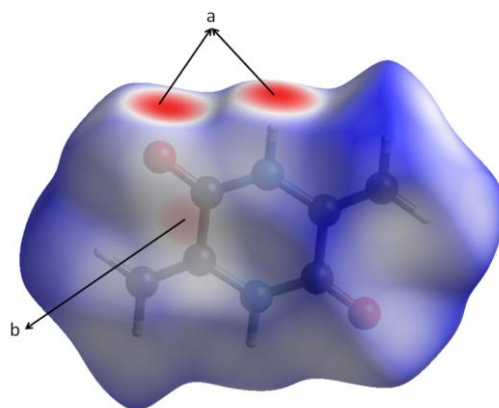


Figure 5.21. Hirshfeld surface mapped with d_{norm} showing all close contacts in DMDKP.

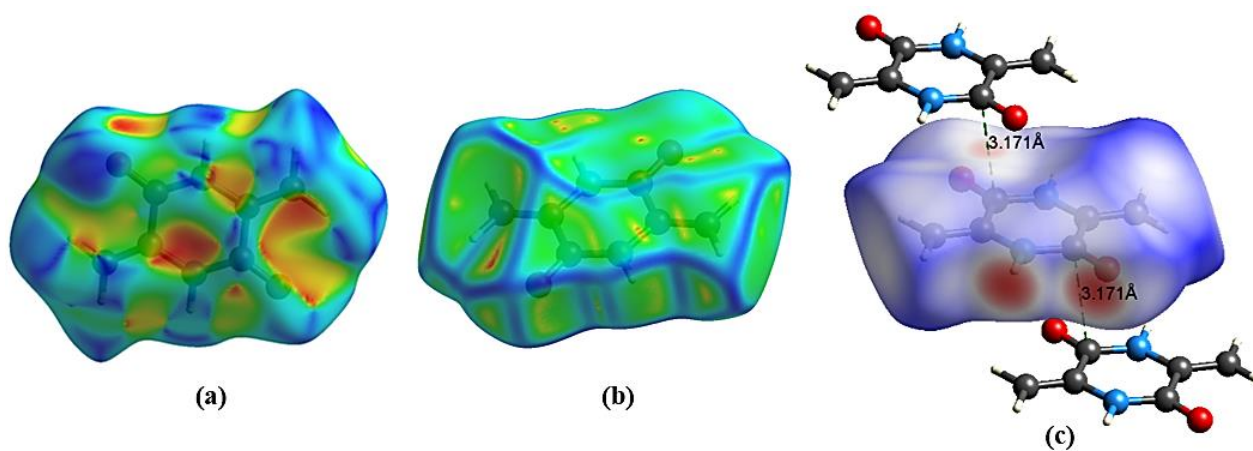


Figure 5.22. Hirshfeld surfaces of DMDKP mapped with (a) shape index (b) curvedness (c) stacking interactions in DMDKP.

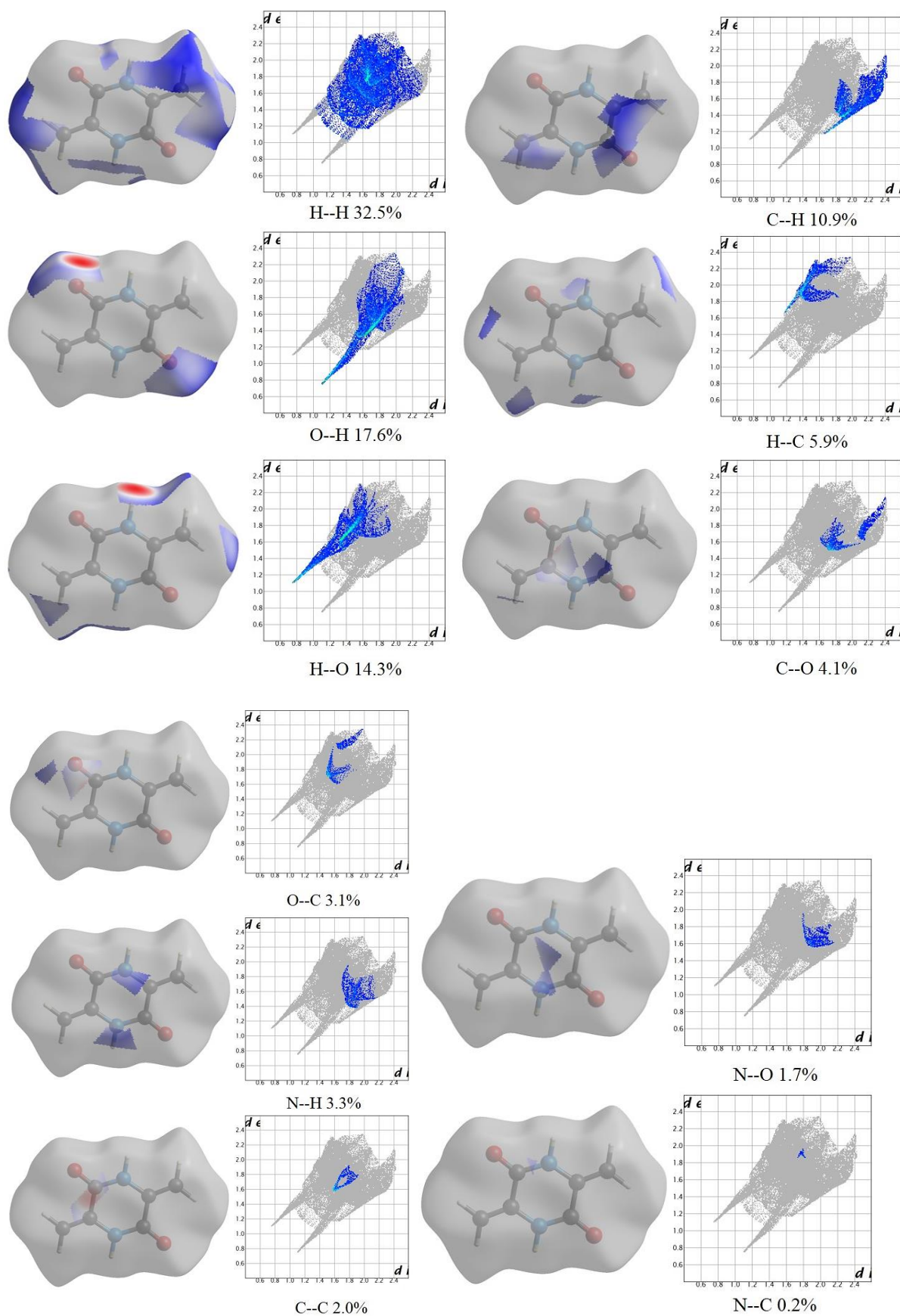


Figure 5.23. 2D Fingerprint plots for the intermolecular contacts in DMDKP.

5.8. Conclusions

An IR and Raman spectroscopic study on the degradation products of D-cycloserine (AMDKP and DMDKP) was carried out in the solid state and solution state (AMDKP only). There is no available X-ray data for AMDKP but DFT calculations suggests that the DKP ring in AMDKP molecule adopts a boat conformation with C_2 symmetry. The X-ray and calculated structures of DMDKP suggest that the DKP ring adopts a planar conformation with C_{2h} symmetry. From our observations, it is suggested that in AMDKP the N-H bonds in the DKP ring participate in intermolecular hydrogen bonding and hence appear at lower wavenumber compared with NH_2 vibrations. The assignments of the amide I and II modes and the nature of the amide vibrations of the *cis* peptide groups in AMDKP and DMDKP have been confirmed by the spectroscopic data and DFT calculations. The effect of differing ring conformations can have a dramatic influence on the location of the *cis* amide II band, which is observed at 1502 cm^{-1} . This band appears at 1518 cm^{-1} in solution state Raman spectrum of AMDKP. The increase in strain on the DKP ring due to the attachment of bulky substituents on the C_α atoms may also influence the location of the amide II mode. Theoretically from calculated PEDs and experimentally from *N*-deuteration shifts in IR and Raman spectra, it is suggested that assumptions on the *cis* amide I mode in DMDKP cannot be made from the experimental data. However, the planar conformation of DKP ring in DMDKP with C_{2h} symmetry has been confirmed by the mutual exclusion rule which appears to hold for the IR and Raman spectra of DMDKP in the solid state. The *cis* amide II mode in DMDKP is found at 1499 cm^{-1} and shifts to lower wavenumber ($\sim 50\text{ cm}^{-1}$) on *N*-deuteration. This is a very unusual observation for a planar DKP molecule to have such a low wavenumber for a *cis* amide II mode and its greater shift on *N*-deuteration compared to other DKPs.¹⁶ The assignment of the *cis* amide II mode at 1427 cm^{-1} from the calculated PEDs also shows a wavenumber shift ($\sim 30\text{ cm}^{-1}$) on *N*-deuteration. Hence, it is hypothesised that, due to strong coupling of out of phase C_α -C-N stretch with N-H in plane bending in *cis* amide II mode and also because of the presence of high N-H character may have a significant effect on the wavenumber of the *cis* amide II mode in DMDKP, with a greater shift on *N*-deuteration compared with planar or near-planar DKPs.¹⁶

HOMO and LUMO analysis has been carried out to elucidate the information related to the charge transfer within the molecule. The HOMO-LUMO gap of AMDKP and DMDKP was found to be about 6.38 eV and 4.76 eV, which implies that both compounds possesses relatively high chemical stability. The MEP analysis reveals that the most negative potential site is around the oxygen atoms of the DKP ring and the side chains (AMDKP), while the positive potential site is located around

the nitrogen, hydrogen atoms. The Hirshfeld surface analysis and 2D fingerprint plots enabled investigations of the types of intermolecular interactions present in the reported crystal structure of DMDKP.

Table 5.6. Definitions of symmetry-adapted internal coordinates for AMDKP and DMDKP.

AMDKP

A symmetry

$$v_s(\text{NH})=1/\sqrt{2}[r(\text{N5H17}) + r(\text{N6H18})]$$

$$v_s(\text{C=O})=1/\sqrt{2}[r(\text{C11O3}) + r(\text{C12O4})]$$

$$v_s(\text{CN})=1/\sqrt{2}[r(\text{N5C12}) + r(\text{N6C11})]$$

$$v_s(\text{NC}_\alpha)=1/\sqrt{2}[r(\text{N5C9}) + r(\text{N6C10})]$$

$$v_s(\text{CC}_\alpha)=1/\sqrt{2}[r(\text{C12C10}) + r(\text{C9C11})]$$

$$v_s(\text{C}_\alpha\text{C}) = 1/\sqrt{2}[r(\text{C9C13}) + r(\text{C10C14})]$$

$$v_s(\text{C-O}) = 1/\sqrt{2}[r(\text{C13O1}) + r(\text{C14O2})]$$

$$v_s(\text{O-N}) = 1/\sqrt{2}[r(\text{O1N7}) + r(\text{O2N8})]$$

$$v_s(\text{CH}) = 1/\sqrt{2}[r(\text{C9H15}) + r(\text{C10H16})]$$

$$v_s(\text{NH}_2) = 1/2[r(\text{N7H23}) + r(\text{N7H24}) + r(\text{N8H25}) + r(\text{N8H26})]$$

$$v_{as}(\text{NH}_2) = 1/2[r(\text{N7H23}) - r(\text{N7H24}) + r(\text{N8H25}) - r(\text{N8H26})]$$

$$v_s(\text{CH}_2) = 1/2[r(\text{C13H19}) + r(\text{C13H20}) + r(\text{C14H21}) + r(\text{C14H22})]$$

$$v_{as}(\text{CH}_2) = 1/2[r(\text{C13H19}) - r(\text{C13H20}) + r(\text{C14H21}) - r(\text{C14H22})]$$

$$\delta_{ip}(\text{NH})=1/2[\theta(\text{C9N5H17}) - \theta(\text{C12N5H17}) + \theta(\text{C11N6H18}) - \theta(\text{C10N6H18})]$$

$$\delta_{ip}(\text{CO})=1/2[\theta(\text{N5C12O4}) - \theta(\text{C10C12O4}) + \theta(\text{N6C11O3}) - \theta(\text{C9C11O3})]$$

$$\delta(\text{CH}_2) = 1/2\sqrt{6}[(\sqrt{6} + 2)\theta(\text{H19C13H20}) - (\sqrt{6} - 2)\theta(\text{C9C13O1}) - \theta(\text{C9C13H19}) - \theta(\text{C9C13H20}) - \theta(\text{O1C13H19}) - \theta(\text{O1C13H20}) + (\sqrt{6} + 2)\theta(\text{H21C14H22}) - (\sqrt{6} - 2)\theta(\text{C10C14O2}) - \theta(\text{C10C14H21}) - \theta(\text{C10C14H22}) - \theta(\text{O2C14H21}) - \theta(\text{O2C14H22})]$$

$$\rho(\text{CH}_2) = 1/2\sqrt{2}[(\theta(\text{C9C13H19}) - \theta(\text{C9C13H20}) + \theta(\text{O1C13H19}) - \theta(\text{O1C13H20}) + \theta(\text{C10C14H21}) - \theta(\text{C10C14H22}) + \theta(\text{O2C14H21}) - \theta(\text{O2C14H22})]$$

$$\omega(\text{CH}_2) = 1/2\sqrt{2}[(\theta(\text{C9C13H19}) + \theta(\text{C9C13H20}) - \theta(\text{O1C13H19}) - \theta(\text{O1C13H20}) + \theta(\text{C10C14H21}) + \theta(\text{C10C14H22}) - \theta(\text{O2C14H21}) - \theta(\text{O2C14H22})]$$

$$\tau(\text{CH}_2) = 1/2\sqrt{2}[(\theta(\text{C9C13H19}) - \theta(\text{C9C13H20}) - \theta(\text{O1C13H19}) + \theta(\text{O1C13H20}) + \theta(\text{C10C14H21}) - \theta(\text{C10C14H22}) - \theta(\text{O2C14H21}) + \theta(\text{O2C14H22})]$$

$$\delta(\text{NH}_2) = 1/2\sqrt{3}[(2\theta(\text{H23N7H24}) - \theta(\text{O1N7H23}) - \theta(\text{O1N7H24}) + 2\theta(\text{H25N8H26}) - \theta(\text{O2N8H25}) - \theta(\text{O2N8H26})]$$

$$\rho(\text{NH}_2) = 1/2[(\theta(\text{O1N7H23}) - \theta(\text{O1N7H24}) + \theta(\text{O2N8H25}) - \theta(\text{O2N8H26})]$$

$$\begin{aligned}
\omega(\text{NH}_2) &= 1/\sqrt{6}[(\theta(\text{H23N7H24}) + \theta(\text{O1N7H23}) + \theta(\text{O1N7H24}) + \theta(\text{H25N8H26}) + \theta(\text{O2N8H25}) + \theta(\text{O2N8H26})] \\
\rho(\text{CCH}) &= 1/2\sqrt{2}[(\theta(\text{N5C9H15}) - \theta(\text{N5C9C13}) + \theta(\text{C11C9H15}) - \theta(\text{C11C9C13}) + (\theta(\text{N6C10H16}) - \theta(\text{N6C10C14}) + \theta(\text{C12C10H16}) - \theta(\text{C12C10C14})] \\
\omega(\text{CCH}) &= 1/2\sqrt{2}[(\theta(\text{N5C9H15}) + \theta(\text{N5C9C13}) - \theta(\text{C11C9H15}) - \theta(\text{C11C9C13}) + (\theta(\text{N6C10H16}) + \theta(\text{N6C10C14}) - \theta(\text{C12C10H16}) - \theta(\text{C12C10C14})] \\
\tau(\text{CCH}) &= 1/2\sqrt{2}[(\theta(\text{N5C9H15}) - \theta(\text{N5C9C13}) - \theta(\text{C11C9H15}) + \theta(\text{C11C9C13}) + (\theta(\text{N6C10H16}) - \theta(\text{N6C10C14}) - \theta(\text{C12C10H16}) + \theta(\text{C12C10C14})] \\
\delta(\text{CCH}) &= 1/\sqrt{2}[\theta(\text{C13C9H15}) + \theta(\text{C14C10H16})] \\
\delta_{\text{op}}(\text{CO}) &= 1/\sqrt{2}[\tau(\text{O4C12N5C10}) + \tau(\text{O3C11N6C9})] \\
\delta_{\text{op}}(\text{NH}) &= 1/\sqrt{2}[\tau(\text{H17N5C12C9}) + \tau(\text{H18N6C11C10})] \\
\delta(\text{CCO}) &= 1/2\sqrt{6}[(-\sqrt{6} - 2)\theta(\text{H19C13H20}) + (\sqrt{6} + 2)\theta(\text{C9C13O1}) - \theta(\text{C9C13H19}) - \theta(\text{C9C13H20}) - \theta(\text{O1C13H19}) - \theta(\text{O1C13H20}) - (\sqrt{6} - 2)\theta(\text{H21C14H22}) \\
&\quad + (\sqrt{6} + 2)\theta(\text{C10C14O2}) - \theta(\text{C10C14H21}) - \theta(\text{C10C14H22}) - \theta(\text{O2C14H21}) - \theta(\text{O2C14H22})] \\
\delta(\text{NOC}) &= 1/\sqrt{2}[\theta(\text{C13O1N7}) + \theta(\text{C14O2N8})] \\
\tau(\text{CC}) &= 1/3\sqrt{2}[\tau(\text{H15C9C13O1}) + \tau(\text{H15C9C13H19}) + \tau(\text{H15C9C13H20}) + \tau(\text{N5C9C13O1}) + \tau(\text{N5C9C13H19}) + \tau(\text{N5C9C13H20}) + \tau(\text{C11C9C13O1}) \\
&\quad + \tau(\text{C11C9C13H19}) + \tau(\text{C11C9C13H20}) + \tau(\text{H16C10C14O2}) + \tau(\text{H16C10C14H21}) + \tau(\text{H16C10C14H22}) + \tau(\text{N6C10C14O2}) + \tau(\text{N6C10C14H21}) \\
&\quad + \tau(\text{N6C10C14H22}) + \tau(\text{C12C10C14O2}) + \tau(\text{C12C10C14H21}) + \tau(\text{C12C10C14H22})] \\
\tau(\text{C-O}) &= 1/\sqrt{6}[\tau(\text{C9C13O1N7}) + \tau(\text{H19C13O1N7}) + \tau(\text{H20C13O1N7}) + \tau(\text{C10C14O2N8}) + \tau(\text{H21C14O2N8}) + \tau(\text{H22C14O2N8})] \\
\tau(\text{ON}) &= 1/2[\tau(\text{C13O1N7H23}) + \tau(\text{C13O1N7H24}) + \tau(\text{C14O2N8H25}) + \tau(\text{C14O2N8H26})] \\
\delta_{\text{ip}}(\text{Ring-1}) &= 1/\sqrt{12}[2\theta(\text{C11C9N5}) - \theta(\text{C9N5C12}) - \theta(\text{N5C12C10}) + 2\theta(\text{C12C10N6}) - \theta(\text{C10N6C11}) - \theta(\text{N6C11C9})] \\
\delta_{\text{ip}}(\text{Ring-2}) &= 1/2[\theta(\text{C9N5C12}) - \theta(\text{N5C12C10}) + \theta(\text{C10N6C11}) - \theta(\text{N6C11C9})] \\
\delta_{\text{op}}(\text{Ring-2}) &= 1/\sqrt{12}[2\tau(\text{C10C12N5C9}) - \tau(\text{C12N5C9C11}) - \tau(\text{N5C9C11N6}) + 2\tau(\text{C9C11N6C10}) - \tau(\text{C11N6C10C12}) - \tau(\text{N6C10C12N5})] \\
\delta_{\text{op}}(\text{Ring-3}) &= 1/2[\tau(\text{C12N5C9C11}) - \tau(\text{N5C9C11N6}) + \tau(\text{C11N6C10C12}) - \tau(\text{N6C10C12N5})]
\end{aligned}$$

B symmetry

$$\begin{aligned}
v_{\text{as}}(\text{NH}) &= 1/\sqrt{2}[r(\text{N5H17}) - r(\text{N6H18})] \\
v_{\text{as}}(\text{C=O}) &= 1/\sqrt{2}[r(\text{C11O3}) - r(\text{C12O4})] \\
v_{\text{as}}(\text{CN}) &= 1/\sqrt{2}[r(\text{N5C12}) - r(\text{N6C11})] \\
v_{\text{as}}(\text{NC}_\alpha) &= 1/\sqrt{2}[r(\text{N5C9}) - r(\text{N6C10})] \\
v_{\text{as}}(\text{CC}_\alpha) &= 1/\sqrt{2}[r(\text{C12C10}) - r(\text{C9C11})]
\end{aligned}$$

$$\begin{aligned}
v_{\text{as}}(\text{C}\alpha\text{C}) &= 1/\sqrt{2}[r(\text{C9C13}) - r(\text{C10C14})] \\
v_{\text{as}}(\text{C-O}) &= 1/\sqrt{2}[r(\text{C13O1}) - r(\text{C14O2})] \\
v_{\text{as}}(\text{O-N}) &= 1/\sqrt{2}[r(\text{O1N7}) - r(\text{O2N8})] \\
v_{\text{as}}(\text{CH}) &= 1/\sqrt{2}[r(\text{C9H15}) - r(\text{C10H16})] \\
v_{\text{s}}(\text{NH}_2) &= 1/2[r(\text{N7H23}) + r(\text{N7H24}) - r(\text{N8H25}) - r(\text{N8H26})] \\
v_{\text{as}}(\text{NH}_2) &= 1/2[r(\text{N7H23}) - r(\text{N7H24}) - r(\text{N8H25}) + r(\text{N8H26})] \\
v_{\text{s}}(\text{CH}_2) &= 1/2[r(\text{C13H19}) + r(\text{C13H20}) - r(\text{C14H21}) - r(\text{C14H22})] \\
v_{\text{as}}(\text{CH}_2) &= 1/2[r(\text{C13H19}) - r(\text{C13H20}) - r(\text{C14H21}) + r(\text{C14H22})] \\
\delta_{\text{ip}}(\text{NH}) &= 1/2[\theta(\text{C9N5H17}) - \theta(\text{C12N5H17}) - \theta(\text{C11N6H18}) + \theta(\text{C10N6H18})] \\
\delta_{\text{ip}}(\text{CO}) &= 1/2[\theta(\text{N5C12O4}) - \theta(\text{C10C12O4}) - \theta(\text{N6C11O3}) + \theta(\text{C9C11O3})] \\
\delta(\text{CH}_2) &= 1/2\sqrt{6}[(\sqrt{6} + 2)\theta(\text{H19C13H20}) - (\sqrt{6} - 2)\theta(\text{C9C13O1}) - \theta(\text{C9C13H19}) - \theta(\text{C9C13H20}) - \theta(\text{O1C13H19}) - \theta(\text{O1C13H20}) - (\sqrt{6} + 2)\theta(\text{H21C14H22}) \\
&\quad + (\sqrt{6} - 2)\theta(\text{C10C14O2}) + \theta(\text{C10C14H21}) + \theta(\text{C10C14H22}) + \theta(\text{O2C14H21}) + \theta(\text{O2C14H22})] \\
\rho(\text{CH}_2) &= 1/2\sqrt{2}[(\theta(\text{C9C13H19}) - \theta(\text{C9C13H20}) + \theta(\text{O1C13H19}) - \theta(\text{O1C13H20}) - \theta(\text{C10C14H21}) + \theta(\text{C10C14H22}) - \theta(\text{O2C14H21}) + \theta(\text{O2C14H22})] \\
\omega(\text{CH}_2) &= 1/2\sqrt{2}[(\theta(\text{C9C13H19}) + \theta(\text{C9C13H20}) - \theta(\text{O1C13H19}) - \theta(\text{O1C13H20}) - \theta(\text{C10C14H21}) - \theta(\text{C10C14H22}) + \theta(\text{O2C14H21}) + \theta(\text{O2C14H22})] \\
\tau(\text{CH}_2) &= 1/2\sqrt{2}[(\theta(\text{C9C13H19}) - \theta(\text{C9C13H20}) - \theta(\text{O1C13H19}) + \theta(\text{O1C13H20}) - \theta(\text{C10C14H21}) + \theta(\text{C10C14H22}) + \theta(\text{O2C14H21}) - \theta(\text{O2C14H22})] \\
\delta(\text{NH}_2) &= 1/\sqrt{6}[(2\theta(\text{H23N7H24}) - \theta(\text{O1N7H23}) - \theta(\text{O1N7H24}) - 2\theta(\text{H25N8H26}) + \theta(\text{O2N8H25}) + \theta(\text{O2N8H26})] \\
\rho(\text{NH}_2) &= 1/2[(\theta(\text{O1N7H23}) - \theta(\text{O1N7H24}) - \theta(\text{O2N8H25}) + \theta(\text{O2N8H26})] \\
\omega(\text{NH}_2) &= 1/\sqrt{6}[(\theta(\text{H23N7H24}) + \theta(\text{O1N7H23}) + \theta(\text{O1N7H24}) - \theta(\text{H25N8H26}) - \theta(\text{O2N8H25}) - \theta(\text{O2N8H26})] \\
\rho(\text{CCH}) &= 1/2\sqrt{2}[(\theta(\text{N5C9H15}) - \theta(\text{N5C9C13}) + \theta(\text{C11C9H15}) - \theta(\text{C11C9C13}) - \theta(\text{N6C10H16}) + \theta(\text{N6C10C14}) - \theta(\text{C12C10H16}) + \theta(\text{C12C10C14})] \\
\omega(\text{CCH}) &= 1/2\sqrt{2}[(\theta(\text{N5C9H15}) + \theta(\text{N5C9C13}) - \theta(\text{C11C9H15}) - \theta(\text{C11C9C13}) - \theta(\text{N6C10H16}) - \theta(\text{N6C10C14}) + \theta(\text{C12C10H16}) + \theta(\text{C12C10C14})] \\
\tau(\text{CCH}) &= 1/2\sqrt{2}[(\theta(\text{N5C9H15}) - \theta(\text{N5C9C13}) - \theta(\text{C11C9H15}) + \theta(\text{C11C9C13}) - \theta(\text{N6C10H16}) + \theta(\text{N6C10C14}) + \theta(\text{C12C10H16}) - \theta(\text{C12C10C14})] \\
\delta(\text{CCH}) &= 1/\sqrt{2}[\theta(\text{C13C9H15}) - \theta(\text{C14C10H16})] \\
\delta_{\text{op}}(\text{CO}) &= 1/\sqrt{2}[\tau(\text{O4C12N5C10}) - \tau(\text{O3C11N6C9})] \\
\delta_{\text{op}}(\text{NH}) &= 1/\sqrt{2}[\tau(\text{H17N5C12C9}) - \tau(\text{H18N6C11C10})] \\
\delta(\text{CCO}) &= 1/2\sqrt{6}[(-\sqrt{6} - 2)\theta(\text{H19C13H20}) + (\sqrt{6} + 2)\theta(\text{C9C13O1}) - \theta(\text{C9C13H19}) - \theta(\text{C9C13H20}) - \theta(\text{O1C13H19}) - \theta(\text{O1C13H20}) + (\sqrt{6} - 2)\theta(\text{H21C14H22}) \\
&\quad - (\sqrt{6} + 2)\theta(\text{C10C14O2}) + \theta(\text{C10C14H21}) + \theta(\text{C10C14H22}) + \theta(\text{O2C14H21}) + \theta(\text{O2C14H22})]
\end{aligned}$$

$$\delta(\text{NOC})=1/\sqrt{2}[\theta(\text{C13O1N7})-\theta(\text{C14O2N8})]$$

$$\begin{aligned} \tau(\text{CC})= & 1/3\sqrt{2}[\tau(\text{H15C9C13O1})+\tau(\text{H15C9C13H19})+\tau(\text{H15C9C13H20})+ \tau(\text{N5C9C13O1}) +\tau(\text{N5C9C13H19}) + \tau(\text{N5C9C13H20}) +\tau(\text{C11C9C13O1}) \\ & + \tau(\text{C11C9C13H19}) +\tau(\text{C11C9C13H20})- \tau(\text{H16C10C14O2}) -\tau(\text{H16C10C14H21}) -\tau(\text{H16C10C14H22}) -\tau(\text{N6C10C14O2}) -\tau(\text{N6C10C14H21}) \\ & -\tau(\text{N6C10C14H22}) -\tau(\text{C12C10C14O2}) -\tau(\text{C12C10C14H21}) -\tau(\text{C12C10C14H22})] \end{aligned}$$

$$\tau(\text{C-O})=1/\sqrt{6}[\tau(\text{C9C13O1N7}) +\tau(\text{H19C13O1N7}) + \tau(\text{H20C13O1N7}) -\tau(\text{C10C14O2N8}) - \tau(\text{H21C14O2N8}) -\tau(\text{H22C14O2N8})]$$

$$\tau(\text{ON})=1/2[\tau(\text{C13O1N7H23})+\tau(\text{C13O1N7H24}) - \tau(\text{C14O2N8H25}) -\tau(\text{C14O2N8H26})]$$

$$\delta_{\text{ip}}(\text{Ring-3}) = 1/\sqrt{6}[\theta(\text{C11C9N5}) - \theta(\text{C9N5C12}) + \theta(\text{N5C12C10}) - \theta(\text{C12C10N6}) + \theta(\text{C10N6C11}) - \theta(\text{N6C11C9})]$$

$$\delta_{\text{op}}(\text{Ring-1}) = 1/\sqrt{6}[\tau(\text{C10C12N5C9}) - \tau(\text{C12N5C9C11}) +\tau(\text{N5C9C11N6}) - \tau(\text{C9C11N6C10}) + \tau(\text{C11N6C10C12}) - \tau(\text{N6C10C12N5})]$$

DMDKP

AG symmetry

$$v_s(\text{NH})=1/\sqrt{2}[r(\text{N5H6}) + r(\text{N7H8})]$$

$$v_s(\text{CH}_2) = 1/2[r(\text{C11H12}) + r(\text{C11H13})+ r(\text{C14H15}) + r(\text{C14H16})]$$

$$v_{\text{as}}(\text{CH}_2) = 1/2[r(\text{C11H12}) - r(\text{C11H13})+ r(\text{C14H15}) - r(\text{C14H16})]$$

$$v_s(\text{C=O})=1/\sqrt{2}[r(\text{C1O9}) + r(\text{C3O10})]$$

$$v_s(\text{NC})=1/\sqrt{2}[r(\text{N5C1}) + r(\text{N7C3})]$$

$$v_s(\text{NC}_\alpha)=1/\sqrt{2}[r(\text{N5C4}) + r(\text{N7C2})]$$

$$v_s(\text{C}_\alpha\text{C})=1/\sqrt{2}[r(\text{C2C1}) + r(\text{C4C3})]$$

$$v_s(\text{C=C}) = 1/\sqrt{2}[r(\text{C2C11}) + r(\text{C4C14})]$$

$$\delta_{\text{ip}}(\text{NH})=1/2[\theta(\text{C1N5H6}) - \theta(\text{C4N5H6}) + \theta(\text{C3N7H8}) - \theta(\text{C2N7H8})]$$

$$\delta_{\text{ip}}(\text{CO})=1/2[\theta(\text{N5C1O9}) - \theta(\text{C2C1O9}) + \theta(\text{N7C3O10}) - \theta(\text{C4C3O10})]$$

$$\delta_{\text{ip}}(\text{C=CH}_2)=1/2[\theta(\text{C1C2C11}) - \theta(\text{N7C2C11}) + \theta(\text{C3C4C14}) - \theta(\text{N5C4C14})]$$

$$\delta(\text{CH}_2)= 1/\sqrt{12}[(2\theta(\text{H12C11H13}) - \theta(\text{C2C11H12}) - \theta(\text{C2C11H13}) + 2\theta(\text{H15C14H16}) - \theta(\text{C4C14H15}) - \theta(\text{C4C14H16})]$$

$$\rho(\text{CH}_2)= 1/2[(\theta(\text{C2C11H12}) - \theta(\text{C2C11H13}) + \theta(\text{C4C14H15}) - \theta(\text{C4C14H16})]$$

$$\delta_{\text{ip}}(\text{Ring-1}) = 1/\sqrt{12}[2\theta(\text{C1C2N7}) - \theta(\text{C2N7C3}) - \theta(\text{N7C3C4}) + 2\theta(\text{C3C4N5}) - \theta(\text{C4N5C1}) - \theta(\text{N5C1C2})]$$

$$\delta_{\text{ip}}(\text{Ring-2}) = 1/2[\theta(\text{C2N7C3}) - \theta(\text{N7C3C4}) + \theta(\text{C4N5C1}) - \theta(\text{N5C1C2})]$$

BG symmetry

$$\delta_{\text{op}}(\text{NH})= 1/\sqrt{2}[\tau(\text{H6N5C1C4}) - \tau(\text{H8N7C3C2})]$$

$$\delta_{\text{op}}(\text{CO})= 1/\sqrt{2}[\tau(\text{O9C1N5C2}) - \tau(\text{O10C3N7C4})]$$

$$\delta_{\text{op}}(\text{C}=\text{CH}_2)= 1/\sqrt{2}[\tau(\text{C11C2C1N7}) - \tau(\text{C14C4C3N5})]$$

$$\delta_{\text{op}}(\text{CH}_2)= 1/\sqrt{2}[\tau(\text{C2C11H12H13}) - \tau(\text{C4C14H15H16})]$$

$$\tau(\text{CH}_2)= 1/2\sqrt{2}[\tau(\text{C1C2C11H12}) + \tau(\text{C1C2C11H13}) + \tau(\text{N7C2C11H12}) + \tau(\text{N7C2C11H13}) - \tau(\text{C3C4C14H15}) - \tau(\text{C3C4C14H16}) - \tau(\text{N5C4C14H15}) - \tau(\text{N5C4C14H16})]$$

$$\delta_{\text{op}}(\text{Ring-3}) = 1/\sqrt{6}[\tau(\text{C4N5C1C2}) - \tau(\text{N5C1C2N7}) + \tau(\text{C1C2N7C3}) - \tau(\text{N7C3C4N5}) + \tau(\text{C3C4N5C1}) - \tau(\text{C4N5C1C2})]$$

AU symmetry

$$\delta_{\text{op}}(\text{NH})= 1/\sqrt{2}[\tau(\text{H6N5C1C4}) + \tau(\text{H8N7C3C2})]$$

$$\delta_{\text{op}}(\text{CO})= 1/\sqrt{2}[\tau(\text{O9C1N5C2}) + \tau(\text{O10C3N7C4})]$$

$$\delta_{\text{op}}(\text{C}=\text{CH}_2)= 1/\sqrt{2}[\tau(\text{C11C2C1N7}) + \tau(\text{C14C4C3N5})]$$

$$\delta_{\text{op}}(\text{CH}_2)= 1/\sqrt{2}[\tau(\text{C2C11H12H13}) + \tau(\text{C4C14H15H16})]$$

$$\tau(\text{CH}_2)= 1/2\sqrt{2} [\tau(\text{C1C2C11H12}) + \tau(\text{C1C2C11H13}) + \tau(\text{N7C2C11H12}) + \tau(\text{N7C2C11H13}) + \tau(\text{C3C4C14H15}) + \tau(\text{C3C4C14H16}) + \tau(\text{N5C4C14H15}) + \tau(\text{N5C4C14H16})]$$

$$\delta_{\text{op}}(\text{Ring-2}) = 1/2[\tau(\text{N5C1C2N7}) + \tau(\text{C1C2N7C3}) + \tau(\text{C3C4N5C1}) - \tau(\text{C4N5C1C2})]$$

$$\delta_{\text{op}}(\text{Ring-1}) = 1/\sqrt{12}[2\tau(\text{C4N5C1C2}) - \tau(\text{N5C1C2N7}) - \tau(\text{C1C2N7C3}) + 2\tau(\text{N7C3C4N5}) - \tau(\text{C3C4N5C1}) - \tau(\text{C4N5C1C2})]$$

BU symmetry

$$v_s(\text{NH})=1/\sqrt{2}[r(\text{N5H6}) - r(\text{N7H8})]$$

$$v_s(\text{CH}_2) = 1/2[r(\text{C11H12}) + r(\text{C11H13}) - r(\text{C14H15}) - r(\text{C14H16})]$$

$$v_{\text{as}}(\text{CH}_2) = 1/2[r(\text{C11H12}) - r(\text{C11H13}) - r(\text{C14H15}) + r(\text{C14H16})]$$

$$v_s(\text{C}=\text{O})=1/\sqrt{2}[r(\text{C1O9}) - r(\text{C3O10})]$$

$$v_s(\text{NC})=1/\sqrt{2}[r(\text{N5C1}) - r(\text{N7C3})]$$

$$v_s(\text{NC}_\alpha)=1/\sqrt{2}[r(\text{N5C4}) - r(\text{N7C2})]$$

$$v_s(C_{\alpha}C) = 1/\sqrt{2}[r(C2C1) - r(C4C3)]$$

$$v_s(C=C) = 1/\sqrt{2}[r(C2C11) - r(C4C14)]$$

$$\delta_{ip}(NH) = 1/2[\theta(C1N5H6) - \theta(C4N5H6) - \theta(C3N7H8) + \theta(C2N7H8)]$$

$$\delta_{ip}(CO) = 1/2[\theta(N5C1O9) - \theta(C2C1O9) - \theta(N7C3O10) + \theta(C4C3O10)]$$

$$\delta_{ip}(C=CH_2) = 1/2[\theta(C1C2C11) - \theta(N7C2C11) - \theta(C3C4C14) + \theta(N5C4C14)]$$

$$\delta(CH_2) = 1/\sqrt{12}[(2\theta(H12C11H13) - \theta(C2C11H12) - \theta(C2C11H13) - 2\theta(H15C14H16) + \theta(C4C14H15) + \theta(C4C14H16)]$$

$$\rho(CH_2) = 1/2[(\theta(C2C11H12) - \theta(C2C11H13) - \theta(C4C14H15) + \theta(C4C14H16)]$$

$$\delta_{ip}(\text{Ring-3}) = 1/\sqrt{6}[\theta(C1C2N7) - \theta(C2N7C3) + \theta(N7C3C4) - \theta(C3C4N5) + \theta(C4N5C1) - \theta(N5C1C2)]$$

5.9. References

1. (a) K. Hayashi, C. G. Skinner, W. J. Shive. *Org. Chem.*, 1961, 26, 1167; (b) M. F. Gordeev, G. W. Luehr, H. C. Hui, E. M. Gordon, D. V. Patel. *Tetrahedron*, 1998, 54, 15879.
2. S. J. David. *Antimicrob. Chemother.*, 2001, 47, 203.
3. M. G. Kushner, S. W. Kim, C. Donahue, P. Thuras, D. Adson, M. Kotlyar, J. McCabe, J. Peterson, E. B. Foa, *Biol. Psychiatry.*, 2007, 62, 835.
4. J. E. Baldwin, A. J. Pratt, *Tetrahedron Lett.*, 1987, 28, 4319.
5. (a) A. J. Guastella, R. Richardson, P. F. Lovibond, R. M. Rapee, J. E. Gaston, P. Mitchell, M. R. Dadds, *Biol. Psychiatry.*, 2008, 63, 544. (b) D. C. Goff, C. Cather, J. D. Gottlieb, A. E. Evins, J. Waish, L. Raeke, M. W. Otto, D. Schoenfeld, M. F. Green, *Schizophr. Res.*, 2008, 106, 320.
6. M. P. Lambert, F. C. Neuhaus, *J. Bacteriology*, 1972, 110, 978.
7. D. Perez-Sala, M. S. Ayuso, M. Rico, R. Parilla, *Biochem Pharmacol.*, 1989, 38, 1037.
8. J. Michalsky, J. Ctvrtnik, Z. Horakova, V. Bydzovsky, *Experientia*, 1962, 18, 217.
9. M. Y. Karpeisky, R. M. Khomutov, E. S. Severin, Y. N. Breusov, "Chemical and Biological Aspects of Pyridoxal Catalysis" (E. E. Snell, P. M. Fasella, A. Braunstein & A. Rossi Fanelli, Eds.), Pergamon Press, Oxford, 1963.
10. W. G. Clark, "Metabolic Inhibitors" (Eds. R. M. Hochster and J. H. Quastel), Academic Press, New York. 1963.
11. H. H. Lee, H. Yamaguchi, H. Senda, S. Maeda, A. Kuwae, K. Hanai, *Spectroscopy Letts.*, 1997, 30, 685.
12. H. H. Lee, N. Takeuchi, H. Senda, A. Kuwae, K. Hanai, *Spectroscopy Letts.*, 1998, 31, 1217.
13. C. H. Stammer, F. O. Lassen, *J. Org. Chem.*, 1971, 36, 2631.
14. J. L. Miller, F. C. Neuhaus, F. O. Lassen, C. H. Stammer, *J. Org. Chem.*, 1968, 33, 3908.
15. Spartan'14 for Windows. Wavefunction, Inc; Irvine, CA, USA: 2013.
16. A. P. Mendham, T. J. Dines, M. J. Snowden, R. Withnall, B. Z. Chowdhry, *J. Raman Spectrosc.*, 2009, 40, 1478.
17. Y. Zhu, M. Tang, X. Shi, Y. Zhao, *Int. J. Quantum Chem.*, 2007, 107, 745.
18. D. A. Clemente, *Tetrahedron*, 2003, 59, 8445.
19. K. H. Ongania, G. Granozzi, V. Buseti, M. Casarin, D. Ajò, *Tetrahedron*, 1985, 41, 2015.

20. T. C. Cheam, S. Krimm, *Spectrochim. Acta*, 1984, 40A, 481.
21. A. P. Mendham, R. A. Palmer, B. S. Potter, T. J. Dines, M. J. Snowden, R. Withnall, B. Z. Chowdhry, *J. Raman Spectrosc.*, 2010, 41, 148.
22. T. C. Cheam, S. Krimm, *Spectrochim. Acta*, 1988, 44A, 182.
23. A. P. Mendham, T. J. Dines, M. J. Snowden, R. Withnall, B. Z. Chowdhry, *J. Raman Spectrosc.*, 2009, 40, 1508.
24. A. P. Mendham, T. J. Dines, J. C. Mitchell, R. Withnall, B. Z. Chowdhry, *J. Raman Spectrosc.*, 2009, 40, 1498.
25. A. P. Mendham, R. A. Palmer, B. S. Potter, T. J. Dines, M. J. Snowden, R. Withnall, B. Z. Chowdhry, *J. Raman Spectrosc.*, 2010, 41, 288.

Chapter 6: Vibrational Spectroscopic Studies of the Diketopiperazines *N, N'*-Diacetyl-cyclo(Gly-Gly) and *N, N'*-Dimethyl-cyclo(Gly-Gly)

6.1. Introduction

Diketopiperazines (DKPs) and their derivatives are proving to be of significant interdisciplinary scientific interest, particularly, with respect to novel drug design and development.^{1,2} *N*-acetylation of DKP has been shown to be a popular and simple, initial, step in the synthesis of structurally diverse DKP derivatives. Indeed, a number of such molecules have been patented for possible future medical applications as e.g., inhibitors of plasminogen activator inhibitor.^{3,4}

The X-ray structures for both, *N, N'*-diacetyl-cyclo(Gly-Gly) (DAGG) and *N, N'*-dimethyl-cyclo(Gly-Gly) (DMGG) have been reported.^{5,6} The structure and conformation of a number of DKPs have been investigated, in the solid state, by X-ray, indicating that the DKP ring adopts either a planar or boat conformation.^{7,8} Semi-empirical calculations and studies using density functional theory (DFT) have indicated that the minimum energy structure, for a number of different DKPs, is a boat conformation in the gaseous state.⁹⁻¹¹ It has been hypothesised that hydrogen bonding and/or crystal packing forces can sometimes constrain the DKP ring into the higher energy, planar conformation in the solid (powdered) state.¹² Vibrational spectroscopic studies have been reported on a number of DKPs, for example cyclo(GlyGly), cyclo(D-Ala-L-Ala), cyclo(L-Ala-Gly), cyclo(L-Ala-L-Ala),¹² cyclo(L-Met-L-Met),¹³ cyclo(L-Ser-L-Ser),¹⁴ cyclo(L-Asp-L-Asp)¹⁵ and cyclo(L-Glu-L-Glu),¹⁶ cyclo(Gly-Val),¹⁷ cyclo(His-Phe)¹⁸ as well as cyclo(Leu-Gly).¹⁹ The results have highlighted the *cis* amide characteristics of these molecules, and the effect on the vibrational spectra as a consequence of differing DKP ring conformations.

To our knowledge no vibrational spectroscopic studies have been reported for either DAGG or DMGG. Herein, the spectroscopic (Raman and FTIR) and X-ray structures of DAGG and DMGG are compared with those of the parent DKP, cyclo(Gly-Gly), from both an experimental and theoretical perspective in order to determine the effect of *N*-acetylation and *N*-methylation on the vibrational spectroscopic/physicochemical properties of the DKP ring.

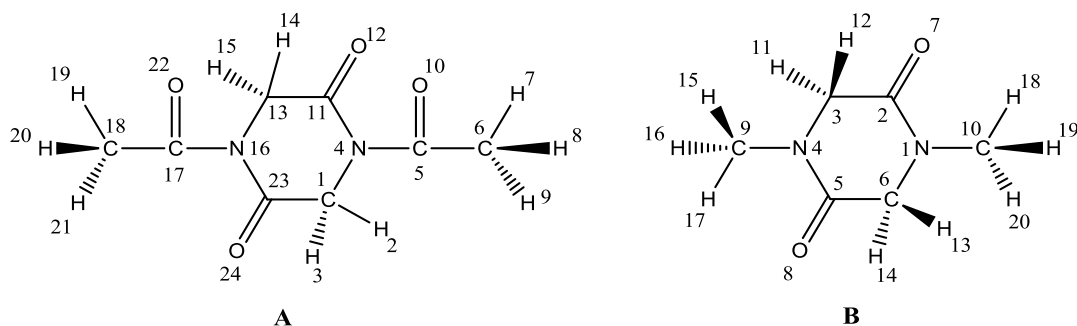


Figure 6.1. Atom numbering scheme for (A) DAGG and (B) DMGG.

6.2. Experimental

6.2.1. Materials

See sections 3.1 to 3.1.2 in Chapter 3.

6.2.2. Synthesis

Cyclo(Gly-Gly), (99% purity), acetic anhydride, absolute ethanol and decolorising charcoal were supplied by Sigma-Aldrich (Dorset, UK) and used without further purification. DAGG was synthesised by a literature procedure.³ *N*-acetylation was carried out by refluxing the parent DKP in acetic anhydride for 2 hr. The volume of acetic anhydride was reduced to a quarter of its original volume and the resulting solid product was recrystallized from hot absolute ethanol. Decolorising charcoal was used to remove any charred by-products. DMGG was obtained from Alfa Aesar (Lancashire, UK) and used without further purification. The purity and structure of all the DKPs used were checked and ascertained by elemental analysis, NMR and mass spectrometry (see Appendix).

6.2.3. Vibrational spectroscopy and Instrumental details

See sections 3.2, 3.2.1, 3.2.2, 3.2.3 and 3.2.4 in Chapter 3.

6.2.4. DFT calculations

See section 3.5 in Chapter 3

6.3. Results and discussion

6.3.1. Geometry optimization

The atom numbering scheme and computed molecular geometries for DAGG and DMGG are shown in Figs. 6.1-6.3. Bond distances, valence bond angles and selected torsional angles are compared with experimental values in Tables 6.1 and 6.2. Assuming that both molecules have C_2 symmetry we would expect a total of 66 normal modes (34 with A symmetry and 32 with B symmetry) for DAGG, and a total of 54 normal modes (28 with A symmetry and 26 with B symmetry) for DMGG.

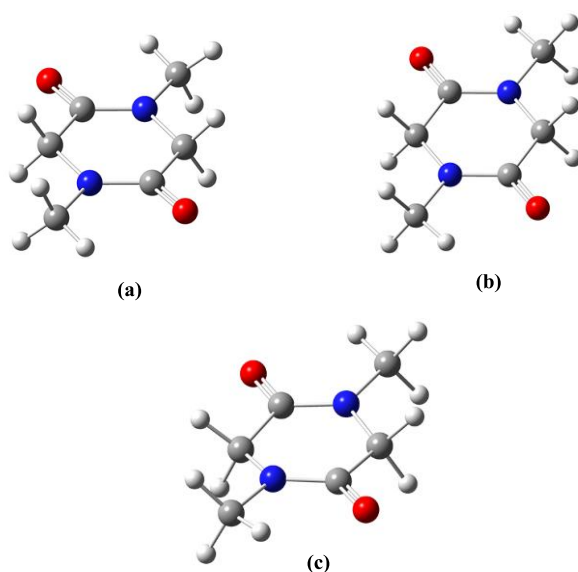


Figure 6.2. Experimental (a) and calculated (planar (b) and boat (c)) structure of DMGG.

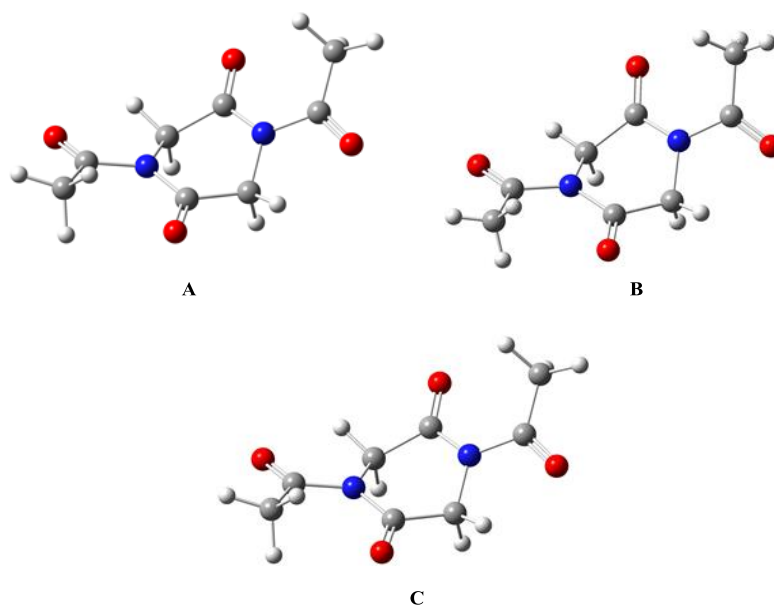


Figure 6.3. Experimental (A and B) and calculated (C) structure of DAGG.

The X-ray structure⁵ results for DAGG reveal there are two inequivalent molecules in the unit cell, termed molecules A and B and that the ω , ϕ , and ψ peptide torsional angles are: 5.4° and 8.1° (4.7° and 3.2°), -51.8° and -49.1° (-46.4° and -47.6°), and 43.9° and 41.1° (41.8° and 43.1°), respectively. As there is a slight twist to the DKP ring, two different sets of angles for both of the peptide bonds in the ring are obtained. Our calculated structure for DAGG has a ring boat conformation with C₂ symmetry, where the corresponding calculated ω , ϕ and ψ peptide torsional angles are: 8.5°, -46.4° and 37°, respectively. The degree of buckling, β , of the DKP ring is -47.6° (-45.6°) (X-ray structure) and -42.5° (calculated structure). These torsional angles indicate there is a close relationship between the ring geometries of the experimental and calculated structure.

In the case of DMGG, the X-ray structure⁶ results reveal that the ω , ϕ , and ψ peptide torsional angles are: 7.3°, 7.2° and 6.8°, respectively. As the molecule has C_i symmetry the other set of peptide torsional angles are also -7.3°, -7.2° and -6.83°, respectively.⁶ The calculated structure for an isolated DMGG molecule displays a boat conformation with C₂ symmetry; it is noted that the calculation performed by constraining the DKP ring to a planar conformation with C₂ symmetry results in an imaginary frequency (Table 6.4), which shows that DMGG cannot have a planar DKP ring as the lowest energy conformation in the gas phase. As expected the boat conformation was found to be slightly lower in energy compared to the planar conformation (-0.04 kJ mol⁻¹) because the calculations are based on a single molecule in the gas phase and do not take into account possible intermolecular forces. The corresponding calculated ω , ϕ and ψ peptide torsional angles are: 5.3°, -14.9° and 9.3° for the boat and 0°, 0° and 0° for the planar conformation, respectively. The degree of buckling, β , of the DKP ring is 0° (X-ray structure) and -12.3° and 0° (calculated boat and planar structures, respectively). These torsional angles indicate there is a close relationship between the ring geometries of the experimental X-ray structure and the calculated structure for DMGG.

Table 6.1. Comparison of calculated bond lengths for DAGG with the X-ray geometry.⁵

Bond lengths (Å)	Molecule A ⁵	Molecule B ⁵	Calculated
O(24)-C(23)	1.2150	1.2153	1.2093
C(23)-N(16)	1.3883	1.3872	1.5207
C(23)-C(1)	1.5058	1.5085	1.3895
O(22)-C(17)	1.2113	1.2129	1.2096
H(21)-C(18)	0.9602	0.9596	1.0886
H(20)-C(18)	0.9604	0.9597	1.0878
H(19)-C(18)	0.9595	0.9604	1.0861
C(18)-C(17)	1.4879	1.4872	1.5021

C(17)-N(16)	1.4100	1.4143	1.4254
N(16)-C(13)	1.4742	1.4689	1.4675
H(15)-C(13)	0.9696	0.9704	1.0952
H(14)-C(13)	0.9709	0.9700	1.0827
C(13)-C(11)	1.5081	1.5119	1.5207
O(12)-C(11)	1.2088	1.2142	1.2093
C(11)-N(4)	1.3837	1.3806	1.3895
O(10)-C(5)	1.2184	1.2166	1.2096
H(9)-C(6)	0.9602	0.9593	1.0886
H(8)-C(6)	0.9596	0.9604	1.0878
H(7)-C(6)	0.9599	0.9597	1.0861
C(6)-C(5)	1.4934	1.4926	1.5021
C(5)-N(4)	1.4129	1.4150	1.4254
N(4)-C(1)	1.4718	1.4739	1.4675
H(3)-C(1)	0.9699	0.9704	1.0952
H(2)-C(1)	0.9700	0.9700	1.0827
Bond angles (°)			
O(24)-C(23)-N(16)	124.9610	124.9415	125.1569
O(24)-C(23)-C(1)	121.9301	121.7199	120.8001
N(16)-C(23)-C(1)	113.0597	113.2627	114.0194
C(17)-C(18)-H(19)	109.4709	109.4519	107.1292
C(17)-C(18)-H(20)	109.4558	109.5022	111.8329
C(17)-C(18)-H(21)	109.4419	109.4866	110.5285
H(19)-C(18)-H(20)	109.5126	109.4149	110.8676
H(19)-C(18)-H(21)	109.4692	109.4478	110.1918
H(20)-C(18)-H(21)	109.4769	109.5239	106.3300
N(16)-C(17)-C(18)	119.9275	118.7021	118.9109
N(16)-C(17)-O(22)	118.1878	118.6300	118.6035
C(18)-C(17)-O(22)	121.8843	122.6413	122.4761
C(17)-N(16)-C(23)	126.2619	126.1632	125.6896
C(17)-N(16)-C(13)	117.2839	117.0434	116.6243
C(23)-N(16)-C(13)	116.0977	116.7895	117.4821
H(14)-C(13)-H(15)	107.8499	107.7274	107.3266
H(14)-C(13)-N(16)	109.2258	109.0366	108.3902
H(14)-C(13)-C(11)	109.1867	109.0662	107.9623
H(15)-C(13)-N(16)	109.2369	109.0083	110.5915
H(15)-C(13)-C(11)	109.2585	109.0559	108.5335
N(16)-C(13)-C(11)	111.9921	112.8193	113.8097
O(12)-C(11)-C(13)	122.0433	121.1547	120.8001
O(12)-C(11)-N(4)	125.4076	125.1209	125.1569
C(13)-C(11)-N(4)	112.5130	113.7125	114.0194
C(5)-C(6)-H(7)	109.4850	109.4239	107.1292
C(5)-C(6)-H(8)	109.5069	109.4087	111.8329
C(5)-C(6)-H(9)	109.4539	109.4928	110.5285

H(7)-C(6)-H(8)	109.4644	109.5067	110.8676
H(7)-C(6)-H(9)	109.4304	109.4807	110.1918
H(8)-C(6)-H(9)	109.4866	109.5145	106.3300
N(4)-C(5)-C(6)	118.5346	119.6244	118.9109
N(4)-C(5)-O(10)	119.0668	118.2262	118.6035
C(6)-C(5)-O(10)	122.3799	122.1402	122.4761
C(5)-N(4)-C(11)	125.2010	125.4468	125.6896
C(5)-N(4)-C(1)	117.3911	117.8266	116.6243
C(11)-N(4)-C(1)	117.0284	116.5138	117.4821
H(2)-C(1)-H(3)	107.8216	107.7300	107.3266
H(2)-C(1)-C(23)	109.0828	108.8272	107.9623
H(2)-C(1)-N(4)	109.0896	108.8583	108.3902
H(3)-C(1)-C(23)	109.1205	108.8506	108.5335
H(3)-C(1)-N(4)	109.0749	108.8611	110.5915
C(23)-C(1)-N(4)	112.5398	113.5564	113.8097
Dihedral angles (°)			
C(1)-C(23)-N(16)-C(13)	8.1204	4.7530	8.5968
C(1)-C(23)-N(16)-C(17)	-178.9596	-175.9912	-176.7867
O(24)-C(23)-N(16)-C(13)	-169.3606	-172.1147	-169.6376
O(24)-C(23)-N(16)-C(17)	3.5595	7.1411	4.9789
N(16)-C(23)-C(1)-N(4)	41.0938	41.8484	37.0085
N(16)-C(23)-C(1)-H(3)	-80.1295	-79.5846	-86.5905
N(16)-C(23)-C(1)-H(2)	162.3095	163.2611	157.3767
O(24)-C(23)-C(1)-N(4)	-141.3387	-141.1700	-144.6721
O(24)-C(23)-C(1)-H(3)	97.4380	97.3970	91.7290
O(24)-C(23)-C(1)-H(2)	-20.1230	-19.7573	-24.3039
H(21)-C(18)-C(17)-O(22)	115.5490	105.7768	112.0055
H(21)-C(18)-C(17)-N(16)	-64.6834	-76.1249	-69.1316
H(20)-C(18)-C(17)-O(22)	-124.4714	-134.1303	-129.7358
H(20)-C(18)-C(17)-N(16)	55.2961	43.9680	49.1272
H(19)-C(18)-C(17)-O(22)	-4.4304	-14.1921	-8.0661
H(19)-C(18)-C(17)-N(16)	175.3372	163.9062	170.7969
O(22)-C(17)-N(16)-C(13)	0.8162	7.7826	3.1292
O(22)-C(17)-N(16)-C(23)	-172.0294	-171.4716	-171.5284
C(18)-C(17)-N(16)-C(13)	-178.9598	-170.3930	-175.7782
C(18)-C(17)-N(16)-C(23)	8.1946	10.3528	9.5642
C(23)-N(16)-C(13)-C(11)	-51.8819	-47.6372	-46.4313
C(23)-N(16)-C(13)-H(15)	69.2951	73.6674	76.0430
C(23)-N(16)-C(13)-H(14)	-172.9608	-168.9748	-166.5586
C(17)-N(16)-C(13)-C(11)	134.5385	133.0373	138.4585
C(17)-N(16)-C(13)-H(15)	-104.2845	-105.6580	-99.0672
C(17)-N(16)-C(13)-H(14)	13.4596	11.6997	18.3312
N(16)-C(13)-C(11)-N(4)	43.9448	43.0624	37.0085
N(16)-C(13)-C(11)-O(12)	-138.1292	-138.1295	-144.6721

H(15)-C(13)-C(11)-N(4)	-77.2197	-78.2152	-86.5905
H(15)-C(13)-C(11)-O(12)	100.7064	100.5928	91.7290
H(14)-C(13)-C(11)-N(4)	165.0463	164.3833	157.3767
H(14)-C(13)-C(11)-O(12)	-17.0276	-16.8087	-24.3039
C(13)-C(11)-N(4)-C(1)	5.4022	3.2464	8.5968
C(13)-C(11)-N(4)-C(5)	178.1207	-171.3143	-176.7867
O(12)-C(11)-N(4)-C(1)	-172.4408	-175.5065	-169.6376
O(12)-C(11)-N(4)-C(5)	0.2777	9.9328	4.9789
H(9)-C(6)-C(5)-O(10)	102.3296	124.1923	112.0055
H(9)-C(6)-C(5)-N(4)	-79.2596	-54.6838	-69.1316
H(8)-C(6)-C(5)-O(10)	-137.6403	-115.7797	-129.7358
H(8)-C(6)-C(5)-N(4)	40.7705	65.3441	49.1272
H(7)-C(6)-C(5)-O(10)	-17.6183	4.1965	-8.0661
H(7)-C(6)-C(5)-N(4)	160.7925	-174.6796	170.7969
O(10)-C(5)-N(4)-C(1)	11.7951	-2.2283	3.1292
O(10)-C(5)-N(4)-C(11)	-160.8995	172.2678	-171.5284
C(6)-C(5)-N(4)-C(1)	-166.6693	176.6917	-175.7782
C(6)-C(5)-N(4)-C(11)	20.6360	-8.8122	9.5642
C(11)-N(4)-C(1)-C(23)	-49.0712	-46.3986	-46.4313
C(11)-N(4)-C(1)-H(3)	72.1781	75.0285	76.0430
C(11)-N(4)-C(1)-H(2)	-170.2830	-167.7939	-166.5586
C(5)-N(4)-C(1)-C(23)	137.6273	128.5920	138.4585
C(5)-N(4)-C(1)-H(3)	-101.1234	-109.9809	-99.0672
C(5)-N(4)-C(1)-H(2)	16.4155	7.1967	18.3312

Table 6.2. Comparison of calculated bond lengths for DMGG with the X-ray geometry.⁶

Bond lengths (Å)	Experimental ⁶	Calc. boat	Calc. planar
H(20)-C(10)	0.9798	1.0929	1.0922
H(19)-C(10)	0.9800	1.0914	1.0922
H(18)-C(10)	0.9803	1.0847	1.0845
H(17)-C(9)	0.9803	1.0847	1.0845
H(16)-C(9)	0.9800	1.0929	1.0922
H(15)-C(9)	0.9798	1.0914	1.0922
H(14)-C(6)	0.9899	1.0958	1.0938
H(13)-C(6)	0.9898	1.0915	1.0938
H(12)-C(3)	0.9899	1.0915	1.0938
H(11)-C(3)	0.9898	1.0958	1.0938
C(10)-N(1)	1.4545	1.4551	1.4551
C(9)-N(4)	1.4545	1.4551	1.4551
O(8)-C(5)	1.2327	1.2215	1.2217
O(7)-C(2)	1.2327	1.2215	1.2217
C(6)-N(1)	1.4516	1.4522	1.4514
C(6)-C(5)	1.4974	1.5184	1.5175
C(5)-N(4)	1.3313	1.3547	1.3544

N(4)-C(3)	1.4516	1.4522	1.4514
C(3)-C(2)	1.4974	1.5184	1.5175
C(2)-N(1)	1.3313	1.3547	1.3544
Bond angles (°)			
N(1)-C(10)-H(18)	109.4447	108.6710	108.6789
N(1)-C(10)-H(19)	109.4649	109.9839	110.2478
N(1)-C(10)-H(20)	109.4763	110.5670	110.2469
H(18)-C(10)-H(19)	109.4748	109.7779	109.5914
H(18)-C(10)-H(20)	109.5028	109.2963	109.5919
H(19)-C(10)-H(20)	109.4638	108.5340	108.4735
N(4)-C(9)-H(15)	109.4795	109.9839	110.2478
N(4)-C(9)-H(16)	109.4649	110.5670	110.2469
N(4)-C(9)-H(17)	109.4455	108.6710	108.6789
H(15)-C(9)-H(16)	109.4611	108.5340	108.4735
H(15)-C(9)-H(17)	109.5066	109.7779	109.5914
H(16)-C(9)-H(17)	109.4697	109.2963	109.5919
H(13)-C(6)-H(14)	107.2704	106.3046	106.2090
H(13)-C(6)-N(1)	108.0252	109.2649	109.8026
H(13)-C(6)-C(5)	108.0348	105.9319	106.2013
H(14)-C(6)-N(1)	108.0074	110.4288	109.8026
H(14)-C(6)-C(5)	107.9847	106.7578	106.2014
N(1)-C(6)-C(5)	117.1289	117.5206	117.9525
O(8)-C(5)-C(6)	118.1646	118.4513	118.1691
O(8)-C(5)-N(4)	123.5662	124.0434	123.9805
C(6)-C(5)-N(4)	118.2595	117.5052	117.8504
C(9)-N(4)-C(5)	120.2939	119.8970	119.9135
C(9)-N(4)-C(3)	115.1769	116.0738	115.8895
C(5)-N(4)-C(3)	124.2244	123.7013	124.1971
H(11)-C(3)-H(12)	107.2744	106.3046	106.2090
H(11)-C(3)-N(4)	108.0211	110.4288	109.8026
H(11)-C(3)-C(2)	108.0354	106.7578	106.2014
H(12)-C(3)-N(4)	108.0074	109.2649	109.8026
H(12)-C(3)-C(2)	107.9847	105.9319	106.2013
N(4)-C(3)-C(2)	117.1289	117.5206	117.9525
O(7)-C(2)-C(3)	118.1646	118.4513	118.1691
O(7)-C(2)-N(1)	123.5661	124.0434	123.9805
C(3)-C(2)-N(1)	118.2595	117.5052	117.8504
C(10)-N(1)-C(6)	115.1769	116.0738	115.8895
C(10)-N(1)-C(2)	120.2939	119.8970	119.9135
C(6)-N(1)-C(2)	124.2244	123.7013	124.1971
Dihedral angles (°)			
H(20)-C(10)-N(1)-C(2)	-136.0194	-112.8488	-120.1393
H(20)-C(10)-N(1)-C(6)	50.0579	60.8177	59.8613
H(19)-C(10)-N(1)-C(2)	103.9904	127.3027	120.1221

H(19)-C(10)-N(1)-C(6)	-69.9323	-59.0308	-59.8772
H(18)-C(10)-N(1)-C(2)	-15.9939	7.1080	-0.0086
H(18)-C(10)-N(1)-C(6)	170.0835	-179.2254	179.9921
H(17)-C(9)-N(4)-C(3)	-170.0892	-179.2254	179.9921
H(17)-C(9)-N(4)-C(5)	15.9881	7.1080	-0.0086
H(16)-C(9)-N(4)-C(3)	69.9323	60.8177	59.8613
H(16)-C(9)-N(4)-C(5)	-103.9904	-112.8488	-120.1393
H(15)-C(9)-N(4)-C(3)	-50.0566	-59.0308	-59.8772
H(15)-C(9)-N(4)-C(5)	136.0208	127.3027	120.1221
C(5)-C(6)-N(1)-C(2)	7.2865	-14.9185	0.0000
C(5)-C(6)-N(1)-C(10)	-179.0610	171.6824	179.9993
H(14)-C(6)-N(1)-C(2)	129.3833	107.8333	121.7888
H(14)-C(6)-N(1)-C(10)	-56.9642	-65.5658	-58.2119
H(13)-C(6)-N(1)-C(2)	-114.8911	-135.5810	121.7888
H(13)-C(6)-N(1)-C(10)	58.7615	51.0199	-58.2119
N(1)-C(6)-C(5)-N(4)	-6.8378	9.3561	0.0000
N(1)-C(6)-C(5)-O(8)	174.2547	-170.6603	-179.9992
H(14)-C(6)-C(5)-N(4)	-128.9464	-115.2494	-123.6121
H(14)-C(6)-C(5)-O(8)	52.1462	64.7342	56.3887
H(13)-C(6)-C(5)-N(4)	115.3348	131.7425	123.6120
H(13)-C(6)-C(5)-O(8)	-63.5727	-48.2739	-56.3872
C(6)-C(5)-N(4)-C(3)	7.3628	5.2934	0.0000
C(6)-C(5)-N(4)-C(9)	-179.2915	178.4530	-179.9993
O(8)-C(5)-N(4)-C(3)	-173.7932	-174.6892	179.9992
O(8)-C(5)-N(4)-C(9)	-0.4474	-1.5296	-0.0001
C(5)-N(4)-C(3)-C(2)	-7.2865	-14.9185	0.0000
C(5)-N(4)-C(3)-H(12)	-129.3833	-135.5810	-121.7886
C(5)-N(4)-C(3)-H(11)	114.8885	107.8333	121.7888
C(9)-N(4)-C(3)-C(2)	179.0610	171.6824	179.9993
C(9)-N(4)-C(3)-H(12)	56.9642	51.0199	58.2107
C(9)-N(4)-C(3)-H(11)	-58.7640	-65.5658	-58.2119
N(4)-C(3)-C(2)-N(1)	6.8378	9.3561	0.0000
N(4)-C(3)-C(2)-O(7)	-174.2590	-170.6603	-179.9992
H(12)-C(3)-C(2)-N(1)	128.9464	131.7425	123.6120
H(12)-C(3)-C(2)-O(7)	-52.1505	-48.2739	-56.3872
H(11)-C(3)-C(2)-N(1)	-115.3298	-115.2494	-123.6121
H(11)-C(3)-C(2)-O(7)	63.5734	64.7342	56.3887
C(3)-C(2)-N(1)-C(6)	-7.3628	5.2934	0.0000
C(3)-C(2)-N(1)-C(10)	179.2915	178.4530	-179.9993
O(7)-C(2)-N(1)-C(6)	173.7977	-174.6892	179.9992
O(7)-C(2)-N(1)-C(10)	0.4520	-1.5296	-0.0001

6.3.2. Vibrational assignments

Experimental solid state and calculated IR and Raman spectra of DAGG and DMGG are shown in Figs. 6.4-6.7. Solution state IR and Raman spectra for DAGG and DMGG are shown in Figs. 6.8 and 6.9, respectively. A comparison of calculated bond lengths with X-ray geometry bond lengths for cyclo(Gly-Gly)⁷ are shown Tables 6.3 and 6.4. Detailed experimental and calculated vibrational data for DAGG and DMGG in the solid and solution phases are shown in Tables 6.5 and 6.6. Spectral assignments were made with reference to the calculated data, group frequency considerations and by comparison with previous experimental work.¹²⁻¹⁶

6.3.3. Wavenumber region > 2000 cm⁻¹

The bands found in this region are due to N-H, and C-H stretching modes. Bands between 3150 and 3300 cm⁻¹ are typical for the location of the N-H stretching vibration of a secondary amide and the absence of these confirms that substitution has taken place and the parent compound has been *N*-acetylated or *N*-methylated. C-H stretching vibrations can clearly be detected in both the Raman and IR spectra between 2870 and 3050 cm⁻¹ although they are more intense in the Raman than in the IR spectra. Previously, theoretical *ab initio* calculations have hypothesized a relationship between the conformation of the DKP ring and the extent of splitting between the asymmetric and symmetric C-H stretching vibrations.¹² Results showed that a splitting of these normal modes by ~30 cm⁻¹, predicted a DKP ring with a planar conformation and by ~90 cm⁻¹, a boat conformation. From both the solid state and aqueous solution Raman spectra it has been shown that cyclo(Gly-Gly) has a splitting of ~30 cm⁻¹, which would indicate a planar ring conformation in both the solid and aqueous states.¹² This result agrees well with the experimental structure (solid state) and NMR and CD results for the solution state conformations. The C-H stretching region is more complicated in both DAGG and DMGG, because of the presence of CH₃ stretching vibrations arising from the acetyl groups, and in the case of DMGG the CH₃ stretching vibrations arising from the *N*-methyl group. Due to this problem, in the case of both DAGG and DMGG it was not possible to ascertain the degree of splitting between the symmetric and asymmetric stretches found for the C_αH₂ group. To attempt to alleviate this problem, DAGG-d₆ (both methyl groups on the *N*-acetyl are deuterated (CD₃)) was synthesised. The product and purity of this derivative were checked by using both mass spectroscopy and NMR. The solid state Raman results of DAGG-d₆ were recorded and it was clearly seen that the C-H stretching region had become a lot simpler. This is because of the isotopic shift of the CD₃ group, down to the ~2200 cm⁻¹ region. The result shows that in the solid state Raman spectrum of DAGG the asymmetric CH stretching appears at 3042 cm⁻¹ and the symmetric stretch

at 2930 cm⁻¹, which shows a split of ~110 cm⁻¹. The DFT calculations and normal coordinate analysis would infer that the DKP ring of DAGG-d₆ has a boat conformation in the solid state.¹³

Table 6.3. Comparison of calculated bond lengths for DAGG with the X-ray geometry bond lengths for cyclo(Gly-Gly).⁷

	Calculated bond lengths for DAGG (Å)			X-ray geometry bond lengths for cyclo(Gly-Gly) (Å) ⁷
	boat	A	B	
N16-C17= N4-C5	1.425	1.410,1.412	1.414,1.419	
N16- ^α C13 = N4- ^α C1	1.467	1.474,1.471	1.468,1.473	1.449
N16-C23= N4-C11	1.389	1.388,1.383	1.387,1.380	1.325
C17-O22= C5-O10	1.209	1.211,1.218	1.212,1.216	
C17-C18= C5-C6	1.502	1.487,1.493	1.487,1.492	
^α C13-H14 = ^α C1-H2	1.082	0.97,0.97	0.97,0.97	0.93
^α C13-H15= ^α C1-H3	1.095	0.97,0.97	0.97,0.97	0.95
^α C13-C11 = ^α C1-C23	1.520	1.508,1.505	1.511,1.508	1.499
C11-O12= C23-O24	1.209	1.208,1.215	1.214,1.215	1.239
C18-H19= C6-H7	1.086	0.96,0.96	0.96,0.96	
C18-H20= C6-H8	1.087	0.96,0.96	0.96,0.96	
C18-H21 = C6-H9	1.088	0.96,0.96	0.96,0.96	

Table 6.4. Comparison of calculated and experimental bond lengths for DMGG with X-ray geometry bond lengths for cyclo(Gly-Gly).⁷

	Calculated and experimental bond lengths for DMGG (Å)			X-ray geometry bond lengths for cyclo(Gly-Gly) (Å) ⁷
	boat	planar	Expt.	
N-C ^{methyl}	1.455	1.455	1.454	
N-C _α	1.452	1.451	1.451	1.449
N-CO	1.345	1.354	1.331	1.325
C9-H15	1.091	1.092	0.979	
C9-H16	1.092	1.092	0.979	
C9-H17	1.084	1.084	0.980	
^α C3-H11	1.095	1.093	0.989	0.93
^α C3-H12	1.091	1.093	0.989	0.95
C _α -CO	1.518	1.517	1.497	1.499
C2-O7	1.221	1.221	1.232	1.239

6.3.4. Wavenumber region 1200-1700 cm⁻¹

Bands found in this region are attributed to normal modes involving the following: C=O stretch, C-N stretch, C-H bending, C_αH bends, CH₂ wagging and CH₂ torsion. Five bands associated with C=O stretching vibrations of DAGG can be detected between 1700-1736 cm⁻¹ in the solid state Raman spectrum (Fig. 6.5). It is predicted that for a molecule with C₂ symmetry there would be a total of 4 vibrational modes found for the acetyl and amide C=O stretching (2 having A symmetry and 2 having B symmetry). Additional bands may be observed due to factor group splitting, which is the result of there being more than one molecule per crystallographic unit cell.⁵ It is also very difficult to assign which bands are due to C=O stretching of the acetyl group or the ring amide group. The calculations predict that both acetyl and ring C=O bond distances are equal, but the PED results infer that the ring amide C=O stretching vibration should be ~7-10 cm⁻¹ higher than that found for the acetyl C=O stretch. The C=O stretching modes are also found in the solution Raman spectrum; however, only a very broad singlet at 1716 cm⁻¹ is observed (Fig. 6.8). The C=O stretching vibrations in the IR spectrum are detected as very intense, broad bands centred at 1723 cm⁻¹, with a shoulder at 1701 cm⁻¹ (Fig. 6.4). In the IR spectrum it is not possible to ascertain the location of both the amide and acetyl C=O stretching vibrations due to the broad nature of this band. The C=O stretching vibration (amide I mode) is typically found in the 1620-1700 cm⁻¹ region for secondary amides. For example the amide I mode of solid cyclo(Gly-Gly) is located at ~1655 cm⁻¹ in the solid state Raman spectrum. It is apparent that the ring C=O stretch of DAGG appears at a significantly higher wavenumber (~40 cm⁻¹), and has a significantly higher Raman intensity than found in other CDAPs, including cyclo(Gly-Gly).^{12-16,20} This can be explained by the shortening of the ring C=O bond distance after acetylation, which is attributed to the delocalization of the lone pairs on the nitrogen atoms towards the exo, from the endocyclic amide linkages²¹ (Table 6.3).

In the case of DMGG, the Raman spectrum (Fig. 6.6) shows two sharper, factor group split vibrations, with a higher relative intensity than their DKP counterparts and occur at 1640 and 1666 cm⁻¹ (1650 and 1644 cm⁻¹ in IR), they are predominantly C=O stretching modes, but do not contain any N-H bending character. The Raman spectrum of cyclo(Gly-Gly)¹² contains two weak, factor group split, broad, *cis* amide I vibrations located at 1621 and 1655 cm⁻¹. The *cis* amide I mode of DKP is predominantly a C=O stretching vibration which is coupled to the N-H bending mode. The sharper, and higher relative intensity of the C=O stretching band of DMGG to that of cyclo(Gly-Gly) is attributed to the lack of hydrogen bonding in DMGG. It is noteworthy that in DMGG there is a difference of around ~50-60 cm⁻¹ in the location of C=O stretching band compared to DAGG.

This can be attributed to the presence of some C-N stretching character associated with the C=O stretch in the amide I mode. The calculated PEDs suggest that there is a small contribution from the C-N stretch (~8%) associated with C=O stretching vibration in DMGG.

The C-N stretch, a *cis* amide II mode, is found at ~1517 cm⁻¹ in the solid state Raman spectrum of cyclo(Gly-Gly). This mode is, apparently, mainly an out-of-phase C^α-C-N stretch with a lower degree of contribution from the N-H in plane bend than in the *trans* amide II mode.¹² The *cis* amide II mode, unlike its amide I mode counterpart, is not sensitive to different hydrogen bonding strengths found in the crystal lattices of CDAPs.¹² There is no band in the 1500 cm⁻¹ region for DAGG unlike that found in the parent compound i.e. cyclo(Gly-Gly), Figs 6.4-6.7. This shows the absence of the *cis* amide II mode; thereby, confirming the absence of N-H in-plane-bending. The amide C-N stretching vibration of DAGG occurs at 1370 and 1360 cm⁻¹ (Raman and IR, respectively). There is a very large difference between the location of the C-N stretching vibration of the *cis* amide II mode of cyclo(Gly-Gly) and the amide C-N stretch of DAGG. One reason for this has been explained already, by the fact that after *N*-acetylation the amide C-N stretching vibration cannot possibly mix with N-H in-plane-bending. Additionally, it has also been stated that after *N*-acetylation there is a delocalization of the lone pairs on the nitrogen atoms towards the exo, from the endocyclic, amide linkages. This in turn means that the ring, amide C-N bond distance increases (1.33 → 1.38 Å) after acetylation. Indeed, this is predicted by our calculations shown in Table 6.3. Therefore, as found from our experimental results, as the ring amide C-N bond distance increases there will be a significant decrease in the wavenumber of the C-N stretching vibration. The acetyl C-N stretching vibration is observed at 1271 and 1261 cm⁻¹ in the Raman and IR spectra, respectively. The calculated results show that the C-N acetyl bond distance is 1.425 Å. Additionally, the PEDs predict that this motion couples with stretching of the NC_α bond, which has a calculated distance of 1.467 Å. This coupling and bond lengthening explains why there is a downward shift of ~100 cm⁻¹ between the ring amide C-N and C-N acetyl stretching vibrations. The bands in the 1370-1470 cm⁻¹ region can be assigned to C-H bending, due to either symmetric or asymmetric CH₃ and/or CH₂ bending vibrations. In the IR spectrum the CH₃ and/or CH₂ bending vibrations occur between 1374 and 1454 cm⁻¹, and in the solid state Raman spectrum between 1383 and 1457 cm⁻¹. These are also present in the solution phase Raman spectrum between 1374 and 1434 cm⁻¹ (Figs. 6-8-6.9). Between ~1280-1310 cm⁻¹ it is common place to find CH₂ wagging vibrations, and between ~1220-1250 cm⁻¹ CH₂ twisting vibrations are detected in both the Raman and IR spectra. Both of these assignments are confirmed by results from our calculated data and with reference to the vibrational spectra of cyclo(Gly-Gly).¹²

For DMGG, the band located at 1535 cm^{-1} in the Raman and 1496 cm^{-1} in the IR can be assigned to a mode involving C-N stretching coupled to CH_2 bending. The tertiary amide C-N stretch of DMGG, obviously, cannot have any N-H character, unlike cyclo(Gly- Gly) and other cyclic di-amino acid derivatives. It appears that there is no significant difference, on comparing the experimental amide C-N bond lengths of cyclo(Gly-Gly) and DMGG (1.32 and 1.33 \AA , respectively) (Table 6.4). Therefore, unlike DAGG, no changes in delocalization of the lone pair of electrons on the nitrogen atoms are observed. The apparent $\sim 20\text{ cm}^{-1}$ upward shift of the amide C-N stretching vibration in DMGG compared with cyclo (Gly-Gly) must, therefore, be the result of the change in mixing of this normal mode, namely the absence of a contribution from N-H in-plane-bending. In the aqueous solution IR and Raman spectra this band occurs at 1505 cm^{-1} and 1544 cm^{-1} , respectively. There is an apparent upward shift of 10 cm^{-1} on aqueous solvation for the C-N stretching vibration which can be attributed to possible alleviation in ring strain on going from the solid to the aqueous state. CH_2 and CH_3 symmetric and asymmetric bending vibrations are observed between 1445 and 1398 cm^{-1} in the IR spectrum and in the Raman spectrum they appear between 1442 and 1401 cm^{-1} . Bands found between 1340 and 1256 cm^{-1} in the Raman and IR spectra of DMGG are attributed to modes which show a significant contribution from CH_2 wagging. These vibrations are generally quite mixed and also show contributions from either NC_α or N-Me stretching.

6.3.5. Wavenumber region $900\text{-}1200\text{ cm}^{-1}$

The NC_α stretching vibrations are found between 1130 and 1190 cm^{-1} ; occurring at considerably lower wavenumber than either the C-N (of amide) and C-N' (of acetyl) stretching vibrations, due to its longer bond length. In the region between 900 and 1080 cm^{-1} the assignments are tentative because there is considerable mixing of the vibrational modes. However, it is common to find C-C stretching, CH_3 and CH_2 rocking modes and also CO out-of-plane bending vibrational modes in this region.

The N-Me and NC_α stretching vibrations in DMGG are found between 1160 and 1230 cm^{-1} . This can be explained by comparing the experimental bond distances for the N-Me and NC_α for DMGG and the bond distance for NC_α of cyclo(Gly-Gly) (1.45 , 1.454 and 1.45 \AA , respectively). It is apparent that the foregoing N-C bond distances are similar, thereby explaining the commonality of the location of these vibrational modes. The CH_3 out-of-plane rocking vibrations occurs at $\sim 1132\text{ cm}^{-1}$, in both the Raman and IR spectra. It is worth noting that our calculations predict this to be quite a pure mode, having a high percentage PEDs for the CH_3 out-of-plane rock. In the region

between 880 and 1100 cm^{-1} the assignments are also tentative because of the considerable mixing of the vibrational modes. However, it is common to find CH_3 and CH_2 twisting and also CO out-of-plane bending modes in this region.

6.3.7. Wavenumber region 500-900 cm^{-1}

In this region C=O bending modes, ring stretching, ring bending vibrations and ring stretching modes occur. Ring bending vibrations occur at 732 and 814 cm^{-1} (IR) and 731 cm^{-1} (Raman), and at 728 cm^{-1} in the solution Raman spectrum of DAGG. In the solid Raman spectrum of DAGG a strong band is found at 731 cm^{-1} which is tentatively assigned to a symmetric ring stretching vibration, and likewise an intense signal is observed at 719 cm^{-1} in the Raman spectrum of DMGG. These correspond to the strong band observed in the 750 cm^{-1} region of the Raman spectrum of cyclo(Gly-Gly).^{12, 20} These bands are assigned to ring stretching but are actually mixed with other types of motion. It has been hypothesized that the planar ring geometry gives very strong Raman signals for the ring stretching vibration.¹² The aqueous Raman spectrum of DMGG has a very intense signal at 730 cm^{-1} which is also assigned to the same ring stretching vibration. It is therefore suggested that the six membered ring of DMGG adopts a planar or near planar conformation in the aqueous and solid states, in contrast to the DFT optimized geometry of an isolated molecule in the gas phase. It is hypothesized that intermolecular forces constrain the ring geometry to be planar in both the solid and aqueous phases.

Bands attributed to vibrations involving significant contributions from carbonyl in-plane or out-of-plane bending are found in the Raman and IR spectra of DAGG, between 540 and 770 cm^{-1} . This is contrary to previous results for CDAP's containing a secondary *cis* amide, where the ring amide C=O in-plane and out-of-plane bending vibrations occur between $\sim 550 - 670 \text{ cm}^{-1}$.^{12, 20} For DMGG, the bands at 634 (Raman) and 602 cm^{-1} (IR) are assigned to modes that are predominantly C=O in-plane-bending. The Raman band at 584 cm^{-1} is assigned to the C=O out-of-plane bending vibration. These locations are quite similar to those observed for cyclo(Gly-Gly), where the C=O in-plane bend and out-of-plane bend occur at 610 and 561 cm^{-1} , respectively, in the Raman spectrum. As previously stated, there are no changes in the direction of delocalization of the lone pair electrons on the nitrogen atom on going from the endo to the exocyclic amide linkage as there is little difference between the experimental C=O bond distances for both compounds. Any difference between the location of the C=O in-plane-bending and out-of-plane bending for these two molecules can-possibly-be attributed to differences in the mixing of the modes or to changes in

the strong intermolecular hydrogen bonding involved in solid cyclo(Gly-Gly), and interatomic van der Waals interactions in solid DMGG.

6.3.8. Wavenumber region < 500 cm⁻¹

In the 400 to 499 cm⁻¹ region of the Raman spectra there are several bands attributable to vibrations which have C=O, C-N, and C-C bending contributions. Assignments are tentative due to the close proximity of a number of bands. In Raman spectra of DAGG, at 439 cm⁻¹ ring bending coupled with N-C-C bending vibrations are observed, at 386 cm⁻¹, N-C-C bending coupled with C=O bending vibrations are also observed, N-Ac in-plane and out-of-plane bending vibrations are found in the 200 to 400 cm⁻¹ region. Ring torsion and lattice vibrational modes are found at wavenumbers below 180 cm⁻¹. In DMGG, the 300 to 499 cm⁻¹ region of the spectra there are quite a few bands, which have C=O, C-N bending and C-C, N-C stretching and ring bending contributions. All these vibrations are fairly mixed. Assignments are tentative due to the close proximity of a number of bands. Between 200 and 300 cm⁻¹ in the Raman spectrum, mixed modes of vibrations for *N*-Me occur that include in- and out-of-plane bending and torsional vibrations. Torsional modes occur below 200 cm⁻¹ (Table 6.2) as well as lattice vibrations.

Table 6.5. Experimental and calculated wavenumber assignments (in cm⁻¹) for DAGG vibrational bands (carbonyl of the acetyl group are designated with a prime).

IR solid	IR aq.	Raman solid	Raman aq.	Calc.	% P.E.D
3053		3056			
3041		3043	3037		
3020		3021		3009 A	$\nu_s(\text{CH}_2)$ (37), $\nu_{as}(\text{CH}_2)$ (63)
		3001		3007 B	$\nu_s(\text{CH}_2)$ (37), $\nu_{as}(\text{CH}_2)$ (63)
2997				2989 B	$\nu_{as}(\text{CH}_3)$ (99)
2980				2988 A	$\nu_{as}(\text{CH}_3)$ (99)
2971				2966 A	$\nu_{as}'(\text{CH}_3)$ (99)
2946		2945	2949	2965 B	$\nu_{as}'(\text{CH}_3)$ (99)
2928		2930		2929 B	$\nu_s(\text{CH}_3)$ (100)
		2905		2929 A	$\nu_s(\text{CH}_3)$ (100)
2877				2870 A	$\nu_s(\text{CH}_2)$ (63), $\nu_{as}(\text{CH}_2)$ (37)
				2868 B	$\nu_s(\text{CH}_2)$ (63), $\nu_{as}(\text{CH}_2)$ (37)
		1741		1742 A	$\nu_s(\text{CO})$ (86)
1723		1731		1737 B	$\nu_s(\text{CO})$ (85)
		1717		1735 A	$\nu_s(\text{CO}')$ (86)
1701		1704	1716	1732 B	$\nu_s(\text{CO}')$ (87)
		1702			
		1668	1644		

			1628		
1454 1431	1436	1457	1434	1458 A	$\delta(\text{CH}_2)$ (94)
		1441		1447 B	$\delta(\text{CH}_2)$ (97)
	1425	1430		1428 B	$\delta_{\text{as}}(\text{CH}_3)$ (89)
		1416	1421	1420 A	$\delta_{\text{as}}(\text{CH}_3)$ (89)
1415				1411 A	$\delta_{\text{as}}(\text{CH}_3)$ (82)
		1383 1373	1374	1411 B 1371 B	$\delta_{\text{as}}(\text{CH}_3)$ (83) $\delta_{\text{s}}(\text{CH}_3)$ (85)
	1373			1370 A	$\delta_{\text{s}}(\text{CH}_3)$ (86)
1357				1357 B	$\nu(\text{NC})$ (23), $\rho(\text{CH}_2)$ (50)
		1362		1354 A	$\nu(\text{NC})$ (16), $\nu(\text{CC}_\alpha)$ (10), $\rho(\text{CH}_2)$ (46)
1305	1314	1312 1284	1314	1286 B	$\nu(\text{NC})$ (14), $\nu(\text{CC}_\alpha)$ (11), $\rho(\text{CH}_2)$ (32), $\omega(\text{CH}_2)$ (32)
1261	1271	1261	1257	1252 A 1251 A	$\nu(\text{NC})$ (21), $\rho(\text{CH}_2)$ (34), $\omega(\text{CH}_2)$ (16) $\nu(\text{NAC})$ (11), $\nu(\text{NC}_\alpha)$ (18), $\omega(\text{CH}_2)$ (26)
1224		1225		1225 B	$\nu(\text{NAC})$ (19), $\nu(\text{NC}_\alpha)$ (20), $\delta_{\text{ip}}(\text{CO}')$ (12)
	1201			1211 A	$\nu(\text{NAC})$ (10), $\delta_{\text{ip}}(\text{CO}')$ (10) $\omega(\text{CH}_2)$ (48)
1179		1188		1177 B	$\nu(\text{NAC})$ (11), $\nu(\text{NC}_\alpha)$ (10), $\omega(\text{CH}_2)$ (41), $\rho_{\text{ip}}(\text{CH}_3)$ (12)
		1154		1141 A	$\nu(\text{NC}_\alpha)$ (29), $\nu(\text{CC}_\alpha)$ (12), $\rho_{\text{ip}}(\text{CH}_3)$ (18)
1129	1135	1133	1135	1122 B	$\nu(\text{NC}_\alpha)$ (24), $\nu(\text{CC}_\alpha)$ (18), $\delta_{\text{ip}}(\text{CO})$ (22)
	1092				
1078	1078	1077		1063 B	$\tau(\text{CH}_2)$ (26), $\delta_{\text{ip}}(\text{ring-3})$ (17)
		1039	1033	1042 A	$\rho_{\text{op}}(\text{CH}_3)$ (69), $\delta_{\text{op}}(\text{CO}')$ (22)
1040	1042			1042 B	$\rho_{\text{op}}(\text{CH}_3)$ (69), $\delta_{\text{op}}(\text{CO}')$ (22)
		982	987	965 A	$\tau(\text{CH}_2)$ (57), $\delta_{\text{ip}}(\text{CO})$ (20)
		955		960 A	$\nu(\text{CC}')$ (18), $\tau(\text{CH}_2)$ (10), $\rho_{\text{ip}}(\text{CH}_3)$ (40)
974				960 B	$\nu(\text{NC}_\alpha)$ (16), $\nu(\text{CC}')$ (28), $\rho_{\text{ip}}(\text{CH}_3)$ (36)
947 924		924		946 B	$\nu(\text{CC}_\alpha)$ (15), $\tau(\text{CH}_2)$ (38), $\delta_{\text{ip}}(\text{CO})$ (18)
			891	899 A	$\nu(\text{NAC})$ (27), $\nu(\text{CC}_\alpha)$ (25), $\nu(\text{CC}')$ (15)
			879		
814		812	800	805 B	$\nu(\text{NC}_\alpha)$ (13), $\nu(\text{CC}_\alpha)$ (11), $\nu(\text{CC}')$ (10), $\delta_{\text{op}}(\text{CO})$ (12), $\delta_{\text{ip}}(\text{ring-3})$ (31)
732 690		731 690	728	713 A	$\nu(\text{NC}_\alpha)$ (19), $\nu(\text{CC}')$ (16), $\delta_{\text{op}}(\text{CO})$ (16), $\delta_{\text{ip}}(\text{ring-1})$ (20)
665		662	660	667 B	$\nu(\text{NAC})$ (28), $\nu(\text{CC}')$ (19), $\delta_{\text{op}}(\text{CO})$ (10)
				655 A	$\nu(\text{CC}_\alpha)$ (11), $\delta_{\text{ip}}(\text{NAC})$ (13), $\delta_{\text{ip}}(\text{CO})$ (42)
621		621 599	623	618 A	$\delta_{\text{op}}(\text{CO})$ (28), $\delta_{\text{op}}(\text{CO}')$ (23), $\delta_{\text{op}}(\text{NAC})$ (11)
597		591	594	590 A	$\delta_{\text{ip}}(\text{CO})$ (26), $\delta_{\text{ip}}(\text{CO}')$ (32)
590				587 B	$\rho_{\text{op}}(\text{CH}_3)$ (20), $\delta_{\text{op}}(\text{CO}')$ (68)
565		566		573 B	$\delta_{\text{ip}}(\text{CO}')$ (48), $\tau(\text{CH}_2)$ (11), $\delta_{\text{op}}(\text{CO})$ (17)
550		549	551	543 B	$\nu(\text{CC}_\alpha)$ (11), $\delta_{\text{ip}}(\text{CO})$ (29), $\delta_{\text{ip}}(\text{CO}')$ (10), $\delta_{\text{ip}}(\text{ring-3})$ (11)
				543 A	$\nu(\text{NC}_\alpha)$ (14), $\delta_{\text{ip}}(\text{CO})$ (29), $\delta_{\text{ip}}(\text{CO}')$ (12), $\delta_{\text{ip}}(\text{ring-2})$ (13)
468		439	482		

			438	436 A	$\delta(\text{NCC}') (12), \delta_{\text{ip}}(\text{ring-1}) (37), \delta_{\text{ip}}(\text{ring-2}) (20)$
		414		406 B	$\delta(\text{NCC}') (67)$
				380 B	$\nu(\text{NC}) (12), \nu(\text{NAc}) (13), \nu(\text{NC}_\alpha) (10), \delta_{\text{ip}}(\text{CO}) (44)$
		386	390	373 A	$\delta_{\text{ip}}(\text{CO}) (24), \delta(\text{NCC}') (46)$
		313	311	288 A	$\nu(\text{NAc}) (21), \nu(\text{CC}_\alpha) (12), \delta_{\text{ip}}(\text{ring-1}) (14), \delta_{\text{ip}}(\text{ring-2}) (29)$
		262		274 A	$\delta_{\text{ip}}(\text{NAc}) (46), \delta_{\text{op}}(\text{NAc}) (19), \delta(\text{NCC}') (11)$
				227 B	$\delta_{\text{ip}}(\text{NAc}) (46), \delta_{\text{op}}(\text{NAc}) (19), \delta_{\text{op}}(\text{ring-1}) (16)$
		231		231 A	$\delta_{\text{ip}}(\text{NAc}) (21), \delta_{\text{op}}(\text{NAc}) (23), \delta_{\text{op}}(\text{ring-2}) (13), \delta_{\text{op}}(\text{ring-3}) (28)$
		214		196 B	$\delta_{\text{ip}}(\text{NAc}) (36), \delta_{\text{op}}(\text{NAc}) (30), \delta_{\text{op}}(\text{ring-1}) (13)$
			156	159 B	$\tau(\text{CC}') (95)$
		106	127 107	149 A	$\tau(\text{CC}') (95)$
		93		74 B	$\delta_{\text{op}}(\text{NAc}) (34), \delta_{\text{op}}(\text{ring-1}) (50), \tau(\text{NAc}) (13)$
		79		69 A	$\delta_{\text{op}}(\text{NAc}) (14), \delta_{\text{op}}(\text{ring-2}) (17), \delta_{\text{op}}(\text{ring-3}) (38), \tau(\text{NAc}) (23)$
				57 B	$\tau(\text{NAc}) (80), \delta_{\text{op}}(\text{ring-1}) (18)$
				48 A	$\tau(\text{NAc}) (74), \delta_{\text{op}}(\text{ring-3}) (21)$
				16 A	$\delta_{\text{op}}(\text{NAc}) (25), \delta_{\text{op}}(\text{ring-2}) (70)$

Table 6.6. Experimental and calculated wavenumber assignments (in cm^{-1}) for DMGG vibrational bands.

IR solid	Raman solid	IR aq.	Raman aq.	Calc. planar	% P.E.D. planar	Calc. boat	% P.E.D. boat
3024	3025			2997 B 2996 A	$\nu_s(\text{CH}_3) (11), \nu_{\text{as}}(\text{CH}_3) (22), \nu_{\text{as}}'(\text{CH}_3) (67)$ $\nu_s(\text{CH}_3) (11), \nu_{\text{as}}(\text{CH}_3) (22), \nu_{\text{as}}'(\text{CH}_3) (67)$	2997 A 2997 B	$\nu_s(\text{CH}_3) (11), \nu_{\text{as}}(\text{CH}_3) (25), \nu_{\text{as}}'(\text{CH}_3) (64)$ $\nu_s(\text{CH}_3) (11), \nu_{\text{as}}(\text{CH}_3) (25), \nu_{\text{as}}'(\text{CH}_3) (64)$
2967	2970						
2937	2937		2947	2907 A 2907 B	$\nu_{\text{as}}(\text{CH}_3) (74), \nu_{\text{as}}'(\text{CH}_3) (25)$ $\nu_{\text{as}}(\text{CH}_3) (75), \nu_{\text{as}}'(\text{CH}_3) (25)$	2895 A 2897 B	$\nu_{\text{as}}(\text{CH}_3) (72), \nu_{\text{as}}'(\text{CH}_3) (22)$ $\nu_{\text{as}}(\text{CH}_3) (73), \nu_{\text{as}}'(\text{CH}_3) (22)$
2924							
2871				2898 B	$\nu_{\text{as}}(\text{CH}_2) (99)$	2900 A	$\nu_s(\text{CH}_2) (29), \nu_{\text{as}}(\text{CH}_2) (67)$
	2915		2925	2897 A	$\nu_{\text{as}}(\text{CH}_2) (99)$	2900 B	$\nu_s(\text{CH}_2) (29), \nu_{\text{as}}(\text{CH}_2) (68)$
			2885	2893 A 2892 B	$\nu_s(\text{CH}_2) (34), \nu_s(\text{CH}_3) (58)$ $\nu_s(\text{CH}_2) (24), \nu_s(\text{CH}_3) (67)$	2889 A 2885 B	$\nu_s(\text{CH}_3) (85), \nu_{\text{as}}'(\text{CH}_3) (14)$ $\nu_s(\text{CH}_3) (85), \nu_{\text{as}}'(\text{CH}_3) (14)$
2857	2850		2849	2877 B 2877 A	$\nu_s(\text{CH}_2) (66), \nu_s(\text{CH}_3) (31)$ $\nu_s(\text{CH}_2) (22), \nu_s(\text{CH}_3) (76)$	2862 B 2861 A	$\nu_s(\text{CH}_2) (70), \nu_{\text{as}}(\text{CH}_2) (29)$ $\nu_s(\text{CH}_2) (70), \nu_{\text{as}}(\text{CH}_2) (29)$
2784	2785		2808				
1742							
	1666			1695 B	$\nu_{\text{as}}(\text{CO}) (78)$	1693 B	$\nu_{\text{as}}(\text{CO}) (78)$
1650				1695 A	$\nu_s(\text{CO}) (82)$	1690 A	$\nu_s(\text{CO}) (82)$
1644	1640		1645				
1615	1617						
1556							
	1535		1544	1507 A	$\nu_s(\text{CN}) (19), \delta(\text{CH}_2) (22), \rho(\text{CH}_2) (11), \delta_{\text{as}}(\text{CH}_3) (15)$	1511 A	$\nu_s(\text{CN}) (18), \delta(\text{CH}_2) (23), \rho(\text{CH}_2) (10), \delta_{\text{as}}(\text{CH}_3) (15)$

1496		1505		1490 B	$\nu_{\text{as}}(\text{CN})$ (15), $\delta(\text{CH}_2)$ (10), $\rho(\text{CH}_2)$ (10), $\delta_{\text{as}}(\text{CH}_3)$ (33), $\rho_{\text{ip}}(\text{CH}_3)$ (11)	1493 B	$\nu_{\text{as}}(\text{CN})$ (14), $\delta(\text{CH}_2)$ (11), $\rho(\text{CH}_2)$ (10), $\delta_{\text{as}}(\text{CH}_3)$ (34), $\rho_{\text{ip}}(\text{CH}_3)$ (11)
1458	1460		1456	1460 B	$\delta_{\text{as}}'(\text{CH}_3)$ (92)	1457 B	$\delta_{\text{as}}'(\text{CH}_3)$ (90)
		1452		1458 A	$\delta_{\text{as}}'(\text{CH}_3)$ (92)	1456 A	$\delta_{\text{as}}'(\text{CH}_3)$ (86)
1444	1441	1439		1455 A	$\delta_{\text{s}}(\text{CH}_2)$ (34), $\delta_{\text{as}}(\text{CH}_3)$ (58)	1453 A	$\delta_{\text{s}}(\text{CH}_2)$ (34), $\delta_{\text{as}}(\text{CH}_3)$ (53)
				1451 B	$\delta_{\text{s}}(\text{CH}_2)$ (79), $\delta_{\text{as}}(\text{CH}_3)$ (20)	1452 B	$\delta_{\text{s}}(\text{CH}_2)$ (77), $\delta_{\text{as}}(\text{CH}_3)$ (20)
			1432	1425 B	$\nu_{\text{as}}(\text{CN})$ (20), $\delta(\text{CH}_2)$ (12), $\rho(\text{CH}_2)$ (14), $\delta_{\text{as}}(\text{CH}_3)$ (38)	1429 B	$\nu_{\text{as}}(\text{CN})$ (20), $\delta(\text{CH}_2)$ (12), $\rho(\text{CH}_2)$ (14), $\delta_{\text{as}}(\text{CH}_3)$ (36)
		1412	1414	1422 A	$\nu_{\text{s}}(\text{CN})$ (11), $\delta(\text{CH}_2)$ (43), $\rho(\text{CH}_2)$ (10), $\delta_{\text{as}}(\text{CH}_3)$ (17)	1418 A	$\nu_{\text{s}}(\text{CN})$ (11), $\delta(\text{CH}_2)$ (40), $\rho(\text{CH}_2)$ (10), $\delta_{\text{as}}(\text{CH}_3)$ (18)
	1402			1400 A	$\delta_{\text{s}}(\text{CH}_3)$ (90)	1406 A	$\delta_{\text{s}}(\text{CH}_3)$ (36)
		1349					
1395				1401 B	$\delta_{\text{s}}(\text{CH}_3)$ (86)	1407 B	$\delta_{\text{s}}(\text{CH}_3)$ (36)
	1332		1335	1315 A	$\nu_{\text{s}}(\text{CN})$ (10), $\nu_{\text{s}}(\text{NC}_{\alpha})$ (19), $\rho(\text{CH}_2)$ (47)	1320 A	$\nu_{\text{s}}(\text{CN})$ (10), $\nu_{\text{s}}(\text{NC}_{\alpha})$ (12), $\rho(\text{CH}_2)$ (48)
1336 1296				1316 B	$\nu_{\text{as}}(\text{CN})$ (14), $\nu_{\text{as}}(\text{NC}_{\alpha})$ (14), $\nu_{\text{as}}(\text{CC}_{\alpha})$ (16), $\rho(\text{CH}_2)$ (53)	1309 B	$\nu_{\text{as}}(\text{CN})$ (14), $\nu_{\text{as}}(\text{NC}_{\alpha})$ (14), $\nu_{\text{as}}(\text{CC}_{\alpha})$ (16), $\rho(\text{CH}_2)$ (53)
1250				1241 B	$\omega(\text{CH}_2)$ (93)	1249 A	$\nu_{\text{s}}(\text{NMe})$ (15), $\nu_{\text{s}}(\text{NC}_{\alpha})$ (18), $\rho(\text{CH}_2)$ (25)
	1255	1264	1262	1240 A	$\nu_{\text{s}}(\text{NMe})$ (15), $\nu_{\text{s}}(\text{NC}_{\alpha})$ (20), $\rho(\text{CH}_2)$ (27)	1247 B	$\omega(\text{CH}_2)$ (76)
				1236 A	$\omega(\text{CH}_2)$ (96)	1242 A	$\omega(\text{CH}_2)$ (86)
1231				1225 B	$\nu_{\text{as}}(\text{NMe})$ (13), $\nu_{\text{as}}(\text{NC}_{\alpha})$ (22), $\delta_{\text{ip}}(\text{CO})$ (16), $\rho_{\text{ip}}(\text{CH}_3)$ (21)	1238 B	$\nu_{\text{as}}(\text{NMe})$ (11), $\nu_{\text{as}}(\text{NC}_{\alpha})$ (17), $\delta_{\text{ip}}(\text{CO})$ (14), $\omega(\text{CH}_2)$ (16), $\rho_{\text{ip}}(\text{CH}_3)$ (17)
1161		1161		1147 B	$\nu_{\text{as}}(\text{NMe})$ (38), $\nu_{\text{as}}(\text{CC}_{\alpha})$ (13), $\rho_{\text{ip}}(\text{CH}_3)$ (16), $\delta_{\text{ip}}(\text{Ring-3})$ (11)	1152 B	$\nu_{\text{as}}(\text{NMe})$ (37), $\nu_{\text{as}}(\text{CC}_{\alpha})$ (13), $\rho_{\text{ip}}(\text{CH}_3)$ (16), $\delta_{\text{ip}}(\text{Ring-3})$ (11)
1132	1131		1124	1134 A	$\rho_{\text{op}}(\text{CH}_3)$ (86)	1133 A	$\rho_{\text{op}}(\text{CH}_3)$ (86)
				1125 B	$\rho_{\text{op}}(\text{CH}_3)$ (87)	1126 B	$\rho_{\text{op}}(\text{CH}_3)$ (87)
	1097		1092	1074 A	$\nu_{\text{s}}(\text{NMe})$ (28), $\rho_{\text{ip}}(\text{CH}_3)$ (41)	1074 A	$\nu_{\text{s}}(\text{NMe})$ (28), $\rho_{\text{ip}}(\text{CH}_3)$ (40)
1014	1041	1018	1035	1007 A	$\nu_{\text{s}}(\text{NMe})$ (33), $\nu_{\text{s}}(\text{CC}_{\alpha})$ (26), $\rho_{\text{ip}}(\text{CH}_3)$ (24)	1013 A	$\nu_{\text{s}}(\text{NMe})$ (33), $\nu_{\text{s}}(\text{NC}_{\alpha})$ (10), $\nu_{\text{s}}(\text{CC}_{\alpha})$ (26), $\rho_{\text{ip}}(\text{CH}_3)$ (24)
990				998 B	$\nu_{\text{as}}(\text{NC}_{\alpha})$ (25), $\delta_{\text{ip}}(\text{CO})$ (10), $\rho_{\text{ip}}(\text{CH}_3)$ (39), $\delta_{\text{ip}}(\text{Ring-3})$ (10)	1001 B	$\nu_{\text{as}}(\text{NC}_{\alpha})$ (24), $\tau(\text{CH}_2)$ (10), $\rho_{\text{ip}}(\text{CH}_3)$ (35)
	989		986	983 A	$\tau(\text{CH}_2)$ (78), $\delta_{\text{op}}(\text{CO})$ (24)	985 A	$\tau(\text{CH}_2)$ (77), $\delta_{\text{op}}(\text{CO})$ (24)
				980 B	$\tau(\text{CH}_2)$ (85), $\delta_{\text{op}}(\text{CO})$ (17)	982 B	$\tau(\text{CH}_2)$ (73), $\delta_{\text{op}}(\text{CO})$ (17)
838	787			819 B	$\nu_{\text{as}}(\text{CN})$ (26), $\nu_{\text{as}}(\text{CC}_{\alpha})$ (27), $\delta_{\text{ip}}(\text{ring-3})$ (15)	823 B	$\nu_{\text{as}}(\text{CN})$ (25), $\nu_{\text{as}}(\text{CC}_{\alpha})$ (27), $\delta_{\text{ip}}(\text{ring-3})$ (15)
736			730	729 B	$\nu_{\text{as}}(\text{NMe})$ (35), $\delta_{\text{ip}}(\text{Ring-3})$ (49)	725 B	$\nu_{\text{as}}(\text{NMe})$ (34), $\delta_{\text{ip}}(\text{Ring-3})$ (47)
	719			703 A	$\nu_{\text{s}}(\text{CN})$ (38), $\nu_{\text{s}}(\text{NC}_{\alpha})$ (17), $\delta_{\text{ip}}(\text{Ring-1})$ (21)	697 A	$\nu_{\text{s}}(\text{CN})$ (38), $\nu_{\text{s}}(\text{NC}_{\alpha})$ (17), $\delta_{\text{ip}}(\text{Ring-1})$ (22)
	634		639	628 A	$\nu_{\text{s}}(\text{CC}_{\alpha})$ (17), $\delta_{\text{ip}}(\text{CO})$ (48), $\delta_{\text{ip}}(\text{NMe})$ (19)	630 A	$\nu_{\text{s}}(\text{CC}_{\alpha})$ (13), $\delta_{\text{ip}}(\text{CO})$ (46), $\delta_{\text{ip}}(\text{NMe})$ (18)
602			605	601 A	$\tau(\text{CH}_2)$ (18), $\delta_{\text{op}}(\text{CO})$ (88), $\delta_{\text{op}}(\text{NMe})$ (15)	598 A	$\tau(\text{CH}_2)$ (15), $\delta_{\text{op}}(\text{CO})$ (77), $\delta_{\text{op}}(\text{NMe})$ (13)
	584		580	586 B	$\tau(\text{CH}_2)$ (12), $\delta_{\text{op}}(\text{CO})$ (97)	588 B	$\tau(\text{CH}_2)$ (13), $\delta_{\text{op}}(\text{CO})$ (93)
			352				

	458		464	451 A	$\nu_s(\text{CC}_\alpha)$ (11), $\nu_s(\text{NC}_\alpha)$ (19), $\delta_{\text{ip}}(\text{Ring-1})$ (40), $\delta_{\text{ip}}(\text{Ring-2})$ (19)	452 A	$\nu_s(\text{CC}_\alpha)$ (10), $\nu_s(\text{NC}_\alpha)$ (19), $\delta_{\text{ip}}(\text{Ring-1})$ (39), $\delta_{\text{ip}}(\text{Ring-2})$ (20)
	392		398	411 B	$\nu_{\text{as}}(\text{NC}_\alpha)$ (11), $\delta_{\text{ip}}(\text{CO})$ (60), $\delta_{\text{op}}(\text{NMe})$ (10)	410 B	$\nu_{\text{as}}(\text{NC}_\alpha)$ (11), $\delta_{\text{ip}}(\text{CO})$ (60)
				386 A	$\nu_s(\text{NMe})$ (10), $\nu_s(\text{CC}_\alpha)$ (11), $\delta_{\text{ip}}(\text{Ring-1})$ (16), $\delta_{\text{ip}}(\text{Ring-2})$ (57)	388 A	$\nu_s(\text{NMe})$ (10), $\nu_s(\text{CC}_\alpha)$ (11), $\delta_{\text{ip}}(\text{Ring-1})$ (17), $\delta_{\text{ip}}(\text{Ring-2})$ (55)
	343		349	337 A	$\delta_{\text{ip}}(\text{CO})$ (16), $\delta_{\text{ip}}(\text{NMe})$ (69)	346 A	$\delta_{\text{ip}}(\text{CO})$ (16), $\delta_{\text{ip}}(\text{NMe})$ (69)
	246		249	295 B	$\nu_{\text{as}}(\text{CC}_\alpha)$ (16), $\delta_{\text{ip}}(\text{NMe})$ (71)	296 B	$\nu_{\text{as}}(\text{CC}_\alpha)$ (15), $\delta_{\text{ip}}(\text{NMe})$ (71)
	194			209 B	$\delta_{\text{op}}(\text{NMe})$ (123)	206 B	$\delta_{\text{op}}(\text{NMe})$ (122)
			162	177 A	$\delta_{\text{op}}(\text{NMe})$ (115), $\tau(\text{NMe})$ (19)	173 A	$\delta_{\text{op}}(\text{NMe})$ (113), $\tau(\text{NMe})$ (13)
	93		128	166 B	$\tau(\text{NMe})$ (31), $\tau(\text{ring-1})$ (92)	151 B	$\tau(\text{NMe})$ (26), $\tau(\text{ring-1})$ (97)
			105	125 A	$\delta_{\text{op}}(\text{NMe})$ (40), $\tau(\text{NMe})$ (74)	88 A	$\delta_{\text{op}}(\text{NMe})$ (31), $\tau(\text{NMe})$ (74)
				94 B	$\tau(\text{NMe})$ (62), $\tau(\text{ring-1})$ (60)	65 B	$\tau(\text{NMe})$ (67), $\tau(\text{ring-1})$ (52)
	78			82 A	$\tau(\text{ring-2})$ (126), $\tau(\text{ring-3})$ (10)	77 A	$\tau(\text{ring-2})$ (125)
				26 Ai	$\delta_{\text{op}}(\text{NMe})$ (47)	39 A	$\tau(\text{ring-2})$ (23), $\tau(\text{ring-3})$ (108)

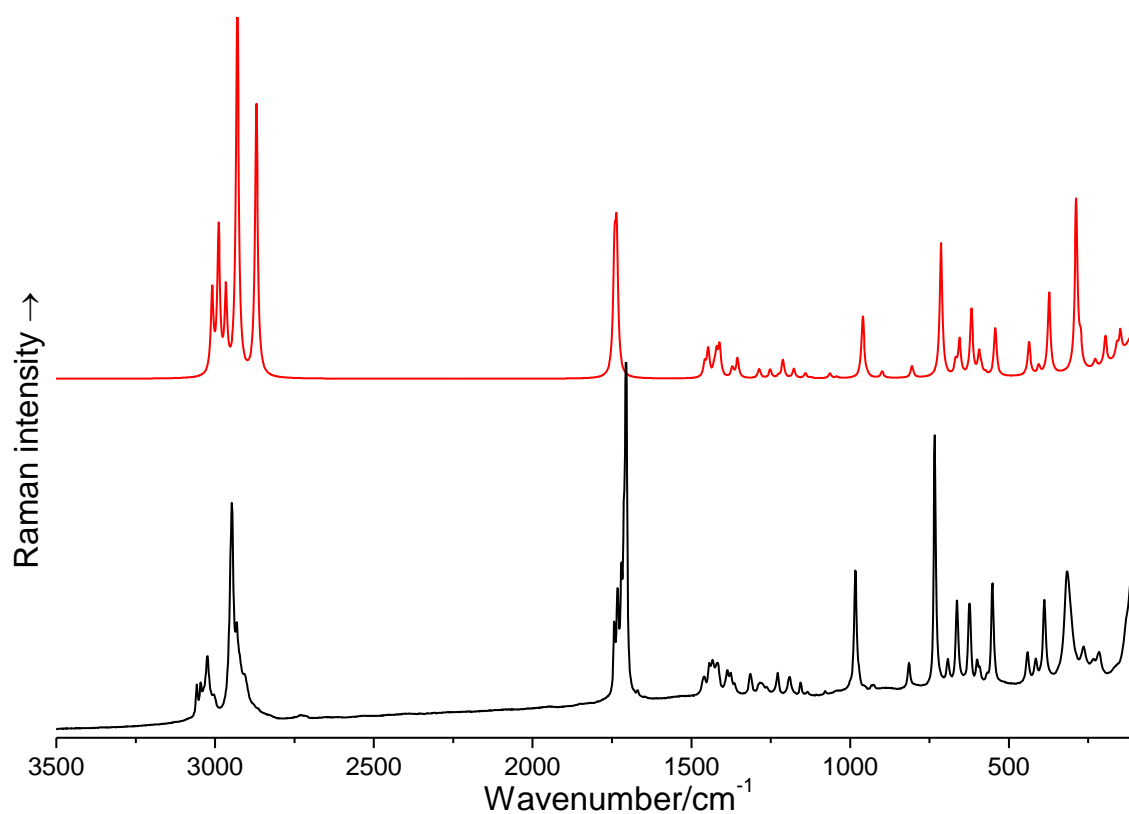


Figure 6.4. Calculated (top) and experimental (bottom) solid state Raman spectra for DAGG.

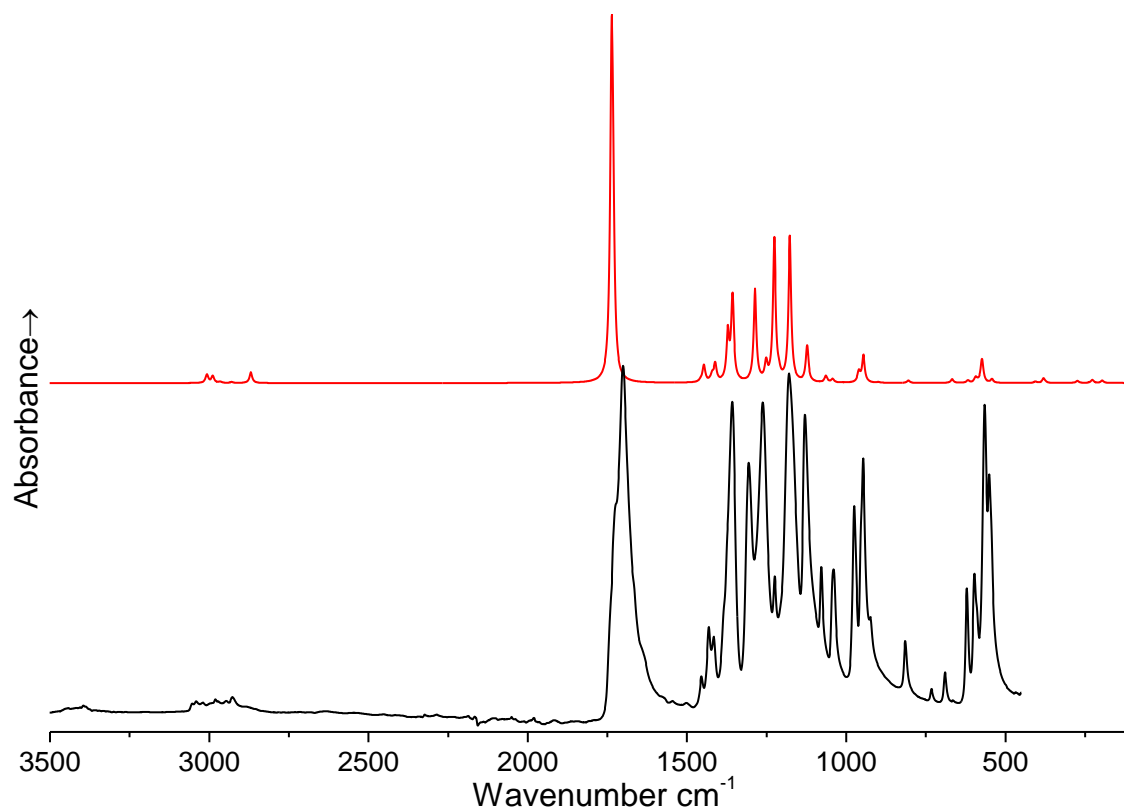


Figure 6.5. Calculated (top) and experimental (bottom) solid state IR spectra for DAGG.

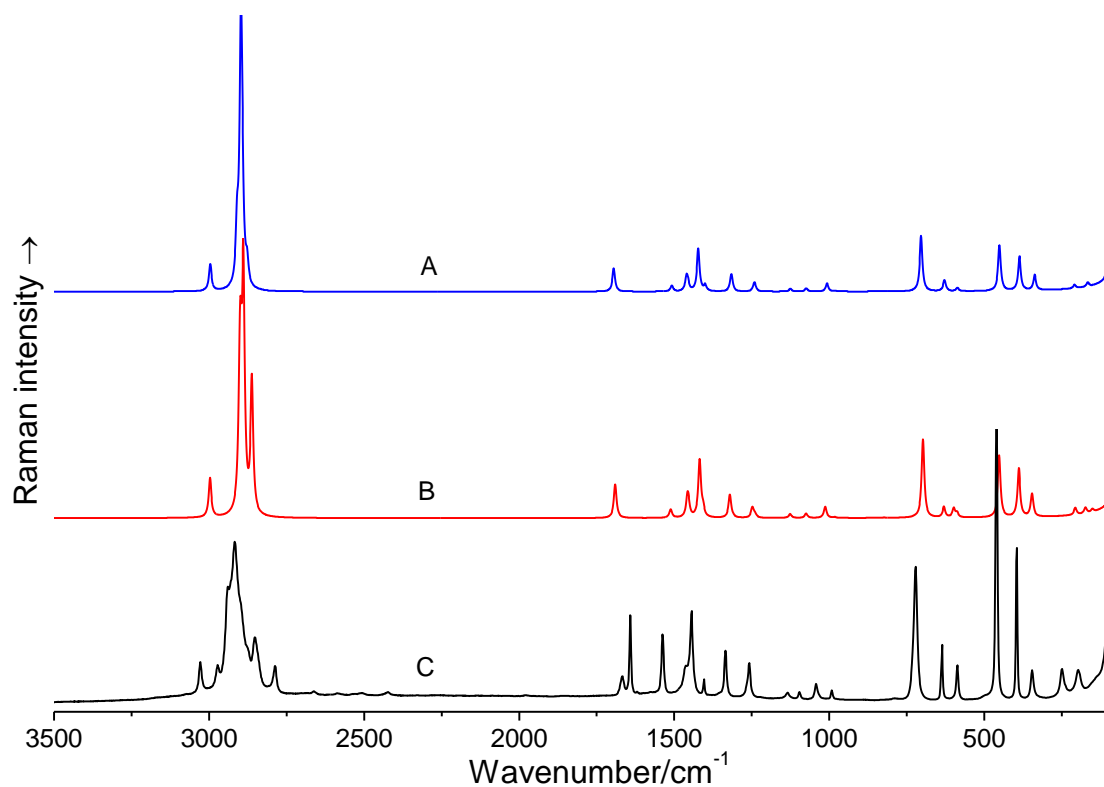


Figure 6.6. Calculated (A) planar (B) boat conformers and (C) experimental solid state Raman spectra of DMGG.

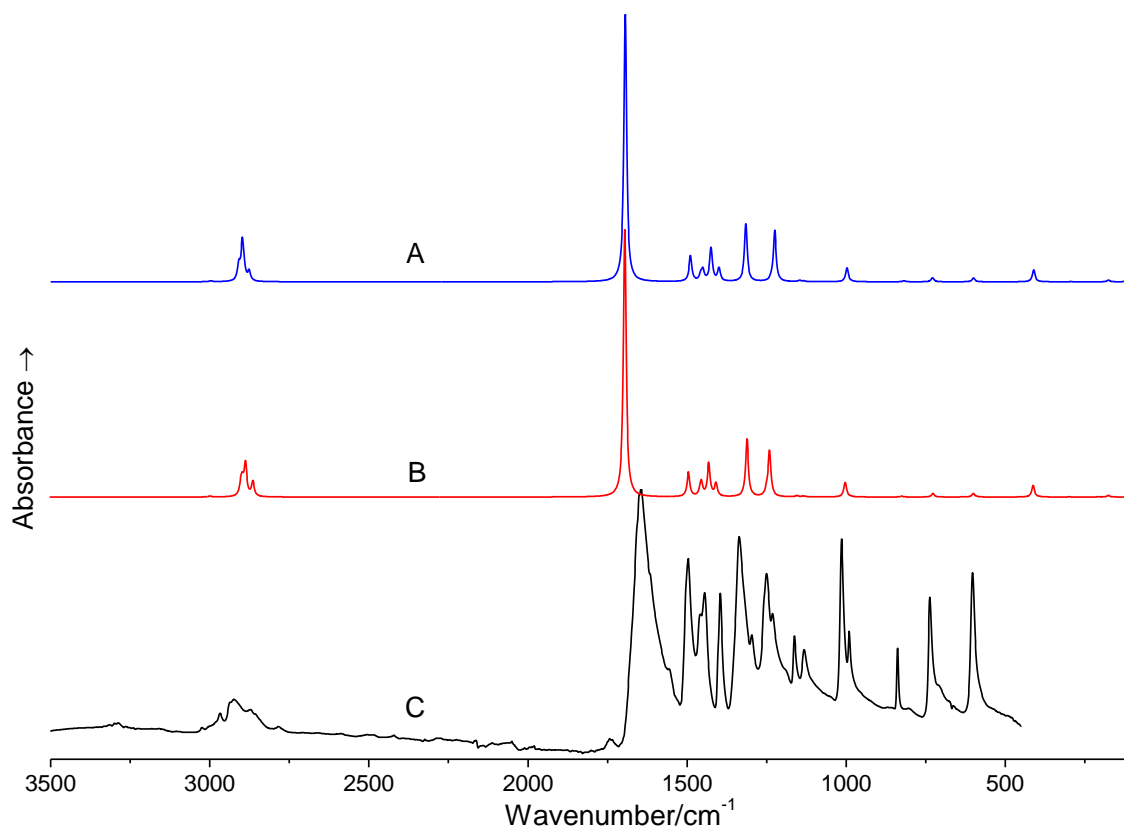


Figure 6.7. Calculated (A) planar (B) boat conformers and (C) experimental solid state IR spectra of DMGG.

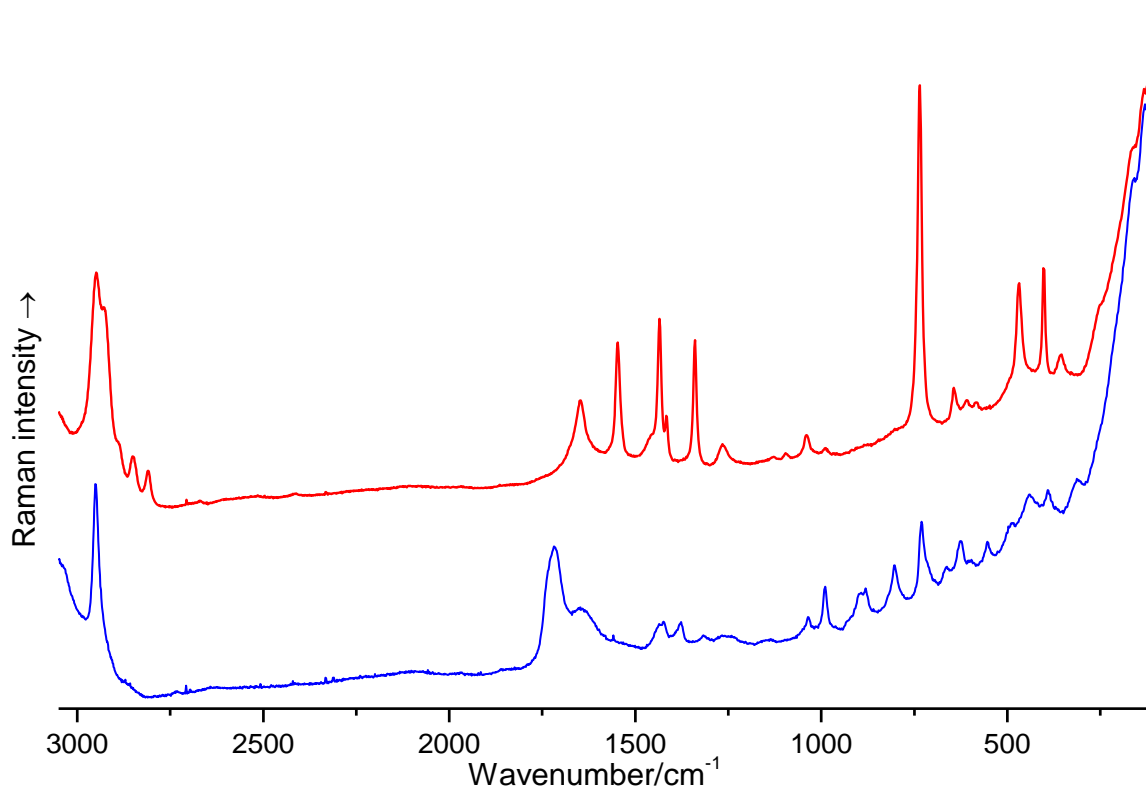


Figure 6.8. Solution state Raman spectra of (top) DMGG and (bottom) DAGG.

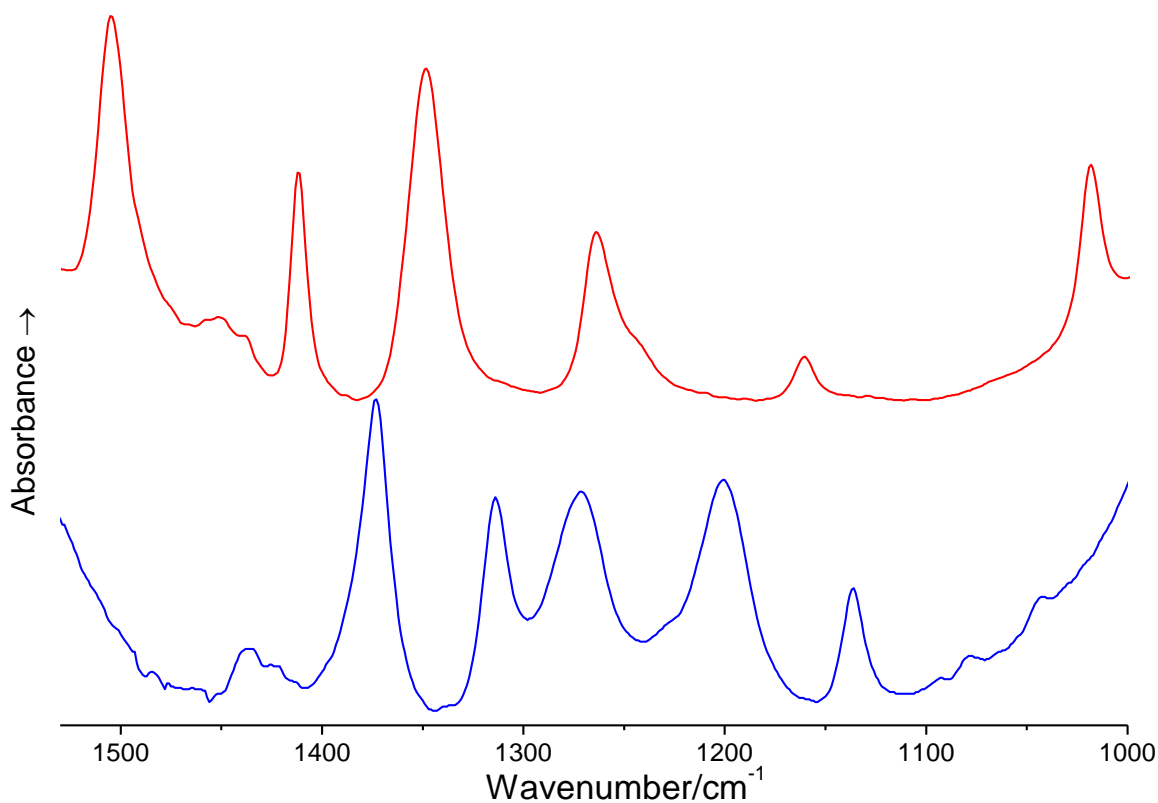


Figure 6.9. Solution state IR spectra of (top) DMGG and (bottom) DAGG.

6.4. Molecular orbital analysis

The highest occupied molecular orbital (HOMO) and lowest unoccupied molecular orbital (LUMO) energies of DAGG and DMGG were calculated for the optimised structures at the B3LYP/aug-cc-pVTZ level. The HOMO energies of DAGG and DMGG are -7.827 eV and -7.054 eV, respectively whereas, the LUMO energies are -1.721 eV and -0.560 eV, respectively. The composition of HOMO and LUMO are shown in Fig. 6.10. The analyses of molecular orbitals of DAGG and DMGG show that the HOMO is localized on the oxygen, nitrogen, C_{α} and carbonyl carbon atoms of the DKP ring, partly on the oxygen (DAGG) and carbon atoms (DMGG) on the side-chains (DAGG) whereas the LUMO is localized on the carbonyl carbon, hydrogen (DMGG) atoms on the DKP ring, carbon (both DAGG and DMGG) and oxygen atoms (DAGG) on the side chains and partly on the nitrogen and oxygen atoms on the DKP ring. The computed HOMO–LUMO energy gap corresponds to 6.105 eV (DAGG) and 6.494 eV (DMGG). The plots of HOMO and LUMO are shown in Figs. 6.10 and 6.11.

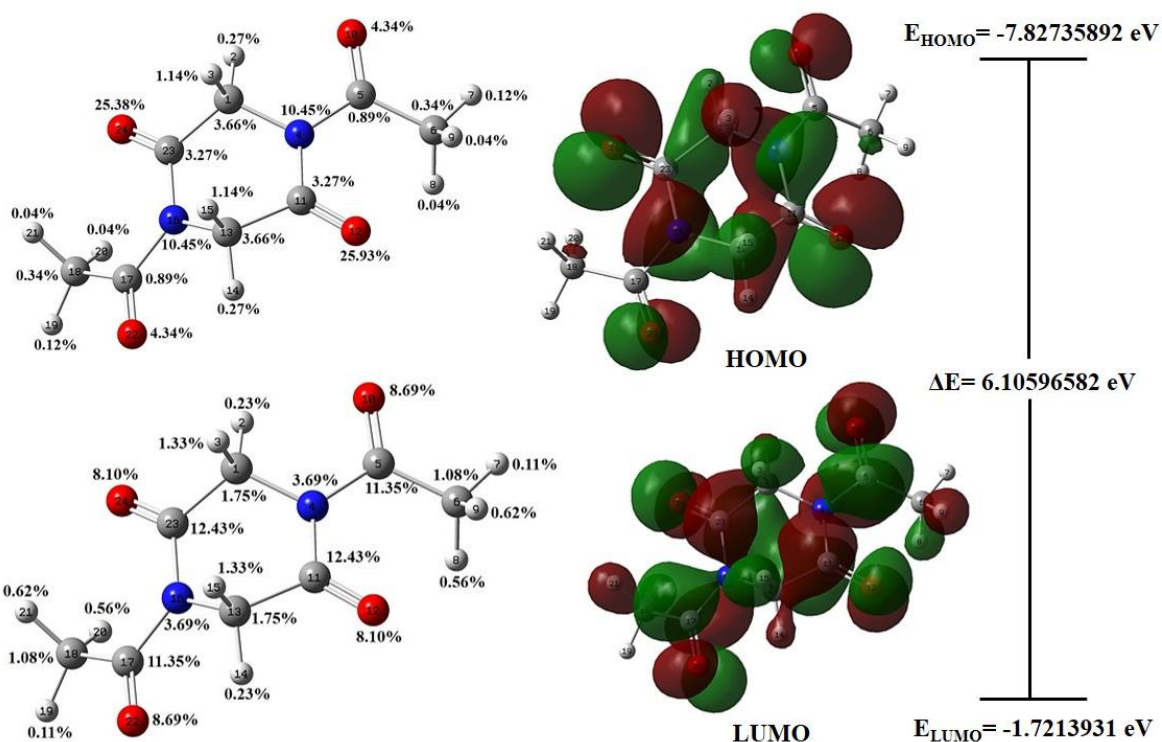


Figure 6.10. HOMO-LUMO plots with orbital compositions of DAGG.

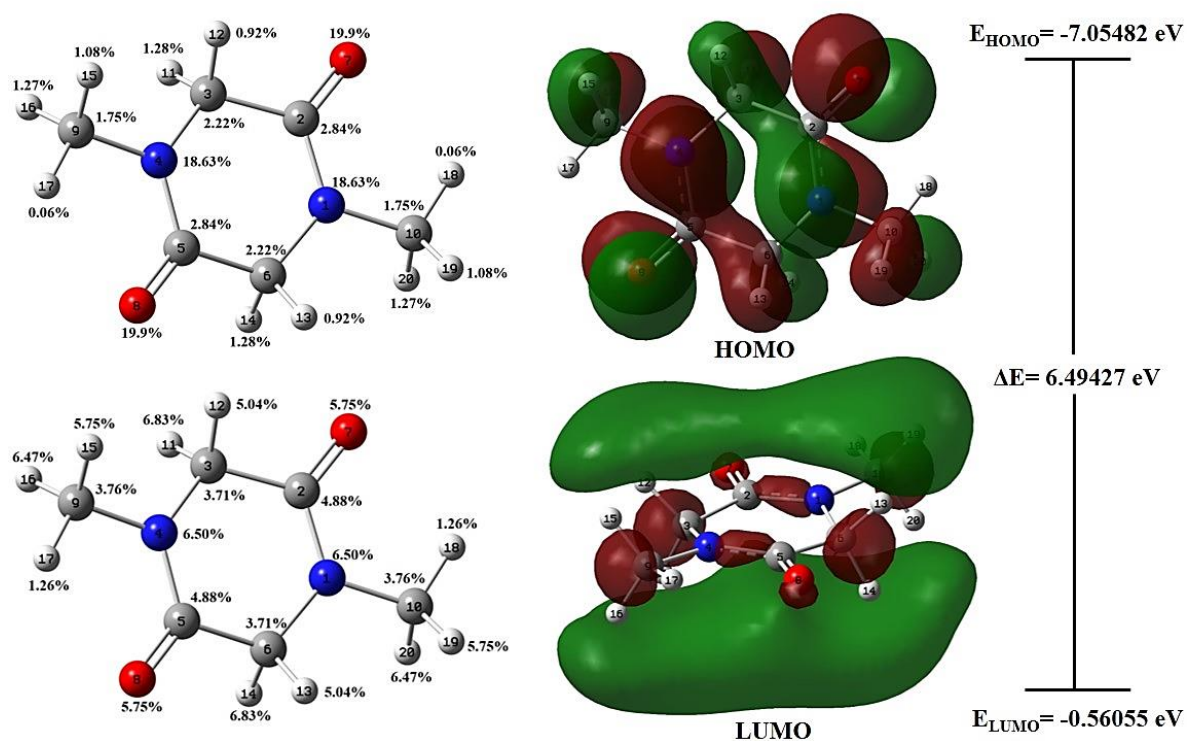


Figure 6.11. HOMO-LUMO plots with orbital compositions of DMGG.

6.5. Molecular electrostatic potential

The total electron density mapped using the molecular electrostatic potential (MEP) surface and the contour map of the electrostatic potential (ESP) have been plotted for DAGG (Fig. 6.12) and DMGG (Fig. 6.13) molecules at the B3LYP/aug-cc-pVTZ level. The MEP surfaces are in the range between -4.78 (arb. units) (deepest red) and 4.78 (arb. units) (deepest blue) for DAGG and between -5.13 (arb. units) (deepest red) and 5.13 (arb. units) (deepest blue) for DMGG. The red area indicates the strongest electrostatic repulsion and the blue coloured area indicates the strongest attraction. From the MEP maps of DAGG (Fig. 6.12a) and DMGG (Fig. 6.13b), the increase in negative potential is shown from yellow to red colour, with the maximum negative potential in red colour (preferred site for electrophilic attack), green represent the zero potentials and the maximum positive region, (preferred site for nucleophilic attack) is represented in deep blue colour. The calculated results shows that the negative potentials are mainly around the electronegative oxygen atoms on the DKP ring, the oxygen atoms of the N',N' -diacetyl side-chains (in the case of DAGG) and a positive potential over the nitrogen atoms of the DKP ring and partly on the hydrogen atoms in both DAGG and DMGG. This information can be useful in investigating possible sites for intermolecular interactions. The contour map of the MEP also clearly indicates the electron rich (red lines) are around the oxygen and nitrogen atoms and the electron deficient (yellow lines) are around the hydrogen and carbon atoms in both DAGG (Fig. 6.12b) and DMGG (Fig. 6.13b).

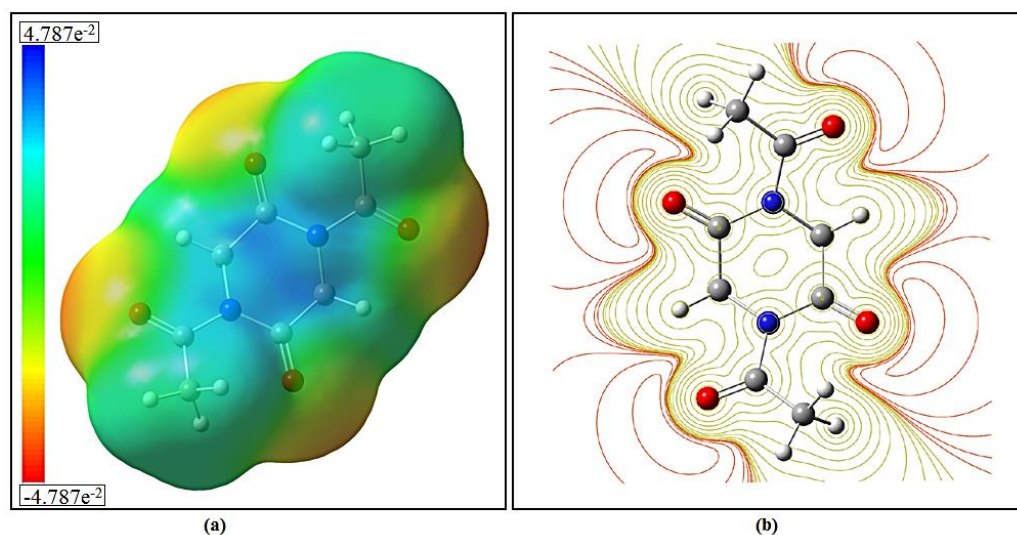


Figure 6.12. (a) Molecular electrostatic potential energy surface and (b) contour map (MEP) of DAGG.

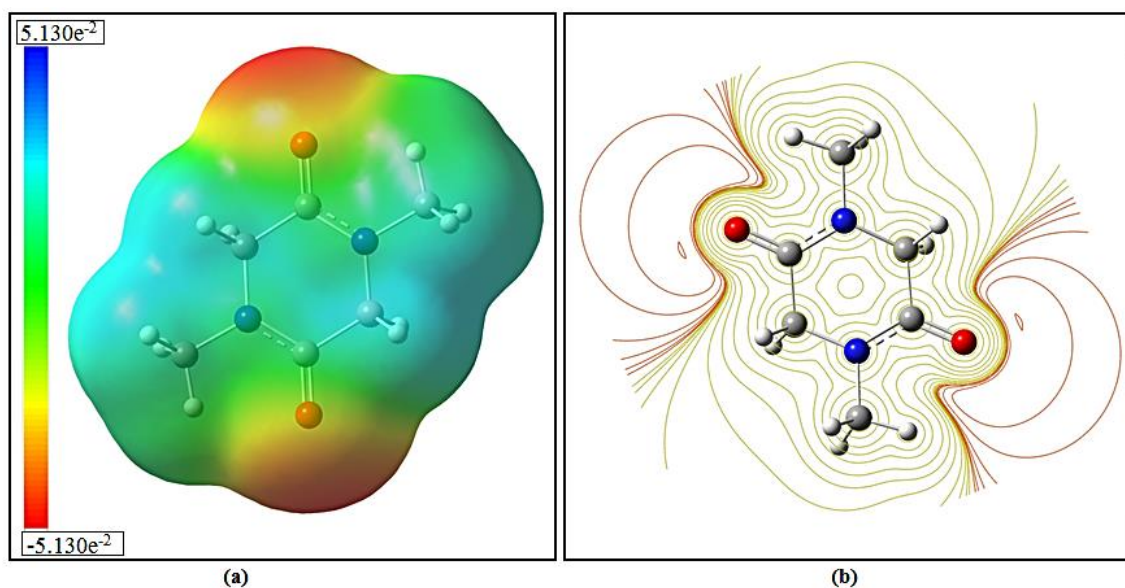


Figure 6.13. (a) Molecular electrostatic potential energy surface and (b) contour map (MEP) of DMGG.

6.6. Hirshfeld surface analysis

The Hirshfeld surfaces of DAGG and DMGG are illustrated in Figs. 6.14 and 6.15 showing the mapped surface over d_{norm} , curvedness and shape index in Figs. 6.16 and 6.17. The interactions between the carbonyl carbon atoms and the oxygen atoms of the side-chains C--O/O--C (3.0 and 3.6%) can be seen as the bright red areas on the Hirshfeld surface of molecule A and B of DAGG respectively (Fig. 6.14, labelled as a and b). The light red spots are due to O--N (2.3%) interactions between the oxygen atoms of the side-chains and nitrogen atoms of the DKP ring (Fig. 6.14, labelled as d). In DMGG the interactions between the hydrogens of the C $_{\alpha}$ -carbon atoms and the oxygen atoms of the DKP ring O--H/O--H (18.9%) interactions can be seen as the bright red areas (Fig. 6.15, labelled as a and b). The light red spots are due to the interactions between oxygen atoms of the DKP ring and the hydrogens of the N'-N'-dimethyl side chains on the Hirshfeld surface of DMGG (Fig. 6.15, labelled as c). The H--H and O--H intermolecular interactions appear as separate spikes in the 2D fingerprint plot (Fig. 6.18). Corresponding regions are visible in the fingerprint plots where one molecule acts as an acceptor ($d_e < d_i$) and the other acts as a donor ($d_e > d_i$). The small broad spikes with ($d_e + d_i$) values around 2.2 Å, pointing toward the lower left of the plots are due to H--H hydrogen interactions, encompassing 43.7% and 38% in A and B of DAGG and 52.5% (DMGG) of the total Hirshfeld surface.

The O--H interactions can be easily located around the corners, resembling “wings” (DAGG) and sharp spikes (DMGG) on the 2D fingerprint plot (Fig. 6.18 and 6.19). They comprise about 23.2 % (A) and 21.6% (B) in DAGG and 18.9 % (DMGG) of the total Hirshfeld surface with a high ($d_e + d_i$) value of 2.4 Å. The shortest contact i.e., the minimum ($d_e + d_i$) value on the Hirshfeld surface is ~ 2.2 Å which shows the importance of H--H interactions in both A and B of DAGG and O--H interactions (2.3 Å) in DMGG. From the fingerprint plots, the contributions involving different interactions includes O--C/N/O, C--H and N--H on the fingerprint plots of A and B of DAGG and DMGG comprises C--O/O--C (3.0%, 3.6% and 0.2%), N--O/O--N (2.3%, 2.3% and 0.5%), C--H (1.7%, 2.2% (Fig. 6.14, labelled as c) and 3.7%) and N--H (0.5%, 0.4% and 2.9%) of the total Hirshfeld surface area (Fig 6.18 and 6.19). Curvedness and shape index can also be used to identify the ways by which the neighbouring molecules contact each another and the characteristic packing modes. The shape indexes of DAGG and DMGG shows a red concave region on the surface around the acceptor atom and a blue region around the donor H-atom. (Figs. 6.16 and 6.17a). Curvedness is a function of the RMS curvature of the surface and the curvedness maps on the Hirshfeld surface show no flat surface patches which indicates that there is no stacking interaction between the DAGG molecules (Fig. 6.16) or the DMGG molecules (Fig. 6.17b). The type and nature of the interaction of the DAGG molecule is more easily understood using Hirshfeld surface, the results showcase the power of the analysis in mapping such interactions.

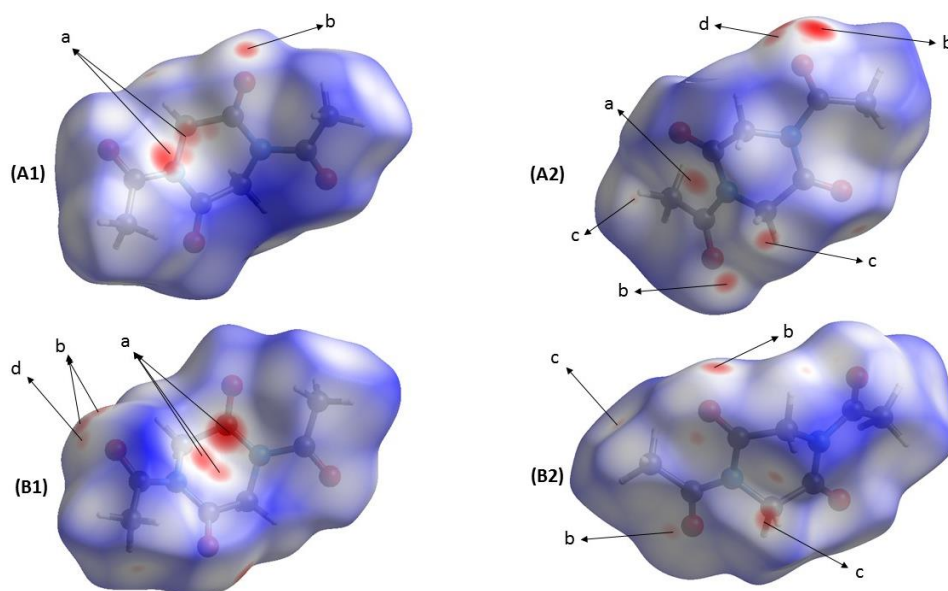


Figure 6.14. Hirshfeld surface mapped with dnorm showing all close contacts in (A1, B1) front view and (A2, B2) back view of molecules A and B of DAGG, respectively.

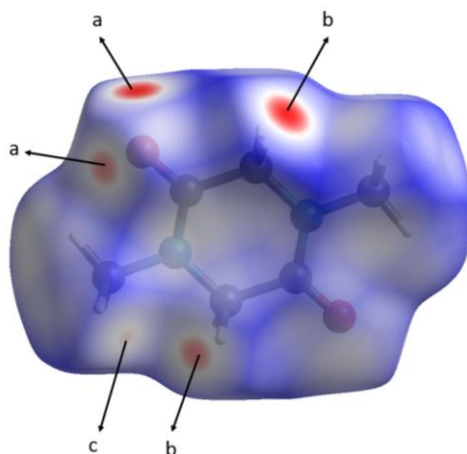


Figure 6.15. Hirshfeld surface mapped with d_{norm} showing all close contacts in DMGG.

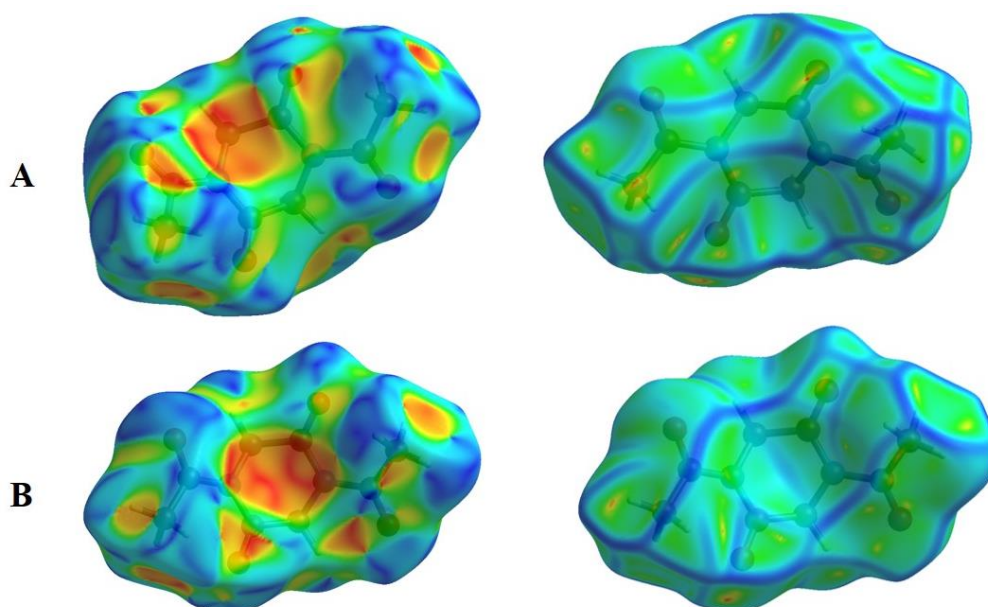


Figure 6.16. Hirshfeld surfaces mapped with shape index (left) and curvedness (right) for molecules **A** and **B** of DAGG.

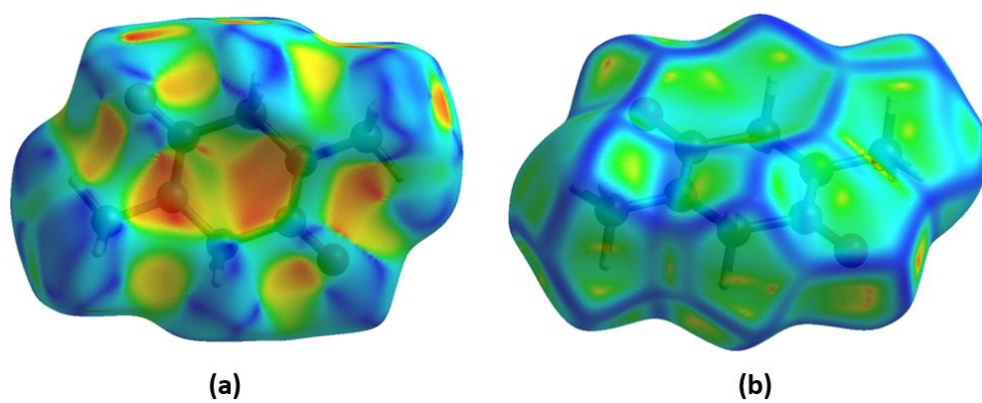


Figure 6.17. Hirshfeld surfaces of DMGG mapped with (a) shape index (b) curvedness.

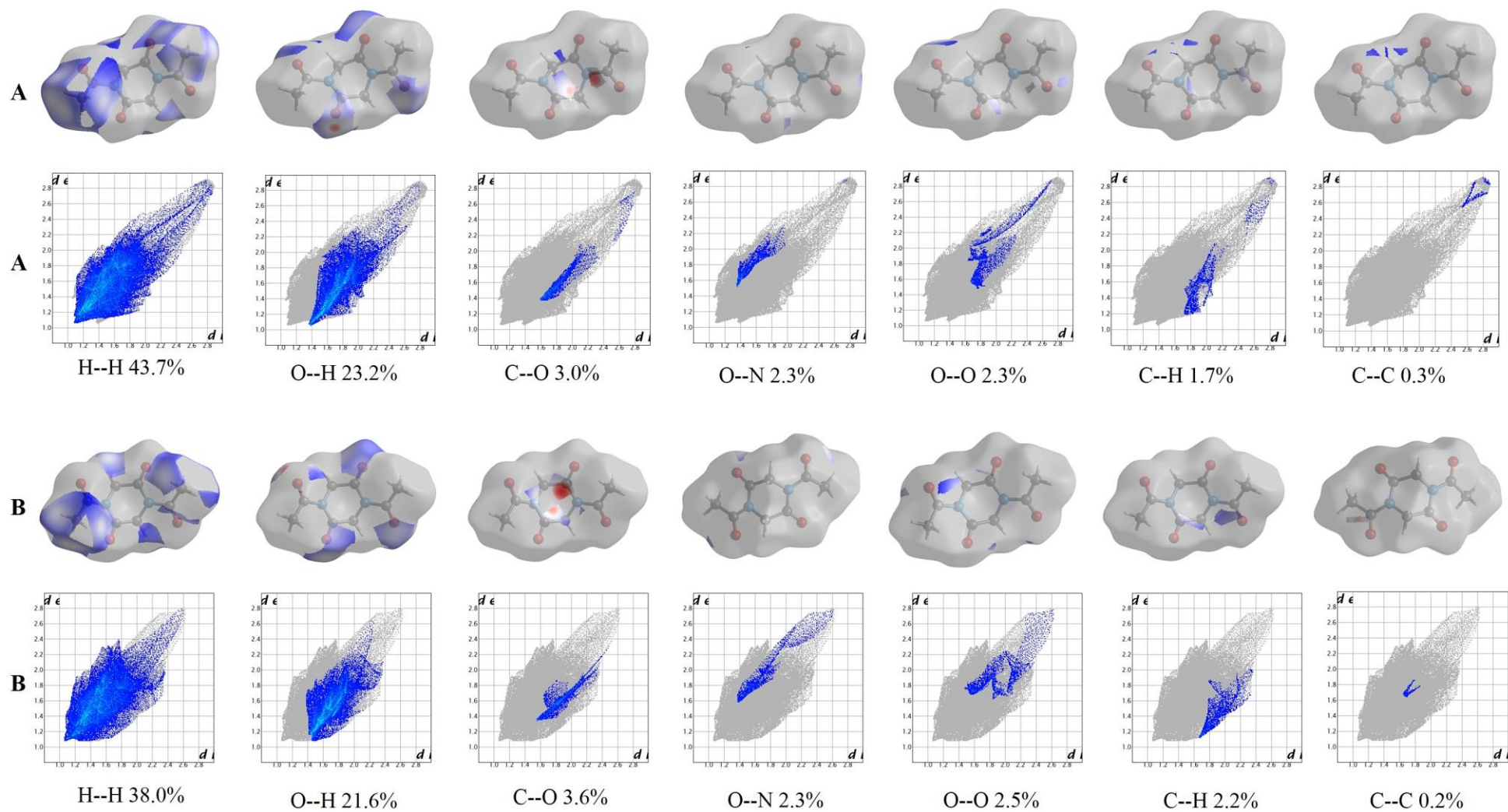


Figure 6.18. 2D Fingerprint plots for all the intermolecular contacts in molecules **A** and **B** of DAGG.

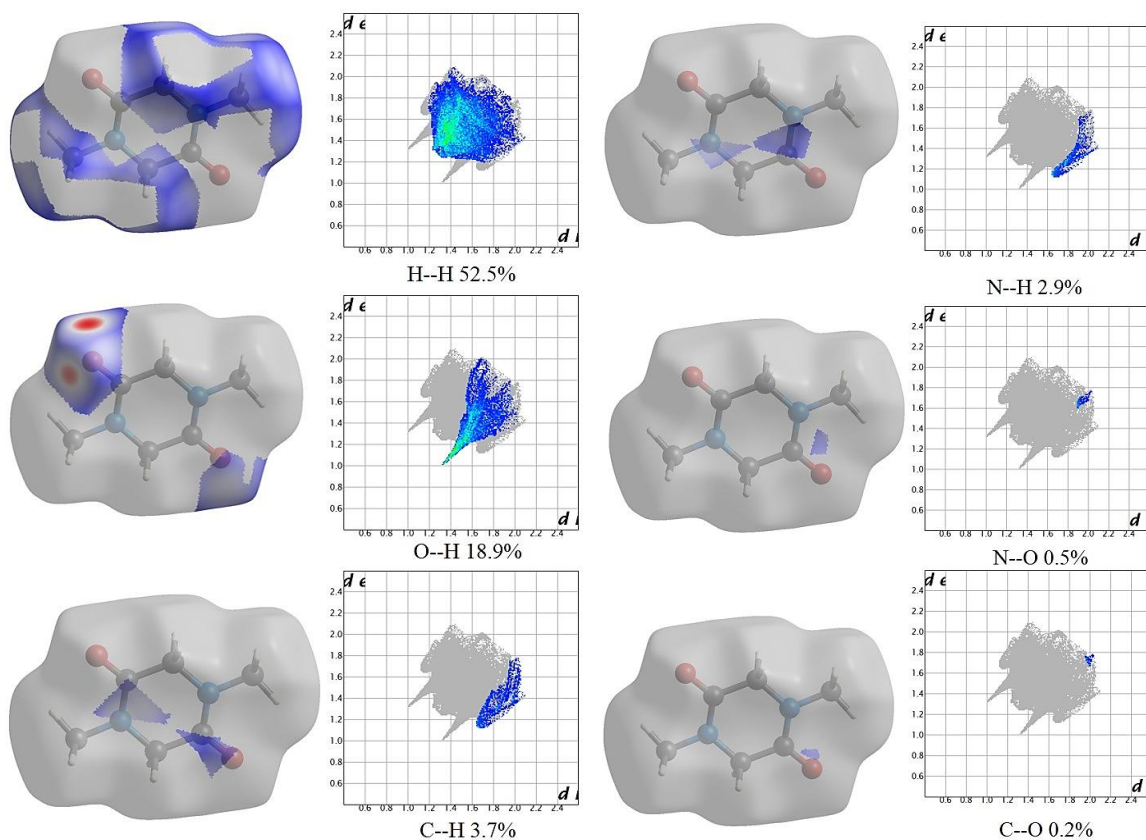


Figure 6.19. 2D Fingerprint plots for all the intermolecular contacts in DMGG.

6.7. Conclusions

A theoretical and experimental vibrational spectroscopic study of *N*-acetylated and *N*-methylated derivatives of cyclo(Gly-Gly) namely, DAGG and DMGG has provided an insight into the molecular geometry of these molecules. The calculated minimum energy structures of DAGG and DMGG predicts a boat conformation for isolated molecules in the gas phase with C_2 symmetry and shows a good fit with the previously reported X-ray data.^{5,6} However, calculations performed by constraining the DKP ring to a planar structure in DMGG reveals an imaginary frequency which shows that DMGG is unlikely to exhibit a planar conformation in the gas phase. The Raman and IR spectra for DAGG shows that the ring C=O stretching mode of DAGG appears at a significantly higher wavenumber ($\sim 40\text{ cm}^{-1}$), and has a significantly higher Raman intensity than observed in other CDAPs, including cyclo(Gly-Gly).^{12-16, 20} This can be explained by the shortening of the ring C=O bond distance after acetylation, which is attributed to the delocalization of the lone pairs on the nitrogen atoms towards the exo, from the endocyclic amide linkages.²¹ It is noteworthy that in DMGG there is a difference of around $\sim 50\text{-}60\text{ cm}^{-1}$ in the location of the C=O stretching band (1666 cm^{-1} in Raman and 1650 cm^{-1} in IR) compared to

DAGG. This can be attributed to the presence of C-N stretching character, instead of N-H in-plane-bending, associated with C=O stretch in the amide I mode. However, it is noted that there is a $\sim 20\text{ cm}^{-1}$ upward shift of the amide C-N stretching vibration in DMGG compared to cyclo(Gly-Gly) which must be due to the mixing of the C-N stretching with the CH_2 bending modes. It appears that there is no significant difference in the C-N bond lengths of DMGG, compared to those of cyclo(Gly-Gly). Therefore, unlike DAGG, no change in delocalization of the lone pairs of electrons on the nitrogen atoms occur. Furthermore, HOMO and LUMO analysis has been carried out to elucidate the information related to the charge transfer within the molecules. The HOMO-LUMO gap of DAGG and DMGG were found to be about 6.105 eV and 6.494 eV, respectively which implies that both compounds possess relatively high chemical stability. The MEP analysis of DAGG and DMGG reveals that the most negative potential site is around the oxygen atoms of the DKP ring and the side-chains (DAGG), while the positive potential site is located around the nitrogen and hydrogen atoms. The Hirshfeld surface analysis and 2D fingerprint plots enabled us to investigate the types of intermolecular interactions present in the crystal structures of DAGG and DMGG.

Table 6.7. Definitions of symmetry-adapted internal coordinates for DAGG and DMGG.

DAGG

A symmetry

$$v_s(\text{CO})=1/\sqrt{2}[r(\text{C11O12}) + r(\text{C23C24})]$$

$$v_s(\text{CO}')=1/\sqrt{2}[r(\text{C5O10}) + r(\text{C17O22})]$$

$$v_s(\text{NC})=1/\sqrt{2}[r(\text{N4C11}) + r(\text{N16C23})]$$

$$v_s(\text{NAc})=1/\sqrt{2}[r(\text{N4C5}) + r(\text{N16C17})]$$

$$v_s(\text{NC}_\alpha)=1/\sqrt{2}[r(\text{N4C1}) + r(\text{N16C13})]$$

$$v_s(\text{CC}_\alpha)=1/\sqrt{2}[r(\text{C23C1}) + r(\text{C11C13})]$$

$$v(\text{CC}') = 1/\sqrt{2}[r(\text{C5C6}) + r(\text{C17C18})]$$

$$v_s(\text{CH}_2) = 1/2[r(\text{C1H2}) + r(\text{C1H3}) + r(\text{C13H14}) + r(\text{C13C15})]$$

$$v_{as}(\text{CH}_2) = 1/2[r(\text{C1H2}) - r(\text{C1H3}) + r(\text{C13H14}) - r(\text{C13C15})]$$

$$v_s(\text{CH}_3) = 1/\sqrt{6}[r(\text{C6H7}) + r(\text{C6H8}) + r(\text{C6H9}) + r(\text{C18CH19}) + r(\text{C18H20}) + r(\text{C18H21})]$$

$$v_{as}(\text{CH}_3) = 1/\sqrt{12}[2r(\text{C6H7}) - r(\text{C6H8}) - r(\text{C6H9}) + 2r(\text{C18CH19}) - r(\text{C18H20}) - r(\text{C18H21})]$$

$$v_{as}'(\text{CH}_3) = 1/2[r(\text{C6H8}) - r(\text{C6H9}) + r(\text{C18H20}) - r(\text{C18H21})]$$

$$\delta_{ip}(\text{CO})=1/2[\theta(\text{N4C11O12}) - \theta(\text{C13C11O12}) + \theta(\text{N16C23O24}) - \theta(\text{C1C23O24})]$$

$$\delta_{ip}(\text{CO}')=1/2[\theta(\text{C6C5O10}) - \theta(\text{N4C5O10}) + \theta(\text{C18C17O22}) - \theta(\text{N16C17O22})]$$

$$\delta(\text{CH}_2) = 1/2\sqrt{10}[4\theta(\text{C1H2H3}) - \theta(\text{N4C1H2}) - \theta(\text{N4C1H3}) - \theta(\text{C23C1H2}) - \theta(\text{C23C1H3}) + 4\theta(\text{C13H14H15}) - \theta(\text{N16C13H14}) - \theta(\text{N16C13H15}) - \theta(\text{C11C13H14}) - \theta(\text{C11C13H15})]$$

$$\rho(\text{CH}_2) = 1/2\sqrt{2}[\theta(\text{N4C1H2}) - \theta(\text{N4C1H3}) + \theta(\text{C23C1H2}) - \theta(\text{C23C1H3}) + \theta(\text{N16C13H14}) - \theta(\text{N16C13H15}) + \theta(\text{C11C13H14}) - \theta(\text{C11C13H15})]$$

$$\omega(\text{CH}_2) = 1/2\sqrt{2}[\theta(\text{N4C1H2}) + \theta(\text{N4C1H3}) - \theta(\text{C23C1H2}) - \theta(\text{C23C1H3}) + \theta(\text{N16C13H14}) + \theta(\text{N16C13H15}) - \theta(\text{C11C13H14}) - \theta(\text{C11C13H15})]$$

$$\tau(\text{CH}_2) = 1/2\sqrt{2}[\theta(\text{N4C1H2}) - \theta(\text{N4C1H3}) - \theta(\text{C23C1H2}) + \theta(\text{C23C1H3}) + \theta(\text{N16C13H14}) - \theta(\text{N16C13H15}) - \theta(\text{C11C13H14}) + \theta(\text{C11C13H15})]$$

$$\delta_s(\text{CH}_3) = 1/2\sqrt{3}[\theta(\text{C5C6H7}) + \theta(\text{C5C6H8}) + \theta(\text{C5C6H9}) - \theta(\text{H7C6H8}) - \theta(\text{H7C6H9}) - \theta(\text{H8C6H9}) + \theta(\text{C17C18H19}) + \theta(\text{C17C18H20}) + \theta(\text{C17C18H21}) - \theta(\text{H19C18H20}) - \theta(\text{H19C18H21}) - \theta(\text{H20C18H21})]$$

$$\delta_{as}(\text{CH}_3) = 1/\sqrt{12}[2\theta(\text{H7C6H8}) - \theta(\text{H7C6H9}) - \theta(\text{H8C6H9}) + 2\theta(\text{H19C18H20}) - \theta(\text{H19C18H21}) - \theta(\text{H20C18H21})]$$

$$\begin{aligned}
\delta_{\text{as}}(\text{CH}_3) &= 1/2[\theta(\text{H7C6H9}) - \theta(\text{H8C6H9}) + \theta(\text{H19C18H21}) - \theta(\text{H20C18H21})] \\
\rho_{\text{ip}}(\text{CH}_3) &= 1/\sqrt{12}[2\theta(\text{C5C6H7}) - \theta(\text{C5C6H8}) - \theta(\text{C5C6H9}) + 2\theta(\text{C17C18H19}) - \theta(\text{C17C18H20}) - \theta(\text{C17C18H21})] \\
\rho_{\text{op}}(\text{CH}_3) &= 1/2[\theta(\text{C5C6H8}) - \theta(\text{C5C6H9}) + \theta(\text{C17C18H20}) - \theta(\text{C17C18H21})] \\
\delta_{\text{op}}(\text{CO}) &= 1/\sqrt{2}[\tau(\text{O12C11N4C13}) + \tau(\text{O24C23N16C1})] \\
\delta_{\text{op}}(\text{CO}') &= 1/\sqrt{2}[\tau(\text{O10C5N4C6}) + \tau(\text{O22C17N16C18})] \\
\delta_{\text{ip}}(\text{NAc}) &= 1/2[\theta(\text{C5N4C11}) - \theta(\text{C5N4C1}) + \theta(\text{C17N16C23}) - \theta(\text{C17N16C13})] \\
\delta_{\text{op}}(\text{NAc}) &= 1/\sqrt{2}[\tau(\text{C5N4C1C11}) + \tau(\text{C17N16C13C23})] \\
\tau(\text{CC}') &= 1/2\sqrt{3}[\tau(\text{H7C6C5O10}) + \tau(\text{H7C6C5N4}) + \tau(\text{H8C6C5O10}) + \tau(\text{H8C6C5N4}) + \tau(\text{H9C6C5O10}) + \tau(\text{H9C6C5N4}) + \tau(\text{H19C18C17O22}) + \tau(\text{H19C18C17N16}) \\
&\quad + \tau(\text{H20C18C17O22}) + \tau(\text{H20C18C17N16}) + \tau(\text{H21C18C17O22}) + \tau(\text{H21C18C17N16})] \\
\tau(\text{NAc}) &= 1/2\sqrt{3}[\tau(\text{C1N4C5C6}) + \tau(\text{C11N4C5C6}) + \tau(\text{C1N4C5O10}) + \tau(\text{C11N4C5O10}) + \tau(\text{C13N16C17C18}) + \tau(\text{C23N16C17C18}) + \tau(\text{C13N16C17O22}) \\
&\quad + \tau(\text{C23N16C17O22})] \\
\delta(\text{NCC}') &= 1/\sqrt{2}[\theta(\text{N4C5C6}) + \theta(\text{N16C17C18})] \\
\delta_{\text{ip}}(\text{Ring-1}) &= 1/\sqrt{12}[2\theta(\text{N4C1C23}) - \theta(\text{C1C23N16}) - \theta(\text{C23N16C13}) + 2\theta(\text{N16C13C11}) - \theta(\text{C13C11N4}) - \theta(\text{C11N4C1})] \\
\delta_{\text{ip}}(\text{Ring-2}) &= 1/2[\theta(\text{C1C23N16}) - \theta(\text{C23N16C13}) + \theta(\text{C13C11N4}) - \theta(\text{C11N4C1})] \\
\delta_{\text{op}}(\text{Ring-2}) &= 1/\sqrt{12}[-\tau(\text{C11N4C1C23}) + 2\tau(\text{N4C1C23N16}) - \tau(\text{C1C23N16C13}) - \tau(\text{C23N16C13C11}) + 2\tau(\text{N16C13C11N4}) - \tau(\text{C13C11N4C1})] \\
\delta_{\text{op}}(\text{Ring-3}) &= 1/2[\tau(\text{C11N4C1C23}) - \tau(\text{C1C23N16C13}) + \tau(\text{C23N16C13C11}) - \tau(\text{C13C11N4C1})]
\end{aligned}$$

B symmetry

$$\begin{aligned}
v_{\text{as}}(\text{CO}) &= 1/\sqrt{2}[r(\text{C11O12}) - r(\text{C23C24})] \\
v_{\text{as}}(\text{CO}') &= 1/\sqrt{2}[r(\text{C5O10}) - r(\text{C17C22})] \\
v_{\text{as}}(\text{NC}) &= 1/\sqrt{2}[r(\text{N4C11}) - r(\text{N16C23})] \\
v_{\text{as}}(\text{NAc}) &= 1/\sqrt{2}[r(\text{N4C5}) - r(\text{N16C17})] \\
v_{\text{as}}(\text{NC}_\alpha) &= 1/\sqrt{2}[r(\text{N4C1}) - r(\text{N16C13})] \\
v_{\text{as}}(\text{CC}_\alpha) &= 1/\sqrt{2}[r(\text{C23C1}) - r(\text{C11C13})] \\
v_{\text{as}}(\text{CC}') &= 1/\sqrt{2}[r(\text{C54C6}) - r(\text{C17C18})] \\
v_{\text{s}}(\text{CH}_2) &= 1/2[r(\text{C1H2}) + r(\text{C1H3}) - r(\text{C13H14}) - r(\text{C13C15})]
\end{aligned}$$

$$\begin{aligned}
v_{as}(\text{CH}_2) &= 1/2[r(\text{C1H2}) - r(\text{C1H3}) - r(\text{C13H14}) + r(\text{C13C15})] \\
v_s(\text{CH}_3) &= 1/\sqrt{6}[r(\text{C6H7}) + r(\text{C6H8}) + r(\text{C6H9}) - r(\text{C18CH19}) - r(\text{C18H20}) - r(\text{C18H21})] \\
v_{as}(\text{CH}_3) &= 1/\sqrt{12}[2r(\text{C6H7}) - r(\text{C6H8}) - r(\text{C6H9}) - 2r(\text{C18CH19}) + r(\text{C18H20}) + r(\text{C18H21})] \\
v_{as}'(\text{CH}_3) &= 1/2[r(\text{C6H8}) - r(\text{C6H9}) - r(\text{C18H20}) + r(\text{C18H21})] \\
\delta_{ip}(\text{CO}) &= 1/2[\theta(\text{N4C11O12}) - \theta(\text{C13C11O12}) - \theta(\text{N16C23O24}) + \theta(\text{C1C23O24})] \\
\delta_{ip}(\text{CO}') &= 1/2[\theta(\text{C6C5O10}) - \theta(\text{N4C5O10}) - \theta(\text{C18C17O22}) + \theta(\text{N16C17O22})] \\
\delta(\text{CH}_2) &= 1/2\sqrt{10}[4\theta(\text{C1H2H3}) - \theta(\text{N4C1H2}) - \theta(\text{N4C1H3}) - \theta(\text{C23C1H2}) - \theta(\text{C23C1H3}) - 4\theta(\text{C13H14H15}) + \theta(\text{N16C13H14}) + \theta(\text{N16C13H15}) + \theta(\text{C11C13H14}) \\
&\quad + \theta(\text{C11C13H15})] \\
\rho(\text{CH}_2) &= 1/2\sqrt{2}[\theta(\text{N4C1H2}) - \theta(\text{N4C1H3}) + \theta(\text{C23C1H2}) - \theta(\text{C23C1H3}) - \theta(\text{N16C13H14}) + \theta(\text{N16C13H15}) - \theta(\text{C11C13H14}) + \theta(\text{C11C13H15})] \\
\omega(\text{CH}_2) &= 1/2\sqrt{2}[\theta(\text{N4C1H2}) + \theta(\text{N4C1H3}) - \theta(\text{C23C1H2}) - \theta(\text{C23C1H3}) - \theta(\text{N16C13H14}) - \theta(\text{N16C13H15}) + \theta(\text{C11C13H14}) + \theta(\text{C11C13H15})] \\
\tau(\text{CH}_2) &= 1/2\sqrt{2}[\theta(\text{N4C1H2}) - \theta(\text{N4C1H3}) - \theta(\text{C23C1H2}) + \theta(\text{C23C1H3}) - \theta(\text{N16C13H14}) + \theta(\text{N16C13H15}) + \theta(\text{C11C13H14}) - \theta(\text{C11C13H15})] \\
\delta_s(\text{CH}_3) &= 1/2\sqrt{3}[\theta(\text{C5C6H7}) + \theta(\text{C5C6H8}) + \theta(\text{C5C6H9}) - \theta(\text{H7C6H8}) - \theta(\text{H7C6H9}) - \theta(\text{H8C6H9}) - \theta(\text{C17C18H19}) - \theta(\text{C17C18H20}) - \theta(\text{C17C18H21}) + \theta(\text{H19C18H20}) \\
&\quad + \theta(\text{H19C18H21}) + \theta(\text{H20C18H21})] \\
\delta_{as}(\text{CH}_3) &= 1/\sqrt{12}[2\theta(\text{H7C6H8}) - \theta(\text{H7C6H9}) - \theta(\text{H8C6H9}) - 2\theta(\text{H19C18H20}) + \theta(\text{H19C18H21}) + \theta(\text{H20C18H21})] \\
\delta_{as}'(\text{CH}_3) &= 1/2[\theta(\text{H7C6H9}) - \theta(\text{H8C6H9}) - \theta(\text{H19C18H21}) + \theta(\text{H20C18H21})] \\
\rho_{ip}(\text{CH}_3) &= 1/\sqrt{12}[2\theta(\text{C5C6H7}) - \theta(\text{C5C6H8}) - \theta(\text{C5C6H9}) - 2\theta(\text{C17C18H19}) + \theta(\text{C17C18H20}) + \theta(\text{C17C18H21})] \\
\rho_{op}(\text{CH}_3) &= 1/2[\theta(\text{C5C6H8}) - \theta(\text{C5C6H9}) - \theta(\text{C17C18H20}) + \theta(\text{C17C18H21})] \\
\delta_{op}(\text{CO}) &= 1/\sqrt{2}[\tau(\text{O12C11N4C13}) - \tau(\text{O24C23N16C1})] \\
\delta_{op}(\text{CO}') &= 1/\sqrt{2}[\tau(\text{O10C5N4C6}) - \tau(\text{O22C17N16C18})] \\
\delta_{ip}(\text{NAc}) &= 1/2[\theta(\text{C5N4C11}) - \theta(\text{C5N4C1}) - \theta(\text{C17N16C23}) + \theta(\text{C17N16C13})] \\
\delta_{op}(\text{NAc}) &= 1/2\sqrt{2}[\tau(\text{C5N4C1C11}) - \tau(\text{C17N16C13C23})] \\
\tau(\text{CC}') &= 1/2\sqrt{3}[\tau(\text{H7C6C5O10}) + \tau(\text{H7C6C5N4}) + \tau(\text{H8C6C5O10}) + \tau(\text{H8C6C5N4}) + \tau(\text{H9C6C5O10}) + \tau(\text{H9C6C5N4}) - \tau(\text{H19C18C17O22}) - \tau(\text{H19C18C17N16}) \\
&\quad - \tau(\text{H20C18C17O22}) - \tau(\text{H20C18C17N16}) - \tau(\text{H21C18C17O22}) - \tau(\text{H21C18C17N16})] \\
\tau(\text{NAc}) &= 1/2\sqrt{3} [\tau(\text{C1N4C5C6}) + \tau(\text{C11N4C5C6}) + \tau(\text{C1N4C5O10}) + \tau(\text{C11N4C5O10}) - \tau(\text{C13N16C17C18}) - \tau(\text{C23N16C17C18}) - \tau(\text{C13N16C17O22}) \\
&\quad - \tau(\text{C23N16C17O22})] \\
\delta(\text{NCC}') &= 1/\sqrt{2}[\theta(\text{N4C5C6}) - \theta(\text{N16C17C18})]
\end{aligned}$$

$$\delta_{ip}(\text{Ring-3}) = 1/\sqrt{6}[\theta(\text{N4C1C23}) - \theta(\text{C1C23N16}) + \theta(\text{C23N16C13}) - \theta(\text{N16C13C11}) + \theta(\text{C13C11N4}) - \theta(\text{C11N4C1})]$$

$$\delta_{op}(\text{Ring-1}) = 1/\sqrt{6}[\tau(\text{C11N4C1C23}) - \tau(\text{N4C1C23N16}) + \tau(\text{C1C23N16C13}) - \tau(\text{C23N16C13C11}) + \tau(\text{N16C13C11N4}) - \tau(\text{C13C11N4C1})]$$

DMGG

A symmetry

$$v_s(\text{CO})=1/\sqrt{2}[r(\text{C5O8}) + r(\text{C23C24})]$$

$$v_s(\text{NC})=1/\sqrt{2}[r(\text{N4C5}) + r(\text{N1C6})]$$

$$v_s(\text{NMe})=1/\sqrt{2}[r(\text{N4C9}) + r(\text{N1C10})]$$

$$v_s(\text{NC}_\alpha)=1/\sqrt{2}[r(\text{N4C3}) + r(\text{N1C6})]$$

$$v_s(\text{CC}_\alpha)=1/\sqrt{2}[r(\text{C2C3}) + r(\text{C5C6})]$$

$$v_s(\text{CH}_2) = 1/2[r(\text{C3H12}) + r(\text{C3H11}) + r(\text{C6H13}) + r(\text{C6C14})]$$

$$v_{as}(\text{CH}_2) = 1/2[r(\text{C3H12}) - r(\text{C3H11}) + r(\text{C6H13}) - r(\text{C6C14})]$$

$$v_s(\text{CH}_3) = 1/\sqrt{6}[r(\text{C9H15}) + r(\text{C9H16}) + r(\text{C9H17}) + r(\text{C10CH18}) + r(\text{C10H19}) + r(\text{C10H20})]$$

$$v_{as}(\text{CH}_3) = 1/\sqrt{12}[2r(\text{C9H15}) - r(\text{C9H16}) - r(\text{C9H17}) + 2r(\text{C10CH18}) - r(\text{C10H19}) - r(\text{C10H20})]$$

$$v_{as}'(\text{CH}_3) = 1/2[r(\text{C9H16}) - r(\text{C9H17}) + r(\text{C10H19}) - r(\text{C10H20})]$$

$$\delta_{ip}(\text{CO})=1/2[\theta(\text{N4C5O8}) - \theta(\text{C6C5O8}) + \theta(\text{N1C2O7}) - \theta(\text{C3C2O7})]$$

$$\delta(\text{CH}_2) = 1/2\sqrt{10}(4\theta(\text{H12C3H11}) - \theta(\text{N4C3H12}) - \theta(\text{N4C3H11}) - \theta(\text{C2C3H12}) - \theta(\text{C2C3H11}) + 4\theta(\text{H13C6H14}) - \theta(\text{N1C6H13}) - \theta(\text{N1C6H14}) - \theta(\text{C5C6H13}) - \theta(\text{C5C6H14})]$$

$$\rho(\text{CH}_2) = 1/2\sqrt{2}[\theta(\text{N4C3H12}) - \theta(\text{N4C3H11}) + \theta(\text{C2C3H12}) - \theta(\text{C2C3H11}) + \theta(\text{N1C6H13}) - \theta(\text{N1C6H14}) + \theta(\text{C5C6H13}) - \theta(\text{C5C6H14})]$$

$$\omega(\text{CH}_2) = 1/2\sqrt{2}[\theta(\text{N4C3H12}) + \theta(\text{N4C3H11}) - \theta(\text{C2C3H12}) - \theta(\text{C2C3H11}) + \theta(\text{N1C6H13}) + \theta(\text{N1C6H14}) - \theta(\text{C5C6H13}) - \theta(\text{C5C6H14})]$$

$$\tau(\text{CH}_2) = 1/2\sqrt{2}[\theta(\text{N4C3H12}) - \theta(\text{N4C3H11}) - \theta(\text{C2C3H12}) + \theta(\text{C2C3H11}) + \theta(\text{N1C6H13}) - \theta(\text{N1C6H14}) - \theta(\text{C5C6H13}) + \theta(\text{C5C6H14})]$$

$$\delta_s(\text{CH}_3) = 1/2\sqrt{3}[\theta(\text{N4C9H15}) + \theta(\text{N4C9H16}) + \theta(\text{N4C9H17}) - \theta(\text{H15C9H16}) - \theta(\text{H16C9H17}) - \theta(\text{H15C9H17}) + \theta(\text{N1C10H18}) + \theta(\text{N1C10H19}) + \theta(\text{N1C10H20}) - \theta(\text{H18C10H19}) - \theta(\text{H19C10H20}) - \theta(\text{H18C10H20})]$$

$$\delta_{as}(\text{CH}_3) = 1/\sqrt{12}[2\theta(\text{H15C9H16}) - \theta(\text{H15C9H17}) - \theta(\text{H16C9H17}) + 2\theta(\text{H18C10H19}) - \theta(\text{H18C10H20}) - \theta(\text{H19C10H20})]$$

$$\delta_{as}'(\text{CH}_3) = 1/2[\theta(\text{H15C9H17}) - \theta(\text{H16C9H17}) + \theta(\text{H18C10H20}) - \theta(\text{H19C10H20})]$$

$$\begin{aligned}
\rho_{ip}(\text{CH}_3) &= 1/\sqrt{12}[2\theta(\text{N4C9H15}) - \theta(\text{N4C9H16}) - \theta(\text{N4C9H17}) + 2\theta(\text{N1C10H18}) - \theta(\text{N1C10H19}) - \theta(\text{N1C10H20})] \\
\rho_{op}(\text{CH}_3) &= 1/2[\theta(\text{N4C9H16}) - \theta(\text{N4C9H17}) + \theta(\text{N1C10H19}) - \theta(\text{N1C10H20})] \\
\delta_{op}(\text{CO}) &= 1/\sqrt{2}[\tau(\text{O8C5N4C6}) + \tau(\text{O7C2N1C3})] \\
\delta_{ip}(\text{NMe}) &= 1/2[\theta(\text{C3N4C9}) - \theta(\text{C5N4C9}) + \theta(\text{C6N1C10}) - \theta(\text{C2N1C10})] \\
\delta_{op}(\text{NAc}) &= 1/\sqrt{2}[\tau(\text{C9N4C3C5}) + \tau(\text{C10N1C6C2})] \\
\tau(\text{NMe}) &= 1/2\sqrt{3}[\tau(\text{H15C9N4C5}) + \tau(\text{H16C9N4C5}) + \tau(\text{H17C9N4C5}) + \tau(\text{H15C9N4C3}) + \tau(\text{H16C9N4C3}) + \tau(\text{H17C9N4C3}) + \tau(\text{H18C10N1C2}) \\
&\quad + \tau(\text{H19C10N1C2}) + \tau(\text{H20C10N1C2}) + \tau(\text{H18C10N1C6}) + \tau(\text{H19C10N1C6}) + \tau(\text{H20C10N1C6})] \\
\delta_{ip}(\text{Ring-1}) &= 1/\sqrt{12}[2\theta(\text{N4C3C2}) - \theta(\text{C3C2N1}) - \theta(\text{C2N1C6}) + 2\theta(\text{N1C6C5}) - \theta(\text{C6C5N4}) - \theta(\text{C5N4C3})] \\
\delta_{ip}(\text{Ring-2}) &= 1/2[\theta(\text{C3C2N1}) - \theta(\text{C2N1C6}) + \theta(\text{C6C5N4}) - \theta(\text{C5C4C3})] \\
\delta_{op}(\text{Ring-2}) &= 1/\sqrt{12}[-\tau(\text{C5N4C3C2}) + 2\tau(\text{N4C3C2N1}) - \tau(\text{C3C2N1C6}) - \tau(\text{C2N1C6C5}) + 2\tau(\text{N1C6C5N4}) - \tau(\text{C6C5N4C3})] \\
\delta_{op}(\text{Ring-3}) &= 1/2[\tau(\text{C5N4C3C2}) - \tau(\text{C3C2N1C6}) + \tau(\text{C2N1C6C5}) - \tau(\text{C6C5N4C3})]
\end{aligned}$$

B symmetry

$$\begin{aligned}
v_{as}(\text{CO}) &= 1/\sqrt{2}[r(\text{C5O8}) - r(\text{C23C24})] \\
v_{as}(\text{NC}) &= 1/\sqrt{2}[r(\text{N4C5}) - r(\text{N1C6})] \\
v_{as}(\text{NMe}) &= 1/\sqrt{2}[r(\text{N4C9}) - r(\text{N1C10})] \\
v_{as}(\text{NC}_\alpha) &= 1/\sqrt{2}[r(\text{N4C3}) - r(\text{N1C6})] \\
v_{as}(\text{CC}_\alpha) &= 1/\sqrt{2}[r(\text{C2C3}) - r(\text{C5C6})] \\
v_s(\text{CH}_2) &= 1/2[r(\text{C3H12}) + r(\text{C3H11}) - r(\text{C6H13}) - r(\text{C6C14})] \\
v_{as}(\text{CH}_2) &= 1/2[r(\text{C3H12}) - r(\text{C3H11}) - r(\text{C6H13}) + r(\text{C6C14})] \\
v_s(\text{CH}_3) &= 1/\sqrt{6}[r(\text{C9H15}) + r(\text{C9H16}) + r(\text{C9H17}) - r(\text{C10CH18}) - r(\text{C10H19}) - r(\text{C10H20})] \\
v_{as}(\text{CH}_3) &= 1/\sqrt{12}[2r(\text{C9H15}) - r(\text{C9H16}) - r(\text{C9H17}) - 2r(\text{C10CH18}) + r(\text{C10H19}) + r(\text{C10H20})] \\
v_{as}'(\text{CH}_3) &= 1/2[r(\text{C9H16}) - r(\text{C9H17}) - r(\text{C10H19}) + r(\text{C10H20})] \\
\delta_{ip}(\text{CO}) &= 1/2[\theta(\text{N4C5O8}) - \theta(\text{C6C5O8}) - \theta(\text{N1C2O7}) + \theta(\text{C3C2O7})] \\
\delta(\text{CH}_2) &= 1/2\sqrt{10}[4\theta(\text{H12C3H11}) - \theta(\text{N4C3H12}) - \theta(\text{N4C3H11}) - \theta(\text{C2C3H12}) - \theta(\text{C2C3H11}) - 4\theta(\text{H13C6H14}) + \theta(\text{N1C6H13}) + \theta(\text{N1C6H14}) + \theta(\text{C5C6H13}) \\
&\quad + \theta(\text{C5C6H14})]
\end{aligned}$$

$$\begin{aligned}
\rho(\text{CH}_2) &= 1/2\sqrt{2}[\theta(\text{N4C3H12}) - \theta(\text{N4C3H11}) + \theta(\text{C2C3H12}) - \theta(\text{C2C3H11}) - \theta(\text{N1C6H13}) + \theta(\text{N1C6H14}) - \theta(\text{C5C6H13}) + \theta(\text{C5C6H14})] \\
\omega(\text{CH}_2) &= 1/2\sqrt{2}[\theta(\text{N4C3H12}) + \theta(\text{N4C3H11}) - \theta(\text{C2C3H12}) - \theta(\text{C2C3H11}) - \theta(\text{N1C6H13}) - \theta(\text{N1C6H14}) + \theta(\text{C5C6H13}) + \theta(\text{C5C6H14})] \\
\tau(\text{CH}_2) &= 1/2\sqrt{2}[\theta(\text{N4C3H12}) - \theta(\text{N4C3H11}) - \theta(\text{C2C3H12}) + \theta(\text{C2C3H11}) - \theta(\text{N1C6H13}) + \theta(\text{N1C6H14}) + \theta(\text{C5C6H13}) - \theta(\text{C5C6H14})] \\
\delta_s(\text{CH}_3) &= 1/2\sqrt{3}[\theta(\text{N4C9H15}) + \theta(\text{N4C9H16}) + \theta(\text{N4C9H17}) - \theta(\text{H15C9H16}) - \theta(\text{H16C9H17}) - \theta(\text{H15C9H17}) - \theta(\text{N1C10H18}) - \theta(\text{N1C10H19}) - \theta(\text{N1C10H20}) \\
&\quad + \theta(\text{H18C10H19}) + \theta(\text{H19C10H20}) + \theta(\text{H18C10H20})] \\
\delta_{as}(\text{CH}_3) &= 1/\sqrt{12}[2\theta(\text{H15C9H16}) - \theta(\text{H15C9H17}) - \theta(\text{H16C9H17}) - 2\theta(\text{H18C10H19}) + \theta(\text{H18C10H20}) + \theta(\text{H19C10H20})] \\
\delta_{as'}(\text{CH}_3) &= 1/2[\theta(\text{H15C9H17}) - \theta(\text{H16C9H17}) - \theta(\text{H18C10H20}) + \theta(\text{H19C10H20})] \\
\rho_{ip}(\text{CH}_3) &= 1/\sqrt{12}[2\theta(\text{N4C9H15}) - \theta(\text{N4C9H16}) - \theta(\text{N4C9H17}) - 2\theta(\text{N1C10H18}) + \theta(\text{N1C10H19}) + \theta(\text{N1C10H20})] \\
\rho_{op}(\text{CH}_3) &= 1/2[\theta(\text{N4C9H16}) - \theta(\text{N4C9H17}) - \theta(\text{N1C10H19}) + \theta(\text{N1C10H20})] \\
\delta_{op}(\text{CO}) &= 1/\sqrt{2}[\tau(\text{O8C5N4C6}) - \tau(\text{O7C2N1C3})] \\
\delta_{ip}(\text{NMe}) &= 1/2[\theta(\text{C3N4C9}) - \theta(\text{C5N4C9}) - \theta(\text{C6N1C10}) + \theta(\text{C2N1C10})] \\
\delta_{op}(\text{NAc}) &= 1/\sqrt{2}[\tau(\text{C9N4C3C5}) - \tau(\text{C10N1C6C2})] \\
\tau(\text{NMe}) &= 1/2\sqrt{3}[\tau(\text{H15C9N4C5}) + \tau(\text{H16C9N4C5}) + \tau(\text{H17C9N4C5}) + \tau(\text{H15C9N4C3}) + \tau(\text{H16C9N4C3}) + \tau(\text{H17C9N4C3}) - \tau(\text{H18C10N1C2}) \\
&\quad - \tau(\text{H19C10N1C2}) - \tau(\text{H20C10N1C2}) - \tau(\text{H18C10N1C6}) - \tau(\text{H19C10N1C6}) - \tau(\text{H20C10N1C6})] \\
\delta_{ip}(\text{Ring-3}) &= 1/\sqrt{6}[\theta(\text{N4C3C2}) - \theta(\text{C3C2N1}) + \theta(\text{C2N1C6}) - \theta(\text{N1C6C5}) + \theta(\text{C6C5N4}) - \theta(\text{C5N4C3})] \\
\delta_{op}(\text{Ring-1}) &= 1/\sqrt{6}[\tau(\text{C5N4C3C2}) - \tau(\text{N4C3C2N1}) + \tau(\text{C3C2N1C6}) - \tau(\text{C2N1C6C5}) + \tau(\text{N1C6C5N4}) - \tau(\text{C6C5N4C3})]
\end{aligned}$$

6.8. References

1. S. W. Larsen, M. Ankersen, C. Larsen, *Eur. J. Pharm. Sci.*, 2004, 22, 399.
2. A. D. Borthwick, J. Liddle, *Med. Res. Rev.*, 2011, 31, 576.
3. A. P. N. Franchimont, H. Friedmann, *Recl. Trav. Chim. Pays. Bays.*, 1908, 27, 192.
4. S. Wang, J. Golec, W. Miller, S. Milutinovic, A. Folkes, S. Williams, T. Brooks, K. Hardman, P. Charlton, S. Wren, J. Spencer, *Bioorg. Med. Chem. Lett.*, 2002, 12, 2367.
5. A. P. Mendham, J. Spencer, M. Mujahid, R. A. Palmer, G. J. Tizzard, T. J. Dines, S. J. Coles, B. Z. Chowdhry, *J. Chem. Crystallogr.*, 2011, 41, 1323.
6. M. Jainta, M. Nieger, S. Bräse, *Eur. J. Org. Chem.*, 2008, 32, 5418.
7. R. Degeilh, R. E. Marsh, *Acta Crystallogr.*, 1959, 12, 1007.
8. E. Sletten, *J. Am. Chem. Soc.*, 1970, 92, 172.
9. J. D. Hirst, B. J. Persson, *J. Phys. Chem. A.*, 1998, 102, 7519.
10. F. L. Bettens, R. P. A. Bettens, R. D. Brown, P. D. Godfrey, *J. Am. Chem. Soc.*, 2000, 122, 5856.
11. Y. Zhu, M. Tang, X. Shi, Y. Zhao, *Int. J. Quantum Chem.*, 2007, 107, 745.
12. A. P. Mendham, T. J. Dines, M. J. Snowden, R. Withnall, B. Z. Chowdhry, *J. Raman Spectrosc.*, 2009, 40, 1478.
13. A. P. Mendham, R. A. Palmer, B. S. Potter, T. J. Dines, J.C. Mitchell, R. Withnall, B. Z. Chowdhry, *J. Raman Spectrosc.*, 2010, 41, 148.
14. A. P. Mendham, T. J. Dines, M. J. Snowden, R. Withnall, B. Z. Chowdhry, *J. Raman Spectrosc.*, 2009, 40, 1508.
15. A. P. Mendham, T. J. Dines, J. C. Mitchell, R. Withnall, B. Z. Chowdhry, *J. Raman Spectrosc.*, 2009, 40, 1498.
16. A. P. Mendham, R. A. Palmer, B. S. Potter, T. J. Dines, M. J. Snowden, R. Withnall, B. Z. Chowdhry, *J. Raman Spectrosc.*, 2010, 41, 288.
17. S. Celik, A. E. Ozel, S. Akyuz, G. Agaeva, *J. Mol. Struct.*, 2011, 993, 341.
18. S. Celik, A. E. Ozel, S. Akyuz, S. Kecel, *Vib. Spectrosc.*, 2012, 61, 54.
19. S. Celik, A. E. Ozel, S. Akyuz, *Vib. Spectrosc.*, 2016, 83, 57.
20. T. C. Cheam, S. Krimm, *Spectrochim. Acta*, 1984, 40A, 481.
21. C. L. L. Chai, D. C. R. Hockless, A. R. King, *Aust. J. Chem.*, 1996, 49, 1229.

Chapter 7: Vibrational Spectroscopic Studies of Histidine Containing DKPs in the Solid State and in Aqueous Solution: Conformational Analysis and DFT Calculations

7.1. Introduction

Cyclo(His-pro) (CHP) also known as histidine-proline diketopiperazine, is a naturally occurring endogenous cyclic dipeptide produced in the hypothalamus as one of the primary metabolites by the proteolysis of thyrotropin-releasing hormone (TRH) by an enzyme pyroglutamate aminopeptidase.¹ It is also found in cerebrospinal fluid (CSF), the spinal cord, blood and gastrointestinal track (GIT) of humans^{1, 2} and has a stereospecific receptor in the liver.³ CHP has been reported to be the most potent cyclic dipeptide amongst several other cyclic dipeptides possessing inhibitory properties against enzymes,⁴ e.g. preventing formation of the infectious filamentous form of *Candida albicans* and affecting cell separation in *Saccharomyces cerevisiae*. Other properties includes inhibition of prolactin secretion,⁵ antagonism to ethanol necrosis⁶ and induction of hypothermic effects in rats.⁷ CHP is also recognised for its several biological roles in the CNS.⁸ Among these, the most promising and innovative feature is its neuroprotective activity for future applications. CHP and some of its synthesized derivatives are potentially used for the treatment of neurodegenerative disorders because of their ability to prevent neuronal death induced by calcium mobilization, free radicals and traumatic injury.⁹ Minelli and co-workers¹⁰ investigated the effect of cellular proliferation induced by CHP *in vitro* in rat PC12 cell cultures in the presence of experimental conditions that cause cellular stress and to prevent apoptosis.¹¹ It has been hypothesised that CHP acts *via* a receptor dually coupled to stimulatory and inhibitory G-proteins, but the binding characteristics of this receptor system are still not completely clear.¹⁰ *In vitro* studies suggests that CHP safeguards the H₂O₂-injured cells against oxidative stress via a mechanism that leads to an increase in glutathione levels and a decrease in reactive oxygen species (ROS) generation.¹² The cytoprotective/anti-inflammatory effect of CHP appears to occur via a mechanism involving both the activation of the Nrf2-EpRE/ARE pathway, which enhances the antioxidant defensive response, and the suppression of NF-κB signalling, which depresses the pro-inflammatory response in rat adrenal pheochromocytoma PC12 cells.¹³ Previous studies on cyclo(Ala-His) and cyclo(Gly-His) suggests that both histidine containing DKPs show promising results in thrombin inhibition, marked effects on heart rate and coronary flow rate in the isolated rat heart and are effective against *S. aureus*.¹⁴ Moreover, these DKPs are also recognised for their general antimicrobial and anticancer activities.¹⁵

Previously reported NMR and X-ray diffraction studies suggests that DKPs containing histidine, tyrosine and phenylalanine tend to have folded conformations with the aromatic side-chain facing the DKP ring.^{16, 17} This preferred conformation is mainly due to the magnetic shielding effects about the α and β bonds of the aromatic side-chain in cyclic dipeptides which brings them closer to the DKP ring.¹⁸ It appears that the induced dipole-dipole interaction between the aromatic side-chain and the DKP ring have a great influence on the overall molecular conformation in cyclic dipeptides.^{19, 20} Kojima *et al.* have studied the folded and unfolded conformation of cyclo(L-His-L-His) in solid and solution state using X-ray diffraction and NMR techniques, respectively. The DKP ring in cyclo(L-His-L-His) has a flagpole boat conformation with *cis* α -carbons in the quasi-axial orientation in the solid state.²¹ The two imidazole ring are attached on either side of DKP ring, one being folded back over the ring and another kept away from the DKP ring. This flagpole boat conformation is commonly found in substituted DKP with aromatic side chains.^{19, 22} There are three possible conformations for cyclo(L-His-L-His) in the solution state namely: a folded-folded conformation (two imidazole rings lie over DKP ring), folded-unfolded conformation (same as the conformation in the solid state) and an unfolded-unfolded conformation (two imidazole rings facing away from the DKP ring). However, the ¹H-NMR measurements show that the folded-unfolded conformation appears to be consistent for cyclo(L-His-L-His) in the solution state.²¹ In the case of cyclo(L-Thr-L-His), ¹H-NMR studies have concluded that the hydroxyl group of the L-Thr side-chain points above the DKP ring, and keeps the L-His side-chain away from the DKP ring (unfolded state) due to the effect of hydration on the conformation of cyclo(L-Thr-L-His).²³ This phenomenon was also explained by Cotrait *et al.*, in the solid state; the formation of hydrogen bonds between the hydroxyl group of L-Thr and the imidazole ring of L-His side-chains is prohibited due to the presence of an intramolecular water molecule, this also precludes the existence of a folded form with the L-His side-chain facing the DKP ring.²⁴

The switching propensity of CHP and its interaction with neurotoxins in solution state have been studied using molecular dynamics simulations and DFT. From the calculations, it is suggested that the unfolded conformation of CHP is predicted to be the dominant conformer in the solution state and the interaction of the DKP ring with neurotoxins is expected to play a significant role in reducing oxidative stress and prevent cell death caused by neurotoxins.²⁵ Knowledge of the conformational properties of the biologically active cyclic dipeptides/DKPs are essential in order to examine their functional structure which is related to their vibrational and electronic properties. However, very few vibrational spectroscopic studies have been carried out on histidine containing DKPs in the solid state.²⁶ Despite their interesting biological properties no reports on the

vibrational spectroscopic studies of CHP has yet been reported. As a continuation of previous studies on DKP derivatives, herein, IR and Raman spectroscopic studies on the solid and solution state of cyclo(L-His-L-Pro) (CHP), cyclo(D-His-L-Pro) (CDHP) and cyclo(L-Ala-L-His) (CAH) (Fig. 7.1) are reported, together with their conformational analysis and vibrational assignments from density functional (DFT) theory calculations.

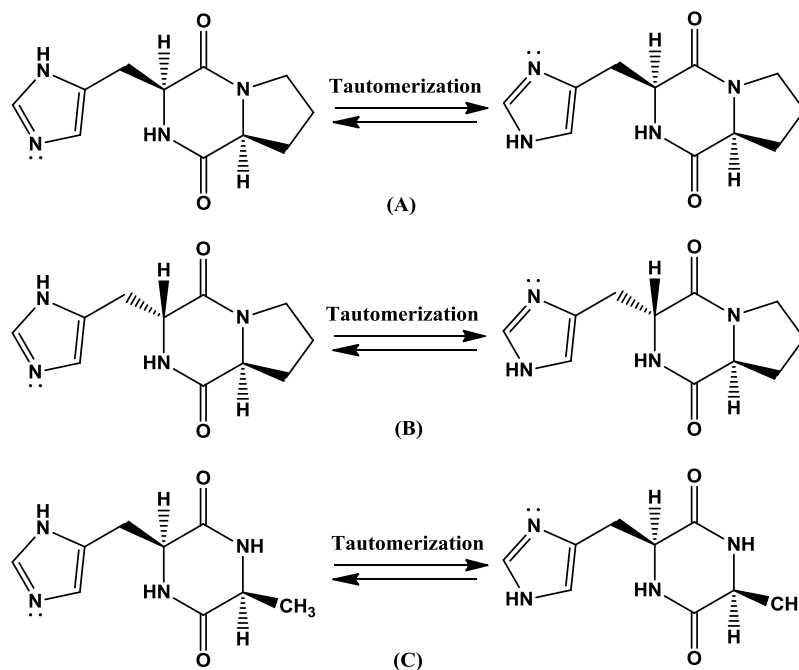


Figure 7.1. Structures of (A) CHP (B) CDHP and (C) CAH with their tautomeric forms.

7.2. Experimental

7.2.1. Materials

See sections 3.1 to 3.1.2 in Chapter 3.

CHP, CDHP and CAH were supplied by Bachem (Saint Helens, UK) and used without further purification. Spectroscopic grade deuterium oxide (99.98 atom %) were obtained from Sigma-Aldrich Ltd (Poole, Dorset, UK). Deuteration was carried out by dissolving 5 mg of CAH in 5 ml D₂O and the powdered *N*-deuterated isotopomer was recovered after evaporation of D₂O followed by drying (60 °C) using a hot air oven. The deuteration of CHP and CDHP results in hygroscopic products. Hence, the vibrational spectroscopic studies of *N*-deuterated isotopomers of CHP and CDHP could not be carried out.

7.2.2. Vibrational spectroscopy and Instrumental details

See sections 3.2, 3.2.1, 3.2.2, 3.2.3 and 3.2.4 in Chapter 3.

7.2.3. DFT calculations

See section 3.5 in Chapter 3

Previously reported solid-state chemical shift (^{15}N , ^{13}C , and ^1H) NMR spectroscopic studies on histidine, recrystallized from aqueous solution at various pH values from 4.5 to 11, suggest that small changes in the environmental pH can readily change the charged state of histidine. 2-D homo- and heteronuclear correlation spectra indicates that ^{15}N , ^{13}C , and ^1H chemical shifts are sensitive to tautomeric structures and protonation state.²⁷ At low pH, the imidazole ring on the histidine side-chain exist in cationic form with two protonated nitrogen atoms on the imidazolium ring. At about pH 7, two neutral tautomers exist: the N1H-protonated and the N3H-protonated tautomers.^{27,28} Hence, from the aforementioned statements the imidazole ring on the L-His side-chain in histidine containing cyclic dipeptides can exist as N11-protonated (N^ϵ) and N17-protonated (N^δ) tautomers for CHP and CDHP and N13-protonated (N^ϵ) and N15-protonated (N^δ) tautomers for CAH (Fig. 7.1). Hence, two calculation strategies were employed for CHP, CDHP and CAH by shifting the proton on two nitrogen atoms in the imidazole ring of the L-His side chain.

7.3. Results and discussion

7.3.1. Geometry optimization

The atom number schemes for CHP, CDHP and CAH are shown in Fig. 7.2. The calculated bond distances, bond angles and dihedral angles are shown in Tables 7.5-7.6. It is noteworthy that the calculations are based on the single molecule in the gas phase, and do not account for intermolecular interactions that appear in the solid and solution state. In order to verify the minimum energy conformations of the L-His side-chain of the tautomers (N^ϵ and N^δ) of CHP, CDHP and CAH, energy profile calculations were conducted by rotating the torsional angles $\tau(\text{H4C3C7C10})$ i.e., $\text{C}_\alpha\text{-C}_\beta$ in CHP and CDHP and $\tau(\text{H18C4C9C11})$ in CAH using the HF/321-G basis set in the Spartan'14 program.²⁹ The potential energy plots, shown in Figs. 7.3-7.8, reveal that there are three minimum energy structures for each N^ϵ and N^δ -tautomeric form of CHP, CDHP and CAH in the region of $\tau(\text{H4C3C7C10}) = \pm 180^\circ$ (CHP and CDHP) and $\tau(\text{H18C4C9C11})$

$= \pm 180^\circ$ (CAH), corresponding to three possible conformations I, II and III. Additionally, energy profile calculations were also performed by rotating the dihedral angles $\tau(\text{C3C7C10N11})$ (CHP,CDHP) and $\tau(\text{C4C9C11N13})$ (CAH), known as $\text{C}_\beta\text{-C}_\gamma$, using initial geometries of the calculated minimum energy conformers. DFT calculations were carried out using Gaussian 09 at the B3LYP/aug-cc-pVTZ level using initial geometries from the Spartan'14 outputs leading to the optimised geometries tabulated in Tables 7.1-7.3, together with their computed energies, dihedral angles ($\text{C}_\alpha\text{-C}_\beta$ and $\text{C}_\beta\text{-C}_\gamma$) and degree of folding (β). These optimised geometries correspond to energy minima, as evidenced by the lack of imaginary frequencies.

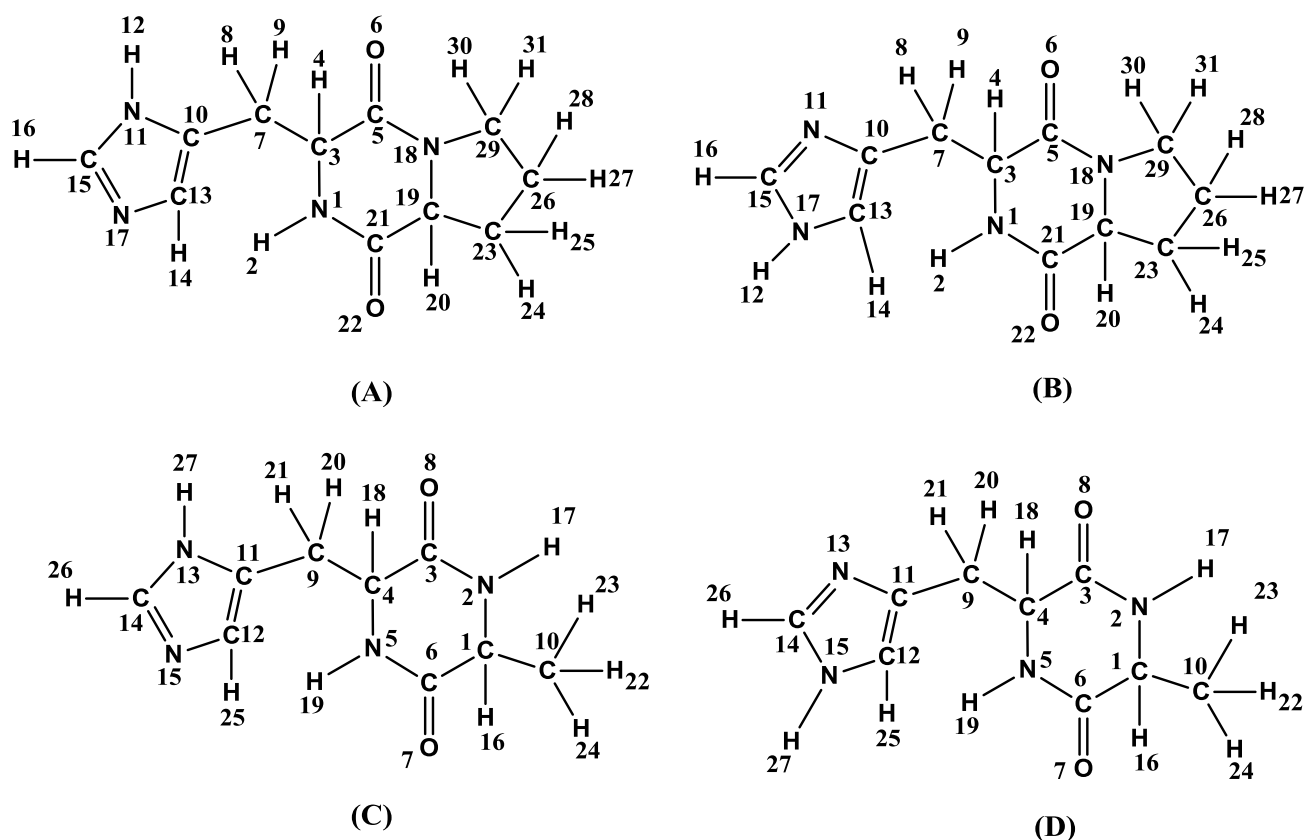


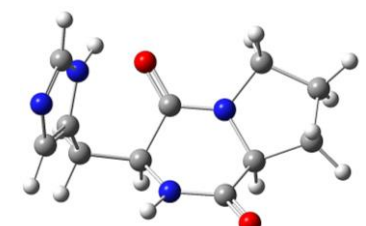
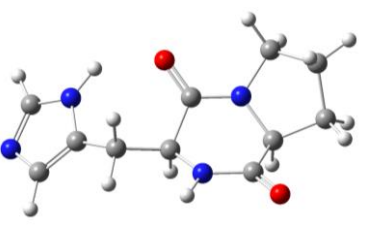
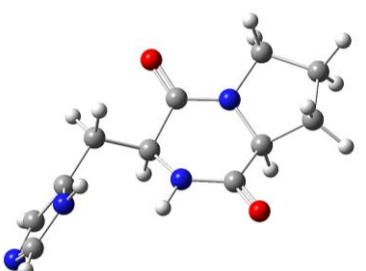
Figure 7.2. Atom numbering scheme for (A) N^ϵ -protonated (B) N^δ -protonated tautomers of CHP and CDHP and (C) N^ϵ -protonated (D) N^δ -protonated tautomers of CAH.

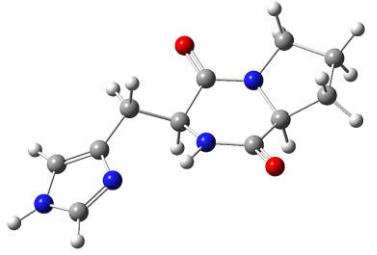
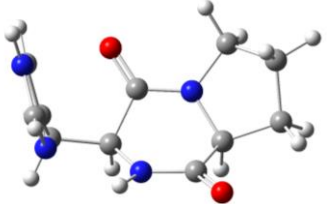
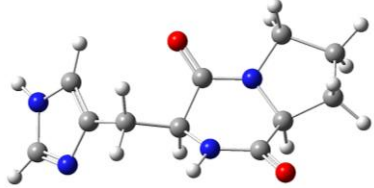
7.3.2 Conformational analysis

In the case of CHP, the L-His side chains in the N^ϵ -tautomeric forms favours the folded conformation as the minimum energy conformation (conformer I). The imidazole ring is almost perpendicular to the DKP ring with the N11-H12 closer to the $\text{C}=\text{O}$ peptide bond of the DKP ring. The dihedral angles $\text{C}_\alpha\text{-C}_\beta$ and $\text{C}_\beta\text{-C}_\gamma$ of the L-His side-chain are 178° and 69.5° and the degree of folding $\beta=41.5^\circ$, respectively. Conformers II and III are slightly higher in energy, described as an

open form, obtained for $C_{\alpha}-C_{\beta}$ (-40.7° , 62.6°), $C_{\beta}-C_{\gamma}$ (-66.9° , 95.7°) and $\beta = 44.4^{\circ}$, 31.6° for II and III, respectively. The N11 atom of the imidazole ring interacts with the N-H group of the DKP ring. In all three minimum energy conformers of the N^{ϵ} -tautomeric forms of CHP the DKP ring exists in a bowsprit boat conformation. Interestingly, $\beta > 41^{\circ}$ in conformers I and II involving interaction between N-H of the imidazole ring and C=O group of the DKP ring (I and II) and folded conformation of the L-His side-chain (I). For the N^{δ} -tautomeric forms of CHP the DKP ring, in all three energy minimized molecules, exists in the bowsprit boat conformation with the L-His side-chains extended away from the DKP ring except for conformer II, where the side-chain is perpendicular to the DKP ring. In this case the electrostatic interaction significantly effects the conformational stability of the three conformers. The importance of electrostatic interactions in stabilizing the conformers of histidine containing cyclic dipeptides have been previously studied.³⁰ The dihedral angles obtained are $C_{\alpha}-C_{\beta}$ (55.4° , 168.8° and -35.5°), $C_{\beta}-C_{\gamma}$ (58.3° , -78° and 90.4°) and $\beta = 33.5^{\circ}$, 44.7° and 40.4° for the three δ -tautomeric minimum energy conformers of CHP. Similarly, $\beta > 41^{\circ}$ in conformer II of δ -tautomeric-CHP where the L-His side-chain is perpendicular to the DKP ring.

Table 7.1. Calculated structures and conformational energies of CHP.

Conformation	$C_{\alpha}-C_{\beta} / C_{\beta}-C_{\gamma}$	β	E/H	Structure
N^{ϵ} (I)	177.1° 69.5°	41.5°	$E = -797.38431961$ H	
N^{ϵ} (II)	-40.7° -66.9°	44.6°	$E = -797.38392493$ H	
N^{ϵ} (III)	62.6° 95.7°	31.6°	$E = -797.37828600$ H	

N^δ (I)	55.4° 58.3°	33.5°	$E = -797.38582549$ H	
N^δ (II)	168.8° -78.0°	44.7°	$E = -797.38300591$ H	
N^δ (III)	-35.5° 90.4°	40.4°	$E = -797.38029390$ H	

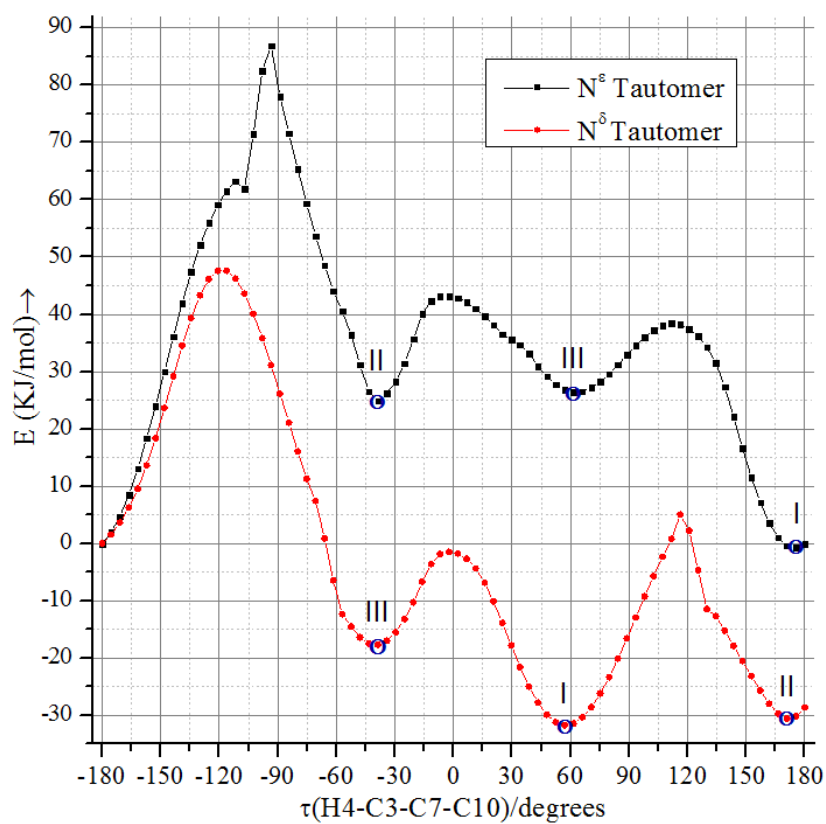


Figure 7.3. Potential energy scan of CHP.

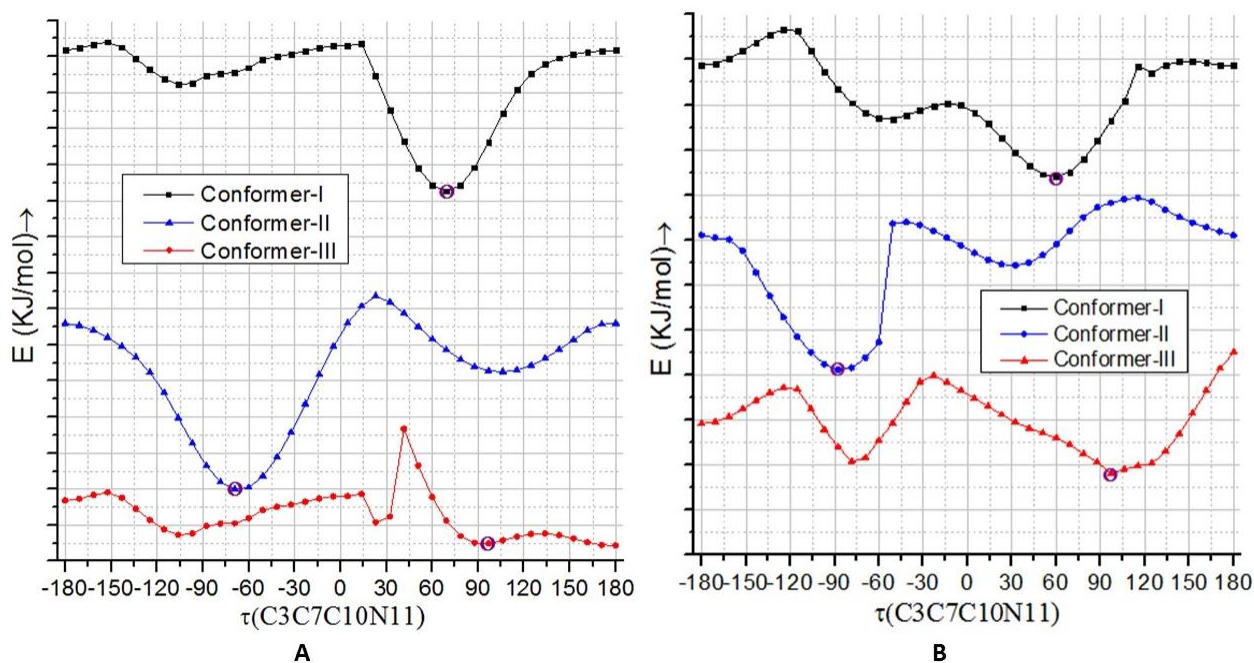


Figure 7.4. Potential energy scans of (A) N^ϵ and (B) N^δ -tautomeric forms of CHP.

In the case of CDHP, the side-chains of D-His and L-Pro are arranged in opposite directions (one facing up and other facing down) unlike CHP where both the side-chains are on the same side of the DKP ring. Hence, the minimum conformers obtained for CDHP are different than those obtained for CHP. In the N^ϵ -tautomeric forms of CDHP, conformers I and II involve interactions between the N-H of the imidazole ring and C=O group of the DKP ring. However, the D-His side-chain exists in an open form (I and III) and folded form (II) with the dihedral angles C_α - C_β (33.5° , 163.9° and -59.5°), C_β - C_γ (46.3° , -78.6° and -78.3°) and $\beta=27.6^\circ$, 22.3° and 35.6° for conformer I, II and III, respectively. It is noteworthy that $\beta < 24^\circ$ for conformer II, where the D-His side-chain is folded over the DKP ring. In all three conformers of N^ϵ -tautomeric forms the DKP ring exists in a bowsprit boat conformation. For the δ -tautomeric forms of CDHP, the D-His side-chain in I and II faces away from the DKP ring. The N17 atom of the imidazole ring interacts with the N-H group of the DKP ring in I and the D-His side-chain faces over the DKP ring in III. The obtained dihedral angles for all three conformers are -49.0° , 45.1° , -171.1° (C_α - C_β), -42.0° , -69° , -59.2° (C_β - C_γ) and $\beta=20.4^\circ$, 38.2° , 24.2° , respectively and the DKP ring exists in a bowsprit conformation.

Table 7.2. Calculated structures and conformational energies of CDHP.

Conformation	$C_{\alpha}-C_{\beta} / C_{\beta}-C_{\gamma}$	β	E/H	Structure
N ^ε (I)	33.5° 46.3°	27.6°	$E = -797.38307021$ H	
N ^ε (II)	163.9° -78.6°	22.3°	$E = -797.38054761$ H	
N ^ε (III)	-59.5° -78.3°	35.6°	$E = -797.37757460$ H	
N ^δ (I)	-49.2° -42.0°	20.4°	$E = -797.38351007$ H	
N ^δ (II)	45.1° -69.0°	38.2°	$E = -797.38100335$ H	
N ^δ (III)	-171.1° -59.2°	24.2°	$E = -797.37967541$ H	

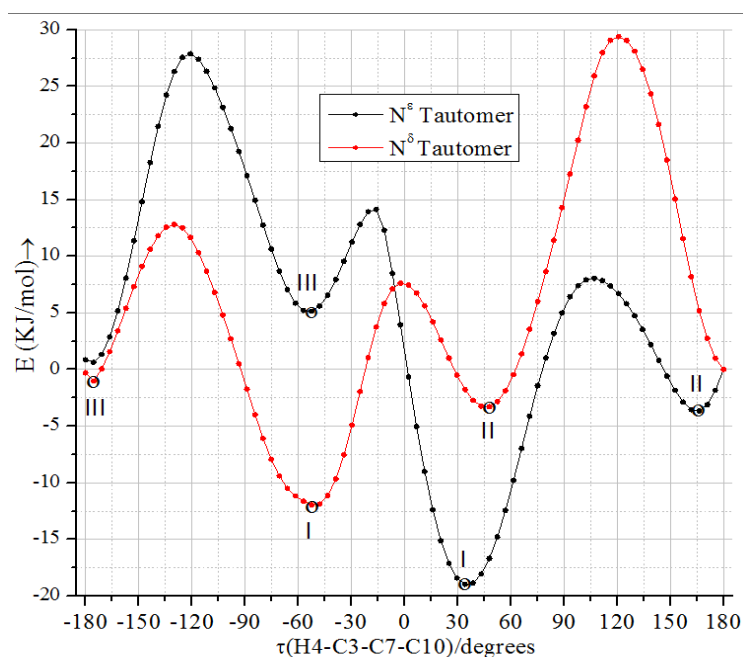


Figure 7.5. Potential energy scan of CDHP.

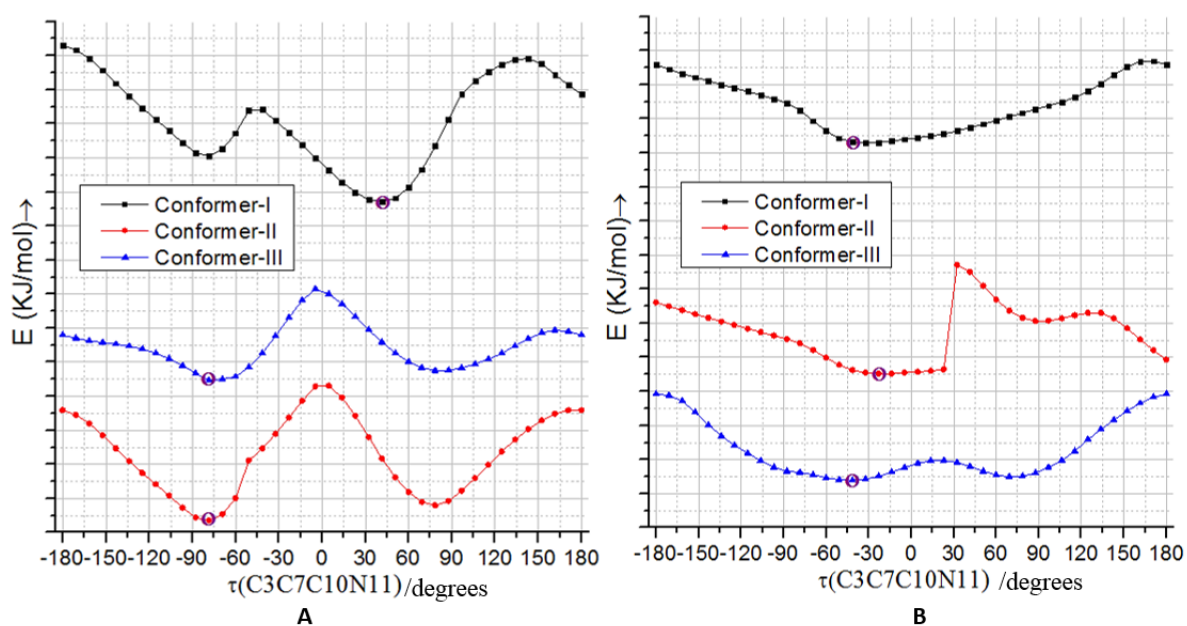
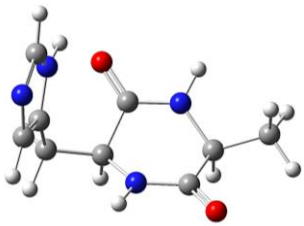
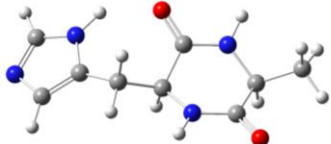
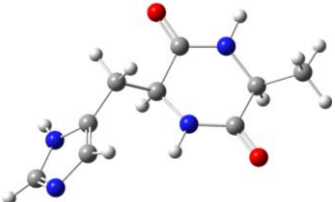
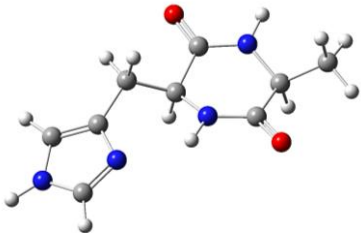
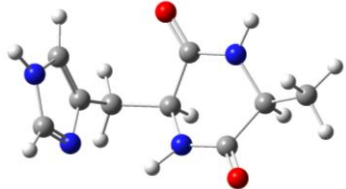
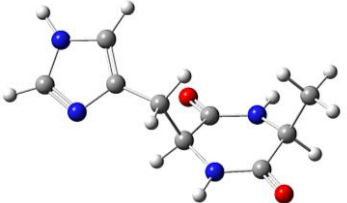


Figure 7.6. Potential energy scan of (A) N^ϵ and (B) N^δ -tautomeric forms of CDHP.

The potential energy surface for CAH is very similar to CHP, except the calculated energies for conformers II and III of both N^ϵ and N^δ -tautomeric forms (Figs. 7.7 and 7.8). Various geometries of the side-chains can slightly influence the stability of the conformation of the DKP ring. Previously reported empirical calculations on cyclic dipeptides suggests that the L-Thr and L-His side-chains are folded over a bowsprit boat DKP ring whereas in the flagpole boat DKP ring the side-chains extend away to eliminate steric hindrance.³¹

Table 7.3. Calculated structures and conformational energies of CAH.

Conformation	$C_{\alpha}-C_{\beta} / C_{\beta}-C_{\gamma}$	β	E/H	Structure
N ^ε (I)	178.84° 69.7°	39.8°	$E = -719.94445838$ H	
N ^ε (II)	-37.7° -64.5°	35.4°	$E = -719.94354359$ H	
N ^ε (III)	57.4° -79.4°	21.8°	$E = -719.94121270$ H	
N ^δ (I)	54.5° 55.9°	28.7°	$E = -719.94715489$ H	
N ^δ (II)	169.6° -79.8°	39.5°	$E = -719.94449853$ H	
N ^δ (III)	-39.03° 66.9°	21.2°	$E = -719.93985020$ H	

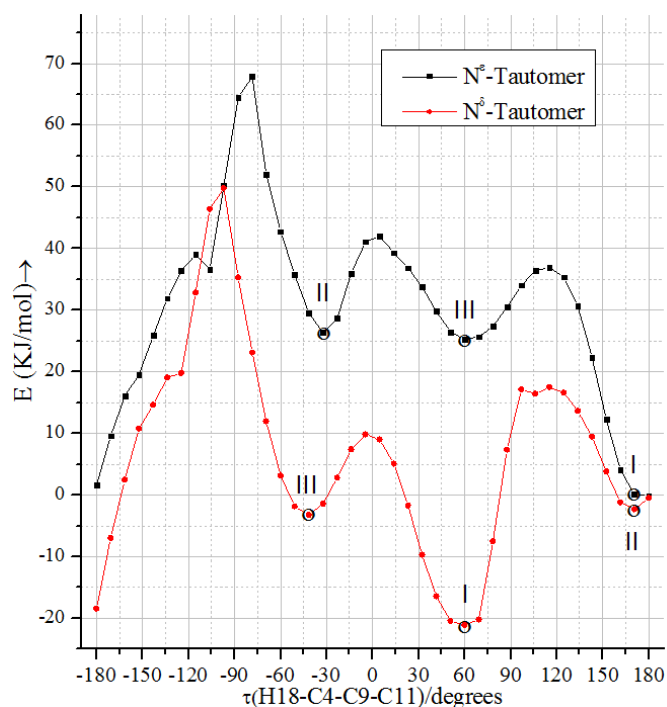


Figure 7.7. Potential energy scan of CAH.

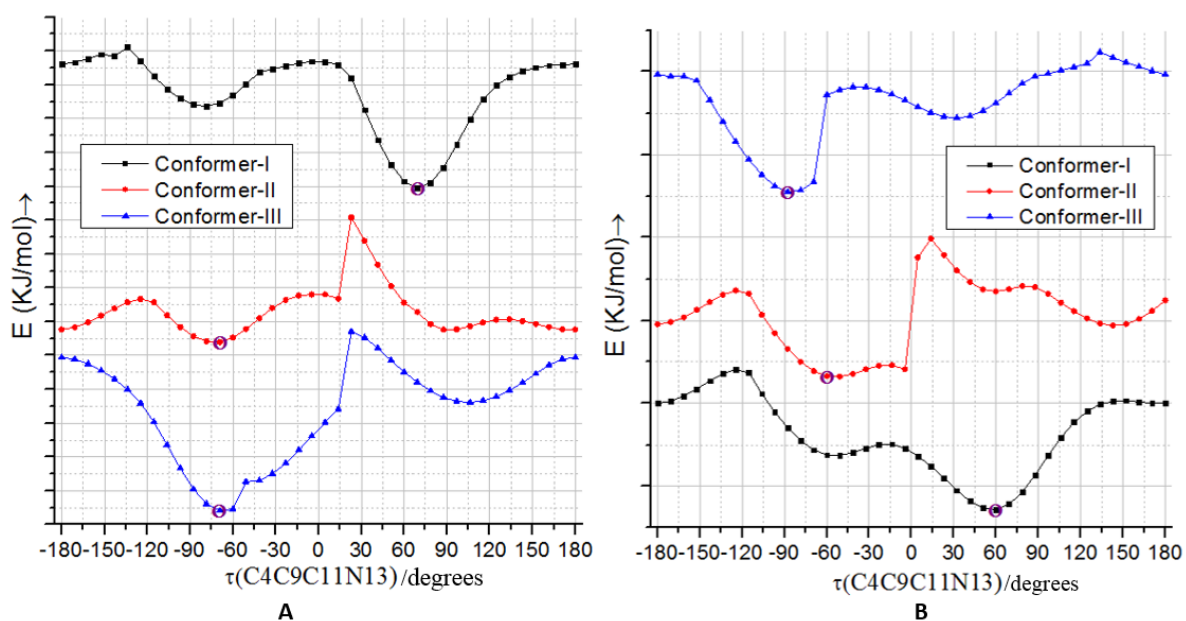


Figure 7.8. Potential energy scan of (A) N^ϵ and (B) N^δ -tautomeric forms of CAH.

The DKP ring dihedral angles of the lowest energy conformers of CHP, CDHP and CAH are tabulated in Table 7.4. Unfortunately, there is no X-ray data for CHP, CDHP and CAH for comparison. Hence, the DKP ring geometry of the calculated molecules are compared with the DKP ring geometries of the un-substituted DKP and other histidine-containing DKPs (Table 7.4). From previous X-ray studies on various histidine-containing DKPs, it is suggested that the N-H group of the imidazole ring and the amide groups of the DKP ring participate in

inter-molecular hydrogen bonding.^{21-24, 34-38} The calculated structures of CHP, CDHP and CAH predict a boat conformation as the minimum energy conformers in the gas phase and agrees well with the previously reported *ab-initio* calculations on a range of DKP derivatives; i.e., the boat conformation was, consistently, shown to be the most stable conformation in the gas-phase.^{32,33}

The three dihedral angles ω , ψ , ϕ are mainly responsible for determining the geometry of the peptide units in the DKP ring. David and Khaled first reported the degree of folding (β) for the simplest DKP cyclo(Gly-Gly).³³ By examining the dihedral angles $C_\alpha-N-C'-C_\alpha$, $N-C'-C_\alpha-N$ and $C'-N-C_\alpha-C'$ the geometry of the ring can be determined. A good measure of folding of the DKP ring can be established by taking the average of $N-C_\alpha-C_\alpha-N$ (β_1) and $C_\alpha-C'-C'-C_\alpha$ (β_2). Interestingly, in DKP derivatives II-VII (Table 7.4) the DKP ring is nearly planar (except IV) with a slight deviation from planarity $\beta \sim 16^\circ$ in II and V, $\sim 10^\circ$ in VII and $\sim 2^\circ$ in III and VI. The presence of intra-molecular water molecules in DKPs (II-VII) is responsible for stabilizing the DKP ring in a planar/near-planar conformation in the solid state.^{21,22,34-36} However, in compounds VIII and IX (proline containing DKPs) the DKP ring exists in a boat conformation with $\beta = 41^\circ$ and 52° , respectively.^{44,45} From the aforementioned statements it is, therefore, hypothesised that in the absence of the intra-molecular water molecule(s) the DKP ring in CHP, CDHP and CAH may exist in a boat conformation in the solid state. Furthermore, the attachment of L-Pro and L-His side-chains on either side of the DKP ring and the orientation of the imidazole ring of the L-His side-chains may also effect the conformation of the DKP ring in the solid state.

Table 7.4. Comparison of the DKP ring geometries of the lowest energy conformers of the calculated structures with other DKPs.

Dihedral angles (°)	Calculated						X-ray									
	N ^c CHP	N ^d CHP	N ^c CDHP	N ^d CDHP	N ^c CAH	N ^d CAH	I	II	III	IV	V	VI	VII	VIII	IX	
ω_1	-3.3	0.1	1.9	2.8	1.4	8.7	1.3	-9.5	3.7	6.2	-7.5	-0.7	-5.7	6.2	-4.5	
ω_2	2.6	6.9	3.4	3.5	5.3	8.9	-1.3	-9.1	1.5	-6.2	-5.2	-1.9	-4.7	6.3	-0.4	
Ψ_1	39.8	31.3	23.9	17.3	35.6	21.8	-1.2	-10.1	-2.9	-5.3	-10.8	2.1	12.5	33.7	49.8	
Ψ_2	34.8	25.7	23.2	17.0	32.0	21.4	1.2	-10.4	-0.9	5.3	-12.2	3.1	11.7	33.6	46.1	
ϕ_1	-40.9	-36.3	-27.6	-21.1	-40.4	-31.7	1.3	19.8	0.3	5.9	17.3	-0.7	-7.5	-41.5	-48.3	
ϕ_2	-35.3	-29.7	-26.7	-20.7	-36.5	-31.3	-1.3	20.1	-1.7	-5.9	19.0	-1.8	-6.6	-41.6	-44.3	
β	41.5	33.5	27.6	20.4	39.8	28.7	0.0	16.2	-1.1	0.0	15.9	2.1	10.5	41.1	52.3	

Where, (I= cyclo(Gly-Gly), II= cyclo(L-Leu-L-His),³⁴ III= cyclo(L-His-L-Asp),^{20a} IV=cyclo(L-His-D-His),³¹ V= cyclo(L-His-L-His),¹⁹ VI= cyclo(L-Ser-L-His),³² VII= cyclo(L-Thr-L-His).²² VIII = cyclo(L-Leu-L-Pro),³⁵ and IX= cyclo(L-Phe-L-Pro)³⁶.

Table 7.5. The calculated bond lengths, bond angles and dihedral angles of the lowest energy conformer of N^ε and N^δ- tautomeric forms of CHP and CDHP.

Bond lengths (Å)	N ^ε -CHP	N ^δ -CHP	N ^ε -CDHP	N ^δ -CDHP
H(31)-C(29)	1.0886	1.0895	1.0904	1.0905
H(30)-C(29)	1.0920	1.0915	1.0892	1.0900
C(29)-C(26)	1.5329	1.5361	1.5371	1.5399
C(29)-N(18)	1.4695	1.4686	1.4720	1.4697
H(28)-C(26)	1.0880	1.0883	1.0878	1.0882
H(27)-C(26)	1.0914	1.0914	1.0908	1.0910
C(26)-C(23)	1.5349	1.5350	1.5357	1.5360
H(25)-C(23)	1.0901	1.0907	1.0862	1.0863
H(24)-C(23)	1.0866	1.0864	1.0908	1.0911
C(23)-C(19)	1.5291	1.5291	1.5294	1.5298
O(22)-C(21)	1.2167	1.2203	1.2175	1.2212
C(21)-C(19)	1.5272	1.5222	1.5179	1.5182
C(21)-N(1)	1.3561	1.3523	1.3569	1.3515
H(20)-C(19)	1.0983	1.0993	1.0980	1.0986
C(19)-N(18)	1.4721	1.4665	1.4664	1.4636
N(18)-C(5)	1.3419	1.3465	1.3396	1.3460
N(17)-C(13)	1.3737	1.3777	1.3728	1.3774
N(17)-C(15)	1.3118	1.3581	1.3124	1.3577
H(16)-C(15)	1.0774	1.077	1.0773	1.0770
C(15)-N(11)	1.3596	1.3104	1.3595	1.3108
H(14)-C(13)	1.0780	1.0749	1.0778	1.0749
C(13)-C(10)	1.3722	1.3686	1.3724	1.3688
H(12)-N(11)	1.0101	1.0047	1.0149	1.0048
N(11)-C(10)	1.3769	1.3819	1.3771	1.3812
C(10)-C(7)	1.4913	1.4947	1.4943	1.4975
H(9)-C(7)	1.0912	1.0874	1.0955	1.0898
H(8)-C(7)	1.0908	1.0928	1.0902	1.0942
C(7)-C(3)	1.5364	1.5344	1.5569	1.5447
O(6)-C(5)	1.2288	1.2238	1.2313	1.2248
C(5)-C(3)	1.5378	1.5361	1.5299	1.5271
H(4)-C(3)	1.0990	1.0995	1.0899	1.0912
C(3)-N(1)	1.4592	1.4607	1.4589	1.4577
H(2)-N(1)	1.0089	1.0155	1.0094	1.0135
Bond angles (°)				
H(30)-C(29)-H(31)	107.6486	107.3336	107.4507	107.2554
H(30)-C(29)-C(26)	112.1517	112.5096	113.2955	112.9618

H(30)-C(29)-N(18)	109.5160	109.3128	110.6788	110.9758
H(31)-C(29)-C(26)	113.7720	113.3692	112.7661	112.9346
H(31)-C(29)-N(18)	110.4101	110.7163	108.9022	108.8742
C(26)-C(29)-N(18)	103.2780	103.5670	103.6875	103.8110
H(27)-C(26)-H(28)	107.6384	107.5162	107.5270	107.4606
H(27)-C(26)-C(29)	110.0282	110.0832	110.1309	110.1515
H(27)-C(26)-C(23)	110.2414	110.0137	109.9566	109.8830
H(28)-C(26)-C(29)	112.0458	111.9819	111.8567	111.8453
H(28)-C(26)-C(23)	112.7474	112.8225	112.7141	112.7424
C(29)-C(26)-C(23)	104.1395	104.4277	104.6633	104.7678
H(24)-C(23)-H(25)	107.5681	107.7553	107.8936	108.0083
H(24)-C(23)-C(26)	113.6094	113.7435	111.2161	111.1187
H(24)-C(23)-C(19)	112.0298	112.1843	109.4393	109.3563
H(25)-C(23)-C(26)	111.2270	111.1350	113.7270	113.7764
H(25)-C(23)-C(19)	109.2669	109.3045	112.1136	112.2087
C(26)-C(23)-C(19)	103.0992	102.6547	102.3791	102.2826
O(22)-C(21)-C(19)	122.5688	121.2552	121.6270	120.3121
O(22)-C(21)-N(1)	124.2875	124.0832	123.4091	123.5908
C(19)-C(21)-N(1)	113.1416	114.6536	114.9519	116.0661
H(20)-C(19)-C(21)	107.1005	106.2710	106.2121	105.4705
H(20)-C(19)-C(23)	110.0233	109.2669	109.0745	108.7120
H(20)-C(19)-N(18)	109.7572	109.8627	109.6605	109.6653
C(21)-C(19)-C(23)	114.9525	115.2656	115.5551	115.6719
C(21)-C(19)-N(18)	111.6411	113.1961	113.4168	114.5723
C(23)-C(19)-N(18)	103.3258	102.9381	102.8480	102.6540
C(5)-N(18)-C(29)	123.3749	122.4383	122.2304	121.8570
C(5)-N(18)-C(19)	123.7632	125.0278	125.6626	125.9761
C(29)-N(18)-C(19)	112.5830	112.3989	111.9773	111.8159
C(13)-N(17)-C(15)	105.2082	107.3868	105.1835	107.3749
H(16)-C(15)-N(17)	125.7922	122.7875	125.7954	122.7834
H(16)-C(15)-N(11)	122.4657	126.0386	122.3421	125.9996
N(17)-C(15)-N(11)	111.7421	111.1739	111.8614	111.2168
H(14)-C(13)-N(17)	121.4500	122.2948	121.5597	122.2671
H(14)-C(13)-C(10)	127.6781	131.9743	127.6356	132.0171
N(17)-C(13)-C(10)	110.8629	105.7301	110.8035	105.7149
H(12)-N(11)-C(15)	128.8887	126.3227	128.6122	126.3474
H(12)-N(11)-C(10)	123.5950	126.2895	123.7655	126.2751
C(15)-N(11)-C(10)	107.4787	106.2895	107.2982	106.2310
C(7)-C(10)-C(13)	131.9843	128.7976	130.8428	128.3917
C(7)-C(10)-N(11)	123.2865	121.7790	124.2874	122.1474
C(13)-C(10)-N(11)	104.7075	109.4196	104.8501	109.4608
H(8)-C(7)-H(9)	106.7340	106.8584	106.1123	107.5419
H(8)-C(7)-C(3)	106.8639	108.1130	107.5331	108.4465
H(8)-C(7)-C(10)	110.5672	109.9301	107.4206	110.3399

H(9)-C(7)-C(3)	107.7806	107.7561	108.6652	108.1494
H(9)-C(7)-C(10)	108.1810	110.2401	111.3407	109.3359
C(3)-C(7)-C(10)	116.2908	113.6847	115.3005	112.8645
O(6)-C(5)-N(18)	123.5361	123.1779	122.5200	123.0918
O(6)-C(5)-C(3)	123.0024	122.0613	120.7748	119.9140
N(18)-C(5)-C(3)	113.4545	114.7550	116.7041	116.9821
H(4)-C(3)-C(7)	106.6354	107.9816	108.2064	107.5217
H(4)-C(3)-C(5)	105.8842	106.3991	105.3750	104.0588
H(4)-C(3)-N(1)	109.4924	110.0420	107.4205	107.7739
C(7)-C(3)-C(5)	113.1875	110.3843	111.4305	110.8186
C(7)-C(3)-N(1)	111.4655	110.4674	112.4385	112.5809
C(5)-C(3)-N(1)	109.9228	111.4298	111.5774	113.5031
H(2)-N(1)-C(21)	117.0114	117.4803	114.8656	116.3561
H(2)-N(1)-C(3)	118.9922	116.0659	117.6598	115.1504
C(21)-N(1)-C(3)	123.9855	125.1173	127.1765	127.0410
Dihedral angles (°)				
N(18)-C(29)-C(26)-C(23)	-27.9911	-24.0311	-22.0905	-19.8285
N(18)-C(29)-C(26)-H(28)	-150.1467	-146.4263	-144.4346	-142.2676
N(18)-C(29)-C(26)-H(27)	90.1458	94.0248	96.0521	98.2961
H(31)-C(29)-C(26)-C(23)	-147.6925	-144.0765	95.5422	97.9292
H(31)-C(29)-C(26)-H(28)	90.1520	93.5283	-26.8019	-24.5100
H(31)-C(29)-C(26)-H(27)	-29.5556	-26.0207	-146.3153	-143.9462
H(30)-C(29)-C(26)-C(23)	89.8274	93.8916	-142.1284	-140.1271
H(30)-C(29)-C(26)-H(28)	-32.3282	-28.5036	95.5275	97.4337
H(30)-C(29)-C(26)-H(27)	-152.0357	-148.0526	-23.9858	-22.0025
C(26)-C(29)-N(18)-C(19)	8.3825	1.9937	-1.0547	-4.1171
C(26)-C(29)-N(18)-C(5)	-177.4850	177.9650	175.0212	169.4615
H(31)-C(29)-N(18)-C(19)	130.3693	123.8312	-121.3448	-124.6562
H(31)-C(29)-N(18)-C(5)	-55.4983	-60.1975	54.7312	48.9224
H(30)-C(29)-N(18)-C(19)	-111.2656	-118.1307	120.7473	117.5167
H(30)-C(29)-N(18)-C(5)	62.8668	57.8406	-63.1767	-68.9047
C(29)-C(26)-C(23)-C(19)	37.1534	36.5726	36.2137	35.3474
C(29)-C(26)-C(23)-H(25)	-79.8360	-80.1742	157.3757	156.5878
C(29)-C(26)-C(23)-H(24)	158.6196	158.0080	-80.5752	-81.2502
H(28)-C(26)-C(23)-C(19)	158.8448	158.4159	157.9968	157.2013
H(28)-C(26)-C(23)-H(25)	41.8555	41.6690	-80.8412	-81.5583
H(28)-C(26)-C(23)-H(24)	-79.6889	-80.1488	41.2080	40.6037
H(27)-C(26)-C(23)-C(19)	-80.8370	-81.5307	-82.0474	-82.9595
H(27)-C(26)-C(23)-H(25)	162.1737	161.7225	39.1145	38.2810
H(27)-C(26)-C(23)-H(24)	40.6293	39.9047	161.1637	160.4430
C(26)-C(23)-C(19)-N(18)	-31.4171	-34.6132	-36.0747	-37.0713
C(26)-C(23)-C(19)-C(21)	-153.3028	-158.3455	-160.1914	-162.5772
C(26)-C(23)-C(19)-H(20)	85.7160	82.1051	80.2846	79.0452
H(25)-C(23)-C(19)-N(18)	86.9507	83.4345	-158.3407	-159.3856

H(25)-C(23)-C(19)-C(21)	-34.9351	-40.2978	77.5426	75.1085
H(25)-C(23)-C(19)-H(20)	-155.9162	-159.8472	-41.9813	-43.2691
H(24)-C(23)-C(19)-N(18)	-153.9471	-157.1074	81.9829	80.7890
H(24)-C(23)-C(19)-C(21)	84.1672	79.1603	-42.1339	-44.7169
H(24)-C(23)-C(19)-H(20)	-36.8140	-40.3891	-161.6578	-163.0944
N(1)-C(21)-C(19)-N(18)	34.8610	25.7720	23.2082	17.0424
N(1)-C(21)-C(19)-C(23)	152.1259	143.9103	141.6121	136.1888
N(1)-C(21)-C(19)-H(20)	-85.3080	-94.9015	-97.3060	-103.6549
O(22)-C(21)-C(19)-N(18)	-145.6479	-155.2154	-158.0074	-164.9120
O(22)-C(21)-C(19)-C(23)	-28.3830	-37.0771	-39.6035	-45.7656
O(22)-C(21)-C(19)-H(20)	94.1831	84.1111	81.4785	74.3907
C(19)-C(21)-N(1)-C(3)	2.6792	6.9151	3.4860	3.5043
C(19)-C(21)-N(1)-H(2)	-176.1065	173.1533	177.0179	168.9957
O(22)-C(21)-N(1)-C(3)	-176.8017	-172.0657	-175.2741	-174.4703
O(22)-C(21)-N(1)-H(2)	4.4126	-5.8276	-1.7422	-8.9789
C(23)-C(19)-N(18)-C(29)	14.6545	20.7941	23.6880	26.2892
C(23)-C(19)-N(18)-C(5)	-159.4514	-155.0535	-152.2261	-146.9697
C(21)-C(19)-N(18)-C(29)	138.7375	145.8862	149.2051	152.5084
C(21)-C(19)-N(18)-C(5)	-35.3683	-29.9614	-26.7090	-20.7505
H(20)-C(19)-N(18)-C(29)	-102.6658	-95.4996	-92.2517	-89.1402
H(20)-C(19)-N(18)-C(5)	83.2283	88.6528	91.8341	97.6009
C(19)-N(18)-C(5)-C(3)	-3.2913	0.1169	1.9045	2.8347
C(19)-N(18)-C(5)-O(6)	177.6459	-179.0203	-177.7150	-178.4365
C(29)-N(18)-C(5)-C(3)	-176.7719	-175.3334	-173.6156	-169.7938
C(29)-N(18)-C(5)-O(6)	4.1654	5.5294	6.7649	8.9350
C(15)-N(17)-C(13)-C(10)	0.0489	-0.1579	-0.2705	0.3821
C(15)-N(17)-C(13)-H(14)	-178.9384	-179.8636	-179.9022	-179.3279
C(13)-N(17)-C(15)-N(11)	0.1043	0.1614	0.5394	-0.2670
C(13)-N(17)-C(15)-H(16)	-179.9360	-179.8373	-179.0795	179.5819
N(17)-C(15)-N(11)-C(10)	-0.2172	-0.0941	-0.6104	0.0355
N(17)-C(15)-N(11)-H(12)	-178.0197	-179.4867	-174.1799	-179.7098
H(16)-C(15)-N(11)-C(10)	179.8216	179.9045	179.0237	-179.8075
H(16)-C(15)-N(11)-H(12)	2.0191	0.5147	5.4542	0.1390
N(17)-C(13)-C(10)-N(11)	-0.1754	0.1047	-0.0874	-0.3695
N(17)-C(13)-C(10)-C(7)	-178.4756	-179.1868	-178.4903	179.7563
H(14)-C(13)-C(10)-N(11)	178.7330	179.7701	179.5162	179.3004
H(14)-C(13)-C(10)-C(7)	0.4328	0.4786	1.1134	-0.5738
C(15)-N(11)-C(10)-C(13)	0.2304	-0.0095	0.4023	0.2135
C(15)-N(11)-C(10)-C(7)	178.7189	179.341	178.9400	-179.9029
H(12)-N(11)-C(10)-C(13)	178.1770	179.4903	174.3595	179.8254
H(12)-N(11)-C(10)-C(7)	-3.3345	-0.2154	-7.1028	0.1155
N(11)-C(10)-C(7)-C(3)	69.5410	58.3911	46.3791	-42.0300
N(11)-C(10)-C(7)-H(9)	-169.0762	179.5004	-78.0052	-162.4435
N(11)-C(10)-C(7)-H(8)	-52.5299	-62.9522	166.2179	79.4741

C(13)-C(10)-C(7)-C(3)	-112.4259	-122.3950	-135.4895	137.8299
C(13)-C(10)-C(7)-H(9)	8.9568	-1.2856	100.1262	17.4164
C(13)-C(10)-C(7)-H(8)	125.5031	116.2617	-15.6507	-100.6660
C(10)-C(7)-C(3)-N(1)	57.6899	-64.8853	152.0620	69.2912
C(10)-C(7)-C(3)-C(5)	-66.8345	171.4232	-81.8148	-162.3776
C(10)-C(7)-C(3)-H(4)	177.1423	55.4942	33.5854	-49.2628
H(9)-C(7)-C(3)-N(1)	-63.9050	172.6258	-82.1665	-169.6186
H(9)-C(7)-C(3)-C(5)	171.5706	48.9343	43.9566	-41.2874
H(9)-C(7)-C(3)-H(4)	55.5474	-66.9947	159.3568	71.8274
H(8)-C(7)-C(3)-N(1)	-178.3093	57.4666	32.2849	-53.2781
H(8)-C(7)-C(3)-C(5)	57.1663	-66.2249	158.4081	75.0532
H(8)-C(7)-C(3)-H(4)	-58.8569	177.8460	-86.1917	-171.8320
N(18)-C(5)-C(3)-N(1)	39.8110	31.3607	23.9841	17.3106
N(18)-C(5)-C(3)-C(7)	165.1695	154.4937	-102.6118	-110.5200
N(18)-C(5)-C(3)-H(4)	-78.3629	-88.5920	140.2565	134.1862
O(6)-C(5)-C(3)-N(1)	-141.1205	-149.4915	-156.3893	-161.4607
O(6)-C(5)-C(3)-C(7)	-15.7620	-26.3585	77.0148	70.7087
O(6)-C(5)-C(3)-H(4)	100.7055	90.5559	-40.1169	-44.5851
C(5)-C(3)-N(1)-C(21)	-40.9079	-36.3596	-27.6769	-21.1753
C(5)-C(3)-N(1)-H(2)	137.8552	157.2286	158.9495	173.1836
C(7)-C(3)-N(1)-C(21)	-167.2453	-159.4452	98.3669	105.7370
C(7)-C(3)-N(1)-H(2)	11.5178	34.1430	-75.0068	-59.9041
H(4)-C(3)-N(1)-C(21)	75.0117	81.4171	-142.6954	-135.8569
H(4)-C(3)-N(1)-H(2)	-106.2252	-84.9947	43.9310	58.5020

Table 7.6. The calculated bond lengths, bond angles and dihedral angles of the lowest energy conformer of the N^ε and N^δ-tautomeric forms of CAH.

Bond lengths (Å)	N ^ε -CAH	N ^δ -CAH
H(27)-N(13)	1.0095	1.0048
H(26)-C(14)	1.0773	1.0770
H(25)-C(12)	1.0780	1.0749
H(24)-C(10)	1.0863	1.0864
H(23)-C(10)	1.0896	1.0898
H(22)-C(10)	1.0908	1.0912
H(21)-C(9)	1.0908	1.0875
H(20)-C(9)	1.0912	1.0931
H(19)-N(5)	1.0088	1.0158
H(18)-C(4)	1.0996	1.0993
H(17)-N(2)	1.0089	1.0094
H(16)-C(1)	1.0983	1.0985
N(15)-C(14)	1.3116	1.3580
N(15)-C(12)	1.3734	1.3776

C(14)-N(13)	1.3600	1.3105
N(13)-C(11)	1.3776	1.3818
C(12)-C(11)	1.3718	1.3685
C(11)-C(9)	1.4912	1.4949
C(10)-C(1)	1.5203	1.5233
C(9)-C(4)	1.5370	1.5364
O(8)-C(3)	1.2244	1.2203
O(7)-C(6)	1.2161	1.2200
C(6)-N(5)	1.3559	1.3515
C(6)-C(1)	1.5365	1.5320
N(5)-C(4)	1.4568	1.4573
C(4)-C(3)	1.5328	1.5293
C(3)-N(2)	1.3483	1.3537
N(2)-C(1)	1.4645	1.4606
Bond angles (°)		
C(14)-N(15)-C(12)	105.2415	107.4050
H(26)-C(14)-N(15)	125.8241	122.7944
H(26)-C(14)-N(13)	122.4507	126.0352
N(15)-C(14)-N(13)	111.7252	111.1704
H(27)-N(13)-C(14)	128.6622	126.2803
H(27)-N(13)-C(11)	123.8579	126.3146
C(14)-N(13)-C(11)	107.4535	106.2739
H(25)-C(12)-N(15)	121.4466	122.3008
H(25)-C(12)-C(11)	127.6713	131.9891
N(15)-C(12)-C(11)	110.8746	105.7097
C(9)-C(11)-N(13)	123.2798	121.8245
C(9)-C(11)-C(12)	131.9967	128.7331
N(13)-C(11)-C(12)	104.7047	109.4405
C(1)-C(10)-H(22)	110.3980	110.3938
C(1)-C(10)-H(23)	110.7587	110.6500
C(1)-C(10)-H(24)	109.6938	109.6618
H(22)-C(10)-H(23)	109.0799	108.7892
H(22)-C(10)-H(24)	108.7889	108.8437
H(23)-C(10)-H(24)	108.0646	108.4542
H(20)-C(9)-H(21)	106.6885	107.1883
H(20)-C(9)-C(4)	107.7770	108.0591
H(20)-C(9)-C(11)	108.2487	110.0074
H(21)-C(9)-C(4)	106.8426	107.6968
H(21)-C(9)-C(11)	110.6125	110.1714
C(4)-C(9)-C(11)	116.2448	113.4895
O(7)-C(6)-N(5)	123.7295	120.7672
O(7)-C(6)-C(1)	122.2644	123.3683

N(5)-C(6)-C(1)	113.9998	115.8591
H(19)-N(5)-C(6)	116.4686	116.9053
H(19)-N(5)-C(4)	118.8280	115.5309
C(6)-N(5)-C(4)	124.6164	126.1701
H(18)-C(4)-C(9)	106.6150	107.7814
H(18)-C(4)-N(5)	109.7516	110.0502
H(18)-C(4)-C(3)	105.4414	105.5280
C(9)-C(4)-N(5)	111.6535	110.6281
C(9)-C(4)-C(3)	113.0859	110.4728
N(5)-C(4)-C(3)	110.0162	112.1708
O(8)-C(3)-C(4)	122.9153	121.6768
O(8)-C(3)-N(2)	123.3162	122.8680
C(4)-C(3)-N(2)	113.7590	115.4499
H(17)-N(2)-C(3)	116.2056	114.6832
H(17)-N(2)-C(1)	118.4624	117.6632
C(3)-N(2)-C(1)	125.2300	126.5089
C(10)-C(1)-H(16)	108.7033	108.3173
C(10)-C(1)-C(6)	111.6671	111.3380
C(10)-C(1)-N(2)	110.4331	110.2941
H(16)-C(1)-C(6)	106.1673	105.3959
H(16)-C(1)-N(2)	109.4207	109.6169
C(6)-C(1)-N(2)	110.3278	111.7043
Dihedral angles (°)		
C(12)-N(15)-C(14)-N(13)	0.0990	0.2275
C(12)-N(15)-C(14)-H(26)	-179.9404	-179.7840
C(14)-N(15)-C(12)-C(11)	0.0566	-0.2268
C(14)-N(15)-C(12)-H(25)	-179.0186	179.9692
N(15)-C(14)-N(13)-C(11)	-0.2159	-0.1285
N(15)-C(14)-N(13)-H(27)	-178.3778	-179.6498
H(26)-C(14)-N(13)-C(11)	179.8220	179.8835
H(26)-C(14)-N(13)-H(27)	1.6601	0.3386
C(14)-N(13)-C(11)-C(12)	0.2338	-0.0202
C(14)-N(13)-C(11)-C(9)	178.8233	179.5132
H(27)-N(13)-C(11)-C(12)	178.5055	179.6506
H(27)-N(13)-C(11)-C(9)	-2.9050	-0.1533
N(15)-C(12)-C(11)-N(13)	-0.1823	0.1544
N(15)-C(12)-C(11)-C(9)	-178.5956	-179.3374
H(25)-C(12)-C(11)-N(13)	178.8209	179.9315
H(25)-C(12)-C(11)-C(9)	0.4076	0.4397
C(12)-C(11)-C(9)-C(4)	-112.0464	-124.5657
C(12)-C(11)-C(9)-H(21)	125.9088	-3.7181
C(12)-C(11)-C(9)-H(20)	9.3526	114.2388

N(13)-C(11)-C(9)-C(4)	69.7895	55.9983
N(13)-C(11)-C(9)-H(21)	-52.2553	176.8459
N(13)-C(11)-C(9)-H(20)	-168.8114	-65.1972
H(24)-C(10)-C(1)-N(2)	179.1866	179.8074
H(24)-C(10)-C(1)-C(6)	56.0313	55.2127
H(24)-C(10)-C(1)-H(16)	-60.7646	-60.2273
H(23)-C(10)-C(1)-N(2)	59.9846	60.2114
H(23)-C(10)-C(1)-C(6)	-63.1707	-64.3834
H(23)-C(10)-C(1)-H(16)	-179.9666	-179.8233
H(22)-C(10)-C(1)-N(2)	-60.9405	-60.2748
H(22)-C(10)-C(1)-C(6)	175.9042	175.1304
H(22)-C(10)-C(1)-H(16)	59.1083	59.6905
C(11)-C(9)-C(4)-C(3)	-65.7407	169.3388
C(11)-C(9)-C(4)-N(5)	58.9786	-65.8451
C(11)-C(9)-C(4)-H(18)	178.8404	54.5151
H(21)-C(9)-C(4)-C(3)	58.2706	47.1079
H(21)-C(9)-C(4)-N(5)	-177.0102	171.9240
H(21)-C(9)-C(4)-H(18)	-57.1483	-67.7158
H(20)-C(9)-C(4)-C(3)	172.6102	-68.3789
H(20)-C(9)-C(4)-N(5)	-62.6705	56.4371
H(20)-C(9)-C(4)-H(18)	57.1913	176.7973
C(1)-C(6)-N(5)-C(4)	5.3471	8.9472
C(1)-C(6)-N(5)-H(19)	-178.0972	174.8044
O(7)-C(6)-N(5)-C(4)	-173.7567	-170.2071
O(7)-C(6)-N(5)-H(19)	2.7990	-4.3499
N(5)-C(6)-C(1)-N(2)	32.0164	21.4888
N(5)-C(6)-C(1)-H(16)	-86.4462	-97.4845
N(5)-C(6)-C(1)-C(10)	155.2315	145.2869
O(7)-C(6)-C(1)-N(2)	-148.8651	-159.3332
O(7)-C(6)-C(1)-H(16)	92.6723	81.6934
O(7)-C(6)-C(1)-C(10)	-25.6499	-35.5351
C(6)-N(5)-C(4)-C(3)	-40.4914	-31.7378
C(6)-N(5)-C(4)-C(9)	-166.9064	-155.5834
C(6)-N(5)-C(4)-H(18)	75.0960	85.4208
H(19)-N(5)-C(4)-C(3)	143.0281	162.2355
H(19)-N(5)-C(4)-C(9)	16.6131	38.3899
H(19)-N(5)-C(4)-H(18)	-101.3845	-80.6059
N(5)-C(4)-C(3)-N(2)	35.6086	21.8472
N(5)-C(4)-C(3)-O(8)	-145.4820	-158.9660
C(9)-C(4)-C(3)-N(2)	161.2124	145.7795
C(9)-C(4)-C(3)-O(8)	-19.8782	-35.0337
H(18)-C(4)-C(3)-N(2)	-82.6702	-97.9852

H(18)-C(4)-C(3)-O(8)	96.2392	81.2016
C(4)-C(3)-N(2)-C(1)	1.4922	8.7485
C(4)-C(3)-N(2)-H(17)	177.7486	176.1439
O(8)-C(3)-N(2)-C(1)	-177.4122	-170.4276
O(8)-C(3)-N(2)-H(17)	-1.1559	-3.0322
C(3)-N(2)-C(1)-C(6)	-36.5770	-31.3765
C(3)-N(2)-C(1)-H(16)	79.8759	85.0608
C(3)-N(2)-C(1)-C(10)	-160.5076	-155.7610
H(17)-N(2)-C(1)-C(6)	147.2439	161.5602
H(17)-N(2)-C(1)-H(16)	-96.3033	-82.0025
H(17)-N(2)-C(1)-C(10)	23.3132	37.1756

7.3.3. Vibrational assignments

The experimental solid state and calculated IR and Raman spectra of CHP, CDHP and CAH are shown in Figs. 7.9-7.12. The solution state spectra are shown in Figs. 7.13-7.16. The experimental solid state and calculated IR and Raman spectra of *N*-deuterated CAH are shown in Figs. 7.17-7.20. The experimental and calculated wavenumbers (cm^{-1}) and potential energy distribution (PEDs) of vibrational modes of the lowest energy conformer of CHP, CDHP and CAH and its *N*-deuterated isotopomer (CAH) are given in Tables 7.7-7.10. The vibrational band assignments for CDHP, CHP and CAH are compared with the calculated wavenumbers and the shifts of the vibrational band wavenumbers on deuteration of CAH. As previously stated the *N*-deuterated isotopomers of CHP and CDHP could not be obtained.

7.3.4. Spectral region $>2000 \text{ cm}^{-1}$

The vibrational bands found in this region are mainly due to N-H, C-H and N-D stretching modes. The vibrational wavenumbers for the N-H stretching bands for CDHP, CHP and CAH are located in the $3100\text{-}3300 \text{ cm}^{-1}$ region. The N-H stretching vibration of the imidazole ring in the L-His side-chain are assigned to the bands at 3175 , 3313 and 3222 cm^{-1} in the IR spectra and 3181 , 3313 and 3181 cm^{-1} in the Raman spectra of CHP, CDHP and CAH, respectively. On *N*-deuteration, this band shifts considerably down in wavenumber and appears at 2372 and 2375 cm^{-1} in IR and Raman spectra, respectively of *N*-deuterated CAH. The N-H stretching band in the IR spectrum is more intense compared to its Raman counterpart. The N-H stretching vibration of the DKP ring appears at 3135 , 3168 and 3188 cm^{-1} in the IR spectra and at 3135 , 3170 and 3181 cm^{-1} in the Raman spectra of CHP, CDHP and CAH, respectively. These modes shift down in wavenumber and appear at 2352 and 2351 in the IR and Raman spectra of *N*-deuterated CAH, respectively.

However, from the IR spectra of CAH, it is evident that complete *N*-deuteration of the N-H groups of the DKP and imidazole ring could not be obtained. As previously stated, the N-H atoms on the imidazole ring of the L-His side-chain and the N-H atoms of the DKP ring participate in hydrogen bonding. It is, therefore, hypothesised that the two N-H atoms in all three DKPs (CHP, CDHP and CAH) are involved in hydrogen bonding, but of different strengths. The group of bands in the 3000-3100 cm⁻¹ region is recognized for *sp*² C-H stretching modes and the vibrational bands between 2800 and 2990 cm⁻¹ are assigned to *sp*³ C-H stretching modes in all three molecules. These bands are more intense in the Raman than in the IR spectra. These vibrational bands can be assigned by PEDs from the DFT calculations and lack of shift of C-H modes on *N*-deuteration in CAH.

7.3.5. Spectral region 1250-1700 cm⁻¹

The vibrational bands found in this region are attributed to amide group vibrations (C=O stretch, C-N stretch and N-H in-plane bending,) C-H bending, C_α-H bending, CH₂ scissoring, twisting and wagging modes. The strong bands at 1645 and 1648 cm⁻¹ observed in the IR and at 1649 and 1650 cm⁻¹ in the Raman spectra of CHP and CDHP are assigned to the (C=O) stretching mode (*cis* amide 1 mode). This band reveals a shoulder ~1666 cm⁻¹ in both IR and Raman spectra of CHP and at 1633 cm⁻¹ in the Raman spectrum of CDHP. Previous studies on DKPs derivatives [cyclo(L-Met-L-Met),³⁹ cyclo(L-Asp-L-Asp)⁴⁰ and cyclo(L-Ser-L-Ser)⁴¹] also show splitting of the *cis* amide 1 mode in the order of 15-20 cm⁻¹ as a result of factor group splitting for cyclo(L-Asp-L-Asp) and cyclo(L-Ser-L-Ser) and resonance effects (cyclo(L-Met-L-Met), which mainly arise from the interaction between more than one neighbouring molecule in a crystallographic unit cell.²⁶

In the case of CAH, the *cis* amide 1 appears at 1671 cm⁻¹ in the IR spectrum and at 1662 cm⁻¹ in the Raman spectrum. On *N*-deuteration this band shifts down to lower wavenumber, and appears at 1667 cm⁻¹ in the IR and at 1638 cm⁻¹ in the Raman spectra of *N*-deuterated CAH. From the previous observations³³ it is suggested that the coupling of C=O stretch with the N-H in-plane bending is higher in compounds with a *cis* amide group compared to the *trans* amide group and, hence, on *N*-deuteration the *cis* amide I band shifts down to lower wavenumber to a greater extent. It is noteworthy that the *cis* amide I mode shows a downward shift of around 20 cm⁻¹ in the solid state Raman spectrum of CAH. This can be attributed to weaker coupling and the low N-H character of the *cis* amide I mode (Tables 7.9 and 7.10). The *N*-deuteration shift, of around 25 cm⁻¹, in the amide I mode is typical of the *cis* amide I conformation and this indicates that the

C=O stretch is not an independent mode but a coupling vibration, coupled with C-N stretching and N-H bending modes. In contrast, the *trans* amide I vibrational mode has significantly lower N-H character. Hence, it is observed that in linear L-Met-L-Met the *trans* amide I mode shows a downward shift of only 6 cm⁻¹ upon *N*-deuteration.³³ However, in the solution state Raman spectra of CHP, CDHP and CAH this mode is detected at ~1650 cm⁻¹. Compared to its Raman counterpart in D₂O solution, it is noteworthy that the *cis* amide I mode does not show a downward shift. This is attributed to the hydrogen bonding effects in the solid state compared to that in solution.^{33,42}

The band due to C=C stretching vibrations of the imidazole ring can be easily located around 1580 cm⁻¹ in both IR and Raman spectra of CHP, CDHP and CAH. On *N*-deuteration this mode shifts down in wavenumber and appears at 1563 cm⁻¹ and reveals a shoulder at 1575 cm⁻¹ in the *N*-deuterated solid-state Raman spectra of CAH. This suggests that C=C stretching vibration is coupled with the N-H in-plane-bending vibration of the imidazole ring. As previously mentioned, complete deuteration of CAH could not be obtained. Hence, this band splits into two bands in the *N*-deuterated Raman spectra of CAH. This mode (C=C stretching) is in good agreement with the previously reported C=C stretching vibrations coupled with the N-H in-plane bending mode in a histidine-containing DKP.²⁶ This mode is observed at ~1570 cm⁻¹ in the aqueous solution-state Raman spectra and shows a downward shift in wavenumber and appears at 1562 cm⁻¹ in the Raman spectra of CHP, CDHP and CAH in D₂O.

The *cis* amide II mode is found at 1495, 1498 and 1496 cm⁻¹ in the solid-state Raman spectrum of CHP, CDHP and CAH, respectively. This mode is mainly due to the out of plane C_α-C-N stretch, with a decreased contribution from the N-H in-plane bending vibration compared to the *trans* amide II mode. This band fits well with the *cis* amide II mode location (cm⁻¹) found in other DKPs where the ring essentially adopts a boat conformation.^{26,39,40} In other DKPs, such as cyclo(Gly-Gly), cyclo(D-Ala-L-Ala) and cyclo(L-Ala-Gly), the *cis* amide II mode was found at ~1520 cm⁻¹ where the DKP ring is planar or near planar.³³ From previous studies on DKPs which show a boat conformation, it is suggested that the increase in the strain on the DKP ring due the attachment of bulky substituents on the C_α atoms may also influence the location of the *cis* amide II mode.^{39,40} In the case of cyclo(His-Phe), this mode is observed at 1481 cm⁻¹ in the solid-state Raman spectrum.²⁶ Unfortunately, the *cis* amide II vibration could not be assigned from our calculated PEDs of CHP, CDHP and CAH. This is ascribed to the overlap of the *cis* amide II mode with the intense C-H bending vibrations, as the vibrational modes observed in the 1400-1500 cm⁻¹ region relate mostly to C-H bending vibrations. The *cis* amide II band in CAH shifts down to lower

wavenumber on *N*-deuteration by 19 cm⁻¹ and appears as a weak band at 1477 cm⁻¹ and reveals a shoulder at 1468 cm⁻¹ in the Raman spectrum. This shift is in good agreement with both our calculated wavenumbers and *cis* amide II mode shifts observed in other DKPs (the expected *N*-deuterium shift is ~18 cm⁻¹) after *N*-deuteration.^{33,42} In contrast, the *trans* amide II vibrational mode has a significantly higher N-H character. Hence, in linear L-Met-L-Met the *trans* amide II mode shows a downward shift of 66 cm⁻¹ upon *N*-deuteration.³³ In the solution state, this band is found at 1518, 1512 and 1523 cm⁻¹ in the Raman spectrum of CHP, CDHP and CAH, respectively. This mode shows a downward shift of ~10-20 cm⁻¹ in the Raman spectrum of CHP, CDHP and CAH in D₂O solution.

IR and Raman bands in the 1440-1510 cm⁻¹ region can be assigned to CH and CH₂ bending modes of CHP, CDHP and CAH. These vibrations are predominantly due to CH₂ deformation modes and have been assigned with reference to our calculated PEDs. From our calculated PEDs, the N-H bending vibrations of the DKP ring are found in the 1360 to 1401 cm⁻¹ region in CHP, CDHP and CAH. This agrees well with previous observations in DKPs^{33,39,40} and other histidine containing DKPs e.g., cyclo(His-Phe).²⁶ The band located at 1330 cm⁻¹ in the IR and Raman spectrum has been assigned to the N-H in-plane bending vibration in CAH. However, minor shifts are observed (~7 cm⁻¹) in this region for N-H bending modes on *N*-deuteration in the solid state IR and Raman spectra of CAH. From the calculated PEDs and previously reported data on DKPs,²⁶ the bands at ~1350 cm⁻¹ in the solid state IR and Raman spectra of CHP and CDHP are tentatively assigned to C-N and N-C stretching coupled with C-H wagging vibrations of the imidazole ring. IR and Raman vibrational bands located between 1230 and 1340 cm⁻¹ appear to be quite complex and can be assigned to mixed vibrations. As shown by the calculated wavenumbers these bands are mainly due to a combination of C_α-H bending, C_α-H wagging, C_α-H twisting, CH₂ wagging and CH₂ twisting vibrations. Generally most of the bands due to C-H bending vibrations show little shift on *N*-deuteration; but some bands are shifted down by 5-10 cm⁻¹ in CAH. Unfortunately, no vibrational modes due to N-H bending vibrations are observed in the solution state.

7.3.6. Spectral region 850-1350 cm⁻¹

The vibrations observed in this region are due to C-C, N-C_α stretching as well as CH₂ rocking vibrations. The band located at 1160 cm⁻¹ in both IR and Raman spectra of CHP and CDHP and at 1168 cm⁻¹ in CAH is assigned to mixed N-C_α stretching vibrations of the DKP ring together with contributions from CH₂ rocking vibrations. This band appears at ~1163 cm⁻¹ in the solution state IR and Raman spectra of CHP, CDHP and CAH. The bands at ~1105 cm⁻¹ (1108 cm⁻¹ in

CAH) in both solid and solution-state IR and Raman spectra of CHP and CDHP have been assigned to C-N stretching with little contribution from C-H in-plane-bending and N-H in-plane bending vibrations of the imidazole ring. This mode fits well with the previously reported imidazole ring bands in this region.²⁶ Additionally, the N-C α stretching vibration of the DKP ring is also observed at 1090 cm⁻¹ in the IR spectra and at 1095, 1099 and 1090 cm⁻¹ in the solid-state Raman spectra of CHP, CDHP and CAH, respectively. Other IR and Raman bands observed in the 850–1070 cm⁻¹ region appear quite complex and are also assigned to mixed vibrations. From our calculated PEDs these vibrations are due to a combination of N-C α , C-C stretching as well as CH₂ rocking vibrations.

7.3.7. Spectral region 500-850 cm⁻¹

In this region, there are two peptide group vibrations (C=O bending and N-H out-of-plane bending) and C-H out-of-plane bending modes. Other modes in this region include ring deformation and ring stretching vibrations. Bands due to C-H out-of-plane bending modes have been assigned on the basis of the data obtained from calculated spectra and also from the previous IR and Raman data relating to other histidine containing DKPs.²⁶ The band found at 789 cm⁻¹ and ~790 cm⁻¹ in the solid-state IR and Raman spectra, respectively of CHP, CDHP and CAH can be assigned to C-H out-of-plane bending modes. The N-H out-of-plane bending vibration is assigned to the band at ~730 cm⁻¹ in the solid-state IR and Raman spectra of CHP and CDHP. In the case of CAH, the bands at 824, 764, 639, 619 cm⁻¹ in IR and at 826, 804, 736, 619 cm⁻¹ in the Raman spectra shift considerably on *N*-deuteration and appear at 570 and 545 cm⁻¹ in the *N*-deuterated IR and Raman spectra of CAH, respectively indicative of N-H-out-of plane bending vibrations. Previous work on other DKPs has shown that the NH out-of-plane bending band is quite difficult to detect and has a wide (broad)-ranging feature centred ~820 cm⁻¹ in the IR spectrum.^{33,39-42} The vibrations from 500 to 750 cm⁻¹ are of mixed character and cannot be easily assigned to a particular vibration. The medium intensity Raman bands located from 520 to 780 cm⁻¹ can be assigned to C=O in and out-of-plane bending vibrations, although these vibrations are quite mixed, they do contain a significant contribution with respect to the C=O in- and out-of-plane bending vibrations and N-H out-of-plane bending motions.

7.3.8. Spectral region < 500 cm⁻¹

There are some weak bands observed in the Raman spectrum below 500 cm⁻¹, which are due to vibrations from C=O, C-N, C-C bending motions together with ring stretching and ring bending

vibrations of the DKP, proline and imidazole rings and ring buckling vibrations. Normally, the bands in this region appear to be complex but the assignments have been made possible by comparison with the calculated PEDs. A medium intensity band centred at 484, 484 and 478 cm^{-1} in IR and 485, 483 and 472 cm^{-1} in the Raman spectra of CHP, CDHP and CAH, respectively is tentatively assigned to the proline and DKP ring vibrations. On *N*-deuteration, it increases in intensity and shifts down in wavenumber by 5 cm^{-1} indicative of a small contribution from N-H out-of-plane bending in CAH. The bands in the 50-400 cm^{-1} region of the Raman spectrum are predominantly due to C-C and C=O bending motions; the attachment of the side-chain on the C_α atom also shows C-C-C bending vibrations in this region as well as the bending modes of the DKP, proline and imidazole rings with ring buckling vibrations. The bands located below 200 cm^{-1} are mainly due to torsional vibrations of the aliphatic side chain attached to the C_α atom, ring torsional vibrations and lattice vibrations.

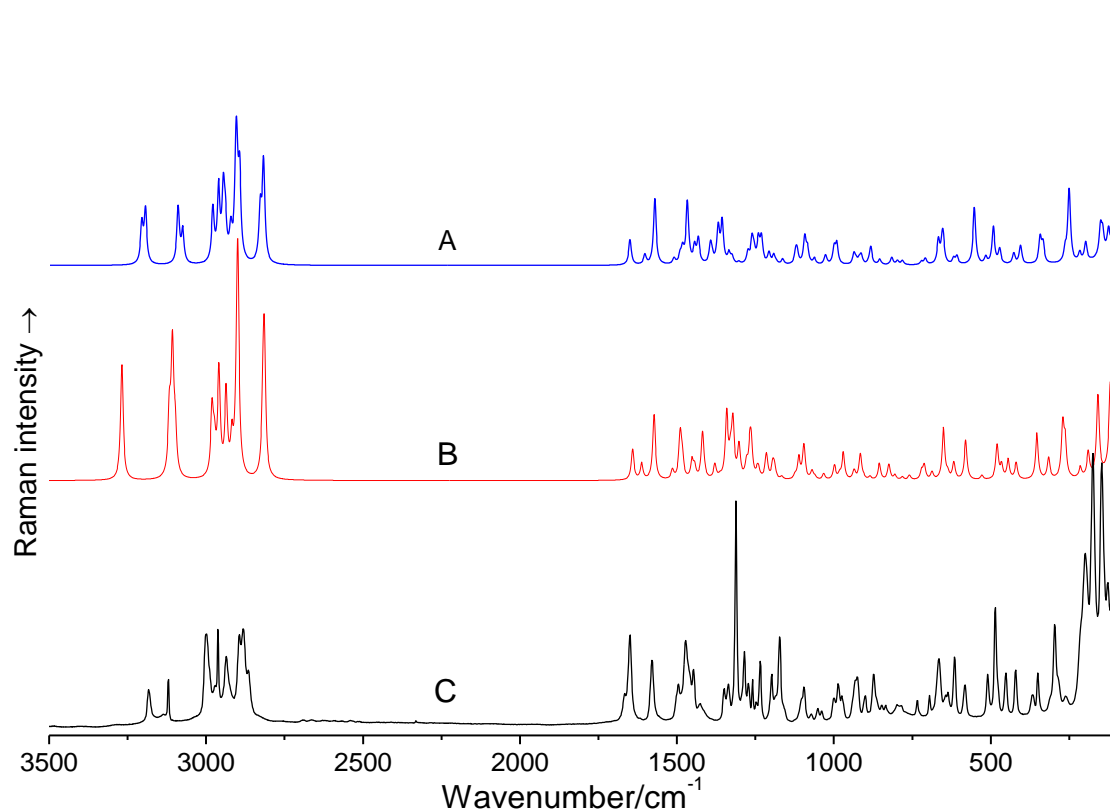


Figure 7.9. Calculated (A) N^ϵ -protonated (B) N^δ -protonated tautomers and (C) experimental solid state Raman spectra of CHP.

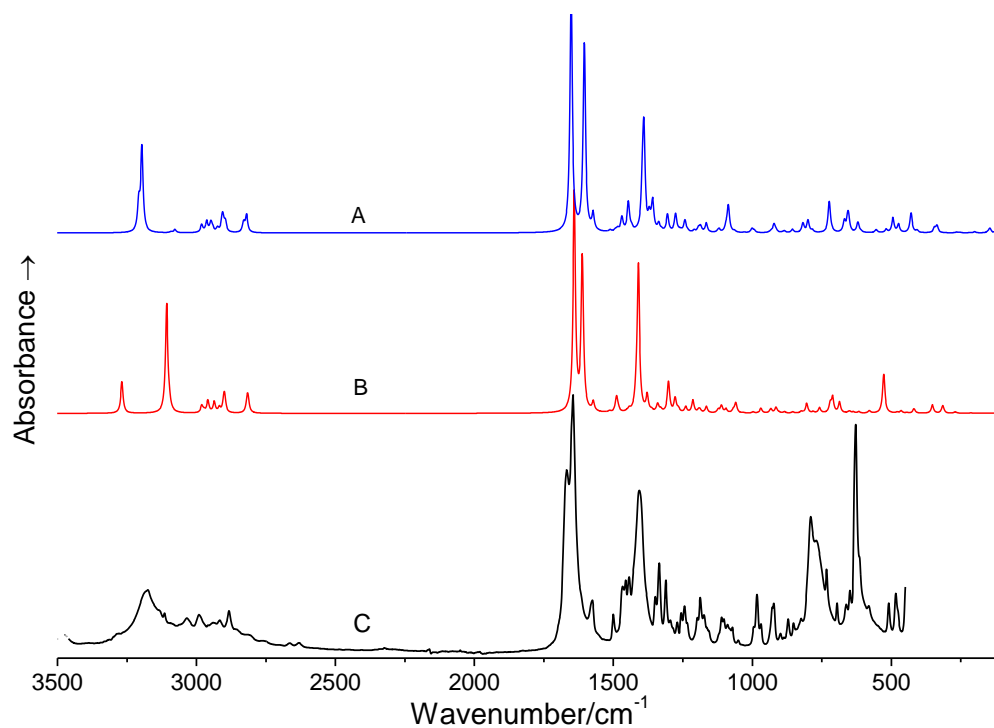


Figure 7.10. Calculated (A) N^{ϵ} -protonated (B) N^{δ} -protonated tautomers and (C) experimental solid state IR spectra of CHP.

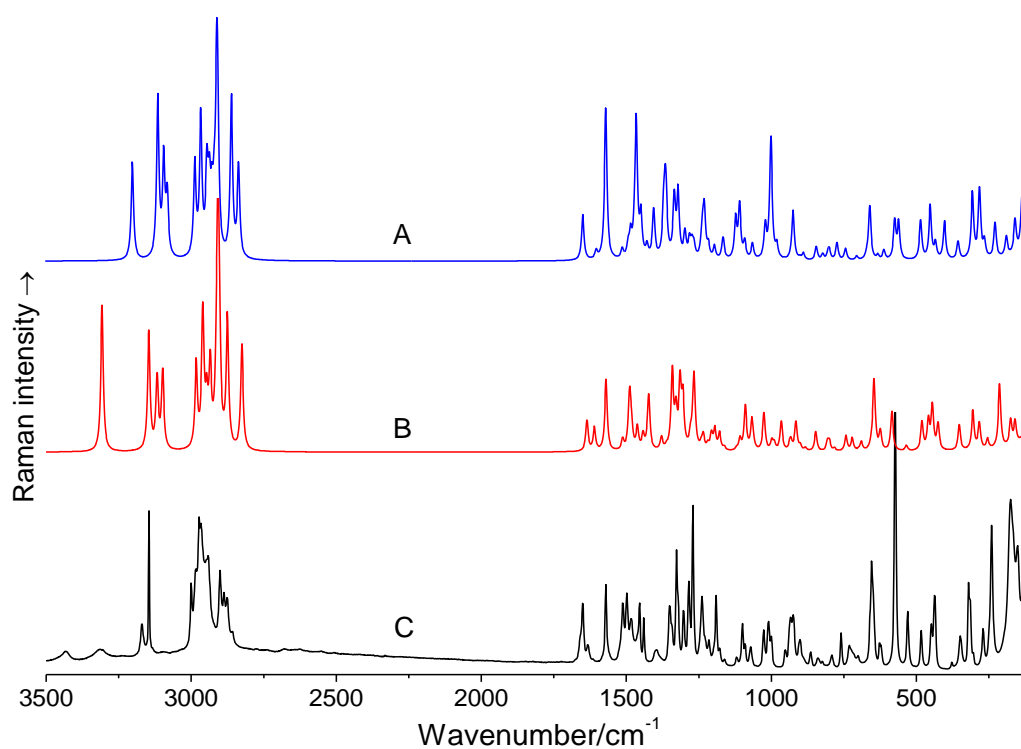


Figure 7.11. Calculated (A) N^{ϵ} -protonated (B) N^{δ} -protonated tautomers and (C) experimental solid state Raman spectra of CDHP.

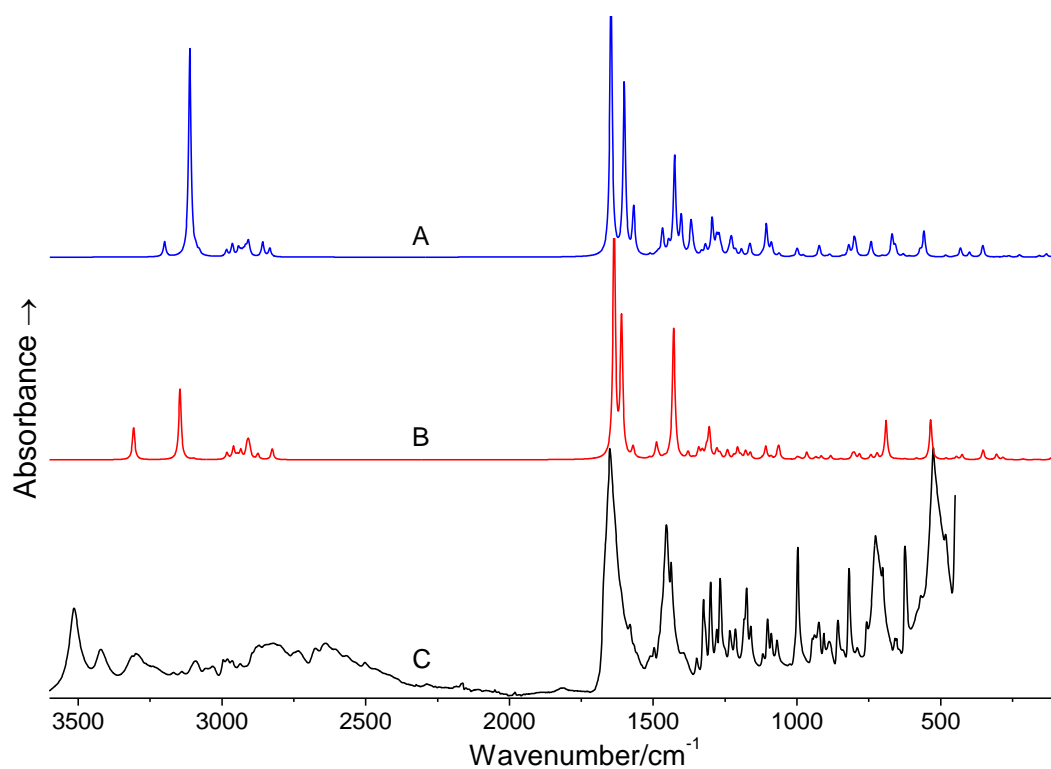


Figure 7.12. Calculated (A) N^ε-protonated (B) N^δ-protonated tautomers and (C) experimental solid state IR spectra of CDHP.

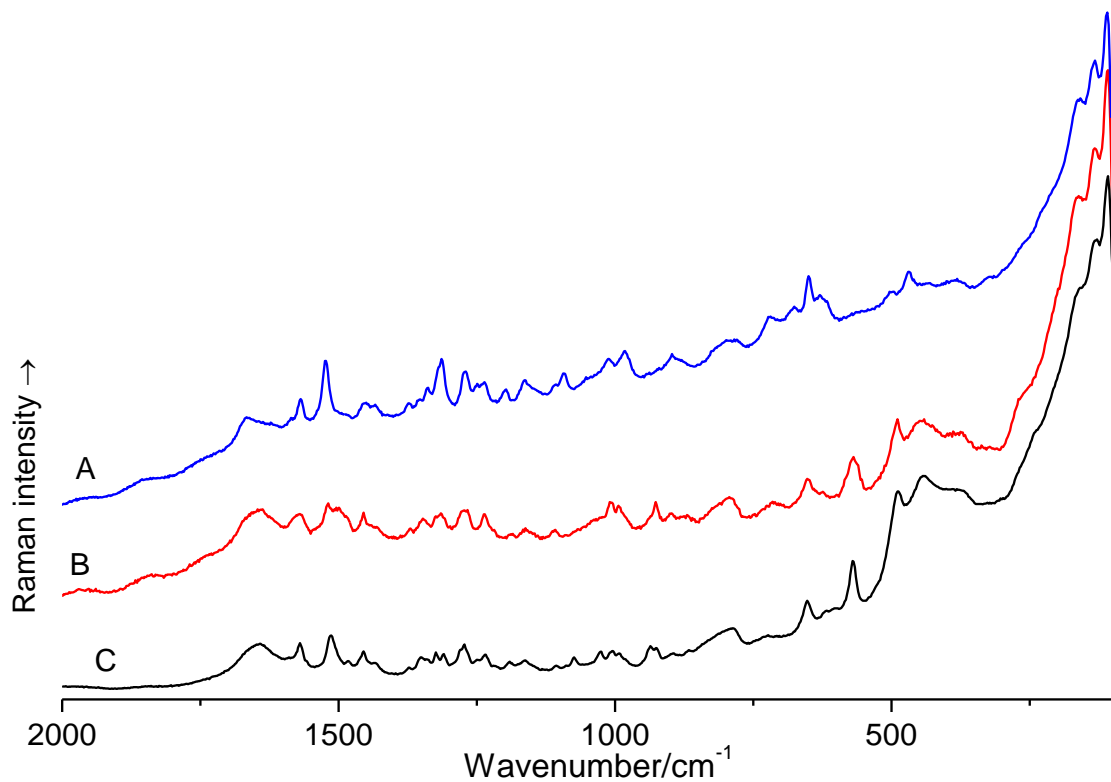


Figure 7.13. Solution state Raman spectra of (A) CAH (B) CHP and (C) CDHP in H₂O.

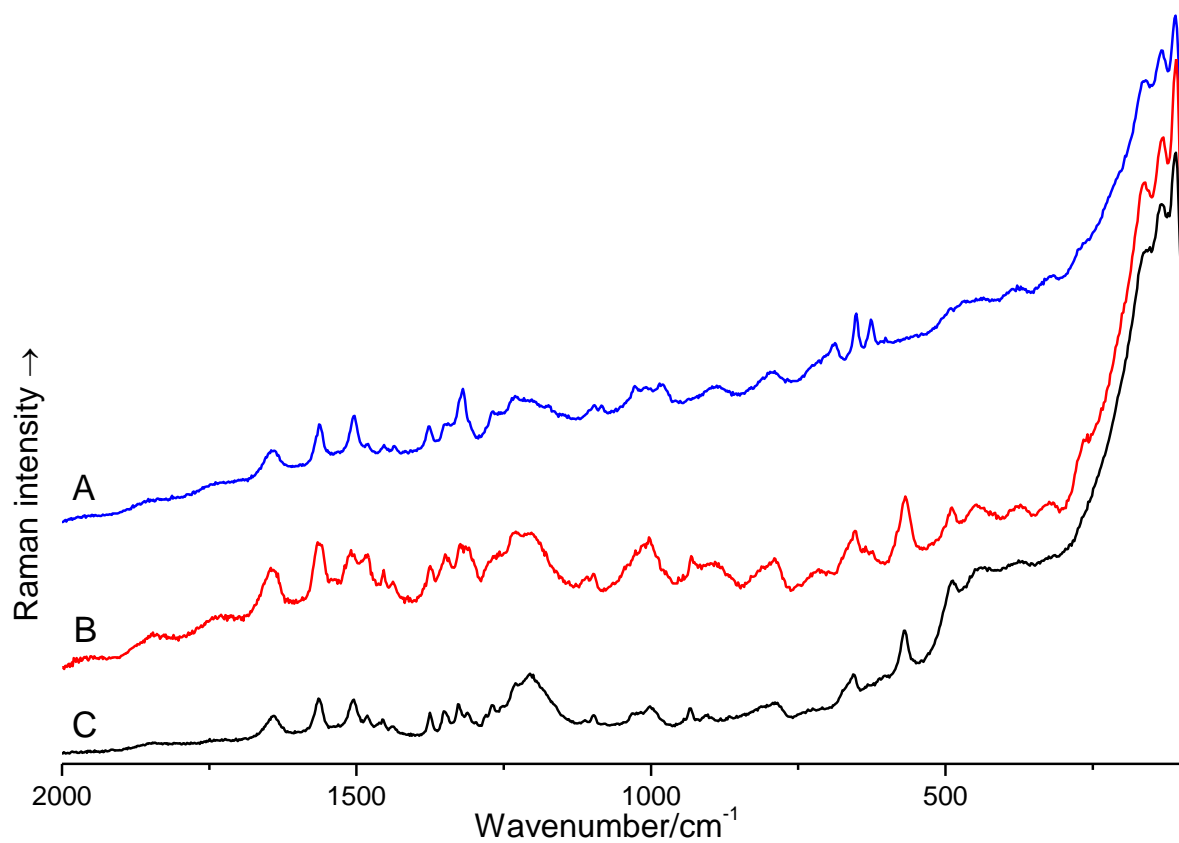


Figure 7.14. Solution state Raman spectra of (A) CAH (B) CHP and (C) CDHP in D₂O.

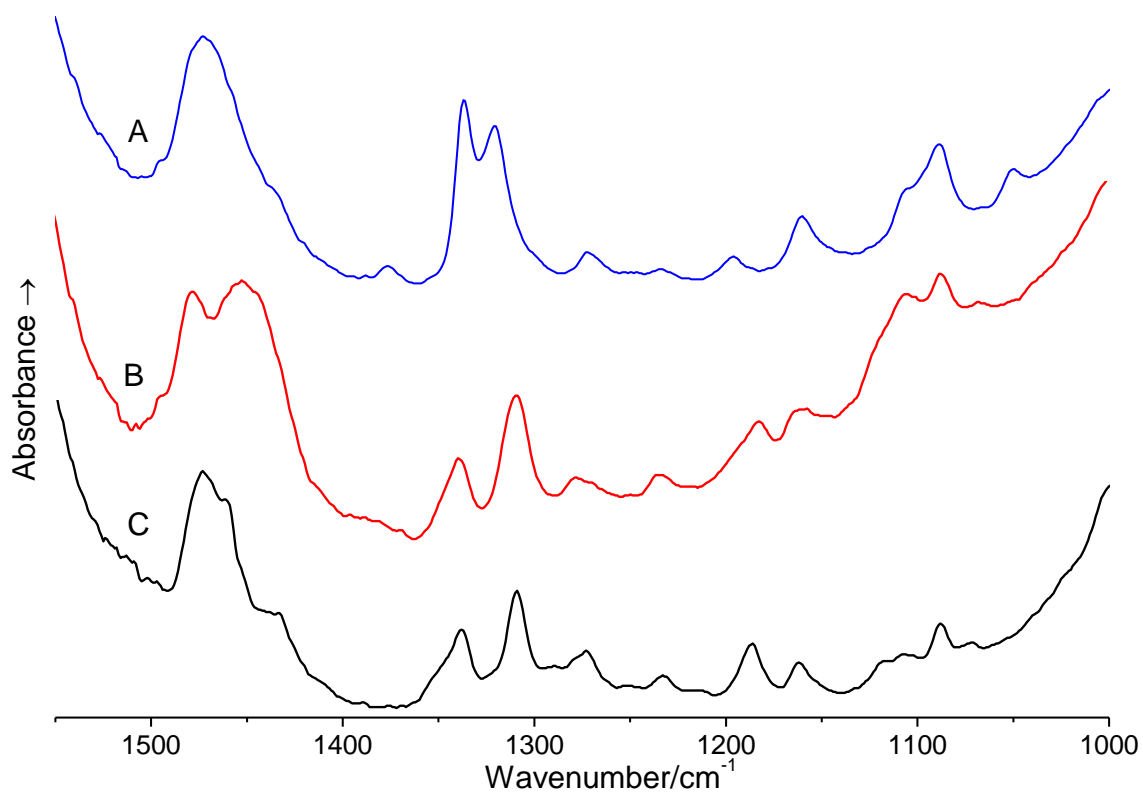


Figure 7.15. Solution state IR spectra of (A) CAH (B) CHP and (C) CDHP in H₂O.

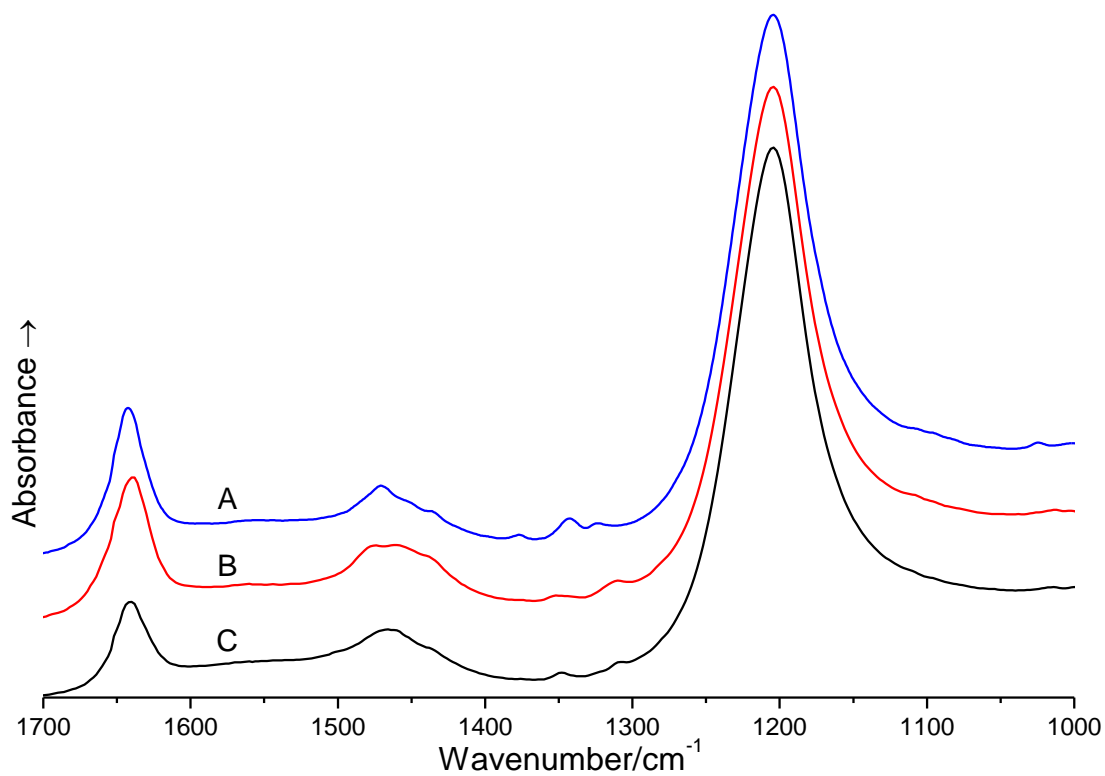


Figure 7.16. Solution state IR spectra of (A) CAH (B) CHP and (C) CDHP in D₂O.

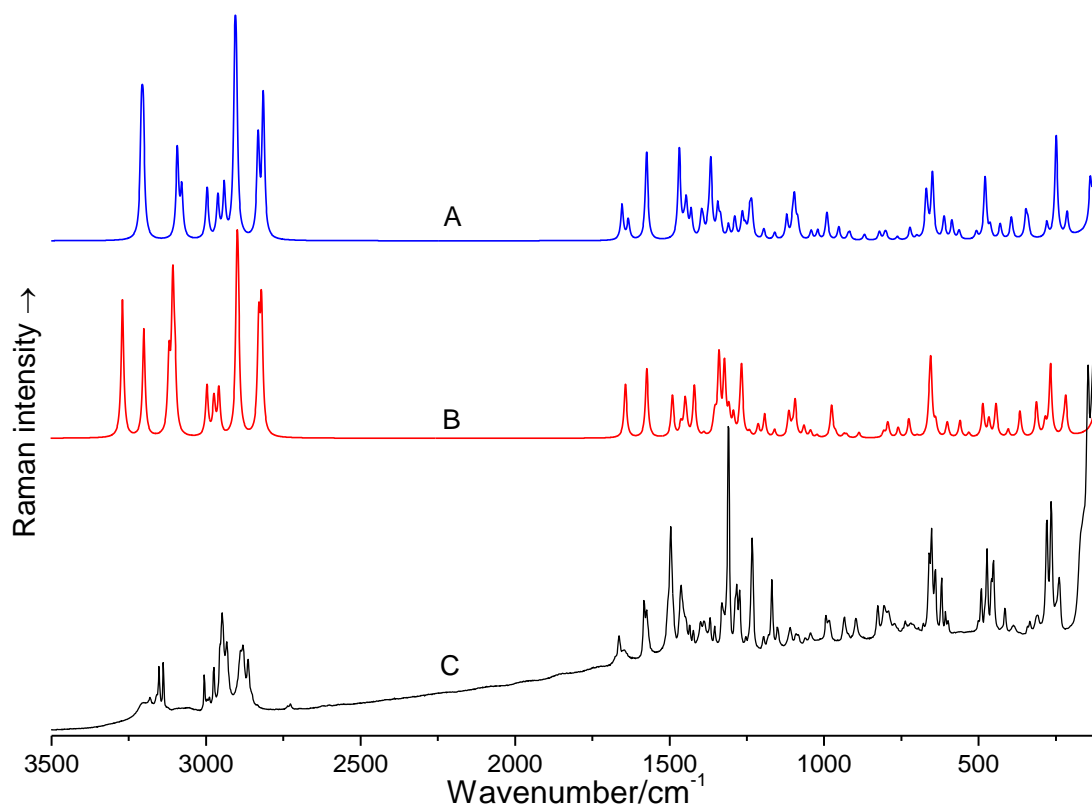


Figure 7.17. Calculated (A) N^ε-protonated (B) N^δ-protonated tautomers and (C) experimental solid state Raman spectra of CAH.

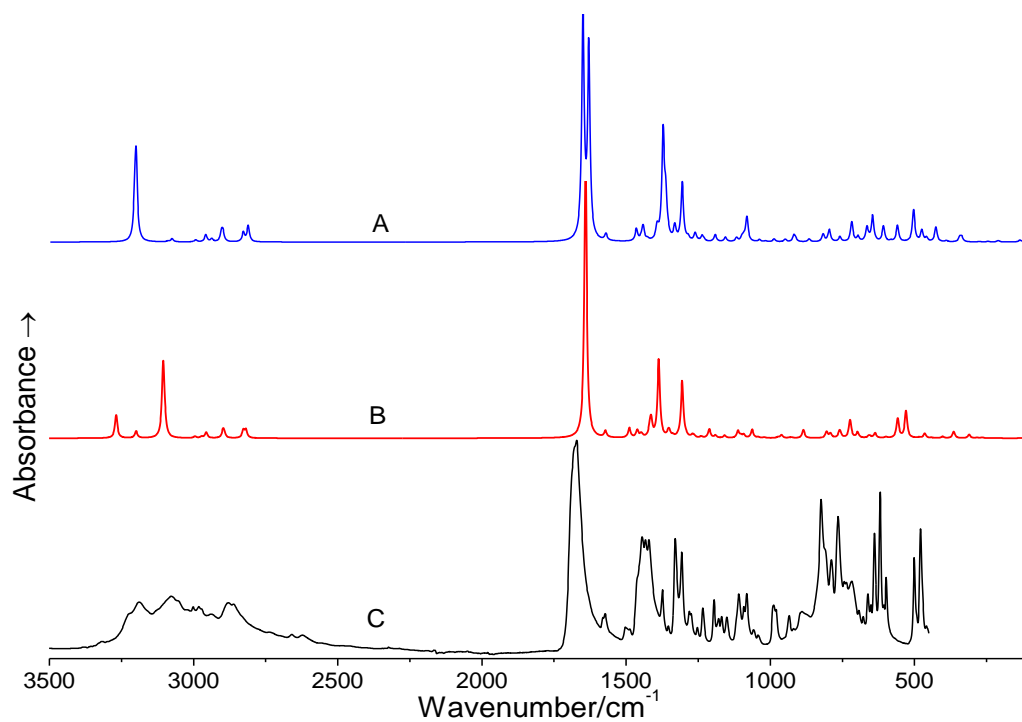


Figure 7.18. Calculated (A) N^{ϵ} -protonated (B) N^{δ} -protonated tautomers and (C) experimental solid state IR spectra of CAH.

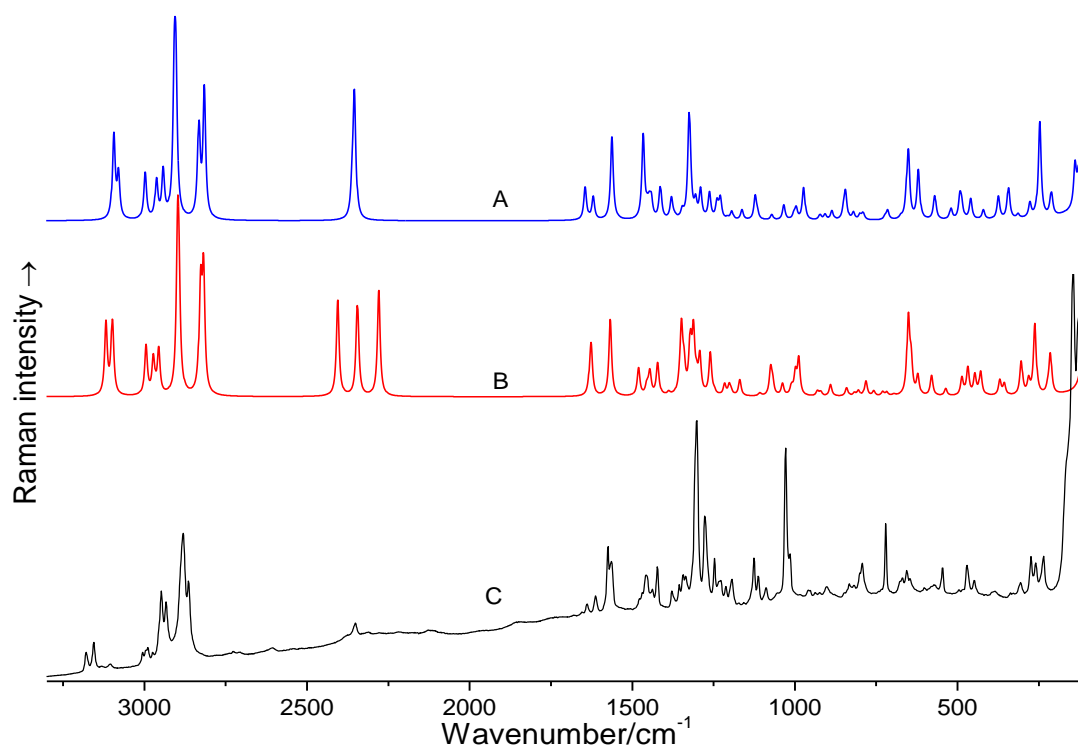


Figure 7.19. Calculated (A) N^{ϵ} -deuterated (B) N^{δ} -deuterated tautomers of CHP and (C) experimental solid state Raman spectra of *N*-deuterated CAH.

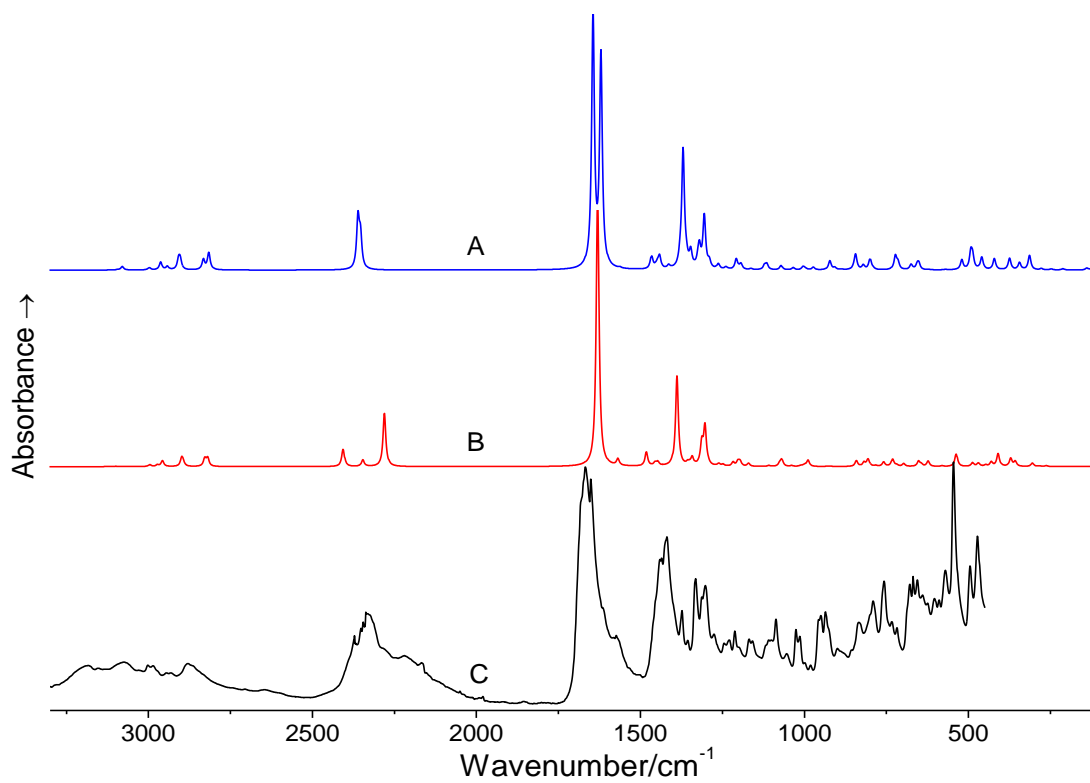


Figure 7.20. Calculated (A) N^{ϵ} -deuterated (B) N^{δ} -deuterated tautomers and (C) experimental solid state IR spectra of *N*-deuterated CAH.

Table 7.7. Experimental and calculated vibrational band wavenumbers (cm⁻¹) for CHP.

IR solid	Raman solid	IR H ₂ O	Raman H ₂ O	IR D ₂ O	Raman D ₂ O		N ^c -protonated		N ^δ -protonated
3282									
3175	3181					3196	99% v(N11H12)	3268	99% v(N17H12)
3135	3135					3208	99% v(N1H2)	3107	97% v(N1H2)
3114	3119								
3090						3092	97% v(C15H16)	3117	98% v(C13H14)
3061						3077	98% v(C13H14)	3098	96% v(C15H16)
3034									
2991	2998					2981	13% v _s (CH _{2a}), 84% v _{as} (CH _{2a})	2981	16% v _s (CH _{2a}), 81% v _{as} (CH _{2a})
	2972					2963	14% v _s (CH _{2b}), 73% v _{as} (CH _{2b})	2973	25% v _s (CH ₂), 76% v _{as} (CH ₂)
2957	2962					2948	20% v _s (CH _{2c}), 71% v _{as} (CH _{2c})	2959	14% v _s (CH _{2b}), 75% v _{as} (CH _{2b})
2940	2935					2941	100% v _{as} (CH ₂)	2936	11% v _s (CH _{2c}), 78% v _{as} (CH _{2c})
2916						2924	81% v _s (CH _{2a}), 13% v _{as} (CH _{2a})	2918	77% v _s (CH _{2a}), 15% v _{as} (CH _{2a})
						2907	99% v _s (CH ₂)	2902	59% v _s (CH _{2b}), 13% v _{as} (CH _{2b}), 23% v _s (CH _{2c})
						2905	69% v _s (CH _{2b}), 15% v _{as} (CH _{2b}), 12% v _s (CH _{2c})	2899	11% v _s (CH _{2b}), 65% v _s (CH _{2c}), 14% v _{as} (CH _{2c})
	2894					2896	68% v _s (CH _{2c}), 21% v _{as} (CH _{2c})	2898	74% v _s (CH ₂), 24% v _{as} (CH ₂)
2882	2881								
2858	2865								
						2830	97% v(C19H20)	2818	92% v(C19H20)
2815						2820	97% v(C3H4)	2814	92% v(C3H4)
2757									
2664									
2631									
1667	1666								
1645	1649		1642	1638	1646	1652	73% v(C21O22)	1641	68% v(C21O22), 12% v(C21N1)
						1605	65% v(C5O6), 14% v(C5N18)	1612	74% v(C5O6), 12% v(C5N18)
1576	1579		1569		1562	1573	44% v(C13C10), 14% v(C7C10)	1572	57% v(C13C10), 14% v(C7C10)

			1518		1509	1512	10% $\delta(\text{CH}_{2b})$, 80% $\delta(\text{CH}_{2c})$	1514	85% $\delta(\text{CH}_{2c})$
1499	1495		1501			1492	27% $\delta(\text{CH}_{2a})$, 53% $\delta(\text{CH}_{2b})$, 17% $\delta(\text{CH}_{2c})$	1491	26% $\delta(\text{CH}_{2a})$, 60% $\delta(\text{CH}_{2b})$ 13% $\delta(\text{CH}_{2c})$
					1481	1485	58% $\delta(\text{CH}_{2a})$, 35% $\delta(\text{CH}_{2b})$	1488	50% $\nu(\text{N11C15})$, 20% $\delta_{ip}(\text{C15H16})$
1467	1471	1478		1476		1469	41% $\nu(\text{C15N17})$, 23% $\delta_{ip}(\text{C15H16})$	1482	61% $\delta(\text{CH}_{2a})$, 31% $\delta(\text{CH}_{2b})$
1456		1452	1453		1454				
1442	1446				1438	1446	19% $\nu(\text{C5N18})$, 45% $\delta(\text{CH}_2)$	1451	18% $\nu(\text{C5N18})$, 21% $\delta_{ip}(\text{N1H2})$
	1425		1428			1434	17% $\nu(\text{C5N18})$, 48% $\delta(\text{CH}_2)$	1443	92% $\delta(\text{CH}_2)$
		1395				1395	22% $\nu(\text{C10N11})$, 16% $\nu(\text{N11C15})$ 11% $\nu(\text{C13C10})$, 23% $\delta_{ip}(\text{N11H12})$	1418	33% $\nu(\text{C15N17})$ 41% $\delta_{ip}(\text{N17H12})$
1406		1388				1390	21% $\nu(\text{C21N1})$, 13% $\nu(\text{C5N18})$ 26% $\delta_{ip}(\text{N1H2})$	1410	12% $\nu(\text{C21N1})$, 31% $\nu(\text{C5N18})$ 16% $\delta_{ip}(\text{N1H2})$
		1381				1371	10% $\nu(\text{N11C15})$, 10% $\omega(\text{CH}_2)$	1378	23% $\nu(\text{C21N1})$, 16% $\nu(\text{C19C21})$ 26% $\delta_{ip}(\text{N1H2})$, 11% $\delta_{ip}(\text{C21O22})$
		1368	1370		1375	1361	66% $\omega(\text{CH}_{2c})$	1362	68% $\omega(\text{CH}_{2c})$
1348	1349		1346	1351	1349	1358	11% $\nu(\text{C15N17})$, 13% $\delta_{ip}(\text{N1H2})$	1341	12% $\nu(\text{N11C15})$, 12% $\nu(\text{N17C13})$, 41% $\omega(\text{CH}_2)$
1335	1336	1339				1337	10% $\delta(\text{C7C3H4})$, 42% $\omega(\text{CH}_2)$	1332	68% $\omega(\text{CH}_{2b})$
						1334	68% $\omega(\text{CH}_{2b})$	1328	10% $\rho(\text{CH})$, 26% $\omega(\text{CH}_{2a})$
					1324	1327	16% $\rho(\text{C7C3H4})$, 27% $\omega(\text{CH}_{2a})$	1321	16% $\nu(\text{C10N11})$, 13% $\nu(\text{N11C15})$, 13% $\tau(\text{CH}_2)$
1311	1312	1309	1314	1310		1305	27% $\rho(\text{C7C3H4})$, 13% $\tau(\text{C7C3H4})$ 13% $\omega(\text{CH}_{2a})$, 11% $\tau(\text{CH}_{2b})$	1302	26% $\rho(\text{C7C3H4})$, 11% $\tau(\text{C7C3H4})$
1295					1229				
1285	1284	1278	1271			1276	36% $\omega(\text{CH})$, 13% $\rho(\text{CH})$, 21% $\tau(\text{CH}_{2a})$	1278	30% $\omega(\text{CH})$, 20% $\rho(\text{CH})$, 15% $\tau(\text{CH}_{2a})$
1270	1272					1263	23% $\delta(\text{C7C3H4})$, 12% $\omega(\text{C7C3H4})$, 12% $\tau(\text{CH}_2)$	1267	18% $\nu(\text{C10N11})$, 15% $\nu(\text{N17C13})$, 14% $\nu(\text{C7C10})$, 13% $\delta_{ip}(\text{C15H16})$
1255	1259					1257	32% $\omega(\text{CH})$, 18% $\rho(\text{CH})$	1263	34% $\omega(\text{CH})$, 20% $\rho(\text{CH})$
1244	1247					1243	14% $\delta_{ip}(\text{C13H14})$, 23% $\delta_{ip}(\text{C15H16})$, 11% $\tau(\text{CH}_2)$, 12% $\tau(\text{CH}_{2c})$	1243	22% $\delta(\text{C7C3H4})$ 13% $\rho(\text{C7C3H4})$, 12% $\tau(\text{C7C3H4})$, 16% $\omega(\text{CH}_2)$
						1242	11% $\delta_{ip}(\text{C15H16})$, 32% $\tau(\text{CH}_{2c})$	1239	40% $\tau(\text{CH}_{2c})$
1234	1234	1234	1235			1233	36% $\nu(\text{N17C13})$, 11% $\nu(\text{C7C10})$ 20% $\delta_{ip}(\text{C13H14})$, 13% $\omega(\text{CH}_2)$	1215	15% $\nu(\text{N18C19})$, 14% $\tau(\text{CH}_{2b})$ 13% $\tau(\text{CH}_{2c})$
					1203	1209	10% $\omega(\text{CH})$, 13% $\omega(\text{CH}_{2a})$, 26% $\tau(\text{CH}_{2b})$	1213	15% $\delta_{ip}(\text{C13H14})$, 13% $\delta_{ip}(\text{C15H16})$, 17% $\tau(\text{CH}_2)$

1197	1197		1189			1194	15% $\tau(\text{CH}_2)$	1194	10% $\nu(\text{N18C19})$ 11% $\omega(\text{CH}_{2a})$ 16% $\tau(\text{CH}_{2a})$ 16% $\tau(\text{CH}_{2b})$
1187	1186	1183				1186	13% $\nu(\text{N18C19})$, 12% $\tau(\text{CH}_{2a})$ 14% $\tau(\text{CH}_{2c})$	1188	13% $\delta_{ip}(\text{C13H14})$, 16% $\delta_{ip}(\text{C15H16})$, 14% $\tau(\text{CH}_2)$
1173	1173								
1163	1161	1160	1161			1166	15% $\nu(\text{N18C19})$, 12% $\tau(\text{CH}_{2a})$, 16% $\rho(\text{CH}_{2c})$	1165	10% $\nu(\text{N18C19})$, 15% $\tau(\text{CH}_{2a})$ 19% $\rho(\text{CH}_{2c})$, 12% $\tau(\text{CH}_{2c})$
1156									
1120						1124	19% $\nu(\text{C19C23})$, 15% $\rho(\text{CH}_{2a})$ 17% $\rho(\text{CH}_{2b})$, 17% $\rho(\text{CH}_{2c})$	1123	23% $\nu(\text{C19C23})$, 12% $\rho(\text{CH}_{2a})$ 17% $\rho(\text{CH}_{2b})$, 16% $\rho(\text{CH}_{2c})$
1110	1103	1106	1110	1105	1109	1120	36% $\nu(\text{N17C13})$, 16% $\delta_{ip}(\text{C13H14})$, 10% Im $\delta_{ip}(\text{ring-1})$	1111	38% $\nu(\text{C15N17})$, 10% $\nu(\text{N1C3})$ 19% $\delta_{ip}(\text{N17H12})$, 10% $\delta_{ip}(\text{C15H16})$
1102									
1088	1095	1088			1098	1095	38% $\nu(\text{N1C3})$, 20% $\tau(\text{CH}_2)$	1095	10% $\nu(\text{C15N17})$, 21% $\nu(\text{N1C3})$ 16% $\nu(\text{C3C7})$, 13% $\delta_{ip}(\text{N17H12})$
1072	1072	1067				1086	35% $\nu(\text{N11C15})$, 34% $\delta_{ip}(\text{N11H12})$	1069	13% $\nu(\text{N17C13})$, 13% $\nu(\text{C3C7})$
1050	1051					1064	13% $\nu(\text{C3C5})$, 17% $\nu(\text{C3C7})$, 10% $\delta(\text{C7C3H4})$	1060	24% $\nu(\text{N17C13})$, 26% $\delta_{ip}(\text{C13H14})$
	1037			1012		1029	11% $\nu(\text{C19C23})$, 13% $\nu(\text{C23C26})$ 16% $\nu(\text{C28C29})$	1032	11% $\nu(\text{C23C26})$, 16% $\nu(\text{C28C29})$, 16% $\nu(\text{C3C7})$
994	1000		1004	1002	1003	1001	25% Im $\delta_{ip}(\text{ring-1})$	997	18% $\nu(\text{C19C23})$, 10% $\nu(\text{C28C29})$
983	986					993	18% $\nu(\text{C28C29})$	981	11% $\nu(\text{C3C5})$, 11% $\nu(\text{C23C26})$ 11% $\nu(\text{C29N18})$, 10% $\rho(\text{CH}_2)$
968	974		972			938	19% $\nu(\text{C23C26})$, 17% $\nu(\text{C3C7})$	969	22% $\nu(\text{C10N11})$, 12% $\nu(\text{C13C10})$, 31% Im $\delta_{ip}(\text{ring-1})$
928	931				932	931	10% $\nu(\text{C19C21})$, 17% $\nu(\text{C29N18})$ 25% $\rho(\text{CH}_2)$	935	12% $\nu(\text{C23C26})$, 24% Im $\delta_{ip}(\text{ring-2})$
922	926					922	12% $\nu(\text{C10N11})$, 61% Im $\delta_{ip}(\text{ring-2})$	933	54% Im $\delta_{ip}(\text{ring-2})$
						915	27% $\nu(\text{C23C26})$, 11% $\nu(\text{C28C29})$	915	28% $\nu(\text{C23C26})$, 16% $\nu(\text{C28C29})$
898	899		897			892	17% $\nu(\text{C28C29})$, 14% $\rho(\text{CH}_{2a})$ 11% $\tau(\text{CH}_{2b})$, 19% $\rho(\text{CH}_{2c})$	904	10% $\nu(\text{C29N18})$, 10% $\rho(\text{CH}_2)$ 13% $\rho(\text{CH}_{2a})$, 13% $\rho(\text{CH}_{2c})$
885						885	11% $\nu(\text{C19C21})$, 10% $\nu(\text{C28C29})$ 13% $\rho(\text{CH}_2)$	884	12% $\nu(\text{C28C29})$, 12% $\rho(\text{CH}_2)$
870	874								
851	846					857	15% $\rho(\text{CH}_2)$, 10% $\delta_{op}(\text{C5O6})$	854	25% $\rho(\text{CH}_{2b})$, 19% Pro $\delta_{ip}(\text{ring-2})$

824	834				855	27% $\rho(\text{CH}_2\text{b})$, 14% Pro $\delta_{\text{ip}}(\text{ring-2})$	824	13% $\delta_{\text{op}}(\text{C5O6})$		
	799		796		791	818	87% $\delta_{\text{op}}(\text{C13H14})$	804	90% $\delta_{\text{op}}(\text{C15H16})$	
789						800	96% $\delta_{\text{op}}(\text{C15H16})$	781	24% pep $\delta_{\text{ip}}(\text{ring-3})$, 27% $\delta_{\text{op}}(\text{C21O22})$	
	785					784	22% pep $\delta_{\text{ip}}(\text{ring-3})$, 32% $\delta_{\text{op}}(\text{C21O22})$	758	24% $\delta_{\text{op}}(\text{C13H14})$, 12% $\delta_{\text{op}}(\text{C10C7})$, 18% $\delta_{\text{op}}(\text{C5O6})$ 20% Im $\delta_{\text{op}}(\text{ring-2})$	
769										
732	733					723	30% $\delta_{\text{op}}(\text{N11H12})$, 25% Im $\delta_{\text{op}}(\text{ring-2})$	720	45% $\delta_{\text{op}}(\text{C13H14})$	
695	695		714			711	34% $\delta_{\text{op}}(\text{N11H12})$, 13% $\delta_{\text{op}}(\text{C5O6})$, 20% Im $\delta_{\text{op}}(\text{ring-1})$	711	77% $\delta_{\text{op}}(\text{N1H2})$, 12% $\delta_{\text{op}}(\text{C13H14})$	
661	664					669	11% $\delta_{\text{op}}(\text{C21O22})$, 31% Im $\delta_{\text{op}}(\text{ring-1})$, 18% Im $\delta_{\text{op}}(\text{ring-2})$	686	12% pep $\delta_{\text{ip}}(\text{ring-3})$, 10% $\delta_{\text{op}}(\text{N1H2})$, 14% Im $\delta_{\text{op}}(\text{ring-1})$ 23% Im $\delta_{\text{op}}(\text{ring-2})$	
						657	11% $\delta_{\text{op}}(\text{N11H12})$, 24% Im $\delta_{\text{op}}(\text{ring-1})$	654	74% Im $\delta_{\text{op}}(\text{ring-1})$	
648	643		653			654	13% $\nu(\text{C7C10})$, 19% pep $\delta_{\text{ip}}(\text{ring-3})$, 10% Im $\delta_{\text{ip}}(\text{ring-1})$	650	18% $\delta_{\text{ip}}(\text{C21O22})$, 12% $\delta_{\text{op}}(\text{C21O22})$	
628	636					624	620	11% $\nu(\text{C7C10})$, 19% $\delta_{\text{op}}(\text{N11H12})$ 13% Im $\delta_{\text{op}}(\text{ring-1})$, 25% Im $\delta_{\text{op}}(\text{ring-2})$	636	15% $\nu(\text{C3C5})$, 12% $\nu(\text{C7C10})$ 11% $\delta_{\text{ip}}(\text{C5O6})$
613	615					610	10% $\rho(\text{CH}_2\text{b})$, 19% Pro $\delta_{\text{ip}}(\text{ring-2})$ 13% $\delta_{\text{ip}}(\text{C21O22})$	617	12% pep $\delta_{\text{ip}}(\text{ring-3})$, 15% Pro $\delta_{\text{ip}}(\text{ring-2})$, 18% $\delta_{\text{op}}(\text{C5O6})$ 15% Im $\delta_{\text{op}}(\text{ring-2})$	
580	581					568	555	11% $\nu(\text{C3C5})$, 18% Pro $\delta_{\text{ip}}(\text{ring-2})$	579	31% Pro $\delta_{\text{ip}}(\text{ring-2})$, 12% $\delta_{\text{op}}(\text{C5O6})$
509	510		517			518	518	10% $\nu(\text{C7C10})$, 14% $\delta_{\text{op}}(\text{C5O6})$	527	95% $\delta_{\text{op}}(\text{N17H12})$
484	485		490			489	494	18% Pro $\delta_{\text{ip}}(\text{ring-1})$, 31% $\delta_{\text{op}}(\text{N1H2})$	479	42% pep $\delta_{\text{ip}}(\text{ring-1})$, 16% Pro $\delta_{\text{ip}}(\text{ring-1})$
475										
475						474	10% $\nu(\text{C3C5})$, 58% pep $\delta_{\text{ip}}(\text{ring-1})$	465	10% $\nu(\text{C19C21})$, 10% $\omega(\text{C7C3H4})$, 12% Pro $\delta_{\text{ip}}(\text{ring-1})$, 17% $\delta_{\text{ip}}(\text{C21O22})$	
	452		442			447				
	420					429	12% $\nu(\text{C19C21})$, 11% pep $\delta_{\text{ip}}(\text{ring-1})$, 10% $\delta_{\text{ip}}(\text{C21O22})$, 41% $\delta_{\text{op}}(\text{N1H2})$	444	19% pep $\delta_{\text{ip}}(\text{ring-1})$, 19% pep $\delta_{\text{ip}}(\text{ring-1})$	
						408	40% pep $\delta_{\text{ip}}(\text{ring-1})$, 11% pep $\delta_{\text{op}}(\text{ring-2})$	418	31% pep $\delta_{\text{ip}}(\text{ring-1})$, 11% pep $\delta_{\text{op}}(\text{ring-3})$	
	367		373			373	345	14% pep $\delta_{\text{ip}}(\text{ring-1})$, 10% $\delta_{\text{ip}}(\text{C5O6})$, 38% $\delta_{\text{ip}}(\text{C10C7})$	352	10% $\nu(\text{C5N18})$, 25% $\delta_{\text{ip}}(\text{C5O6})$
	350					324	336	16% $\delta_{\text{ip}}(\text{C5O6})$, 10% $\tau(\text{C3C7})$	315	27% $\delta_{\text{ip}}(\text{C10C7})$, 26% $\delta_{\text{op}}(\text{C10C7})$, 14% Im $\delta_{\text{op}}(\text{ring-2})$
	296					265	13% $\delta_{\text{ip}}(\text{C21O22})$, 23% Pro $\delta_{\text{op}}(\text{ring-2})$, 26% Ring buckl	270	11% $\delta_{\text{ip}}(\text{C21O22})$, 18% $\delta_{\text{ip}}(\text{C10C7})$	

	262		263		259	253	11% $\nu(\text{C3C7})$, 13% $\omega(\text{C7C3H4})$ 12% $\delta(\text{C3C7C10})$, 23% $\delta_{\text{op}}(\text{C10C7})$, 12% Im $\delta_{\text{op}}(\text{ring-2})$	262	10% pep $\delta_{\text{ip}}(\text{ring-1})$, 13% pep $\delta_{\text{op}}(\text{ring-3})$, 10% Pro $\delta_{\text{op}}(\text{ring-2})$ 10% Ring buckl
						219	10% $\tau(\text{C7C3H4})$, 35% Pro $\delta_{\text{op}}(\text{ring-1})$, 17% Pro $\delta_{\text{op}}(\text{ring-2})$	214	12% $\rho(\text{C7C3H4})$, 16% $\tau(\text{C7C3H4})$, 11% Pro $\delta_{\text{op}}(\text{ring-1})$, 10% Pro $\delta_{\text{op}}(\text{ring-2})$, 22% Ring buckl
	199					200	12% $\rho(\text{C7C3H4})$, 20% $\tau(\text{C7C3H4})$, 16% $\delta_{\text{ip}}(\text{C10C7})$, 23% Pro $\delta_{\text{op}}(\text{ring-1})$	189	41% Pro $\delta_{\text{op}}(\text{ring-1})$, 22% Pro $\delta_{\text{op}}(\text{ring-2})$
	174		166			161	14% Pro $\delta_{\text{op}}(\text{ring-2})$, 60% Ring buckl	158	14% Pro $\delta_{\text{op}}(\text{ring-2})$, 60% Ring buckl
	146					145	11% $\delta(\text{C3C7C10})$, 10% $\delta_{\text{op}}(\text{C10C7})$, 22% pep $\delta_{\text{op}}(\text{ring-1})$ 25% pep $\delta_{\text{op}}(\text{ring-2})$, 22% $\tau(\text{C3C7})$	118	23% pep $\delta_{\text{op}}(\text{ring-1})$, 45% pep $\delta_{\text{op}}(\text{ring-2})$, 10% Ring buckl
	126 108		134 108			130 108	15% $\delta_{\text{op}}(\text{C10C7})$, 36% pep $\delta_{\text{op}}(\text{ring-2})$, 26% Ring buckl	105	38% pep $\delta_{\text{op}}(\text{ring-1})$, 48% pep $\delta_{\text{op}}(\text{ring-2})$
	95					93	21% pep $\delta_{\text{op}}(\text{ring-1})$, 13% Pro $\delta_{\text{op}}(\text{ring-1})$, 39% $\tau(\text{C7C10})$	84	24% $\delta(\text{C3C7C10})$, 17% pep $\delta_{\text{op}}(\text{ring-1})$, 14% $\tau(\text{C7C10})$
	81					73	10% pep $\delta_{\text{op}}(\text{ring-1})$, 12% $\tau(\text{C3C7})$ 49% $\tau(\text{C7C10})$	69	12% pep $\delta_{\text{op}}(\text{ring-3})$, 10% Pro $\delta_{\text{op}}(\text{ring-1})$, 23% $\tau(\text{C3C7})$, 40% $\tau(\text{C7C10})$
						45	14% $\delta(\text{C3C7C10})$, 16% $\delta_{\text{op}}(\text{C10C7})$, 10% pep $\delta_{\text{op}}(\text{ring-1})$, 15% pep $\delta_{\text{op}}(\text{ring-2})$, 36% $\tau(\text{C3C7})$	47	12% pep $\delta_{\text{op}}(\text{ring-2})$, 58% $\tau(\text{C3C7})$, 24% $\tau(\text{C7C10})$
						31	10% $\omega(\text{C7C3H4})$, 19% pep $\delta_{\text{op}}(\text{ring-2})$, 49% pep $\delta_{\text{op}}(\text{ring-3})$, 10% Ring buckl	32	40% pep $\delta_{\text{op}}(\text{ring-3})$, 17% Ring buckl 17% $\tau(\text{C7C10})$

Table 7.8. Experimental and calculated vibrational band wavenumbers (cm^{-1}) for CDHP.

IR solid	Raman solid	IR H ₂ O	Raman H ₂ O	IR D ₂ O	Raman D ₂ O	Calc.	N ^c -protonated	Calc.	N ^d -protonated
3421									
3313	3313					3113	98% $\nu(\text{N11H12})$	3268	99% $\nu(\text{N17H12})$
3299									
3168	3170					3201	100% $\nu(\text{N11H2})$	3146	100% $\nu(\text{N11H2})$
3139	3145								
3091	3096					3093	96% $\nu(\text{C15H16})$	3118	98% $\nu(\text{C13H14})$
						3081	97% $\nu(\text{C13H14})$	3098	98% $\nu(\text{C15H16})$

3056 3031									
2995	2999								
2981	2983					2985	17% $v_s(\text{CH}_{2a})$, 80% $v_{as}(\text{CH}_{2a})$	2983	18% $v_s(\text{CH}_{2a})$, 79% $v_{as}(\text{CH}_{2a})$
	2973								
2965	2966					2965	12% $v_s(\text{CH}_{2b})$, 74% $v_{as}(\text{CH}_{2b})$	2960	12% $v_s(\text{CH}_{2b})$, 75% $v_{as}(\text{CH}_{2b})$
	2947					2944	82% $v_{as}(\text{CH}_{2c})$	2947	22% $v_s(\text{CH}_2)$, 77% $v_{as}(\text{CH}_2)$
2935	2941					2935	11% $v_s(\text{C}_3\text{H}_4)$, 24% $v_s(\text{CH}_2)$, 65% $v_{as}(\text{CH}_2)$	2934	11% $v_s(\text{CH}_{2b})$, 85% $v_{as}(\text{CH}_{2c})$
						2927	88% $v_s(\text{C}_3\text{H}_4)$	2914	68% $v_s(\text{CH}_{2a})$, 14% $v_{as}(\text{CH}_{2a})$, 15% $v_s(\text{CH}_{2b})$
						2919	72% $v_s(\text{CH}_{2a})$, 14% $v_{as}(\text{CH}_{2a})$, 12% $v_s(\text{CH}_{2b})$	2911	94% $v_s(\text{C}_3\text{H}_4)$
						2911	94% $v_s(\text{CH}_{2c})$	2907	83% $v_s(\text{CH}_{2c})$
	2901					2907	66% $v_s(\text{CH}_{2b})$, 19% $v_{as}(\text{CH}_{2b})$	2903	56% $v_s(\text{CH}_{2b})$, 15% $v_{as}(\text{CH}_{2b})$, 16% $v_s(\text{CH}_{2c})$
	2887								
2871	2876					2859	69% $v_s(\text{CH}_2)$, 30% $v_{as}(\text{CH}_2)$	2875	73% $v_s(\text{CH}_2)$, 23% $v_{as}(\text{CH}_2)$
2845									
2820	2858					2835	99% $v(\text{C}_{19}\text{H}_{20})$	2825	99% $v(\text{C}_{19}\text{H}_{20})$
2734 2674									
2639 2604 2566 2501									
1815									
1648	1650		1643	1641	1638	1648	71% $v(\text{C}_{21}\text{O}_{22})$, 10% $\delta_{ip}(\text{N}_{11}\text{H}_2)$	1636	66% $v(\text{C}_{21}\text{O}_{22})$, 12% $v(\text{N}_{11}\text{C}_{21})$ 10% $\delta_{ip}(\text{N}_{11}\text{H}_2)$
	1633								
						1602	57% $v(\text{C}_5\text{O}_6)$, 17% $v(\text{N}_{18}\text{C}_5)$	1610	71% $v(\text{C}_5\text{O}_6)$, 14% $v(\text{N}_{18}\text{C}_5)$
1580	1570		1568		1562	1569	40% $v(\text{C}_{13}\text{C}_{10})$, 13% $v(\text{C}_7\text{C}_{10})$, 11% $\delta_{ip}(\text{N}_{11}\text{H}_{12})$	1568	57% $v(\text{C}_{13}\text{C}_{10})$, 14% $v(\text{C}_7\text{C}_{10})$
1509	1512		1512		1502	1512	11% $\delta(\text{CH}_{2b})$, 81% $\delta(\text{CH}_{2c})$	1513	11% $\delta(\text{CH}_{2b})$, 82% $\delta(\text{CH}_{2c})$

1495	1498					1491	34% $\delta(\text{CH}_{2a})$, 55% $\delta(\text{CH}_{2b})$, 17% $\delta(\text{CH}_{2c})$	1491	11% $\nu(\text{C}23\text{C}26)$, 13% $\tau(\text{CH}_{2a})$, 58% $\delta(\text{CH}_{2b})$, 15% $\delta(\text{CH}_{2c})$, 12% Ring buckl
	1484	1472	1481	1466	1479	1483	81% $\delta(\text{CH}_{2a})$, 33% $\delta(\text{CH}_{2b})$, 10% Pro $\delta_{ip}(\text{ring-1})$	1487	48% $\nu(\text{N}11\text{C}15)$, 20% $\delta_{ip}(\text{C}15\text{H}16)$
		1460			1457	1469	24% $\nu(\text{C}15\text{N}17)$, 11% $\nu(\text{N}18\text{C}5)$, 14% $\delta_{ip}(\text{C}15\text{H}16)$	1482	36% $\delta(\text{CH}_{2a})$, 19% $\omega(\text{CH}_{2a})$, 30% $\delta(\text{CH}_{2b})$, 23% Pro $\delta_{ip}(\text{ring-2})$
1453	1454		1453			1464	14% $\nu(\text{C}15\text{N}17)$, 15% $\nu(\text{N}18\text{C}5)$, 11% $\delta(\text{CH}_2)$	1462	10% $\nu(\text{N}1\text{C}21)$, 21% $\nu(\text{N}18\text{C}5)$, 14% $\delta_{ip}(\text{N}1\text{H}2)$
						1448	85% $\delta(\text{CH}_2)$	1442	94% $\delta(\text{CH}_2)$
1437	1439	1433	1432		1439	1426	10% $\nu(\text{C}5\text{O}6)$, 19% $\nu(\text{N}1\text{C}21)$, 20% $\nu(\text{N}18\text{C}5)$	1429	16% $\nu(\text{N}1\text{C}21)$, 29% $\nu(\text{N}18\text{C}5)$
1391	1396	1388				1404	14% $\nu(\text{C}10\text{N}11)$, 20% $\nu(\text{N}11\text{C}15)$, 14% $\nu(\text{C}13\text{C}10)$, 33% $\delta_{ip}(\text{N}11\text{H}12)$	1418	33% $\nu(\text{C}15\text{N}17)$, 40% $\delta_{ip}(\text{N}17\text{H}12)$
			1374		1376	1369	11% $\nu(\text{C}19\text{C}21)$, 30% $\delta_{ip}(\text{N}1\text{H}2)$, 10% $\omega(\text{CH}_{2a})$	1379	16% $\nu(\text{C}19\text{C}21)$, 42% $\delta_{ip}(\text{N}1\text{H}2)$
						1364	13% $\nu(\text{C}10\text{N}11)$, 14% $\nu(\text{C}15\text{N}17)$, 29% $\omega(\text{CH}_{2c})$	1361	68% $\omega(\text{CH}_{2c})$
1347	1351		1351	1347	1349	1360	34% $\omega(\text{CH}_{2c})$	1343	15% $\nu(\text{N}11\text{C}15)$, 11% $\nu(\text{N}17\text{C}13)$, 37% $\omega(\text{CH}_2)$
		1337				1333	10% $\omega(\text{CH}_{2a})$, 13% $\tau(\text{CH}_{2a})$, 40% $\omega(\text{CH}_{2b})$, 12% $\tau(\text{CH}_{2b})$	1331	71% $\omega(\text{CH}_{2b})$
1324	1327		1324		1326	1332	20% $\omega(\text{CH}_{2a})$, 32% $\omega(\text{CH}_{2b})$	1329	13% $\rho(\text{CH})$, 30% $\delta(\text{CH}_{2a})$, 11% $\omega(\text{CH}_{2a})$
						1320	27% $\omega(\text{CH}_2)$, 22% $\omega(\text{CH}_{2a})$	1315	29% $\delta(\text{C}7\text{C}3\text{H}4)$, 13% $\tau(\text{CH}_2)$
1300	1303	1309	1310	1309	1307	1296	20% $\rho(\text{C}7\text{C}3\text{H}4)$, 14% $\tau(\text{CH}_2)$	1305	19% $\rho(\text{C}7\text{C}3\text{H}4)$
1278	1284	1289				1280	16% $\omega(\text{CH})$, 19% $\rho(\text{CH})$, 10% $\tau(\text{CH}_{2a})$	1279	16% $\omega(\text{CH})$, 31% $\rho(\text{CH})$, 19% $\tau(\text{CH}_{2a})$, 14% $\tau(\text{CH}_{2b})$
	1270	1273	1273		1271	1272	15% $\delta(\text{C}7\text{C}3\text{H}4)$, 26% $\omega(\text{CH})$, 15% $\omega(\text{CH}_2)$	1269	47% $\omega(\text{CH})$, 14% $\rho(\text{CH})$
1266						1265	11% $\nu(\text{N}1\text{C}21)$, 22% $\omega(\text{CH})$, 21% $\rho(\text{CH})$	1268	18% $\nu(\text{C}10\text{N}11)$, 17% $\nu(\text{N}17\text{C}13)$, 15% $\nu(\text{C}7\text{C}10)$, 15% $\delta_{ip}(\text{C}15\text{H}16)$, 10% $\omega(\text{CH}_2)$
	1238					1238	10% $\omega(\text{CH})$, 40% $\tau(\text{CH}_{2c})$	1242	23% $\delta(\text{C}7\text{C}3\text{H}4)$, 10% $\omega(\text{C}7\text{C}3\text{H}4)$, 14% $\omega(\text{CH}_2)$
1233		1233	1236		1229	1234	33% $\nu(\text{N}17\text{C}13)$, 10% $\nu(\text{C}7\text{C}10)$, 15% $\delta_{ip}(\text{C}15\text{H}16)$	1235	11% $\tau(\text{CH}_{2a})$, 44% $\tau(\text{CH}_{2c})$
						1229	31% $\delta_{ip}(\text{C}13\text{H}14)$, 20% $\delta_{ip}(\text{C}15\text{H}16)$, 11% $\omega(\text{CH}_2)$	1219	19% $\nu(\text{N}18\text{C}19)$, 12% $\omega(\text{CH}_{2a})$, 13% $\tau(\text{CH}_{2b})$, 18% $\tau(\text{CH}_{2c})$

1214	1216	1211			1200	1215	15% v(N18C19), 10% v(C29N18), 20% τ (CH _{2b}), 14% τ (CH _{2c})	1207	18% δ_{ip} (C13H14), 17% δ_{ip} (C15H16), 10% ω (CH ₂), 23% τ (CH ₂)
1183	1190	1186	1192			1194	11% v(N18C19), 22% τ (CH _{2a}), 12% τ (CH _{2b})	1195	22% ω (CH _{2a}), 16% τ (CH _{2b}), 10% Pro δ_{ip} (ring-1)
1175	1177					1166	28% τ (CH ₂)	1179	12% δ_{ip} (C15H16), 10% τ (C7C3H4), 27% τ (CH ₂)
1160	1161	1161	1161			1164	18% τ (CH ₂), 11% ρ (CH _{2c})	1162	12% v(N18C19), 22% τ (CH _{2a}), 15% ρ (CH _{2c}), 12% τ (CH _{2c})
1117	1120	1117				1122	22% v(C19C23), 16% ρ (CH _{2b}), 15% ρ (CH _{2c})	1121	17% v(C19C23), 22% ρ (CH _{2a}), 15% ρ (CH _{2b}), 14% ρ (CH _{2c})
						1121	14% v(N11C15), 27% v(N17C13), 12% δ_{ip} (C13H14) 15% δ_{ip} (C15H16)	1111	26% v(C15N17), 14% v(N1C3), 13% δ_{ip} (N17H12)
1102	1099	1107	1106		1099	1107	25% v(N11C15), 10% v(N17C13), 24% δ_{ip} (N11H12), 11% δ_{ip} (C13H14)	1099	21% v(C15N17), 45% δ_{ip} (N17H12), 15% v(N1C3)
1089		1087				1090	26% v(N1C3), 14% τ (CH ₂)	1067	11% v(C3C5), 10% v(C29N18), 12% v(C3C7)
1068	1072	1071	1073			1063	10% v(C3C5)	1063	36% v(N17C13), 32% δ_{ip} (C13H14)
1024	1026		1025	1014		1019	34% v(C3C7)	1026	34% v(C3C7), 11% ρ (CH ₂)
	1009		1002	1000	1001	1001	12% v(C23C26), 20% v(C28C29), 14% ρ (CH _{2a})	999	13% v(C23C26), 17% v(C28C29), 16% ω (C7C3H4), 10% ω (CH _{2b}), 15% pep δ_{ip} (ring-3)
997	999					999	12% v(C10N11), 28% Im δ_{ip} (ring-1)	990	19% v(C19C23), 18% ρ (CH ₂), 14% δ (CH _{2a}), 11% pep δ_{ip} (ring-1)
946	951					979	20% v(C19C23), 10% v(C3C7), 10% ω (C7C3H4), 11% ρ (CH _{2a})	967	22% v(C10N11), 12% v(C13C10), 33% Im δ_{ip} (ring-1)
938	934		936		932	926	11% v(C19C21), 19% v(C23C26), 16% C29N18 v	936	12% v(C23C26), 27% Im δ_{ip} (ring-2)
923	924		926			924	76% Im δ_{ip} (ring-2)	933	50% Im δ_{ip} (ring-2)
906	901					923	31% v(C23C26), 13% v(C28C29), 11% ρ (CH ₂)	915	21% v(C23C26), 25% v(C28C29), 19% δ (CH _{2a})
						899	11% τ (CH _{2b}), 22% ρ (CH _{2c})	900	18% v(C28C29), 11% ρ (CH _{2a}), 12% τ (CH _{2a}), 14% ρ (CH _{2c})
887			893			888	24% v(C28C29), 18% ρ (CH ₂), 25% ρ (CH _{2a})	883	11% v(C28C29) 11% v(C29N18), 11% v(C3C7), 13% ρ (CH ₂)
857	864								

838	838					843	30% $\rho(\text{CH}_2\text{b})$, 12% $\rho(\text{CH}_2\text{c})$, 19% Pro $\delta_{\text{ip}}(\text{ring-2})$	847	25% $\rho(\text{CH}_2\text{b})$, 12% Pro $\delta_{\text{ip}}(\text{ring-2})$, 11% Ring buckl
819	824					821	81% $\delta_{\text{op}}(\text{C13H14})$	807	35% $\delta_{\text{op}}(\text{C15H16})$
						802	33% pep $\delta_{\text{ip}}(\text{ring-3})$, 13% $\delta_{\text{op}}(\text{C13H14})$	800	57% $\delta_{\text{op}}(\text{C15H16})$
789	791		788		788	798	97% $\delta_{\text{op}}(\text{C15H16})$	783	23% pep $\delta_{\text{ip}}(\text{ring-3})$, 24% $\delta_{\text{op}}(\text{C21O22})$
757	759					772	12% pep $\delta_{\text{ip}}(\text{ring-1})$, 26% $\delta_{\text{op}}(\text{C21O22})$	743	49% $\delta_{\text{op}}(\text{C13H14})$, 10% $\delta_{\text{op}}(\text{C10C7})$, 14% Im $\delta_{\text{op}}(\text{ring-2})$
726	731					744	74% $\delta_{\text{op}}(\text{N11H12})$	721	13% pep $\delta_{\text{ip}}(\text{ring-1})$, 11% pep $\delta_{\text{ip}}(\text{ring-3})$
						741	61% $\delta_{\text{op}}(\text{C5O6})$	700	37% $\delta_{\text{op}}(\text{C13H14})$, 15% $\delta_{\text{op}}(\text{C5O6})$, 10% Im $\delta_{\text{op}}(\text{ring-1})$, 21% Im $\delta_{\text{op}}(\text{ring-2})$
701	701					704	15% $\nu(\text{C7C10})$, 17% pep $\delta_{\text{ip}}(\text{ring-3})$, 16% Im $\delta_{\text{ip}}(\text{ring-1})$	690	83% $\delta_{\text{op}}(\text{N1H2})$
						670	75% Im $\delta_{\text{op}}(\text{ring-1})$, 19% Im $\delta_{\text{op}}(\text{ring-2})$	661	14% $\delta_{\text{op}}(\text{C5O6})$, 56% Im $\delta_{\text{op}}(\text{ring-1})$
658									
652	654		653		653	659	14% $\delta_{\text{op}}(\text{N1H2})$, 35% $\delta_{\text{op}}(\text{C21O22})$	646	13% $\delta_{\text{ip}}(\text{C21O22})$, 22% $\delta_{\text{op}}(\text{C21O22})$, 17% Ring buckl
644									
	626		618			631	11% $\delta_{\text{op}}(\text{N11H12})$, 15% Im $\delta_{\text{op}}(\text{ring-1})$, 44% Im $\delta_{\text{op}}(\text{ring-2})$	644	13% $\nu(\text{C3C7})$, 11% Im $\delta_{\text{ip}}(\text{ring-1})$, 25% Im $\delta_{\text{op}}(\text{ring-1})$, 17% Im $\delta_{\text{op}}(\text{ring-2})$
623	622					610	14% Pro $\delta_{\text{ip}}(\text{ring-2})$, 13% $\delta_{\text{ip}}(\text{C5O6})$, 18% $\delta_{\text{ip}}(\text{C21O22})$	624	12% $\nu(\text{C3C5})$, 13% Pro $\delta_{\text{ip}}(\text{ring-1})$, 14% $\delta_{\text{ip}}(\text{C5O6})$, 10% $\delta_{\text{op}}(\text{C5O6})$, 16% Im $\delta_{\text{op}}(\text{ring-2})$
569	572		569		567	573	10% $\nu(\text{C3C5})$, 31% Pro $\delta_{\text{ip}}(\text{ring-2})$, 13% $\delta_{\text{op}}(\text{N1H2})$	584	40% Pro $\delta_{\text{ip}}(\text{ring-2})$
525	529					559	66% $\delta_{\text{op}}(\text{N1H2})$	528	95% $\delta_{\text{op}}(\text{N17H12})$
483	483		488		487	483	13% $\nu(\text{C19C21})$, 16% pep $\delta_{\text{ip}}(\text{ring-1})$, 19% pep $\delta_{\text{ip}}(\text{ring-1})$, 25% Pro $\delta_{\text{ip}}(\text{ring-1})$	481	12% $\nu(\text{C19C21})$, 12% pep $\delta_{\text{ip}}(\text{ring-1})$, 42% Pro $\delta_{\text{ip}}(\text{ring-1})$
	447		443		439	450	10% $\nu(\text{N18C19})$, 20% pep $\delta_{\text{ip}}(\text{ring-1})$, 43% pep $\delta_{\text{ip}}(\text{ring-1})$	459	11% $\omega(\text{C7C3H4})$, 21% pep $\delta_{\text{ip}}(\text{ring-1})$, 18% pep $\delta_{\text{ip}}(\text{ring-1})$
	437					432	12% pep $\delta_{\text{ip}}(\text{ring-1})$, 20% $\delta_{\text{ip}}(\text{C21O22})$, 11% $\delta_{\text{op}}(\text{C21O22})$, 10% Pro $\delta_{\text{op}}(\text{ring-2})$	445	26% pep $\delta_{\text{ip}}(\text{ring-1})$, 15% $\delta_{\text{ip}}(\text{C21O22})$
						401	19% $\omega(\text{C7C3H4})$, 10% $\delta(\text{C3C7C10})$, 22% $\delta_{\text{ip}}(\text{C10C7})$	425	13% $\omega(\text{C7C3H4})$, 17% pep $\delta_{\text{ip}}(\text{ring-1})$, 11% $\delta_{\text{ip}}(\text{C21O22})$, 13% Pro $\delta_{\text{op}}(\text{ring-2})$

	378		372						
	348					354	14% pep $\delta_{ip}(\text{ring-1})$, 30% $\delta_{ip}(\text{C5O6})$	352	15% pep $\delta_{ip}(\text{ring-1})$, 31% $\delta_{ip}(\text{C5O6})$
	320 314								
	303					305	10% $\nu(\text{C3C7})$, 12% $\rho(\text{C7C3H4})$, 17% $\tau(\text{C7C3H4})$, 12% $\delta_{ip}(\text{C10C7})$	305	10% $\delta(\text{C3C7C10})$, 37% $\delta_{op}(\text{C10C7})$, 19% Im $\delta_{op}(\text{ring-2})$
	270					281	13% $\delta(\text{C3C7C10})$, 10% $\delta_{ip}(\text{C10C7})$, 38% $\delta_{op}(\text{C10C7})$, 14% Im $\delta_{op}(\text{ring-2})$	283	46% $\delta_{ip}(\text{C10C7})$
	240					264	11% $\delta_{ip}(\text{C21O22})$, 20% Pro $\delta_{op}(\text{ring-2})$, 24% Ring buckl	255	16% Pro $\delta_{op}(\text{ring-2})$, 31% Ring buckl
						227	13% $\rho(\text{C7C3H4})$, 17% $\tau(\text{C7C3H4})$, 17% $\delta_{ip}(\text{C10C7})$, 14% Pro $\delta_{op}(\text{ring-1})$, 21% Ring buckl	213	10% $\rho(\text{C7C3H4})$, 14% $\tau(\text{C7C3H4})$, 10% Pro $\delta_{op}(\text{ring-1})$, 34% Ring buckl
	174		161		160	188	11% pep $\delta_{op}(\text{ring-1})$, 34% Pro $\delta_{op}(\text{ring-1})$, 34% Pro $\delta_{op}(\text{ring-2})$	175	42% Pro $\delta_{op}(\text{ring-1})$, 35% Pro $\delta_{op}(\text{ring-2})$
	150					158	75% Ring buckl	160	12% pep $\delta_{ip}(\text{ring-1})$, 49% Ring buckl
	128		129		128	133	39% $\delta(\text{C3C7C10})$, 19% $\delta_{ip}(\text{C10C7})$, 15% $\delta_{op}(\text{C10C7})$, 24% pep $\delta_{op}(\text{ring-2})$, 11% $\tau(\text{C3C7})$	116	25% $\delta(\text{C3C7C10})$, 10% $\delta_{op}(\text{C10C7})$ 35% pep $\delta_{op}(\text{ring-2})$, 15% Ring buckl
	99		108		106	108	11% $\delta_{op}(\text{C10C7})$, 33% pep $\delta_{op}(\text{ring-1})$, 26% pep $\delta_{op}(\text{ring-2})$, 18% $\tau(\text{C7C10})$	88	58% pep $\delta_{op}(\text{ring-1})$, 20% pep $\delta_{op}(\text{ring-2})$, 10% $\tau(\text{C3C7})$
						73	26% pep $\delta_{op}(\text{ring-1})$, 10% pep $\delta_{op}(\text{ring-2})$, 13% Pro $\delta_{op}(\text{ring-1})$, 47% $\tau(\text{C7C10})$	79	11% $\delta(\text{C3C7C10})$, 16% pep $\delta_{op}(\text{ring-1})$, 62% pep $\delta_{op}(\text{ring-2})$, 12% Pro $\delta_{op}(\text{ring-1})$
						71	45% pep $\delta_{op}(\text{ring-2})$, 20% pep $\delta_{op}(\text{ring-3})$, 32% $\tau(\text{C3C7})$	55	12% pep $\delta_{op}(\text{ring-2})$, 66% $\tau(\text{C3C7})$
						57	17% pep $\delta_{op}(\text{ring-2})$, 36% $\tau(\text{C3C7})$, 19% $\tau(\text{C7C10})$	40	11% $\tau(\text{C3C7})$, 76% $\tau(\text{C7C10})$
						28	10% pep $\delta_{op}(\text{ring-1})$, 44% pep $\delta_{op}(\text{ring-3})$, 19% Ring buckl, 18% $\tau(\text{C3C7})$	23	60% pep $\delta_{op}(\text{ring-3})$, 26% Ring buckl, 14% $\tau(\text{C7C10})$

Table 7.9. Experimental and calculated vibrational band wavenumbers (cm⁻¹) for non-deuterated CAH.

IR solid	Raman solid	IR sol	Raman sol	Calc.	N ^c -protonated	Calc.	N ^δ -protonated
3222	3201			3203	94% v(N13H27)	3269	99% v(N15H27)
3188	3181			3209	93% v _{ss} (NH)	3199	100% v(N2H17)
	3159			3207	95% v _{as} (NH)	3105	95% v(N5H19)
	3152						
	3138						
	3005			3093	97% v(C14H26)	3118	98% v(C12H25)
3075				3079	98% v(C12H25)	3098	94% v(C14H26)
3054							
3021							
3001	2996			2997	31% v _{as} (CH ₃), 63% v _{as} (CH ₃)'	2995	33% v _{as} (CH ₃), 62% v _{as} (CH ₃)'
2981	2989						
2972	2974			2962	68% v _{as} (CH ₃), 30% v _{as} (CH ₃)'	2972	25% v _s (CH ₂), 75% v _{as} (CH ₂)
	2954						
2940	2947			2941	100% v _{as} (CH ₂)	2956	67% v _{as} (CH ₃), 31% v _{as} (CH ₃)'
	2932			2907	100% v _s (CH ₂)	2898	92% v _s (CH ₃)
	2888			2902	93% v _s (CH ₃)	2894	75% v _s (CH ₂), 25% v _{as} (CH ₂)
2879	2880						
2860	2864						
2736							
2659							
2621							
				2832	99% v(C1H16)	2827	99% v(C1H16)
				2815	99% v(C4H18)	2818	98% v(C4H18)
1678	1675						
1671	1662		1661	1654	72% v(C6O7)	1641	66% v(C6O7), 12% v(C6N5), 10% δ _{ip} (N5H19)

	1647			1634	64% v(C3O8), 12% v(C3N2)	1640	68% v(C3O8), 10% v(C3N2), 10% δ_{ip} (N2H15)
1580	1582		1586				
1572	1574			1574	46% v(C11C12), 15% v(C9C11), 10% δ_{ip} (N13H27)	1572	57% v(C11C12), 14% v(C9C11)
1502	1496		1523	1469	42% v(C14N15), 23% δ_{ip} (C14H26)	1489	49% v(N13C14), 20% δ_{ip} (C14H26)
1486		1473	1498				
1461	1462			1454	12% δ_{as} (CH ₃), 57% δ_{as} (CH ₃)'	1461	10% δ_{as} (CH ₃), 30% δ_{as} (CH ₃)'
1444	1447		1450	1448	52% δ_{as} (CH ₃), 28% δ_{as} (CH ₃)'	1449	10% δ (CH ₂), 55% δ_{as} (CH ₃)'
				1445	53% δ (CH ₂), 23% δ_{as} (CH ₃)	1447	18% δ (CH ₂), 64% δ_{as} (CH ₃)
1432	1435	1435	1434	1430	11% v(C3N2), 11% δ_{ip} (N5H19), 30% δ (CH ₂)	1444	69% δ (CH ₂)
1420	1423			1397	11% v(N13C14) 30% δ_{ip} (N5H19), 15% δ_{ip} (N13H27)	1418	33% v(C14N15), 41% δ_{ip} (N15H27)
				1399	16% v(C11N13), 26% δ_{ip} (N2H17)	1414	28% δ_{ip} (N2H17), 23% δ_{ip} (N5H19)
	1388	1388		1376	24% v(C6N5), 22% v(C3N2)	1387	25% v(C6N5), 25% v(C3N2)
1373	1368	1376	1372	1367	14% v(N13C14), 15% v(C14N15), 11% δ_{ip} (N13H27)	1354	74% δ_s (CH ₃)
1353	1354		1352	1358	82% δ_s (CH ₃)	1351	14% δ_{ip} (N2H17), 11% δ_{ip} (N5H19), 17% δ_s (CH ₃)
				1344	20% δ_{ip} (N2H17), 15% ω (CH ₂), 12% ω (C9C4H18)	1338	10% v(N13C14), 10% v(N15C12), 30% ω (CH ₂)
1330	1330	1337	1337	1335	11% δ_{ip} (N2H17), 38% ω (CH ₂)	1320	16% v(C11N13), 13% v(N13C14), 12% ω (CH ₂), 17% τ (CH ₂), 14% δ (C9C4H18)
1308	1310	1320	1314	1310	30% ω (C10C1H16), 14% τ (C10C1H16), 16% ω (C9C4H18)	1306	22% ω (C10C1H16), 10% τ (C10C1H16), 17% ω (C9C4H18)
1281	1288			1289	37% δ (C10C1H16), 14% ρ (C10C1H16)	1291	39% δ (C10C1H16), 18% ρ (C10C1H16)
	1282						
1273	1273	1272	1269	1265	13% ω (C10C1H16), 14% δ (C9C4H18)	1271	17% ω (C10C1H16)
1252	1253		1249	1255	22% τ (CH ₂), 11% δ (C9C4H18)	1265	11% v(C11N13), 12% v(N15C12), 13% δ_{ip} (C14H26), 14% ω (CH ₂)
				1241	22% δ_{ip} (C12H25), 27% δ_{ip} (C14H26), 10% δ (C9C4H18)	1239	11% ω (CH ₂), 22% δ (C9C4H18), 16% ω (C9C4H18), 16% τ (C9C4H18)
1234	1232	1233	1236	1235	36% v(N15C12), 11% v(C9C11), 17% δ_{ip} (C12H25), 14% ω (CH ₂)	1212	16% δ_{ip} (C12H25), 15% δ_{ip} (C14H26), 11% ω (CH ₂), 19% τ (CH ₂)
1194	1195	1195	1197	1195	20% τ (CH ₂), 12% τ (C9C4H18)	1190	13% v(N5C4), 13% δ_{ip} (C12H25), 15% δ_{ip} (C14H26), 13% τ (CH ₂)10% τ (C9C4H18)
1179	1180						

1168	1168	1160	1163	1160	33% v(N2C1), 18% $\rho_{op}(CH_3)$, 15% $\tau(C10C1H16)$	1158	26% v(N2C1), 15% $\rho_{op}(CH_3)$, 18% $\tau(C10C1H16)$
1150	1152						
1108	1109	1106		1121	41% v(N15C12), 18% $\delta_{ip}(C12H25)$, 10% $\delta_{ip}(C14H26)$ 11% Im $\delta_{ip}(ring-1)$	1112	33% v(C14N15), 13% v(N5C4), 16% $\delta_{ip}(N15H27)$, 10% $\delta_{ip}(C14H26)$
				1103	39% v(C1C10), 17% $\rho_{ip}(CH_3)$	1102	24% v(C1C10)
1090	1090	1088	1094	1096	35% v(N5C4), 21% $\tau(CH_2)$	1092	12% v(N5C4), 15% v(C1C10), 15% $\rho_{ip}(CH_3)$
1081	1083			1085	36% v(N13C14), 35% $\delta_{ip}(N13H27)$	1063	36% v(N15C12), 30% $\delta_{ip}(C12H25)$
1056	1062						
1041	1043	1049		1042	26% v(C4C9)	1042	30% v(C4C9)
	1020	1004	1010	1021	14% v(C1C10), 15% $\rho_{ip}(CH_3)$, 13% $\rho_{op}(CH_3)$, 10% $\rho(C10C1H16)$	1021	15% v(C1C10), 14% $\rho_{ip}(CH_3)$, 14% $\rho_{op}(CH_3)$, 11% $\rho(C10C1H16)$
	993			991	11% v(C4C9), 33% Im $\delta_{ip}(ring-1)$	974	10% v(C11N13), 10% v(C11C12), 17% Im $\delta_{ip}(ring-1)$
988	984		982				
979				953	15% v(N2C1), 11% $\rho_{ip}(CH_3)$, 32% $\rho_{op}(CH_3)$	961	12% v(C11N13), 15% $\rho_{op}(CH_3)$ 15% Im $\delta_{ip}(ring-1)$
933	934			922	12% v(C11N13), 68% Im $\delta_{ip}(ring-2)$	934	78% Im $\delta_{ip}(ring-2)$
920	922			917	40% $\rho(CH_2)$	925	23% $\rho(CH_2)$, 15% Pep $\delta_{ip}(ring-3)$
891	897		897	870	11% $\delta(C4C9C11)$, 11% $\rho(CH_2)$, 14% $\rho(C9C4H18)$, 21% $\delta_{op}(C3O8)$	885	11% v(C4C3), 14% $\rho(CH_2)$
824	826			821	90% $\delta_{op}(C12H25)$	805	10% $\delta_{op}(C12H25)$, 90% $\delta_{op}(C14H26)$
807	804			804	18% v(C1C6), 11% $\rho_{ip}(CH_3)$, 21% $\delta_{op}(C6O7)$	792	13% $\rho_{ip}(CH_3)$, 34% $\delta_{op}(C6O7)$
788	790		798	799	96% $\delta_{op}(C14H26)$	761	14% Pep $\delta_{ip}(ring-3)$, 12% $\delta_{op}(C12H25)$, 19% $\delta_{op}(C3O8)$, 12% Im $\delta_{op}(ring-1)$
764	770			763	16% v(C4C3), 10% Pep $\delta_{ip}(ring-3)$, 22% $\delta_{op}(C6O7)$	758	10% v(C4C3), 13% $\delta_{op}(C12H25)$, 12% Im $\delta_{op}(ring-1)$
744							
735	736						
717	718		718	722	13% $\delta(C4C9C11)$, 12% $\delta_{op}(C3O8)$, 22% Im $\delta_{op}(ring-1)$	724	11% Im $\delta_{ip}(ring-1)$, 17% $\delta_{op}(N5H19)$, 40% $\delta_{op}(C12H25)$
				700	44% $\delta_{op}(N13H27)$, 37% Im $\delta_{op}(ring-2)$	723	65% $\delta_{op}(N5H19)$
692	694			669	11% $\delta_{op}(C3O8)$, 29% Im $\delta_{op}(ring-2)$	697	25% $\delta_{op}(C12H25)$, 28% Im $\delta_{op}(ring-1)$
677	678		676	663	24% Pep $\delta_{ip}(ring-3)$	658	13% $\delta_{op}(C3O8)$, 59% Im $\delta_{op}(ring-2)$
661	659						
651	652		649	650	22% $\delta_{op}(N13H27)$, 28% Imd $\delta_{op}(ring-2)$	653	12% v(C1C6), 12% v(C1C10), 20% $\delta_{op}(C6O7)$

639	639						
619	619		629	612	10% v(C9C11), 27% δ_{op} (N13H27), 31% Im δ_{op} (ring-1)	637	12% δ_{op} (N2H17), 19% δ_{op} (C3O8), 15% Im δ_{op} (ring-1), 29% Im δ_{op} (ring-2)
606	607						
597	598			586	51% δ_{ip} (C6O7)	599	11% v(C1C6), 22% δ_{ip} (C6O7), 26% δ_{ip} (C3O8)
				563	55% δ_{op} (N2H17)	558	68% δ_{op} (N2H17), 10% δ_{ip} (C3O8)
500	502		503	507	29% Pep δ_{ip} (ring-2), 36% δ_{op} (N5H19)	529	94% δ_{op} (N15H27)
	491						
478	472		468	479	25% Pep δ_{ip} (ring-2), 20% δ_{op} (N5H19)	484	39% Pep δ_{ip} (ring-2)
458	457			463	12% Pep δ_{ip} (ring-1), 31% δ_{op} (N2H17)	464	18% δ_{ip} (C6O7), 10% δ_{ip} (C3O8)
453	451		432	430	29% δ_{op} (N5H19), 32% δ_{ip} (C3O8)	442	33% Pep δ_{ip} (ring-1), 12% Pep δ_{ip} (ring-2)
	415			394	44% Pep δ_{ip} (ring-1), 26% Pep δ_{op} (ring-3)	402	15% ρ (C9C4H18), 13% Pep δ_{ip} (ring-1), 17% Pep δ_{op} (ring-3) 10% ρ (C4C9)
	387		381				
	341			347	32% δ_{ip} (C11C9)	364	10% δ (C10C1H16), 22% ρ (C10C1H16), 10% δ_{ip} (C6O7), 12% δ_{ip} (C3O8)
	334			340	15% ρ (C10C1H16), 13% δ_{ip} (C11C9), 12% δ_{ip} (C3O8)	310	24% δ_{ip} (C11C9), 31% δ_{op} (C11C9), 14% Imd δ_{op} (ring-1)
	308						
	278			279	25% ω (C10C1H16), 37% τ (C10C1H16)	283	25% ω (C10C1H16), 35% τ (C10C1H16)
	265			249	10% δ (C4C9C11), 17% ρ (C9C4H18), 26% δ_{op} (C11C9) 12% Im δ_{op} (ring-1)	265	11% v(C4C9), 11% ρ (C9C4H18), 25% δ_{ip} (C11C9), 10% Pep δ_{ip} (ring-1)
	239			215	62% ρ (C1C10)	224	81% ρ (C1C10)
				213	14% ω (C9C4H18), 23% τ (C9C4H18), 16% δ_{ip} (C11C9) 28% ρ (C1C10)	216	13% ω (C9C4H18), 23% τ (C9C4H18), 12% ρ (C1C10)
	145		158	139	11% δ (C4C9C11), 13% δ_{op} (C11C9), 60% Pep δ_{op} (ring-1)	112	50% Pep δ_{op} (ring-1), 24% Pep δ_{op} (ring-3)
	127		132	127	13% δ_{op} (C11C9), 65% Pep δ_{op} (ring-3)	106	30% Pep δ_{op} (ring-1), 60% Pep δ_{op} (ring-3)
	107		110	110	20% Pep δ_{op} (ring-1), 19% ρ (C9C11), 34% ρ (C4C9)	90	34% δ (C4C9C11), 19% δ_{op} (C11C9), 13% Pep δ_{op} (ring-1)
	76			74	74% ρ (C9C11)	69	39% ρ (C9C11), 44% ρ (C4C9)
				44	15% δ (C4C9C11), 16% δ_{op} (C11C9), 11% Pep δ_{op} (ring-1) 18% Pep δ_{op} (ring-3), 33% ρ (C4C9)	49	20% Pep δ_{op} (ring-2), 31% ρ (C9C11), 41% ρ (C4C9)
				29	76% Pep δ_{op} (ring-2)	28	60% Pep δ_{op} (ring-2), 11% Pep δ_{op} (ring-3), 18% ρ (C9C11)

Table 7.10. Experimental and calculated vibrational band wavenumbers (cm⁻¹) for *N*-deuterated CAH.

IR solid	Raman solid	IR sol	Raman sol	Calc.	N ^c -protonated	Calc.	N ^δ -protonated
3185	3178						
3152	3155						
	3104			3093	98% v(C14H26)	3118	98% v(C12H25)
3073				3079	98% v(C12H25)	3099	98% v(C14H26)
3029							
3001	3005						
	2995			2997	31% v _{as} (CH ₃), 63% v _{as} (CH ₃)'	2995	33% v _{as} (CH ₃), 62% v _{as} (CH ₃)'
2986	2989						
	2974			2962	68% v _{as} (CH ₃), 30% v _{as} (CH ₃)'	2972	25% v _s (CH ₂), 75% v _{as} (CH ₂)
2945	2947			2941	100% v _{as} (CH ₂)	2956	67% v _{as} (CH ₃), 31% v _{as} (CH ₃)'
2930	2932			2907	100% v _s (CH ₂)	2898	92% v _s (CH ₃)
				2902	93% v _s (CH ₃)	2894	75% v _s (CH ₂), 25% v _{as} (CH ₂)
				2832	99% v(C1H16)	2827	99% v(C1H16)
2880	2880			2815	99% v(C4H18)	2818	98% v(C4H18)
2864	2864						
2372	2375			2360	95% v(N13D27)	2405	97% v(N15D27)
2352	2351			2353	83% v _{ss} (ND), 14% v _{as} (ND)	2345	99% v(N2D17)
2345				2352	13% v _{ss} (ND), 85% v _{as} (ND)	2279	98% v(N5D19)
2220							
1667							
	1654						
1651	1640	1641	1645	1644	78% v(C6O7)	1630	62% v(C6O7), 12% v(C3O8), 10% v(C6N5)
1613	1612			1619	72% v(C3O8), 12% v(C3N2)	1627	13% v(C6O7), 64% v(C3O8)
1574	1574						
	1563	1561	1562	1561	51% v(C11C12), 17% v(C9C11), 10% δ _{ip} (C12H25)	1568	59% v(C11C12), 16% v(C9C11)

			1503				
	1477	1470	1480	1465	46% v(C14N15), 22% $\delta_{ip}(C14H26)$	1481	57% v(N13C14), 22% $\delta_{ip}(C14H26)$
	1469						
	1457	1453	1453	1453	81% $\delta_{as}(CH_3)'$	1455	10% $\delta_{as}(CH_3)$, 73% $\delta_{as}(CH_3)'$
				1447	84% $\delta_{as}(CH_3)$	1447	80% $\delta_{as}(CH_3)$, 12% $\delta_{as}(CH_3)'$
1441	1437	1436	1435	1441	92% $\delta(CH_2)$	1445	96% $\delta(CH_2)$
1435							
1418	1423			1413	10% v(C4C3), 26% v(C3N2)	1422	18% v(C6N5), 16% v(C3N2)
1373	1378	1375	1377	1378	34% v(C11N13), 11% $\tau(CH_2)$	1388	23% v(C6N5), 29% v(C3N2)
	1356			1369	29% v(C6N5), 14% v(C3N2), 16% $\delta_s(CH_3)$	1355	91% $\delta_s(CH_3)$
1355	1343	1342	1344	1358	80% $\delta_s(CH_3)$	1349	44% v(C14N15), 13% v(N15C12), 15% $\delta_{ip}(N15D27)$
				1345	53% $\omega(CH_2)$, 18% $\delta(C9C4H18)$	1341	14% v(N15C12), 40% $\omega(CH_2)$
1333	1336	1324	1319	1324	42% v(N13C14), 18% v(C14N15), 10% $\delta_{ip}(N13D27)$	1322	18% v(C11N13), 16% v(N13C14), 19% $\tau(CH_2)$, 13% $\delta(C9C4H18)$
1312				1320	31% $\omega(C9C4H18)$, 11% $\tau(C9C4H18)$	1312	21% $\omega(C9C4H18)$, 10% $\tau(C9C4H18)$
1301	1301			1304	30% $\delta(C10C1H16)$, 13% $\rho(C10C1H16)$, 20% $\omega(C10C1H16)$, 11% $\tau(C10C1H16)$	1302	32% $\delta(C10C1H16)$, 15% $\rho(C10C1H16)$, 15% $\omega(C10C1H16)$
				1289	17% $\omega(C10C1H16)$, 11% $\omega(C9C4H18)$	1292	10% v(N5C4), 19% $\omega(C10C1H16)$
1274	1277		1269	1262	10% $\omega(CH_2)$, 12% $\tau(CH_2)$, 21% $\delta(C9C4H18)$, 14% $\rho(C9C4H18)$	1260	15% v(C11N13), 21% v(N15C12), 14% v(C9C11), 16% $\delta_{ip}(C14H26)$
1245	1247			1238	35% $\delta_{ip}(C12H25)$, 16% $\delta_{ip}(C14H26)$	1247	20% $\omega(CH_2)$, 17% $\delta(C9C4H18)$
1228	1228		1230	1229	24% v(N15C12), 10% $\delta_{ip}(C14H26)$, 12% $\omega(CH_2)$, 14% $\tau(CH_2)$	1216	17% $\tau(CH_2)$, 10% $\tau(C9C4H18)$
1212	1212			1206	17% v(N5C4), 20% $\delta_{ip}(C14H26)$	1202	21% $\delta_{ip}(C12H25)$, 21% $\delta_{ip}(C14H26)$
1199	1193			1193	30% v(N2C1)	1195	14% v(N5C4), 11% $\delta_{ip}(N5D19)$, 15% $\delta(C9C4H18)$
1169	1170		1174	1162	22% $\tau(CH_2)$	1169	10% $\delta_{ip}(C12H25)$, 11% $\delta_{ip}(C14H26)$, 26% $\tau(CH_2)$
1157	1157						
	1126			1121	31% v(N15C12), 13% $\delta_{ip}(C12H25)$	1108	18% v(C1C10), 19% $\rho_{ip}(CH_3)$, 10% $\rho_{op}(CH_3)$
1118	1113			1114	16% v(N15C12), 14% v(C1C10), 11% $\delta_{ip}(C12H25)$, 13% $\rho_{ip}(CH_3)$	1075	11% v(C14N15), 10% v(C1C10), 11% $\rho_{ip}(CH_3)$, 13% $\rho_{op}(CH_3)$
1109							

1110							
1086	1088		1095	1070	12% v(C1C10), 10% $\rho_{ip}(\text{CH}_3)$, 28% $\rho_{op}(\text{CH}_3)$	1068	15% v(C14N15), 14% v(N15C12), 14% $\delta_{ip}(\text{C12H25})$, 13% $\rho_{op}(\text{CH}_3)$
1054	1052						
1025	1028	1024	1027	1033	28% v(C4C9)	1038	48% v(C4C9)
1013	1014	1000	1008	1003	12% v(C1C10), 17% $\delta_{ip,as}(\text{ND})$, 10% $\rho_{ip}(\text{CH}_3)$	1010	28% $\delta_{ip}(\text{N5D19})$
998				995	13% v(C1C10), 16% $\delta_{ip,s}(\text{ND})$, 13% $\rho_{ip}(\text{CH}_3)$	999	22% v(C1C10), 16% $\rho_{ip}(\text{CH}_3)$
981	982		985	972	16% v(C11N13) 38% Im $\delta_{ip}(\text{ring-1})$	988	17% v(C11N13), 17% Im $\delta_{ip}(\text{ring-1})$
956	959						
949	953						
935	937			922	77% Im $\delta_{ip}(\text{ring-2})$	930	25% $\rho(\text{CH}_2)$, 13% $\rho(\text{C9C4H18})$, 10% Pep $\delta_{ip}(\text{ring-3})$, 11% $\delta_{op}(\text{C3O8})$
926	924			907	13% $\rho(\text{CH}_2)$, 13% $\rho(\text{C9C4H18})$, 17% $\delta_{op}(\text{C3O8})$	921	12% v(C11N13), 66% Im $\delta_{ip}(\text{ring-2})$
899	901						
888			888	885	23% v(N2C1), 28% $\delta_{ip,as}(\text{ND})$, 28% $\rho_{op}(\text{CH}_3)$	890	22% v(N2C1), 27% $\delta_{ip}(\text{N15D27})$, 32% $\rho_{op}(\text{CH}_3)$
856				849	22% $\rho(\text{CH}_2)$, 12% $\delta_{op}(\text{C3O8})$	841	10% v(N5C4), 13% $\delta_{ip}(\text{N5D19})$, 24% $\delta_{ip}(\text{N15D27})$, 11% $\rho(\text{CH}_2)$
833	832			843	58% $\delta_{ip}(\text{N13D27})$, 11% $\rho(\text{CH}_2)$	817	48% $\delta_{ip}(\text{N15D27})$
	818			819	86% $\delta_{op}(\text{C12H25})$	805	10% $\delta_{op}(\text{C12H25})$, 91% $\delta_{op}(\text{C14H26})$
799	800						
790	792		789	799	96% $\delta_{op}(\text{C14H26})$	782	16% $\rho_{ip}(\text{CH}_3)$ 38% $\delta_{op}(\text{C6O7})$
757				789	17% $\rho_{ip}(\text{CH}_3)$, 39% $\delta_{op}(\text{C6O7})$	757	26% $\delta_{op}(\text{C12H25})$, 10% $\delta_{op}(\text{C3O8})$, 12% $\delta_{op}(\text{C11C9})$, 23% Im $\delta_{op}(\text{ring-1})$
733	720			722	15% v(C1C6), 13% v(C4C3), 18% $\delta_{ip,s}(\text{ND})$, 14% Pep $\delta_{ip}(\text{ring-3})$, 10% $\delta_{op}(\text{C3O8})$	730	11% v(C1C6), 19% Pep $\delta_{ip}(\text{ring-3})$, 17% $\delta_{op}(\text{C12H25})$
717				714	13% $\delta(\text{C4C9C11})$, 14% Im $\delta_{op}(\text{ring-1})$	718	13% v(C4C3), 11% v(C9C11), 16% Im $\delta_{ip}(\text{ring-1})$, 25% $\delta_{op}(\text{C12H25})$
678	676		687	673	98% Im $\delta_{op}(\text{ring-2})$	696	24% $\delta_{op}(\text{C12H25})$, 28% Im $\delta_{op}(\text{ring-1})$
668	668						
655	656		651	655	13% v(C9C11), 12% Im $\delta_{ip}(\text{ring-1})$, 14% Pep $\delta_{ip}(\text{ring-3})$ 18% $\delta_{op}(\text{C3O8})$	651	13% v(C1C6), 13% v(C1C10), 11% Pep $\delta_{ip}(\text{ring-3})$, 27% $\delta_{op}(\text{C6O7})$
640	645			650	10% v(C1C6), 10% v(C1C10), 16% $\delta_{op}(\text{C6O7})$, 20% Im $\delta_{op}(\text{ring-1})$	643	21% $\delta_{op}(\text{C3O8})$, 17% Im $\delta_{op}(\text{ring-1})$, 38% Im $\delta_{op}(\text{ring-2})$

623							
602	602		626	619	12% ν (C9C11), 46% Im δ_{op} (ring-1)	622	13% δ_{op} (C3O8), 69% Im δ_{op} (ring-2)
589							
570	572			569	52% δ_{ip} (C6O7)	580	10% ν (C1C6), 21% δ_{ip} (C6O7), 29% δ_{ip} (C3O8)
545	545			519	11% ν (C9C11), 13% δ_{op} (N2D17), 17% δ_{op} (C3O8)	536	91% δ_{op} (N5D19)
495	495			492	37% Pep δ_{ip} (ring-2), 45% δ_{op} (N13D27)	486	30% Pep δ_{ip} (ring-2), 14% δ_{ip} (C3O8)
471	470		467	486	23% Pep δ_{ip} (ring-2), 63% δ_{op} (N13D27)	469	15% ρ (C9C4H18), 19% Pep δ_{ip} (ring-2)
	449			459	18% ρ (C10C1H16), 22% δ_{ip} (C3O8)	447	12% δ (C4C9C11), 19% Pep δ_{ip} (ring-1), 11% Pep δ_{ip} (ring-2)
				420	47% Pep δ_{ip} (ring-1), 20% δ_{op} (N2D17)	429	20% Pep δ_{ip} (ring-1), 34% δ_{op} (N2D17), 11% δ_{ip} (C6O7)
	385		378	373	20% δ_{op} (N2D17), 20% δ_{op} (N5D19), 21% δ_{ip} (C3O8)	408	105% δ_{op} (N15D27)
				343	12% Pep δ_{ip} (ring-1), 36% δ_{op} (N2D17)	370	11% Pep δ_{ip} (ring-1), 24% δ_{op} (N2D17)
	336			342	36% δ_{ip} (C11C9), 12% δ_{op} (N2D17), 10% τ (C4C9)	356	19% ρ (C10C1H16), 12% δ_{op} (N2D17), 16% Pep δ_{op} (ring-3)
	306		316	313	10% ρ (C10C1H16), 60% δ_{op} (N5D19)	304	21% δ_{ip} (C11C9), 28% δ_{op} (C11C9), 14% Im δ_{op} (ring-1)
	274			276	21% ω (C10C1H16), 33% τ (C10C1H16)	282	25% ω (C10C1H16), 35% τ (C10C1H16)
	259			246	17% ρ (C9C4H18), 26% δ_{op} (C11C9), 12% Im δ_{op} (ring-1)	262	11% ν (C4C9), 11% ρ (C9C4H18), 26% δ_{ip} (C11C9), 10% Pep δ_{ip} (ring-1)
	235			213	88% τ (C1C10)	223	86% τ (C1C10)
				210	19% ω (C9C4H18), 31% τ (C9C4H18), 23% δ_{ip} (C11C9)	215	14% ω (C9C4H18), 25% τ (C9C4H18)
	145		159	138	10% δ (C4C9C11), 12% δ_{op} (C11C9), 61% Pep δ_{op} (ring-1)	110	48% Pep δ_{op} (ring-1), 28% Pep δ_{op} (ring-3)
	127		133	127	14% δ_{op} (C11C9), 67% Pep δ_{op} (ring-3)	106	33% Pep δ_{op} (ring-1), 10% Pep δ_{op} (ring-2), 60% Pep δ_{op} (ring-3)
	107		109	108	23% Pep δ_{op} (ring-1), 19% τ (C9C11), 33% τ (C4C9)	89	33% δ (C4C9C11), 18% δ_{op} (C11C9), 16% Pep δ_{op} (ring-1)
	89						
	76			72	75% τ (C9C11)	68	39% τ (C9C11), 43% τ (C4C9)
				44	15% δ (C4C9C11), 16% δ_{op} (C11C9), 11% Pep δ_{op} (ring-1) 18% Pep δ_{op} (ring-3), 34% τ (C4C9)	49	20% Pep δ_{op} (ring-2), 30% τ (C9C11), 42% τ (C4C9)
				28	75% Pep δ_{op} (ring-2)	28	59% Pep δ_{op} (ring-2), 11% Pep δ_{op} (ring-3), 19% τ (C9C11)

Table 7.11. Definitions of symmetry-adapted internal coordinates for CHP, CDHP and CAH.

CHP and CDHP

$$v(\text{N1H2}) = r(\text{N1H2})$$

$$v(\text{C5O6}) = r(\text{C5O6})$$

$$v(\text{C21O22}) = r(\text{C21O22})$$

$$v(\text{N18C19}) = r(\text{N18C19})$$

$$v(\text{N1C3}) = r(\text{N1C3})$$

$$v(\text{C21N1}) = r(\text{C21N1})$$

$$v(\text{C5N18}) = r(\text{C5N18})$$

$$v(\text{C3C5}) = r(\text{C3C5})$$

$$v(\text{C19C21}) = r(\text{C19C21})$$

$$v(\text{C19C23}) = r(\text{C19C23})$$

$$v(\text{C29N18}) = r(\text{C29N18})$$

$$v(\text{C3C7}) = r(\text{C3C7})$$

$$v(\text{C3H4}) = r(\text{C3H4})$$

$$v(\text{C19H20}) = r(\text{C19H20})$$

$$v(\text{C23C26}) = r(\text{C23C26})$$

$$v(\text{C26C29}) = r(\text{C26C29})$$

$$v_s(\text{CH}_2) = 1/\sqrt{2}[r(\text{C7H8}) + r(\text{C7H9})]$$

$$v_{as}(\text{CH}_2) = 1/\sqrt{2}[r(\text{C7H8}) - r(\text{C7H9})]$$

$$v_s(\text{CH}_{2a}) = 1/\sqrt{2}[r(\text{C23H24}) + r(\text{C23H25})]$$

$$v_{as}(\text{CH}_{2a}) = 1/\sqrt{2}[r(\text{C23H24}) - r(\text{C23H25})]$$

$$v_s(\text{CH}_{2b}) = 1/\sqrt{2}[r(\text{C26H27}) + r(\text{C26H28})]$$

$$v_{as}(\text{CH}_{2b}) = 1/\sqrt{2}[r(\text{C26H27}) - r(\text{C26H28})]$$

$$v_s(\text{CH}_{2c}) = 1/\sqrt{2}[r(\text{C29H30}) + r(\text{C29H31})]$$

$$v_{as}(\text{CH}_{2c}) = 1/\sqrt{2}[r(\text{C29H30}) - r(\text{C29H31})]$$

$$v(\text{N11H12}) = r(\text{N11H12})$$

$$\begin{aligned}
v(\text{N17H12}) &= r(\text{N11H12}) \\
v(\text{C13H14}) &= r(\text{C13H14}) \\
v(\text{C15H16}) &= r(\text{C15H16}) \\
v(\text{C10N11}) &= r(\text{C10N11}) \\
v(\text{N11C15}) &= r(\text{N11C15}) \\
v(\text{C15N17}) &= r(\text{C15N17}) \\
v(\text{N17C13}) &= r(\text{N17C13}) \\
v(\text{C13C10}) &= r(\text{C13C10}) \\
\delta_{\text{ip}}(\text{N11H12}) &= 1/\sqrt{2}[\theta(\text{C10N11H12}) - \theta(\text{C15N11H12})] \\
\delta_{\text{op}}(\text{N11H12}) &= \tau(\text{H12N11C10C15}) \\
\delta_{\text{ip}}(\text{N17H12}) &= 1/\sqrt{2}[\theta(\text{C13N17H12}) - \theta(\text{C15N17H12})] \\
\delta_{\text{op}}(\text{N17H12}) &= \tau(\text{H12N17C13C15}) \\
\delta_{\text{ip}}(\text{C13H14}) &= 1/\sqrt{2}[\theta(\text{C10C13H14}) - \theta(\text{N17C13H14})] \\
\delta_{\text{op}}(\text{C13H14}) &= \tau(\text{H14C13C10N17}) \\
\delta_{\text{ip}}(\text{C15H16}) &= 1/\sqrt{2}[\theta(\text{N11C15H16}) - \theta(\text{N17C15H16})] \\
\delta_{\text{op}}(\text{C15H16}) &= \tau(\text{H16C15N11N17}) \\
\delta_{\text{op}}(\text{C7C10}) &= \tau(\text{C7C10C13N11}) \\
\delta_{\text{ip}}(\text{N1H2}) &= 1/\sqrt{2}[\theta(\text{C3N1H2}) - \theta(\text{C21N1H2})] \\
\delta_{\text{op}}(\text{N1H2}) &= \tau(\text{H2N1C3C21}) \\
\delta_{\text{ip}}(\text{C5O6}) &= 1/\sqrt{2}[\theta(\text{N18C5O6}) - \theta(\text{C3C5O6})] \\
\delta_{\text{ip}}(\text{C21O22}) &= 1/\sqrt{2}[\theta(\text{N1C21O22}) - \theta(\text{C19C2O22})] \\
\delta_{\text{op}}(\text{C5O6}) &= \tau(\text{O6C5N18C3}) \\
\delta_{\text{op}}(\text{C21O22}) &= \tau(\text{O22C21N1C19}) \\
\delta(\text{C3C7C10}) &= 1/2\sqrt{6}[-(\sqrt{6}-2)\theta(\text{H8C7H9}) + (\sqrt{6}+2)\theta(\text{C3C7C10}) - \theta(\text{C3C7H8}) - \theta(\text{C3C7H9}) - \theta(\text{C10C7H8}) - \theta(\text{C10C7H9})] \\
\delta(\text{CH}_2) &= 1/2\sqrt{6}[(\sqrt{6}+2)\theta(\text{H8C7H9}) - (\sqrt{6}-2)\theta(\text{C3C7C10}) - \theta(\text{C3C7H8}) - \theta(\text{C3C7H9}) - \theta(\text{C10C7H8}) - \theta(\text{C10C7H9})] \\
\rho(\text{CH}_2) &= 1/2[\theta(\text{C3C7H8}) - \theta(\text{C3C7H9}) + \theta(\text{C10C7H8}) - \theta(\text{C10C7H9})] \\
\omega(\text{CH}_2) &= 1/2[\theta(\text{C3C7H8}) + \theta(\text{C3C7H9}) - \theta(\text{C10C7H8}) - \theta(\text{C10C7H9})]
\end{aligned}$$

$$\begin{aligned}
\tau(\text{CH}_2) &= 1/2[\theta(\text{C3C7H8}) - \theta(\text{C3C7H9}) - \theta(\text{C10C7H8}) + \theta(\text{C10C7H9})] \\
\delta(\text{CH}_{2a}) &= 1/2\sqrt{6}[(\sqrt{6} + 2)\theta(\text{H24C23H25}) - (\sqrt{6} - 2)\theta(\text{C19C23C26}) - \theta(\text{C19C23H24}) - \theta(\text{C19C23H25}) - \theta(\text{C26C23H24}) - \theta(\text{C26C23H25})] \\
\rho(\text{CH}_{2a}) &= 1/2[\theta(\text{C19C23H24}) - \theta(\text{C19C23H25}) + \theta(\text{C26C23H24}) - \theta(\text{C26C23H25})] \\
\omega(\text{CH}_{2a}) &= 1/2[\theta(\text{C19C23H24}) + \theta(\text{C19C23H25}) - \theta(\text{C26C23H24}) - \theta(\text{C26C23H25})] \\
\tau(\text{CH}_{2a}) &= 1/2[\theta(\text{C19C23H24}) - \theta(\text{C19C23H25}) - \theta(\text{C26C23H24}) + \theta(\text{C26C23H25})] \\
\delta(\text{CH}_{2b}) &= 1/2\sqrt{6}[(\sqrt{6} + 2)\theta(\text{H27C26H28}) - (\sqrt{6} - 2)\theta(\text{C23C26C29}) - \theta(\text{C23C26H27}) - \theta(\text{C23C26H28}) - \theta(\text{C29C26H27}) - \theta(\text{C29C26H28})] \\
\rho(\text{CH}_{2b}) &= 1/2[\theta(\text{C23C26H27}) - \theta(\text{C23C26H28}) + \theta(\text{C29C26H27}) - \theta(\text{C29C26H28})] \\
\omega(\text{CH}_{2b}) &= 1/2[\theta(\text{C23C26H27}) + \theta(\text{C23C26H28}) - \theta(\text{C29C26H27}) - \theta(\text{C29C26H28})] \\
\tau(\text{CH}_{2b}) &= 1/2[\theta(\text{C23C26H27}) - \theta(\text{C23C26H28}) - \theta(\text{C29C26H27}) + \theta(\text{C29C26H28})] \\
\delta(\text{CH}_{2c}) &= 1/2\sqrt{6}[(\sqrt{6} + 2)\theta(\text{H30C29H31}) - (\sqrt{6} - 2)\theta(\text{N18C29C26}) - \theta(\text{C26C29H30}) - \theta(\text{C26C29H31}) - \theta(\text{N18C29H30}) - \theta(\text{N18C29H31})] \\
\rho(\text{CH}_{2c}) &= 1/2[\theta(\text{C26C29H30}) - \theta(\text{C26C29H31}) + \theta(\text{N18C29H30}) - \theta(\text{N18C29H31})] \\
\omega(\text{CH}_{2c}) &= 1/2[\theta(\text{C26C29H30}) + \theta(\text{C26C29H31}) - \theta(\text{N18C29H30}) - \theta(\text{N18C29H31})] \\
\tau(\text{CH}_{2c}) &= 1/2[\theta(\text{C26C29H30}) - \theta(\text{C26C29H31}) - \theta(\text{N18C29H30}) + \theta(\text{N18C29H31})] \\
\omega(\text{CH}) &= 1/\sqrt{6}[2\theta(\text{N18C19H20}) - \theta(\text{C21C19H20}) - \theta(\text{C23C19C20})] \\
\rho(\text{CH}) &= 1/\sqrt{2}[\theta(\text{C21C19H20}) - \theta(\text{C23C19C20})] \\
\rho(\text{C7C3H4}) &= 1/2[(\theta(\text{N1C3H4}) - \theta(\text{N1C3C7}) + \theta(\text{C5C3H4}) - \theta(\text{C5C3C7})] \\
\omega(\text{C7C3H4}) &= 1/2[(\theta(\text{N1C3H4}) + \theta(\text{N1C3C7}) - \theta(\text{C5C3H4}) - \theta(\text{C5C3C7})] \\
\tau(\text{C7C3H4}) &= 1/2[(\theta(\text{N1C3H4}) - \theta(\text{N1C3C7}) - \theta(\text{C5C3H4}) + \theta(\text{C5C3C7})] \\
\delta(\text{C7C3H4}) &= 1/\sqrt{10}[4\theta(\text{C7C3H4}) - \theta(\text{N1C3H4}) - \theta(\text{N1C3C7}) - \theta(\text{C5C3H4}) - \theta(\text{C5C3C7})] \\
\text{Pro } \delta_{ip}(\text{ring-1}) &= {}^2/\sqrt{7}[\theta(\text{N18C19C23}) + a\theta(\text{C19C23C26}) + b\theta(\text{C23C26C29}) + b\theta(\text{C26C29N18}) + a\theta(\text{C29N18C19})] \\
\text{Pro } \delta_{ip}(\text{ring-2}) &= {}^2/\sqrt{p} [(a - b)\theta(\text{C19C23C26}) + (1 - a)\theta(\text{C23C26C29}) - (1 - a)\theta(\text{C26C29N18}) - (a - b)\theta(\text{C29N18C19})] \\
\text{Pro } \delta_{op}(\text{ring-1}) &= {}^2/\sqrt{7} [b\tau(\text{C19C23C26C29}) + a\tau(\text{C23C26C29N18}) + \tau(\text{C26C29N18C19}) + a\tau(\text{C29N18C19C23}) + b\tau(\text{N18C19C23C26})] \\
\text{Pro } \delta_{op}(\text{ring-2}) &= {}^2/\sqrt{p} [-(1 - a)\tau(\text{C19C23C26C29}) - (a - b)\tau(\text{C23C26C29N18}) + (a - b)\tau(\text{C29N18C19C23}) + (1 - a)\tau(\text{N18C19C23C26})] \\
\text{Ring buckling vibration} &= {}^1/2[(\tau(\text{C5N18C29C26}) - \tau(\text{C29C26C5C3}) + \tau(\text{C21C19C23C26}) - \tau(\text{C23C19C21N1})] \\
\tau(\text{C3C7}) &= 1/3 [\tau(\text{N1C3C7H8}) + \tau(\text{N1C3C7H9}) + \tau(\text{N1C3C7C10}) + \tau(\text{H4C3C7C8}) + \tau(\text{H4C3C7H9}) + \tau(\text{H4C3C7C10}) + \tau(\text{C5C3C7H8}) + \tau(\text{C5C3C7H9}) \\
&\quad + \tau(\text{C5C3C7C10})]
\end{aligned}$$

$$\begin{aligned}
\tau(\text{C7C10}) &= 1/\sqrt{6}[\tau(\text{N11C10C7C3}) + \tau(\text{N11C10C7H8}) + \tau(\text{N11C10C7H9}) + \tau(\text{C13C10C7C3}) + \tau(\text{C13C10C7H8}) + \tau(\text{C13C10C7H9})] \\
\text{Im } \delta_{\text{ip}}(\text{ring-1}) &= 2/\sqrt{7}[\theta(\text{N11C10C13}) + a\theta(\text{C10C13N17}) + b\theta(\text{C13N17C15}) + b\theta(\text{N17C15N11}) + a\theta(\text{C15N11C10})] \\
\text{Im } \delta_{\text{ip}}(\text{ring-2}) &= 2/\sqrt{p}[(a-b)\theta(\text{C10C13N17}) + (1-a)\theta(\text{C13N17C15}) - (1-a)\theta(\text{N17C15N11}) - (a-b)\theta(\text{C15N11C10})] \\
\text{Im } \delta_{\text{op}}(\text{ring-1}) &= 2/\sqrt{7}[b\tau(\text{N11C10C13N17}) + a\tau(\text{C10C13N17C15}) + \tau(\text{C13N17C15N11}) + a\tau(\text{N17C15N11C10}) + b\tau(\text{C15N11C10C13})] \\
\text{Im } \delta_{\text{op}}(\text{ring-2}) &= 2/\sqrt{p}[-(1-a)\tau(\text{N11C10C13N17}) - (a-b)\tau(\text{C10C13N17C15}) + (a-b)\tau(\text{N17C15N11C10}) + (1-a)\tau(\text{C15N11C10C13})] \\
\text{Pep } \delta_{\text{ip}}(\text{ring-1}) &= 1/\sqrt{12}[-2\theta(\text{N18C19C21}) + \theta(\text{C19C21N1}) + \theta(\text{C21N1C3}) - 2\theta(\text{N1C3C5}) + \theta(\text{C3C5N18}) + \theta(\text{C5N18C19})] \\
\text{Pep } \delta_{\text{ip}}(\text{ring-2}) &= 1/2[\theta(\text{C19C21N1}) - \theta(\text{C21N1C3}) + \theta(\text{C3C5N18}) - \theta(\text{C5N18C19})] \\
\text{Pep } \delta_{\text{ip}}(\text{ring-3}) &= 1/\sqrt{6}[-\theta(\text{N18C19C21}) + \theta(\text{C19C21N1}) - \theta(\text{C21N1C3}) + \theta(\text{N1C3C5}) - \theta(\text{C3C5N18}) + \theta(\text{C5N18C19})] \\
\text{Pep } \delta_{\text{op}}(\text{ring-1}) &= 1/\sqrt{6}[\tau(\text{C5N18C19C21}) - \tau(\text{N18C19C21N1}) + \tau(\text{C19C21N1C3}) - \tau(\text{C21N1C3C5}) + \tau(\text{N1C3C5N18}) - \tau(\text{C3C5N18C19})] \\
\text{Pep } \delta_{\text{op}}(\text{ring-2}) &= 1/\sqrt{12}[-\tau(\text{C5N18C19C21}) + 2\tau(\text{N18C19C21N1}) - \tau(\text{C19C21N1C3}) - \tau(\text{C21N1C3C5}) + 2\tau(\text{N1C3C5N18}) - \tau(\text{C3C5N18C19})] \\
\text{Pep } \delta_{\text{op}}(\text{ring-3}) &= 1/2[\tau(\text{C5N18C19C21}) - \tau(\text{C19C21N1C3}) + \tau(\text{C21N1C3C5}) - \tau(\text{C3C5N18C19})]
\end{aligned}$$

CAH

$$\begin{aligned}
v(\text{N2C1}) &= r(\text{N2C1}) \\
v(\text{N5C4}) &= r(\text{N5C4}) \\
v(\text{C6N5}) &= r(\text{C6N5}) \\
v(\text{C3N2}) &= r(\text{C3N2}) \\
v(\text{C4C3}) &= r(\text{C4C3}) \\
v(\text{C1C6}) &= r(\text{C1C6}) \\
v(\text{C1C10}) &= r(\text{C1C10}) \\
v(\text{C4C9}) &= r(\text{C4C9}) \\
v(\text{N5H19}) &= r(\text{N5H19}) \\
v(\text{N2H17}) &= r(\text{N2H17}) \\
v_{\text{s}}(\text{NH}) &= 1/\sqrt{2}[r(\text{N5H19}) + r(\text{N2H17})] \\
v_{\text{as}}(\text{NH}) &= 1/\sqrt{2}[r(\text{N5H19}) - r(\text{N2H17})] \\
v(\text{C3O8}) &= r(\text{C3O8})
\end{aligned}$$

$$\begin{aligned}
v(\text{C6O7}) &= r(\text{C6O7}) \\
v(\text{C1H16}) &= r(\text{C1H16}) \\
v(\text{C4H18}) &= r(\text{C4H18}) \\
v_s(\text{CH}_2) &= 1/\sqrt{2}[r(\text{C9H20}) + r(\text{C9H21})] \\
v_{as}(\text{CH}_2) &= 1/\sqrt{2}[r(\text{C9H20}) - r(\text{C9H21})] \\
v_s(\text{CH}_3) &= 1/\sqrt{3}[r(\text{C10H22}) + r(\text{C10H23}) + r(\text{C10H24})] \\
v_{as}(\text{CH}_3) &= 1/\sqrt{6}[2r(\text{C10H22}) - r(\text{C10H23}) - r(\text{C10H24})] \\
v_{as}(\text{CH}_3)' &= 1/\sqrt{2}[r(\text{C10H23}) - r(\text{C10H24})] \\
v(\text{N13H27}) &= r(\text{N13H27}) \\
v(\text{N15H27}) &= r(\text{N15H27}) \\
v(\text{C12H25}) &= r(\text{C12H25}) \\
v(\text{C14H26}) &= r(\text{C14H26}) \\
v(\text{C11N13}) &= r(\text{C11N13}) \\
v(\text{N13C14}) &= r(\text{N13C14}) \\
v(\text{C14N15}) &= r(\text{C14N15}) \\
v(\text{N15C12}) &= r(\text{N15C12}) \\
v(\text{C12C11}) &= r(\text{C12C11}) \\
v(\text{C9C11}) &= r(\text{C9C11}) \\
\delta_{ip}(\text{N13H27}) &= 1/\sqrt{2} [\theta(\text{C11N13H27}) - \theta(\text{C14N13H27})] \\
\delta_{op}(\text{N13H27}) &= \tau(\text{H27N13C11C14}) \\
\delta_{ip}(\text{N15H27}) &= 1/\sqrt{2} [\theta(\text{C12N15H27}) - \theta(\text{C14N15H27})] \\
\delta_{op}(\text{N15H27}) &= \tau(\text{H27N15C12C14}) \\
\delta_{ip}(\text{C12H25}) &= 1/\sqrt{2} [\theta(\text{C11C12H25}) - \theta(\text{N15C12H25})] \\
\delta_{op}(\text{C12H25}) &= \tau(\text{H25C12C11N15}) \\
\delta_{ip}(\text{C14H26}) &= 1/\sqrt{2} [\theta(\text{N13C14H26}) - \theta(\text{N15C14H26})] \\
\delta_{op}(\text{C14H26}) &= \tau(\text{H26C14N13N15}) \\
\delta_{op}(\text{C9C11}) &= \tau(\text{C9C11N12N13})
\end{aligned}$$

$$\begin{aligned}
\delta_{ip}(N5H19) &= 1/\sqrt{2}[\theta(C4N5H19) - \theta(C6N5H19)] \\
\delta_{op}(N5H19) &= \tau(H19N5C6C4) \\
\delta_{ip}(N2H17) &= 1/\sqrt{2}[\theta(C3N2H17) - \theta(C1N2H17)] \\
\delta_{op}(N2H17) &= \tau(H17N2C3C1) \\
\delta_{ip}(C3O8) &= 1/\sqrt{2}[\theta(N2C3O8) - \theta(C4C3O8)] \\
\delta_{ip}(C6O7) &= 1/\sqrt{2}[\theta(N5C6O7) - \theta(C1C6O7)] \\
\delta_{op}(C3O8) &= \tau(O8C3N2C4) \\
\delta_{op}(C6O7) &= \tau(O7C6N5C1) \\
\delta(C4C9C11) &= 1/2\sqrt{6}[-(\sqrt{6}-2)\theta(H20C9H21) + (\sqrt{6}+2)\theta(C4C9C11) - \theta(C4C9H20) - \theta(C4C9H21) - \theta(C11C9H20) - \theta(C11C9H21)] \\
\delta(CH_2) &= 1/2\sqrt{6}[(\sqrt{6}+2)\theta(H20C9H21) - (\sqrt{6}-2)\theta(C4C9C11) - \theta(C4C9H20) - \theta(C4C9H21) - \theta(C11C9H20) - \theta(C11C9H21)] \\
\rho(CH_2) &= 1/2[\theta(C4C9H20) - \theta(C4C9H21) + \theta(C11C9H20) - \theta(C11C9H21)] \\
\omega(CH_2) &= 1/2[\theta(C4C9H20) + \theta(C4C9H21) - \theta(C11C9H20) - \theta(C11C9H21)] \\
\tau(CH_2) &= 1/2[\theta(C4C9H20) - \theta(C4C9H21) - \theta(C11C9H20) + \theta(C11C9H21)] \\
\rho(C10C1H16) &= 1/2[(\theta(N2C1H16) - \theta(N2C1C10) + \theta(C6C1H16) - \theta(C6C1C10)] \\
\omega(C10C1H16) &= 1/2[(\theta(N2C1H16) + \theta(N2C1C10) - \theta(C6C1H16) - \theta(C6C1C10)] \\
\tau(C10C1H16) &= 1/2[(\theta(N2C1H16) - \theta(N2C1C10) - \theta(C6C1H16) + \theta(C6C1C10)] \\
\delta(C10C1H16) &= 1/\sqrt{10}[4\theta(C10C1H16) - \theta(N2C1H16) - \theta(N2C1C10) - \theta(C6C1H16) - \theta(C6C1C10)] \\
\rho(C9C4H18) &= 1/2[(\theta(N5C4H18) - \theta(N5C4C9) + \theta(C3C4H18) - \theta(C3C4C9)] \\
\omega(C9C4H18) &= 1/2[(\theta(N5C4H18) + \theta(N5C4C9) - \theta(C3C4H18) - \theta(C3C4C9)] \\
\tau(C9C4H18) &= 1/2[(\theta(N5C4H18) - \theta(N5C4C9) - \theta(C3C4H18) + \theta(C3C4C9)] \\
\delta(C9C4H18) &= 1/\sqrt{10}[4\theta(C9C4H18) - (\theta(N5C4H18) - \theta(N5C4C9) - \theta(C3C4H18) - \theta(C3C4C9)] \\
\delta_s(CH_3) &= 1/\sqrt{6}[\theta(C1C10H22) + \theta(C1C10H23) + \theta(C1C10H24) - \theta(H22C10H23) - \theta(H22C10H24) - \theta(H23C10H24)] \\
\delta_{as}(CH_3) &= 1/\sqrt{6}[2\theta(H22C10H23) - \theta(H22C10H24) - \theta(H23C10H24)] \\
\delta_{as}(CH_3)' &= 1/\sqrt{2}[\theta(H22C10H24) - \theta(H23C10H24)] \\
\rho_{ip}(CH_3) &= 1/\sqrt{6}[2\theta(C1C10H22) - \theta(C1C10H23) - \theta(C1C10H24)] \\
\rho_{op}(CH_3) &= 1/\sqrt{2}[\theta(C1C10H23) - \theta(C1C10H24)] \\
\text{Im } \delta_{ip}(\text{ring-1}) &= \sqrt[2]{\sqrt{7}}[\theta(N13C11C12) + a\theta(C11C12N15) + b\theta(C12N15C14) + b\theta(N15C14N13) + a\theta(C14N13C11)]
\end{aligned}$$

$$\begin{aligned}
\text{Im } \delta_{ip}(\text{ring-2}) &= \frac{2}{\sqrt{p}} [(a - b)\theta(\text{C11C12N15}) + (1 - a)\theta(\text{C12N15C14}) - (1 - a)\theta(\text{N15C14N13}) - (a - b)\theta(\text{C14N13C11})] \\
\text{Im } \delta_{op}(\text{ring-1}) &= \frac{2}{\sqrt{7}} [b\tau(\text{N13C11C12N15}) + a\tau(\text{C11C12N15C14}) + \tau(\text{C12N15C14N13}) + a\tau(\text{N15C14N13C11}) + b\tau(\text{C14N13C11C12})] \\
\text{Im } \delta_{op}(\text{ring-2}) &= \frac{2}{\sqrt{p}} [-(1 - a)\tau(\text{N13C11C12N15}) - (a - b)\tau(\text{C11C12N15C14}) + (a - b)\tau(\text{N15C14N13C11}) + (1 - a)\tau(\text{C14N13C11C12}) \\
\tau(\text{C4C9}) &= \frac{1}{3} [\tau(\text{N5C4C9C11}) + \tau(\text{N5C4C9H20}) + \tau(\text{N5C4C9H21}) + \tau(\text{H18C4C9C11}) + \tau(\text{H18C4C9H20}) + \tau(\text{H18C4C9H21}) + \tau(\text{C3C4C9C11}) + \tau(\text{C3C4C9H20}) \\
&\quad + \tau(\text{C3C4C9H21})] \\
\tau(\text{C9C11}) &= \frac{1}{\sqrt{6}} [\tau(\text{C4C9C11N13}) + \tau(\text{C4C9C11C12}) + \tau(\text{H20C9C11N13}) + \tau(\text{H21C9C11C12}) + \tau(\text{H21C9C11N13}) + \tau(\text{H21C9C11C12})] \\
\text{Pep } \delta_{ip}(\text{ring-1}) &= \frac{1}{\sqrt{12}} [-2\theta(\text{N2C1C6}) + \theta(\text{C1C6N5}) + \theta(\text{C6N5C4}) - 2\theta(\text{N5C4C3}) + \theta(\text{C4C3N2}) + \theta(\text{C3N2C1})] \\
\text{Pep } \delta_{ip}(\text{ring-2}) &= \frac{1}{2} [\theta(\text{C1C6N5}) - \theta(\text{C6N5C4}) + \theta(\text{C4C3N2}) - \theta(\text{C3N2C1})] \\
\text{Pep } \delta_{ip}(\text{ring-3}) &= \frac{1}{\sqrt{6}} [-\theta(\text{N2C1C6}) + \theta(\text{C1C6N5}) - \theta(\text{C6N5C4}) + \theta(\text{N5C4C3}) - \theta(\text{C4C3N2}) + \theta(\text{C3N2C1})] \\
\text{Pep } \delta_{op}(\text{ring-1}) &= \frac{1}{\sqrt{6}} [\tau(\text{C3N2C1C6}) - \tau(\text{N2C1C6N5}) + \tau(\text{C1C6N5C4}) - \tau(\text{C6N5C4C3}) + \tau(\text{N5C4C3N2}) - \tau(\text{C4C3N2C1})] \\
\text{Pep } \delta_{op}(\text{ring-2}) &= \frac{1}{\sqrt{12}} [-\tau(\text{C3N2C1C6}) + 2\tau(\text{N2C1C6N5}) - \tau(\text{C1C6N5C4}) - \tau(\text{C6N5C4C3}) + 2\tau(\text{N5C4C3N2}) - \tau(\text{C4C3N2C1})] \\
\text{Pep } \delta_{op}(\text{ring-3}) &= \frac{1}{2} [\tau(\text{C3N2C1C6}) - \tau(\text{C1C6N5C4}) + \tau(\text{C6N5C4C3}) - \tau(\text{C4C3N2C1})]
\end{aligned}$$

N.B $-a = \cos 144^\circ = -0.8090$, $b = \cos 72^\circ = 0.3090$, $p = \frac{1}{2} (7 - 5 \cos 144^\circ)$, $1 - a = 1.8090$, $a - b = -1.1180$.

7.4. Molecular orbital analysis

The highest occupied molecular orbital (HOMO) and lowest unoccupied molecular orbital (LUMO) energies were calculated for the minimum energy conformers of CHP, CDHP and CAH (both N^{ϵ} and N^{δ} -tautomeric forms) (Figs. 7.21-7.23). The HOMO energies of the N^{ϵ} and N^{δ} -tautomeric forms are -6.326 eV, -6.566 eV (CHP), -6.185 eV, -6.612 eV (CDHP) and -6.380 eV, -6.762 eV (CAH), respectively whereas, the LUMO energies are -0.772 eV, -0.709 eV (CHP), -0.872 eV, -0.709 eV (CDHP) and -0.828 eV, -0.733 eV (CAH), respectively. The composition of HOMO and LUMO are given in Tables 7.12 and 7.13. The analysis of molecular orbitals of the N^{ϵ} -tautomeric forms of CHP, CDHP and CAH show that the HOMO is localized on the imidazole ring of the L-His side-chains, whereas the LUMO is localized on the DKP ring. The N^{δ} -tautomeric forms of CHP, CDHP and CAH show that the HOMO is localized on the oxygen, nitrogen atoms and partly on the carbon atoms of the DKP ring in all three molecules and the carbon atoms of the imidazole ring in CAH. Whereas the LUMO is localized on the N^{δ} -H $^{\delta}$ of the imidazole ring in CHP, CDHP and CAH. The computed HOMO-LUMO energy gap for the N^{ϵ} and N^{δ} -tautomeric forms corresponds to 5.553 eV, 5.856 eV (CHP), 5.313 eV, 5.902 eV (CDHP) and 5.551 eV, 6.028 eV (CAH), respectively. Since the HOMO-LUMO gap value is relatively large, it is expected that both tautomeric forms of CHP, CDHP and CAH are not very reactive or polarizable, and therefore, chemically relatively stable molecules.

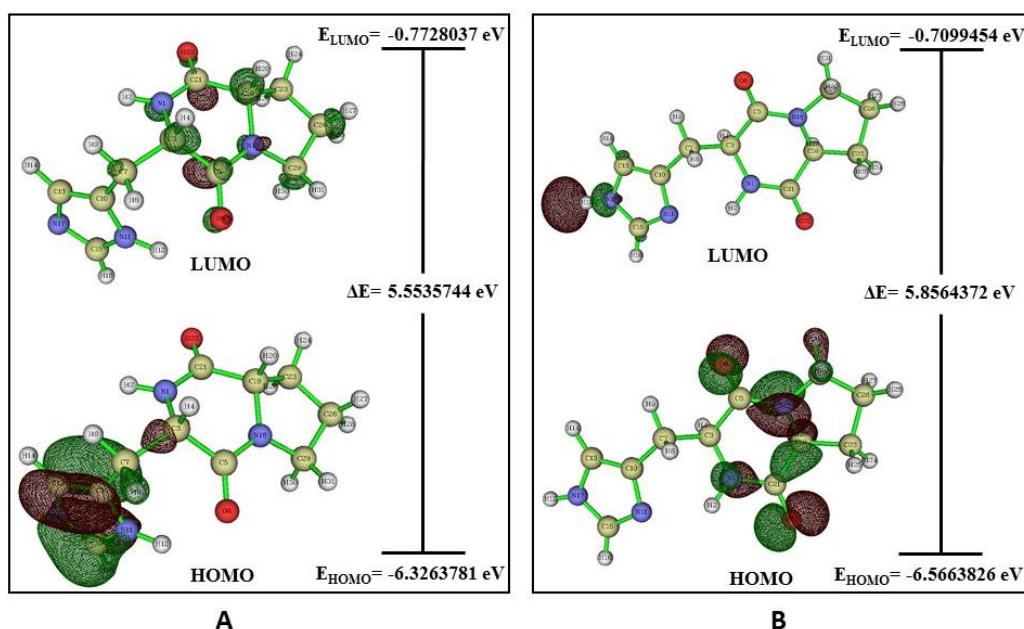


Figure 7.21. HOMO-LUMO plots of lowest energy conformer of (A) N^{ϵ} and (B) N^{δ} -tautomeric forms of CHP.

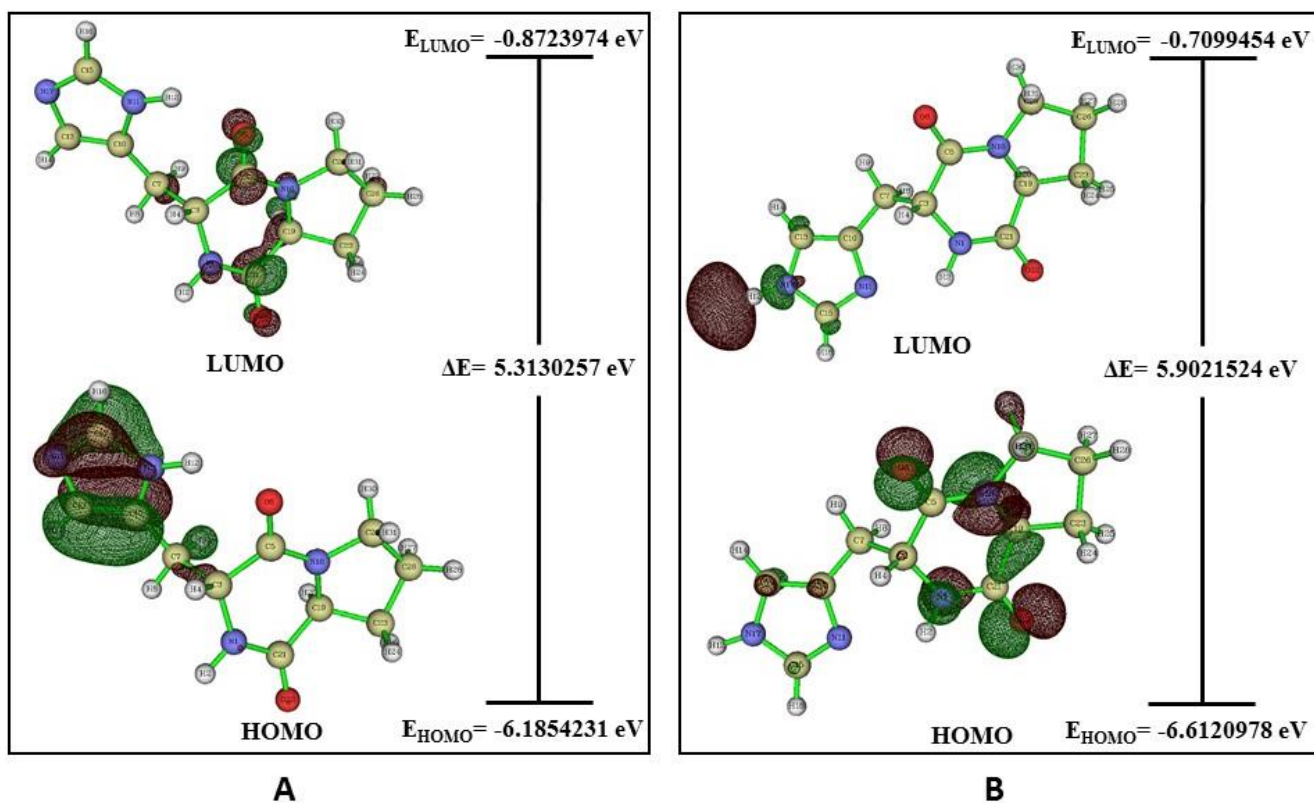


Figure 7.22. HOMO-LUMO plots of the lowest energy conformer of (A) N^ϵ and (B) N^δ -tautomeric forms of CDHP.

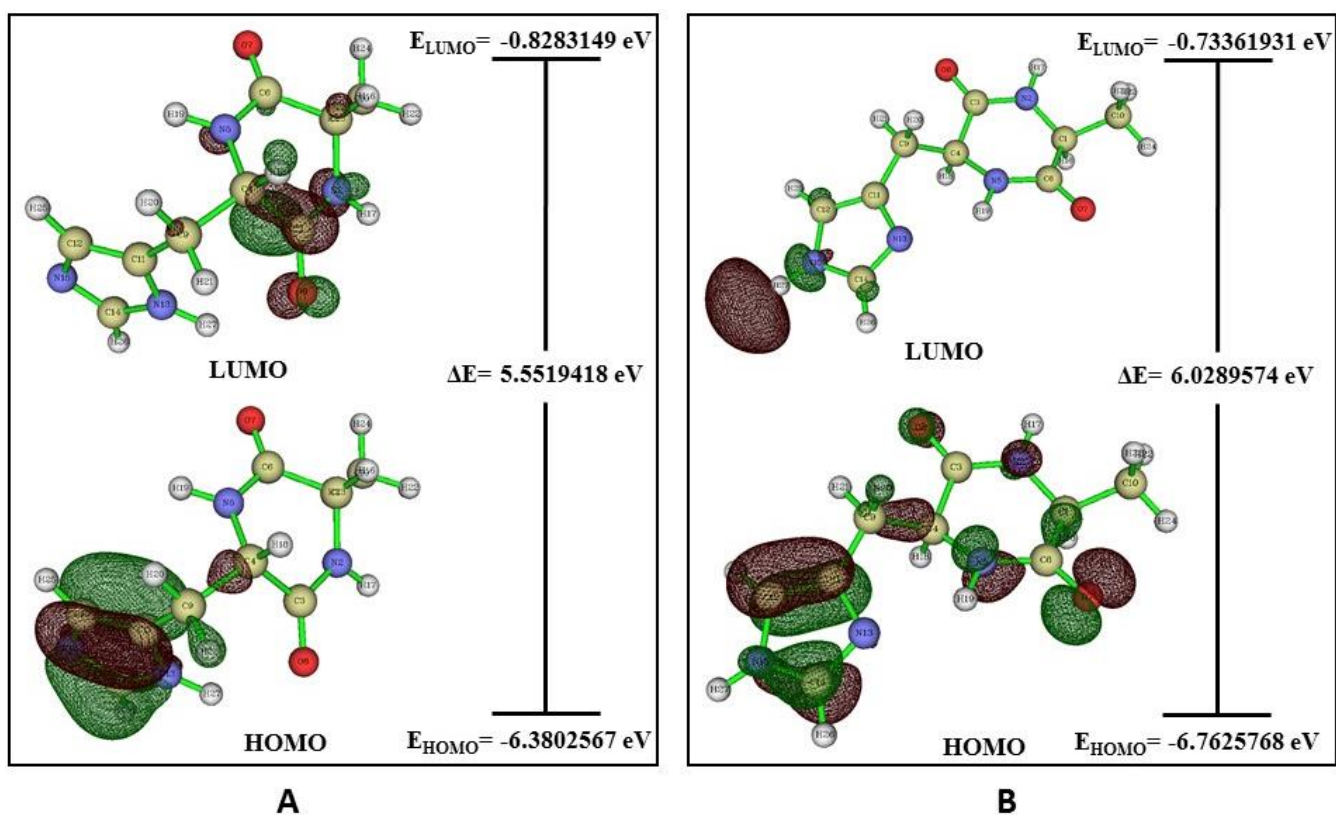


Figure 7.23. HOMO-LUMO plots of the lowest energy conformer of (A) N^ϵ and (B) N^δ -tautomeric forms of CAH.

Table 7.12. HOMO-LUMO composition of the lowest energy conformers of N^ε- and N^δ-tautomeric forms of CHP and CDHP.

Atoms	CHP				CDHP			
	HOMO (N ^ε)	LUMO (N ^ε)	HOMO (N ^δ)	LUMO (N ^δ)	HOMO (N ^ε)	LUMO (N ^ε)	HOMO (N ^δ)	LUMO (N ^δ)
1(N)	0.687%	5.729%	6.632%	0.286%	0.793%	3.141%	8.746%	0.180%
2(H)	0.167%	1.260%	0.180%	0.072%	0.017%	1.996%	0.220%	0.111%
3(C)	2.075%	2.792%	0.839%	0.116%	1.427%	1.600%	1.426%	0.060%
4(H)	0.076%	10.039%	0.140%	0.497%	0.140%	1.476%	0.656%	0.173%
5(C)	0.108%	5.141%	2.942%	0.133%	0.113%	6.798%	2.633%	0.034%
6(O)	0.166%	5.484%	14.441%	0.317%	0.065%	5.181%	16.454%	0.318%
7(C)	2.521%	1.982%	0.443%	0.246%	2.866%	2.973%	0.746%	0.297%
8(H)	1.451%	2.112%	0.014%	0.113%	0.184%	2.604%	0.398%	0.231%
9(H)	0.098%	3.929%	0.093%	0.334%	2.097%	4.666%	0.017%	0.340%
10(C)	30.225%	0.507%	0.261%	0.834%	29.808%	1.468%	2.228%	0.854%
11(N)	4.360%	1.103%	0.238%	1.715%	4.420%	0.951%	0.245%	1.829%
12(H)	0.057%	0.138%	0.003%	44.364%	0.062%	0.042%	0.019%	44.655%
13(C)	25.289%	0.661%	0.328%	7.500%	25.242%	1.017%	2.757%	7.229%
14(H)	0.655%	0.618%	0.010%	9.199%	0.678%	0.478%	0.077%	9.203%
15(C)	24.126%	0.586%	0.200%	6.833%	23.955%	0.225%	1.605%	6.875%
16(H)	0.770%	0.174%	0.009%	8.010%	0.782%	0.033%	0.056%	8.297%
17(N)	6.718%	0.188%	0.084%	18.845%	6.537%	0.147%	0.679%	18.731%
18(N)	0.082%	7.178%	21.760%	0.083%	0.055%	7.331%	18.333%	0.055%
19(C)	0.025%	2.797%	6.146%	0.025%	0.052%	3.946%	4.641%	0.028%
20(H)	0.005%	10.166%	2.669%	0.076%	0.022%	13.065%	2.013%	0.069%
21(C)	0.088%	4.111%	4.352%	0.086%	0.181%	7.115%	3.619%	0.105%
22(O)	0.204%	3.664%	31.891%	0.194%	0.479%	6.191%	27.140%	0.195%
23(C)	0.009%	2.175%	0.756%	0.009%	0.011%	2.983%	0.770%	0.014%
24(H)	0.000%	3.603%	0.032%	0.009%	0.003%	0.889%	0.123%	0.012%
25(H)	0.001%	1.138%	0.149%	0.008%	0.000%	4.533%	0.041%	0.014%
26(C)	0.008%	3.165%	0.196%	0.012%	0.002%	2.886%	0.213%	0.014%
27(H)	0.000%	6.821%	0.045%	0.019%	0.000%	7.619%	0.025%	0.023%
28(H)	0.005%	3.718%	0.024%	0.016%	0.001%	1.922%	0.041%	0.014%
29(C)	0.021%	2.813%	2.197%	0.016%	0.006%	2.372%	1.756%	0.015%
30(H)	0.003%	3.033%	1.269%	0.020%	0.001%	3.597%	1.446%	0.014%
31(H)	0.000%	3.174%	1.657%	0.014%	0.000%	0.754%	0.879%	0.012%

Table 7.13. HOMO-LUMO composition of the lowest energy conformer of N^ε and N^δ-tautomeric forms of CAH.

Atoms	CAH			
	HOMO (N ^ε)	LUMO (N ^ε)	HOMO (N ^δ)	LUMO (N ^δ)
1(C)	0.021%	2.361%	2.053%	0.029%
2(N)	0.083%	9.425%	2.997%	0.085%
3(C)	0.107%	14.128%	0.595%	0.136%
4(C)	2.076%	4.949%	2.569%	0.114%
5(N)	0.652%	7.152%	7.554%	0.276%
6(C)	0.083%	3.124%	2.255%	0.071%
7(O)	0.196%	2.921%	18.077%	0.186%
8(O)	0.145%	10.329%	3.464%	0.372%
9(C)	2.519%	3.051%	2.544%	0.244%
10(C)	0.006%	1.392%	0.228%	0.014%
11(C)	30.349%	0.755%	15.374%	0.854%
12(C)	25.265%	0.874%	19.593%	7.450%
13(N)	4.385%	0.808%	2.098%	1.756%
14(C)	24.138%	0.240%	12.393%	6.898%
15(N)	6.705%	0.164%	4.150%	18.905%
16(H)	0.004%	5.670%	0.487%	0.062%
17(H)	0.015%	3.509%	0.205%	0.039%
18(H)	0.085%	13.339%	0.725%	0.467%
19(H)	0.139%	2.187%	0.184%	0.075%
20(H)	0.099%	5.779%	1.216%	0.121%
21(H)	1.442%	2.831%	0.074%	0.296%
22(H)	0.001%	3.322%	0.015%	0.020%
23(H)	0.002%	0.235%	0.049%	0.004%
24(H)	0.001%	0.582%	0.034%	0.004%
25(H)	0.652%	0.772%	0.549%	9.073%
26(H)	0.771%	0.025%	0.415%	8.063%
27(H)	0.060%	0.077%	0.102%	44.387%

7.5. Conclusions

Vibrational spectroscopy studies of histidine containing DKPs-CHP, CDHP and CAH-were undertaken using IR and Raman spectroscopic techniques in the solid state and in aqueous solution. Energy profile calculations were performed on both N^ε and N^δ- tautomeric forms for the conformational analysis of L-His/D-His side-chains attached to the DKP ring, by rotating the C_α-C_β and C_β-C_γ dihedral angles. DFT calculations at the B3LYP/aug-cc-pVTZ level for the conformers of each N^ε and N^δ- tautomeric forms of these molecules have enabled the structures and energies of each of these conformers to be determined and the observed IR and Raman spectra

to be attributed, in each case, to the lowest energy conformer. From our calculations it is suggested that the lowest energy conformers of the N^δ- tautomeric forms has a lower energy compared to the N^ε-tautomers of each molecule. The vibrational band assignments for the amide I and II modes and the imidazole ring as well as the nature of the amide vibrations of the *cis* peptide groups in all three molecules has been confirmed by the spectroscopic data and DFT calculations. The attachment of bulky side-chains on either side of the DKP ring may effect the conformation of the DKP ring. The band located at ~1495 cm⁻¹ agrees well with previous observations for DKP derivatives which exhibit boat conformations, where the *cis* amide II mode was found ~1491 cm⁻¹. Furthermore, HOMO and LUMO analysis has been carried out to elucidate information related to charge transfer within the molecules. The computed HOMO-LUMO energy gap corresponds to (~5.3-6.0 eV) which implies that all three molecules possesses relatively high chemical stability.

7.6. References

1. R. Scharfmann, J. L. Morgat, S. Aratan-Spire, *Neuroendocrinology*, 1989, 49, 442.
2. C. Prasad, *Neurosci & Biobehav. Rev.*, 1988, 12, 19.
3. C. W. Hilton, C. Prasad, F. Svec, P. Vo, S. Reddy, *Lancet*, 1990, 336, 1455.
4. D. R. Houston, S. Bjørnar, V. G. H. Eijsink, M. J. R. Stark, I. M. Eggleston, D. M. F. van Aalten. *J Med Chem.*, 2004, 47, 5713.
5. (a) K. Bauer, K. J. Graf, A. Faivre-Bauman, S. Beier, A. Tixier-Vidal, H. Kleinkauf, *Nature*, 1978, 274, 174. (b) A. Enjalbert, M. Ruberg, S. Atancigia, M. Priam, K. Bauer, C. Kordon, *Europ. J. Pharmacol.*, 1979, 58, 97.
6. (a) C. Prasad, T. Masui, A. Peterkofsky, *Nature*, 1977, 268, 142. (b) T. Yanagisawa, C. Prasad, J. Williams and A. Peterkofsky, *Biochem. Biophys. Res. Commun.*, 1979, 86, 1146.
7. C. Prasad, T. Masui, J. Williams, A. Peterkofsky, *Biochem. Biophys. Res. Commun.*, 1978, 85, 1582.
8. (a) A. Peterkofsky, F. Battaini, *Neuropeptides*, 1980, 1, 105. (b) A. Peterkofsky, F. Battaini, Y. Koch, Y. Takahara, P. Dannies, *Mol. Cell. Biochem.*, 1982, 42, 45.
9. K. R. Prakash, Y. Tang, A. P. Kozikowski, J. L. Flippen-Anderson, S. M. Knoblach, A. I. Faden, *Bioorg. Med. Chem.*, 2002, 10, 3043.
10. A. Minelli, I. Bellezza, S. Grottelli, F. Pinnen, L. Brunetti, M. Vacca, *Peptides*, 2006, 27, 105.
11. G. W. Carlile, R. M. Chalmers-Redman, N. A. Tatton, A. Pong, K. E. Borden, W. G. Tatton, *Mol. Pharmacol.*, 2000, 57, 2.

12. A. Minelli, I. Bellezza, S. Grottelli, F. Galli, *Amino Acids*, 2008, 35, 283.
13. A. Minelli, S. Grottelli, A. Mierla, F. Pinnen, I. Cacciatore, I. Bellezza, *Int. J. Biochem. Cell Biol.*, 2012, 44, 525.
14. F. R. Lucietto, P. J. Milne, G. Kilian, C. L. Frost, M. Van De Venter, *Peptides*, 2006, 27, 2706.
15. G. Kilian, H. Davids, P. J. Milne, *Pharmazie*, 2013, 68, 207.
16. K. D. Kopple and M. Ohnishi, *J. Am. Chem. Soc.*, 1969, 91, 962.
17. G. Gawne, G.W. Kenner, N. H. Rogerts, R.C. Sheppard, K. Titelstad, "Peptides", E. Bricas, Ed, Wiley, New York, NY, 1968.
18. K. D. Kopple, D. H. Marr, *J. Am. Chem. Soc.*, 1967, 89, 6193.
19. C. F. Lin , L. E. Webb, *J. Am. Chem. Soc.*, 1973, 95, 6803.
20. Y. Imanishi, *Adv. Polym. Sci.*, 1976, 20, 1.
21. Y. Kojima, T. Yamashita, S. Nihide, K. Hirotsu, T. Higuchi, *Bull. Chem. Soc. Jpn.* 1985, 58, 409.
22. (a) R. Ramani, K. Venkatesan, R. E. Marsh, *J. Am. Chem. Soc.*, 1978, 100, 949. (b) E. Benedetti, R. E. Marsh, M. Goodman, *J. Am. Chem. Soc.*, 1976, 98, 6676. (c) I. Tanaka, T. Iwata, N. Takahashi, T. Ashida, *Acta Crystallogr. Sect. B.*, 1977, 33, 3902.
23. M. Ptak, A. Heitz, *Org. Magn. Reson*, 1974, 6, 358.
24. M. Cotrait, M. Ptak, B. Busetta, A. Heitz, *J. Am. Chem. Soc.*, 1976, 98, 1073.
25. A. Abiram, P. Kolandaivel, *J. Mol. Model.*, 2010, 16, 193.
26. S. Celik, A. E. Ozel, S. Kecel, S. Akyuz, *Vib. Spectrosc.*, 2012, 61, 54.
27. S. Li, M. Hong, *J. Am. Chem. Soc.*, 2011, 133, 1534.
28. J. A. Vila, Y. A. Arnautova, Y. Vorobjev , H. A. Scheraga, *Proc. Natl. Acad. Sci.*, 2011, 108, 14.
29. Spartan'14 for Windows. Wavefunction, Inc; Irvine, CA, USA: 2013.
30. P. E. Grebow, T. M. Hooker Jr, *Biopolymers*, 1974, 13, 2349.
31. M. Genest, M. Ptak, *Int. J. Peptide Protein Res.*, 1978, 11, 194.
32. Y. Zhu, M. Tang, X. Shi, Y. Zhao, *Int. J. Quantum Chem.*, 2007, 107, 745.
33. A. P. Mendham, T. J. Dines, M. J. Snowden, R. Withnall, B. Z. Chowdhry, *J. Raman Spectrosc.*, 2009, 40, 1478.
34. E. Benedetti, A. Bavoso, B. Di blasio, V. Pavone, C. Pedone, L. Paolillo, M. D'alagni, *Int. J. Peptide Protein Res.*, 1988, 31, 220.
35. M. Cotrait, M. Ptak, *Acta Cryst. B.*, 1978, 34, 528.
36. I. Tanaka, T. Iwata, N. Takahashi, T. Ashida, M. Tanihara, *Acta Cryst. B.*, 1977, 33, 3902.

37. I. L. Karle, *J. Am. Chem. Soc.*, 1972, 94, 81.
38. F. Mazza, *Acta Cryst*, 1984, C40, 1974.
39. A. P. Mendham, R. A. Palmer, B. S. Potter, T. J. Dines, J. C. Mitchell, R. Withnall, B. Z. Chowdhry, *J. Raman Spectrosc.*, 2010, 41, 148.
40. A. P. Mendham, T. J. Dines, J. C. Mitchell, R. Withnall, B. Z. Chowdhry, *J. Raman Spectrosc.*, 2009, 40, 1498.
41. A. P. Mendham, T. J. Dines, M. J. Snowden, R. Withnall, B. Z. Chowdhry, *J. Raman Spectrosc.*, 2009, 40, 1508.

Chapter 8: IR and Raman Spectroscopic Studies of the Regioisomers of Diketopiperazine: Solid state and Aqueous Solution, DFT Calculations, HOMO-LUMO and Hirshfeld Surface Analysis

8.1. Introduction

Diketopiperazines (DKPs), also known as piperazinediones or dioxopiperazines are a class of organic molecules which consists of a 6-membered piperazine ring where the two nitrogen atoms of the ring participating in amide linkages. There are three possible regioisomers for the DKP, depending upon the locations of the two carbonyl groups (C=O) in the ring. Although these isomers share a piperazine ring, the optimal strategies for their synthesis differ.¹ The 2,3-diketopiperazines (2,3-DKPs) also referred to as cyclic oxamides or ethylene oxamides are obtained from 1,2-ethylenediamine.² 2,5-DKPs are cyclic dipeptides often synthesised *via* the condensation of two α -amino acids. 2,6-DKPs may be viewed as cyclic imide derivatives derived from iminodiacetic acids. Of the three regioisomeric DKPs, the 2,5-DKPs have attracted the greatest interest from a scientific and applied perspective.³ Due to the presence of the DKP motif in biologically active natural products, and as a result of structural similarities of DKPs to peptides,⁴ medicinal chemists have been inspired to use DKPs to circumvent the poor physical and metabolic properties of peptides in the course of drug discovery. 2,3-DKP is a metabolite of ketoconazole, a broad-spectrum antifungal drug that inhibits steroid synthetic pathways and is used to treat patients with seborrheic dermatitis.^{5,6}

Potent antibiotics which include the 2,3-DKP ring in their structure include 6 α -formamidopencillin⁷ and piperacillin,⁸ both exhibit potent activity against Gram-negative bacteria. Recent studies on these compounds suggests that the introduction of phenyl or methyl substituents into the 2,3-DKP ring of piperacillin resulted in increased activity against Gram-positive bacteria. Furthermore, the introduction of the 6 α -formamido group in piperacillin improved the stability of the enzyme β -lactamase.⁹ 2,6-DKPs derivatives have been recognised for their potent broad-spectrum anticonvulsant activity in animals.¹⁰ Another important derivative of 2,6-DKP, dexrazoxane hydrochloride (brand name zincard), is known for its potent cardioprotective activity against the cardiotoxic side-effects of chemotherapeutic drugs such as doxorubicin.^{11,12} The structural characterization of diastereomeric pairs, stereochemistry and conformational preferences have been studied in a range of 2,6-DKP derivatives using a combined X-ray diffraction, solid-state NMR and DFT calculation approach.¹³

Single-crystal X-ray crystallographic studies of 2,3-DKP¹⁴ suggest that the six-membered ring adopts a skew-boat conformation in the solid state. The C₂ symmetry, typical for the molecule, is broken in the solid state due to the formation of inter-molecular hydrogen bonds involving only one of the C=O groups in the molecule.¹⁵ Vibrational spectra (both solid and solution state) have also been reported.¹⁵ *Ab initio* calculations in the gas phase were conducted using BRABO, a 4-21G basis set; solid-state geometry calculations were performed using electrostatic crystal-field perturbed *ab initio* calculations.¹⁵ Interestingly, the twisted form/skew-boat form with C₂ symmetry was identified as the minimum energy conformer compared to the planar form.

Although previous spectroscopic studies on 2,3-DKP provided spectral frequencies and IR and Raman profiles, potential energy distributions for vibrational bands were not included.¹⁵ Similarly, to our knowledge, there is no evidence of data pertaining to theoretical and vibrational spectra for 2, 6-DKP in the scientific literature. Hence, as a part of our studies on DKPs, herein we report the theoretical and experimental vibrational spectra (solid state and aqueous solution) of 2,3-DKP, 2,6-DKP and its isomer hexahydropyrimidine-4,5-dione (4,5-HHP) in comparison to the previously reported data on the 2,5-DKP regioisomer. Vibrational assignments are supported by DFT calculations of isolated molecules at the B3LYP/aug-cc-pVTZ level. The current study is part of a long-term program to investigate the relationship between the molecular structure/conformation of 2,3/2,6-DKPs and their derivatives with their experimental vibrational spectroscopic characteristics.

8.2. Experimental

8.2.1. Materials

See sections 3.1 to 3.1.2 in Chapter 3.

8.2.2. Synthesis

2,3-DKP was synthesised by a method reported in the literature² (see Appendix). Whereas, 2,6-DKP and its isomer 4,5-HHP were obtained from Fluorochem (Derbyshire, UK) and were further purified *via* recrystallization with acetone. The purity of the DKPs was checked using ¹H-NMR, ¹³C-NMR, MS and C, H, N analyses were found to be >98% (see Appendix). All other procedures were conducted as previously stated in Chapter 3.

8.2.3. Vibrational spectroscopy and Instrumental details

See sections 3.2, 3.2.1, 3.2.2, 3.2.3 and 3.2.4 in Chapter 3.

8.2.4. DFT calculations

See section 3.5, Chapter 3

8.3. Results and discussion

8.3.1. Geometry optimization

The atom numbering schemes and computed molecular geometries for 2,3-DKP, 2,6-DKP and 4,5-HHP are shown in Figs. 8.1 and 8.2, respectively. Bond distances, valence bond angles and selected torsional angles are compared with experimental values in Tables 8.1-8.3. The calculated minimum energy structures of 2,3-DKP, 2,6-DKP and its isomer 4,5-HHP display C_2 , C_s and C_1 symmetries, respectively. Additionally, the calculations have also been performed by constraining the six membered ring to be planar with C_{2v} (2,3-DKP and 2,6-DKP), C_1 (4,5-HHP). From the aforementioned statements, we would expect a total of 36 normal vibrational modes for all three molecules. The data for the calculated energy values at the B3LYP/aug-cc-pVTZ level, for both non-constrained and constrained molecules, together with their symmetries and respective normal modes are given in Table 8.4.

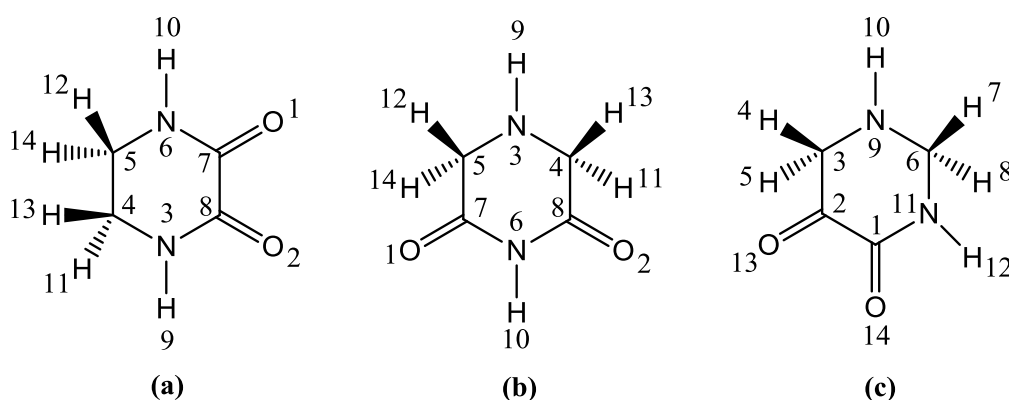


Figure 8.1. Atom numbering schemes for (a) 2,3-DKP (b) 2,6-DKP and (c) 4,5-HHP.

As previously stated, the X-ray structure for 2,3-DKP reveals that the molecule adopts a skew-boat conformation. The C_2 symmetry of the molecule is broken due to the intermolecular hydrogen bonding involving only one of the carbonyl group in the molecule.¹⁴ The bond lengths are 1.32 and 1.33 Å (C-N), 1.45 and 1.45 Å (N-C'), 1.48 Å (C-C'), 1.53 Å (C-C), 1.23 and 1.21 Å (C=O) and

0.90 and 0.87 Å (N-H), respectively. The DKP ring torsional angles are -3.27° and -3.84° (C'-N-C-C'), -15.60° (N-C-C-N), 37.89° and 38.64° (C-N-C'-C') and -52.60° (N-C'-C'-N), respectively. Our calculated minimum energy structure for 2,3-DKP has a skew-boat conformation with C_2 symmetry, where the corresponding calculated bond lengths are 1.36 Å, 1.45 Å, 1.51 Å, 1.55 Å, 1.20 Å and 1.00 Å, respectively and the torsional angles are -9.29° , -8.68° , 40.82° , and -52.60° , respectively. These bond lengths and torsional angles indicate there is a close relationship between the ring geometries of the experimental X-ray structure and the calculated structure for an isolated 2,3-DKP molecule.

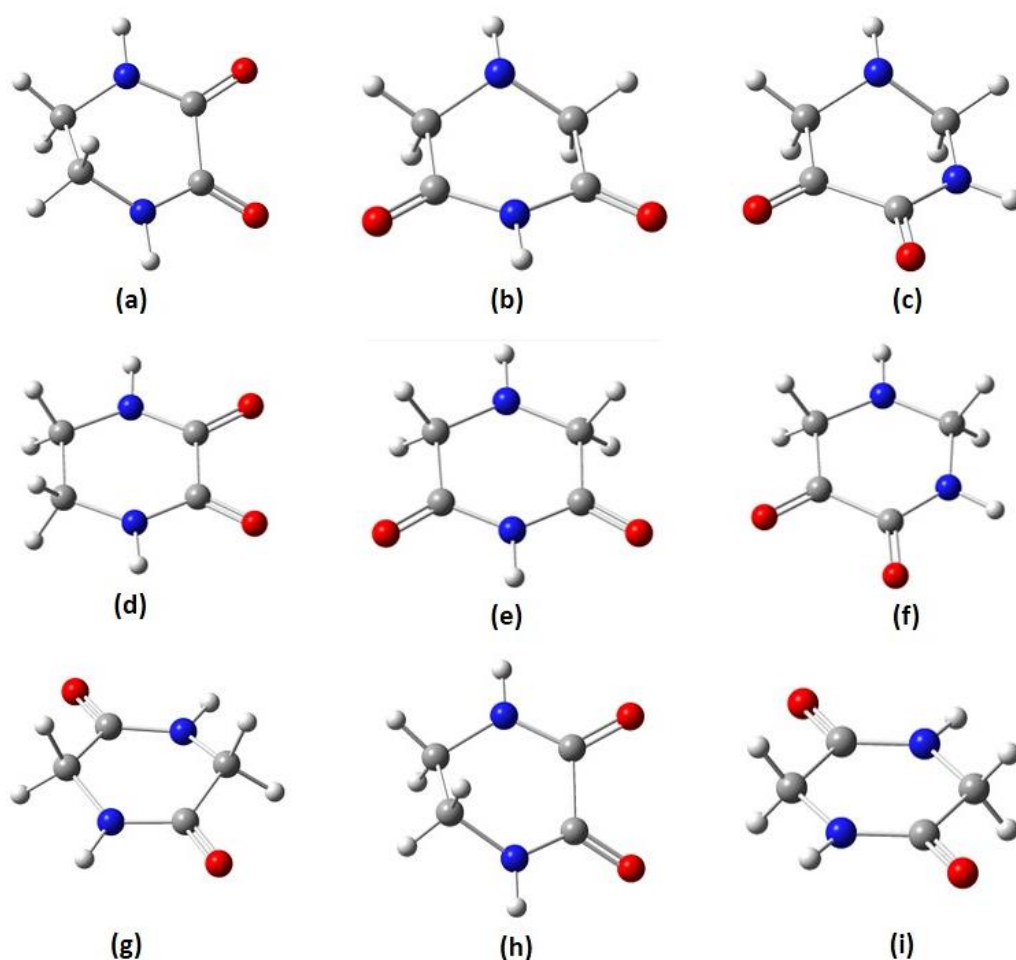


Figure 8.2. Calculated structures of 2,3-DKP (a) skew-boat (d) planar, 2,6-DKP (b) half-chair (e) planar, 4,5-HHP (c) half-chair (f) planar and 2,5-DKP (g) boat together with X-ray structures of (h) 2,3-DKP and (i) 2,5-DKP.

Table 8.1. Calculated bond lengths (Å), bond angles and dihedral angles (°) for 2,3-DKP.

Bond lengths (Å)	X-ray	Skew-boat	Planar
H(14)-C(5)	0.9753	1.0952	1.0916
H(13)-C(4)	0.9728	1.0952	1.0916
H(12)-C(5)	0.9761	1.0892	1.0916
H(11)-C(4)	1.0130	1.0892	1.0916
H(10)-N(6)	0.9064	1.0088	1.0095
H(9)-N(3)	0.8722	1.0088	1.0095
C(8)-N(3)	1.3376	1.3662	1.3607
C(8)-O(2)	1.2150	1.2089	1.2106
C(8)-C(7)	1.5323	1.5551	1.5414
C(7)-N(6)	1.3218	1.3662	1.3607
C(7)-O(1)	1.2302	1.2089	1.2106
N(6)-C(5)	1.4576	1.4552	1.4537
C(5)-C(4)	1.4898	1.5176	1.5435
C(4)-N(3)	1.4512	1.4552	1.4537
Bond angles (°)			
O(2)-C(8)-N(3)	124.9269	123.3273	121.0478
O(2)-C(8)-C(7)	119.1391	120.8964	122.6501
N(3)-C(8)-C(7)	115.9271	115.7684	116.3021
O(1)-C(7)-C(8)	119.2096	120.8964	121.0478
O(1)-C(7)-N(6)	123.4900	123.3273	122.6501
C(8)-C(7)-N(6)	117.2913	115.7684	116.3021
H(10)-N(6)-C(7)	117.1298	114.7607	113.7026
H(10)-N(6)-C(5)	119.8219	119.2970	117.0585
C(7)-N(6)-C(5)	122.8797	124.1210	129.2390
H(12)-C(5)-H(14)	110.7393	108.0542	106.7728
H(12)-C(5)-N(6)	106.8004	108.7218	108.7317
H(12)-C(5)-C(4)	109.8023	109.8955	108.9358
H(14)-C(5)-N(6)	107.3526	111.2949	108.7317
H(14)-C(5)-C(4)	112.8469	109.8780	108.9358
N(6)-C(5)-C(4)	109.0767	108.9770	114.4589
H(11)-C(4)-H(13)	107.9296	108.0542	106.7728
H(11)-C(4)-C(5)	109.0884	109.8955	108.9358
H(11)-C(4)-N(3)	108.6229	108.7218	108.7317
H(13)-C(4)-C(5)	111.0636	109.8780	108.9358
H(13)-C(4)-N(3)	110.2537	111.2949	108.7317
C(5)-C(4)-N(3)	109.8206	108.9770	114.4589
H(9)-N(3)-C(8)	116.1527	114.7607	113.7026
H(9)-N(3)-C(4)	120.4085	119.2970	117.0585
C(8)-N(3)-C(4)	122.7787	124.1210	129.2390

Dihedral angles (°)			
C(7)-C(8)-N(3)-C(4)	-3.8472	-9.2932	0.0000
C(7)-C(8)-N(3)-H(9)	-174.5562	-173.7563	180.0000
O(2)-C(8)-N(3)-C(4)	177.1158	171.7258	180.0000
O(2)-C(8)-N(3)-H(9)	6.4068	7.2626	0.0000
N(3)-C(8)-C(7)-N(6)	-15.6009	-8.6827	0.0000
N(3)-C(8)-C(7)-O(1)	165.4575	170.3251	180.0000
O(2)-C(8)-C(7)-N(6)	163.4952	170.3251	180.0000
O(2)-C(8)-C(7)-O(1)	-15.4464	-10.6671	0.0000
C(8)-C(7)-N(6)-C(5)	-3.2780	-9.2932	0.0000
C(8)-C(7)-N(6)-H(10)	-178.5433	-173.7563	180.0000
O(1)-C(7)-N(6)-C(5)	175.6143	171.7258	180.0000
O(1)-C(7)-N(6)-H(10)	0.3489	7.2626	0.0000
C(7)-N(6)-C(5)-C(4)	37.8950	40.8263	0.0000
C(7)-N(6)-C(5)-H(14)	-84.6855	-80.5024	-122.0517
C(7)-N(6)-C(5)-H(12)	156.5058	160.5958	122.0517
H(10)-N(6)-C(5)-C(4)	-146.9622	-155.3686	180.0000
H(10)-N(6)-C(5)-H(14)	90.4573	83.3027	57.9483
H(10)-N(6)-C(5)-H(12)	-28.3514	-35.5991	-57.9483
N(6)-C(5)-C(4)-N(3)	-52.6072	-52.6042	0.0000
N(6)-C(5)-C(4)-H(13)	69.6106	69.5842	121.9403
N(6)-C(5)-C(4)-H(11)	-171.5494	-171.6441	-121.9403
H(14)-C(5)-C(4)-N(3)	66.6122	69.5842	121.9403
H(14)-C(5)-C(4)-H(13)	-171.1700	-168.2273	-116.1194
H(14)-C(5)-C(4)-H(11)	-52.3300	-49.4556	0.0000
H(12)-C(5)-C(4)-N(3)	-169.3237	-171.6441	-121.9403
H(12)-C(5)-C(4)-H(13)	-47.1059	-49.4556	0.0000
H(12)-C(5)-C(4)-H(11)	71.7341	69.3160	116.1194
C(5)-C(4)-N(3)-C(8)	38.6429	40.8263	0.0000
C(5)-C(4)-N(3)-H(9)	-151.0307	-155.3686	180.0000
H(13)-C(4)-N(3)-C(8)	-84.0551	-80.5024	-122.0517
H(13)-C(4)-N(3)-H(9)	86.2713	83.3027	57.9483
H(11)-C(4)-N(3)-C(8)	157.8709	160.5958	122.0517
H(11)-C(4)-N(3)-H(9)	-31.8027	-35.5991	-57.9483

Table 8.2. Calculated bond lengths (Å), bond angles and dihedral angles (°) for 2,6-DKP.

Bond lengths (Å)	Half-chair	Planar
H(14)-C(5)	1.1037	1.0966
H(13)-C(4)	1.0873	1.0966
H(12)-C(5)	1.0873	1.0966

H(11)-C(4)	1.1037	1.0966
H(10)-N(6)	1.0124	1.0128
H(9)-N(3)	1.0101	1.0013
C(8)-C(4)	1.5160	1.5110
C(8)-N(6)	1.3889	1.3848
C(8)-O(2)	1.2086	1.2097
C(7)-C(5)	1.5160	1.2097
C(7)-O(1)	1.2086	1.5110
C(7)-N(6)	1.3889	1.3848
C(5)-N(3)	1.4541	1.4401
C(4)-N(3)	1.4541	1.4401
Bond angles (°)		
O(2)-C(8)-C(4)	123.6053	122.0644
O(2)-C(8)-N(6)	121.2879	120.7363
C(4)-C(8)-N(6)	115.0831	117.1994
O(1)-C(7)-C(5)	123.6053	122.0644
O(1)-C(7)-N(6)	121.2879	120.7363
C(5)-C(7)-N(6)	115.0831	117.1994
H(10)-N(6)-C(8)	116.3645	115.7607
H(10)-N(6)-C(7)	116.3645	115.7607
C(8)-N(6)-C(7)	127.1831	128.4785
H(12)-C(5)-H(14)	107.6022	106.1091
H(12)-C(5)-C(7)	107.2831	104.9704
H(12)-C(5)-N(3)	110.4185	112.3059
H(14)-C(5)-C(7)	106.5020	104.9704
H(14)-C(5)-N(3)	113.8850	112.3059
C(7)-C(5)-N(3)	110.8471	115.3874
H(11)-C(4)-H(13)	107.6022	106.1091
H(11)-C(4)-C(8)	106.5020	104.9704
H(11)-C(4)-N(3)	113.8850	112.3059
H(13)-C(4)-C(8)	107.2831	104.9704
H(13)-C(4)-N(3)	110.4185	112.3059
C(8)-C(4)-N(3)	110.8471	115.3874
H(9)-N(3)-C(5)	111.1863	116.8260
H(9)-N(3)-C(4)	111.1863	116.8260
C(5)-N(3)-C(4)	112.5852	126.3480
Dihedral angles (°)		
N(6)-C(8)-C(4)-N(3)	26.8913	0.0000
N(6)-C(8)-C(4)-H(13)	147.5186	124.1790
N(6)-C(8)-C(4)-H(11)	-97.4897	-124.1790
O(2)-C(8)-C(4)-N(3)	-154.8627	180.0000
O(2)-C(8)-C(4)-H(13)	-34.2354	-55.8210

O(2)-C(8)-C(4)-H(11)	80.7563	55.8210
C(4)-C(8)-N(6)-C(7)	2.8176	0.0000
C(4)-C(8)-N(6)-H(10)	179.2612	180.0000
O(2)-C(8)-N(6)-C(7)	-175.4729	180.0000
O(2)-C(8)-N(6)-H(10)	0.9707	0.0000
N(6)-C(7)-C(5)-N(3)	-26.8913	0.0000
N(6)-C(7)-C(5)-H(14)	97.4897	124.1790
N(6)-C(7)-C(5)-H(12)	-147.5186	-124.1790
O(1)-C(7)-C(5)-N(3)	154.8627	180.0000
O(1)-C(7)-C(5)-H(14)	-80.7563	-55.8210
O(1)-C(7)-C(5)-H(12)	34.2354	55.8210
C(5)-C(7)-N(6)-C(8)	-2.8176	0.0000
C(5)-C(7)-N(6)-H(10)	-179.2612	180.0000
O(1)-C(7)-N(6)-C(8)	175.4729	180.0000
O(1)-C(7)-N(6)-H(10)	-0.9707	0.0000
C(7)-C(5)-N(3)-C(4)	58.1854	0.0000
C(7)-C(5)-N(3)-H(9)	-176.2924	180.0000
H(14)-C(5)-N(3)-C(4)	-61.8838	-120.2484
H(14)-C(5)-N(3)-H(9)	63.6385	59.7516
H(12)-C(5)-N(3)-C(4)	176.9347	120.2484
H(12)-C(5)-N(3)-H(9)	-57.5431	-59.7516
C(8)-C(4)-N(3)-C(5)	-58.1854	0.0000
C(8)-C(4)-N(3)-H(9)	176.2924	180.0000
H(13)-C(4)-N(3)-C(5)	-176.9347	-120.2484
H(13)-C(4)-N(3)-H(9)	57.5431	59.7516
H(11)-C(4)-N(3)-C(5)	61.8838	120.2484
H(11)-C(4)-N(3)-H(9)	-63.6385	-59.7516

Table 8.3. Calculated bond lengths (Å), bond angles and dihedral angles (°) for 4,5-HHP.

Bond lengths (Å)	Half-chair	Planar
O(14)-C(1)	1.2110	1.2130
O(13)-C(2)	1.1993	1.2015
H(12)-N(11)	1.0084	1.0105
N(11)-C(1)	1.3626	1.3583
N(11)-C(6)	1.4554	1.4574
H(10)-N(9)	1.0106	1.0054
N(9)-C(3)	1.4568	1.4621
N(9)-C(6)	1.4464	1.4524
H(8)-C(6)	1.1036	1.0947
H(7)-C(6)	1.0893	1.0970
H(5)-C(3)	1.1046	1.0927

H(4)-C(3)	1.0884	1.0959
C(3)-C(2)	1.5206	1.5170
C(2)-C(1)	1.5565	1.5396
Bond angles (°)		
H(12)-N(11)-C(1)	115.4478	113.7938
H(12)-N(11)-C(6)	118.9612	116.0164
C(1)-N(11)-C(6)	125.5876	130.1050
H(10)-N(9)-C(3)	111.6263	110.1357
H(10)-N(9)-C(6)	110.9117	109.5079
C(3)-N(9)-C(6)	111.5491	123.0187
H(7)-C(6)-H(8)	108.0415	106.8754
H(7)-C(6)-N(11)	108.5879	106.8958
H(7)-C(6)-N(9)	109.3104	109.9865
H(8)-C(6)-N(11)	109.6253	108.6031
H(8)-C(6)-N(9)	112.5000	109.4338
N(11)-C(6)-N(9)	108.7034	114.7355
H(4)-C(3)-H(5)	107.6425	105.9072
H(4)-C(3)-N(9)	110.5497	110.7325
H(4)-C(3)-C(2)	108.3209	105.2678
H(5)-C(3)-N(9)	113.5081	110.6075
H(5)-C(3)-C(2)	106.6275	105.8414
N(9)-C(3)-C(2)	109.9881	117.7029
O(13)-C(2)-C(3)	122.5731	120.5679
O(13)-C(2)-C(1)	120.1750	120.0056
C(3)-C(2)-C(1)	117.2112	119.4223
O(14)-C(1)-N(11)	123.7074	123.2156
O(14)-C(1)-C(2)	121.5102	121.7620
N(11)-C(1)-C(2)	114.7719	115.0156
Dihedral angles (°)		
C(6)-N(11)-C(1)-C(2)	2.6183	0.0000
C(6)-N(11)-C(1)-O(14)	-178.5505	-179.0608
H(12)-N(11)-C(1)-C(2)	-176.7018	176.4681
H(12)-N(11)-C(1)-O(14)	2.1293	-2.5927
C(1)-N(11)-C(6)-N(9)	29.7990	0.0000
C(1)-N(11)-C(6)-H(8)	-93.5444	-122.7923
C(1)-N(11)-C(6)-H(7)	148.6275	122.2245
H(12)-N(11)-C(6)-N(9)	-150.9026	-176.4038
H(12)-N(11)-C(6)-H(8)	85.7540	60.8039
H(12)-N(11)-C(6)-H(7)	-32.0741	-54.1793
C(6)-N(9)-C(3)-C(2)	60.4637	-0.0001
C(6)-N(9)-C(3)-H(5)	-58.8944	-121.7920
C(6)-N(9)-C(3)-H(4)	-179.9607	121.1158
H(10)-N(9)-C(3)-C(2)	-174.8299	131.4879
H(10)-N(9)-C(3)-H(5)	65.8120	9.6959

H(10)-N(9)-C(3)-H(4)	-55.2543	-107.3963
C(3)-N(9)-C(6)-N(11)	-62.2918	0.0001
C(3)-N(9)-C(6)-H(8)	59.3118	122.3441
C(3)-N(9)-C(6)-H(7)	179.3347	-120.5344
H(10)-N(9)-C(6)-N(11)	172.6032	-131.7426
H(10)-N(9)-C(6)-H(8)	-65.7932	-9.3986
H(10)-N(9)-C(6)-H(7)	54.2297	107.7229
N(9)-C(3)-C(2)-C(1)	-25.5534	0.0000
N(9)-C(3)-C(2)-O(13)	156.7662	179.2556
H(5)-C(3)-C(2)-C(1)	97.9229	124.2094
H(5)-C(3)-C(2)-O(13)	-79.7574	-56.5350
H(4)-C(3)-C(2)-C(1)	-146.4777	-123.9035
H(4)-C(3)-C(2)-O(13)	35.8420	55.3521
C(3)-C(2)-C(1)-N(11)	-4.7276	0.0000
C(3)-C(2)-C(1)-O(14)	176.4130	179.0759
O(13)-C(2)-C(1)-N(11)	173.0112	-179.2598
O(13)-C(2)-C(1)-O(14)	-5.8482	-0.1840

Unfortunately, there is no X-ray data for 2,6-DKP and its isomer (4,5-HHP) with which to compare these results. However, the calculated structures predicts a sofa/half-chair/envelope conformation (four co-planar atoms) as the minimum energy conformers with C_s symmetry (2,6-DKP) and C_1 symmetry (4,5-HHP). It is noted that the calculation performed by constraining the six-membered ring to a planar conformation for all three molecules results in an imaginary frequency, which shows that all three molecules cannot/are unlikely to have a planar six-membered ring as the lowest energy conformation in the gas phase. Moreover, the boat and chair forms are also not preferred as the minimum energy conformers in the gas phase owing to the ring strain/torsional strain on one side of the six membered ring due to the attachment of the carbonyl carbon and nitrogen atoms. The skew-boat (2,3-DKP) and sofa conformations (2,6-DKP and 4,5-HHP) were found to be slightly lower in energy compared to the planar conformation (Table 8.4), because the calculations are based on a single molecule in the gas phase and do not take into account possible intermolecular forces. By comparing the calculated energies of all three regioisomers, the minimum energy boat conformer of 2,5-DKP was found to be the lowest energy conformer.

Table 8.4. Calculated energy values, conformation and vibrational modes for non-constrained and constrained molecules of 2,3-DKP, 2,6-DKP and 4,5-HHP.

Molecule	Conformation/symmetry	Energy (H)/imaginary frequencies	No. of Normal modes
2,3-DKP	Skew-boat (C_2)	-416.16724129 H (0)	19A + 17B
	Planar (C_{2v})	-416.15795063 H (1)	12A ₁ + 7A ₂ + 6B ₁ + 11B ₂
2,6-DKP	Half-chair (C_s)	-416.17027455 H (0)	20A' + 16A''
	Planar (C_{2v})	-416.15949849 H (2)	12A ₁ + 5A ₂ + 8B ₁ + 11B ₂
4,5-HHP	Half-chair (C_1)	-416.13377333 H (0)	36A
	Planar (C_1)	-416.12154984 H (2)	36A
2,5-DKP	Boat (C_2)	-416.17711871 H (0)	19A + 17B

Table 8.5. Comparison of calculated bond lengths for 2,3-DKP, 2,6-DKP and 4,5-HHP with the X-ray geometry bond lengths for 2,5-DKP.²³

Bond	2,3-DKP (Å)			2,6-DKP (Å)		4,5-HHP (Å)		2,5-DKP (Å)
	X-ray ¹⁴	Skew-boat	Planar	Half-chair	Planar	Half-chair	Planar	X-ray ²³
N-H	0.87,0.90	1.00	1.00	1.01	1.00, 1.01	1.00, 1.01	1.00, 1.01	0.85
N-C'	1.45	1.45	1.45	1.45	1.43	1.44, 1.45	1.45, 1.46	1.45
N-CO	1.32,1.33	1.36	1.36	1.38	1.38	1.36	1.35	1.32
C-H ¹	0.97	1.08, 1.09	1.09	1.08, 1.10	1.09	1.08, 1.10	1.09	0.93
C-H ²	0.97,1.01	1.08, 1.09	1.09	1.08, 1.10	1.09	1.08, 1.10	1.09	0.95
C'-CO	-	-	-	1.51	1.51	1.52	1.51	1.50
CO-CO	1.53	1.55	1.54	-	-	1.55	1.53	-
C'-C'	1.48	1.51	1.54	-	-	-	-	-
C=O	1.21,1.23	1.20	1.21	1.20	1.20	1.19, 1.21	1.20, 1.21	1.23

8.3.2. Vibrational assignments

Solid and aqueous phase FTIR and Raman spectra are compared with the regioisomer (2,5-DKP) in Figs. 8.3-8.10, respectively. Calculated Raman and IR spectra for 2,3-DKP, 2,6-DKP and 4,5-HHP are shown in Figs. 8.11-8.14, respectively. A comparison of calculated bond lengths with X-ray geometry bond lengths for 2,3-DKP and 2,5-DKP¹⁷ are shown Table 8.5. Detailed experimental and calculated vibrational data for 2,3-DKP, 2,6-DKP and 4,5-HHP in the solid and solution phases are shown in Tables 8.6-8.11. Spectral assignments were made with reference to the calculated data, group frequency considerations and by comparison with previous experimental work on 2,3-DKP and 2,5-DKP.^{15,16}

8.3.3. Wavenumber region above 2000 cm⁻¹

The bands found in this region are due to N-H, and C-H stretching modes. Bands between 3100 and 3350 cm⁻¹ are typical for the location of the N-H stretching vibration of a secondary amide group. The N-H stretching vibrations can be clearly seen in a broad region between 3120-3330 cm⁻¹ in both IR and Raman spectra of 2,3-DKP and 4,5-HHP. On *N*-deuteration these bands shift down in wavenumber and appear at 2342 and 2390 cm⁻¹ in the IR and at 2330 and 2370 cm⁻¹ in the Raman spectra and this data is in good agreement with previously reported data for *N*-deuterated 2,3-DKP.¹⁵ In 4,5-HHP, on *N*-deuteration these bands are found at ~2320 and 2400 cm⁻¹ in both IR and Raman spectra, respectively. Interestingly, in 2,6-DKP, two N-H stretching bands are observed at different wavenumbers (cm⁻¹) owing to the presence of N-H groups in different locations, one N-H group in between two CH₂ groups and other in between two carbonyl groups (Fig. 8.1). Hence, it has been hypothesised that both N-H groups are involved in hydrogen bonding but at different hydrogen bonding strengths. The N-H stretching vibrations at ~3300 cm⁻¹ is assigned to the N3H9 group and the broad band centred at ~2700 cm⁻¹ in both IR and Raman spectra is assigned to N6H10 stretching vibrations. Unfortunately, these assignments cannot be made from the calculated PEDs. As mentioned earlier, the calculations are performed for a single molecule in the gas phase and do not account for any intermolecular hydrogen bonding effects. On *N*-deuteration, the two N-H groups shift down to two different locations, ~2400 cm⁻¹ for N3D9 stretching and a broad band centred ~2150 cm⁻¹ for N6D10 stretching vibrations in both IR and Raman spectra of *N*-deuterated 2,6-DKP. Despite repeated deuteration, it is evident from IR and Raman spectra that 100% deuteration for all three molecules could not be achieved.

C-H stretching vibrations can clearly be detected in both the solid and solution state IR and Raman spectra of 2,3-DKP, 2,6-DKP and 4,5-HHP between 2850 and 3050 cm⁻¹ although they are more intense in the Raman than in the IR spectra. Compared to 2,5-DKP, the C-H vibrations are separated in the regions ~3000-3010 cm⁻¹ and ~2880-2930 cm⁻¹ (2,3-DKP), ~2970-3000 cm⁻¹ and ~2900-2930 cm⁻¹ (2,6-DKP), ~2990-3025 cm⁻¹ and ~2950-2970 cm⁻¹ (4,5-HHP) in both IR and Raman spectra of 2,3-DKP, 2,6-DKP and 4,5-HHP, respectively. Our calculated PEDs suggests that these modes are a combination of both symmetric and asymmetric C-H stretching vibrations. Previously, theoretical *ab initio* calculations have hypothesized a relationship between the conformation of the symmetrically substituted 2,5-DKP ring and the extent of splitting between the asymmetric and symmetric C-H stretching vibrations.¹⁶ Results showed that a splitting of these normal modes by ~30 cm⁻¹ predicted a DKP ring with a planar conformation, and by ~90 cm⁻¹ a

boat conformation. However, as previously stated, these assumptions cannot be made for other regioisomers of 2,5-DKP; none of the three molecules have planar/boat conformations as the minimum energy conformers but, instead, exist as skew-boat (2,3-DKP) and half-chair/sofa conformations (2,6-DKP and 4,5-HHP) in the gas phase. From our observations, it is hypothesised that DKPs with these conformations may show splitting of symmetric/asymmetric C-H stretching vibrations at two locations in the region between 2880 and 3050 cm^{-1} in both IR and Raman spectra. The calculated PEDs suggest that the minimum energy skew-boat (2,3-DKP) and half-chair/sofa conformations (2,6-DKP and 4,5-HHP) show a difference in the splitting of these modes by $\sim 110\text{ cm}^{-1}$ (2,3-DKP), $\sim 180\text{ cm}^{-1}$ (2,6-DKP) and $\sim 150\text{ cm}^{-1}$ (4,5-HHP) compared to their calculated planar conformers ($\sim 10\text{-}50\text{ cm}^{-1}$). Whereas, the experimental IR and Raman bands show a difference of $\sim 80\text{-}90\text{ cm}^{-1}$ for each molecule.

8.3.4. Wavenumber region 1200-1700 cm^{-1}

Bands found in this region are attributed to normal modes involving the following: C=O stretch, C-N stretch, C-H bending, CH_2 wagging and CH_2 torsion. Four bands associated with C=O stretching vibrations of 2,3-DKP can be detected between 1624 and 1715 cm^{-1} in both solid state IR and Raman spectra (Figs. 8.3 and 8.4). Previous studies on 2,3-DKP suggest that the splitting in this region is mainly due to the presence of two carbonyl groups.¹⁵ Additional bands may be observed due to factor group splitting, which mainly arises due to the interaction between more than one neighbouring molecules per crystallographic unit cell.^{18,19} Cheam and Krimm suggested that the splitting of the C=O stretching bands can also result from Fermi resonance.²⁰ These bands shift on *N*-deuteration and there is good agreement with the previously reported amide I mode and its *N*-deuterated shift of $\sim 15\text{-}30\text{ cm}^{-1}$ observed in the solid state Raman spectra of 2,3-DKP. In fact, this shift agrees well with the *cis* amide I mode shift ($\sim 30\text{ cm}^{-1}$) observed in 2,5-DKP.²² IR spectra also shows decreased frequencies on *N*-deuteration and can be explained by the weak coupling of N-H in-plane-bending with C=O stretching vibrations. In 2,6-DKP these vibrations are detected at ~ 1712 and 1683 cm^{-1} in the IR spectra. They are observed at 1705 and 1693 cm^{-1} in the solid state and at 1725 and 1703 cm^{-1} in the solution state Raman spectra of 2,6-DKP. Compared to the amide I mode of solid 2,5-DKP located at $\sim 1655\text{ cm}^{-1}$ in the solid state Raman spectrum, it is apparent that the ring C=O stretch of 2,6-DKP appears at a significantly higher wavenumber ($\sim 40\text{-}50\text{ cm}^{-1}$), and has a significantly higher Raman intensity than found in other CDAPs, including cyclo(Gly-Gly).^{16,18,19} This can be explained by the shortening of the ring C=O bond distance due to the

presence of the N-H group in between two carbonyl carbons, which is attributed to the delocalization of the lone pairs on the nitrogen atoms (Table 8.5).

On *N*-deuteration the mode at 1683 cm⁻¹ shifts down and appears at 1660 cm⁻¹ in the solid state and 1680 cm⁻¹ in the solution state IR spectra. They are observed at 1675 cm⁻¹ in the solid state and at 1678 cm⁻¹ in the solution state Raman spectra of 2,6-DKP. Both IR and Raman spectra also shows a downward shift of 18-25 cm⁻¹ which is a characteristic shift for *cis* amide I mode on *N*-deuteration.¹⁶ Interestingly, the modes at ~1712 and 1705 cm⁻¹ in the IR and Raman spectra, respectively do not show a downward shift indicative of the absence of N-H character. In the case of 4,5-HHP, the *cis* amide I mode is observed ~1685 and 1620 cm⁻¹ in both solid state IR and Raman spectra. Our calculated PEDs suggests that the mode at ~1685 cm⁻¹ is predominantly due to the C=O stretch of the carbonyl group (C2O13) present in between CH₂ atoms and the amide group with a small contribution from the C1O14 stretch (~7 %). The mode at ~1620 cm⁻¹ is attributed to the C=O stretching vibration of the C1O14 group involved in amide formation; this mode also shows contributions from the C2O13 stretch (~8 %), C-N stretch (~9 %) and N-H-in-plane-bending vibrations (~8%). These bands show a downward shift on *N*-deuteration, appear at ~1651 and 1606 cm⁻¹ and reveal weak shoulders at ~1635 and 1600 cm⁻¹ in both IR and Raman spectra. This suggests that both C=O stretching vibrations are coupled with N-H in-plane bending vibrations and hence, show a downward shifts of ~34 and 15 cm⁻¹, respectively. The band at ~1555 cm⁻¹ (in both the IR and Raman spectra of 4,5-HHP) is assigned to the N-H-in-plane-bending of the N9H10 group coupled with CH₂ bending vibrations as this band shifts on *N*-deuteration and appear at ~1545 cm⁻¹ in both IR and Raman spectra. Unfortunately, the N-H-in-plane-bending modes in 4,5-HHP could not be assigned by our calculated PEDs.

The C-N stretch, a *cis* amide II mode, is found at ~1517 cm⁻¹ in the solid state Raman spectrum of 2,5-DKP. This mode is, apparently, mainly an out-of-phase C_α-C-N stretch with a smaller contribution from the N-H in plane bend than in the *trans* amide II mode.¹⁶ The *cis* amide II mode, unlike its amide I mode counterpart, is not sensitive to different hydrogen bonding strengths found in the crystal lattices of DKPs.²² There is no band in the 1500 cm⁻¹ region for 2,3-DKP and 2,6-DKP, unlike that found in its regioisomer i.e. 2,5-DKP, Figs 8.3-8.10. The bands due to CH₂ bending vibrations are observed at ~1490 and 1470 cm⁻¹ (2,3-DKP), ~1426 and 1414 cm⁻¹ in (2,6-DKP) and ~1470 cm⁻¹ and 1400 cm⁻¹ (4,5-HHP) in both solid and solution state IR and Raman spectra. These assignments have been made possible from our calculated PEDs for the minimum energy conformers of 2,3-DKP and 2,6-DKP. However, in 2,3-DKP, our calculated PEDs for the planar ring conformation suggests that the CH₂ bending vibrations occur at higher wavenumbers

$\sim 1520\text{ cm}^{-1}$. But we know, from the X-ray structure, that 2,3-DKP does not have a planar DKP ring in the solid state.¹⁴ This is of particular interest, as Lenstra *et al.*,¹⁵ in their previous studies on 2,3-DKP suggests that the bands at $\sim 1490\text{ cm}^{-1}$ are due to ring stretching mode with a high contribution from C-N stretching character and bands at $\sim 1470\text{ cm}^{-1}$ are due to the N-C' stretching mode. The bands due to NH-in-plane-bending vibrations (N3H9) are observed as broad signals centered at 1457 cm^{-1} in both solid state IR and Raman spectra of 2,6-DKP. On *N*-deuteration this mode shifts down in wavenumber and appears at $\sim 1340\text{ cm}^{-1}$ in the IR and as a weak broad band at $\sim 1356\text{ cm}^{-1}$ in the Raman spectra of 2,6-DKP. This region appears to be more complex and therefore, assignments have been made by the appearance of intense IR bands in *N*-deuterated 2,6-DKP.

Interestingly, in 4,5-HHP the CH₂ bending vibrations appears at two different locations. The calculated PEDs suggests that the bending vibrations for the CH₂ group (CH_{2a}) present in between C=O and N-H groups occurs at lower wavenumbers ($\sim 1400\text{ cm}^{-1}$) compared to the other CH₂ group (CH_{2b}, $\sim 1470\text{ cm}^{-1}$) present in between two N-H groups in the molecule. The CH_{2b} bending modes shows an upward shift ($10\text{-}12\text{ cm}^{-1}$) on *N*-deuteration in both solid and solution state IR and Raman spectra of *N*-deuterated 4,5-HHP. This can be explained by the downward shifts of the location of the N-D in-plane-bending vibrations to wavenumbers below the CH₂ bending modes. This phenomenon was also observed for the CH₂ bending vibrations on *N*-deuteration in 2,5-DKP.¹⁶ The C-N (amide) stretching vibrations in 2,3-DKP and 4,5-HHP are found at $\sim 1450\text{-}1230\text{ cm}^{-1}$ coupled with NH-in-plane bending, CH₂ wagging, CH₂ twisting and a small contribution from C-C and N-C stretching vibrations. This vibration is observed between $1250\text{ and }1370\text{ cm}^{-1}$ in 2,6-DKP including a small contribution from C=O in-plane-bending vibrations. These bands shows a downward shift of $10\text{-}20\text{ cm}^{-1}$ owing to the presence of NH-in-plane bending character in both solid and solution IR and Raman spectra of 2,3-DKP, 2,6-DKP and 4,5-HHP. However, it was difficult to assign bands to specific vibrations due to their complexity. The reason for the decrease in wavenumber of C-N stretching vibrations in 2,3-DKP and 4,5-HHP can be attributed to the strong coupling of C-N vibrations with N-H in-plane-bending and CH₂ bending vibrations. Whereas, in 2,6-DKP, this can be explained by the delocalisation of partial double bonds on the amide linkages, and hence, decreasing the bond order and increase in bond lengths of the C-N bonds (1.38 \AA) compared to DKP (1.32 \AA) and additionally, due to strong coupling of C-N stretching with N-H-in-plane-bending vibrations. All the above explanations were made possible from our calculated PEDs for all three molecules and in comparison to previous studies undertaken on 2,5-DKPs.¹⁶ Theoretically from the PEDs and experimentally from *N*-deuteration shifts in IR

and Raman spectra, this mode is not a classical *cis* amide II mode due to the presence of high N-H character in all three molecules.

8.3.5. Wavenumber region 900-1200 cm⁻¹

The bands in this region are due to NC_α for 2,6-DKP and NC for 2,3-DKP as well as CH₂ rocking and wagging vibrations in all three molecules, including small NH-in-plane and out-of-plane bending (N3H9) vibrations in 2,6-DKP and small contributions from CO in-plane and out-of-plane bending vibrations in 4,5-HHP. The N-C' stretching vibrations are found at 1000-1190 cm⁻¹ for 2,3-DKP, 920-1140 cm⁻¹ for 2,6-DKP and 920-1150 cm⁻¹ in 4,5-HHP occurring at considerably lower wavenumber than the C-N (of amide) stretching vibrations, due to its longer bond length. The N-C' band at 1164 and 1039 cm⁻¹ shifts considerably on *N*-deuteration and appears at 1141 cm⁻¹ (solid state IR) and ~930 cm⁻¹ in both solid and solution state IR and Raman spectra of 2,3-DKP. In 2,6-DKP, this band is observed at ~1140 cm⁻¹, shows a downward shift on *N*-deuteration and appears at ~953 cm⁻¹ in both solid and solution state IR and Raman spectra. Whereas, in the case of 4,5-HHP this band is observed at ~1150 cm⁻¹ and shows a downward shift on *N*-deuteration and appears at ~990 cm⁻¹ in both solid and state IR and Raman spectra. The NC_α stretching vibrations in 2,5-DKP are found between 1160 and 1230 cm⁻¹. This can be explained by comparing the experimental bond distances for the N-C' in 2,3-DKP and the bond distance for NC_α of 2,5-DKP (1.451, 1.457 and 1.45 Å, respectively).¹⁶ It is apparent that the foregoing N-C bond distances are similar, thereby explaining the commonality of the location of these vibrational modes. Similar hypotheses can be put forward for 2,6-DKP and 4,5-HHP. In the region between 900 and 1080 cm⁻¹ the assignments are tentative because there is considerable mixing of the vibrational modes in all three molecules. However, it is common to find C-C stretching, CH₂ rocking modes and also CO in-plane bending vibrational modes in this region.

8.3.6. Wavenumber region 500-900 cm⁻¹

Various peptide group vibrations are found in this region, especially C=O and N-H out-of-plane bending modes, and also in-plane DKP ring deformation/stretching. The N-H bending modes have been assigned on the basis of *N*-deuteration shifts and also from previous IR and Raman data relating to 2,5-DKPs. Three bands found in the IR spectrum of 2,3-DKP at 803, 773 and 727 cm⁻¹ show significant shifts on deuteration. These bands are found in the Raman spectrum at 765 and 715 cm⁻¹. Previous work on 2,5-DKPs has shown that the N-H out-of-plane bending band is quite difficult to find and has an extensive feature centred ~820 cm⁻¹ in the IR spectrum.^{16,18,19} These

bands shift considerably on *N*-deuteration and appear at 625, 590 and 565 cm^{-1} in IR and at 723 and 715 cm^{-1} in Raman. In 2,6-DKP these bands are observed at ~ 895 , 838 and 688 cm^{-1} in both IR and Raman spectra. These modes shift on *N*-deuteration and appear at 742, 646 cm^{-1} in IR and at 743 and 676 cm^{-1} in the Raman spectra of 2,6-DKP. Whereas, in 4,5-HHP they are observed at 825, 775 cm^{-1} in IR and at 822 and 705 cm^{-1} in the Raman. On *N*-deuteration these modes shift down in wavenumber and appear at 764, 750 and 644 in the IR and at 772, 750 and 650 cm^{-1} in the Raman spectra. Unfortunately, these bands are not accurately assigned by our DFT calculations (due to hydrogen bonding effects). However, the calculated wavenumbers show that the vibrations in this region are of mixed character. Bands attributed to vibrations involving significant contributions from carbonyl in-plane or out-of-plane bending are found in the IR and Raman spectra of 2,3-DKP, 2,6-DKP and 4,5-HHP (between 500 and 800 cm^{-1}). This is contrary to previous results for 2,5-DKPs containing a secondary *cis* amide, where the ring amide C=O in-plane and out-of-plane bending vibrations occur between ~ 550 and 670 cm^{-1} .^{16,18}

8.3.7. Wavenumber region < 500 cm^{-1}

There are some weak bands observed in the Raman spectrum below 500 cm^{-1} , which are due to vibrations from C=O bending motions as well as the bending modes of the DKP ring and pyrimidine ring (4,5-HHP). The bands located between 50 and 200 cm^{-1} are mainly due to ring torsional vibrations and lattice vibrations. These bands show no remarkable shift on *N*-deuteration, indicative of very little N-H contributions to these modes. The bands at 437 and 481 cm^{-1} in the Raman spectra of 2,3-DKP show a downward shift of ~ 15 cm^{-1} , indicative of the presence of N-H out-of-plane bending vibrations. Previous studies on 2,3-DKP also suggest the appearance of N-H out-of-plane bending vibrations for molecules exhibiting intermolecular hydrogen bonding in this region.¹⁵ In 2,6-DKP the modes at 479 and 464 cm^{-1} in Raman spectra show a downward shift on *N*-deuteration and appear at 462 and 434 cm^{-1} , respectively. The calculated PEDs also suggest the presence of NH-out-of-plane bending vibrations in this region. In 4,5-HHP, few bands decrease in wavenumber (cm^{-1}) by ~ 1 -6 cm^{-1} indicating the presence of NH- out-of-plane bending vibrations. The imaginary frequencies for constrained ring (planar) for all three molecules are observed in this region. These vibrations are mainly due to ring bending modes in 2,3-DKP, 2,6-DKP and 4,5-HHP; they also include N-H-out-of-plane bending modes in 2,6-DKP.

Table 8.6. Experimental and calculated vibrational band wavenumbers (cm⁻¹) for non-deuterated 2,3-DKP.

IR s	Raman s	IR sol	Raman sol	Calc.	% PEDs skew boat	Calc.	% PEDs planar
3284							
3201	3213			3208 A	100% v _{ss} (NH)	3198 A ₁	100% v _{ss} (NH)
3156							
3128	3134			3207 B	100% v _{as} (NH)	3197 B ₂	100% v _{as} (NH)
3098							
3077	3010						
3002	3001		3006				
2997							
2924	2928		2954	2945 B	23% v _{ss} (CH ₂), 77% v _{as} (CH ₂)	2917 B ₁	100% v _{as} (CH ₂)
2903	2914			2945 A	37% v _{ss} (CH ₂), 63% v _{as} (CH ₂)	2891 A ₁	100% v _{ss} (CH ₂)
2877	2885		2899	2868 B	77% v _{ss} (CH ₂), 23% v _{as} (CH ₂)	2889 A ₂	100% v _{as} (CH ₂)
2855	2841			2855 A	63% v _{ss} (CH ₂), 37% v _{as} (CH ₂)	2879 B ₂	100% v _{ss} (CH ₂)
2802							
1715	1717						
1681	1697		1690	1692 B	73% v _{as} (CO)	1690 B ₂	71% v _{as} (CO)
1664	1663		1639	1681 A	81% v _{ss} (CO)	1679 A ₁	79% v _{ss} (CO)
	1647						
1624							
1489	1489	1493	1495	1499 A	97% δ(CH ₂)	1536 A ₁	96% δ(CH ₂)
	1484						
1473	1470	1472	1472	1496 B	94% δ(CH ₂)	1517 B ₂	92% δ(CH ₂)
	1459						
	1454						
1449	1443	1438	1443	1449 A	14% v _{ss} (CN), 22% δ _{ip,s} (NH), 42% ω(CH ₂)	1490 A ₁	17% v _{ss} (CN) 17% δ _{ip,s} (NH) 43% ω(CH ₂)
1424	1436			1423 B	11% v _{ss} (CO) 14% v _{as} (CN) 30% δ _{ip,as} (NH) 30% ω(CH ₂)	1459 B ₂	13% v _{as} (CO) 14% v _{as} (CN) 22% δ _{ip,as} (NH) 36% ω(CH ₂)

1386	1387	1387	1387	1374 B	28% $\delta_{ip,as}(NH)$ 52% $\omega(CH_2)$	1389 B ₂	11% $v_{as}(NC)$ 29% $\delta_{ip,as}(NH)$ 51% $\omega(CH_2)$
1377		1364	1367	1365 A	34% $\delta_{ip,s}(NH)$ 22% $\omega(CH_2)$ 26% $\tau(CH_2)$	1376 A ₁	21% $v_{ss}(CN)$ 12% $v(C7C8)$ 48% $\delta_{ip,s}(NH)$ 10% $\delta_{ip,s}(CO)$
	1356						
1348	1351	1338		1349 A	35% $v_{ss}(CN)$ 12% $v(C7C8)$ 15% $\delta_{ip,s}(NH)$ 17% $\tau(CH_2)$	1315 A ₁	20% $v_{ss}(NC)$ 21% $v_{ss}(CN)$ 42% $\omega(CH_2)$
1296	1300	1299		1251 B	10% $\rho(CH_2)$ 81% $\tau(CH_2)$	1283 A ₂	98% $\tau(CH_2)$
1284	1287						
1253	1261		1253	1245 A	18% $v_{ss}(NC)$ 11% $v_{ss}(CN)$ 47% $\tau(CH_2)$ 13% $v(C4C5)$	1281 B ₁	93% $\tau(CH_2)$
1242	1238	1243		1232 B	45% $v_{as}(CN)$ 24% $\delta_{ip,as}(NH)$ 14% $\delta_{ip,as}(CO)$	1264 B ₂	41% $v_{as}(CN)$ 31% $\delta_{ip,as}(NH)$ 12% $\delta_{ip,as}(CO)$
1223							
1188							
1164				1119 A	26% $v_{ss}(NC)$ 11% $\delta_{ip,s}(NH)$ 31% $\rho(CH_2)$ 16% $\omega(CH_2)$	1169 A ₁	34% $v_{ss}(NC)$ 11% $\omega(CH_2)$ 25% $v(C4C5)$
	1139	1136	1132				
1093	1090		1089	1091 A	53% $\rho(CH_2)$ 21% $v(C4C5)$	1105 A ₂	101% $\rho(CH_2)$
1039	1045	1037		1028 B	57% $v_{as}(NC)$ 15% $\delta_{ip,as}(CO)$	1029 B ₂	57% $v_{as}(NC)$ 21% $\delta_{ip,as}(CO)$
967	972	969	973	975 B	47% $\rho(CH_2)$ 29% $\delta_{ip}(\text{Ring-3})$	895 A ₁	14% $v_{ss}(NC)$ 59% $v(C4C5)$
916	920		919	900 A	16% $v_{ss}(NC)$ 54% $v(C4C5)$	865 B ₁	93% $\rho(CH_2)$
819	816		813	812 A	107% $\delta_{op,s}(CO)$	845 B ₂	85% $\delta_{ip}(\text{Ring-3})$
687				691 A	34% $\rho(CH_2)$ 44% $\delta_{ip}(\text{Ring-3})$	805 A ₂	112% $\delta_{op,s}(CO)$
728				691 B	19% $v_{ss}(NC)$ 30% $v_{ss}(CN)$ 32% $v(C7C8)$ 10% $\delta_{ip,s}(CO)$	684 A ₁	24% $v_{ss}(NC)$ 29% $v_{ss}(CN)$ 30% $v(C7C8)$
640							
803	765			609 B	11% $\delta_{ip,as}(CO)$ 51% $\delta_{op,as}(NH)$ 40% $\delta_{op,as}(CO)$	621 B ₁	80% $\delta_{op,as}(NH)$ 45% $\delta_{op,as}(CO)$
773	735		733	550 A	84% $\delta_{op,s}(NH)$ 12% $\delta_{ip}(\text{Ring-1})$	559 A ₂	103% $\delta_{op,s}(NH)$
589	584						
515	516		514	549 B	20% $v_{as}(CN)$ 53% $\delta_{ip,as}(CO)$ 11% $\delta_{op,as}(NH)$	554 B ₂	22% $v_{as}(CN)$ 61% $\delta_{ip,as}(CO)$
506							
475	481		487	486 A	21% $v(C7C8)$ 17% $\delta_{op,s}(NH)$ 46% $\delta_{ip}(\text{Ring-1})$	512 A ₁	25% $v(C7C8)$ 60% $\delta_{ip}(\text{Ring-1})$
	437		430	436 B	82% $\delta_{ip}(\text{Ring-2})$	444 B ₂	12% $v_{as}(NC)$ 79% $\delta_{ip}(\text{Ring-2})$
	377		388	384 B	36% $\delta_{op,as}(NH)$ 53% $\delta_{op,as}(CO)$ 11% $\delta_{op}(\text{Ring-2})$	381 B ₁	28% $\delta_{op,as}(NH)$ 67% $\delta_{op,as}(CO)$

	326			346 A	13% $\nu(\text{C7C8})$ 65% $\delta_{\text{ip,s}}(\text{CO})$ 19% $\delta_{\text{ip}}(\text{Ring-1})$	350 A ₁	11% $\nu(\text{C7C8})$ 66% $\delta_{\text{ip,s}}(\text{CO})$ 20% $\delta_{\text{ip}}(\text{Ring-1})$
	313		313	296 A	31% $\delta_{\text{op}}(\text{Ring-1})$ 64% $\delta_{\text{op}}(\text{Ring-3})$	244i A ₂	46% $\delta_{\text{op}}(\text{Ring-1})$ 59% $\delta_{\text{op}}(\text{Ring-3})$
	198						
	183		161				
	135		130	138 B	110% $\delta_{\text{op}}(\text{Ring-2})$	79 A ₂	58% $\delta_{\text{op}}(\text{Ring-1})$ 56% $\delta_{\text{op}}(\text{Ring-3})$
	112		108				
	95		95	84 A	72% $\delta_{\text{op}}(\text{Ring-1})$ 36% $\delta_{\text{op}}(\text{Ring-3})$	40 B ₁	122% $\delta_{\text{op}}(\text{Ring-2})$

Table 8.7. Experimental and calculated vibrational band wavenumbers (cm^{-1}) for *N*-deuterated 2,3-DKP.

IR s	Raman s	IR sol	Raman sol	Calc.	% PEDs skew boat	Calc.	% PEDs planar
3002	3006		3005				
	3001						
2972	2974						
2942	2943		2955	2945 B	23% $\nu_{\text{ss}}(\text{CH}_2)$ 77% $\nu_{\text{as}}(\text{CH}_2)$	2917 B ₁	100% $\nu_{\text{as}}(\text{CH}_2)$
2927	2926		2903	2945 A	37% $\nu_{\text{ss}}(\text{CH}_2)$ 63% $\nu_{\text{as}}(\text{CH}_2)$	2891 A ₁	100% $\nu_{\text{ss}}(\text{CH}_2)$
2890	2894			2868 B	77% $\nu_{\text{ss}}(\text{CH}_2)$ 23% $\nu_{\text{as}}(\text{CH}_2)$	2889 A ₂	100% $\nu_{\text{as}}(\text{CH}_2)$
2853	2844			2855 A	63% $\nu_{\text{ss}}(\text{CH}_2)$ 37% $\nu_{\text{as}}(\text{CH}_2)$	2879 B ₂	100% $\nu_{\text{ss}}(\text{CH}_2)$
2803	2802						
2392	2370			2352 A	99% $\nu_{\text{ss}}(\text{ND})$	2344 A ₁	99% $\nu_{\text{ss}}(\text{ND})$
2342	2330			2351 B	99% $\nu_{\text{as}}(\text{ND})$	2343 B ₂	99% $\nu_{\text{as}}(\text{ND})$
1715	1706						
1673	1683	1674	1679	1683 B	78% $\nu_{\text{as}}(\text{CO})$	1677 A ₁	77% $\nu_{\text{as}}(\text{CO})$
1659	1639	1634	1629	1672 A	86% $\nu_{\text{ss}}(\text{CO})$	1667 B ₂	85% $\nu_{\text{ss}}(\text{CO})$
1627	1626						
1488	1484	1486	1489	1499 A	97% $\delta(\text{CH}_2)$	1536 A ₁	97% $\delta(\text{CH}_2)$
1474	1479	1470	1465	1496 B	95% $\delta(\text{CH}_2)$	1516 B ₂	95% $\delta(\text{CH}_2)$
1466		1463					

1456	1459						
1435	1440			1428 A	19% $v_{ss}(\text{CN})$ 56% $\omega(\text{CH}_2)$	1471 A ₁	26% $v_{ss}(\text{CN})$ 50% $\omega(\text{CH}_2)$
1401	1405	1409	1412	1401 B	13% $v_{as}(\text{CN})$ 72% $\omega(\text{CH}_2)$	1439 B ₂	16% $v_{as}(\text{CN})$ 66% $\omega(\text{CH}_2)$
1388	1389						
1351	1362	1369	1370	1354 A	10% $v_{ss}(\text{NC})$ 25% $v_{ss}(\text{CN})$ 15% $\omega(\text{CH}_2)$ 42% $\tau(\text{CH}_2)$	1345 B ₂	28% $v_{as}(\text{NC})$ 26% $v_{as}(\text{CN})$ 25% $\omega(\text{CH}_2)$
1325	1331	1333		1314 B	27% $v_{as}(\text{NC})$ 30% $v_{as}(\text{CN})$ 10% $\delta_{ip,as}(\text{ND})$ 14% $\omega(\text{CH}_2)$	1324 A ₁	12% $v_{ss}(\text{NC})$ 33% $v_{ss}(\text{CN})$ 38% $\omega(\text{CH}_2)$
1297				1250 B	10% $\rho(\text{CH}_2)$ 81% $\tau(\text{CH}_2)$	1283 A ₂	98% $\tau(\text{CH}_2)$
1285	1270		1270				
1265	1259		1240	1250 A	15% $v_{ss}(\text{CN})$ 50% $\tau(\text{CH}_2)$ 12% $v(\text{C4C5})$	1281 B ₁	93% $\tau(\text{CH}_2)$
1243	1235						
1198			1201	1213 A	38% $v_{ss}(\text{NC})$ 10% $v(\text{C7C8})$ 20% $\delta_{ip,s}(\text{ND})$ 14% $\delta_{ip,s}(\text{CO})$	1226 A ₁	37% $v_{ss}(\text{NC})$ 12% $v(\text{C7C8})$ 16% $\delta_{ip,s}(\text{ND})$ 14% $\delta_{ip,s}(\text{CO})$
1141	1149		1142	1106 B	16% $v_{as}(\text{NC})$ 19% $v_{as}(\text{CN})$ 22% $\delta_{ip,as}(\text{ND})$ 33% $\delta_{ip,as}(\text{CO})$	1111 B ₂	16% $v_{as}(\text{NC})$ 19% $v_{as}(\text{CN})$ 25% $\delta_{ip,as}(\text{ND})$ 34% $\delta_{ip,as}(\text{CO})$
1091	1088		1091	1096 A	83% $\rho(\text{CH}_2)$ 10% $v(\text{C4C5})$	1105 A ₂	101% $\rho(\text{CH}_2)$
1041	1052		1043	1023 A	27% $\delta_{ip,s}(\text{ND})$ 19% $\omega(\text{CH}_2)$ 38% $v(\text{C4C5})$	1077 A ₁	34% $\delta_{ip,s}(\text{ND})$ 10% $\omega(\text{CH}_2)$ 46% $v(\text{C4C5})$
993	997						
965	968	972	970	976 B	45% $\rho(\text{CH}_2)$ 35% $\delta_{ip}(\text{Ring-3})$	902 B ₂	38% $v_{as}(\text{NC})$ 58% $\delta_{ip,as}(\text{ND})$
929	936	921	892	890 B	37% $v_{as}(\text{NC})$ 57% $\delta_{ip,as}(\text{ND})$	865 B ₁	93% $\rho(\text{CH}_2)$
	918						
	868						
	844		840	815 A	14% $v_{ss}(\text{NC})$ 17% $\delta_{ip,s}(\text{ND})$ 52% $\delta_{op,s}(\text{CO})$ 17% $v(\text{C4C5})$	837 B ₂	86% $\delta_{ip}(\text{Ring-3})$
814	816	817	803	809 A	16% $v_{ss}(\text{NC})$ 17% $\delta_{ip,s}(\text{ND})$ 55% $\delta_{op,s}(\text{CO})$ 12% $v(\text{C4C5})$	804 A ₂	111% $\delta_{op,s}(\text{CO})$
800							
780							
	733						
	723						
712	715		716	685 B	35% $\rho(\text{CH}_2)$ 48% $\delta_{ip}(\text{Ring-3})$	795 A ₁	24% $v_{ss}(\text{NC})$ 37% $\delta_{ip,s}(\text{ND})$ 36% $v(\text{C4C5})$

694				668 A	11% $\nu_{ss}(\text{NC})$ 29% $\nu_{ss}(\text{CN})$ 31% $\nu(\text{C7C8})$ 12% $\delta_{ip,s}(\text{ND})$ 11% $\delta_{ip,s}(\text{CO})$	667 A ₁	17% $\nu_{ss}(\text{NC})$ 30% $\nu_{ss}(\text{CN})$ 31% $\nu(\text{C7C8})$
	613						
565	562		560	564 B	12% $\nu_{as}(\text{CN})$ 31% $\delta_{ip,as}(\text{CO})$ 17% $\delta_{op,as}(\text{ND})$ 39% $\delta_{op,as}(\text{CO})$	544 B ₁	51% $\delta_{op,as}(\text{ND})$ 82% $\delta_{op,as}(\text{CO})$
504	506		510	519 B	11% $\nu_{as}(\text{CN})$ 30% $\delta_{ip,as}(\text{CO})$ 20% $\delta_{op,as}(\text{ND})$ 41% $\delta_{op,as}(\text{CO})$	540 B ₂	23% $\nu_{as}(\text{CN})$ 57% $\delta_{ip,as}(\text{CO})$
493			490	496 A	27% $\nu(\text{C7C8})$ 56% $\delta_{ip}(\text{Ring-1})$	503 A ₁	27% $\nu(\text{C7C8})$ 59% $\delta_{ip}(\text{Ring-1})$
468	470		440				
	422			433 B	80% $\delta_{ip}(\text{Ring-2})$	440 B ₂	12% $\nu_{as}(\text{NC})$ 77% $\delta_{ip}(\text{Ring-2})$
626	723			392 A	90% $\delta_{op,s}(\text{ND})$	412 A ₂	108% $\delta_{op,s}(\text{ND})$
	375		385				
	324		323	342 A	11% $\nu(\text{C7C8})$ 57% $\delta_{ip,s}(\text{CO})$ 21% $\delta_{ip}(\text{Ring-1})$	349 A ₁	11% $\nu(\text{C7C8})$ 65% $\delta_{ip,s}(\text{CO})$ 21% $\delta_{ip}(\text{Ring-1})$
590	715			309 B	71% $\delta_{op,as}(\text{ND})$ 22% $\delta_{op,as}(\text{CO})$	317 B ₁	64% $\delta_{op,as}(\text{ND})$ 31% $\delta_{op,as}(\text{CO})$
	270			295 A	31% $\delta_{op}(\text{Ring-1})$ 65% $\delta_{op}(\text{Ring-3})$	244i A ₂	46% $\delta_{op}(\text{Ring-1})$ 61% $\delta_{op}(\text{Ring-3})$
	194		183				
	181		162				
	132		135	136 B	116% $\delta_{op}(\text{Ring-2})$	79 A ₂	58% $\delta_{op}(\text{Ring-1})$ 59% $\delta_{op}(\text{Ring-3})$
	110		109				
	92		94	83 A	72% $\delta_{op}(\text{Ring-1})$ 37% $\delta_{op}(\text{Ring-3})$	39 B ₁	130% $\delta_{op}(\text{Ring-2})$

Table 8.8. Experimental and calculated vibrational band wavenumbers (cm^{-1}) for non-deuterated 2,6-DKP.

IR s	Raman s	IR sol	Raman sol	Calc.	% PEDs half-chair	Calc.	% PEDs planar
3383							
3293	3301			3180 A'	100% $\nu(\text{N6H10})$	3282 A ₁	100% $\nu(\text{N3H9})$
3163				3175 A'	100% $\nu(\text{N3H9})$	3176 A ₁	100% $\nu(\text{N6H10})$
	3001						
	2997		2997				
2981	2983			2970 A'	42% $\nu_{ss}(\text{CH}_2)$ 58% $\nu_{as}(\text{CH}_2)$	2855 B ₁	100% $\nu_{as}(\text{CH}_2)$

2919	2925		2917	2969 A"	41% $v_{ss}(\text{CH}_2)$ 59% $v_{as}(\text{CH}_2)$	2854 A ₂	100% $v_{as}(\text{CH}_2)$
				2781 A"	59% $v_{ss}(\text{CH}_2)$ 41% $v_{as}(\text{CH}_2)$	2847 A ₁	100% $v_{ss}(\text{CH}_2)$
2905	2905			2780 A'	58% $v_{ss}(\text{CH}_2)$ 42% $v_{as}(\text{CH}_2)$	2842 B ₂	100% $v_{ss}(\text{CH}_2)$
2704	2710						
1747							
1712	1705		1725	1695 A'	86% $v_{ss}(\text{CO})$	1684 A ₁	86% $v_{ss}(\text{CO})$
1683	1693		1703	1682 A"	77% $v_{as}(\text{CO})$ 10% $\delta_{ip}(\text{N6H10})$	1675 B ₂	75% $v_{as}(\text{CO})$ 11% $\delta_{ip}(\text{N6H10})$
1625							
1471	1472						
1457	1457			1435 A"	68% $\delta_{ip}(\text{N3H9})$ 15% $\omega(\text{CH}_2)$	1478 B ₂	11% $v_{as}(\text{NC}_\alpha)$ 59% $\delta_{ip}(\text{N3H9})$ 10% $\delta(\text{CH}_2)$ 14% $\omega(\text{CH}_2)$
1442							
1427	1429	1426	1425	1428 A'	92% $\delta(\text{CH}_2)$	1450 A ₁	92% $\delta(\text{CH}_2)$
1411	1414			1415 A"	97% $\delta(\text{CH}_2)$	1436 B ₂	88% $\delta(\text{CH}_2)$
		1378					
1360	1362			1367 A"	16% $v_{as}(\text{CO})$ 25% $v_{as}(\text{CN})$ 54% $\delta_{ip}(\text{N6H10})$	1374 B ₂	16% $v_{as}(\text{CO})$ 30% $v_{as}(\text{CN})$ 50% $\delta_{ip}(\text{N6H10})$
		1349	1349	1365 A'	15% $v_{ss}(\text{CN})$ 19% $v_{ss}(\text{CC}_\alpha)$ 10% $\delta_{ip}(\text{Ring-1})$ 30% $\omega(\text{CH}_2)$	1369 A ₁	17% $v_{ss}(\text{CN})$ 21% $v_{ss}(\text{CC}_\alpha)$ 10% $\delta_{ip,s}(\text{CO})$ 13% $\delta_{ip}(\text{Ring-1})$ 26% $\omega(\text{CH}_2)$
1338	1336	1336		1328 A'	22% $v_{ss}(\text{CN})$ 18% $\delta_{ip,s}(\text{CO})$ 47% $\omega(\text{CH}_2)$	1341 A ₁	20% $v_{ss}(\text{CN})$ 16% $\delta_{ip,s}(\text{CO})$ 55% $\omega(\text{CH}_2)$
1307	1318	1314	1314	1253 A"	15% $v_{as}(\text{CN})$ 12% $v_{as}(\text{CC}_\alpha)$ 22% $v_{as}(\text{NC}_\alpha)$ 10% $\delta_{ip}(\text{N3H9})$ 20% $\omega(\text{CH}_2)$ 14% $\tau(\text{CH}_2)$	1298 B ₂	18% $v_{as}(\text{CN})$ 20% $v_{as}(\text{CC}_\alpha)$ 46% $v_{as}(\text{NC}_\alpha)$ 10% $\delta_{ip}(\text{N6H10})$
1266		1276		1242 A"	17% $v_{as}(\text{CN})$ 15% $\delta_{ip}(\text{N6H10})$ 51% $\omega(\text{CH}_2)$	1254 B ₂	78% $\omega(\text{CH}_2)$
1183	1194	1198		1236 A'	86% $\tau(\text{CH}_2)$	1219 A ₂	95% $\tau(\text{CH}_2)$
				1157 A"	79% $\tau(\text{CH}_2)$	1189 B ₁	96% $\tau(\text{CH}_2)$
1139	1143	1145	1145	1134 A"	62% $v_{as}(\text{NC}_\alpha)$ 14% $\delta_{ip}(\text{N3H9})$	1185 B ₂	26% $v_{as}(\text{CN})$ 32% $v_{as}(\text{NC}_\alpha)$ 21% $\delta_{ip}(\text{N3H9})$ 10% $\delta_{ip}(\text{N6H10})$
1087	1090		1024				
1017	1010			1025 A'	56% $\rho(\text{CH}_2)$ 16% $\delta_{ip}(\text{Ring-3})$ 11% $\delta_{op,as}(\text{CO})$	987 A ₂	26% $\delta_{op,s}(\text{CO})$ 77% $\rho(\text{CH}_2)$
971	980			962 A'	60% $v_{ss}(\text{NC}_\alpha)$ 11% $\delta_{op}(\text{N3H9})$ 12% $\omega(\text{CH}_2)$	967 A ₁	74% $v_{ss}(\text{NC}_\alpha)$
962	966			961 A"	22% $\delta_{op,s}(\text{CO})$ 75% $\rho(\text{CH}_2)$	960 B ₁	87% $\rho(\text{CH}_2)$ 21% $\delta_{op,as}(\text{CO})$
921	924			916 A'	15% $v_{ss}(\text{NC}_\alpha)$ 16% $\delta_{op}(\text{N3H9})$ 41% $\delta_{ip}(\text{Ring-3})$ 12% $\delta_{op,as}(\text{CO})$	896 A ₁	12% $v_{ss}(\text{CC}_\alpha)$ 74% $\delta_{ip}(\text{Ring-3})$

895	895		889	890 A"	18% $\nu_{as}(\text{CN})$ 47% $\nu_{as}(\text{CC}_\alpha)$ 15% $\delta_{ip,as}(\text{CO})$ 12% $\delta_{ip}(\text{N6H10})$	892 B ₂	17% $\nu_{as}(\text{CN})$ 47% $\nu_{as}(\text{CC}_\alpha)$ 17% $\delta_{ip,as}(\text{CO})$ 12% $\delta_{ip}(\text{N6H10})$
823	824		797				
838	840			739 A'	97% $\delta_{op}(\text{N6H10})$ 24% $\delta_{op,as}(\text{CO})$	752 B ₁	105% $\delta_{op}(\text{N6H10})$ 21% $\delta_{op,as}(\text{CO})$
688	690		681	708 A'	10% $\nu_{ss}(\text{CN})$ 50% $\nu_{ss}(\text{CC}_\alpha)$ 37% $\delta_{op}(\text{N3H9})$	660 A ₁	21% $\nu_{ss}(\text{CN})$ 43% $\nu_{ss}(\text{CC}_\alpha)$ 10% $\nu_{ss}(\text{NC}_\alpha)$ 16% $\delta_{ip}(\text{Ring-3})$
606	609			636 A'	10% $\nu_{ss}(\text{CN})$ 11% $\nu_{ss}(\text{NC}_\alpha)$ 23% $\delta_{op}(\text{N3H9})$ 19% $\delta_{ip}(\text{Ring-3})$ 10% $\delta_{op,as}(\text{CO})$	576 A ₂	85% $\delta_{op,s}(\text{CO})$ 19% $\rho(\text{CH}_2)$
				619 A"	66% $\delta_{op,s}(\text{CO})$ 18% $\rho(\text{CH}_2)$	537 B ₂	20% $\nu_{as}(\text{CC}_\alpha)$ 73% $\delta_{ip,as}(\text{CO})$
	558		552	546 A'	12% $\nu_{ss}(\text{CN})$ 19% $\delta_{ip}(\text{Ring-1})$ 15% $\rho(\text{CH}_2)$ 10% $\delta_{ip}(\text{Ring-3})$ 27% $\delta_{op,as}(\text{CO})$	535 B ₁	10% $\delta_{op}(\text{Ring-2})$ 18% $\rho(\text{CH}_2)$ 62% $\delta_{op,as}(\text{CO})$
545	549			533 A"	21% $\nu_{as}(\text{CC}_\alpha)$ 72% $\delta_{ip,as}(\text{CO})$	498 A ₁	20% $\nu_{ss}(\text{CN})$ 66% $\delta_{ip}(\text{Ring-1})$
480	479						
458	464		460	443 A'	14% $\nu_{ss}(\text{CN})$ 14% $\delta_{ip,s}(\text{CO})$ 34% $\delta_{ip}(\text{Ring-1})$ 10% $\rho(\text{CH}_2)$	466 B ₂	82% $\delta_{ip}(\text{Ring-2})$
	390		388	441 A"	75% $\delta_{ip}(\text{Ring-2})$	377 A ₁	12% $\nu_{ss}(\text{CN})$ 64% $\delta_{ip,s}(\text{CO})$ 17% $\delta_{ip}(\text{Ring-1})$
	313		318	376 A'	54% $\delta_{ip,s}(\text{CO})$ 26% $\delta_{ip}(\text{Ring-1})$	365 i B ₁	79% $\delta_{op}(\text{N3H9})$ 11% $\delta_{op}(\text{Ring-2})$ 13% $\delta_{op}(\text{Ring-1})$
	261			269 A'	58% $\delta_{op}(\text{Ring-2})$ 34% $\delta_{op}(\text{Ring-1})$	196 i B ₁	20% $\delta_{op}(\text{N3H9})$ 48% $\delta_{op}(\text{Ring-2})$ 34% $\delta_{op}(\text{Ring-1})$
	165		159				
	141		132	134 A'	46% $\delta_{op}(\text{Ring-2})$ 56% $\delta_{op}(\text{Ring-1})$	128 B ₁	47% $\delta_{op}(\text{Ring-2})$ 65% $\delta_{op}(\text{Ring-1})$
	110		108	114 A"	102% $\delta_{op}(\text{Ring-3})$	64 A ₂	111% $\delta_{op}(\text{Ring-3})$
	95		95				

Table 8.9. Experimental and calculated vibrational band wavenumbers (cm^{-1}) for *N*-deuterated 2,6-DKP.

IR s	Raman s	IR sol	Raman sol	Calc.	% PEDs half-chair	Calc.	% PEDs planar
2980	2983		2990	2970 A	42% $\nu_{ss}(\text{CH}_2)$ 58% $\nu_{as}(\text{CH}_2)$	2855 B ₁	100% $\nu_{as}(\text{CH}_2)$
2958				2969 B	41% $\nu_{ss}(\text{CH}_2)$ 59% $\nu_{as}(\text{CH}_2)$	2854 A ₂	100% $\nu_{as}(\text{CH}_2)$
2920	2922		2914				
2903	2905						
2850				2781 B	59% $\nu_{ss}(\text{CH}_2)$ 41% $\nu_{as}(\text{CH}_2)$	2847 A ₁	100% $\nu_{ss}(\text{CH}_2)$

				2780 A	58% $v_{ss}(\text{CH}_2)$ 42% $v_{as}(\text{CH}_2)$	2842 B ₂	100% $v_{ss}(\text{CH}_2)$
2446	2451			2332 A	98% $v(\text{N6D10})$	2405 A ₁	99% $v(\text{N3D9})$
2401							
2113	2216			2325 A	99% $v(\text{N3D9})$	2330 A ₁	98% $v(\text{N6D10})$
2081	2148						
1733							
1710	1702	1722	1725	1695 A	86% $v_{ss}(\text{CO})$	1684 A ₁	86% $v_{ss}(\text{CO})$
1660	1675	1680	1678	1667 B	84% $v_{as}(\text{CO})$	1658 B ₂	84% $v_{as}(\text{CO})$
1630							
1468		1467					
1425	1425	1427	1425	1427 A	95% $\delta(\text{CH}_2)$	1450 A ₁	93% $\delta(\text{CH}_2)$
1410	1414		1416	1415 B	99% $\delta(\text{CH}_2)$	1442 B ₂	95% $\delta(\text{CH}_2)$
1360	1362	1373		1354 A	13% $v_{ss}(\text{CN})$ 19% $v_{ss}(\text{CC}_\alpha)$ 37% $\omega(\text{CH}_2)$	1364 B ₂	40% $v_{as}(\text{NC}_\alpha)$ 15% $\delta_{ip}(\text{N3D9})$ 38% $\omega(\text{CH}_2)$
1344	1356	1345	1347				
1334	1336			1322 B	34% $v_{as}(\text{CN})$ 15% $v_{as}(\text{CC}_\alpha)$ 32% $\omega(\text{CH}_2)$	1363 A ₁	12% $v_{ss}(\text{CN})$ 19% $v_{ss}(\text{CC}_\alpha)$ 11% $\delta_{ip}(\text{Ring-1})$ 38% $\omega(\text{CH}_2)$
	1316		1322	1320 A	23% $v_{ss}(\text{CN})$ 19% $\delta_{ip,s}(\text{CO})$ 45% $\omega(\text{CH}_2)$	1334 A ₁	24% $v_{ss}(\text{CN})$ 19% $\delta_{ip,s}(\text{CO})$ 44% $\omega(\text{CH}_2)$
1308	1300		1300	1296 B	36% $v_{as}(\text{CN})$ 47% $\omega(\text{CH}_2)$	1321 B ₂	71% $v_{as}(\text{CN})$ 13% $v_{as}(\text{CC}_\alpha)$
1273	1268			1235 A	87% $\tau(\text{CH}_2)$	1270 B ₂	38% $v_{as}(\text{NC}_\alpha)$ 41% $\omega(\text{CH}_2)$
	1253						
1233			1237	1218 B	60% $v_{as}(\text{NC}_\alpha)$ 19% $\tau(\text{CH}_2)$	1219 A ₂	95% $\tau(\text{CH}_2)$
			1207				
1189	1162			1159 B	17% $v_{as}(\text{NC}_\alpha)$ 71% $\tau(\text{CH}_2)$	1188 B ₁	96% $\tau(\text{CH}_2)$
1144	1143	1137					
1084	1090			1116 B	27% $v_{as}(\text{CC}_\alpha)$ 18% $\delta_{ip,as}(\text{CO})$ 30% $\delta_{ip}(\text{N6D10})$ 11% $\omega(\text{CH}_2)$	1125 B ₂	24% $v_{as}(\text{CC}_\alpha)$ 19% $\delta_{ip,as}(\text{CO})$ 31% $\delta_{ip}(\text{N6D10})$ 13% $\omega(\text{CH}_2)$
1050	1052	1055	1055				
1041							
	1014			1021 A	61% $\rho(\text{CH}_2)$ 13% $\delta_{ip}(\text{Ring-3})$ 13% $\delta_{op,as}(\text{CO})$	987 A ₂	26% $\delta_{op,s}(\text{CO})$ 77% $\rho(\text{CH}_2)$
	997						
985	978						

960	961	964	965	962 B	22% $\delta_{op,s}(CO)$ 73% $\rho(CH_2)$	960 A ₁	75% $v_{ss}(NC_\alpha)$
953	951	954		946 A	79% $v_{ss}(NC_\alpha)$	960 B ₁	86% $\rho(CH_2)$ 21% $\delta_{op,as}(CO)$
	928			930 B	12% $v_{as}(NC_\alpha)$ 58% $\delta_{ip}(N3D9)$ 11% $\delta_{ip}(N6D10)$	946 B ₂	65% $\delta_{ip}(N3D9)$ 13% $\delta_{ip}(N6D10)$
912	912	913					
870	875	881	882	888 A	16% $v_{ss}(CC_\alpha)$ 12% $\delta_{op}(N3D9)$ 43% $\delta_{ip}(Ring-3)$ 13% $\delta_{op,as}(CO)$	885 A ₁	13% $v_{ss}(CC_\alpha)$ 74% $\delta_{ip}(Ring-3)$
835	836	830					
	804		801				
742	743			763 B	16% $v_{as}(CN)$ 28% $v_{as}(CC_\alpha)$ 10% $\delta_{ip}(N3D9)$ 37% $\delta_{ip}(N6D10)$	764 B ₂	15% $v_{as}(CN)$ 30% $v_{as}(CC_\alpha)$ 38% $\delta_{ip}(N6D10)$
705	713		699				
	686		695	675 A	16% $v_{ss}(CN)$ 39% $v_{ss}(CC_\alpha)$ 19% $\delta_{op,as}(CO)$	651 A ₁	23% $v_{ss}(CN)$ 41% $v_{ss}(CC_\alpha)$ 12% $v_{ss}(NC_\alpha)$ 17% $\delta_{ip}(Ring-3)$
646	674			618 A	19% $\delta_{op}(N3D9)$ 37% $\delta_{op}(N6D10)$ 37% $\delta_{op,as}(CO)$	628 B ₁	12% $\rho(CH_2)$ 65% $\delta_{op}(N6D10)$ 60% $\delta_{op,as}(CO)$
633			636				
615							
605	605			617 B	65% $\delta_{op,s}(CO)$ 18% $\rho(CH_2)$	576 A ₂	85% $\delta_{op,s}(CO)$ 19% $\rho(CH_2)$
539	543		539	545 A	11% $v_{ss}(CN)$ 42% $\delta_{op}(N3D9)$ 23% $\delta_{ip}(Ring-1)$ 12% $\delta_{ip}(Ring-3)$	521 B ₂	19% $v_{as}(CC_\alpha)$ 72% $\delta_{ip,as}(CO)$
	522		527				
507	510			517 B	19% $v_{as}(CC_\alpha)$ 71% $\delta_{ip,as}(CO)$	491 A ₁	19% $v_{ss}(CN)$ 65% $\delta_{ip}(Ring-1)$
478	462		460	489 A	10% $\delta_{ip}(Ring-1)$ 58% $\delta_{op}(N6D10)$	470 B ₁	11% $\delta_{op}(Ring-2)$ 48% $\delta_{op}(N6D10)$ 22% $\delta_{op,as}(CO)$
453			456	440 B	76% $\delta_{ip}(Ring-2)$	464 B ₂	83% $\delta_{ip}(Ring-2)$
			451				
	434		437	423 A	14% $v_{ss}(CN)$ 25% $\delta_{ip,s}(CO)$ 13% $\delta_{op}(N3D9)$ 14% $\delta_{ip}(Ring-1)$ 11% $\rho(CH_2)$	374 A ₁	12% $v_{ss}(CN)$ 62% $\delta_{ip,s}(CO)$ 19% $\delta_{ip}(Ring-1)$
	382		377	364 A	42% $\delta_{ip,s}(CO)$ 35% $\delta_{ip}(Ring-1)$	326 <i>i</i> B ₁	59% $\delta_{op}(N3D9)$ 22% $\delta_{op}(Ring-2)$ 22% $\delta_{op}(Ring-1)$
	294		311	255 A	62% $\delta_{op}(Ring-2)$ 32% $\delta_{op}(Ring-1)$	160 <i>i</i> B ₁	40% $\delta_{op}(N3D9)$ 38% $\delta_{op}(Ring-2)$ 24% $\delta_{op}(Ring-1)$
	161		163				
	137		132	132 A	49% $\delta_{op}(Ring-2)$ 58% $\delta_{op}(Ring-1)$	125 B ₁	49% $\delta_{op}(Ring-2)$ 68% $\delta_{op}(Ring-1)$
	108		108	114 B	102% $\delta_{op}(Ring-3)$	64 A ₂	111% $\delta_{op}(Ring-3)$

	95		95				
--	----	--	----	--	--	--	--

Table 8.10. Experimental and calculated vibrational band wavenumbers (cm^{-1}) for non-deuterated 4,5-HHP.

IR s	Raman s	IR sol	Raman sol	Calc.	% PEDs half-chair	Calc.	% PEDs planar
3334	3344						
3287							
3266	3228			3214 A	100% $\nu(\text{N11H12})$	3225 A	100% $\nu(\text{N9H10})$
3165	3170			3174 A	100% $\nu(\text{N9H10})$	3188 A	100% $\nu(\text{N11H12})$
3019	3023						
3005	3009						
2981							
2966	2967			2958 A	41% $\nu_{\text{ss}}(\text{CH}_{2\text{a}})$ 59% $\nu_{\text{as}}(\text{CH}_{2\text{a}})$	2902 A	28% $\nu_{\text{ss}}(\text{CH}_{2\text{a}})$ 72% $\nu_{\text{as}}(\text{CH}_{2\text{a}})$
2952	2955			2935 A	43% $\nu_{\text{ss}}(\text{CH}_{2\text{b}})$ 57% $\nu_{\text{as}}(\text{CH}_{2\text{b}})$	2856 A	69% $\nu_{\text{ss}}(\text{CH}_{2\text{a}})$ 27% $\nu_{\text{as}}(\text{CH}_{2\text{a}})$
2885	2869			2771 A	59% $\nu_{\text{ss}}(\text{CH}_{2\text{a}})$ 40% $\nu_{\text{as}}(\text{CH}_{2\text{a}})$	2854 A	37% $\nu_{\text{ss}}(\text{CH}_{2\text{b}})$ 59% $\nu_{\text{as}}(\text{CH}_{2\text{b}})$
2829				2762 A	56% $\nu_{\text{ss}}(\text{CH}_{2\text{b}})$ 43% $\nu_{\text{as}}(\text{CH}_{2\text{b}})$	2825 A	61% $\nu_{\text{ss}}(\text{CH}_{2\text{b}})$ 39% $\nu_{\text{as}}(\text{CH}_{2\text{b}})$
1686	1688			1700 A	83% $\nu(\text{C2O13})$	1687 A	80% $\nu(\text{C2O13})$
1620	1626		1636	1660 A	68% $\nu(\text{C1O14})$	1658 A	61% $\nu(\text{C1O14})$ 11% $\nu(\text{C2O13})$ 10% $\nu(\text{C1N11})$
1613	1621						
1554	1557		1535				
1462	1470	1483	1465	1469 A	95% $\delta(\text{CH}_{2\text{b}})$	1492 A	97% $\delta(\text{CH}_{2\text{b}})$
1447	1448			1436 A	10% $\nu(\text{C1N11})$ 22% $\delta_{\text{ip}}(\text{N11H12})$ 29% $\delta_{\text{ip}}(\text{N9H10})$	1468 A	11% $\delta_{\text{ip}}(\text{N11H12})$ 52% $\delta_{\text{ip}}(\text{N9H10})$
1433	1436	1432		1424 A	36% $\delta_{\text{ip}}(\text{N9H10})$ 41% $\rho(\text{CH}_{2\text{b}})$	1453 A	33% $\delta_{\text{ip}}(\text{N9H10})$ 40% $\rho(\text{CH}_{2\text{b}})$
1393	1395	1397	1406	1410 A	83% $\delta(\text{CH}_{2\text{a}})$	1421 A	92% $\delta(\text{CH}_{2\text{a}})$
1365	1369			1359 A	22% $\delta_{\text{ip}}(\text{N11H12})$ 21% $\rho(\text{CH}_{2\text{a}})$ 22% $\rho(\text{CH}_{2\text{b}})$	1368 A	33% $\delta_{\text{ip}}(\text{N11H12})$ 11% $\rho(\text{CH}_{2\text{a}})$ 26% $\rho(\text{CH}_{2\text{b}})$
1330	1334	1335	1332				
1320	1323	1322		1314 A	23% $\nu(\text{C1N11})$ 23% $\delta_{\text{ip}}(\text{N11H12})$ 20% $\rho(\text{CH}_{2\text{a}})$	1341 A	19% $\nu(\text{C1N11})$ 20% $\delta_{\text{ip}}(\text{N11H12})$ 35% $\rho(\text{CH}_{2\text{a}})$
1251	1253	1266		1252 A	20% $\tau(\text{CH}_{2\text{a}})$ 66% $\tau(\text{CH}_{2\text{b}})$	1285 A	16% $\nu(\text{C1N11})$ 27% $\rho(\text{CH}_{2\text{a}})$ 16% $\rho(\text{CH}_{2\text{b}})$

		1224	1239	1237 A	15% v(C1N11) 26% ρ(CH _{2a}) 17% ρ(CH _{2b})	1245 A	13% v(C3N9) 18% v(C6N9) 11% ρ(CH _{2a}) 32% τ(CH _{2b})
1200	1205	1201		1182 A	56% τ(CH _{2a}) 16% τ(CH _{2b})	1219 A	20% v(C3N9) 14% v(C6N9) 53% τ(CH _{2b})
1152	1150	1157		1160 A	24% v(C3N9) 25% v(C6N9) 10% ρ(CH _{2a})	1212 A	82% τ(CH _{2a})
			1130	1121 A	11% v(C1C2) 23% v(C2C3) 14% δ _{ip} (C2O13)	1141 A	12% v(C1C2) 31% v(C2C3) 14% δ _{ip} (C2O13)
1072	1075						
	1064			1064 A	50% ω(CH _{2b})	1043 A	93% ω(CH _{2b})
1028	1033		1033	1010 A	19% v(C3N9) 24% v(C6N11) 15% ω(CH _{2b})	1019 A	23% v(C3N9) 31% v(C6N11) 11% δ _{ip} (C1O14) 11% δ _{ip} (C2O13)
952	953			956 A	56% ω(CH _{2a}) 20% δ _{op} (C2O13)	950 A	54% ω(CH _{2a}) 20% δ _{op} (C2O13)
926	930			926 A	23% v(C3N9) 42% v(C6N9) 11% v(C6N11)	899 A	21% v(C3N9) 35% v(C6N9) 11% δ _{ip} (Ring-3)
883	885		882				
826	822		799	861 A	43% δ _{ip} (Ring-3) 27% δ _{op} (N9H10)	848 A	59% δ _{ip} (Ring-3)
702			715	713 A	13% ω(CH _{2a}), 13% δ _{op} (N9H10), 52% δ _{op} (C1O14), 14% δ _{op} (C2O13)	694 A	18% ω(CH _{2a}) 24% δ _{op} (N11H12) 66% δ _{op} (C1O14)
662	670			655 A	35% v(C1C2) 16% v(C2C3) 10% v(C6N11) 13% v(C1N11) 10% δ _{ip} (C1O14)	654 A	30% v(C1C2) 17% v(C2C3) 12% v(C6N11) 14% v(C1N11)
775	705			613 A	18% δ _{ip} (Ring-3) 44% δ _{op} (N9H10)	585 A	61% δ _{op} (N11H12) 16% δ _{op} (C2O13)
597	597			545 A	24% v(C2C3) 24% δ _{ip} (C1O14) 31% δ _{ip} (C2O13)	557 A	45% δ _{op} (N9H10)
	572			545 A	14% δ _{ip} (Ring-1) 54% δ _{op} (N11H12) 14% δ _{op} (C1O14) 17% δ _{op} (C2O13)	547 A	13% v(C2C3) 22% δ _{ip} (C1O14) 17% δ _{ip} (C2O13) 14% δ _{ip} (Ring-1)
504	506						
468	470		486	458 A	22% δ _{ip} (Ring-1) 35% δ _{ip} (Ring-2)	466 A	11% v(C3N9) 13% δ _{ip} (C2O13) 40% δ _{ip} (Ring-1)
	456		442	421 A	11% v(C1C2) 13% δ _{ip} (Ring-1) 39% δ _{ip} (Ring-2)	416 A	70% δ _{ip} (Ring-2)
			391	362 A	13% δ _{op} (Ring-1) 24% δ _{op} (N11H12) 17% δ _{op} (C1O14) 23% δ _{op} (C2O13)	363 A	11% δ _{op} (N11H12) 34% δ _{op} (C1O14) 54% δ _{op} (C2O13)
	326		335	334 A	26% δ _{ip} (C1O14) 23% δ _{ip} (C2O13) 23% δ _{ip} (Ring-1)	344 A	10% v(C1C2) 33% δ _{ip} (C1O14) 31% δ _{ip} (C2O13) 21% δ _{ip} (Ring-1)
	255			307 A	21% δ _{op} (Ring-2) 53% δ _{op} (Ring-3)	279 i A	22% δ _{op} (Ring-1) 20% δ _{op} (Ring-2) 60% δ _{op} (Ring-3)
	205						
	168		162				
	150		113				
	115		95	125 A	11% δ _{op} (Ring-2) 93% δ _{op} (Ring-1)	102 i A	81% δ _{op} (Ring-2) 38% δ _{op} (Ring-1)

	81			61 A	66% $\delta_{op}(\text{Ring-2})$ 32% $\delta_{op}(\text{Ring-3})$	70 A	58% $\delta_{op}(\text{Ring-3})$ 55% $\delta_{op}(\text{Ring-1})$
--	----	--	--	------	---	------	---

Table 8.11. Experimental and calculated vibrational band wavenumbers (cm^{-1}) for *N*-deuterated 4,5-HHP.

IR s	Raman s	IR sol	Raman sol	Calc.	% PEDs half-chair	Calc.	% PEDs planar
3019	3023						
2996	3010						
2979				2958 A	41% $\nu_{ss}(\text{CH}_{2a})$ 59% $\nu_{as}(\text{CH}_{2a})$	2902 A	28% $\nu_{ss}(\text{CH}_{2a})$ 72% $\nu_{as}(\text{CH}_{2a})$
2964	2967						
	2953			2935 A	43% $\nu_{ss}(\text{CH}_{2b})$ 57% $\nu_{as}(\text{CH}_{2b})$	2856 A	70% $\nu_{ss}(\text{CH}_{2a})$ 27% $\nu_{as}(\text{CH}_{2a})$
2883	2856						
2776				2771 A	59% $\nu_{ss}(\text{CH}_{2a})$ 40% $\nu_{as}(\text{CH}_{2a})$	2855 A	37% $\nu_{ss}(\text{CH}_{2b})$ 60% $\nu_{as}(\text{CH}_{2b})$
				2762 A	56% $\nu_{ss}(\text{CH}_{2b})$ 43% $\nu_{as}(\text{CH}_{2b})$	2825 A	61% $\nu_{ss}(\text{CH}_{2b})$ 39% $\nu_{as}(\text{CH}_{2b})$
2498							
2400	2405			2357 A	98% $\nu(\text{N11D12})$	2361 A	99% $\nu(\text{N9D10})$
2345							
2323	2329			2324 A	99% $\nu(\text{N9D10})$	2336 A	99% $\nu(\text{N11D12})$
1657	1651	1681		1699 A	85% $\nu(\text{C2O13})$	1686 A	85% $\nu(\text{C2O13})$
1634	1635	1622					
1615	1615			1651 A	76% $\nu(\text{C1O14})$	1645 A	72% $\nu(\text{C1O14})$ 10% $\nu(\text{C1N11})$
1590	1606						
1590							
1545	1545		1538				
1523							
1472	1479	1472	1473	1468 A	97% $\delta(\text{CH}_{2b})$	1491 A	97% $\delta(\text{CH}_{2b})$
1445	1449			1416 A	58% $\delta(\text{CH}_{2a})$ 25% $\rho(\text{CH}_{2b})$	1442 A	20% $\nu(\text{C1N11})$ 54% $\rho(\text{CH}_{2b})$
1432	1436	1439		1403 A	15% $\nu(\text{C1N11})$ 38% $\delta(\text{CH}_{2a})$ 32% $\rho(\text{CH}_{2b})$	1421 A	90% $\delta(\text{CH}_{2a})$
1390	1391	1405	1406				
1368							

	1333		1344	1333 A	10% v(C6N11) 17% v(C1N11) 35% ρ(CH _{2a}) 14% ρ(CH _{2b})	1349 A	10% v(C6N11) 18% v(C1N11) 27% ρ(CH _{2a}) 23% ρ(CH _{2b})
1314	1326	1318		1304 A	14% δ _{ip} (N9D10) 39% ρ(CH _{2a}) 17% ρ(CH _{2b})	1321 A	13% v(C6N9) 47% ρ(CH _{2a})
	1298						
	1285						
1268	1268						
1253	1255			1251 A	20% τ(CH _{2a}) 64% τ(CH _{2b})	1246 A	11% v(C3N9) 17% v(C6N9) 11% v(C6N11) 40% τ(CH _{2b})
1240	1242						
1214	1209		1211	1211 A	28% v(C3N9) 27% v(C6N9) 11% τ(CH _{2b})	1230 A	11% v(C6N9) 35% τ(CH _{2a}) 25% τ(CH _{2b})
				1206 A	14% v(C1C2) 13% v(C6N11) 12% δ _{ip} (N11D12) 29% τ(CH _{2a})	1221 A	12% v(C1C2) 15% v(C2C3) 10% v(C3N9) 22% τ(CH _{2a}) 12% τ(CH _{2b})
1170	1171			1166 A	30% τ(CH _{2a}) 19% τ(CH _{2b})	1197 A	11% v(C1C2) 11% δ _{ip} (N11D12) 31% τ(CH _{2a}) 19% τ(CH _{2b})
1140	1149			1113 A	20% v(C2C3) 12% δ _{ip} (C1O14) 14% δ _{ip} (C2O13)	1120 A	21% v(C2C3) 23% δ _{ip} (N9D10) 10% δ _{ip} (C1O14) 11% δ _{ip} (C2O13)
1126	1126						
1095	1098						
1071	1066						
1047	1049	1054	1041	1053 A	64% ω(CH _{2b})	1069 A	62% ω(CH _{2b})
1034	1035		1029				
	1003		1003				
991	991			967 A	21% v(C3N9) 24% v(C6N9) 18% δ _{ip} (N11D12)	983	37% δ _{ip} (N9D10) 11% ω(CH _{2a}) 28% ω(CH _{2b})
957	963	960		957 A	49% ω(CH _{2a}) 14% δ _{op} (C2O13)	974 A	28% v(C3N9) 14% v(C6N9) 12% δ _{ip} (N11D12) 13% ω(CH _{2a})
929	926			928 A	21% v(C3N9) 43% δ _{ip} (N9D10)	922 A	14% v(C3N9) 13% δ _{ip} (N9D10) 39% ω(CH _{2a}) 15% δ _{op} (C2O13)
	916						
	908		906				
882	887						
873							

851				843 A	16% v(C6N11) 13% δ_{ip} (N11D12) 17% δ_{ip} (N9D10) 22% δ_{ip} (Ring-3)	841 A	14% v(C6N11) 15% δ_{ip} (N11D12) 47% δ_{ip} (Ring-3)
828	828			803 A	12% v(C6N9), 10% v(C6N11), 20% δ_{ip} (N11D12), 25% δ_{ip} (Ring-3)	796	21% v(C6N9) 10% v(C6N11) 23% δ_{ip} (N11D12) 24% δ_{ip} (Ring-3)
701	700		716	698 A	16% ω (CH _{2a}) 50% δ_{op} (C1O14) 13% δ_{op} (C2O13)	681 A	24% ω (CH _{2a}) 66% δ_{op} (C1O14) 13% δ_{op} (C2O13)
671	672						
	633			638 A	36% v(C1C2) 16% v(C2C3) 11% v(C1N11)	638 A	34% v(C1C2) 16% v(C2C3) 13% v(C1N11)
596	594						
576	576			535 A	16% v(C2C3) 10% v(C1N11) 24% δ_{ip} (C1O14) 23% δ_{ip} (C2O13)	542 A	16% v(C2C3) 10% v(C1N11) 24% δ_{ip} (C1O14) 21% δ_{ip} (C2O13)
764	772		796	521 A	11% v(C2C3) 25% δ_{ip} (Ring-1) 34% δ_{op} (N9D10)	499 A	28% δ_{ip} (Ring-1) 17% δ_{op} (N9D10) 17% δ_{op} (N11D12)
521							
750	750		732	493 A	20% δ_{op} (N9D10) 26% δ_{op} (N11D12) 25% δ_{op} (C1O14) 19% δ_{op} (C2O13)	473 A	47% δ_{op} (N11D12) 24% δ_{op} (C2O13)
492	497		486				
462	459		449				
	434			443 A	10% δ_{ip} (Ring-1) 44% δ_{ip} (Ring-2)	446 A	10% v(C3N9) 11% δ_{ip} (Ring-1) 33% δ_{ip} (Ring-2) 23% δ_{op} (N9D10)
644	650			397 A	13% v(C1C2) 24% δ_{ip} (Ring-2) 19% δ_{op} (N9D10)	398 A	38% δ_{ip} (Ring-2) 45% δ_{op} (N9D10)
	356		372	335 A	28% δ_{ip} (C1O14) 27% δ_{ip} (C2O13) 24% δ_{ip} (Ring-1)	343 A	32% δ_{ip} (C1O14) 30% δ_{ip} (C2O13) 22% δ_{ip} (Ring-1)
	323		321	313 A	11% δ_{op} (Ring-2) 25% δ_{op} (Ring-3) 11% δ_{op} (Ring-1) 40% δ_{op} (N11D12)	329 A	42% δ_{op} (N11D12) 20% δ_{op} (C1O14) 34% δ_{op} (C2O13)
	254		250	284 A	12% δ_{op} (Ring-2) 33% δ_{op} (Ring-3) 28% δ_{op} (N11D12) 18% δ_{op} (C2O13)	258 i A	21% δ_{op} (Ring-1) 22% δ_{op} (Ring-2) 64% δ_{op} (Ring-3)
	220		208				
	200		200				
	167		167				
	147		134				
	114		109	122	10% δ_{op} (Ring-2) 99% δ_{op} (Ring-1)	101 i A	79% δ_{op} (Ring-2) 41% δ_{op} (Ring-1)
	80			61	66% δ_{op} (Ring-2) 31% δ_{op} (Ring-3)	69 A	58% δ_{op} (Ring-3) 58% δ_{op} (Ring-1)

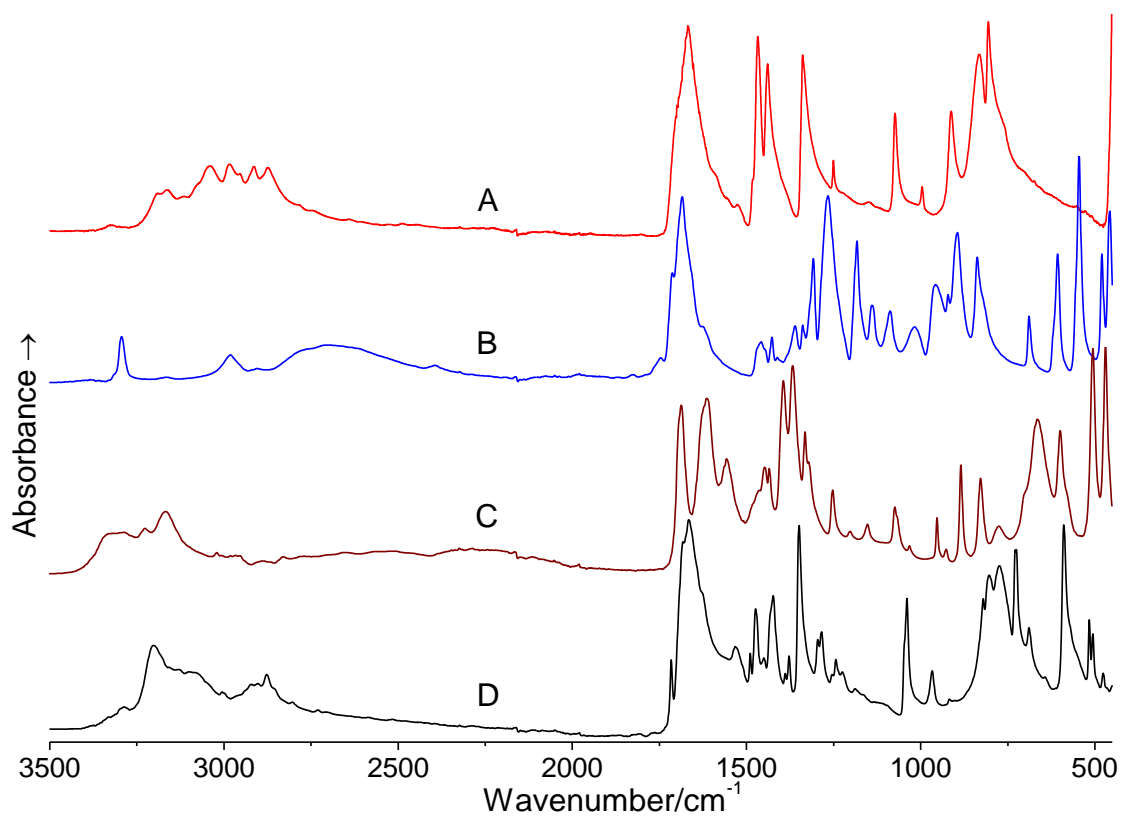


Figure 8.3. Solid state IR spectra of (A) 2,5-DKP, (B) 2,6-DKP, (C) 4,5-HHP and (D) 2,3-DKP.

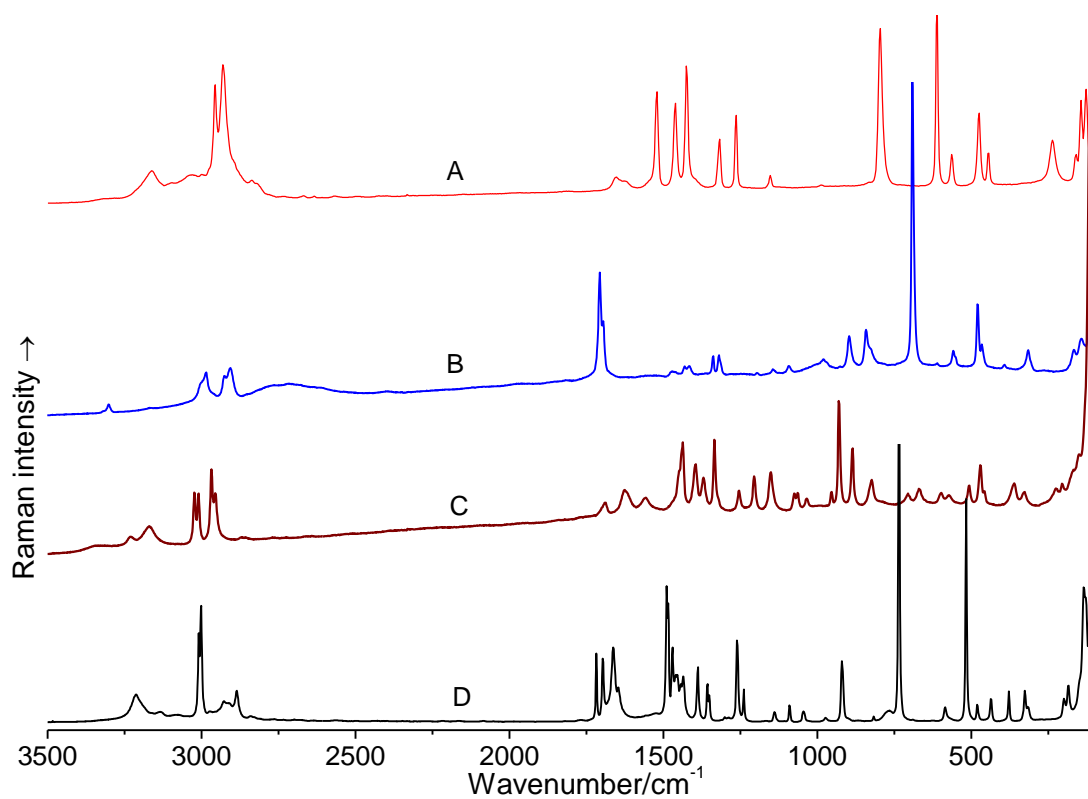


Figure 8.4. Solid state Raman spectra of (A) 2,5-DKP, (B) 2,6-DKP, (C) 4,5-HHP and (D) 2,3-DKP.

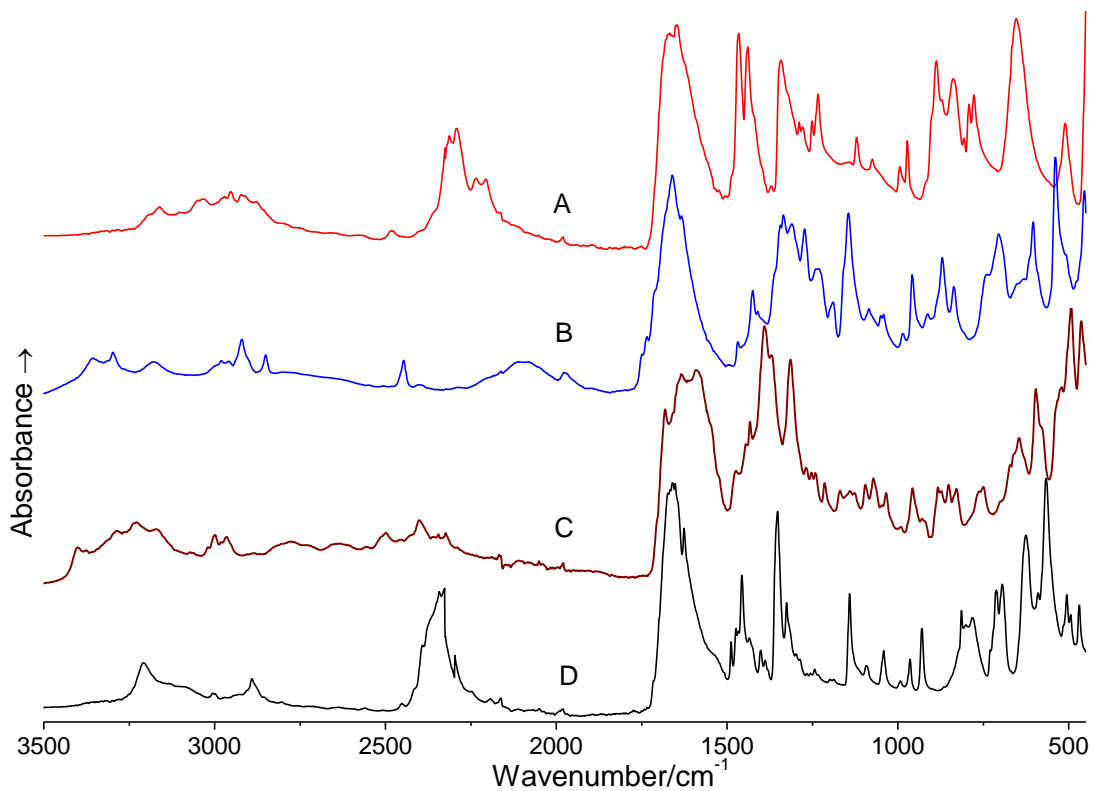


Figure 8.5. Solid state IR spectra of *N*-deuterated (A) 2,5-DKP, (B) 2,6-DKP, (C) 4,5-HHP and (D) 2,3-DKP.

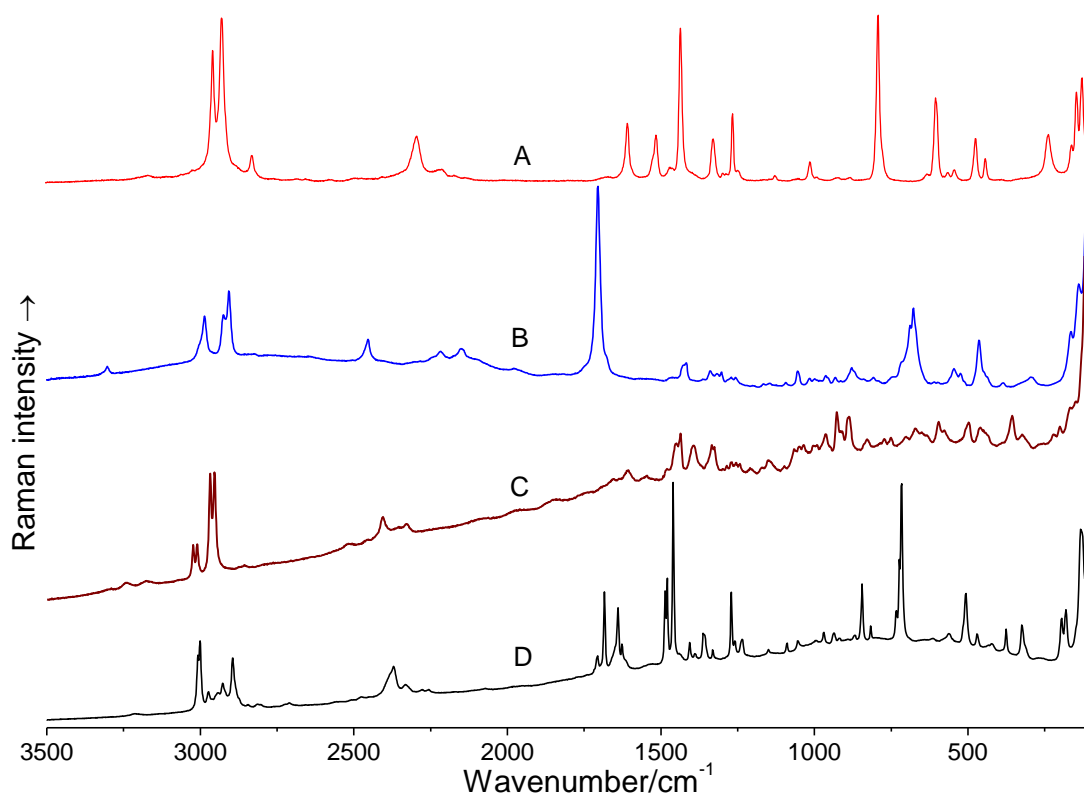


Figure 8.6. Solid state Raman spectra of *N*-deuterated (A) 2,5-DKP, (B) 2,6-DKP, (C) 4,5-HHP and (D) 2,3-DKP.

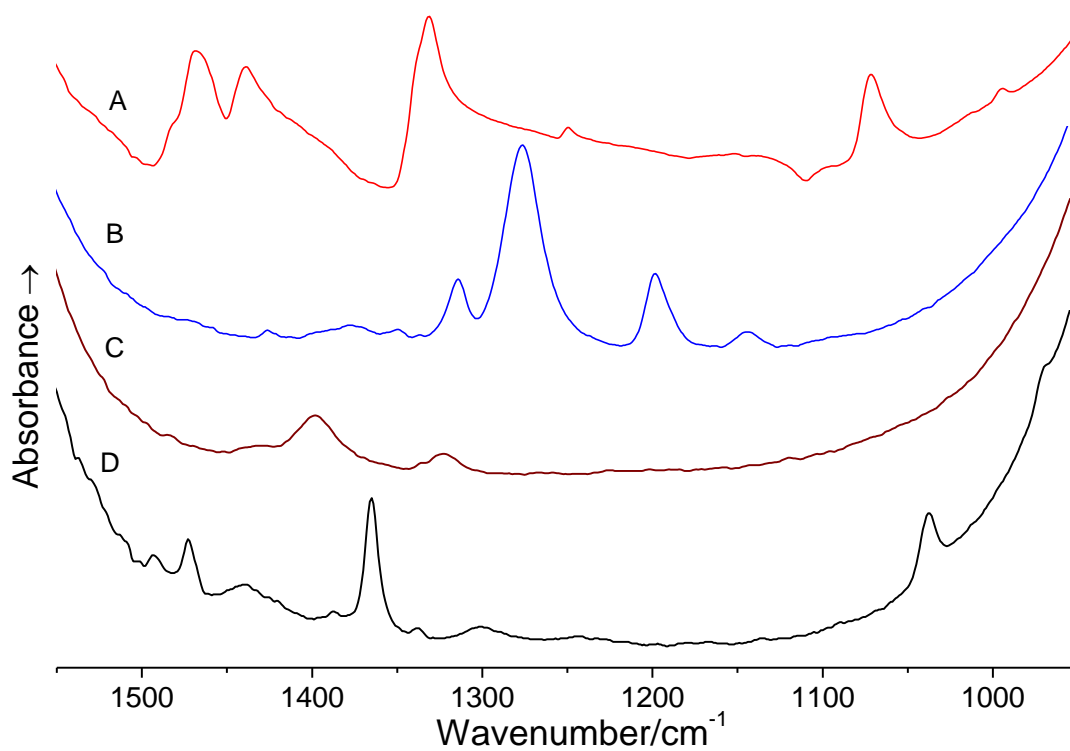


Figure 8.7. Solution state IR spectra of (A) 2,5-DKP, (B) 2,6-DKP, (C) 4,5-HHP and (D) 2,3-DKP.

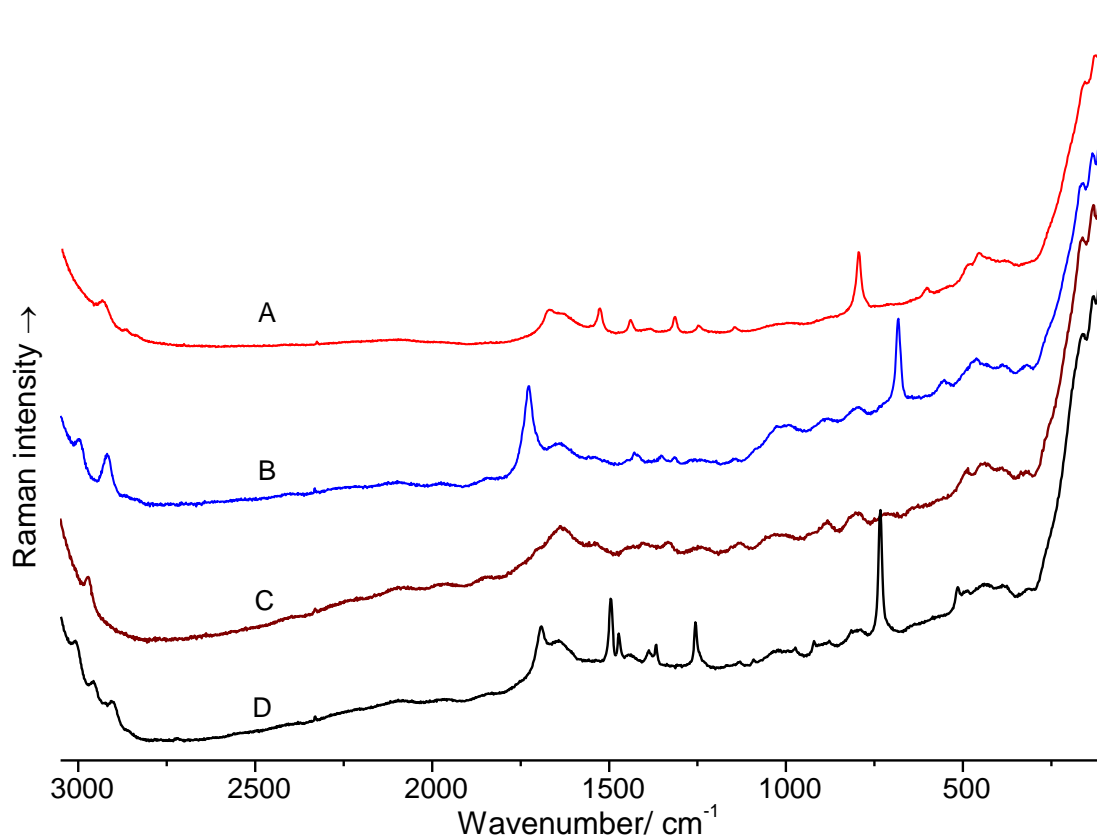


Figure 8.8. Solution state Raman spectra of (A) 2,5-DKP, (B) 2,6-DK, (C) 4,5-HHP and (D) 2,3-DKP.

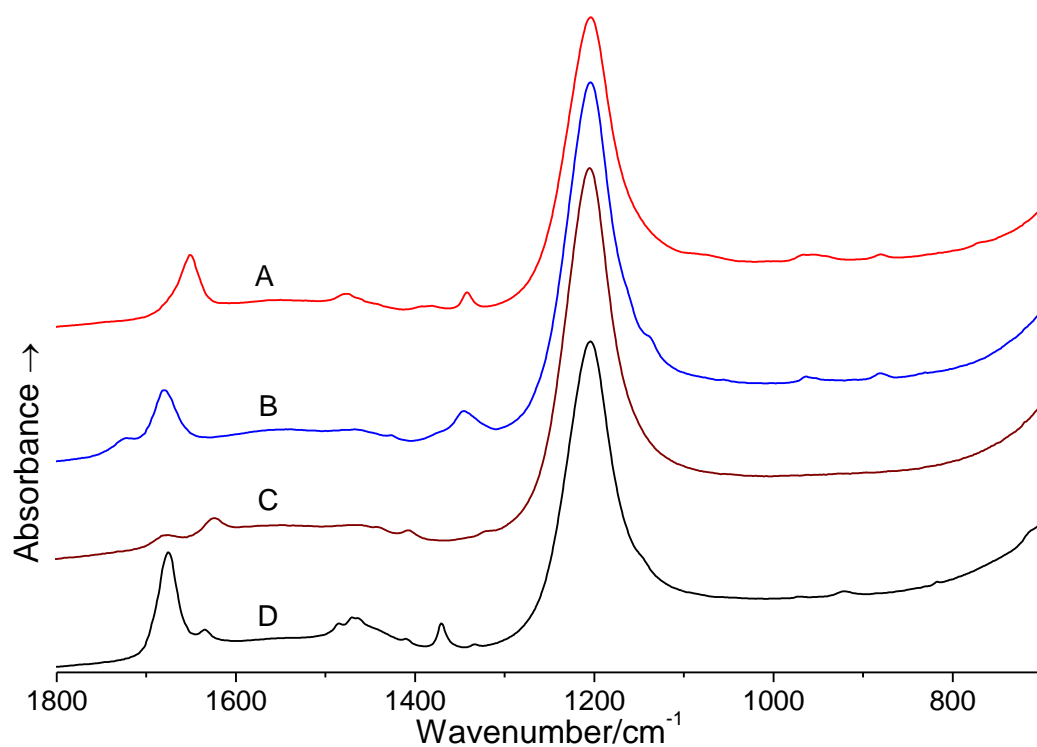


Figure 8.9. Solution state IR spectra of *N*-deuterated (A) 2,5-DKP, (B) 2,6-DKP, (C) 4,5-HHP and (D) 2,3-DKP.

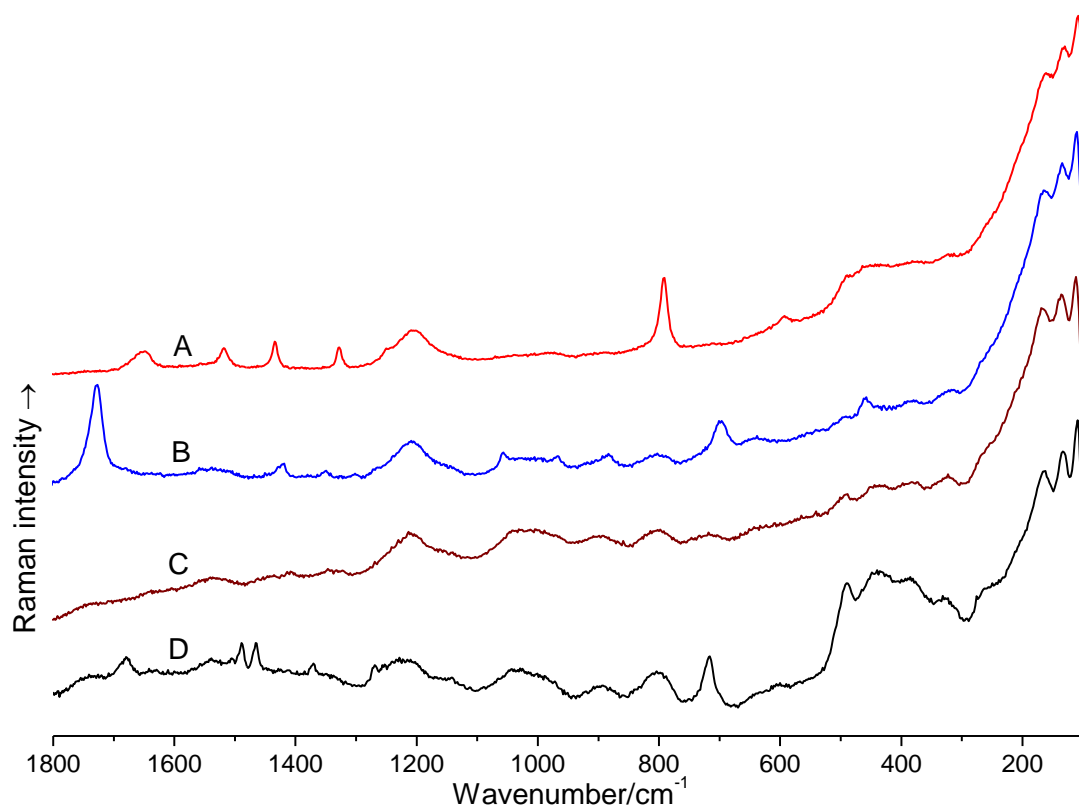


Figure 8.10. Solution state Raman spectra of *N*-deuterated (A) 2,5-DKP, (B) 2,6-DKP, (C) 4,5-HHP and (D) 2,3-DKP.

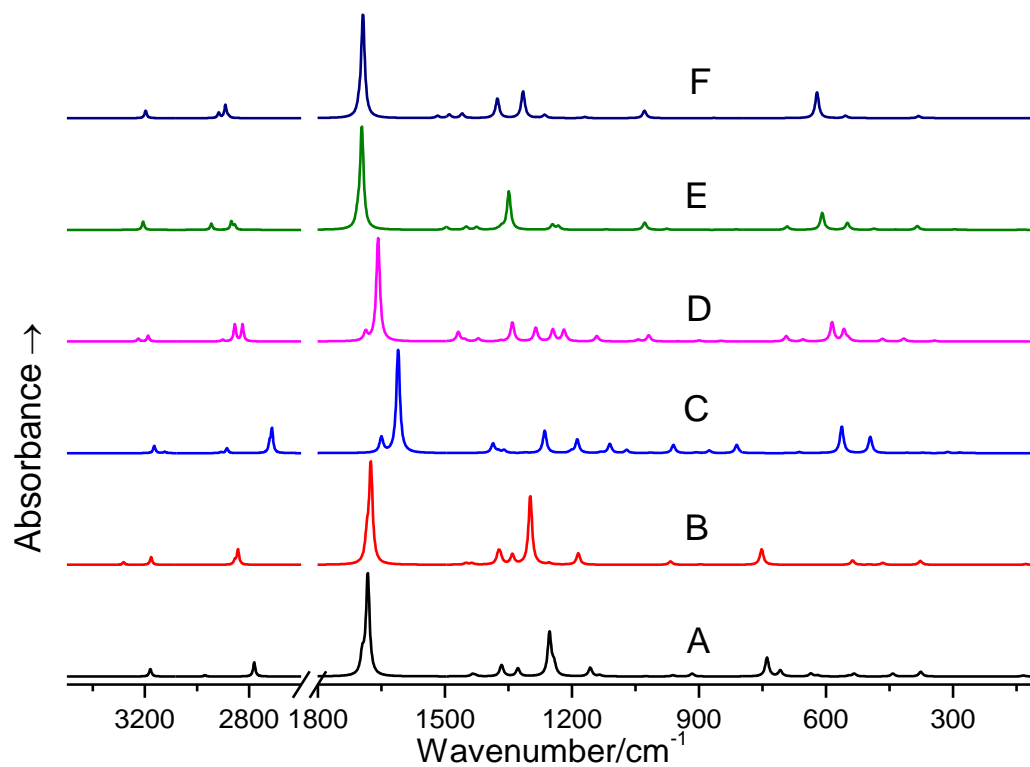


Figure 8.11. Calculated IR spectra of (A) half-chair, (B) planar (2,6-DKP), (C) half-chair, (D) planar (4,5-HHP), (E) skew-boat and (F) planar (2,3-DKP).

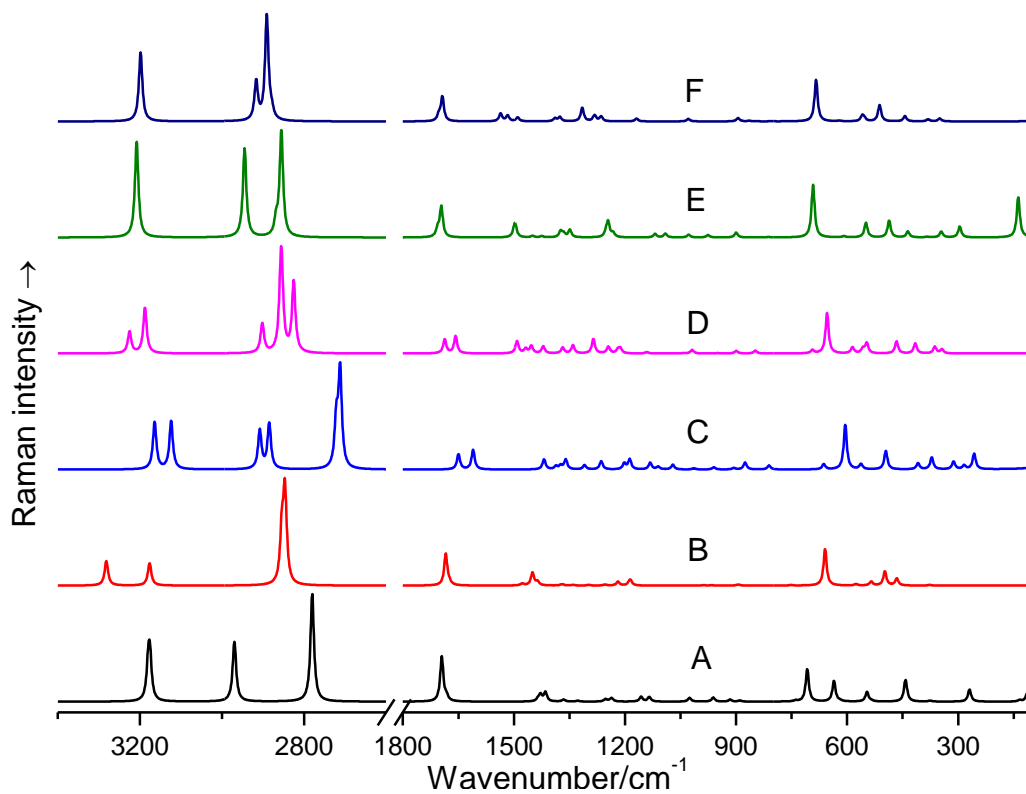


Figure 8.12. Calculated Raman spectra of (A) half-chair, (B) planar (2,6-DKP), (C) half-chair, (D) planar (4,5-HHP), (E) skew-boat (F) and planar (2,3-DKP).

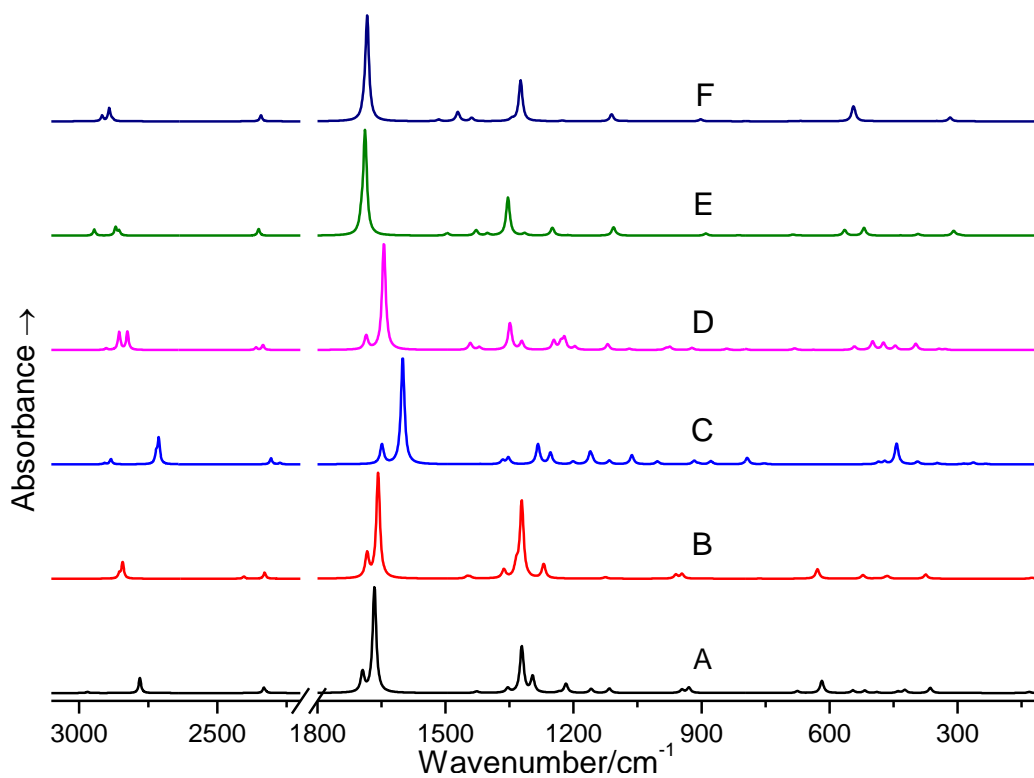


Figure 8.13. Calculated IR spectra of *N*-deuterated (A) half-chair, (B) planar (2,6-DKP), (C) half-chair, (D) planar (4,5-HHP), (E) skew-boat and (F) planar (2,3-DKP).

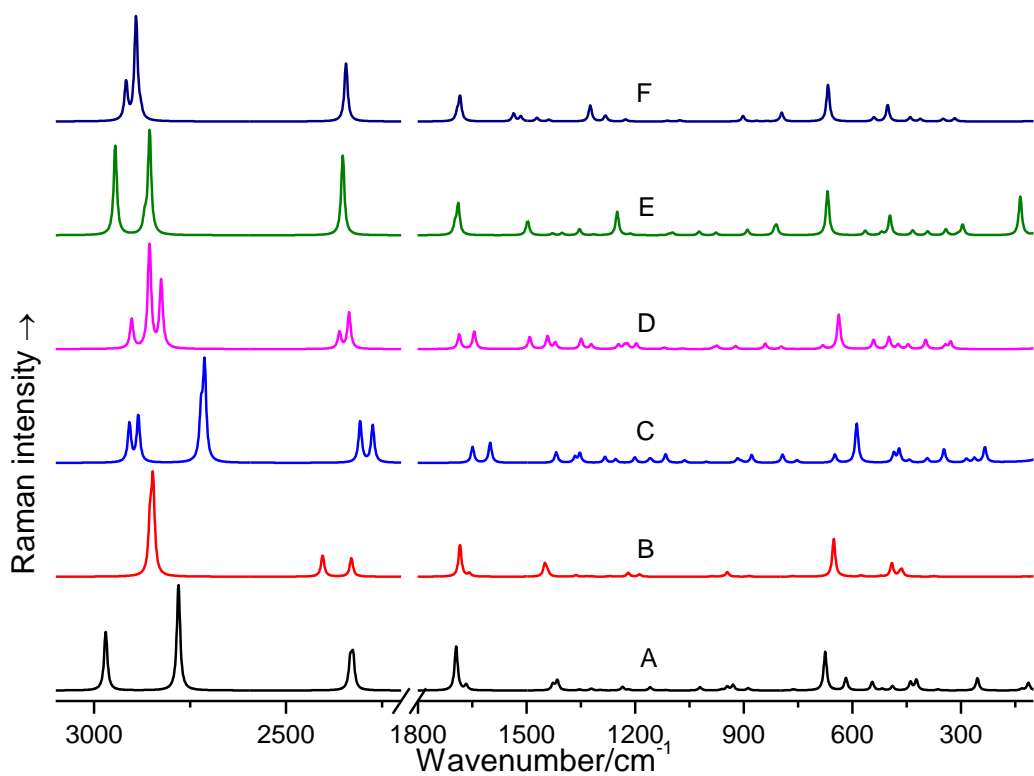


Figure 8.14. Calculated Raman spectra of *N*-deuterated (A) half-chair, (B) planar (2,6-DKP), (C) half-chair, (D) planar (4,5-HHP), (E) skew-boat and (F) planar (2,3-DKP).

8.4. Molecular orbital analysis

The highest occupied molecular orbital (HOMO) and lowest unoccupied molecular orbital (LUMO) energies of 2,3-DKP, 2,5-DKP, 2,6-DKP and 4,5-HHP were calculated at their optimised geometries. The molecular orbitals (HOMO and LUMO) of 2,3-DKP, 2,5-DKP, 2,6-DKP and 4,5-HHP are shown in (Fig. 8.15, labelled as A,B,C,D)). The HOMO energies of 2,3-DKP, 2,5-DKP, 2,6-DKP and 4,5-HHP are -7.135 eV, -7.304 eV, -7.191 eV and -6.999 eV, respectively, whereas, the LUMO energies are -1.486 eV, -0.700 eV, -1.254 eV and -2.193 eV, respectively. The composition of HOMO and LUMO are given in Table 8.12. The analyses of molecular orbitals of 2,3-DKP illustrated that the HOMO and LUMO are localized on the carbonyl carbon, oxygen and nitrogen atoms. The computed HOMO–LUMO energy gap for 2,3-DKP is 5.648 eV. In 2,6-DKP, the HOMO is localized on the nitrogen atom (N3), partly on oxygen, carbon and axial positioned hydrogen atoms of CH₂ groups, whereas the LUMO is predominantly localized on carbonyl carbon, oxygen atoms and partly on nitrogen (N6) atom. The computed HOMO–LUMO energy gap for 2,6-DKP is 5.936 eV.

In the case of 4,5-HHP, the HOMO is localized on oxygen atoms, partly on nitrogen (N9), carbon (C3) and carbonyl carbon atoms; whereas the LUMO is predominantly localized on the carbonyl carbon and oxygen atoms and nitrogen (N11) atoms. The computed HOMO–LUMO energy gap for 4,5-HHP is 4.805 eV. In 2,5-DKP, the HOMO is predominantly localized on oxygen, nitrogen and partly on carbon atoms, whereas the LUMO is predominantly localized on hydrogen atoms, and partly on other atoms in the molecule (Table 8.12). The computed HOMO–LUMO energy gap for 2,5-DKP is 6.604 eV. Since the HOMO-LUMO gap value is relatively large, it is therefore expected that all four molecules are less reactive, less polarizable, and chemically relatively stable molecules. However, a comparison of the HOMO-LUMO gap in all four molecules allows the stability to be given in the order: 2,5-DKP > 2,6-DKP > 2,3-DKP > 4,5-HHP.

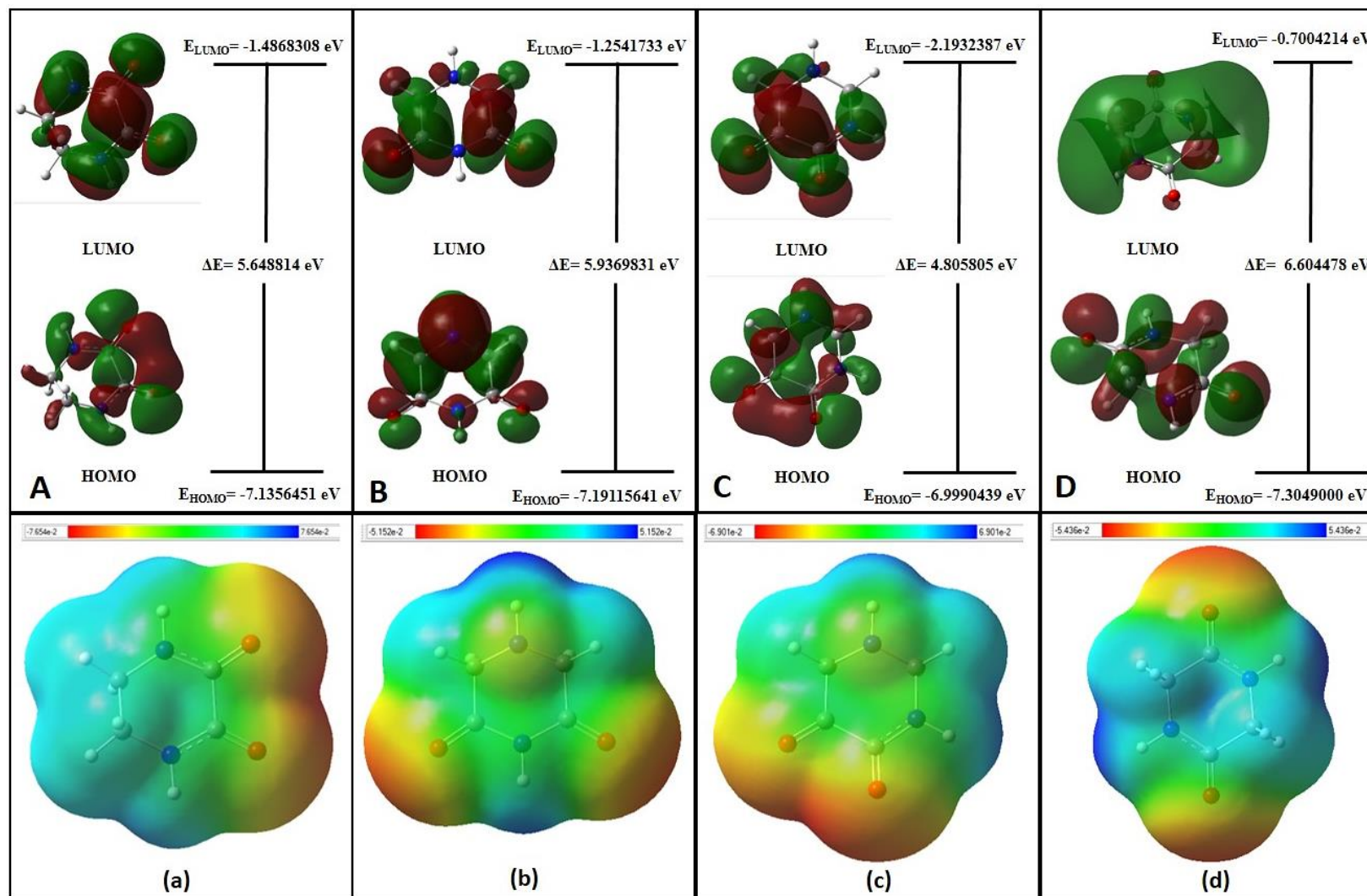


Figure 8.15. HOMO-LUMO plots of (A) 2,3-DKP (B) 2,6-DKP (C) 4,5-HHP and (D) 2,5-DKP and their molecular electrostatic potential energy surface (MEP) are shown in a, b, c and d, respectively.

Table 8.12. HOMO-LUMO composition of the lowest energy conformers of 2,3-DKP, 2,6-DKP, 4,5-HHP and 2,5-DKP.

2,3-DKP	HOMO	LUMO	2,6-DKP	HOMO	LUMO	4,5-HHP	HOMO	LUMO	2,5-DKP	HOMO	LUMO
1(O)	34.5109%	15.8731%	1(O)	4.9004%	17.5634%	1(C)	7.8248%	15.0283%	1(C)	3.1932%	4.1914%
2(O)	34.5109%	15.8731%	2(O)	4.9004%	17.5634%	2(C)	9.0278%	32.5159%	2(C)	3.1932%	4.1914%
3(N)	5.5928%	8.6837%	3(N)	57.4862%	1.0847%	3(C)	8.3364%	3.0082%	3(N)	13.5330%	9.5538%
4(C)	0.5739%	1.2669%	4(C)	6.2672%	2.2876%	4(H)	0.2992%	0.9615%	4(H)	0.3354%	10.1240%
5(C)	0.5739%	1.2669%	5(C)	6.2672%	2.2876%	5(H)	2.0722%	2.0906%	5(N)	13.5330%	9.5538%
6(N)	5.5928%	8.6837%	6(N)	1.4270%	4.3461%	6(C)	1.3335%	0.7124%	6(H)	0.3354%	10.1240%
7(C)	8.2369%	22.8174%	7(C)	2.0243%	24.6231%	7(H)	0.4655%	0.0776%	7(O)	27.6847%	5.8695%
8(C)	8.2369%	22.8174%	8(C)	2.0243%	24.6231%	8(H)	0.8208%	0.3495%	8(O)	27.6847%	5.8695%
9(H)	0.7943%	0.7065%	9(H)	2.5739%	0.0911%	9(N)	10.0350%	1.2887%	9(C)	3.3975%	5.6126%
10(H)	0.7943%	0.7065%	10(H)	0.2602%	0.0098%	10(H)	0.7302%	0.1832%	10(H)	0.6972%	6.5496%
11(H)	0.2176%	0.0962%	11(H)	5.3924%	2.0142%	11(N)	3.8867%	7.3984%	11(H)	1.1587%	8.0987%
12(H)	0.2176%	0.0962%	12(H)	0.5418%	0.7455%	12(H)	0.8362%	0.5317%	12(C)	3.3975%	5.6126%
13(H)	0.0733%	0.5558%	13(H)	0.5418%	0.7455%	13(O)	26.9100%	25.1225%	13(H)	0.6972%	6.5496%
14(H)	0.0733%	0.5558%	14(H)	5.3924%	2.0142%	14(O)	27.4210%	10.7309%	14(H)	1.1587%	8.0987%

8.5. Molecular electrostatic potential

The total electron density mapped with molecular electrostatic potential (MEP) surface have been plotted for 2,3-DKP, 2,5-DKP, 2,6-DKP and 4,5-HHP (Fig. 8.15, labelled as a, b, c and d) molecules at the B3LYP/aug-cc-pVTZ level. The MEP surfaces are in the range between -7.65, -5.43, -5.15 and -6.90 (arb. units) (deepest red) and 7.65, 5.43, 5.15 and 6.90 (arb. units) (deepest blue) for 2,3-DKP, 2,5-DKP, 2,6-DKP and 4,5-HHP, respectively. The red area indicates the strongest electrostatic repulsion and the blue coloured area indicates the strongest attraction. From the MEP maps of 2,3-DKP, 2,5-DKP, 2,6-DKP and 4,5-HHP the increase in negative potential is shown from yellow to red colour, with the maximum negative potential in red colour (preferred site for electrophilic attack), green represent the zero potentials and the maximum positive region, (preferred site for nucleophilic attack) is represented as a deep blue colour.

The negative potentials are mainly over the electronegative oxygen atoms of the six-membered DKP ring (2,3-DKP, 2,5-DKP, 2,6-DKP) and pyrimidine ring (4,5-HHP) and slightly on the nitrogen atoms in 2,6-DKP and 4,5-HHP (Fig. 8.15(b, c)). There is positive potential over the nitrogen and hydrogen atoms all four molecules (Fig. 8.15(a, b, c and d)). This information can be useful in investigating possible sites for intermolecular interactions.

8.6. Hirshfeld surface analysis

The Hirshfeld surfaces of 2,3-DKP (A) and 2,5-DKP (B) are illustrated in Fig. 8.16 showing the mapped surface over d_{norm} , (Fig. 8.16, labelled as a, d), shape index (labelled as b, e) and curvedness (labelled as c, f), respectively. The interactions between the oxygen atoms and the hydrogen atoms O--H (29.3 and 29.0%) (Fig.16, labelled as x) and H--O (24.2 and 23.2%) (Fig.8.16, labelled as y and z) can be seen as the bright red areas on the Hirshfeld surface of molecule A and B, respectively. The H--H and O--H intermolecular interactions appear as separate spikes in the 2D fingerprint plot (Fig. S13). Corresponding regions are visible in the fingerprint plots where one molecule acts as an acceptor ($d_e < d_i$) and the other acts as a donor ($d_e > d_i$). The small broad spikes with $(d_e + d_i)$ values around ~ 2.5 Å, pointing toward the lower left of the plots are due to H--H hydrogen interactions, encompassing 30.1% and 34.0% of the total Hirshfeld surface in A and B, respectively.

The O--H/O--H interactions can be easily located around the corners, resembling sharp spikes on the 2D fingerprint plot (Fig. 8.17). They comprise about 29.3 and 24.2 % (A) and 29.0 and 23.2 % (B) of the total Hirshfeld surface with a high $(d_e + d_i)$ value of ~ 1.8 Å. This is the shortest

contact i.e., the minimum ($d_e + d_i$) value on the Hirshfeld surface, which shows the importance of O--H interactions in both A and B. From the fingerprint plots, the contributions involving different interactions includes C--H/N, N--H/O/N on the fingerprint plots of A and B comprise of C--H (5.6% and 2.4%), N--H (1.7% and 3.1%), N--C (0.6% and 1.2%), O--O (1.2%, in A) and N--O (0.4% in B) of the total Hirshfeld surface area. Curvedness and shape index can also be used to identify the ways by which the neighbouring molecules contact each another and the characteristic packing modes. The shape indexes of A and B show a red concave region on the surface around the acceptor atom and a blue region around the donor H-atom. (Fig. 8.16, labelled as b, e). Curvedness is a function of the RMS curvature of the surface and the curvedness maps on the Hirshfeld surface show no flat surface patches which indicates that there is no stacking interaction between the 2,3-DKP molecules (Fig. 8.16c) or the 2,5-DKP molecules (Fig. 8.16f). The type and nature of the inter-molecular interactions of the 2,3-DKP and 2,5-DKP molecules is more easily understood using Hirshfeld surfaces, the results showcase the power of the analysis in mapping such interactions.

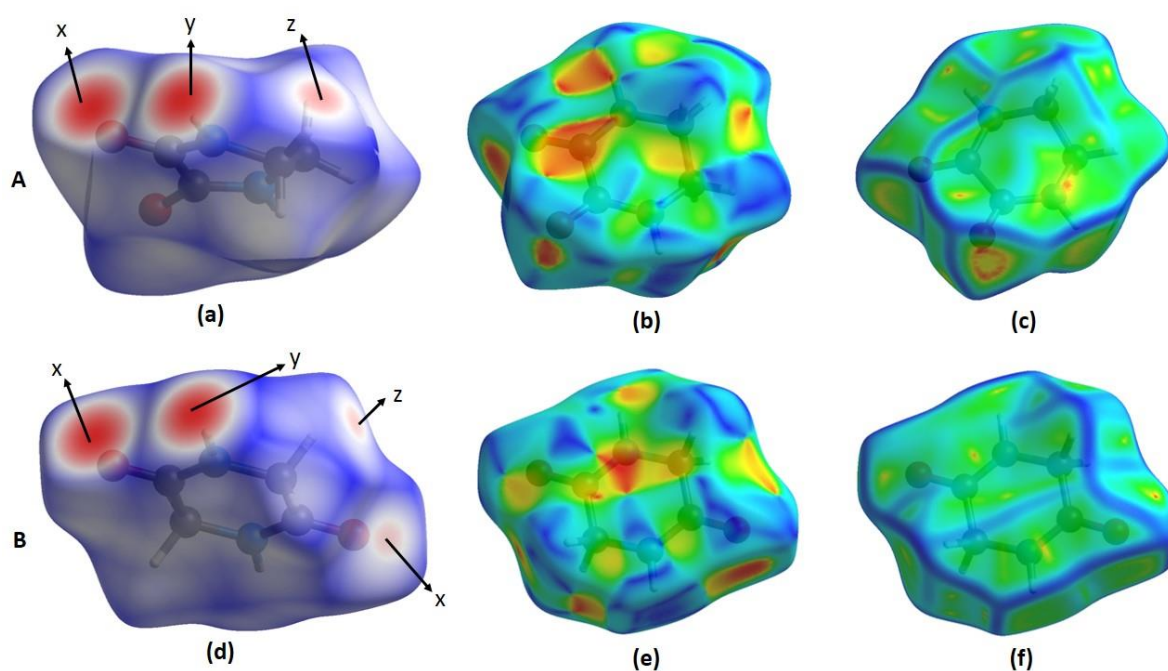


Figure 8.16. Hirshfeld surfaces of (A) 2,3-DKP (B) 2,5-DKP mapped with (a,d) d_{norm} showing all close contacts (b,e) shape index (c,f) curvedness.

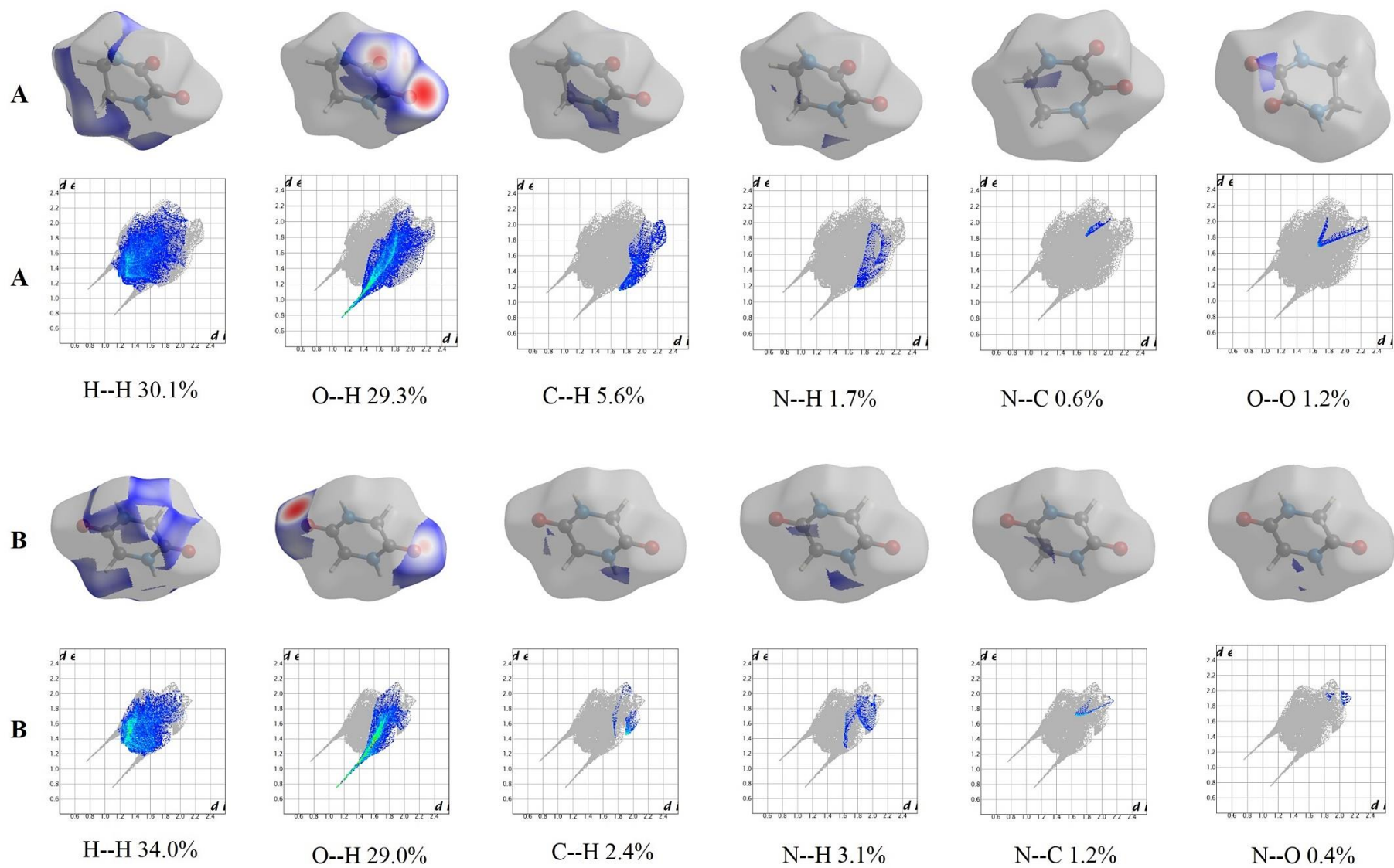


Figure 8.17. 2D Fingerprint plots for all the intermolecular contacts in (A) 2,3-DKP and (B) 2,5-DKP.

Table 8.13. Definitions of symmetry-adapted internal coordinates for 2,6-DKP.

2,6-DKP- C_s

A' symmetry

$$v(\text{N3H9})=r(\text{N3H9})$$

$$v(\text{N6H10})=r(\text{N6H10})$$

$$v_{\text{ss}}(\text{C=O})=1/\sqrt{2}[r(\text{C7O1}) + r(\text{C8O2})]$$

$$v_{\text{s}}(\text{CH}_2)=1/2[r(\text{C4H11}) + r(\text{C4H13})+ r(\text{C5H12}) + r(\text{C5H14})]$$

$$v_{\text{as}}(\text{CH}_2)=1/2[r(\text{C4H11}) - r(\text{C4H13})+ r(\text{C5H12}) - r(\text{C5H14})]$$

$$v_{\text{ss}}(\text{CN})=1/\sqrt{2}[r(\text{N6C8}) + r(\text{N6C7})]$$

$$v_{\text{ss}}(\text{NC}_\alpha)=1/\sqrt{2}[r(\text{N3C4}) + r(\text{N3C5})]$$

$$v_{\text{ss}}(\text{CC}_\alpha)=1/\sqrt{2}[r(\text{C8C4}) + r(\text{C7C5})]$$

$$\delta_{\text{ip,s}}(\text{CO})=1/2[\theta(\text{N6C8O2}) - \theta(\text{C4C8O2}) + \theta(\text{N6C7O1}) - \theta(\text{C5C7O1})]$$

$$\delta_{\text{op,as}}(\text{CO})= 1/2[\tau(\text{O1C7C5N6}) - \tau(\text{O2C8C4N6})]$$

$$\delta_{\text{op}}(\text{N6H10})= \tau(\text{H10N6C7C8})$$

$$\delta_{\text{op}}(\text{N3H9})= \tau(\text{H9N3C4C5})$$

$$\delta(\text{CH}_2)= 1/2\sqrt{10}[4\theta(\text{H11C4H13}) - \theta(\text{C8C4H11}) - \theta(\text{C8C4H13}) - \theta(\text{N3C4H11}) - \theta(\text{N3C4H13})+ 4\theta(\text{H12C5H14}) \\ - \theta(\text{C7C5H12}) - \theta(\text{C7C5H14}) - \theta(\text{N3C5H12}) - \theta(\text{N3C5H14})]$$

$$\rho(\text{CH}_2)= 1/2\sqrt{2}[\theta(\text{C8C4H11}) - \theta(\text{C8C4H13}) + \theta(\text{N3C4H11}) - \theta(\text{N3C4H13})+ \theta(\text{C7C5H12}) - \theta(\text{C7C5H14}) + \theta(\text{N3C5H12}) - \theta(\text{N3C5H14})]$$

$$\omega(\text{CH}_2)= 1/2\sqrt{2}[\theta(\text{C8C4H11}) + \theta(\text{C8C4H13}) - \theta(\text{N3C4H11}) - \theta(\text{N3C4H13})+ \theta(\text{C7C5H12})+ \theta(\text{C7C5H14}) - \theta(\text{N3C5H12}) - \theta(\text{N3C5H14})]$$

$$\tau(\text{CH}_2)= 1/2\sqrt{2}[\theta(\text{C8C4H11}) - \theta(\text{C8C4H13}) - \theta(\text{N3C4H11}) + \theta(\text{N3C4H13})+ \theta(\text{C7C5H12}) - \theta(\text{C7C5H14}) - \theta(\text{N3C5H12}) + \theta(\text{N3C5H14})]$$

$$\delta_{\text{ip}}(\text{Ring-1}) = 1/\sqrt{12}[2\theta(\text{C5N3C4}) - \theta(\text{N3C4C8}) - \theta(\text{C4C8CN6}) + 2\theta(\text{C8N6C7}) - \theta(\text{N6C7C5}) - \theta(\text{C7C5N3})]$$

$$\delta_{\text{op}}(\text{Ring-1}) = 1/\sqrt{6}[\tau(\text{N3C4C8N6}) - \tau(\text{C4C8N6C7}) + \tau(\text{C8N6C7C5}) - \tau(\text{N6C7C5N3}) + \tau(\text{C7C5N3C4}) - \tau(\text{C5N3C4C8})]$$

$$\delta_{\text{ip}}(\text{Ring-3}) = 1/\sqrt{6}[\theta(\text{C5N3C4}) - \theta(\text{N3C4C8}) + \theta(\text{C4C8CN6}) - \theta(\text{C8N6C7}) + \theta(\text{N6C7C5}) - \theta(\text{C7C5N3})]$$

$$\delta_{\text{op}}(\text{Ring-2}) = 1/2[\tau(\text{C4C8N6C7}) - \tau(\text{C8N6C7C5}) + \tau(\text{C7C5N3C4}) - \tau(\text{C5N3C4C8})]$$

A'' symmetry

$$v_{as}(C=O)=1/\sqrt{2}[r(C7O1) - r(C8O2)]$$

$$v_s(CH_2) = 1/2[r(C4H11) + r(C4H13) - r(C5H12) - r(C5H14)]$$

$$v_{as}(CH_2) = 1/2[r(C4H11) - r(C4H13) - r(C5H12) + r(C5H14)]$$

$$v_{as}(CN)=1/\sqrt{2}[r(N6C8) - r(N6C7)]$$

$$v_{as}(NC_\alpha)=1/\sqrt{2}[r(N3C4) - r(N3C5)]$$

$$v_{as}(CC_\alpha)=1/\sqrt{2}[r(C8C4) - r(C7C5)]$$

$$\delta_{ip,as}(CO)=1/2[\theta(N6C8O2) - \theta(C4C8O2) - \theta(N6C7O1) + \theta(C5C7O1)]$$

$$\delta_{op,s}(CO)= 1/2[\tau(O1C7C5N6) + \tau(O2C8C4N6)]$$

$$\delta_{ip}(N6H10)=1/\sqrt{2}[\theta(C7N6H10) - \theta(C8N6H10)]$$

$$\delta_{ip}(N3H9)=1/\sqrt{2}[\theta(C4N3H9) - \theta(C5N3H9)]$$

$$\delta(CH_2)= 1/2\sqrt{10}[4\theta(H11C4H13) - \theta(C8C4H11) - \theta(C8C4H13) - \theta(N3C4H11) - \theta(N3C4H13) - 4\theta(H12C5H14) \\ + \theta(C7C5H12) + \theta(C7C5H14) + \theta(N3C5H12) + \theta(N3C5H14)]$$

$$\rho(CH_2)= 1/2\sqrt{2}[\theta(C8C4H11) - \theta(C8C4H13) + \theta(N3C4H11) - \theta(N3C4H13) - \theta(C7C5H12) + \theta(C7C5H14) - \theta(N3C5H12) + \theta(N3C5H14)]$$

$$\omega(CH_2)= 1/2\sqrt{2}[\theta(C8C4H11) + \theta(C8C4H13) - \theta(N3C4H11) - \theta(N3C4H13) - \theta(C7C5H12) - \theta(C7C5H14) + \theta(N3C5H12) + \theta(N3C5H14)]$$

$$\tau(CH_2)= 1/2\sqrt{2}[\theta(C8C4H11) - \theta(C8C4H13) - \theta(N3C4H11) + \theta(N3C4H13) - \theta(C7C5H12) + \theta(C7C5H14) + \theta(N3C5H12) - \theta(N3C5H14)]$$

$$\delta_{ip}(\text{Ring-2}) = 1/2[\theta(N3C4C8) - \theta(C4C8CN6) + \theta(N6C7C5) - \theta(C7C5N3)]$$

$$\delta_{op}(\text{Ring-3}) = 1/\sqrt{12}[2\tau(N3C4C8N6) - \tau(C4C8N6C7) - \tau(C8N6C7C5) + 2\tau(N6C7C5N3) + \tau(C7C5N3C4) - \tau(C5N3C4C8)]$$

2,6-DKP- C_{2v}

A₁ symmetry

$$v(N3H9)=r(N3H9)$$

$$v(N6H10)=r(N6H10)$$

$$v_{ss}(C=O)=1/\sqrt{2}[r(C7O1) + r(C8O2)]$$

$$v_s(CH_2) = 1/2[r(C4H11) + r(C4H13) + r(C5H12) + r(C5H14)]$$

$$v_{ss}(CN)=1/\sqrt{2}[r(N6C8) + r(N6C7)]$$

$$v_{ss}(NC_\alpha)=1/\sqrt{2}[r(N3C4) + r(N3C5)]$$

$$v_{ss}(CC_{\alpha})=1/\sqrt{2}[r(C8C4) + r(C7C5)]$$

$$\delta_{ip,s}(CO)=1/2[\theta(N6C8O2) - \theta(C4C8O2) + \theta(N6C7O1) - \theta(C5C7O1)]$$

$$\delta(CH_2)= 1/2\sqrt{10}[4\theta(H11C4H13) - \theta(C8C4H11) - \theta(C8C4H13) - \theta(N3C4H11) - \theta(N3C4H13) + 4\theta(H12C5H14) - \theta(C7C5H12) - \theta(C7C5H14) - \theta(N3C5H12) - \theta(N3C5H14)]$$

$$\omega(CH_2)= 1/2\sqrt{2}[\theta(C8C4H11) + \theta(C8C4H13) - \theta(N3C4H11) - \theta(N3C4H13) + \theta(C7C5H12) + \theta(C7C5H14) - \theta(N3C5H12) - \theta(N3C5H14)]$$

$$\delta_{ip}(\text{Ring-1}) = 1/\sqrt{12}[2\theta(C5N3C4) - \theta(N3C4C8) - \theta(C4C8CN6) + 2\theta(C8N6C7) - \theta(N6C7C5) - \theta(C7C5N3)]$$

$$\delta_{ip}(\text{Ring-3}) = 1/\sqrt{6}[\theta(C5N3C4) - \theta(N3C4C8) + \theta(C4C8CN6) - \theta(C8N6C7) + \theta(N6C7C5) - \theta(C7C5N3)]$$

B₁ symmetry

$$v_{as}(CH_2) = 1/2[r(C4H11) - r(C4H13) + r(C5H12) - r(C5H14)]$$

$$\rho(CH_2) = 1/2\sqrt{2}[\theta(C8C4H11) - \theta(C8C4H13) + \theta(N3C4H11) - \theta(N3C4H13) + \theta(C7C5H12) - \theta(C7C5H14) + \theta(N3C5H12) - \theta(N3C5H14)]$$

$$\tau(CH_2) = 1/2\sqrt{2}[\theta(C8C4H11) - \theta(C8C4H13) - \theta(N3C4H11) + \theta(N3C4H13) + \theta(C7C5H12) - \theta(C7C5H14) - \theta(N3C5H12) + \theta(N3C5H14)]$$

$$\delta_{op}(N3H9) = \tau(H9N3C4C5)$$

$$\delta_{op,as}(CO) = 1/2[\tau(O1C7C5N6) - \tau(O2C8C4N6)]$$

$$\delta_{op}(N6H10) = \tau(H10N6C7C8)$$

$$\delta_{op}(\text{Ring-1}) = 1/\sqrt{6}[\tau(N3C4C8N6) - \tau(C4C8N6C7) + \tau(C8N6C7C5) - \tau(N6C7C5N3) + \tau(C7C5N3C4) - \tau(C5N3C4C8)]$$

$$\delta_{op}(\text{Ring-2}) = 1/2[\tau(C4C8N6C7) - \tau(C8N6C7C5) + \tau(C7C5N3C4) - \tau(C5N3C4C8)]$$

A₂ symmetry

$$v_{as}(CH_2) = 1/2[r(C4H11) - r(C4H13) - r(C5H12) + r(C5H14)]$$

$$\delta_{op,s}(CO) = 1/2[\tau(O1C7C5N6) + \tau(O2C8C4N6)]$$

$$\rho(CH_2) = 1/2\sqrt{2}[\theta(C8C4H11) - \theta(C8C4H13) + \theta(N3C4H11) - \theta(N3C4H13) - \theta(C7C5H12) + \theta(C7C5H14) - \theta(N3C5H12) + \theta(N3C5H14)]$$

$$\tau(CH_2) = 1/2\sqrt{2}[\theta(C8C4H11) - \theta(C8C4H13) - \theta(N3C4H11) + \theta(N3C4H13) - \theta(C7C5H12) + \theta(C7C5H14) + \theta(N3C5H12) - \theta(N3C5H14)]$$

$$\delta_{op}(\text{Ring-3}) = 1/\sqrt{12}[2\tau(N3C4C8N6) - \tau(C4C8N6C7) - \tau(C8N6C7C5) + 2\tau(N6C7C5N3) + \tau(C7C5N3C4) - \tau(C5N3C4C8)]$$

B₂ symmetry

$$v_{\text{as}}(\text{C}=\text{O})=1/\sqrt{2}[r(\text{C}7\text{O}1) - r(\text{C}8\text{O}2)]$$

$$v_{\text{s}}(\text{CH}_2) = 1/2[r(\text{C}4\text{H}11) + r(\text{C}4\text{H}13) - r(\text{C}5\text{H}12) - r(\text{C}5\text{H}14)]$$

$$v_{\text{as}}(\text{CN})=1/\sqrt{2}[r(\text{N}6\text{C}8) - r(\text{N}6\text{C}7)]$$

$$v_{\text{as}}(\text{NC}_\alpha)=1/\sqrt{2}[r(\text{N}3\text{C}4) - r(\text{N}3\text{C}5)]$$

$$v_{\text{as}}(\text{CC}_\alpha)=1/\sqrt{2}[r(\text{C}8\text{C}4) - r(\text{C}7\text{C}5)]$$

$$\delta_{\text{ip,as}}(\text{CO})=1/2[\theta(\text{N}6\text{C}8\text{O}2) - \theta(\text{C}4\text{C}8\text{O}2) - \theta(\text{N}6\text{C}7\text{O}1) + \theta(\text{C}5\text{C}7\text{O}1)]$$

$$\delta_{\text{ip}}(\text{N}6\text{H}10)=1/\sqrt{2}[\theta(\text{C}7\text{N}6\text{H}10) - \theta(\text{C}8\text{N}6\text{H}10)]$$

$$\delta_{\text{ip}}(\text{N}3\text{H}9)=1/\sqrt{2}[\theta(\text{C}4\text{N}3\text{H}9) - \theta(\text{C}5\text{N}3\text{H}9)]$$

$$\delta(\text{CH}_2) = 1/2\sqrt{10}[4\theta(\text{H}11\text{C}4\text{H}13) - \theta(\text{C}8\text{C}4\text{H}11) - \theta(\text{C}8\text{C}4\text{H}13) - \theta(\text{N}3\text{C}4\text{H}11) - \theta(\text{N}3\text{C}4\text{H}13) - 4\theta(\text{H}12\text{C}5\text{H}14) \\ + \theta(\text{C}7\text{C}5\text{H}12) + \theta(\text{C}7\text{C}5\text{H}14) + \theta(\text{N}3\text{C}5\text{H}12) + \theta(\text{N}3\text{C}5\text{H}14)]$$

$$\omega(\text{CH}_2) = 1/2\sqrt{2}[\theta(\text{C}8\text{C}4\text{H}11) + \theta(\text{C}8\text{C}4\text{H}13) - \theta(\text{N}3\text{C}4\text{H}11) - \theta(\text{N}3\text{C}4\text{H}13) - \theta(\text{C}7\text{C}5\text{H}12) - \theta(\text{C}7\text{C}5\text{H}14) + \theta(\text{N}3\text{C}5\text{H}12) + \theta(\text{N}3\text{C}5\text{H}14)]$$

$$\delta_{\text{ip}}(\text{Ring}-2) = 1/2[\theta(\text{N}3\text{C}4\text{C}8) - \theta(\text{C}4\text{C}8\text{C}6) + \theta(\text{N}6\text{C}7\text{C}5) - \theta(\text{C}7\text{C}5\text{N}3)]$$

Table 8.14. Definitions of symmetry-adapted internal coordinates for 2,3-DKP.

2,3-DKP- C₂

A symmetry

$$v_{\text{ss}}(\text{NH})=1/\sqrt{2}[r(\text{N}3\text{H}9) + r(\text{N}6\text{H}10)]$$

$$v_{\text{ss}}(\text{CO})=1/\sqrt{2}[r(\text{C}7\text{O}1) + r(\text{C}8\text{O}2)]$$

$$v_{\text{s}}(\text{CH}_2) = 1/2[r(\text{C}4\text{H}11) + r(\text{C}4\text{H}13) + r(\text{C}5\text{H}12) + r(\text{C}5\text{H}14)]$$

$$v_{\text{as}}(\text{CH}_2) = 1/2[r(\text{C}4\text{H}11) - r(\text{C}4\text{H}13) + r(\text{C}5\text{H}12) - r(\text{C}5\text{H}14)]$$

$$v_{\text{ss}}(\text{CN})=1/\sqrt{2}[r(\text{N}3\text{C}8) + r(\text{N}6\text{C}7)]$$

$$v_{\text{ss}}(\text{NC})=1/\sqrt{2}[r(\text{N}3\text{C}4) + r(\text{N}6\text{C}5)]$$

$$v(\text{C}4\text{C}5) = r(\text{C}4\text{C}5)$$

$$v(\text{C}7\text{C}8) = r(\text{C}7\text{C}8)$$

$$\delta_{\text{ip,s}}(\text{CO})=1/2[\theta(\text{N}6\text{C}7\text{O}1) - \theta(\text{C}8\text{C}7\text{O}1) + \theta(\text{N}3\text{C}8\text{O}2) - \theta(\text{C}7\text{C}8\text{O}2)]$$

$$\begin{aligned}
\delta_{\text{op,s}}(\text{CO}) &= 1/\sqrt{2}[\tau(\text{O1C7N6C8}) + \tau(\text{O2C8N3C7})] \\
\delta_{\text{ip,s}}(\text{NH}) &= 1/2[\theta(\text{C5N6H10}) - \theta(\text{C7N6H10}) + \theta(\text{C4N3H9}) - \theta(\text{C8N3H9})] \\
\delta_{\text{op,s}}(\text{NH}) &= 1/\sqrt{2}[\tau(\text{H10N6C5C7}) + \tau(\text{H9N3C4C8})] \\
\delta(\text{CH}_2) &= 1/2\sqrt{10}[4\theta(\text{H11C4H13}) - \theta(\text{C5C4H11}) - \theta(\text{C5C4H13}) - \theta(\text{N3C4H11}) - \theta(\text{N3C4H13}) + 4\theta(\text{H12C5H14}) \\
&\quad - \theta(\text{C4C5H12}) - \theta(\text{C4C5H14}) - \theta(\text{N6C5H12}) - \theta(\text{N6C5H14})] \\
\rho(\text{CH}_2) &= 1/2\sqrt{2}[\theta(\text{C5C4H11}) - \theta(\text{C5C4H13}) + \theta(\text{N3C4H11}) - \theta(\text{N3C4H13}) + \theta(\text{C4C5H12}) - \theta(\text{C4C5H14}) + \theta(\text{N6C5H12}) - \theta(\text{N6C5H14})] \\
\omega(\text{CH}_2) &= 1/2\sqrt{2}[\theta(\text{C5C4H11}) + \theta(\text{C5C4H13}) - \theta(\text{N3C4H11}) - \theta(\text{N3C4H13}) + \theta(\text{C4C5H12}) + \theta(\text{C4C5H14}) - \theta(\text{N6C5H12}) - \theta(\text{N6C5H14})] \\
\tau(\text{CH}_2) &= 1/2\sqrt{2}[\theta(\text{C5C4H11}) - \theta(\text{C5C4H13}) - \theta(\text{N3C4H11}) + \theta(\text{N3C4H13}) + \theta(\text{C4C5H12}) - \theta(\text{C4C5H14}) - \theta(\text{N6C5H12}) + \theta(\text{N6C5H14})] \\
\delta_{\text{ip}}(\text{Ring-1}) &= 1/\sqrt{12}[2\theta(\text{C8N3C4}) - \theta(\text{N3C4C5}) - \theta(\text{C4C5CN6}) + 2\theta(\text{C5N6C7}) - \theta(\text{N6C7C8}) - \theta(\text{C7C8N3})] \\
\delta_{\text{op}}(\text{Ring-1}) &= 1/\sqrt{6}[\tau(\text{N3C8C7N6}) - \tau(\text{C8C7N6C5}) + \tau(\text{C7N6C5C4}) - \tau(\text{N6C5C4N3}) + \tau(\text{C5C4N3C8}) - \tau(\text{C4N3C8C7})] \\
\delta_{\text{op}}(\text{Ring-3}) &= 1/\sqrt{12}[2\tau(\text{N3C8C7N6}) - \tau(\text{C8C7N6C5}) - \tau(\text{C7N6C5C4}) + 2\tau(\text{N6C5C4N3}) - \tau(\text{C5C4N3C8}) - \tau(\text{C4N3C8C7})]
\end{aligned}$$

B symmetry

$$\begin{aligned}
v_{\text{as}}(\text{NH}) &= 1/\sqrt{2}[r(\text{N3H9}) - r(\text{N6H10})] \\
v_{\text{as}}(\text{CO}) &= 1/\sqrt{2}[r(\text{C7O1}) - r(\text{C8O2})] \\
v_{\text{s}}(\text{CH}_2) &= 1/2[r(\text{C4H11}) + r(\text{C4H13}) - r(\text{C5H12}) - r(\text{C5H14})] \\
v_{\text{as}}(\text{CH}_2) &= 1/2[r(\text{C4H11}) - r(\text{C4H13}) - r(\text{C5H12}) + r(\text{C5H14})] \\
v_{\text{as}}(\text{CN}) &= 1/\sqrt{2}[r(\text{N3C8}) - r(\text{N6C7})] \\
v_{\text{as}}(\text{NC}) &= 1/\sqrt{2}[r(\text{N3C4}) - r(\text{N6C5})] \\
\delta_{\text{ip,as}}(\text{CO}) &= 1/2[\theta(\text{N6C7O1}) - \theta(\text{C8C7O1}) - \theta(\text{N3C8O2}) + \theta(\text{C7C8O2})] \\
\delta_{\text{op,as}}(\text{CO}) &= 1/\sqrt{2}[\tau(\text{O1C7N6C8}) - \tau(\text{O2C8N3C7})] \\
\delta_{\text{ip,as}}(\text{NH}) &= 1/2[\theta(\text{C5N6H10}) - \theta(\text{C7N6H10}) - \theta(\text{C4N3H9}) + \theta(\text{C8N3H9})] \\
\delta_{\text{op,as}}(\text{NH}) &= 1/\sqrt{2}[\tau(\text{H10N6C5C7}) - \tau(\text{H9N3C4C8})] \\
\delta(\text{CH}_2) &= 1/2\sqrt{10}[4\theta(\text{H11C4H13}) - \theta(\text{C5C4H11}) - \theta(\text{C5C4H13}) - \theta(\text{N3C4H11}) - \theta(\text{N3C4H13}) - 4\theta(\text{H12C5H14}) \\
&\quad + \theta(\text{C4C5H12}) + \theta(\text{C4C5H14}) + \theta(\text{N6C5H12}) + \theta(\text{N6C5H14})] \\
\rho(\text{CH}_2) &= 1/2\sqrt{2}[\theta(\text{C5C4H11}) - \theta(\text{C5C4H13}) + \theta(\text{N3C4H11}) - \theta(\text{N3C4H13}) - \theta(\text{C4C5H12}) + \theta(\text{C4C5H14}) - \theta(\text{N6C5H12}) + \theta(\text{N6C5H14})] \\
\omega(\text{CH}_2) &= 1/2\sqrt{2}[\theta(\text{C5C4H11}) + \theta(\text{C5C4H13}) - \theta(\text{N3C4H11}) - \theta(\text{N3C4H13}) - \theta(\text{C4C5H12}) - \theta(\text{C4C5H14}) + \theta(\text{N6C5H12}) + \theta(\text{N6C5H14})] \\
\tau(\text{CH}_2) &= 1/2\sqrt{2}[\theta(\text{C5C4H11}) - \theta(\text{C5C4H13}) - \theta(\text{N3C4H11}) + \theta(\text{N3C4H13}) - \theta(\text{C4C5H12}) + \theta(\text{C4C5H14}) + \theta(\text{N6C5H12}) - \theta(\text{N6C5H14})]
\end{aligned}$$

$$\delta_{ip}(\text{Ring-2}) = 1/2[\theta(\text{N3C4C5}) - \theta(\text{C4C5CN6}) + \theta(\text{N6C7C8}) - \theta(\text{C7C8N3})]$$

$$\delta_{ip}(\text{Ring-3}) = 1/\sqrt{6}[\theta(\text{C8N3C4}) - \theta(\text{N3C4C5}) + \theta(\text{C4C5CN6}) - \theta(\text{C5N6C7}) + \theta(\text{N6C7C8}) - \theta(\text{C7C8N3})]$$

$$\delta_{op}(\text{Ring-2}) = 1/2[\tau(\text{C8C7N6C5}) - \tau(\text{C7N6C5C4}) + \tau(\text{C5C4N3C8}) - \tau(\text{C4N3C8C7})]$$

2,3-DKP- C_{2v}

A₁ symmetry

$$v_{ss}(\text{NH}) = 1/\sqrt{2}[r(\text{N3H9}) + r(\text{N6H10})]$$

$$v_{ss}(\text{CO}) = 1/\sqrt{2}[r(\text{C7O1}) + r(\text{C8O2})]$$

$$v_s(\text{CH}_2) = 1/2[r(\text{C4H11}) + r(\text{C4H13}) + r(\text{C5H12}) + r(\text{C5H14})]$$

$$v_{ss}(\text{CN}) = 1/\sqrt{2}[r(\text{N3C8}) + r(\text{N6C7})]$$

$$v_{ss}(\text{NC}) = 1/\sqrt{2}[r(\text{N3C4}) + r(\text{N6C5})]$$

$$v(\text{C4C5}) = r(\text{C4C5})$$

$$v(\text{C7C8}) = r(\text{C7C8})$$

$$\delta_{ip,s}(\text{CO}) = 1/2[\theta(\text{N6C7O1}) - \theta(\text{C8C7O1}) + \theta(\text{N3C8O2}) - \theta(\text{C7C8O2})]$$

$$\delta_{ip,s}(\text{NH}) = 1/2[\theta(\text{C5N6H10}) - \theta(\text{C7N6H10}) + \theta(\text{C4N3H9}) - \theta(\text{C8N3H9})]$$

$$\delta(\text{CH}_2) = 1/2\sqrt{10}[4\theta(\text{H11C4H13}) - \theta(\text{C5C4H11}) - \theta(\text{C5C4H13}) - \theta(\text{N3C4H11}) - \theta(\text{N3C4H13}) + 4\theta(\text{H12C5H14}) \\ - \theta(\text{C4C5H12}) - \theta(\text{C4C5H14}) - \theta(\text{N6C5H12}) - \theta(\text{N6C5H14})]$$

$$\omega(\text{CH}_2) = 1/2\sqrt{2}[\theta(\text{C5C4H11}) + \theta(\text{C5C4H13}) - \theta(\text{N3C4H11}) - \theta(\text{N3C4H13}) + \theta(\text{C4C5H12}) + \theta(\text{C4C5H14}) - \theta(\text{N6C5H12}) - \theta(\text{N6C5H14})]$$

$$\delta_{ip}(\text{Ring-1}) = 1/\sqrt{12}[2\theta(\text{C8N3C4}) - \theta(\text{N3C4C5}) - \theta(\text{C4C5CN6}) + 2\theta(\text{C5N6C7}) - \theta(\text{N6C7C8}) - \theta(\text{C7C8N3})]$$

B₁ symmetry

$$v_{as}(\text{CH}_2) = 1/2[r(\text{C4H11}) - r(\text{C4H13}) + r(\text{C5H12}) - r(\text{C5H14})]$$

$$\delta_{op,s}(\text{CO}) = 1/\sqrt{2}[\tau(\text{O1C7N6C8}) + \tau(\text{O2C8N3C7})]$$

$$\delta_{op,s}(\text{NH}) = 1/\sqrt{2}[\tau(\text{H10N6C5C7}) + \tau(\text{H9N3C4C8})]$$

$$\rho(\text{CH}_2) = 1/2\sqrt{2}[\theta(\text{C5C4H11}) - \theta(\text{C5C4H13}) + \theta(\text{N3C4H11}) - \theta(\text{N3C4H13}) + \theta(\text{C4C5H12}) - \theta(\text{C4C5H14}) + \theta(\text{N6C5H12}) - \theta(\text{N6C5H14})]$$

$$\tau(\text{CH}_2) = 1/2\sqrt{2}[\theta(\text{C5C4H11}) - \theta(\text{C5C4H13}) - \theta(\text{N3C4H11}) + \theta(\text{N3C4H13}) + \theta(\text{C4C5H12}) - \theta(\text{C4C5H14}) - \theta(\text{N6C5H12}) + \theta(\text{N6C5H14})]$$

$$\delta_{\text{op}}(\text{Ring-1}) = 1/\sqrt{6}[\tau(\text{N3C8C7N6}) - \tau(\text{C8C7N6C5}) + \tau(\text{C7N6C5C4}) - \tau(\text{N6C5C4N3}) + \tau(\text{C5C4N3C8}) - \tau(\text{C4N3C8C7})]$$

$$\delta_{\text{op}}(\text{Ring-3}) = 1/\sqrt{12}[2\tau(\text{N3C8C7N6}) - \tau(\text{C8C7N6C5}) - \tau(\text{C7N6C5C4}) + 2\tau(\text{N6C5C4N3}) - \tau(\text{C5C4N3C8}) - \tau(\text{C4N3C8C7})]$$

A₂ symmetry

$$v_{\text{as}}(\text{CH}_2) = 1/2[r(\text{C4H11}) - r(\text{C4H13}) - r(\text{C5H12}) + r(\text{C5H14})]$$

$$\rho(\text{CH}_2) = 1/2\sqrt{2}[\theta(\text{C5C4H11}) - \theta(\text{C5C4H13}) + \theta(\text{N3C4H11}) - \theta(\text{N3C4H13}) - \theta(\text{C4C5H12}) + \theta(\text{C4C5H14}) - \theta(\text{N6C5H12}) + \theta(\text{N6C5H14})]$$

$$\tau(\text{CH}_2) = 1/2\sqrt{2}[\theta(\text{C5C4H11}) - \theta(\text{C5C4H13}) - \theta(\text{N3C4H11}) + \theta(\text{N3C4H13}) - \theta(\text{C4C5H12}) + \theta(\text{C4C5H14}) + \theta(\text{N6C5H12}) - \theta(\text{N6C5H14})]$$

$$\delta_{\text{op,as}}(\text{CO}) = 1/\sqrt{2}[\tau(\text{O1C7N6C8}) - \tau(\text{O2C8N3C7})]$$

$$\delta_{\text{op,as}}(\text{NH}) = 1/\sqrt{2}[\tau(\text{H10N6C5C7}) - \tau(\text{H9N3C4C8})]$$

$$\delta_{\text{op}}(\text{Ring-2}) = 1/2[\tau(\text{C8C7N6C5}) - \tau(\text{C7N6C5C4}) + \tau(\text{C5C4N3C8}) - \tau(\text{C4N3C8C7})]$$

B₂ symmetry

$$v_{\text{as}}(\text{NH}) = 1/\sqrt{2}[r(\text{N3H9}) - r(\text{N6H10})]$$

$$v_{\text{as}}(\text{CO}) = 1/\sqrt{2}[r(\text{C7O1}) - r(\text{C8O2})]$$

$$v_{\text{s}}(\text{CH}_2) = 1/2[r(\text{C4H11}) + r(\text{C4H13}) - r(\text{C5H12}) - r(\text{C5H14})]$$

$$v_{\text{as}}(\text{CN}) = 1/\sqrt{2}[r(\text{N3C8}) - r(\text{N6C7})]$$

$$v_{\text{as}}(\text{NC}) = 1/\sqrt{2}[r(\text{N3C4}) - r(\text{N6C5})]$$

$$\delta_{\text{ip,as}}(\text{CO}) = 1/2[\theta(\text{N6C7O1}) - \theta(\text{C8C7O1}) - \theta(\text{N3C8O2}) + \theta(\text{C7C8O2})]$$

$$\delta_{\text{ip,as}}(\text{NH}) = 1/2[\theta(\text{C5N6H10}) - \theta(\text{C7N6H10}) - \theta(\text{C4N3H9}) + \theta(\text{C8N3H9})]$$

$$\delta(\text{CH}_2) = 1/2\sqrt{10}[4\theta(\text{H11C4H13}) - \theta(\text{C5C4H11}) - \theta(\text{C5C4H13}) - \theta(\text{N3C4H11}) - \theta(\text{N3C4H13}) - 4\theta(\text{H12C5H14})$$

$$\quad + \theta(\text{C4C5H12}) + \theta(\text{C4C5H14}) + \theta(\text{N6C5H12}) + \theta(\text{N6C5H14})]$$

$$\omega(\text{CH}_2) = 1/2\sqrt{2}[\theta(\text{C5C4H11}) + \theta(\text{C5C4H13}) - \theta(\text{N3C4H11}) - \theta(\text{N3C4H13}) - \theta(\text{C4C5H12}) - \theta(\text{C4C5H14}) + \theta(\text{N6C5H12}) + \theta(\text{N6C5H14})]$$

$$\delta_{\text{ip}}(\text{Ring-2}) = 1/2[\theta(\text{N3C4C5}) - \theta(\text{C4C5CN6}) + \theta(\text{N6C7C8}) - \theta(\text{C7C8N3})]$$

$$\delta_{\text{ip}}(\text{Ring-3}) = 1/\sqrt{6}[\theta(\text{C8N3C4}) - \theta(\text{N3C4C5}) + \theta(\text{C4C5CN6}) - \theta(\text{C5N6C7}) + \theta(\text{N6C7C8}) - \theta(\text{C7C8N3})]$$

Table 8.15. Definitions of symmetry-adapted internal coordinates for 4,5-HHP.

4,5-HHP- C₁

A symmetry

$$v(\text{N9H10}) = r(\text{N9H10})$$

$$v(\text{N11H12}) = r(\text{N11H12})$$

$$v(\text{C1O14}) = r(\text{C1O14})$$

$$v(\text{C2O13}) = r(\text{C2O13})$$

$$v(\text{C1N11}) = r(\text{C1N11})$$

$$v(\text{C6N11}) = r(\text{C6N11})$$

$$v(\text{C6N9}) = r(\text{C6N9})$$

$$v(\text{C1C2}) = r(\text{C1C2})$$

$$v(\text{C2C3}) = r(\text{C2C3})$$

$$v(\text{C3N9}) = r(\text{C3N9})$$

$$v_s(\text{CH}_{2a}) = 1/\sqrt{2}[r(\text{C3H4}) + r(\text{C3H5})]$$

$$v_{as}(\text{CH}_{2a}) = 1/\sqrt{2}[r(\text{C3H4}) - r(\text{C3H5})]$$

$$v_s(\text{CH}_{2b}) = 1/\sqrt{2}[r(\text{C6H7}) + r(\text{C6H8})]$$

$$v_{as}(\text{CH}_{2b}) = 1/\sqrt{2}[r(\text{C6H7}) - r(\text{C6H8})]$$

$$\delta_{ip}(\text{C1O14}) = 1/\sqrt{2}[\theta(\text{N11C1O14}) - \theta(\text{C2C1O14})]$$

$$\delta_{ip}(\text{C2O13}) = 1/\sqrt{2}[\theta(\text{C1C2O13}) - \theta(\text{C3C2O13})]$$

$$\delta_{ip}(\text{N9H10}) = 1/\sqrt{2}[\theta(\text{C3N9H10}) - \theta(\text{C6N9H10})]$$

$$\delta_{ip}(\text{N11H12}) = 1/\sqrt{2}[\theta(\text{C1N11H12}) - \theta(\text{C6N11H12})]$$

$$\delta_{op}(\text{C1O14}) = \tau(\text{O14C1C2N11})$$

$$\delta_{op}(\text{C2O13}) = \tau(\text{O13C2C1C3})$$

$$\delta_{op}(\text{N9H10}) = \tau(\text{H10N9C3C6})$$

$$\delta_{op}(\text{N11H12}) = \tau(\text{H12N11C1C6})$$

$$\delta(\text{CH}_{2a}) = 1/2\sqrt{5}[4\theta(\text{H4C3H5}) - \theta(\text{C2C3H4}) - \theta(\text{C2C3H5}) - \theta(\text{N9C3H4}) - \theta(\text{N9C3H5})]$$

$$\rho(\text{CH}_{2a}) = 1/2[\theta(\text{C2C3H4}) - \theta(\text{C2C3H5}) + \theta(\text{N9C3H4}) - \theta(\text{N9C3H5})]$$

$$\omega(\text{CH}_{2a}) = 1/2[\theta(\text{C2C3H4}) + \theta(\text{C2C3H5}) - \theta(\text{N9C3H4}) - \theta(\text{N9C3H5})]$$

$$\tau(\text{CH}_{2a}) = 1/2[\theta(\text{C2C3H4}) - \theta(\text{C2C3H5}) - \theta(\text{N9C3H4}) + \theta(\text{N9C3H5})]$$

$$\delta(\text{CH}_{2b}) = 1/2\sqrt{5}[4\theta(\text{H7C6H8}) - \theta(\text{N11C6H7}) - \theta(\text{N11C6H8}) - \theta(\text{N9C6H7}) - \theta(\text{N9C6H8})]$$

$$\rho(\text{CH}_{2b}) = 1/2[\theta(\text{N11C6H7}) - \theta(\text{N11C6H8}) + \theta(\text{N9C6H7}) - \theta(\text{N9C6H8})]$$

$$\omega(\text{CH}_{2b}) = 1/2[\theta(\text{N11C6H7}) + \theta(\text{N11C6H8}) - \theta(\text{N9C6H7}) - \theta(\text{N9C6H8})]$$

$$\tau(\text{CH}_{2b}) = 1/2[\theta(\text{N11C6H7}) - \theta(\text{N11C6H8}) - \theta(\text{N9C6H7}) + \theta(\text{N9C6H8})]$$

$$\delta_{ip}(\text{Ring-1}) = 1/\sqrt{12}[2\theta(\text{C3N9C6}) - \theta(\text{N9C6N11}) - \theta(\text{C6N11C1}) + 2\theta(\text{C2C1N11}) - \theta(\text{C1C2C3}) - \theta(\text{C2C3N9})]$$

$$\delta_{op}(\text{Ring-1}) = 1/\sqrt{6}[\tau(\text{N9C6N11C1}) - \tau(\text{C6N11C1C2}) + \tau(\text{N11C1C2C3}) - \tau(\text{C1C2C3N9}) + \tau(\text{C2C3N9C6}) - \tau(\text{C3N9C6N11})]$$

$$\delta_{ip}(\text{Ring-3}) = 1/\sqrt{6}[\theta(\text{C3N9C6}) - \theta(\text{N9C6N11}) + \theta(\text{C6N11C1}) - \theta(\text{C2C1N11}) + \theta(\text{C1C2C3}) - \theta(\text{C2C3N9})]$$

$$\delta_{op}(\text{Ring-2}) = 1/2[\tau(\text{C6N11C1C2}) - \tau(\text{N11C1C2C3}) + \tau(\text{C2C3N9C6}) - \tau(\text{C3N9C6N11})]$$

$$\delta_{ip}(\text{Ring-2}) = 1/2[\theta(\text{N9C6N11}) - \theta(\text{C6N11C1}) + \theta(\text{C1C2C3}) - \theta(\text{C2C3N9})]$$

$$\delta_{op}(\text{Ring-3}) = 1/\sqrt{12}[2\tau(\text{N9C6N11C1}) - \tau(\text{C6N11C1C2}) - \tau(\text{N11C1C2C3}) + 2\tau(\text{C1C2C3N9}) + \tau(\text{C2C3N9C6}) - \tau(\text{C3N9C6N11})]$$

8.7. Conclusions

An IR and Raman spectroscopic study of the regioisomers of DKP (2,3-DKP, 2,6-DKP and 4,5-HHP) was carried out in the solid state and solution state and compared and contrasted with previously reported IR and Raman data on 2,5-DKP. There is no X-ray data for 2,6-DKP and 4,5-HHP but DFT calculations suggests that the six-membered ring (DKP) in 2,6-DKP and (pyrimidine) in 4,5-HHP molecules adopts a half-chair/sofa conformation with C_s (2,6-DKP) and C_1 (4,5-HHP) symmetries. The X-ray and calculated structures of 2,3-DKP suggest that the DKP ring adopts a skew-boat conformation with C_1 (X-ray) and C_2 (gas-phase) symmetry. The calculated and experimental data associated with the splitting of C-H asymmetric/asymmetric stretching vibrations also suggests that the skew-boat (2,3-DKP) and half-chair (2,6-DKP and 4,5-HHP) conformations are preferred in the solid state.

From our observations, the N-H stretching vibrations can be clearly seen in a broad region between 3120 and 3330 cm^{-1} in both the IR and Raman spectra of 2,3-DKP and 4,5-HHP. Interestingly, in 2,6-DKP, two N-H stretching bands are observed at different wavenumbers (cm^{-1}) owing to the presence of N-H groups at different environments. Hence, it has been hypothesised that both N-H groups are involved in hydrogen bonding but at different strengths. The assignments of the amide I modes and the nature of the amide vibrations of the *cis* peptide groups in 2,3-DKP and 4,5-HHP have been confirmed by the spectroscopic data and DFT calculations. However, in 2,6-DKP, the amide I vibrations appears at a significantly higher wavenumber ($\sim 40\text{-}50 \text{ cm}^{-1}$), and have a significantly higher Raman intensity than found in other DKPs, including 2,5-DKP.^{16, 18, 19} This can be explained by the presence of less N-H character/contribution in *cis* amide I mode. The assignments of the amide II modes cannot be made due to the decrease in wavenumber (cm^{-1}) of the C-N stretching vibrations in 2,3-DKP and 4,5-HHP; this can be attributed to the strong coupling of C-N vibrations with N-H in-plane-bending and CH_2 bending vibrations. Whereas, in 2,6-DKP, this can be explained by the delocalisation of partial double bonds on amide linkage and hence, decreasing the bond order and increasing bond lengths of the C-N bonds (1.38 Å, Table 8.5) and additionally, due to strong coupling of C-N stretching with N-H-in-plane-bending vibrations. All the aforementioned explanations were made possible from our calculated PEDs for all three molecules and in comparison to the previous studies undertaken on 2,5-DKPs.¹⁶ Theoretically-from PED values-and experimentally from *N*-deuteration shifts in IR and Raman spectra, it is hypothesised that the assumptions (location and coupling of C-N stretch and N-H in-plane bending vibration) relating to *cis* amide II modes cannot be made from the experimental data in all three molecules due to the presence of high N-H character.

HOMO and LUMO analysis has been carried out on the minimum energy conformers of 2,3-DKP, 2,6-DKP, 4,5-HHP and 2,5-DKP to elucidate the information related to the charge transfer within these molecules. The HOMO-LUMO gap for 2,3-DKP, 2,6-DKP, 4,5-HHP and 2,5-DKP was found to be about 5.648, 5.936, 4.805 and 6.604 eV, respectively which implies that all four compounds possess relatively high chemical stability. However, 2,5-DKP was found to be the most stable compound compared to its other regioisomers in the gas phase. The MEP analysis reveals that the most negative potentials are mainly over the electronegative oxygen atoms of the six-membered DKP ring (2,3-DKP, 2,5-DKP, 2,6-DKP) and pyrimidine ring (4,5-HHP) and slightly on the nitrogen atoms in 2,6-DKP and 4,5-HHP. The positive potential is located over the nitrogen and hydrogen atoms in all four molecules. The Hirshfeld surface analysis and 2D fingerprint plots enabled investigations of the nature of the intermolecular interactions present in 2,3-DKP and 2,5-DKP crystal structures.

8.8. References

1. J. C. Dinsmore, D. C. Beshore, *Tetrahedron*, 2002, 58, 3297.
2. (a) Hofmann, *Chem. Ber.*, 1872, 5, 247. (b) Van Alphen, *Rec. Trav. Chim.*, 1986, 64, 937.
3. A. D. Borthwick, *Chem. Rev.*, 2012, 112, 3641.
4. D. T. Witiak, Y. Wei, *Prog. Drug. Res.*, 1990, 35, 249.
5. L.W. Whitehouse, A. Menzies, B. Dawson, T.D. Cyr, A.W. By, D.B. Black, J. Zamecnik, *J. Pharm. Biomed. Anal.*, 1994, 12, 1425.
6. R. Skinner Jr, P. W. Noah, R. M. Taylor, M. D. Zanolli, S. West, J. D. Guin, E. W. Rosenberg, *J. Am. Acad. Dermatol.*, 1985, 12, 852.
7. (a) M. J. Basker, R. A. Edmondson, S. J. Knott, R. J. Ponsford, B. Slocombe, S. J. White, *Antimicrob. Agents Chemother.*, 1984, 26, 734. (b) W. Mandell, H. C. Neu, *Antimicrob. Agents Chemother.*, 1986, 29, 769.
8. S Takano, H. Ochiai , J. Nitta , M. Komatsu , H. Taki , M. Tai , T. Yasuda , I. Saikawa, *Yakugaku Zasshi.*, 1979, 99, 371.
9. D. T. Davies, F. P. Harrington, S. J. knott, R. Southgate, *J. Antibiot.*, 1989, 42, 367.
10. (a) M. Dawidowski, F. Herold, A. Chodkowski, J. Kleps, P. Szulczyk, M. Wilczek, *Eur. J. Med. Chem.*, 2011, 46, 4859. (b) M. Dawidowski, F. Herold, A. Chodkowski, J. Kleps. *Eur. J. Med. Chem.*, 2012, 48, 347.
11. S. E. Lipshultz, N. Rifai, V. M. Dalton, D. E. Levy, L. B. Silverman, S. R. Lipsitz, S. D. Colan, B. L. Asselin, R. D. Barr, L. A. Clavell, C. A. Hurwitz, A. Moghrabi, Y. Samson, M. A. Schorin, R. D. Gelber, S. E. Sallan, *N. Engl. J. Med.*, 2004, 351, 145.

12. S. K. Bjelogrić, J. Radic, S. Radulovic, M. Jokanovic, V. Jovic, *Exp. Biol. Med.*, 2007, 232, 1414.
13. M. Dawidowski, F. Herold, I. Wolska, I. Wawer, *J. Mol. Struct.*, 2010, 975, 78.
14. A. T. H Lenstra, B. Bracke, B. van Dijk, S. Maes, C. Vanhulle, H. O. Desseyn, *Acta Cryst.*, 1998, B54, 851.
15. A. T. H Lenstra, B. Bracke, B. van Dijk, S. Maes, C. Van Alsenoy, H. O. Desseyn, S. P. Perlepes, *Acta Cryst.*, 1998, B54, 859.
16. A. P. Mendham, T. J. Dines, M. J. Snowden, R. Withnall, B. Z. Chowdhry, *J. Raman Spectrosc.* 2009, 40, 1478.
17. R. Degeilh, R. E. Marsh, *Acta Crystallogr.*, 1959, 12, 1007.
18. A. P. Mendham, T. J. Dines, M. J. Snowden, R. Withnall, B. Z. Chowdhry, *J. Raman Spectrosc.* 2009, 40, 1508.
19. A. P. Mendham, T. J. Dines, R. Withnall, J. C. Mitchell, B. Z. Chowdhry, *J. Raman Spectrosc.* 2009, 40, 1498.
20. T. C. Cheam, S. Krimm, *Spectrochim. Acta Part A.*, 1984, 40, 481.

9.0. Overall Conclusions and Future Work

9.1. Overall conclusions

9.1.1. DFT calculations

Geometry optimisation calculations of C-CySH suggests that the minimum energy optimised structure (C_2 symmetry), with energy (-1369.93615495 H) is 2.172 kJ mol⁻¹ lower than that of the asymmetric structure (C_1 symmetry) favoured in the solid state (-1369.93532731 H). However, in both cases the molecule deviates slightly from planarity towards a boat conformation with the two L-homoCySH side-chains folded above the ring. Similarly, DFT calculations of AMDKP, DAGG, DMGG (with C_2 symmetries) also suggests that the boat conformation is preferred as the minimum energy conformation in gas phase. In order to verify the minimum energy conformations of the L-homoCySH side-chains of C-CySH and 3,6-aminoxymethyl side-chains of AMDKP, energy profile calculations were carried out at the HF/3-21G level using the Spartan'14 program,¹ by rotating the CC, CS bonds ($\pm 180^\circ$) in C-CySH and CC, CO bonds ($\pm 180^\circ$) in AMDKP.

In CHP, CDHP, CAH (with C_1 symmetries), the boat conformation is preferred in gas phase calculations. Moreover, two calculation strategies were employed for CHP, CDHP and CAH by shifting the proton on the two nitrogen atoms in the imidazole ring of the L-His side chain. Again, to verify the minimum energy conformations of the L-His and D-His side-chains of the tautomers (N^ϵ and N^δ) of CHP, CDHP and CAH, energy profile calculations were performed for the conformational analysis of L-His/D-His side-chains attached to the DKP ring, by rotating the C_α - C_β and C_β - C_γ dihedral angles at HF/321-G using the Spartan'14 program.¹ The potential energy plots, reveals that there are three minimum energy structures for each N^ϵ and N^δ -tautomeric forms of CHP, CDHP and CAH in the regions of $\tau(\text{H4C3C7C10}) = \pm 180^\circ$ (CHP and CDHP) and $\tau(\text{H18C4C9C11}) = \pm 180^\circ$ (CAH), corresponding to three possible conformations I, II and III. From our calculations it is suggested that the lowest energy conformers of N^δ -tautomeric forms have lower energy compared to the N^ϵ -tautomeric forms for each molecules.

Interestingly, DMDKP exists as planar conformation in the gas phase. This is attributed to the attachment of the dimethylene (alkene) side chains on either side of the DKP ring. The calculated minimum energy structures (at B3LYP/aug-cc-pVTZ) of 2,3-DKP (skew-boat), 2,5-DKP (boat), 2,6-DKP (half chair) and its isomer 4,5-HHP (half chair) have C_2 , C_2 , C_s and C_1 symmetries, respectively. Additionally, the calculations have also been performed by constraining the six membered ring to be planar with C_{2v} (2,3-DKP and 2,6-DKP), C_1 (4,5-HHP) symmetries. This

resulted in an imaginary frequency, which shows that all three molecules cannot have a planar six-membered ring as the lowest energy conformation in the gas phase. By comparing the calculated energies of all three regioisomers of DKP, the minimum energy boat conformer of 2,5-DKP was found to have the lowest energy conformer.

9.1.2. N-H stretching vibrations

N-H stretching vibrations in DKPs appear between 3150 and 3300 cm^{-1} . From previous studies on DKPs, it is suggested that the location (cm^{-1}) of the N-H stretch is sensitive to hydrogen bonding in the solid state and hence, occurs at lower wavenumbers (cm^{-1}) for the DKPs with strong hydrogen bonding.^{2,3} The bands located between $\sim 3342 \text{ cm}^{-1}$ and 3204 cm^{-1} in both the solid state IR and Raman spectra of AMDKP are assigned to the amine NH_2 stretching vibrations. The amide N-H stretching bands in AMDKP appear at 3182 cm^{-1} and 3047 cm^{-1} in the IR spectrum and at 3165 cm^{-1} and 3049 cm^{-1} in the Raman spectrum in the solid state. It is suggested that, in AMDKP the N-H groups on the DKP ring participate in hydrogen bonding and hence appear at lower wavenumber. This hypothesis has been put forward by comparing the location of the amide N-H stretching vibrations and its corresponding shifts on *N*-deuteration in other DKPs.²⁻⁴

Similarly, in CDHP, CHP and CAH the N-H stretching vibrations can be easily located in the region 3300-3100 cm^{-1} . The N-H stretching vibration of the imidazole ring in the L-His side chain is observed at 3175, 3313 and 3222 cm^{-1} in the IR spectra and 3181, 3313 and 3181 cm^{-1} in Raman spectra of CHP, CDHP and CAH respectively. The N-H stretching vibration of the DKP ring appears at 3135, 3168 and 3188 cm^{-1} in the IR spectra and 3135, 3170 and 3181 cm^{-1} in the Raman spectra of CHP, CDHP and CAH. From previous X-ray studies reported on various histidine-containing cyclic dipeptides, it is suggested that the N-H group of the imidazole ring and the amide groups of the DKP ring participate in inter-molecular hydrogen bonding.^{5,6} From our observations, it is therefore hypothesised that the two N-H groups in all three cyclic dipeptides (CHP, CDHP and CAH) are involved in hydrogen bonding in different strengths.

The N-H stretching vibrations can be clearly seen as a broad region in between 3120-3330 cm^{-1} in both IR and Raman spectra of 2,3-DKP and 4,5-HHP. Interestingly, in 2,6-DKP, two N-H stretching bands are observed at different wavenumbers (cm^{-1}) owing to the presence of N-H groups in different locations, one N-H group in between two CH_2 groups and the other in between two carbonyl groups. Hence, it has been hypothesised that both N-H groups are involved in hydrogen bonding but at different strengths. The N-H stretching vibrations at $\sim 3300 \text{ cm}^{-1}$ is assigned to N3H9 group and the broad region centred $\sim 2700 \text{ cm}^{-1}$ in both IR and Raman spectra

is assigned to N6H10 stretching vibrations. On *N*-deuteration, the two N-H groups shifts down at two different locations (cm^{-1}) $\sim 2400 \text{ cm}^{-1}$ for N3D9 stretching and a broad band centred at $\sim 2150 \text{ cm}^{-1}$ for N6D10 stretching vibrations in both IR and Raman spectra of *N*-deuterated 2,6-DKP.

9.1.3. *Cis* amide I vibrations

The *cis* amide mode in DKPs occurs between 1630 and 1690 cm^{-1} .²⁻⁴ In DMDKP, the bands located in the region 1685 and 1600 cm^{-1} are assigned to vibrations that are quite mixed. The band located at 1681 cm^{-1} in both IR and Raman spectra is assigned to a mixed carbonyl C=O stretching and C=C stretching mode. Hence, it can be hypothesised that this is not a typical *cis* amide I mode as observed previously in other DKPs. The Raman and IR spectra for DAGG and 2,6-DKP shows that the ring C=O stretching mode appears at a significantly higher wavenumber ($\sim 40 \text{ cm}^{-1}$), and has a significantly higher Raman intensity than observed in other CDAPs, including cyclo(Gly-Gly).²⁻⁴ This can be explained by the shortening of the ring C=O bond distance after acetylation, which is attributed to the delocalization of the lone pairs on the nitrogen atoms towards the exo, from the endocyclic amide linkages in DAGG and the shortening of the ring C=O bond distance due to the presence of N-H group in between two carbonyl carbons, which is attributed to the delocalization of the lone pairs on the nitrogen atoms in 2,6-DKP. It is noteworthy that in DMGG there is a difference of around $\sim 50\text{-}60 \text{ cm}^{-1}$ in the location of the C=O stretching band (1666 cm^{-1} in Raman and 1650 cm^{-1} in IR) compared to DAGG. This can be attributed to the presence of C-N stretching character, instead of N-H in-plane-bending, associated with C=O stretch in the amide I mode.

Four bands associated with C=O stretching vibrations of 2,3-DKP can be detected between $1715\text{-}1624 \text{ cm}^{-1}$ in both solid state IR and Raman spectra. Previous studies on 2,3-DKP suggest that the splitting in this region is mainly due to the presence of two carbonyl groups.⁷ Additional bands may be observed due to factor group splitting, which mainly arises due to the interaction between more than one neighbouring molecules per crystallographic unit cell.^{4,8} In the case of 4,5-HHP, this mode is observed ~ 1685 and 1620 cm^{-1} in both solid state IR and Raman spectra. Our calculated PEDs suggests that the mode $\sim 1685 \text{ cm}^{-1}$ is predominantly due to the C=O stretch of the carbonyl group (C2O13) present in between CH_2 atoms and the amide group with a little contribution from C1O14 stretch ($\sim 7\%$). The mode $\sim 1620 \text{ cm}^{-1}$ is for the C=O stretching vibration of the C1O14 group involved in amide formation, this mode also shows contributions from C2O13 stretch ($\sim 8\%$), C-N stretch ($\sim 9\%$) and N-H-in-plane-bending vibrations ($\sim 8\%$). The difference of

65 cm⁻¹ of the two C=O stretch can be explained by the shortening of the ring C=O bond distance of C2O13 group due to the presence of C1O14 group next to it, which is attributed to the delocalization of the lone pairs of electrons.

9.1.4. *Cis* amide II vibrations

It has been hypothesised that there appears to be a link between the location of *cis* amide II mode and the conformation of DKP ring. From our observations, it is suggested that the *cis* amide II mode (1506 cm⁻¹ for C-CySH) and ~1502 cm⁻¹ for AMDKP) for the molecules in which DKP ring deviates from planarity towards a boat conformer falls between the *cis* amide II locations of DKP ring with planar conformation (~1520 cm⁻¹ for cyclo(Gly-Gly))² and DKP ring with boat conformation (~1493 cm⁻¹ for cyclo(L-Met-L-Met)).⁹ Despite having the attachment of bulky substituents on the C_α atoms, the DKP ring does not show significant deviation from planarity and it has been observed from our DFT calculations that there is very little difference between the ω , ϕ , ψ and β angles of the calculated structure with the X-ray structure (C-CySH).¹⁰ However, in DMDKP the *cis* amide II mode is located at a much lower wavenumber (~1499 cm⁻¹) compared to cyclo(Gly-Gly).² Coupling of N-H in plane-bending vibrations with C=O stretching in the *cis* amide II mode may influence the location of this mode in the Raman spectrum and its corresponding downward shift on *N*-deuteration (~50 cm⁻¹), this shows that there is a strong coupling of N-H in-plane-bending with C=O stretching vibration. It may also be due to the resonance effect of the dimethylene side chain attached on either side of the DKP ring.

There is no band in the 1500 cm⁻¹ region for DAGG unlike that found in the parent compound i.e. cyclo(Gly-Gly).² This shows the absence of the *cis* amide II mode; thereby, confirming the absence of N-H in-plane-bending. The amide C-N stretching vibration of DAGG occurs at 1370 and 1360 cm⁻¹ (Raman and IR, respectively). There is a very large difference between the location of the C-N stretching vibration of the *cis* amide II mode of cyclo(Gly-Gly) and the amide C-N stretch of DAGG. One reason for this has been explained already, by the fact that after *N*-acetylation the amide C-N stretching vibration cannot possibly mix with N-H in-plane-bending. Additionally, it has also been stated that after *N*-acetylation there is a delocalization of the lone pairs on the nitrogen atoms towards the exo, from the endocyclic, amide linkages. For DMGG, the band located at 1535 cm⁻¹ in the Raman and 1496 cm⁻¹ in the IR can be assigned to a mode involving C-N stretching coupled to CH₂ bending. Therefore, unlike DAGG, no changes in delocalization of the lone pair of electrons on the nitrogen atoms are observed. Although in CHP and CDHP one of the hydrogen atom attached to the nitrogen of the amide group is replaced by

the CH₂ group of the L-Pro cyclic ring, no significant difference in the C-N stretching vibrations of the secondary and tertiary amide of the DKP ring have been seen. Therefore, similar to DMGG, no changes in delocalization of the lone pair of electrons on the nitrogen atoms are observed.

Interestingly, there are no bands in 1500 cm⁻¹ region for 2,3-DKP, 2,6-DKP and 4,5-HHP. The reason for decreased in wavenumbers (cm⁻¹) of C-N stretching vibrations in 2,3-DKP and 4,5-HHP can be attributed to the strong coupling of C-N vibrations with N-H in-plane-bending and CH₂ bending vibrations. Whereas, in 2,6-DKP, one reason for this has been explained already, by the delocalisation of partial double bonds on amide linkage and hence, decreasing the bond order of the C-N bonds and additionally, due to strong coupling of C-N stretching with N-H-in-plane-bending vibrations. All the above explanations were made possible from our calculated PEDs for all three molecules and in comparison to previous studies done on cyclo(Gly-Gly) (2,5-DKP).² Theoretically from PEDs and experimentally from *N*-deuteration shifts in IR and Raman spectra, it is hypothesised that the assumptions on *cis* amide II modes cannot be made from the experimental data in 2,3-DP, 2,6-DKP and 4,5-HHP molecules.

9.2. Future work

It has already been hypothesised that the effect of strong hydrogen bonding can influence the location of N-H and C=O stretching vibrations.^{2,3} From our studies it was found that the regioisomers of DKP (2,3-DKP and 2,6-DKP) are readily soluble in aqueous solution, this could be due to the weak inter-molecular hydrogen bonding between the molecules and irregular hydrogen bonding patterns due to their non-symmetric structures compared to 2,5-DKP. It would be interesting to carry out the IR and Raman studies on their *N-N'*-disubstituted regioisomers (2,3-DKP and 2,6-DKP) in the solid and solution phase. This may provide valuable information with respect to the location of C=O and C-N stretching vibrations.

It has been hypothesised that there appears to be a link between the location of *cis* amide II mode and the conformation of DKP ring and additionally, the attachment of bulky substituents on the C_α atoms on the DKP ring. Our studies on C-CySH and AMDKP served a good example for the DKPs ring with slight deviation from planarity towards a boat conformation. However, in the absence of X-ray structure, the *cis* amide II location in the Raman spectra and its corresponding *N*-deuterated shift could be very useful in determining the nature of the amide group and the conformation of the DKP ring. It would be fruitful to investigate DKP with near-planar/boat conformation with large substituents on C_α atoms.

The vibrational spectroscopic studies on larger (8 and 10 membered rings) cyclic diamides, would also prove interesting in order to draw a comparison of their conformation with DKPs. Moreover, in cyclic diamides with more than six membered ring (DKP) the amide group tends to be in a *trans* configuration due to the absence of ring/torsional strain which is generally seen in conformationally constrained six-membered rings. Hence, it would be interesting to carry out IR and Raman studies to compare and contrast *cis* and *trans* amides in cyclic diamides. Investigation on other proline-containing DKPs with aromatic side chains (Phe or Tyr) in the solid and solution phase should also be investigated as these compounds have several biological and therapeutic applications.^{11,12} These compounds are readily soluble in water due to the replacement of N-H on one *cis* amide with N-CH₂- of the proline side chain on one side of the DKP ring and therefore decrease the effect of hydrogen bonding with neighbouring molecule. Additionally, the aromatic side chains may tend to overlap over the DKP ring and cause steric hindrance which could reflect the band locations (cm⁻¹) in the IR and Raman spectra. Moreover, it would be interesting to carry out the conformational analysis, IR and Raman studies on the mesomeric substituted DKPs, with different enantiomeric substitution (L and D) on either side of the DKP ring.

Computationally, DFT calculations involving implicit solvation can be carried out by the polarizable continuum model (PCM). The effect on the DKP ring conformation under different conditions, (e.g., time (dynamics), temperature, different solvents) can be studied by molecular dynamics.^{13,14} Molecular docking studies could be useful in order to examine the interaction of molecules containing a DKP ring with specific proteins.¹⁵⁻¹⁸

9.3. References

1. Spartan'14 for Windows. Wavefunction, Inc; Irvine, CA, USA: 2013.
2. A. P. Mendham, T. J. Dines, M. J. Snowden, R. Withnall, B. Z. Chowdhry, *J. Raman Spectrosc.*, 2009, 40, 1478.
3. A. P. Mendham, R. A. Palmer, B. S. Potter, T. J. Dines, M. J. Snowden, R. Withnall, B. Z. Chowdhry, *J. Raman Spectrosc.*, 2010, 41, 288.
4. A. P. Mendham, T. J. Dines, M. J. Snowden, R. Withnall, B. Z. Chowdhry, *J. Raman Spectrosc.*, 2009, 40, 1508.
5. Y. Kojima, T. Yamashita, S. Nihide, K. Hirotsu, T. Higuchi, *Bull. Chem. Soc. Jpn.*, 1985, 58, 409.

6. (a) R. Ramani, K. Venkatesan, R. E. Marsh, *J. Am. Chem. Soc.*, 1978, 100, 949. (b) E. Benedetti, R. E. Marsh, M. Goodman, *J. Am. Chem. Soc.*, 1976, 98, 6676. (c) I. Tanaka, T. Iwata, N. Takahashi, T. Ashida, *Acta Crystallogr. Sect. B.*, 1977, 33, 3902.
7. A. T. H. Lenstra et al, *Acta Cryst.*, 1998, B54, 859.
8. A. P. Mendham, T. J. Dines, R. Withnall, J. C. Mitchell, B. Z. Chowdhry, *J. Raman Spectrosc.*, 2009, 40, 1498.
9. A. P. Mendham, B. S. Potter, R. A. Palmer, T. J. Dines, J. C. Mitchell, R. Withnall, B. Z. Chowdhry, *J. Raman Spectrosc.*, 2010, 41, 148.
10. A. P. Mendham, J. Spencer, B. Z. Chowdhry, T. J. Dines, M. Mujahid, R. A. Palmer, G. Tizzard, and S. Coles, *J. Chem. Crystallogr.*, 2011, 41, 1328.
11. E. van der Merwe, D. Huang, D. Peterson, G. Kilian, P.J. Milne, M. Van de Venter, C. Frost, *Peptides*, 2008, 29, 1305.
12. G. Kilian, H. Jamie, S. C. Brauns, K. Dyason, P. J. Milne, *Pharmazie*. 2005, 60, 305.
13. H. Urago, T. Suga, T. Hirata, H. Kodama, M. Unno, *J. Phys. Chem. B.*, 2014, 118, 6767.
14. A. Lewandowska, I. Carmichael, G. Hörner, G.L. Hug, B. Marciniak, *Chem. Phys. Lett.*, 2011, 512, 123.
15. K. T. Nguyen, E. Luethi, S. Syed, S. Urwyler, S. Bertrand, D. Bertrand, J. Reymond, *Bioorg. Med. Chem. Lett.*, 2009, 19, 3832.
16. B. Santoso, *Pharmacon.*, 2012, 13, 24.
17. R. Sharma et al, *Asian J. Biomed. Pharm. Sci.*, 2014, 4, 25.
18. N. Fania, A. Bordbara, Y. Ghayeb, S. Sepehri, *J. Biomol. Struct. Dyn.*, 2015, 33, 2285.

10. Appendix

10.1. Synthesis

10.1.1. Cyclo(L-HomoCySH-L-HomoCySH)

Preparation of isomeric diketopiperazines (DKP) of homocysteine was carried out by dissolving 1 gm of L-homocysteine thiolactone hydrochloride in 7.5 ml of water and 0.54 gm of sodium bicarbonate is added. Nitrogen was bubbled through the solution for 14 hr. The precipitated material was removed by filtration and washed with water. 0.65 gm of the mixture was extracted with 300 ml of hot absolute alcohol in three portions, after the alcoholic solution had been cooled, whetstone-like crystals of cyclo(L-homoCySH-L-homoCySH) (C-CySH) are deposited. The compound was dried in an oven at 60 °C for further analysis.

10.1.2. Degradation products of D-cycloserine

This is a two-step process; first the synthesis of 3,6-bis(aminoxymethyl)-2,5-piperazinedione (AMDKP) was carried out using 2 g of D-cycloserine dissolved in 92.5 ml of absolute ethanol in a 250 ml round bottomed flask. The mixture was stirred on a magnetic stirrer and 3.80 ml of glacial acetic acid was then added, and the suspension was refluxed for 45 min. The white flocculent was removed using vacuum filtration, washed with three 20 ml portions of cold ethanol and dried overnight (product 1, AMDKP). The solution of 0.75 g of product 1 in 148 ml of 0.008M sodium hydroxide was maintained at 25 °C for 2 hr. The product formed was 3,6-dimethylene-2,5-piperazinedione (DMDKP). The products formed were analysed using spectroscopic techniques.

10.1.3. 2,3-DKP

Solutions of 1.85 g of diethyl oxalate in 50 ml of absolute ethyl alcohol and of 0.975 g of ethylenediamine in 50 ml of the same solvent were poured slowly and simultaneously into 150 ml of absolute ethyl alcohol. After about a quarter of an hour, a gelatinous precipitate appeared but when the solution stood for about a week, long, crystalline needles were also formed, which could be mechanically separated from the amorphous product in a practically pure state. The product formed was analysed using spectroscopic techniques.

10.2. NMR Spectroscopy

The JEOL ECP 400 MHz FT NMR Spectrometer, incorporates a tuneable H(5) 400 probe. All samples were dissolved in DMSO-D₆ (C-CySH, AMDKP, DMDKP, 2,3-DKP and 4,5-HHP), CDCl₃ (DAGG and DMGG) and acetone-d₆ (2,6-DKP) and were placed into a 5mm NMR tube made of borosilicate glass. The samples dissolved in the required solvent were spun at 15 Hz. The ¹H-NMR spectra were attained using a single pulse experiment, that had a relaxation delay of 1s, the total number of spectral accumulations were done at 16 scans that had a 90° pulse with a width of 10.5 μ seconds.

The ¹³C-NMR spectra were obtained by using a standard ¹H decoupled pulse sequence, that had a relaxation delay of 1s, the total number of spectral accumulations were 2048 scans that had a 90° pulse width of 18 μ seconds.

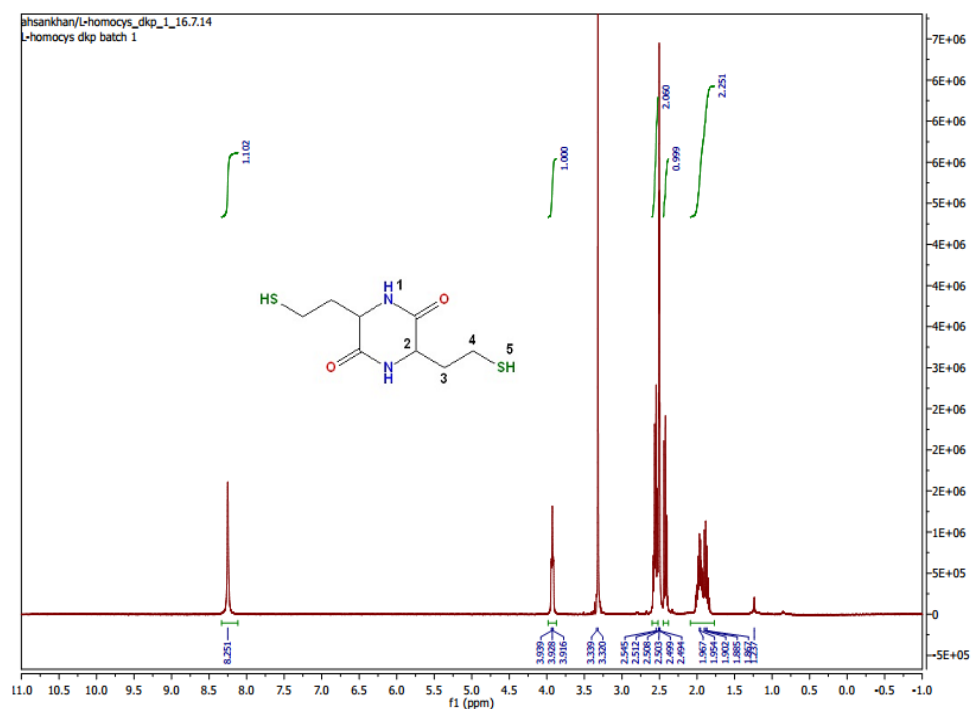


Figure 10.1. ¹H-NMR spectrum of C-CySH.

Table 10.1. ¹H- and ¹³C-NMR shifts for C-CySH.

¹ H Chemical Shift (ppm)	Splitting	Integration	Assignment	¹³ C Chemical Shift	Assignment
8.251	Singlet	1.10	H ₁	168.40	C ₁
3.928	Triplet	1.00	H ₂	53.48	C ₂
2.512	Quartet	2.06	H ₃	39.75	C ₄
2.499	Triplet	0.99	H ₅	20.33	C ₃
1.902	Multiplet	2.25	H ₄		

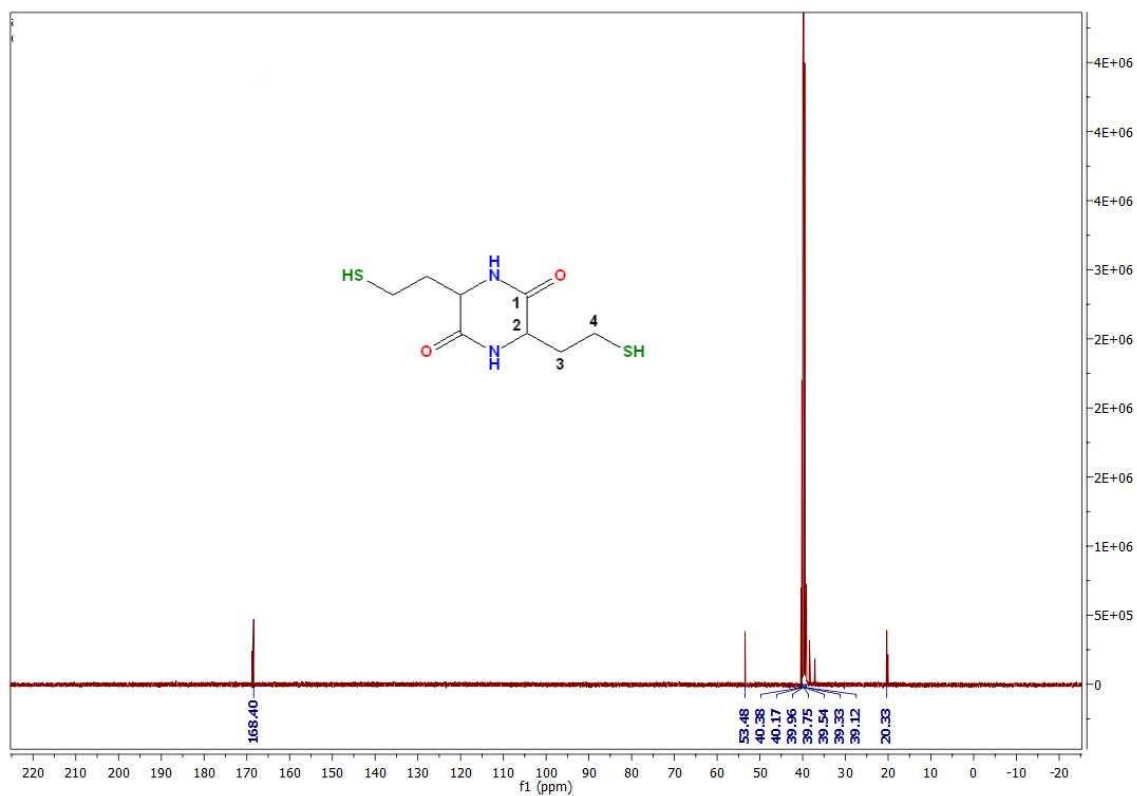


Figure 10.2. ^{13}C -NMR spectrum of C-CySH.

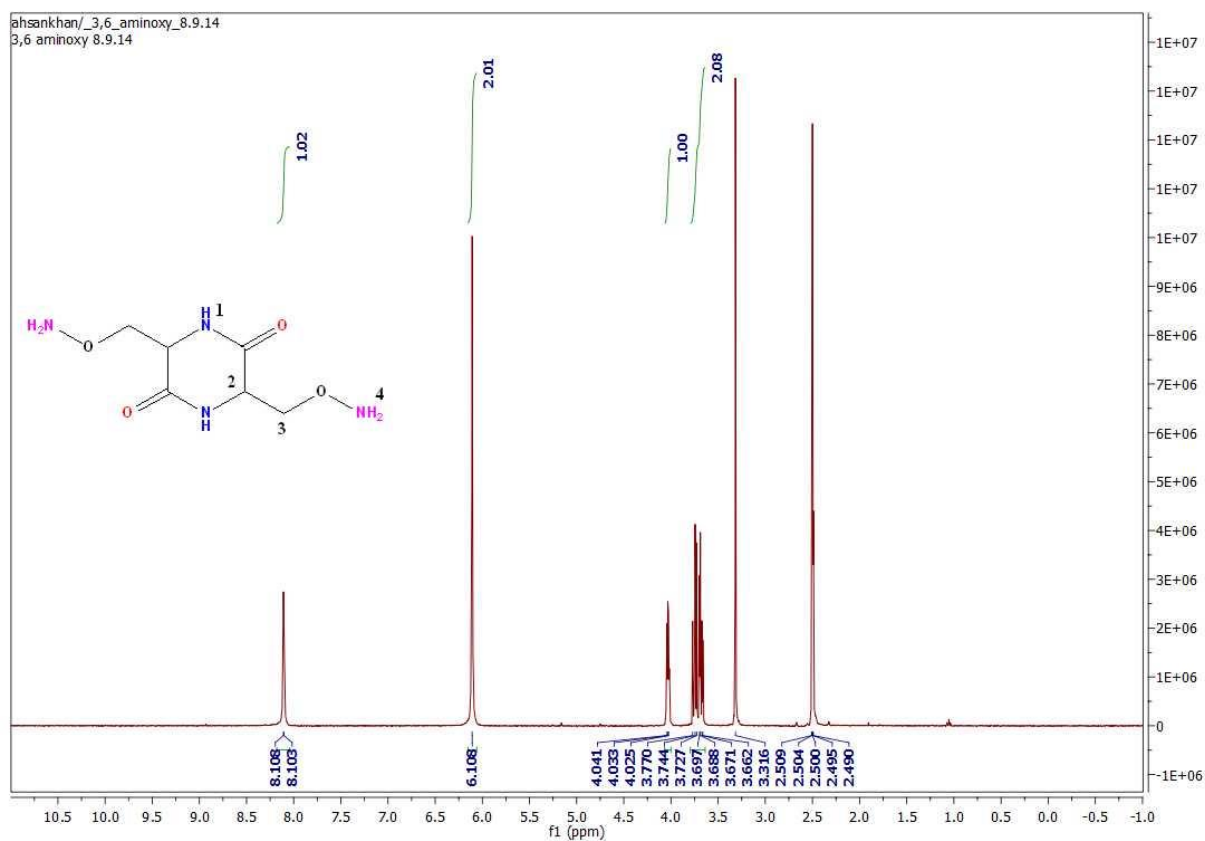


Figure 10.3. ^1H -NMR spectrum of AMDKP.

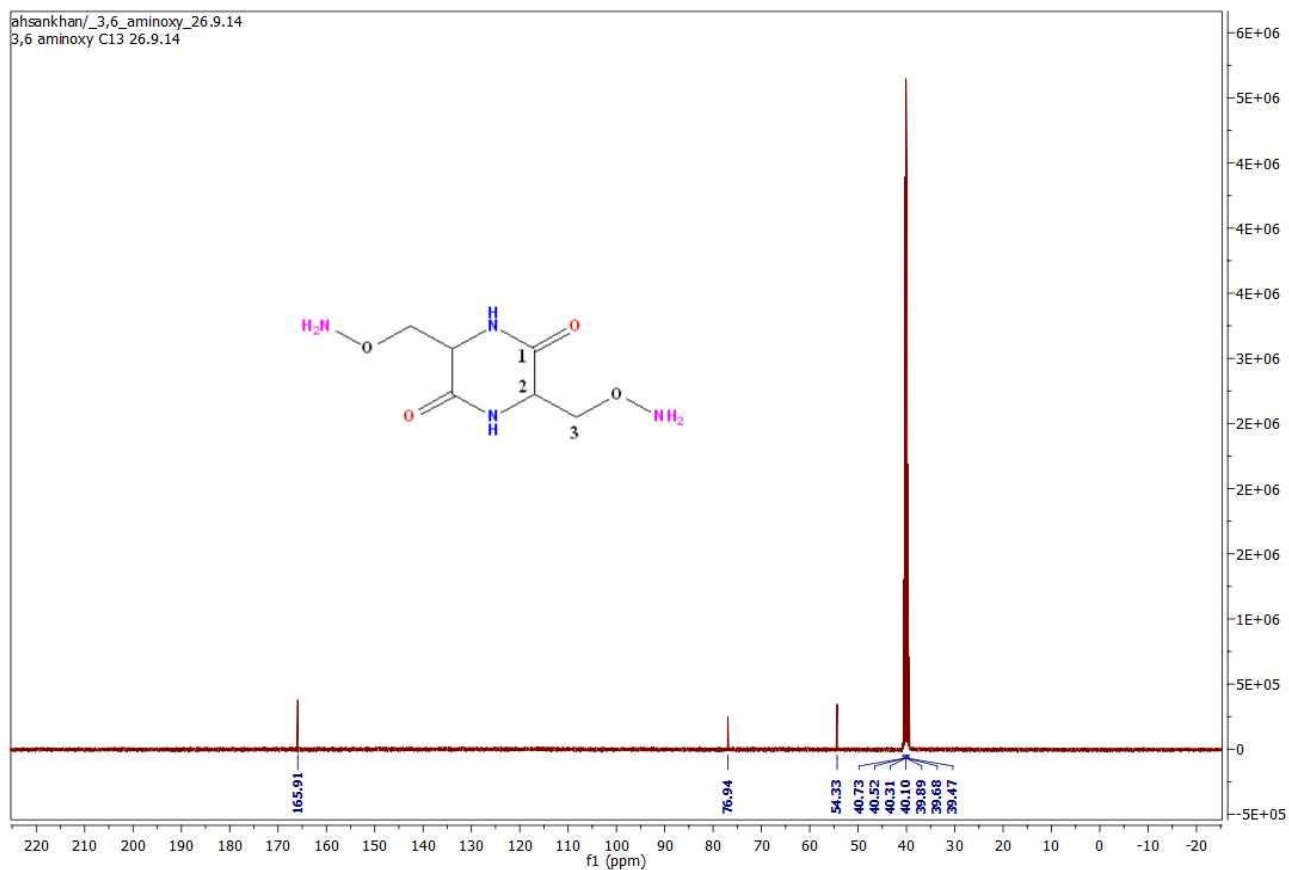


Figure 10.4. ^{13}C -NMR spectrum of AMDKP.

Table 10.2. ^1H - and ^{13}C -NMR shifts of AMDKP.

^1H Chemical Shift (ppm)	Splitting	Integration	Assignment	^{13}C Chemical Shift	Assignment
10.87	Singlet	0.67	H ₁	158.01	C ₁
5.25	Singlet	1.00	H ₂	133.66	C ₂
4.91	Singlet	1.00	H ₃	104.02	C ₃

Table 10.3. ^1H - and ^{13}C -NMR shifts of DMDKP.

^1H Chemical Shift (ppm)	Splitting	Integration	Assignment	^{13}C Chemical Shift	Assignment
8.103	Doublet	1.02	H ₁	165.91	C ₁
6.108	Singlet	2.01	H ₄	76.94	C ₂
4.033	Quintet	1.00	H ₂	54.33	C ₃
3.720	Multiplet	2.08	H ₃		

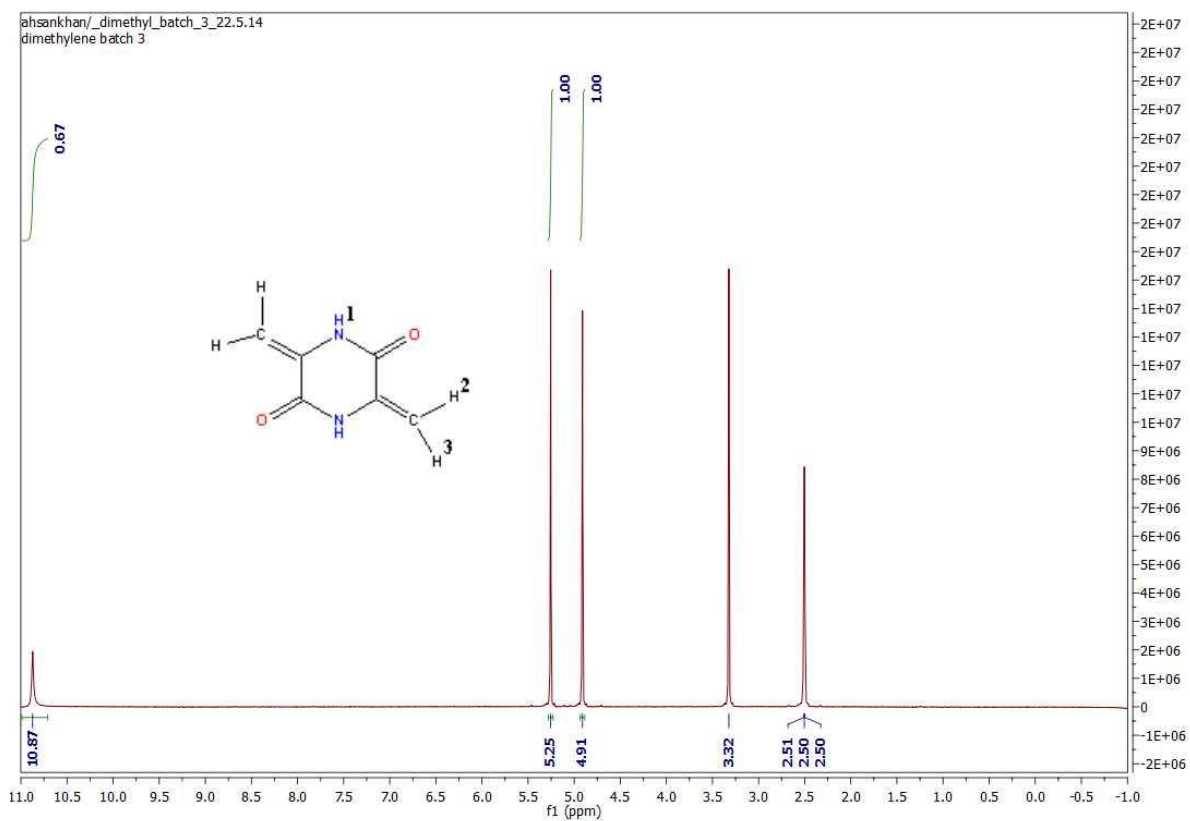


Figure 10.5. The ^1H -NMR spectrum of DMDKP.

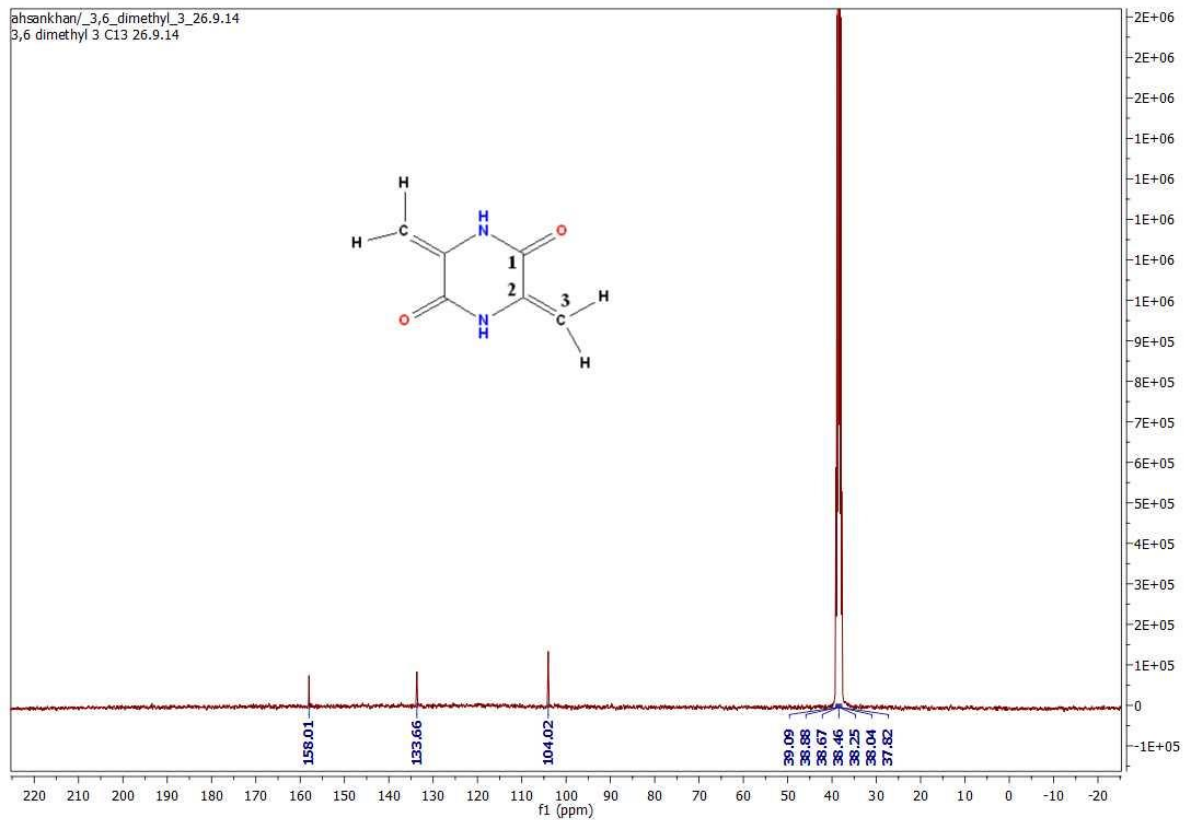


Figure 10.6. ^{13}C -NMR spectrum of DMDKP.

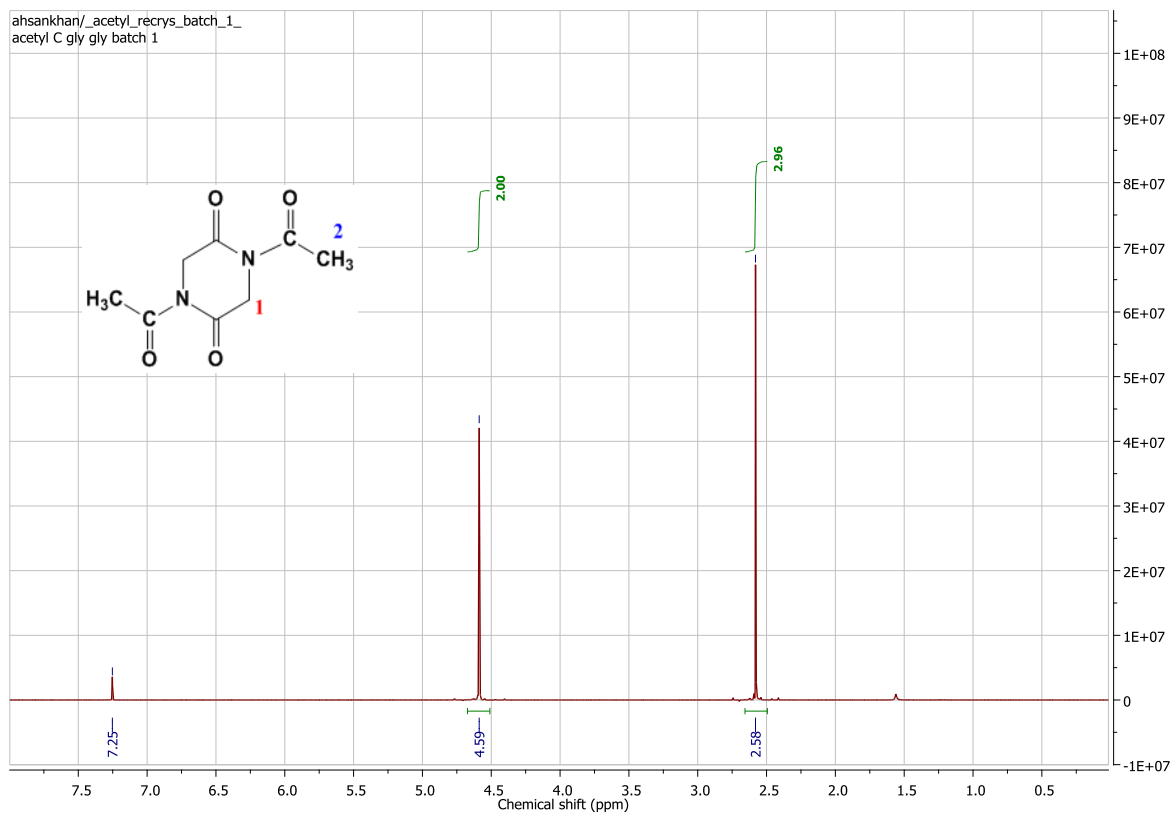


Figure 10.7. ^1H -NMR spectrum of DAGG.

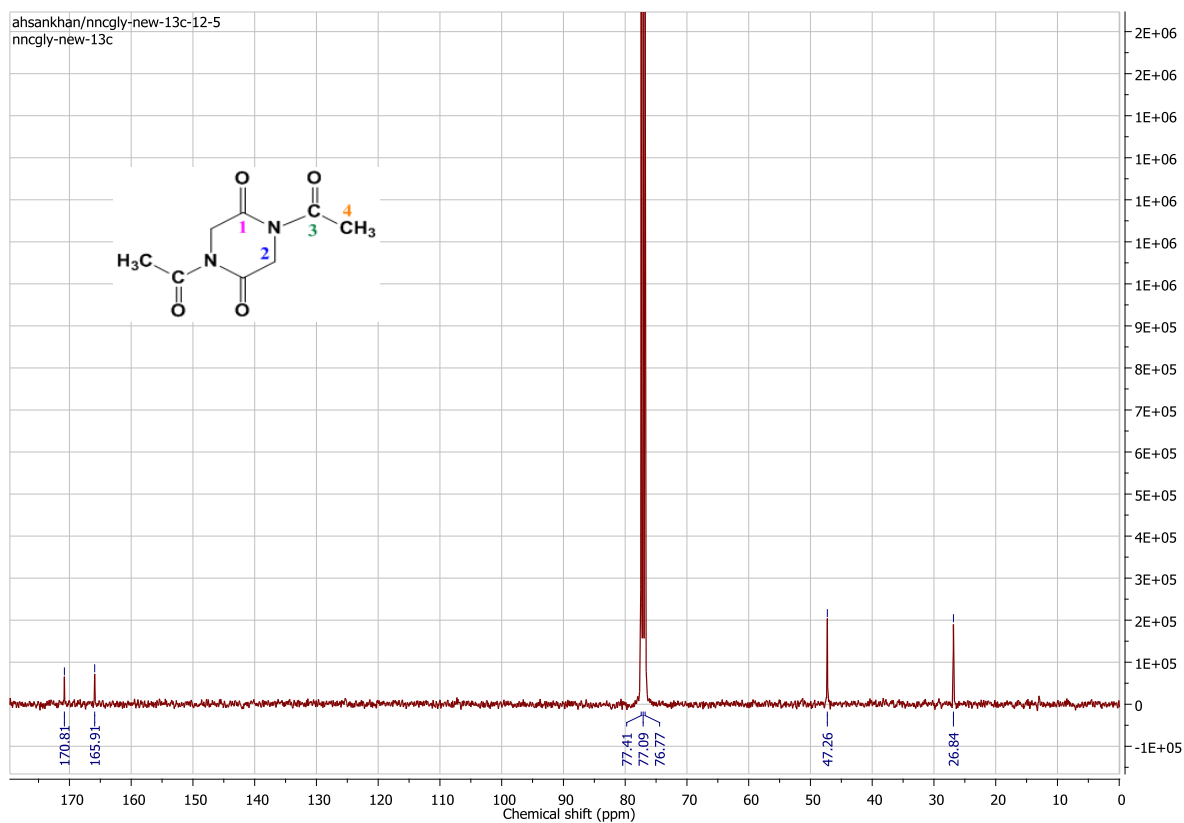


Figure 10.8. ^{13}C -NMR spectrum of DAGG.

Table 10.4. ^1H - and ^{13}C -NMR shifts for DAGG

^1H Chemical Shift (ppm)	Splitting	Integration	Assignment	^{13}C Chemical Shift	Assignment
4.59	Singlet	2.00	H ₁	170.81	C ₃
2.58	Singlet	2.96	H ₂	165.91	C ₁
				47.26	C ₂
				26.84	C ₄

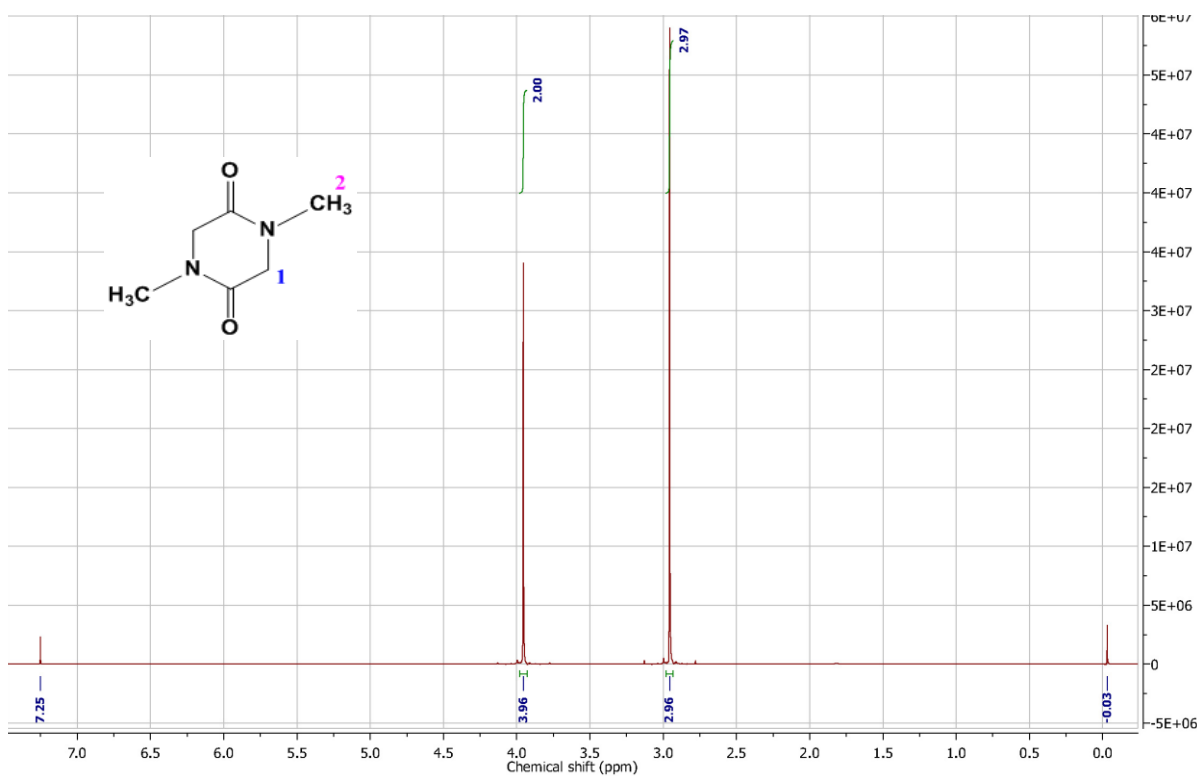


Figure 10.9. ^1H -NMR spectrum of DMGG.

Table 10.5. ^1H - and ^{13}C -NMR shifts for DMGG.

^1H Chemical Shift (ppm)	Splitting	Integration	Assignment	^{13}C Chemical Shift	Assignment
3.96	Singlet	2.00	H ₁	163.16	C ₁
2.96	Singlet	2.97	H ₂	51.73	C ₂
				33.32	C ₃

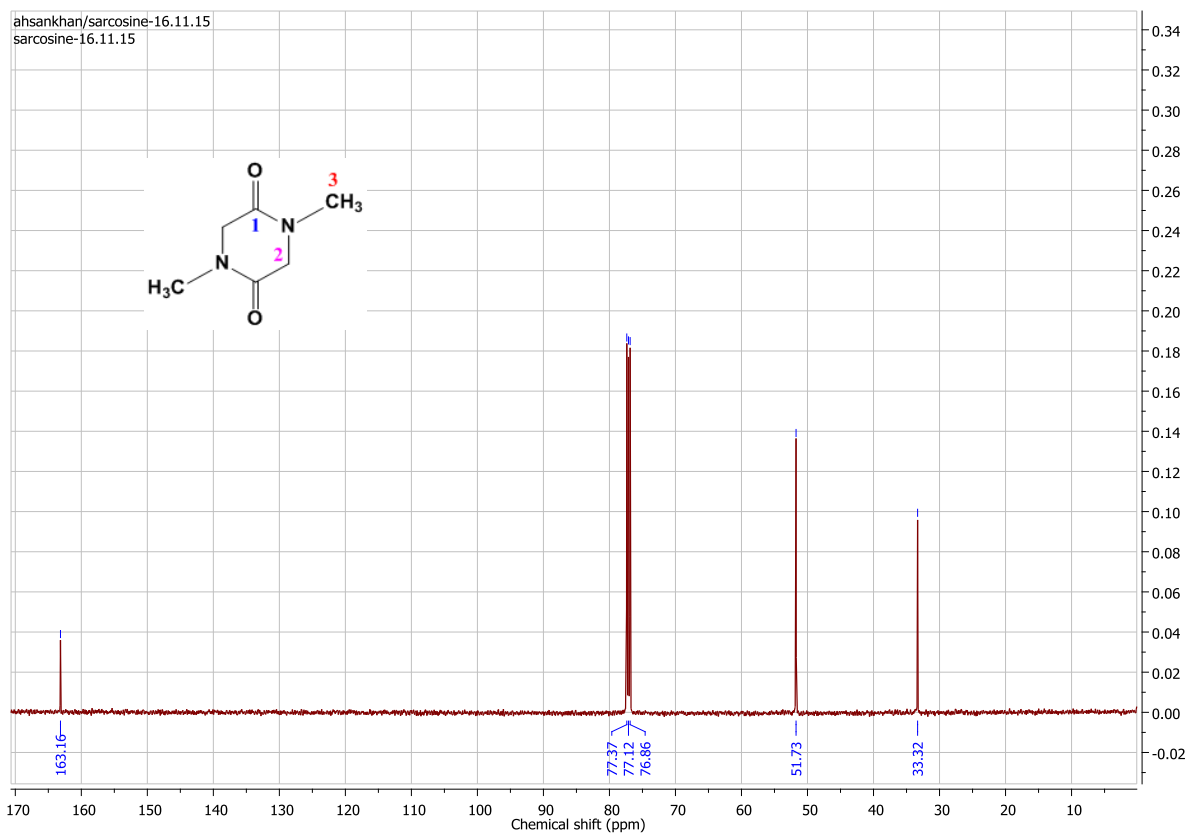


Figure 10.10. ¹³C-NMR spectrum of DMGG.

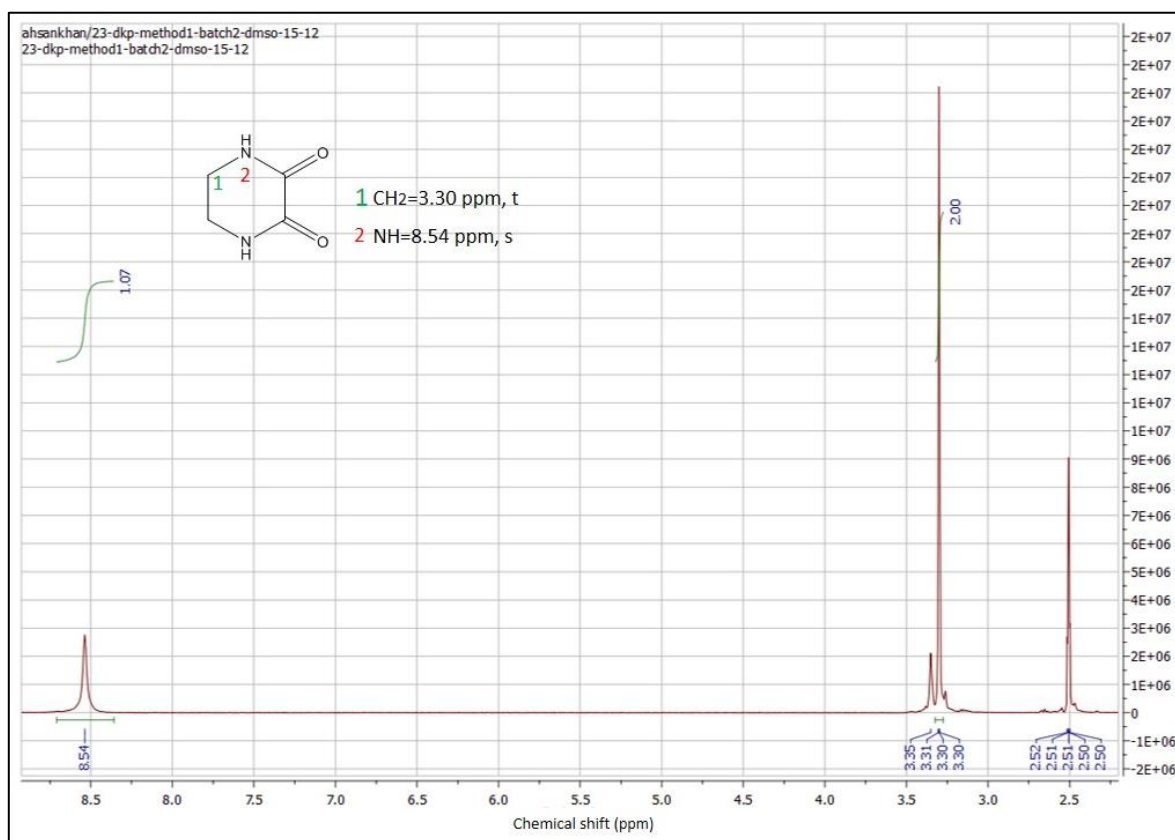


Figure 10.11. ¹H-NMR spectrum of 2,3-DKP.

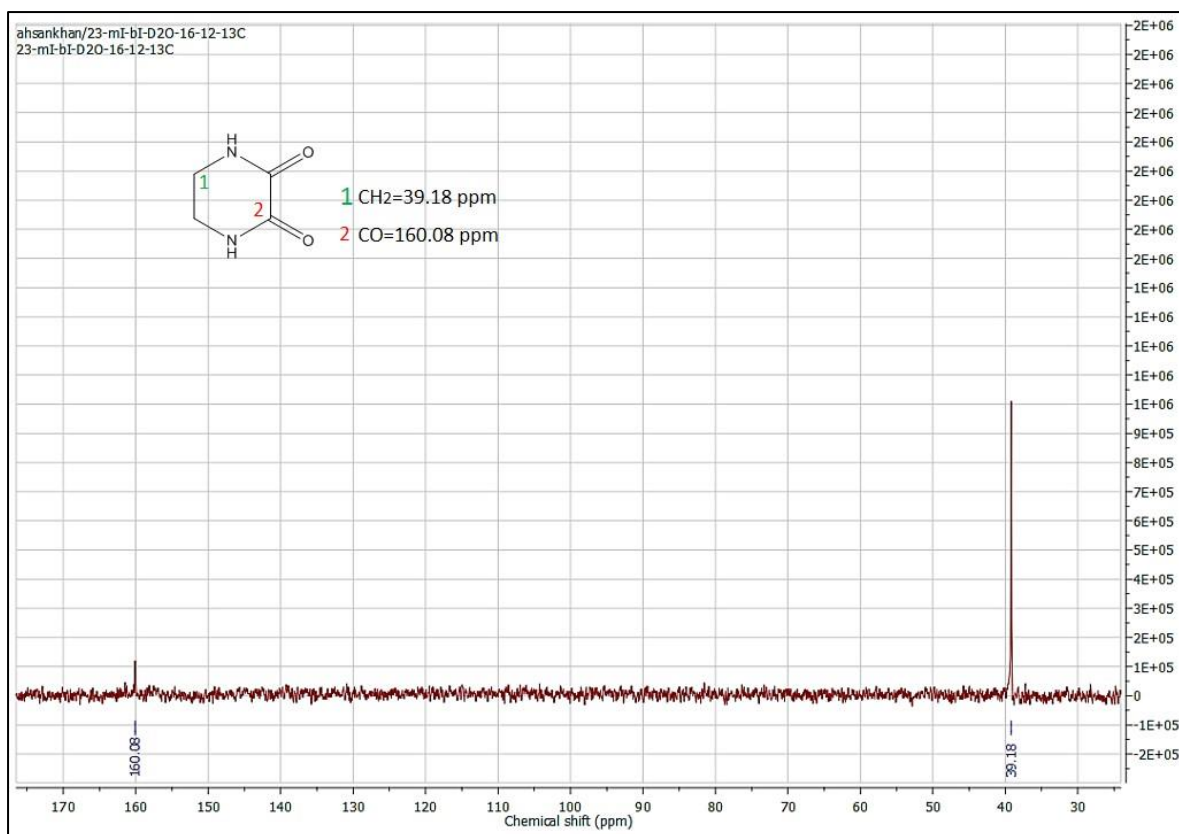


Figure 10.12. ¹³C-NMR spectrum of 2,3-DKP.

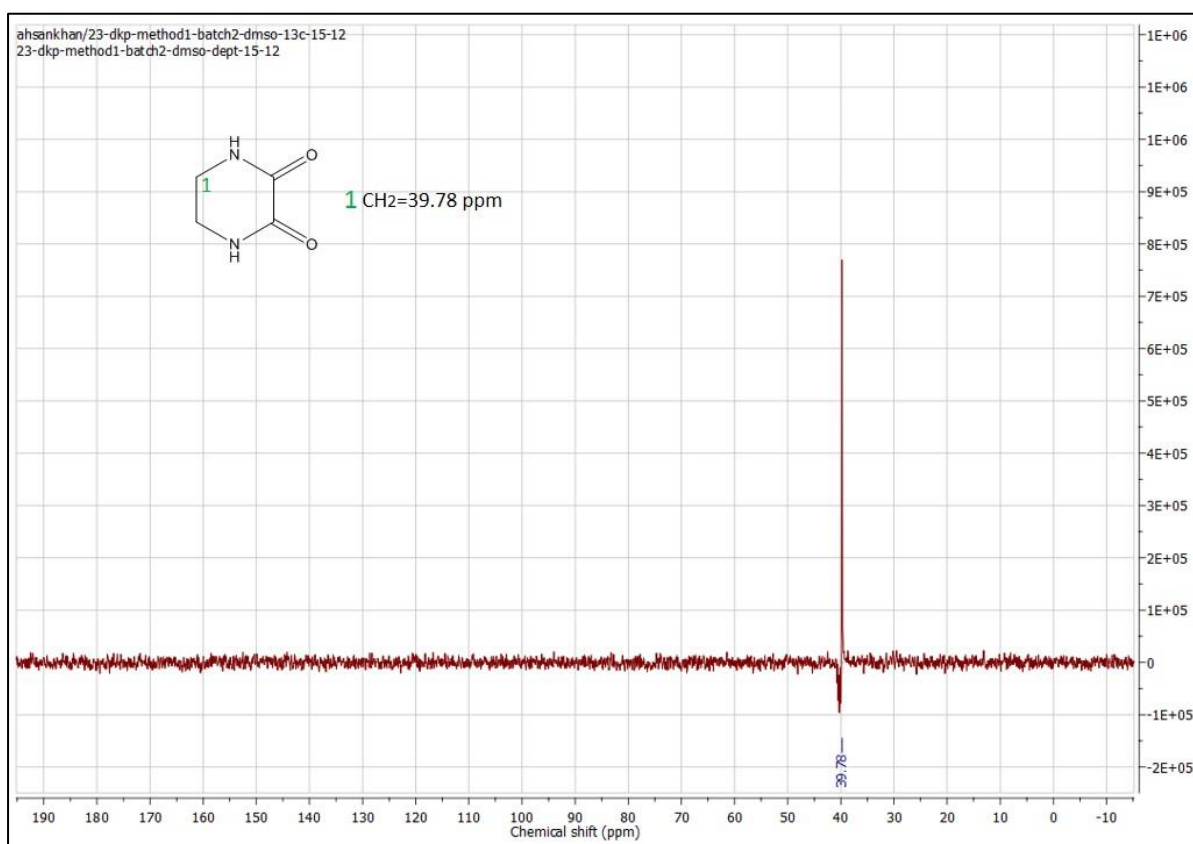


Figure 10.13. DEPT-135 spectrum of 2,3-DKP.

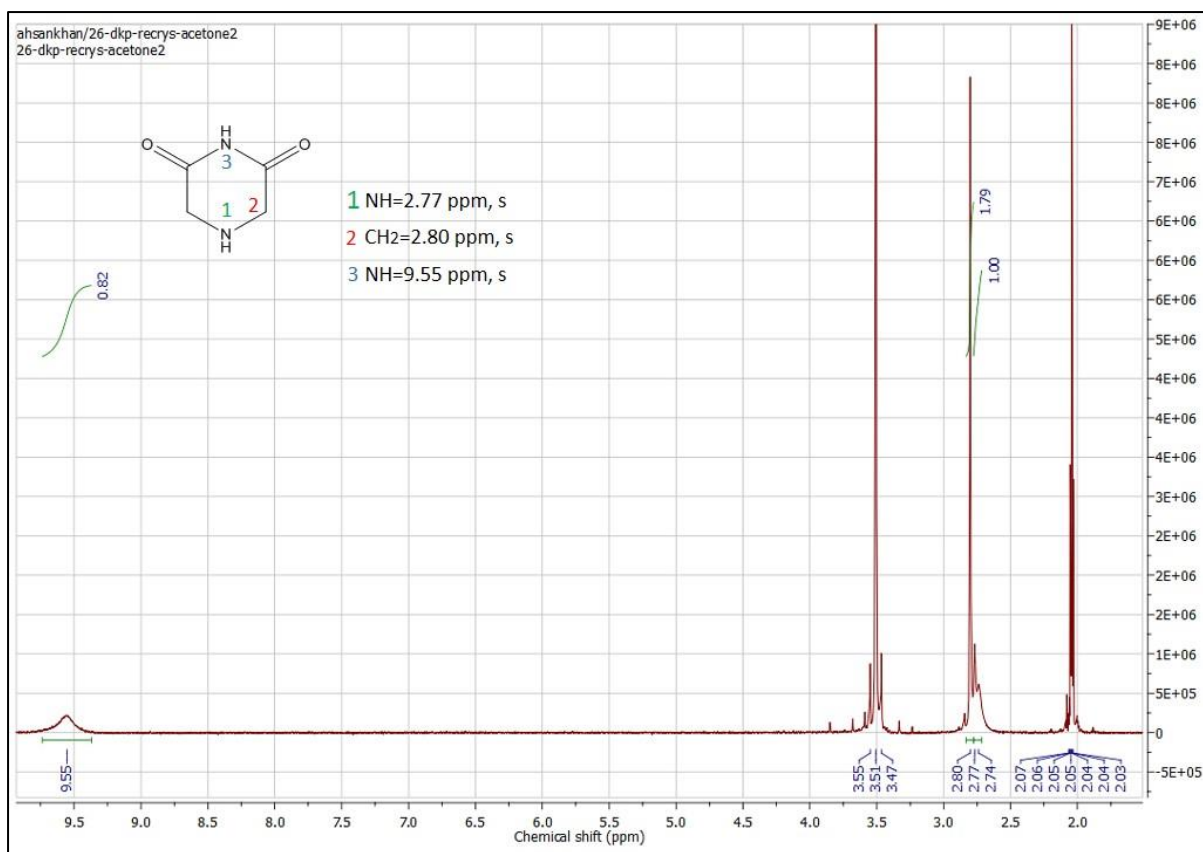


Figure 10.14. ¹H-NMR spectrum of 2,6-DKP.

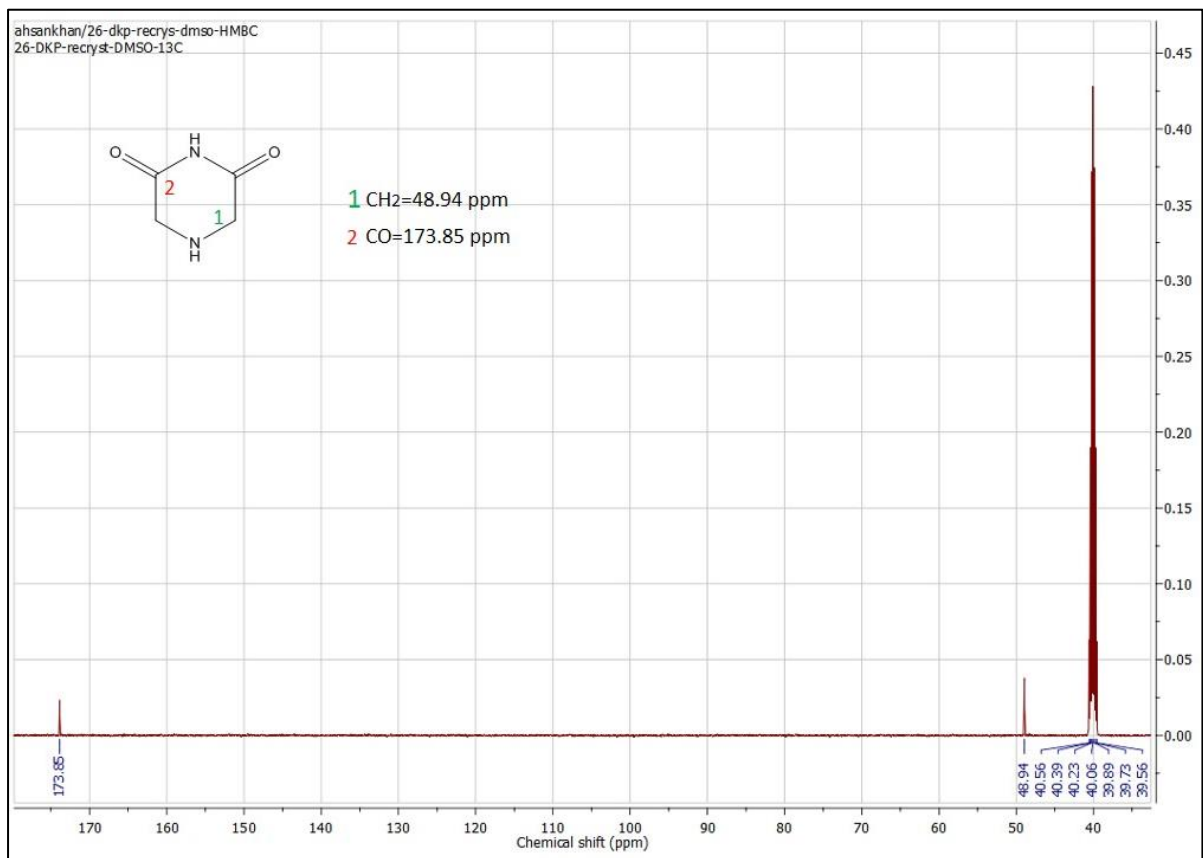


Figure 10.15. ¹³C-NMR spectrum of 2,6-DKP.

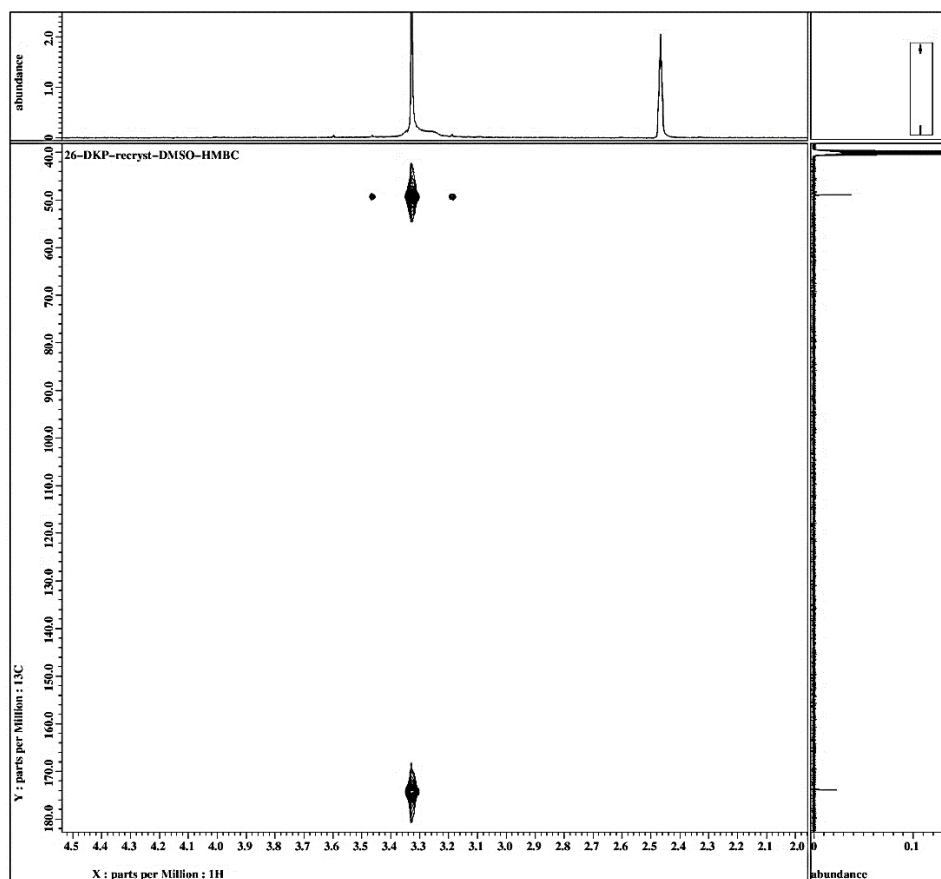


Figure 10.16. HMBC spectrum of 2,6-DKP.

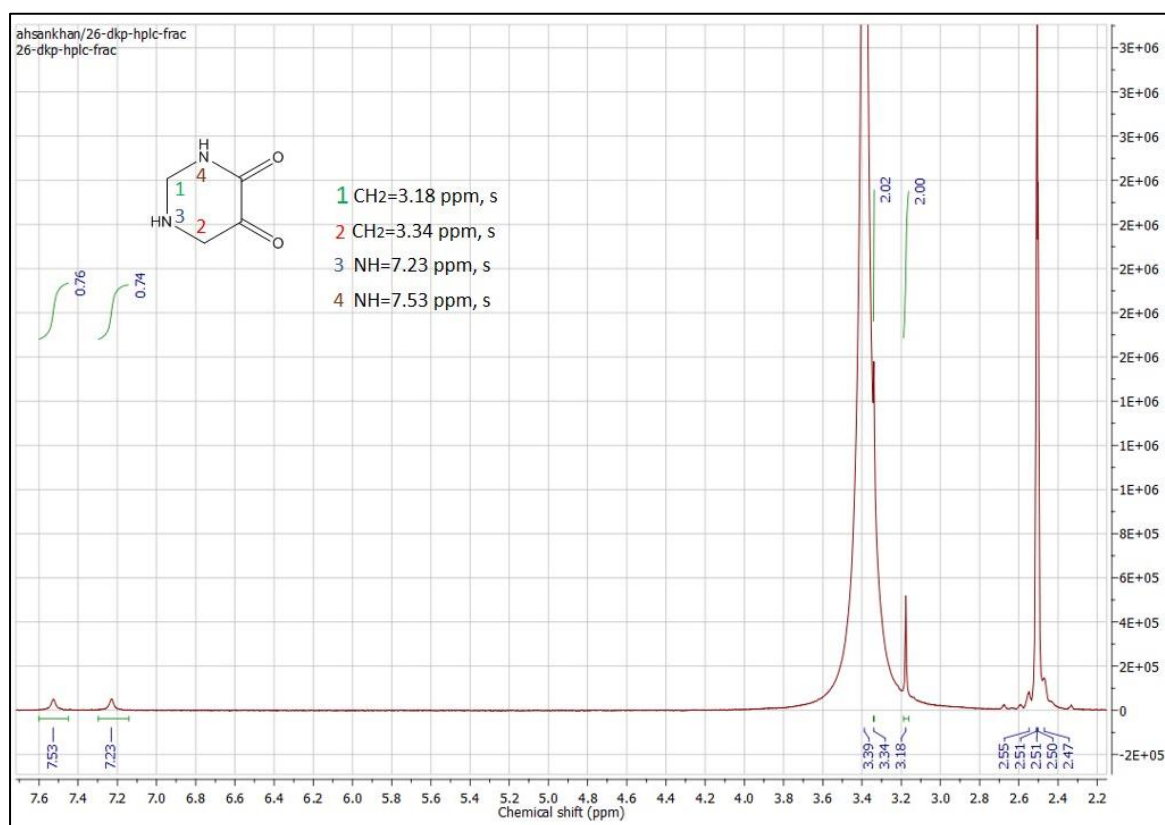


Figure 10.17. ¹H-NMR spectrum of 4,5-HHP.

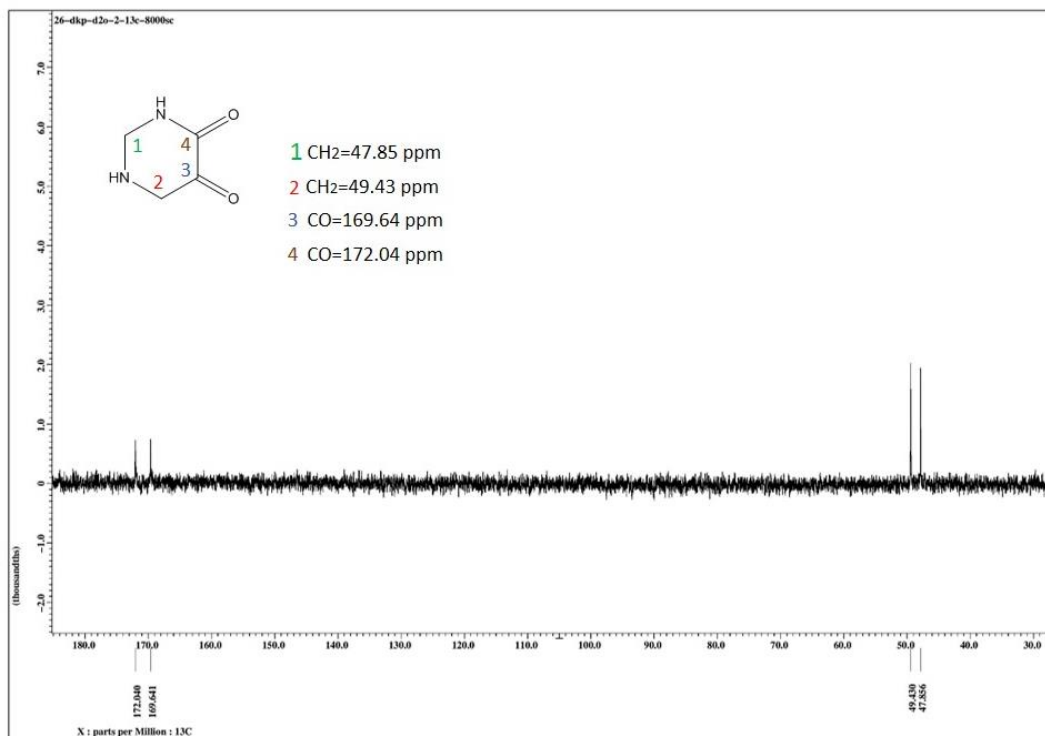


Figure 10.18. ¹³C-NMR spectrum of 4,5-HHP.

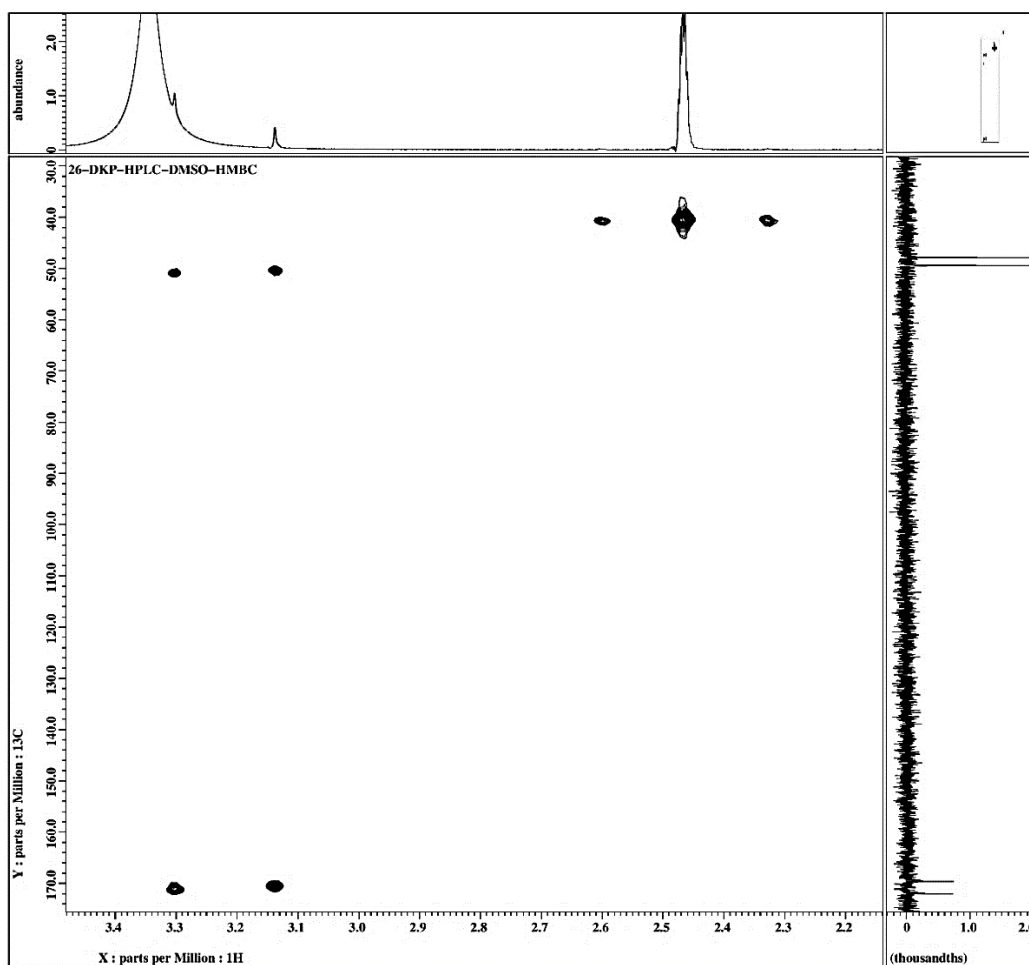


Figure 10.19. HMBC spectrum of 4,5-HHP.

10.3. Mass spectrometry (LC-MS)

Mass spectrometer conditions

A Waters Synapt G2 TOF mass spectrometer (Waters, UK) with an electrospray ionisation probe in electrospray positive and negative mode was used to acquire data over a mass range of 50-800 m.u. A lock spray correction was applied to each acquired data set using the peptide Leu-Enk.

Inlet conditions

An Acquity UPLC system was coupled to an Acquity UPLC BEH C₁₈ 1.7 μ m 2.1 x 50 mm column and UV detection at 220 nm using a Waters TUV detector.

Processing

Processing was carried out using MassLynx 4.1 constraining the possible elements to show the PPM error for the proposed molecular formula.

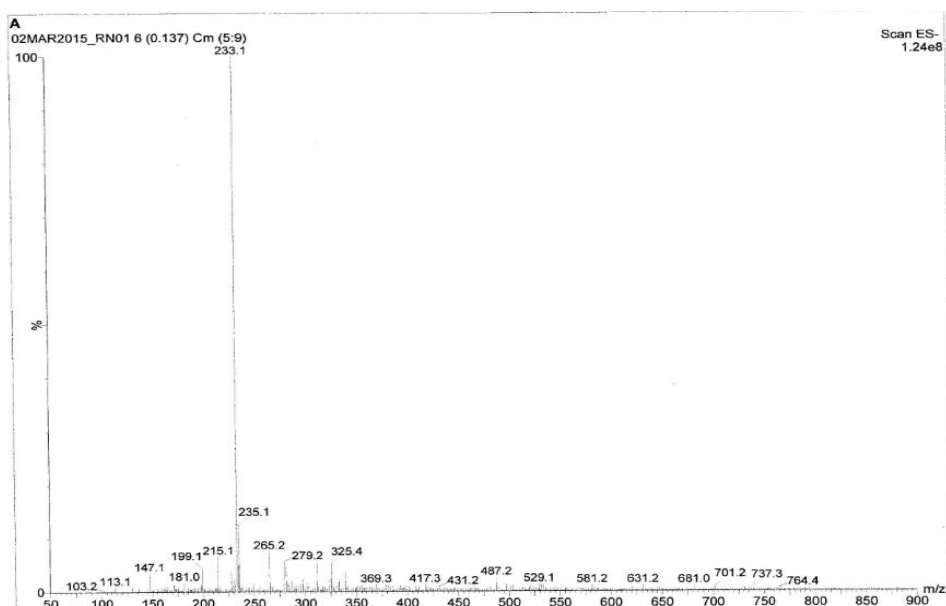
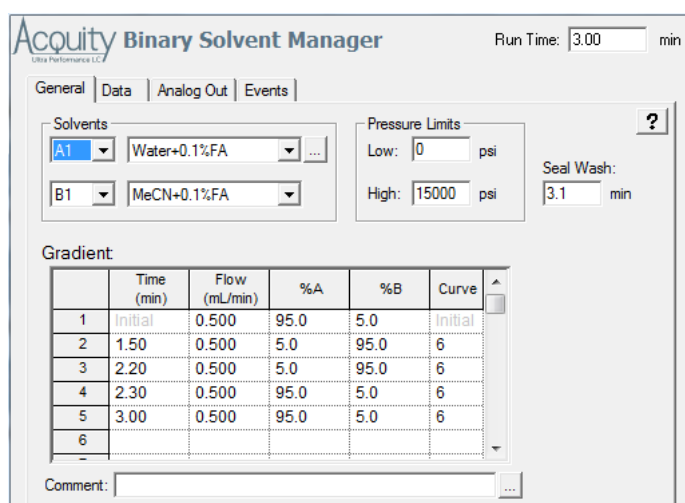


Figure 10.20. The mass spectrum (ES-) of C-CySH.

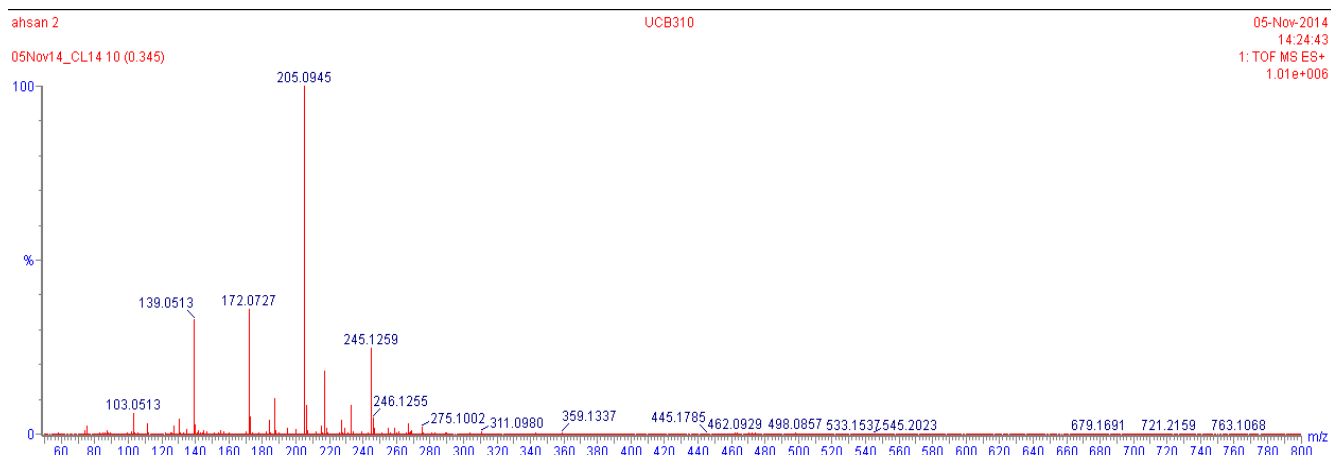


Figure 10.21. MS ES+ spectrum of AMDKP.

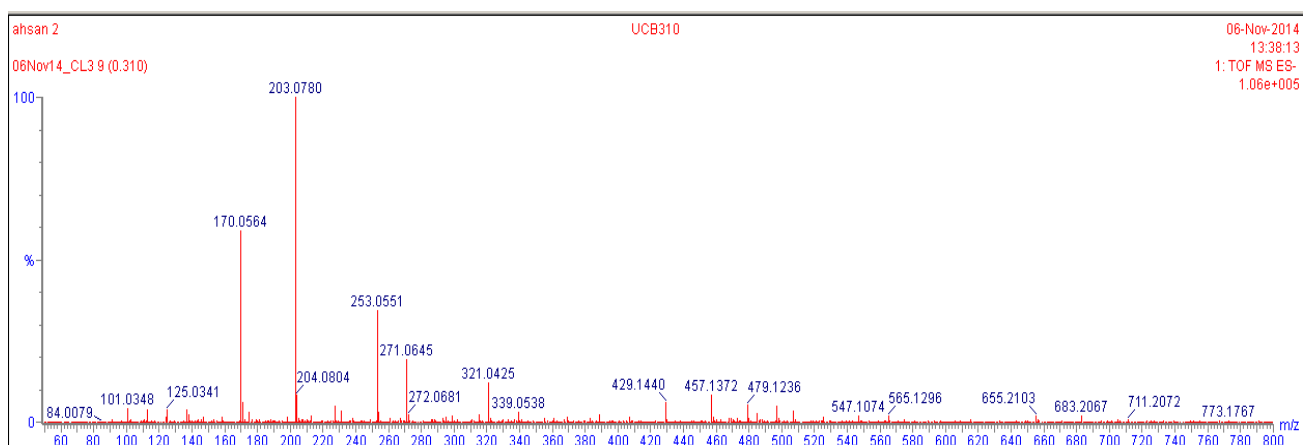


Figure 10.22. MS ES- spectrum of AMDKP.

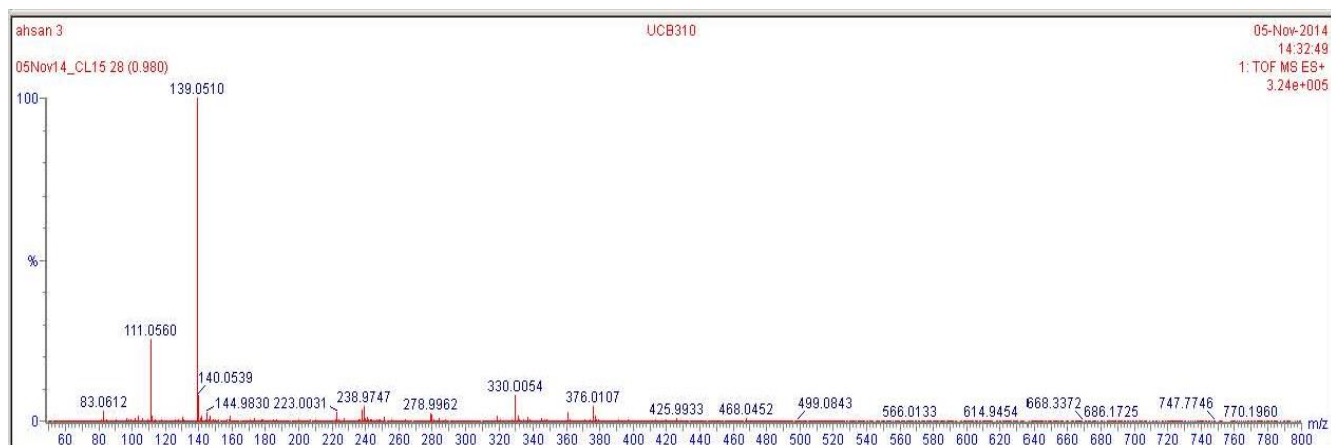


Figure 10.23. MS ES+ spectrum of DMDKP.

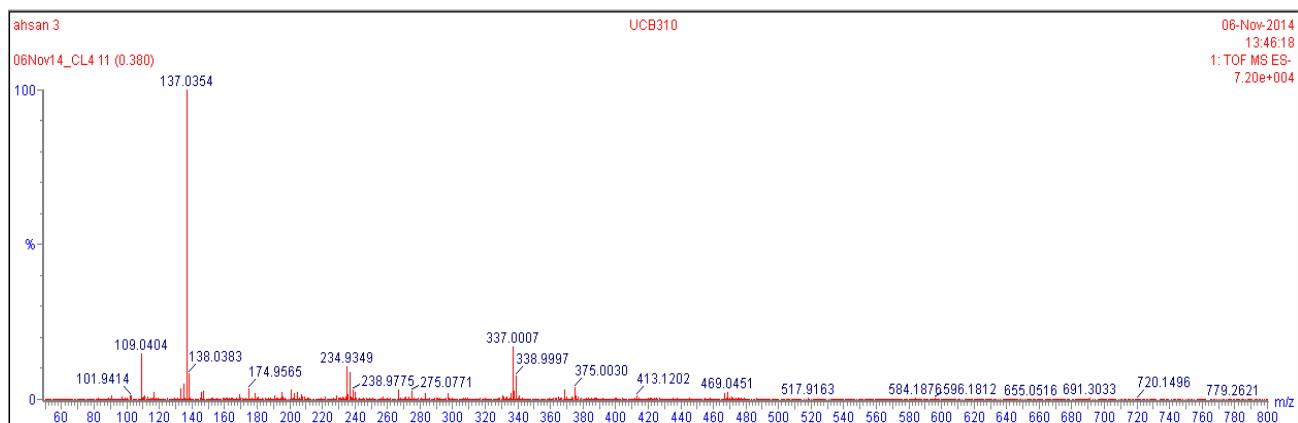


Figure 10.24. MS ES- spectrum of DMDKP.

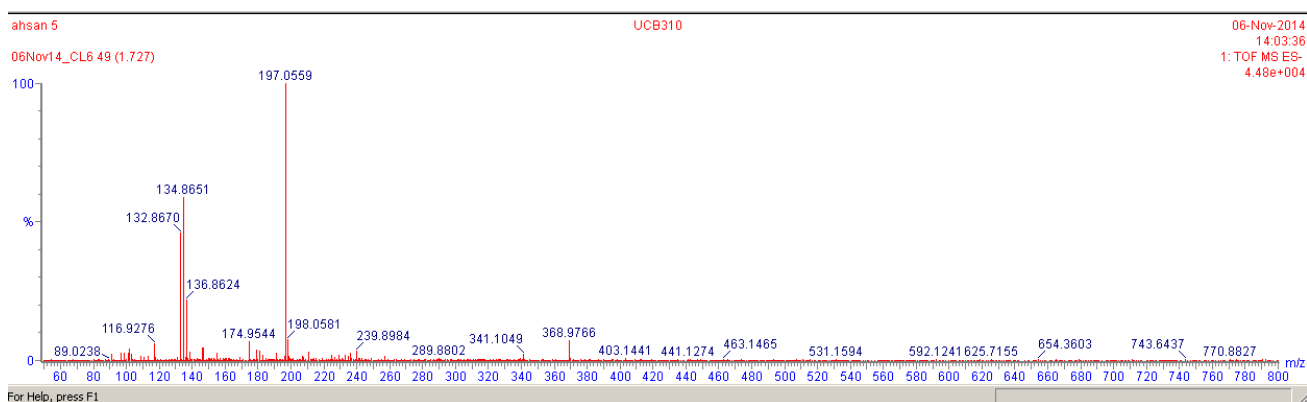


Figure 10.25. MS ES- spectrum of DAGG.

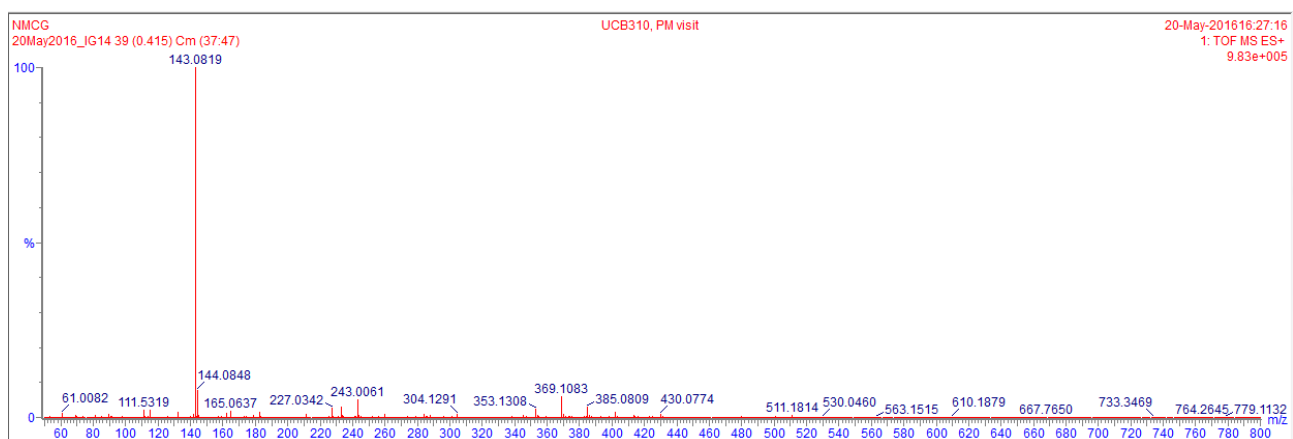
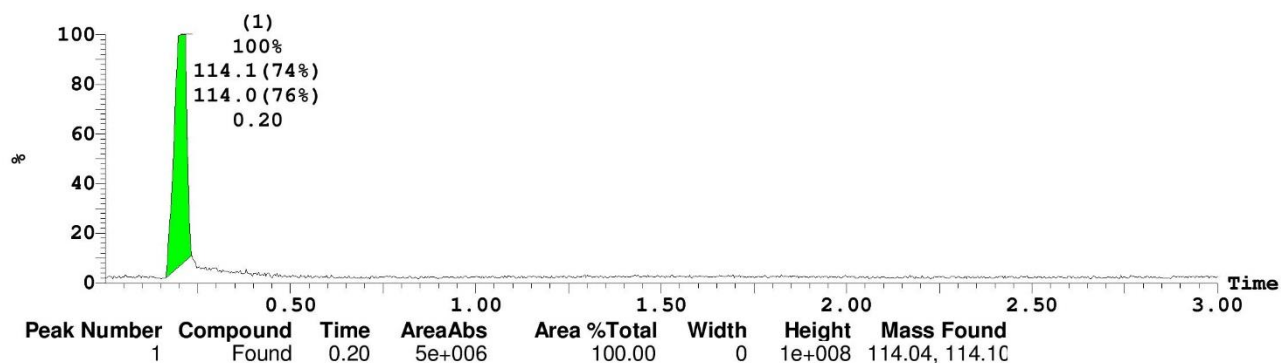
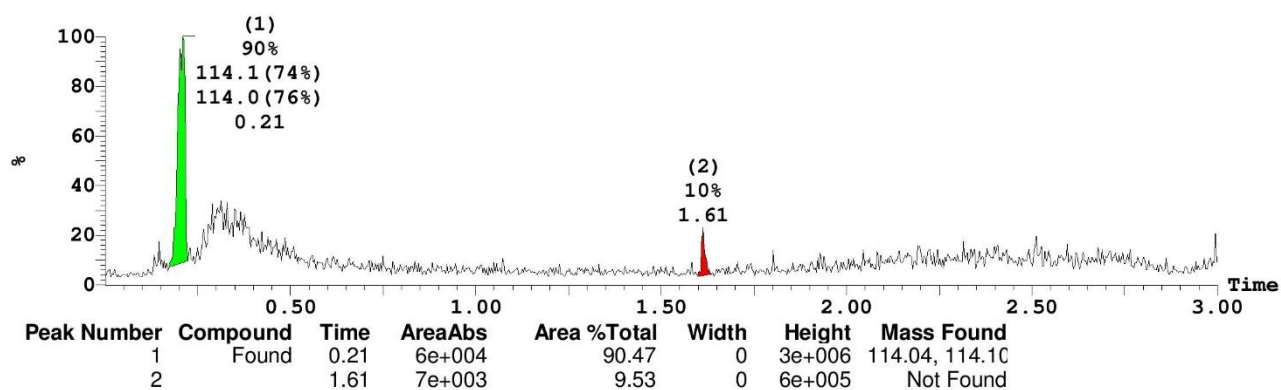


Figure 10.26. MS ES+ spectrum of DMGG.

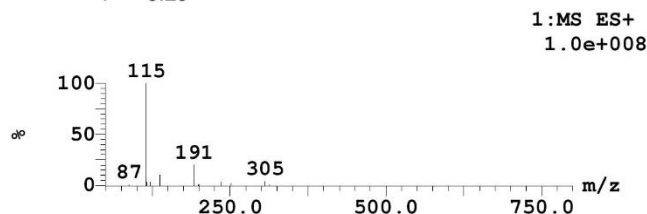
1: MS ES+ :BPI 1.3e+008



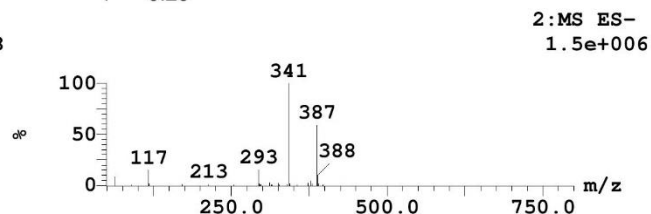
2: MS ES- :BPI 3.0e+006



Peak ID Time
1 0.20



Peak ID Time
1 0.20



Peak ID Time
2 1.61

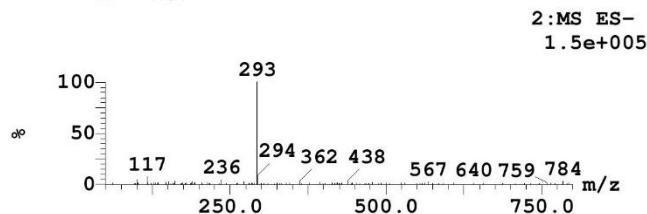
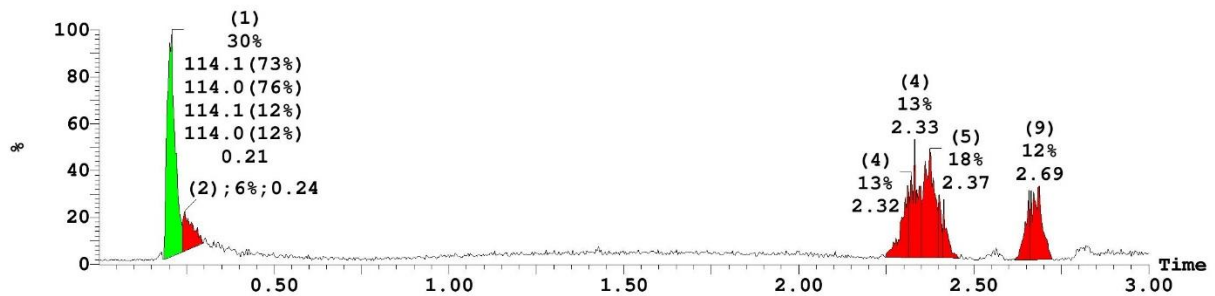


Figure 10.27. The chromatogram and Mass spectrum of 2,3-DKP.

The mass spectrum of 2,3-DKP (molecular weight 114.10 g/mol). Both ES+ and ES- ionization was applied to the compound and the base peak was detected at 115 (m/z) in ES+ which is the molecular weight of 2,3-DKP (+1).

1: MS ES+ :BPI

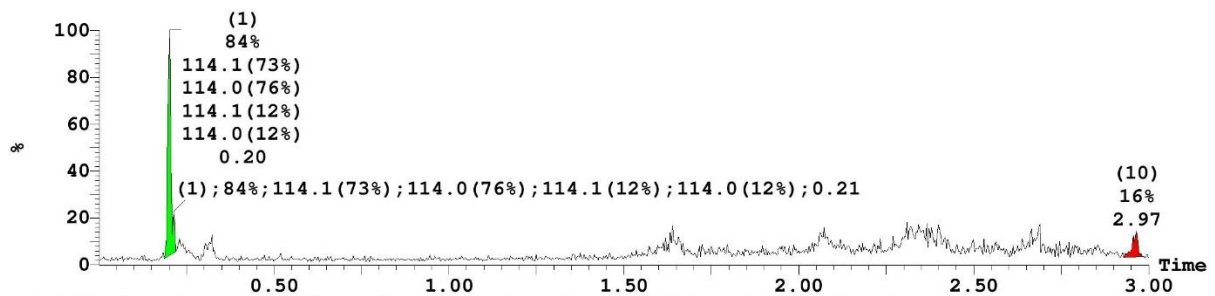
6.4e+007



Peak Number	Compound	Time	AreaAbs	Area %Total	Width	Height	Mass Found
1	Found	0.21	2e+006	30.12	0	6e+007	114.04, 114.10
2		0.24	3e+005	6.13	0	1e+007	Not Found
3		2.31	5e+005	8.54	0	2e+007	Not Found
4		2.33	7e+005	12.87	0	3e+007	Not Found
5		2.37	1e+006	18.10	0	3e+007	Not Found
6		2.40	2e+005	3.20	0	2e+007	Not Found
7		2.41	2e+005	3.79	0	2e+007	Not Found
8		2.66	3e+005	5.02	0	2e+007	Not Found
9		2.69	7e+005	12.24	0	2e+007	Not Found

2: MS ES- :BPI

4.6e+006



Peak Number	Compound	Time	AreaAbs	Area %Total	Width	Height	Mass Found
1	Found	0.20	5e+004	84.25	0	4e+006	114.04, 114.10
10		2.97	9e+003	15.75	0	5e+005	Not Found

Peak ID Time
1 0.21

Peak ID Time
1 0.21

1:MS ES+
2.9e+007

2:MS ES-
1.5e+006

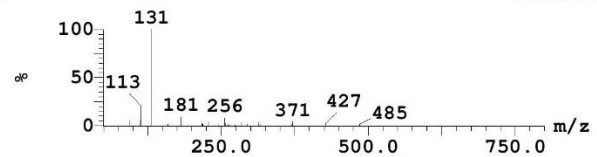
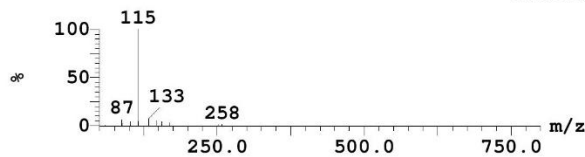
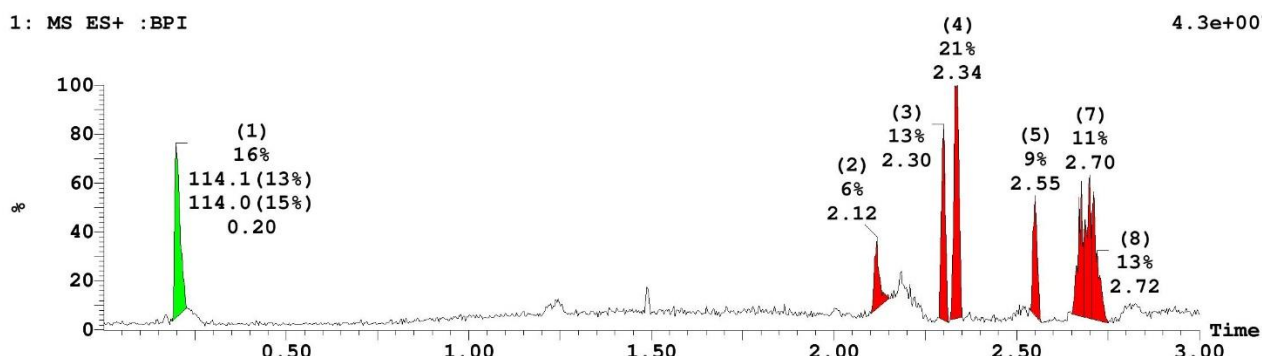


Figure 10.28. The chromatogram and Mass spectrum of 2,6-DKP.

The mass spectrum of 2,6-DKP (molecular weight 114.10 g/mol). Both ES+ and ES- ionization was applied to the compound and the base peak was detected at 115 (m/z) in ES+ and 113 (m/z) in ES- which is the molecular weight of 2,3-DKP (+1 and -1). m/z of 133 in ES+ and 131 in ES- are due to compound + water adduct.

1: MS ES+ :BPI

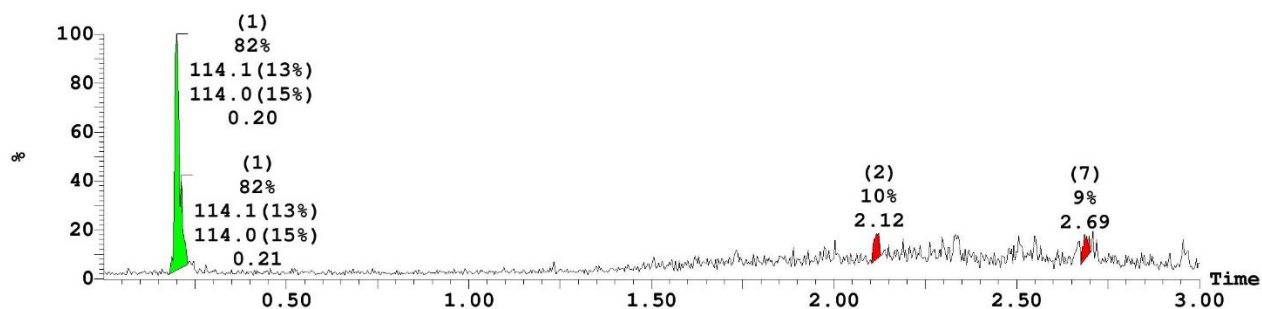
4.3e+007



Peak Number	Compound	Time	AreaAbs	Area %Total	Width	Height	Mass Found
1	Tentative	0.20	5e+005	16.01	0	3e+007	114.04, 114.10
2		2.12	2e+005	6.14	0	1e+007	Not Found
3		2.30	4e+005	13.43	0	3e+007	Not Found
4		2.34	7e+005	21.05	0	4e+007	Not Found
5		2.55	3e+005	8.75	0	2e+007	Not Found
6		2.68	3e+005	10.67	0	2e+007	Not Found
7		2.70	4e+005	11.24	0	3e+007	Not Found
8		2.71	4e+005	12.71	0	2e+007	Not Found

2: MS ES- :BPI

4.0e+006

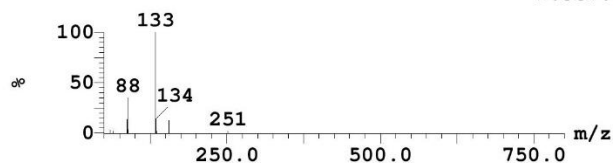


Peak Number	Compound	Time	AreaAbs	Area %Total	Width	Height	Mass Found
1	Tentative	0.20	6e+004	81.81	0	4e+006	114.04, 114.10
2		2.12	8e+003	9.55	0	4e+005	Not Found
7		2.69	7e+003	8.64	0	4e+005	Not Found

Peak ID Time

1 0.20

1:MS ES+
1.3e+007



Peak ID Time

1 0.20

2:MS ES-
1.7e+006

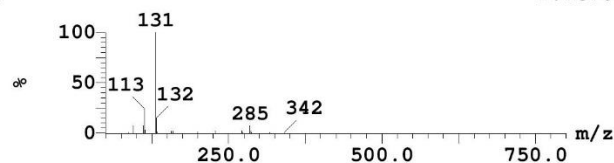


Figure 10.29. The chromatogram and Mass spectrum of 4,5-HHP.

The mass spectrum of 2,6-DKP (molecular weight 114.10 g/mol). Both ES+ and ES- ionization was applied to the compound and the base peak was detected at 113 (m/z) in ES- which is the molecular weight of 2,3-DKP (-1). m/z of 133 in ES+ and 131 in ES- are due to compound + water adduct.

10.4. Elemental Analysis

Thermo electron co-operation – Flash EA 1112 series, CHNS analyser supplied by CE Instruments Ltd.

Cystine (for C-CySH) and acetanilide (for AMDKP, DMDKP, DAGG, 2,3-DKP, 2,6-DKP and 4,5-HHP) were used as reference compounds. Oven temperature was set to 900 °C.

Parameters	Gas flow and system timings
Carrier	130 ml/min
Oxygen	250 ml/min
Reference	100 ml/min
System timings	720 sec cycle
Sampling decay	12 sec
Oxygen injection	5 sec

C-CySH

Anal. Calculated for C₈H₁₄N₂O₂S₂: **C**, 41.00; **H**, 6.02; **N**, 11.95; **S**, 27.37
Found: **C**, 40.45; **H**, 6.08; **N**, 11.72; **S**, 27.02

AMDKP

Anal. Calculated for C₆H₁₂N₄O₄: **C**, 35.28; **H**, 5.93; **N**, 27.44;
Found: **C**, 35.24; **H**, 5.92; **N**, 27.32

DMDKP

Anal. Calculated for C₆H₆N₂O₂: **C**, 52.16; **H**, 4.38; **N**, 20.28;
Found: **C**, 51.94; **H**, 4.39; **N**, 20.17

DAGG

Anal. Calculated for C₈H₁₀N₂O₄: **C**, 48.48; **H**, 5.09; **N**, 14.13;
Found: **C**, 48.18; **H**, 5.05; **N**, 13.98.

2,3-DKP, 2,6-DKP and 4,5-HHP

Anal. Calculated for C₄H₆N₂O₂: **C**, 42.11; **H**, 5.30; **N**, 24.55;
2,3-DKP - Found: **C**, 41.92; **H**, 5.26; **N**, 24.22.
2,6-DKP - Found: **C**, 41.81; **H**, 5.53; **N**, 24.08.
4,5-HHP - Found: **C**, 41.90; **H**, 5.19; **N**, 24.13.